WEATHER RADAR INFORMATION PROCESSING AND REAL-TIME FLOOD FORECASTING

By

Dawei Han, B.Sc, M.Sc.

March 1991

This thesis is submitted

for the degree of Doctor of Philosophy of the

University of Salford

Water Resources Research Group,

Department of Civil Engineering,

University of Salford, U.K.

CONTENTS

LIST OF FIGURES

Chapter 3

Chapter 4

Chapter 5

Chapter 6

Chapter 7

Chapter 8

Chapter 9

LIST OF TABLES

Chapter 1

Chapter 3

LIST OF SYMBOLS

The following is a list of the principle symbols used in this thesis

A,B	Radar equation coefficients
$\in$	Belongs to
$\forall$	For all
α	Volume adjustor
γ	Shape adjustor
τ	Time adjustor
q	Quantisation step
σ^2	Signal power
Q	River flow, quantisation level
U	Quantisation output
h(t)	Impulse response function
z	Z-transform
u	Rainfall data
y	Flow data

ACKNOWLEDGMENTS

Grateful acknowledgement is given to Prof. Ian Cluckie for his supervision, help and encouragement throughout the project.

I should like to give my deepest thanks to:

Mr. Kevin Tilford and Mr. Stephen Burne for their help with many computational and research aspects associated with the project.

Dr Pao-shan Yu, Dr. Marcos Pessoa, Mr. David Viner and Mr. Owen Wedgwood for discussions on various aspects of the project.

Mr. Charles Beaton, Mr. Maurris Baker and Mr. Gordon Mills, Computer Managers of the Department, for their help in computing work.

Gratitude is expressed to the NRA (National Rivers Authority) Wessex Region for funding of the Research Assistantship and the Beijing Economic Management Institute of Water Resources and Electric Power for the first year scholarship.

Finally, I would like to express my gratitude to my parents for their support and assistance and my wife , Kang Wei-ping, for her tolerance and encouragement.

ABSTRACT

This thesis describes research into remotely sensed weather radar information systems and specifically addresses three problems; 1) Weather radar data processing; 2) Real-time flood forecasting models and 3) Computer system design for the realisation of the real-time flood forecasting system using radar data.

Quantitative rainfall measurements utilising weather radar is of high temporal and spatial resolution when compared with traditional rainfall measurements. Analysis was carried out to assess the type of radar data products required for operational use in flood forecasting system. This includes issues of data processing such as quantisation, temporal sampling and spatial sampling. The influence of the data process on hydrological applications is also addressed.

Theoretical analysis was carried out to probe the characteristics of Transfer Function Models and robust flood forecasting modelling procedure is proposed. The proposed model is always stable and physical realisable and is described as PRTF (Physical Realisable Transfer Function model). Algorithms and software for the identification of PRTF are presented. It was found that such a model is easy to identify and more importantly it can be updated robustly in real time. By changing the impulse response of the PRTF, it has been found that significant improvements can be observed in river flow simulation. A RST (Rainfall Separation Tank) model was developed and incorporated into the PRTF model. The adaptivity of the PRTF also has the potential to make use of high spatial resolution radar rainfall data and could be further incorporated into an Expert System suitable for real-time application.

Finally, the thesis includes the development of the WRIP system (Weather Radar Information Processor). Such a system can process weather radar information and use it for the real-time flood forecasting. The system design consists of database design, user interface design and program design. An object-oriented computing concept is used in the program design. The final system is currently in test operation within the N.R.A Wessex Region, including the man machine interface (MMI) incorporating a portable computer based data acquisition and display system known by the acronym 'STORM' (System To Obtain Radar Rainfall Measurements).

PART I INTRODUCTION

CHAPTER 1

INTRODUCTION

1.1 Foreword

Flooding is of universal concern and interest. It is one of the most dramatic interactions between man and his environment, emphasising both the sheer force of natural events and man's inadequate efforts to control them. The ability to provide sufficient advance warning of flood occurrence is important in reducing the potentially disastrous effects of flooding. It may, for example, save lives by giving floodplain residents time to remove themselves and their possessions to safety, and it may save property by allowing time to effect various structural and other adjustments. It is particularly appropriate to note that the 1990's have been designated as international decade for the mitigation of natural hazards of which flooding is one of the most destructive events identified.

During the past few decades the enormous increase in the world-wide availability of computers has influenced virtually all flood forecasting organisations and has made obsolete the classical approach to traditional flood forecasting. Modern high-speed, large-capacity computers make it feasible to model the entire flood-producing process in one operation. This approach has been encouraged not only by developments in computer technology and the complexity of flood calculations, but also by advances in our hydrological understanding of the runoff process.

The real-time flood forecasting system described in this thesis is based on weather radar rainfall data. The weather radar information processing and rainfall runoff modelling comprise the main part of the thesis. In this chapter, a brief introduction is given to illustrate the general research objectives, data access, rainfall runoff modelling developments and the overall structure of the thesis.

1.2 Objective of Real-Time Flood Forecasting

The three watchwords in flood forecasting are accuracy, reliability and timeliness.

Accuracy is clearly important for the forecast. If the forecast of peak river level is substantially in error then a false alarm may be raised or, worse, the system may fail to warn. In contrast to flood estimation for engineering design- where a poor answer is better than none- in flood warning it may be preferable not to issue forecasts than to do so using an inaccurate model.

Reliability of a flood forecasting system is primarily concerned with instrumentation, telemetry and procedural matters. However, no matter how well designed these aspects are, it is inevitable that the forecasting model will have to go through periods of outstation malfunction. It is therefore desirable that the forecasting method should reliably cope with imperfect or missing data: by validation checks, appropriate default values, and models designed for their specifically realtime role.

Accuracy and reliability are fairly obvious requirements; accuracy suggests we need a "good" model, reliability hints that simplicity and robustness may be important. But the requirement that gives flood forecasting a flavour of its own is timeliness.

If warnings are issued consistently late then the system is likely to be of little value, irrespective of the accuracy of its modelling. A balance has to be struck between

issuing a timely but potentially inaccurate forecast and the more cautious approach of compiling a good picture of the event before issuing an accurate but useless forecast (because it leaves insufficient time for dissemination of the warning and effective action by recipients).

1.3 Data Accessing

The variables primarily of interest in flood warning are river flow and rainfall. Advanced methods of flood forecasting may additionally require climate data, soil, moisture measurements and observations of snowpack characteristics. Many factors influence the range of variables monitored, not least modelling philosophy and outstation cost. In this section, weather radar rainfall data is described.

The use of radar in the estimation of precipitation emanated from the Second World War. On February 1941, a shower was tracked to a distance of 7 miles by a 10-cm wavelength radar located on the English coast. From that date on, radar meteorology commenced its development. Radar can produce detailed precipitation information for large areas from a single location in real time. For operational forecasting of river flow and flash floods, dense telemetered raingauge observations are desirable, but their installation has not been practical due to the cost of equipment and operation. Thus there has been considerable interest in utilising weather radar, since it provides spatially and temporally continuous measurements that are immediately available at one location. Although radar has been used experimentally for 40 years to measure rainfall, operational implementation has not been complete. Today we find that data are still not fully utilised quantitatively in hydrology and both confusion and misunderstanding exist about the inherent ability of radar to measure rainfall, about factors that contribute to errors, and about importance of careful calibration and signal processing. Whilst further researches are still needed to improve the performance of weather radar. It is now generally accepted that it provides the best means of remotely

measuring precipitation in both a qualitative and a quantitative manner.

1.3.1 Basic Theory of Radar

First the basic theory should be briefly described (for further introduction see Battan 1973 and Collier 1989). The average power received from a volume of rain-filled atmosphere at range **r** can be expressed as:

$$P_r = \frac{C K Z}{r^2} \qquad (1,1)$$

where **C** is a constant associated with the radar system, i.e., wavelength, transmitted power, antenna gain, beam width and pulse length; **K** is the fractional reduction in the signal strength by attenuation along the path of the propagation; and **Z** (equal to $\sum D_i^6$ with D_i's being diameters of individual raindrops in a unit volume of air) is referred to as the reflectivity factor. It is defined as:

$$Z = A.R^B \qquad (1,2)$$

where **A** and **B** are constants; **R** is the rate of rainfall, in mm/hr.

In reality, the **Z-R** relation varies significantly within storms, and also from storm to storm. Considerable work has been carried out to investigate the relationship between rainfall rate and radar reflectivity. Strictly speaking, if the rain drop size distribution were exponential and known, and vertical air motions were small relative to rain drop terminal velocities, there would be no fundamental limitation to the accuracy of the radar rainfall estimates. However, the drop size distribution is rarely known and it varies in time and space. In addition, vertical air motions are frequently of the same magnitude as the terminal velocities of rain drops (particular

in thunderstorms). More important is the presence of bright band when radar beam intersects the melting layer. The radar reflectivity will be greatly enhanced and the Z-R relationship will be quite different with the radar beam just intersecting rain drops. Thus the Z-R relationship is not unique and we are forced to rely on average empirical relationships. Battan (1973) presents a comprehensive list of **Z-R** relationships derived by a number of investigators. A widely used expression, based on the empirical study of Marshall and Palmer (1948), is

$$Z=200\ R^{1.6} \qquad (1,3)$$

In the U.K., radar rainfall data are derived by the relationship $Z=200*R^{1.6}$ and then modified by gauge calibrated domain maps to change **A** in Eq. (1,2) while retaining a constant value for **B**. There are some problems in this procedure especially when bright band is present.

1.3.2 Error Sources in Radar Estimates of Precipitation

Radar rainfall quantification is a complex matter which involves many parameters. It depends on a number of physical factors, the effects of which may vary significantly from one storm to another and even change within the same storm duration. Both the scatter and attenuation of microwaves by precipitation targets can be bases for estimation of precipitation. Currently, reflectivity data, either alone or in combination with raingauges, are considered most practical for operational measurement of rainfall over large areas. Note that the spatial detail of the rainfall field could not have been defined by a raingauge network. And also unfortunately , radar does not measure rainfall rate directly as do rain gauges, but rather indirectly relating it to the back scattered energy from precipitation particles in an elevated volume of atmosphere.

Some factors affecting radar measurement of surface rainfall have been identified:

(1) The accuracy of measurement of the equivalent radar reflectivity factor; This error source arises primarily from hardware calibration.

(2) Variations in the relationship between back scattered energy and rainfall rate. The relations can be divided into several groups according to rain type and geographic location. It is recognised that variation in the Z-R relationship may occur within storms, as well as from storm to storm. A large error may occur in the presence of bright band when the radar beam intersects the region where ice crystals melt to form rain.

(3) Effects of variation in precipitation with height. Because of curvature of the earth and the elevation of radar beam being above zero degree, the lowest height at which a radar can observe the atmosphere increases greatly with range. Therefore, if either the nature or intensity of the precipitation varies with height, radar indications may not be representative of surface rainfall, especially at large ranges. In fact, sometimes major changes occur to the precipitation before it reaches the ground.

(4) Hail and vertical air motions in convective cells. The presence of hailstones in intense convective storms causes a sharp increase in reflectivity with relatively slight effect on the actual rainfall rate. The presence of an updraft (downdraft) would decrease (increase) the fall speed of the rain drops relative to a stationary horizontal surface so that the value of Z for a given R would be less (greater) than for the same rainfall rate in still air;

(5) Anomalous propagation of the beam. A phenomenon which occurs when a shallow layer of cool moist air at the surface causes downward bending of microwave rays and produces echoes from ground targets that are normally below

the radar horizon.

(6) Discrepancies which result from sampling. Even if there are no actual errors in either gauge or radar measurements, there may be significant discrepancies between indicated amounts of rainfall at any given gauge site because of differences in sampling modes.

1.3.3 Radar Data Process

The rainfall process is a continuously varying signal (or may be pseudo continuous) which is converted from analogue to digital form. The conversion of such an analogue signal to a numerical form involves a double approximation. First, in the time domain, the signal s(t) is replaced by its values at integral time increments T, and is thus converted to s(nT). This process is called *sampling*. Secondly, in terms of signal strength or amplitude, each value of s(nT) is approximated by a whole multiple of an elementary quantity. This process is called *quantisation*. The approximate value thus obtained is then associated with a number. This process is called *coding*, a term often used to describe the whole process by which the value of s(nT) is transformed to the number that represents it. This can be thought of as having digitised the signal by 'level slicing' and that the 'allocation' of a numerical valve to represent each discrete 'slice' consists of the quantisation.

1.3.3.1 Sampling

Considering a continuously varying signal f(t) that is to be converted to digital form. We do this simply by first sampling f(t) periodically at a rate of f_c samples per unit time. The question that immediately arises is: What should the sampling rate be? Are there any limits to the rate at which we sample? One might intuitively feel that the process of sampling has irretrievably distorted the original signal f(t).

Have we lost valuable information in the sampling process?

The answer to this last question, and from this, to the other questions asked, is that under a rather simple assumption (closely approximated in practice), the sampled signal $f_s(t)$ contains within it all information about f(t). Further, f(t) can be uniquely extracted from $f_s(t)$! This rather important and not at all obvious result can be demonstrated through the use of Fourier analysis where $|X(j\omega)|$ represents the frequency spectrum of the continuous signal to be sampled, ω is the frequency and the ω_s is the sampling frequency.

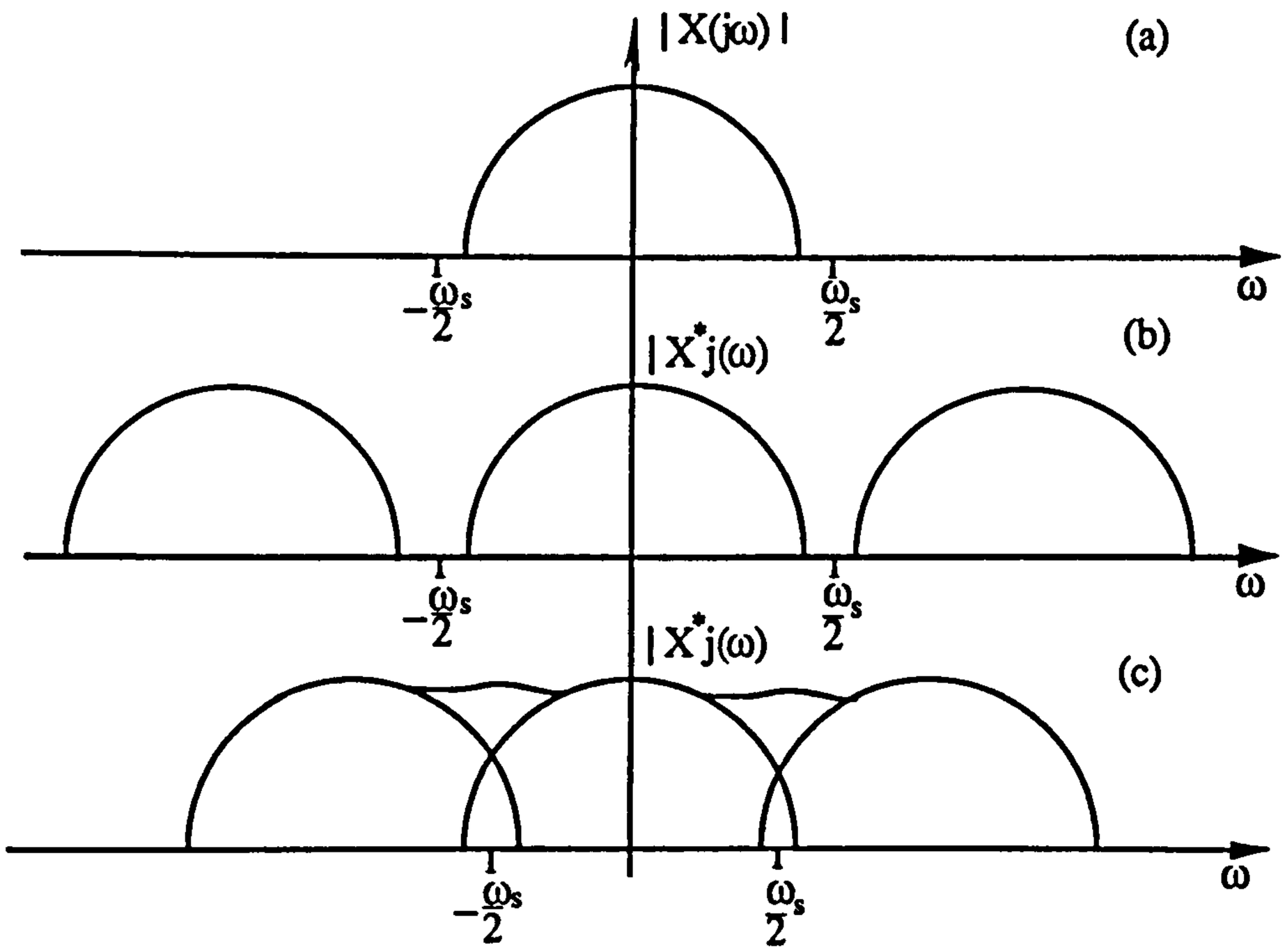

Figure 1.1 (a) Frequency Spectrum of the Continuous Signal; (b) Frequency Spectra of the Sampled Signal; (c) Aliasing of Frequency Spectra

Assuming the rainfall rate signal f(t) is band-limited to B in the frequency domain

(frequency theory will be introduced in the next chapter), it can be shown from sampling theory that sampling the signal does not destroy any information content, provided that the sampling rate $f_s \geq 2B$. The minimum sampling rate of 2B times per unit time is called the *Nyquist sampling rate* and the 1/2B the *Nyquist sampling interval.* The lower, Nyquist , limit on the sampling rate in the case of periodic sampling is highly significant. If we sample at too low a rate, the signal may change radically between sampling times. The phenomenon of overlapping spectra due to too low a sampling rate, and the distortion that results, is termed aliasing. We thus lose information and eventually produce a distorted output.

In the hydrological process, the flood forecasting model sampling rate will have a direct relationship with the catchment response characteristics. It should be kept in mind that the radar rainfall data measurement sampling rate is quite different from the model sampling rate. Too short a model sampling rate will cause strong data collinearity and large errors in model identification. It is never too short for radar data measurement sampling providing it is technical possible and without other cost. It is always possible to use prefiltering techniques to remove the obsolete information and obtain a much improved data set for subsequent hydrological usage.

1.3.3.2 Quantisation

Quantisation is the approximation of each signal value s(t) by a whole multiple of an elementary quantity q which is called the quantising step. If q is constant for all signal amplitudes, the Quantisation is said to be *uniform*, otherwise it is called *nonuniform.* The resultant signals are said to be quantised. Unlike the sampling process (providing the Nyquist frequency is above the maximum process frequency) this results in an irretrievable loss of information since it is impossible to reconstitute the original analogue signal from its quantised version. For practical purposes, there is actually no need to retain all possible signal amplitudes and the

hydrological process may not be sensitive to the noise introduced by an appropriate quantisation procedure.

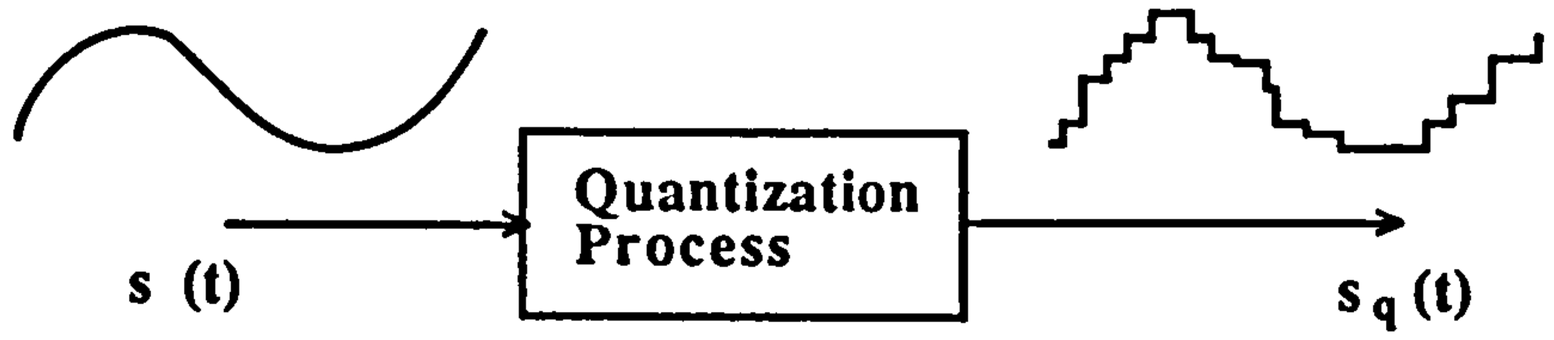

(a) The Quantisation Operation

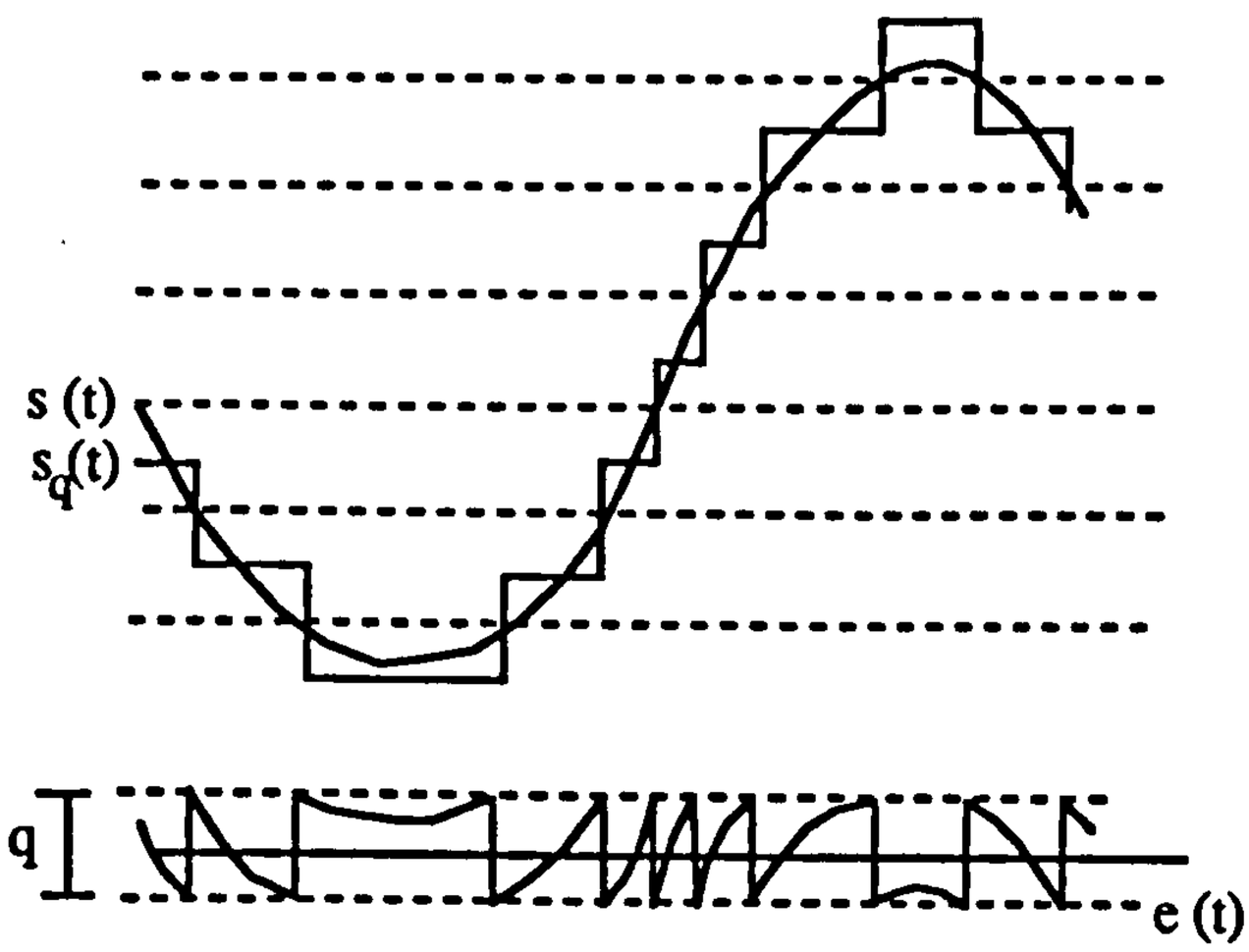

(b) Quantisation error

Figure 1.2 Quantisation Process

The effect of this approximation is to superimpose on the original signal an error signal e(t) called the quantising distortion or, more commonly, the quantising noise. Thus:

$$s(t) = s_q(t) + e(t) \qquad (1,4)$$

Detailed discussion will be carried out in the following chapter about the quantisation properties and its influence on the hydrological process.

1.2.3.3 Coding

The signal which is sampled and quantised in amplitude is represented by a set of numbers which are usually in binary form. If each number has N bits, the maximum number of quantised amplitudes that it is possible to represent is 2^N. This method of representation is called *binary coding*.

Two coding schemes are available: *Fixed-length code* and *Variable-length code* (Grant 1989).

Fixed-length code (also called *the block encoding scheme*) is to assign a unique set of R binary digits to each symbol (or level). The number of binary digits per symbol (or level) required for unique encoding when L (the number of symbols or levels to be represented) is a power of 2 is

$$R = \log_2 L \tag{1,5}$$

and, when L is not a power of 2, it is

$$R = [\log_2 L] + 1 \tag{1,6}$$

The notation [ ] denotes the largest integer contained in it.

Variable-length code is that when the source levels are not equally probable, it is more efficient to use variable-length code words. The levels that occur more frequently are assigned short code bits and the levels that occur infrequently are assigned long bits. The probabilities of occurrence of the different levels are utilised in the selection of the code levels. This type of encoding is called *entropy coding* (Grant 1989).

For simplification, the radar data are encoded into block code at the radar site. That means a fixed number of bits are utilised to represent each radar rainfall intensity level.

A typical identification table for block coding would appear as indicated in Table1.1.

Table 1.1 Typical Identification Table for Block Encoding

Binary Code	
7	111
6	110
5	101
4	100
3	011
2	010
1	001
0	000

As an example, radar data might be restricted to the 16 values, 1,2,4,8,16,.... If one value is 1.9, the quantised output will be 2, the nearest of the allowable values. Each of the 16 values can be represented by a set of four binary symbols. The final signal output would then be sequences of four-digit binary numbers. Transmission errors are less likely with binary symbols than with the original 16-level quantised signal. A compromise will be made between the cost and complexity of smaller quanta and an increased number of levels on the one hand vs. reduced errors. At present, two quantised radar products are available from the Meteorological Office which form the 3-bit and 8-bit data stream.

1.3 The Rainfall Runoff Model

The rainfall runoff process is a complicated natural phenomena. For practical purposes the rainfall-runoff problem is often considered from the phenomenological point of view, mainly on account of the complexity of the various physical phenomena involved and also because of scarcity of the data that would be required for physical simulation. This means that the internal details of the physical mechanism are not examined, but that the catchment is treated as a lumped essentially 'black box' system converting input into output. The main input into the system is rainfall and main output is streamflow. One of the better known methods involving the phenomenological approach is the unit hydrograph, introduced by Sherman [1932] . Later, the TF model (Transfer Function model) was adopted (e.g see typically Box and Jenkins (1970)) to simulate the rainfall runoff process. The transfer function model is efficiently parametrised and naturally suited to real-time use. Researches have been carried out at the University of Birmingham (and lately, following a transfer of period, within the Water Resources Research Group at the University of Salford) , Institute of Hydrology and other Institutions and have indicate that the TF model is a suitable model for exploitation in real time forecasting systems.

The amount of water stored in a hydrologic system, S may be related to the rates of inflow I and outflow Q by the integral equation of continuity (1,7).

$$\frac{dS}{dt} = I - Q \qquad (1,7)$$

Imagine that the water is stored in a hydrologic system, such as a reservoir in Figure 1.3, in which the amount of storage rises and falls with time in response to I and Q and their rates of change with respect to time: dI/dt, d^2I/dt^2,..., dQ/dt,

d^2Q/dt^2,... Thus, the amount of storage at any time can be expressed by a storage function as:

$$S = f\left(I, \frac{dI}{dt}, \frac{d^2I}{dt^2}, \ldots Q, \frac{dQ}{dt}, \frac{d^2Q}{dt^2} \right) \qquad (1,8)$$

The function *f* is determined by the nature of the hydrologic system being examined. For example the storage can be described as S=kQ, where *k* is a constant.

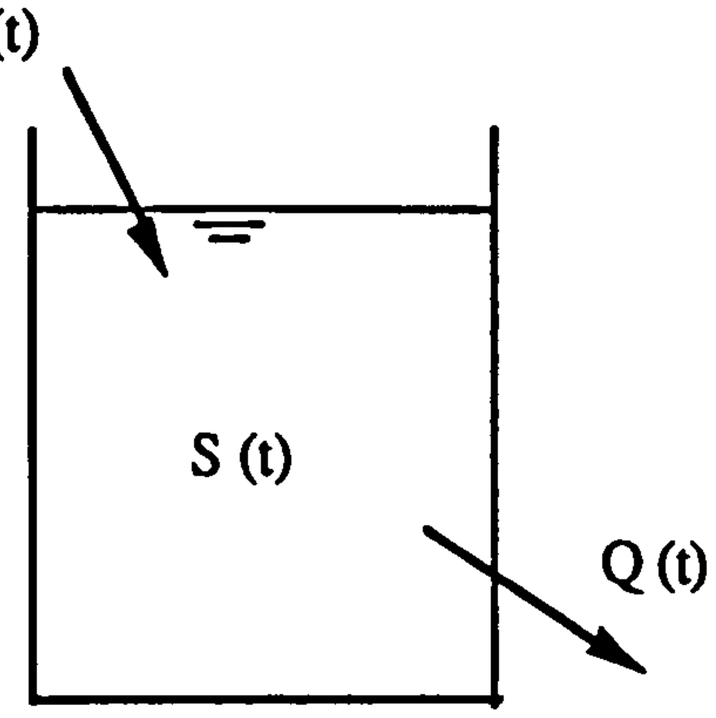

Figure 1.3 Continuity of water stored in a hydrological system

The continuity equation (1,7) and the storage function equation (1,8) must be solved simultaneously so that the output *Q* can be calculated given the input *I*, where *I* and *Q* are both functions of time.

For the storage function to describe a linear system, it must be expressed as a linear equation with constant coefficients

$$S = a_1 Q + a_2 \frac{dQ}{dt} + a_3 \frac{d^2Q}{dt^2} + \ldots + a_n \frac{d^{n-1}Q}{dt^{n-1}}$$
$$+ b_1 I + b_2 \frac{dI}{dt} + b_3 \frac{d^2I}{dt^2} + \ldots + b_m \frac{d^{m-1}I}{dt^{m-1}} \qquad (1,9)$$

in which $a_1, a_2, \ a_n, \ b_1, b_2, \ldots b_m$ are constants and derivatives of higher order than those shown are neglected. Constant coefficients also make the system time-invariant so that the way the system processes input into output does not change with time.

Differentiating (1,9), substitute the result for dS/dt in (1,7), and rearranging yields

$$a_n \frac{d^nQ}{dt^n} + a_{n-1} \frac{d^{n-1}Q}{dt^{n-1}} + \ldots + a_2 \frac{d^2Q}{dt^2} + a_1 \frac{dQ}{dt} =$$
$$I - b_1 \frac{dI}{dt} - b_2 \frac{d^2I}{dt^2} - \ldots - b_{m-1} \frac{d^{m-1}I}{dt^{m-1}} - b_m \frac{d^mI}{dt^m} \qquad (1,10)$$

which may be rewritten in the more compact form

$$N(D)\ Q = M(D)\ I \qquad (1,11)$$

where D= d/dt and N(D) and M(D) are the differential operators

$$N(D) = a_n \frac{d^n}{dt^n} + a_{n-1} \frac{d^{n-1}}{dt^{n-1}} + \ldots + a_2 \frac{d^2}{dt^2} + a_1 \frac{d}{dt} + 1$$

$$M(D) = -b_m \frac{d^m}{dt^m} - b_{m-1} \frac{d^{m-1}}{dt^{m-1}} - \cdots - b_1 \frac{d}{dt} + 1$$

Solving (1,11) for Q yields

$$Q(t) = \frac{M(D)}{N(D)} I(t) \qquad (1,12)$$

The function M(D)/N(D) is called the transfer function of the system; It describes the response of the output to a given input sequence. Equation (1,12) was presented by Chow and Kulandaiswarmy (1971) as a general hydrologic system model.

From the above we can view the hydrological process as a system. According to system theory it is known that if the input time series is x(t) and the output time series is y(t), the system may be described by a system function h(t).

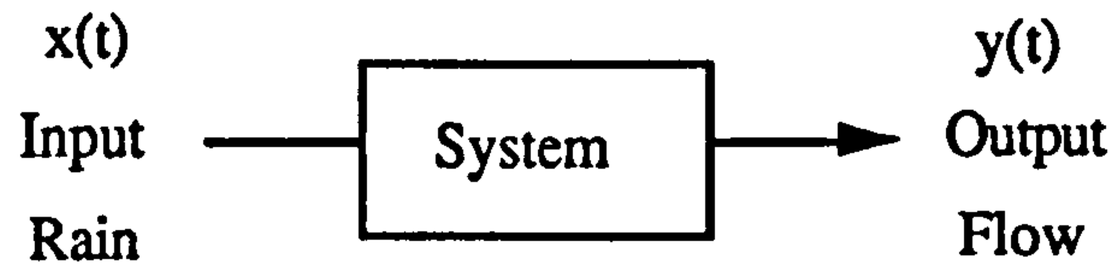

Figure 1.4 A Single-Variabled Dynamic System

Generally speaking, any system is composed of three elements:

1. Input;

2. Output;

3. Translation Operator linking the two.

The rainfall runoff process is a continuous system where the input and output are

continuous variables. In practice the data are transformed into discrete data by sampling from the continuous signals and are called a sampled-data system (a class of discrete variable). If we define two sequences of discrete variables {Ut} and {Yt} and a translation operator *S*, then a system can be characterised by the transformation equation

$$\mathbf{Yt = S(Ut,t)\ Ut} \qquad (1,13)$$

The transformation operator *S* is often termed the *Transfer Function* of the system which has the same meaning as in Equation (1,12). It is that operator which transfers the single variable sequence {Ut} into the single sequence {Yt}. The transfer function thus determines the system output {Yt} at any point in time *t* on the sampling interval. The transfer function that links one input and one output is usually referred to as a univariate system transfer function model. It can also be described as a lumped parameter system as the system is defined at one given point or aggregated over an area of space. A transfer function which describes a spatial system must depict the transformation operations of a variable sequence or set of sequences that are distributed in space and are thus termed a distributed parameter or space-time system.

Two Particular properties of transfer functions deserve special attention: *Linearity and Stationarity.*

(1) Linearity: The transfer function S of a process is said to be linear if *S* remains constant for all magnitudes of input, that is

$$\mathbf{Yt = S\ Ut} \qquad (1,13)$$

The system is said to be nonlinear if the transfer function is a function of the magnitude of the input. That is

$$\mathbf{Yt=S(Ut)\ Ut} \qquad (1,14)$$

(2) Stationarity: If the transformation S is constant in time, the system is said to be stationary and the effect of any input Ut will be the same at any time. The transfer function is nonstationary if it varies as a function of time, that is

$$\mathbf{Yt = S(t)\ Ut} \qquad (1,15)$$

The rainfall runoff process is a class of nonlinear and nonstationary system. For small storms most of the rainfall on a drainage basin is absorbed by the soil and vegetation and it takes a long time for the water to migrate to the outlet of the basin, indeed a large proportion is lost through evaporation and evapotranspiration. For large storms, in contrast, the soil will soon become saturated as the rate of rainfall exceeds the rate of infiltration, and much of the precipitation will flow overground or through the upper levels of the soil. Thus the runoff from large storms reaches the main drainage channel faster than the runoff from smaller storms, which are characterised by a large proportion of flow through intermediate levels of the soil and as groundwater. So the parameters governing the transfer function will thus differ for various magnitudes of input and different time steps.

In practical work, after some restrictions are put upon the magnitude of the input sequence and the time period, a linear and stationary model can often be utilised to describe the system since such a model is easy to set up and usually robust. The TF model has been widely utilised by the research group at Salford and it has proven a very effective model for the flood forecasting process.

1) Rainfall Runoff Simulation

The rainfall runoff process can be simulated by the following formula

$$y_t = a_1 y_{t-1} + a_2 y_{t-2} + \cdots + a_p y_{t-p} + b_0 u_t + b_1 u_{t-1} + b_2 u_{t-2} + \cdots b_q u_{t-q} \quad (1,16)$$

Where

a_i , b_i = Model parameters;

y_t = River flow at time t;

u_t = Rainfall rate at time t.

The system gain is defined as

$$SSG = (b_0 + b_1 + b_2 + \cdots + bq) / (1 - a_1 - a_2 - \cdots - a_p) \quad (1,17)$$

Which represents the percentage runoff of the process.

The simulation model is quite useful when we examine the model performance. In the forecasting processes, the feedback from the observed river flow can easily be incorporated in the model.

2) Runoff Forecasting

During flood forecasting, since the system input is used to forecast the system output, forecasts can be achieved only if the input leads the output in response to changes by a period equal to or greater than the forecasting lead time required. If the input is known ahead in time, then leading indicator forecasts are easy to develop. But if the input is not known ahead in time, a system input must be forecast before forecasting the system output.

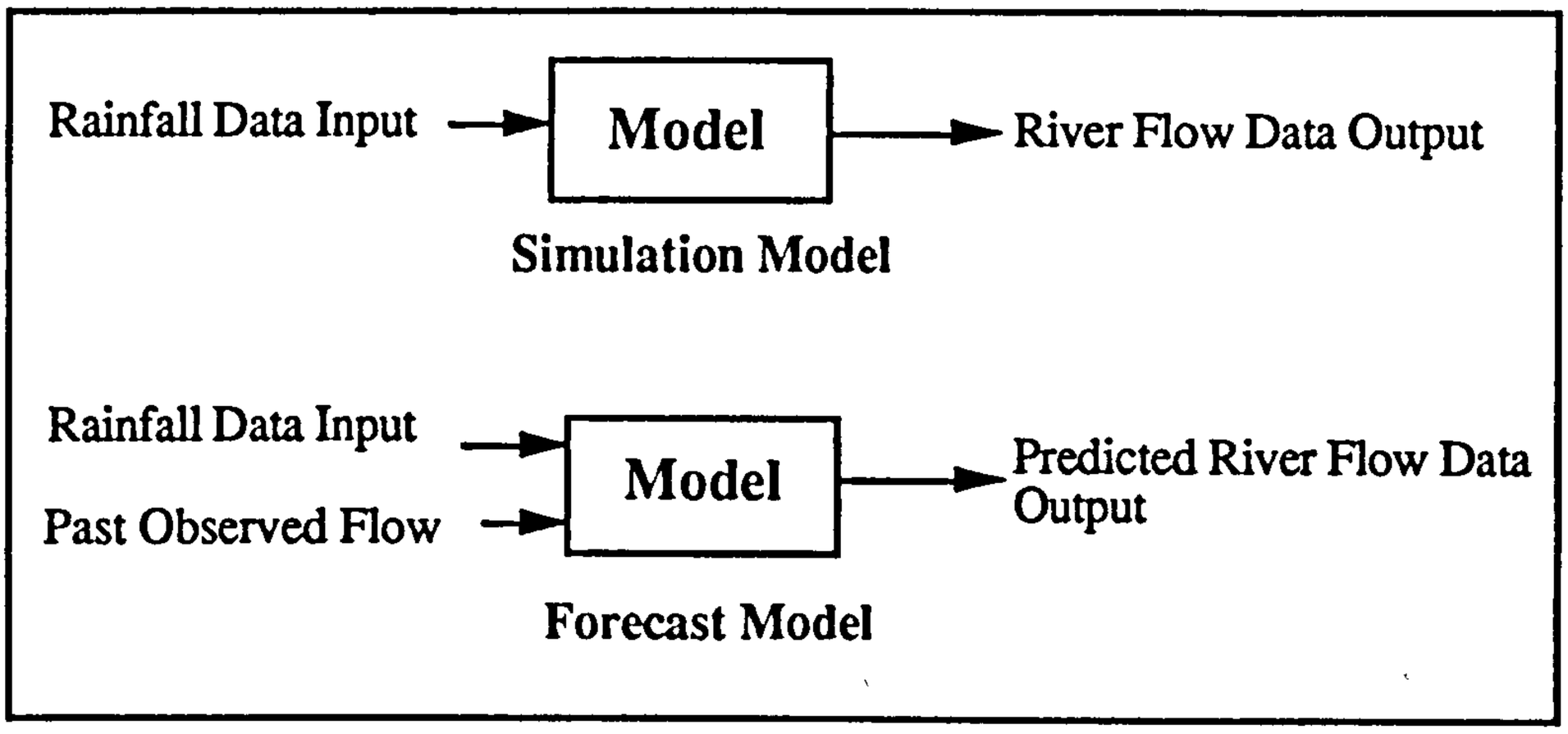

Figure 1.5 TF Model Simulation and Forecasting of Rainfall Runoff Process

If the forecast leading time is 1, then the Transfer Function Forecasting model can be written as

$$Y_{t+1} = a_1 y_t + a_2 y_{t-1} + \ldots + a_p y_{t-p} + b_0 U_{t+1} + b_1 u_t + b_2 u_{t-1} + \ldots b_q u_{t-q} \quad (1,18)$$

Where

Y_{t+1} Predicted flow at leading time 1;

U_{t+1} Predicted Rainfall rate at leading time 1;

y_i & u_i Measured flow and rainfall rate.

The use of a future rainfall scenario is important for single and multi-step ahead forecasting. There are several non-exclusive options which can be chosen:

a) No more rainfall;

b) Data generated by a storm forecasting model;

c) Sequence chosen by the duty hydrologist;

d) Frontiers data (Collier, 1989).

In reality, there usually exists a time delay between the rainfall and the generated flow, so the term U_{t+1} can usually be neglected in practice.

The TF model in Eq (1,18) can also be expressed as

$$H(\omega) = \sum_{k} h_k e^{-i\omega k} \qquad (1,19)$$

The weight function, h_k provides a description of the system response in the time domain. The discrete function $\{h_k\}$ is called the *impulse response function* (some people prefer to call it the unit sample response function). An alternative way of describing a linear system is by means of a function, called the *frequency response function* (Chatfield, 1984), which is the Fourier transform of the impulse response function. It is defined by Equation (1,19).

The frequency response and impulse response functions are equivalent ways of describing a linear system. For some purposes $H(\omega)$ is much more useful than h_k.

1.4 Thesis Structure

This thesis is divided into 5 parts. The introductory paragraphs have outlined the need for accurate real-time flood forecasting. Weather radar is the main provider of real-time rainfall data and the rainfall runoff modelling process is principally addressed by a transfer function approach.

Part II consists of two chapters which describe the radar data process in some detail. Sampling (both temporal and spatial) and quantisation are two main characteristics of radar data utilisation discussed. The conflict between accuracy and cost is addressed by detailed analysis of the various aspects of the digital

processing problem.

Part III concentrates upon the rainfall runoff process. An analysis is carried out to illustrate the principal characteristics of the TF model and a alternative structure is introduced which is easy to identify and has the ability to adapt dynamically to the catchment response. A distributed kinematic wave model is used to simulate the relationship between storm type and catchment response. Finally a new model which incorporates a PRTF (Physical Realisable Transfer Function) and RST (Rainfall Separation Tank) is developed.

Part IV presents the development of the WRIP system (Weather Radar Information Processor). The system structure, database design, user interface design and program design are addressed. Some specific problems related to NRA Wessex region are also described.

The final part presents conclusions which summarise the results from this thesis and suggests further work to be carried out as consequence.

PART II RADAR DATA PROCESSING

CHAPTER 2

TEMPORAL AND SPATIAL SAMPLING OF RADAR DATA

2.1 Introduction

The sampling of radar rainfall data is an important issue for data quality. A dense sampling rate can provide more information for the user but will cost more to process, archive and transmit. This chapter describes some analysis to assess the influence of sampling on radar data quality.

2.2 Sampling Theorem

The operation of sampling a signal f(x) at a single point x=a is achieved with the impulse function $\delta(x)$ and defined by the 'shift integral':

$$\int_{-\infty}^{+\infty} f(x)\,\delta(x-a)\,dx = f(a) \qquad (3,1)$$

Here, the function $\delta(x-a)$ is the sampling impulse. The periodic sampling of a waveform is performed mathematically by means of a sampling impulse train

$$\sum_{k=-\infty}^{+\infty} \delta (t - kT) \qquad (2,2)$$

so that the sampled waveform $f_s(t)$ is given by the relationship

$$f_s(t) = f(t) \sum_{k=-\infty}^{+\infty} \delta (t-KT) \qquad (2,3)$$

According to sampling theory, we must sample at a rate (Nyquist Frequency) which is as least twice the highest frequency in the signal.

$$f_s \geq 2f_m$$

Where f_s is the sample rate and f_m is the maximum frequency component of the signal. In this case, perfect reconstruction can be made by using an ideal low pass filter. The perfect reconstruction referred to by the sampling theorem is much more complicated, since it uses all past and future sample values to compute a single point value. One reconstruction formula that can be shown to provide perfect reconstruction is defined by the infinite sum of weighted sample values

$$f (t) = \sum_{k=-\infty}^{+\infty} f (kt) \frac{\sin [\pi (t - k T)/T]}{\pi (t - k T) / T} \qquad (2,4)$$

The contribution of distant sample values is small, due to the decaying nature of the interpolation function. From the practical point of view, good reconstruction can be produced from a finite set of nearby sample values despite the fact that the mathematical theorem calls for contributions from all past and future samples.

2.3 Spectral Analysis

Spectral analysis can be a useful exploratory diagnostic tool in the analysis of time series. it is essentially a modification of Fourier analysis so as to make it suitable for stochastic rather than deterministic functions of time. Fourier analysis is basically concerned with approximating a function by a sum of sine and cosine terms, called the Fourier series representation.

The power spectrum of a stochastic process, or spectral density function, is defined by the continuous function

$$f(\omega) = (2\pi)^{-1} \left[C_0 + 2 \sum_{k=1}^{\infty} C_k \cos \omega k \right] \qquad (2,5)$$

Where ω, the frequency in radians, may take any value in the range $[-\pi, \pi]$. However, since $f(\omega)$ is symmetric about zero, all the information in the power spectrum is contained in the range $[0, \pi]$. C_i is the autocovariance of the process.

If y_t is white noise, $C(k) = 0$ for $k \neq 0$, and so

$$f(\omega) = \sigma^2 / 2\pi$$

Where σ^2 is the variance of y_t. The process may be regarded as consisting of an infinite number of cyclical components all of which have equal weight. In fact, this effectively provides a definition of white noise in the frequency domain.

In practise, the equation above can't be used to estimate the spectrum from the sampled data. It can be shown that the sample spectrum of a stationary time series may fluctuate radically about the theoretical spectrum since the Fourier series representation requires one to evaluate N parameters from N observations however long the series. There exist several alternative procedures for carrying out a spectral analysis. Each method provides a consistent estimate of the spectrum based on some sort of smoothing procedure.

A popular type of estimation procedure consists of taking a Fourier transform of the truncated sample autocovariance function using a weighting procedure to smooth the sample spectrum which is defined as

$$f(\omega) = (2\pi)^{-1} \left[w_0 C_0 + 2 \sum_{k=1}^{m} w_k C_k \cos \omega k \right] \qquad (2,6)$$

Where $\{ w_k \}$ are a set of weights called the lag window, and m (<the number of sample data) is called the truncation point. The choice of the truncation point, M, is rather difficult and little clear-cut advice is available in the literature. It has to be chosen subjectively so as to balance ' resolution' against ' variance'. The smaller the value of M, the smaller will be the variance of f(ω) but the larger will be the bias. If M is too small, important features of f (w) may be smoothed out, while if M is too large the behaviour of f (w) becomes more like that of the periodogram with erratic variation (refer to Box and Jenkins (1976) for periodogram). Thus a compromise value must be chosen. A useful rough guide is to choose M to be about two times the square root of the number of sampled data. There are several windows available, such as the Turkey window, Parzen window, Barlett window, rectangular window and so on, of which Parzen is generally considered superior to the others and is employed in this thesis. The Parzen window is as follows

$$W_k = 1 - 6K^2 + 6K^3 \qquad 0 <= K <= 0.5$$

$$Wk = 2(1 - K)3 \qquad 0.5 < K < 1$$

The spectral analysis is mainly concerned with estimating the spectrum over the whole range of frequencies and therefore it is an useful tool for the sampling analysis.

2.4 Temporal Sampling of Radar Rainfall Data

Weather radar measures the rainfall field in a discrete form and the UK Meteorological Office uses a shortest interval of 5 minutes to represent quantitative data. In hydrological usage, we usually require half hourly or even hourly rainfall data. The measurement sampling is related to the sampled signal while the flood forecasting model sampling interval will depend on the system response property.

To evaluate a sampling scheme, we must rely on spectral analysis to treat the rainfall rate data as a time series in the frequency domain. As mentioned previously, if the Nyquist frequency is above the highest frequency in the sampled signal, there will be no loss of information otherwise an aliasing error will occur. In the aliasing situation, we not only lose information but also introduce some distortion from the foldback of higher frequencies. The rainfall process sampling rate will differ for different locations and different seasons. A thorough statistical study is needed to obtain an optimum sampling scheme.

An example is given by using Upavon data for an event on the catchment of the River Asker on 26th Dec. 1985. Results show that for the 5 minute interval sampling process, the estimated spectrum approaches zero as the frequency approaches the Nyquist frequency. This suggests that there is no aliasing and that

the choice of the sampling interval is sufficiently small. When the sampling interval is increased to 15 minutes, there is still some spectrum above the Nyquist frequency and we find there is some aliasing effect. As the the proportion of the spectrum above the Nyquist frequency is not large, the error caused by aliasing is reasonable small. When the sampling interval exceeds half an hour a noticeable noise is observed and the spectrum above the Nyquist frequency can't be neglected.

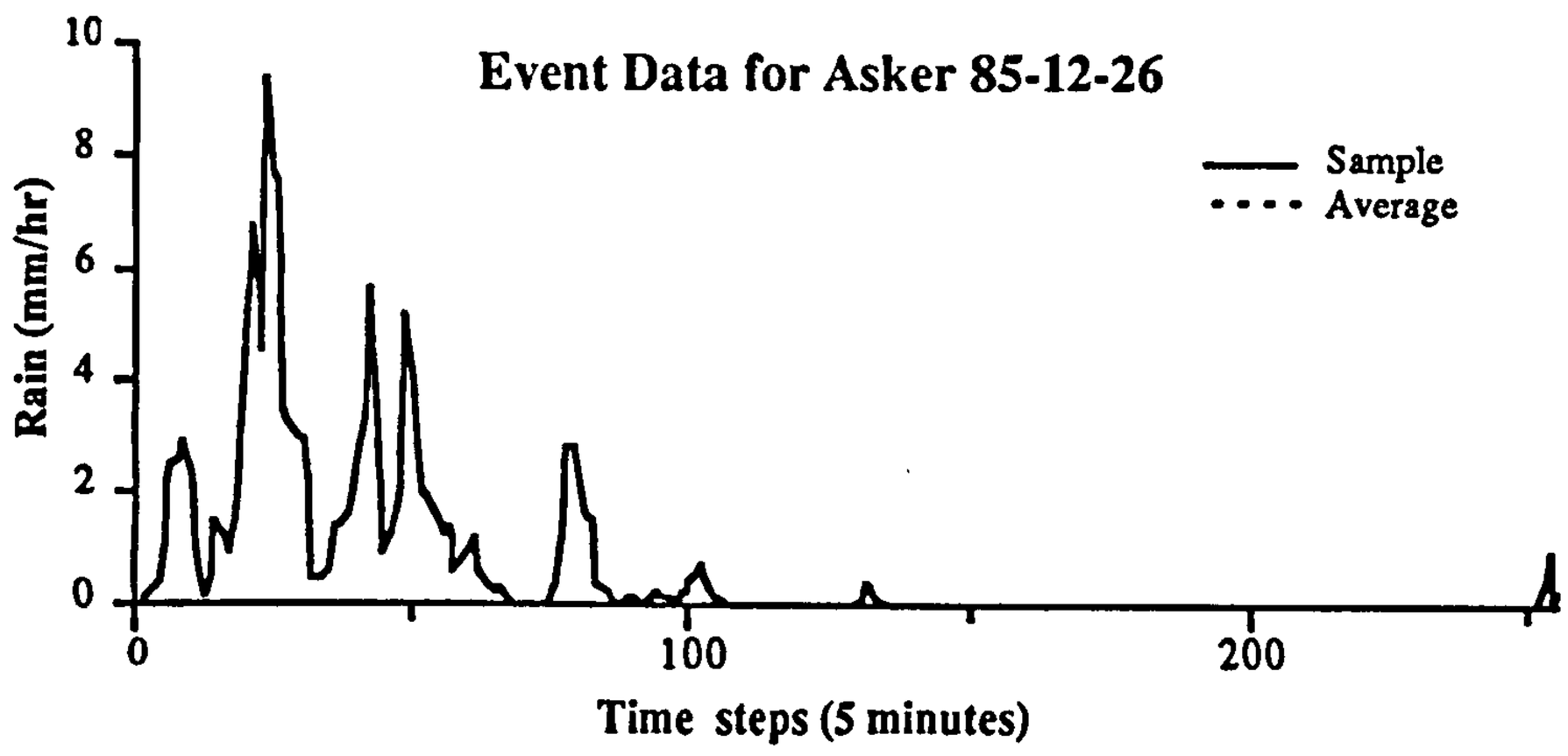

Figure 2.1 Comparison of Rainfall Data by 5 minute Sample and Average (Two curves are overlaid)

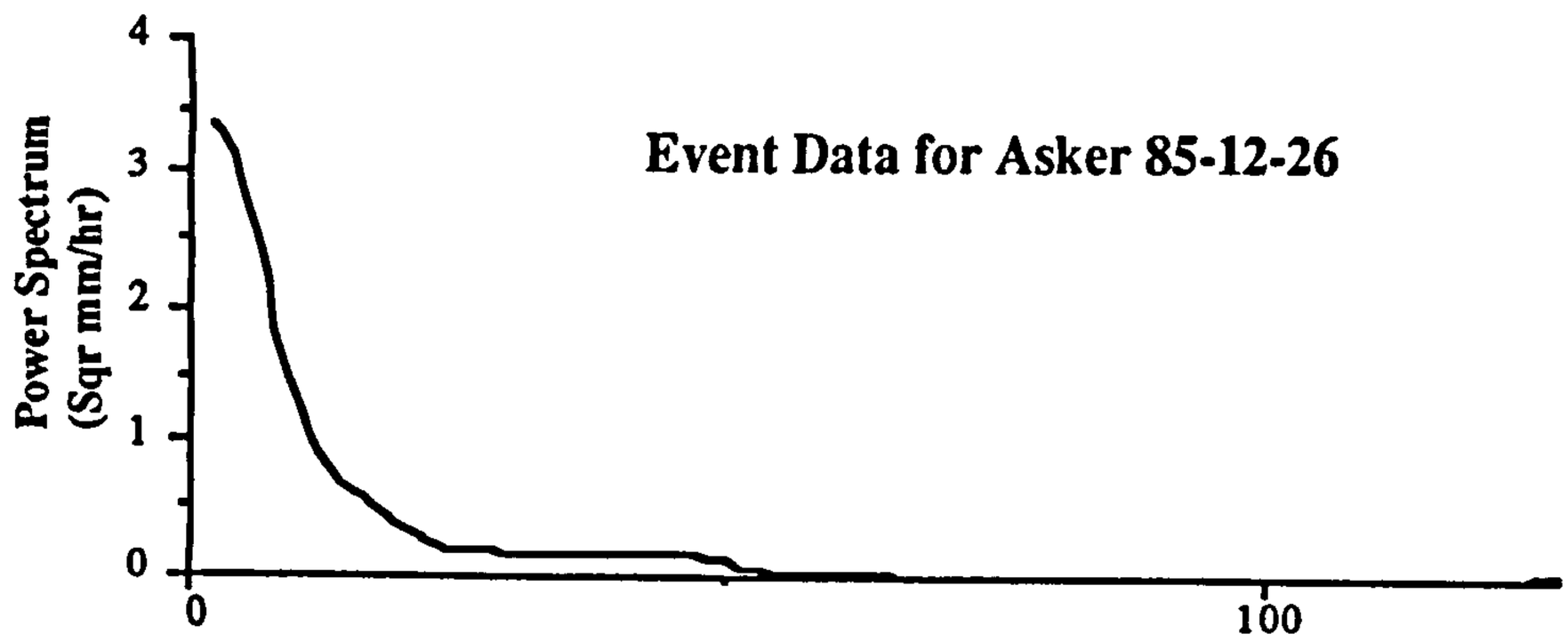

Figure 2.2 Power Spectrum of 5 Minute Rainfall Data

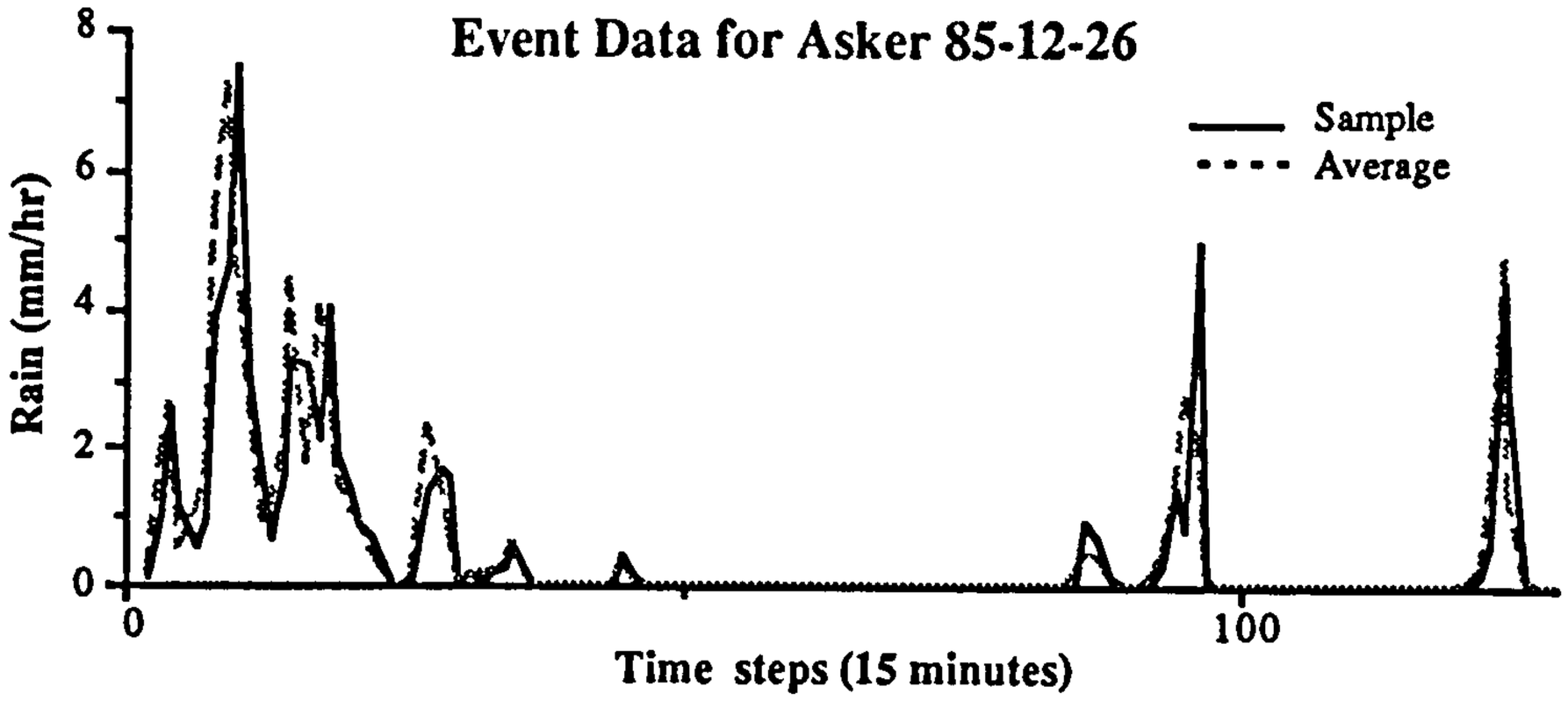

Figure 2.3 Comparison of Rainfall Data by 15 minute Sample and Average

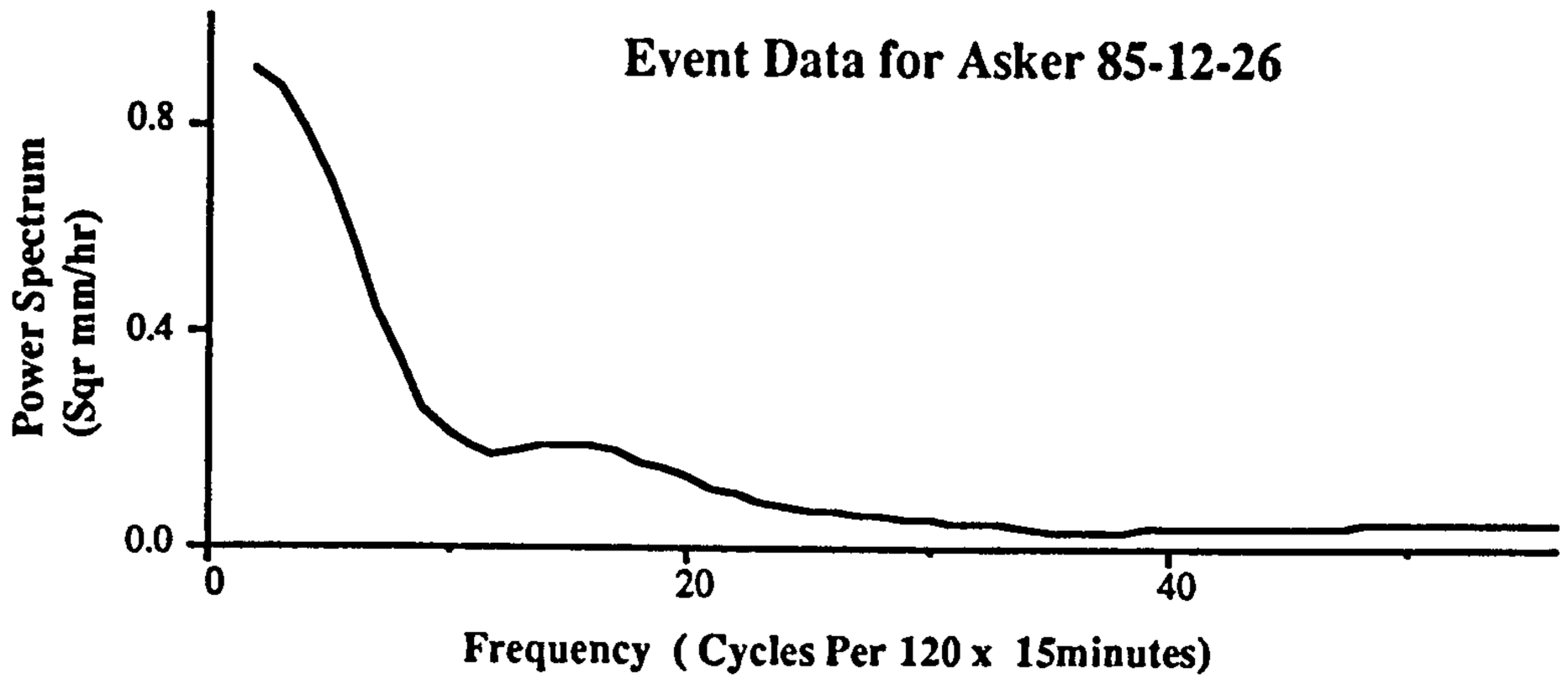

Figure 2.4 Power Spectrum of 15 Minute Rainfall Data

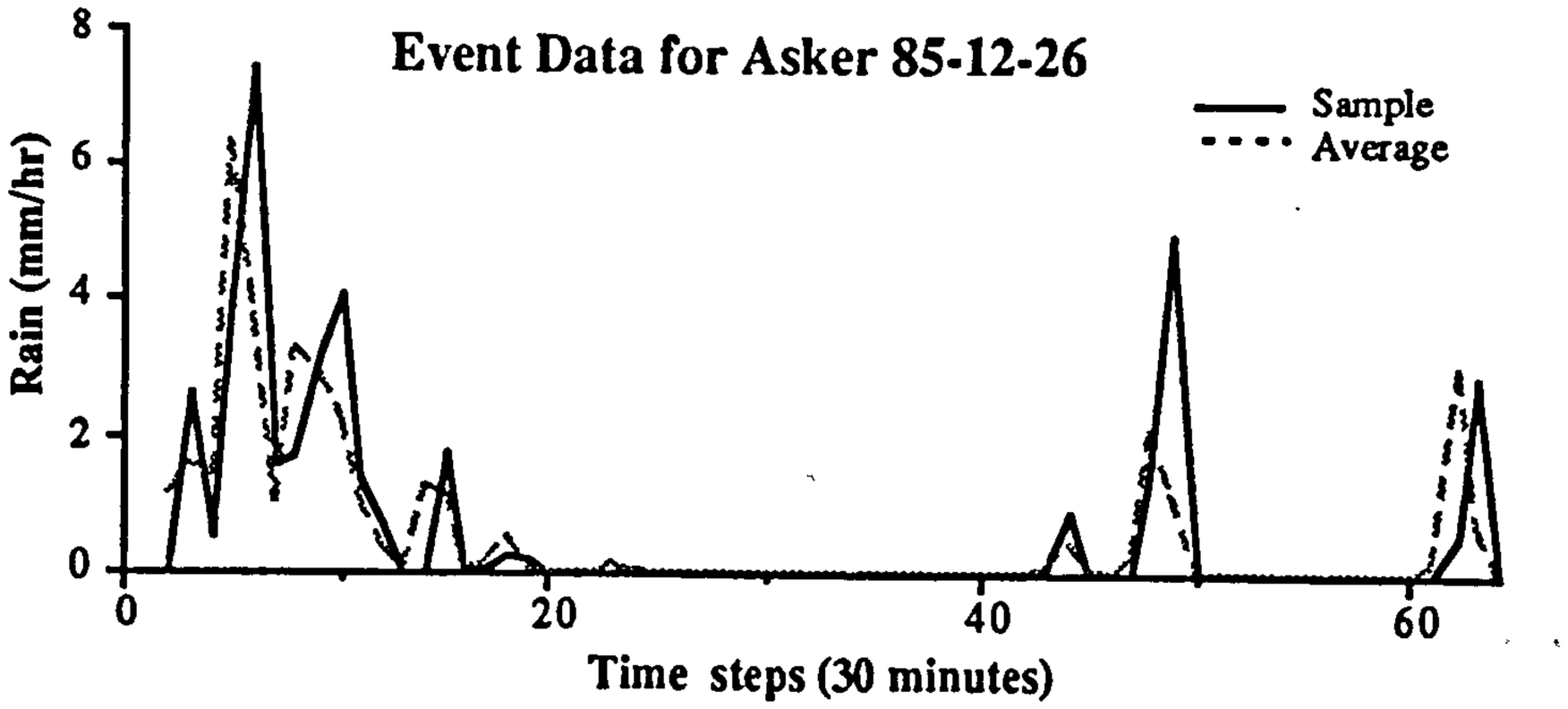

Figure 2.5 Comparison of Rainfall data by 30 minute Sample and Average

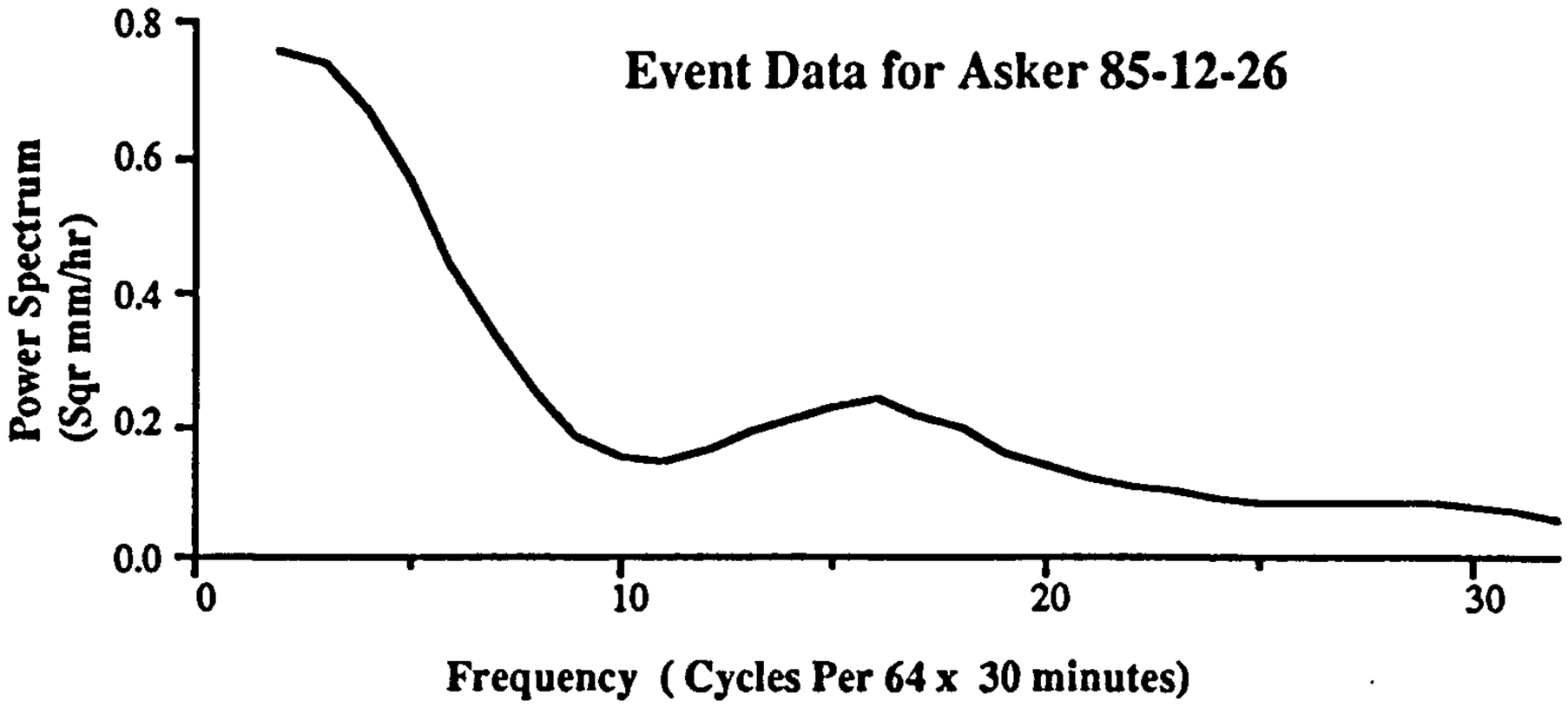

Figure 2.6 Power Spectrum of 30 Minute Rainfall Data

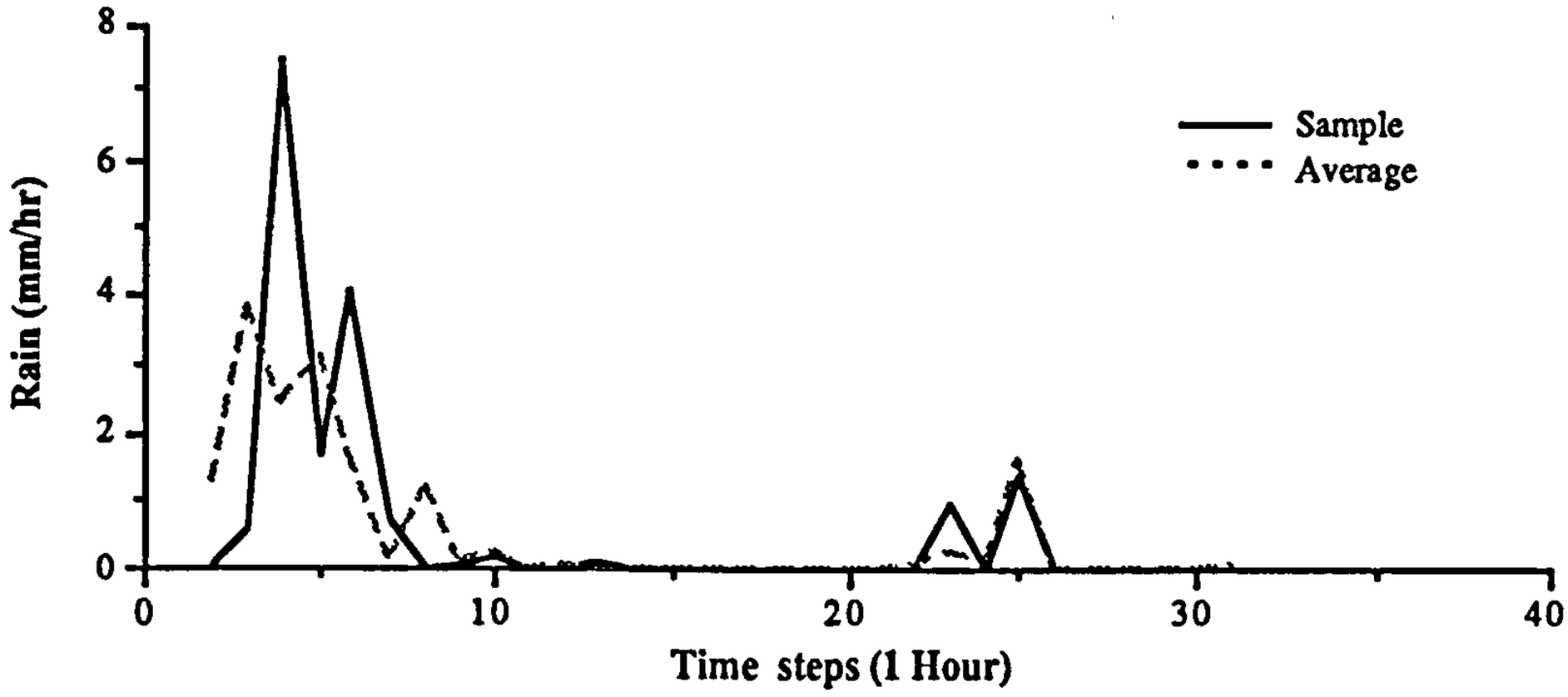

Figure 2.7 Comparison of Rainfall data by 60 minute Sample and Average

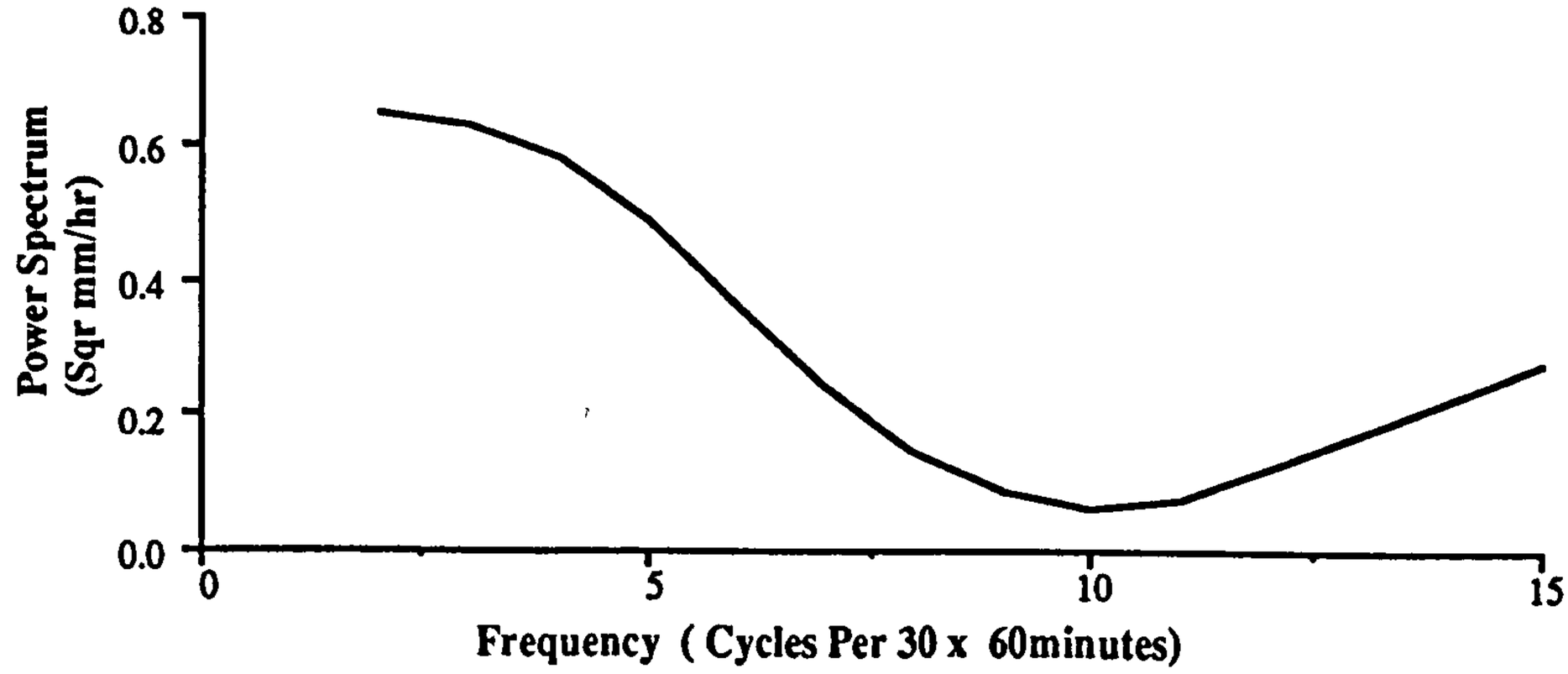

Figure 2.8 Power Spectrum of 60 Minute Rainfall Data

From the example presented above, a sampling interval not more than 15 minutes can be utilised and the aliasing effect is quite small. A further statistical analysis should be used to assess the radar data sampling schemein order to prevent large aliasing errors and possibly decrease the sampling costs by increasing the sampling interval.

2.5 Spatial Sampling of Radar Rainfall Data

The preceding section has been concerned with the temporal sampling. Each system variable has been assumed to be either a lumped characterisation (averaging) of all the effects at that location, or a point sample of events at that location. The specificity of the location itself and the relativistic effect of possible interactions with other locations have both been ignored. In reality the rainfall process is a Space-Time system. Rainfall spatial distribution has a great influence in the larger catchment. Spatial sampling is a very important aspect of the systems analysis.

The spatial sampling process is a 2-D sampling data sequence

$$\mathbf{f = [\ f(n1,n2)]}$$

Which is normally of finite extent,i.e.,

$$0 \le n1 < N1;\ 0 \le n2 < N2$$

In figure 2.9 two radar data spatial sampling schemes are shown and they consist of 76*76 grids (2km data) and 84*84 grids (5 km data) from the Upavon radar data and are typical of the UK radar network.

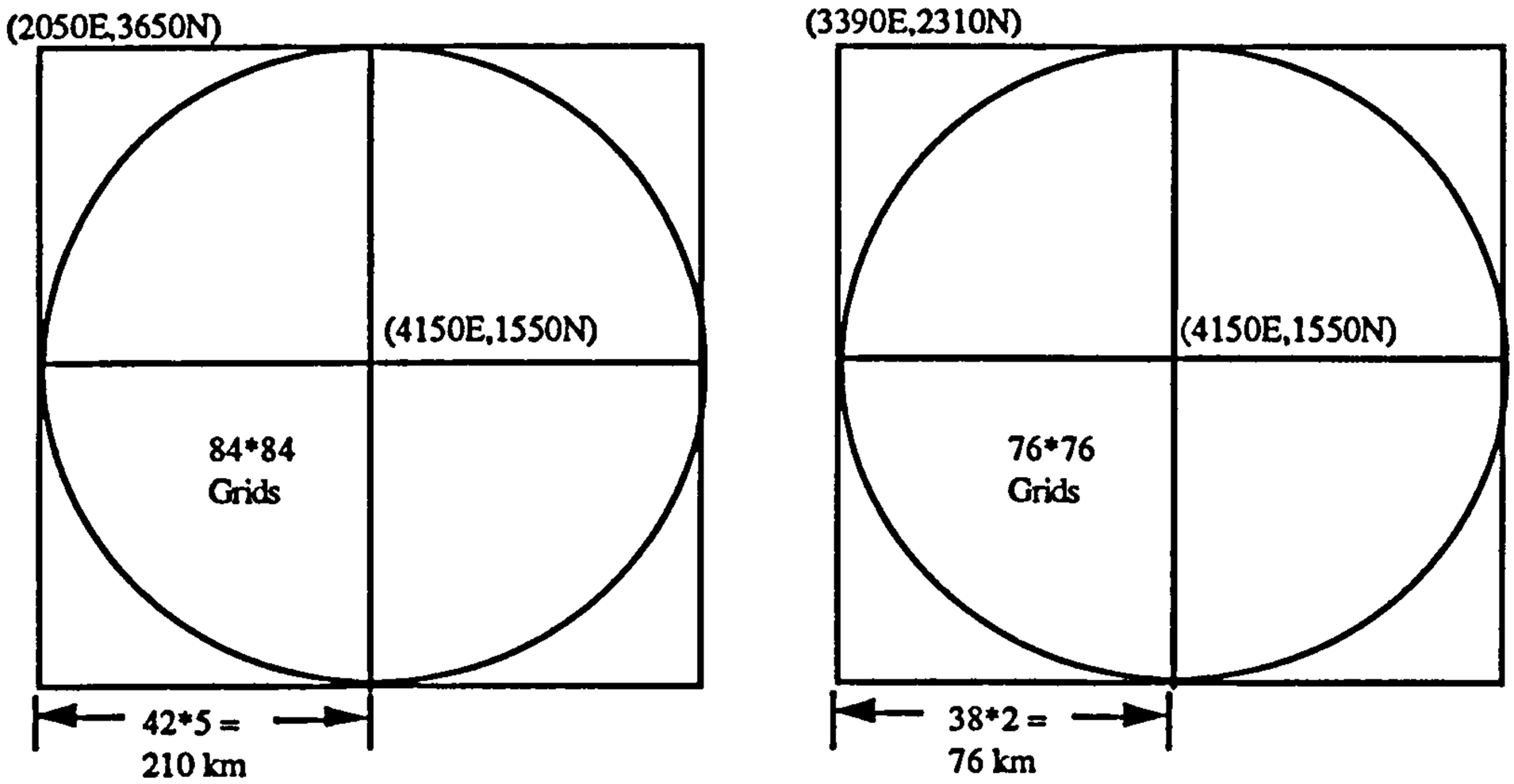

a.) 5 Km Radar Data

b.) 2 Km Radar Data

Figure 2.9 Upavon Radar Data Type (2 km & 5km)

From common sense, the 2km radar data will contain more information than the 5 km radar data and it is also true from the detailed spectral analysis. A spatial sampling scheme is characterised by looking at the signal's frequency response. For a 2-D impulse response $h(n_1,n_2)$ the frequency response is given by the Fourier transform extended into two dimensions, ω1 and ω2.

$$H(\omega 1,\omega 2) = \sum_{n_1=-\infty}^{\infty} \sum_{n_2=-\infty}^{\infty} h(n_1, n_2) \exp(-j\omega_1 n_1) \exp(-j\omega_2 n_2) \qquad (2,9)$$

The impulse function is $h(n_1,n_2)$.

The Nyquist frequency is also applicable in the spatial domain but it depends on the spatial interval instead of the time interval.

When a spatial signal is sampled, the Nyquist frequency should be higher than the

highest spatial frequency in the spatial signal. In the spatial sampling of radar data, a moving average filter is applied before sampling. The aliasing effect has thus been greatly reduced and the accuracy loss will be due to the decreased spatial resolution.

To decide the right data resolution, the purpose of the application will dominate the choice. For the hydrological area, the response of the catchment to the spatial frequency has the same effects as in the time domain. The catchment can be considered as a low pass filter in spatial terms. The high spatial frequency resulting from high spatial resolution radar data will be removed by the catchment filter. In this case, the low resolution data can produce the same result as the high resolution data. To achieve the best utilisation of radar data and minimise the cost, a suitable resolution needs to be decided.

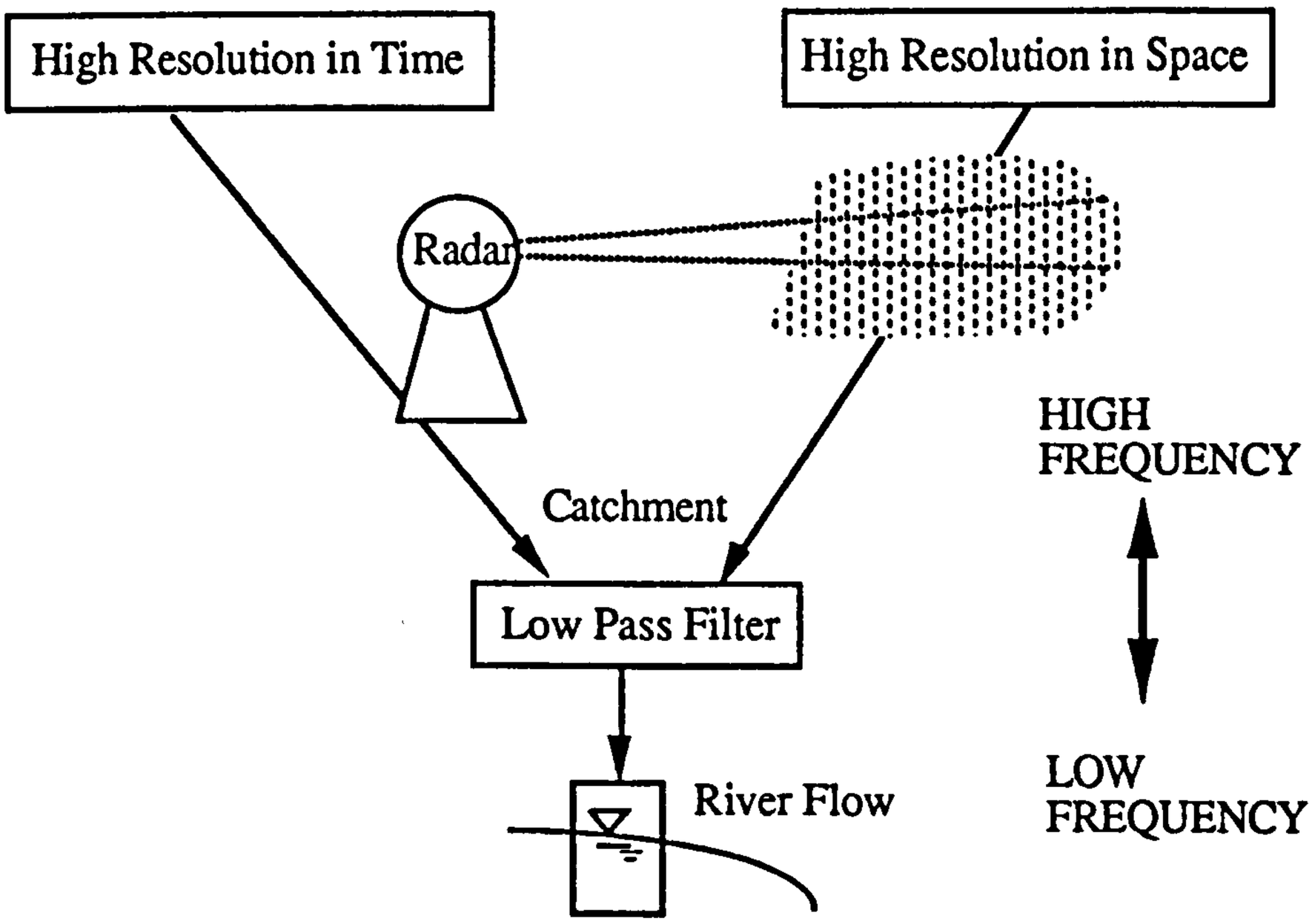

Figure 2.10 Filter Effect by Catchment

As the lumped TF model is utilised in the current research, the spatial frequency information within the catchment is ignored. The input rainfall data is the average rainfall data over the whole catchment. As we know that a spatial moving average filter has been applied to the radar data, the data spatial resolution will not influence the averaged catchment rainfall data very much. A storm event from Hammoon in the Wessex Region has been chosen to illustrate such an effect.

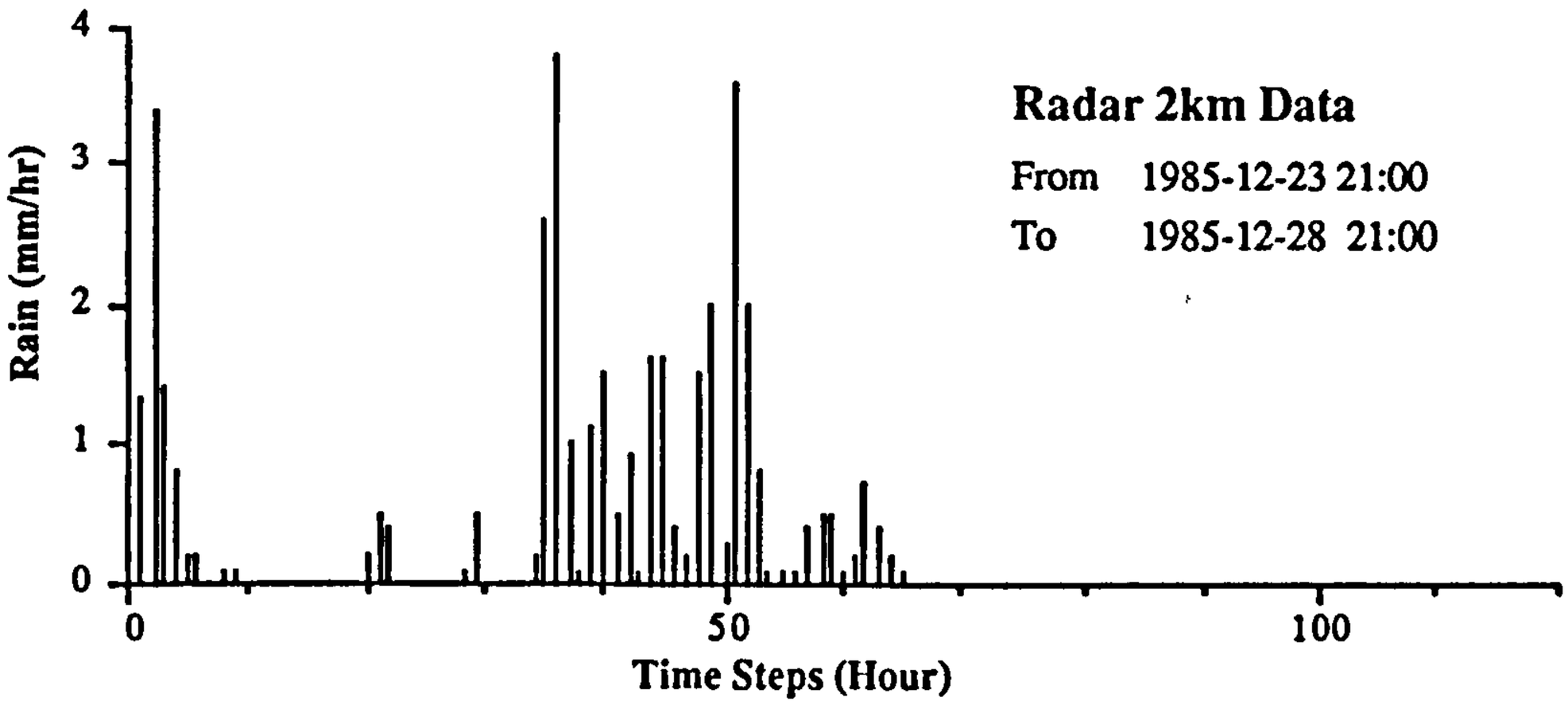

Figure 2.11 2km Event Data for Hammoon 85-12-26 (Area=400km^2)

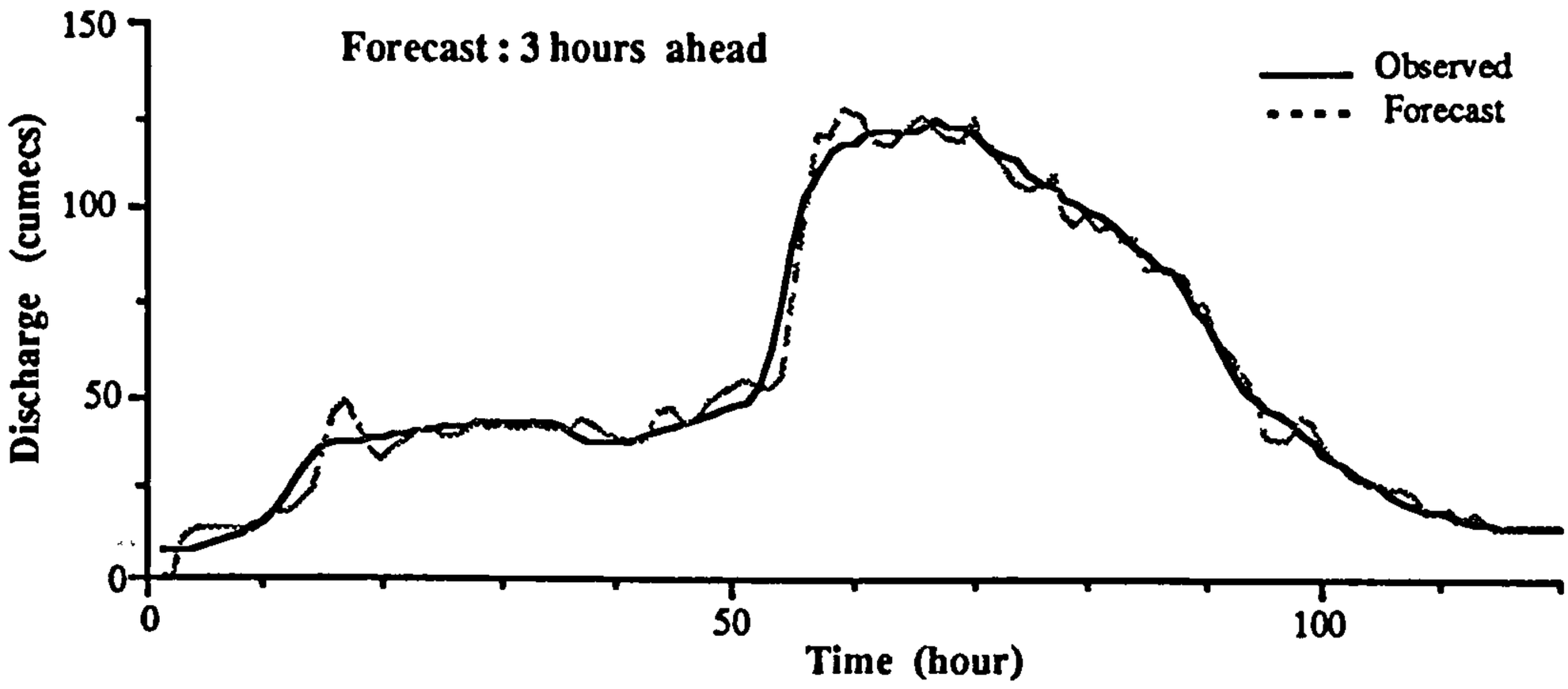

Figure 2.12 3 Step Forecasting by 2km Event Data

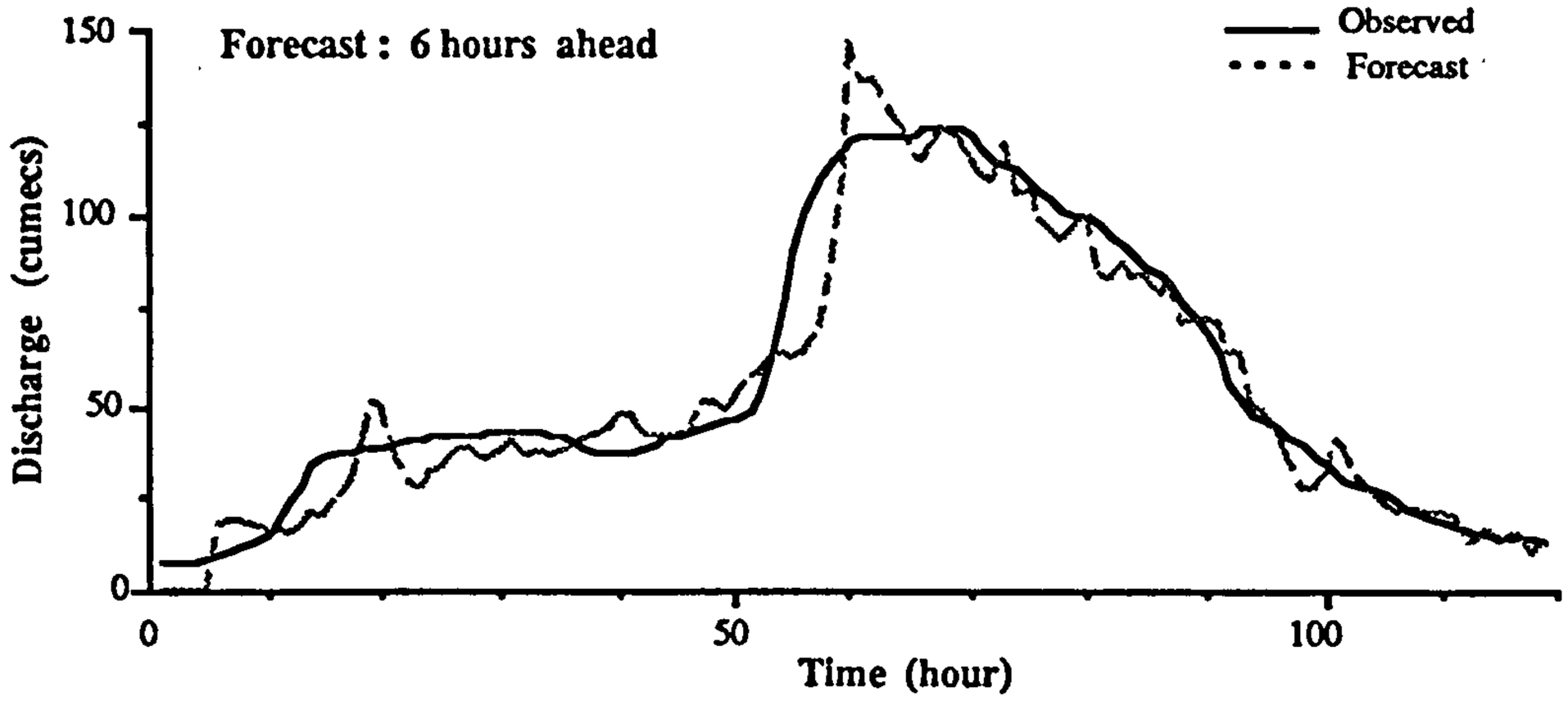

Figure 2.13 6 Step Forecasting by 2km Event Data

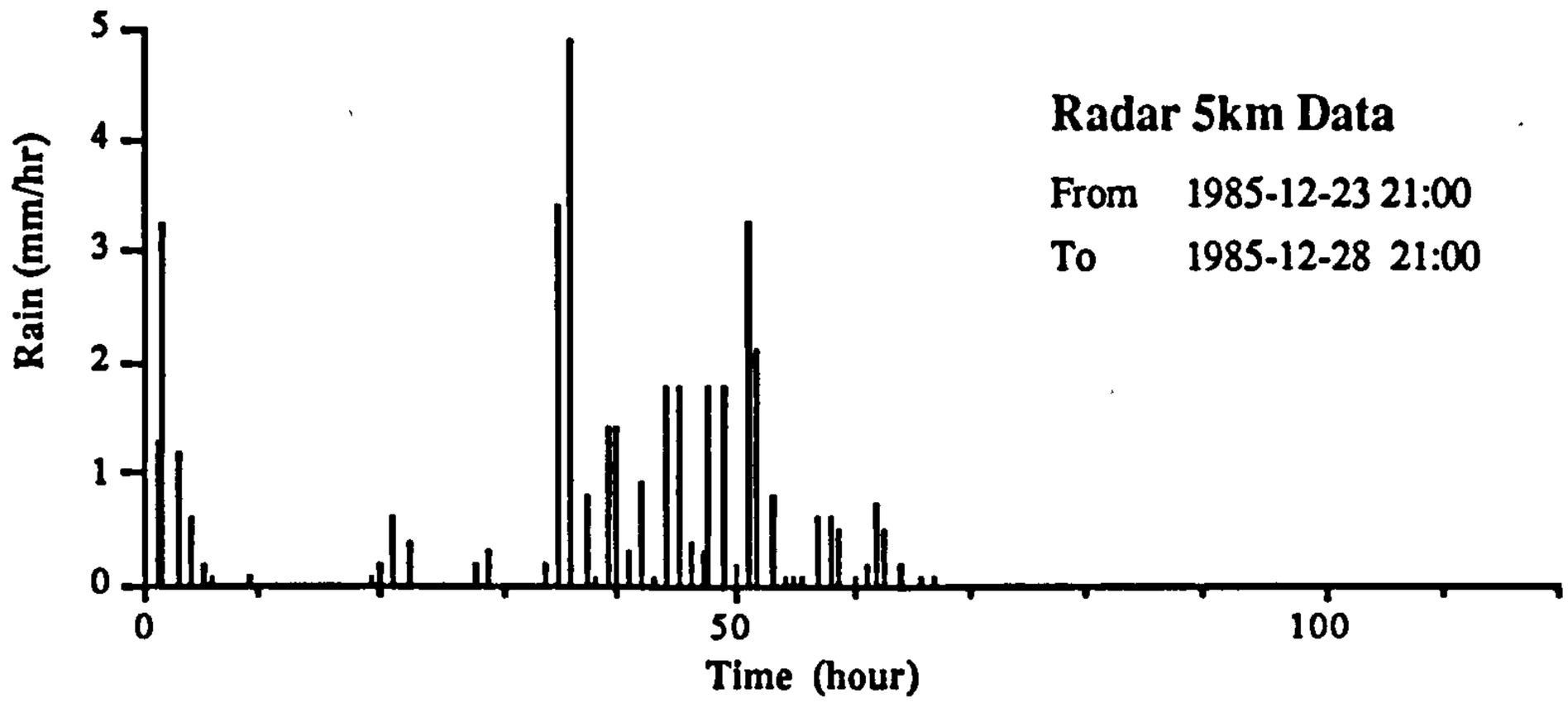

Figure 2.14 5km Event Data for Hammoon 85-12-26

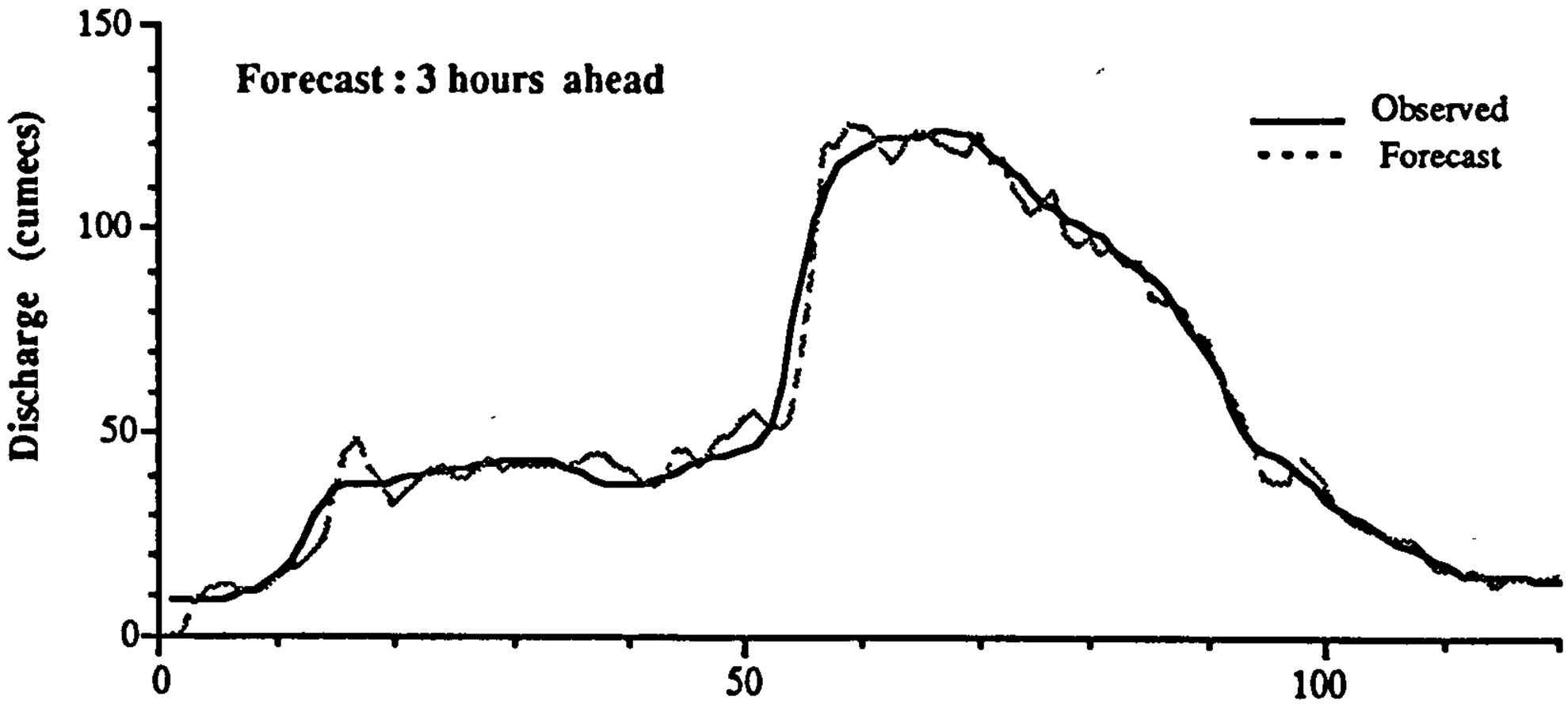

Figure 2.15 3 Step Forecasting by 5km Event Data

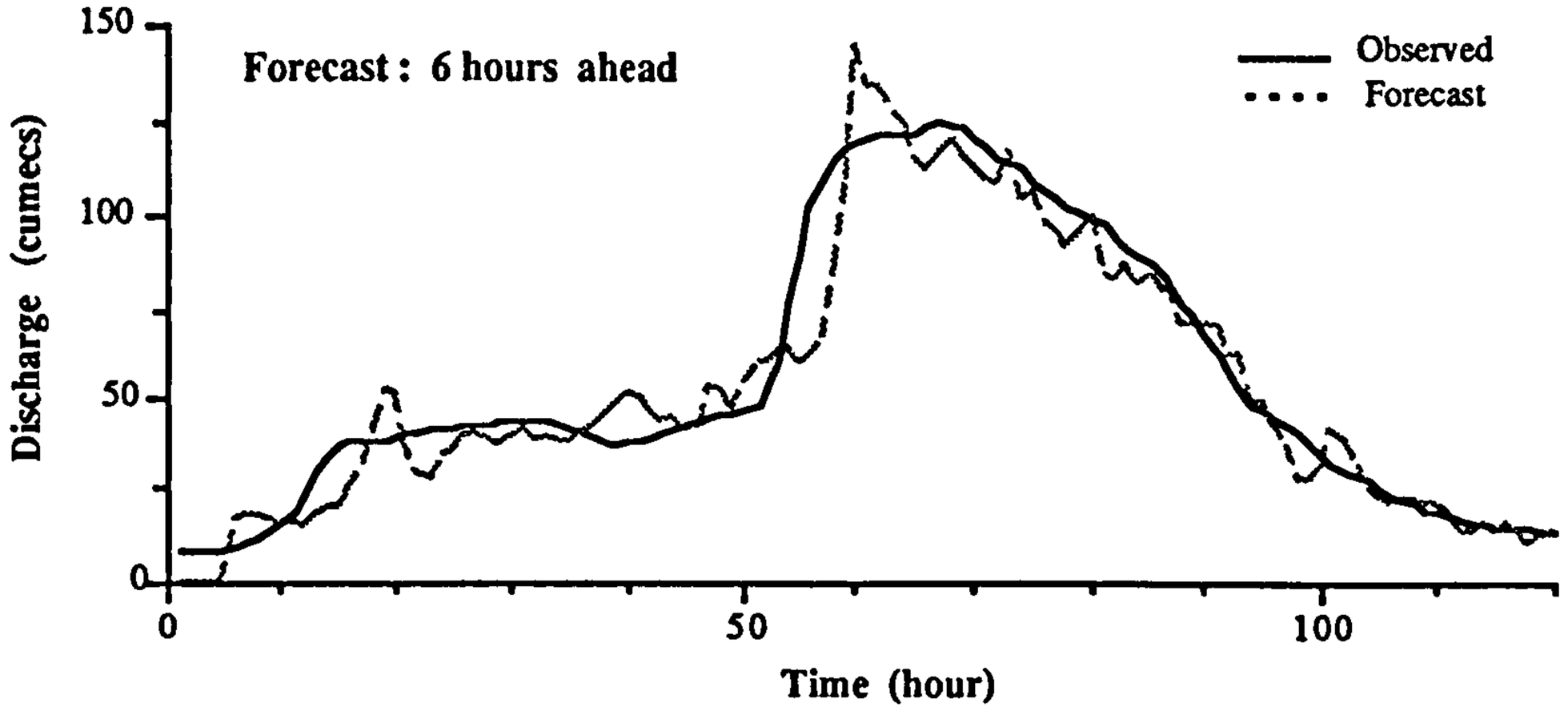

Figure 2.16 6 Step Forecasting by 5km Event Data

The computation results show that the flow forecasting difference between 2km and 5km radar data is very small. It can be understood that the spatial sampling influence to a lumped rainfall runoff model is related to the catchment area. For a catchment with several hundred square kilometres, the difference between 5km and 2km data resolution is small. While for the catchment with 4 or 5 square kilometres area, the difference will be much larger. Figure 2.17 illustrates such an effect.

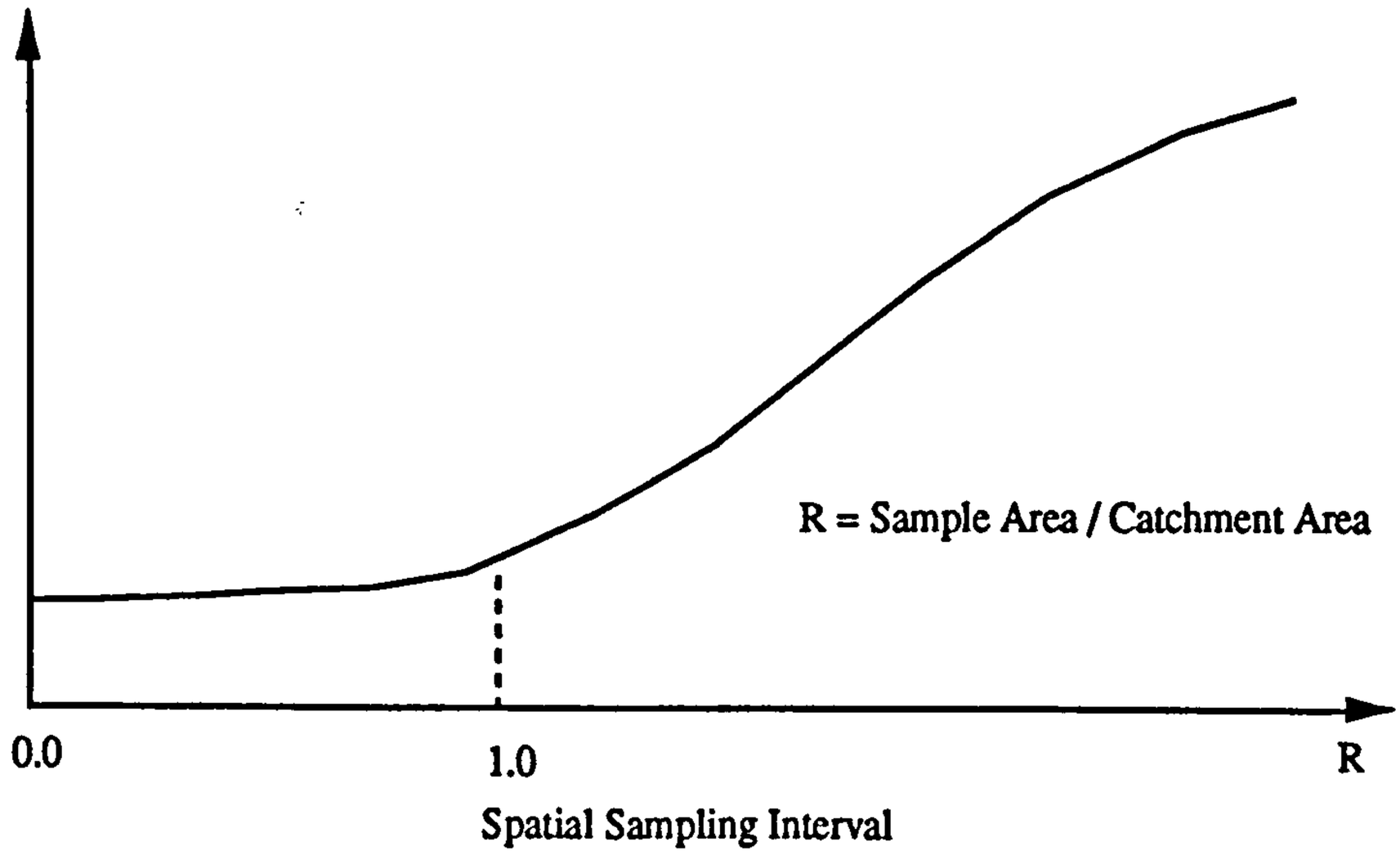

Figure 2.17 Influence of Spatial Sampling to Lumped Rainfall Runoff Model

In reality, the catchment response is not lumped and the influence of spatial sampling will be heavier than the lumped case. More statistical analysis should be carried to examine this influence on distributed catchment models in relation to the availability of remotely sensed data on a grid-square basis.

2.6 Summary

Temporal and spatial sampling of radar rainfall data have been discussed. The measurement sampling rate should be fast enough that the process is well damped above the Nyquist frequency. Although hourly radar data are used in the forecasting model, it has been shown that 5 minute or 15 minute measurement sampling is necessary. A prefilter should be utilised when the radar rainfall data is to be input into a flood forecasting model and this will be discussed in next chapter.

Spatial sampling is quite an important issue for fully distributed forecasting models. It will not affect the lumped TF model providing the sampling area is relatively small compared to the catchment size. Larger catchments can tolerate larger spatial sampling intervals and a low spatial sampling rate will cause some difficulty for the radar data calibration procedure, since it will be difficult to apply pattern recognition techniques to identify storm type and important differences will likely occur between the calibration raingauge data (point measurements) and radar data (spatial average measurements).

CHAPTER 3

RADAR DATA QUANTISATION

3.1 Introduction

As radar data are processed by digital computer, quantisation is inevitable for practical application of radar data. In this chapter, the quantising error and quantisation scheme is described and an adaptive quantisation method is proposed to enhance the accuracy of radar data without using a longer wordlength.

3.2 Uniform and Nonuniform Quantisation

There exist a variety of quantisation methods. Generally speaking, they are characterised by uniform and nonuniform quantisation schemes. It would be helpful to introduce some concepts about the basic properties of different quantisation schemes.

The rounding problem is illustrated in Fig 3.1. It is a case of uniform quantisation. When the variations in the signal are large relative to the quantising step, that is, when quantisation has been carried out sufficiently finely, the error signal e(t) is equivalent to an ensemble of elementary signals which are each formed from a straight-line segment. The power of such an elementary signal of width t is written as :

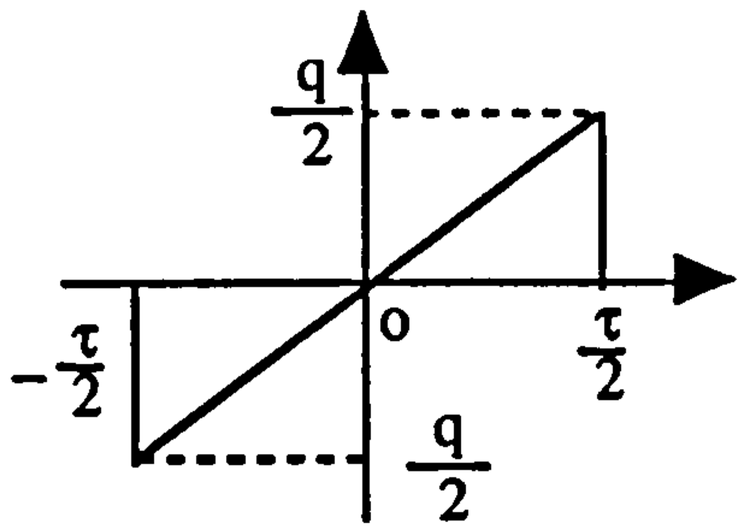

q is quantisation Step

τ is sampling Interval

Figure 3.1 Elementary error signal (from Schwartz,1981)

$$B = \frac{1}{\tau}\int_{-\tau/2}^{\tau/2} e^2(t)\,dt = \frac{1}{\tau}\left[\frac{q}{\tau}\right]^2 \int_{-\tau/2}^{\tau/2} t^2\,dt = \frac{q^2}{12} \qquad (3,1)$$

The value obtained in this way, $B = q^2/12$, is a satisfactory estimate of the power of the quantising noise in the majority of actual cases. Such an equation is popularly utilised to represent the uniform quantisation error power.

In many practical cases such as in hydrological processes, there is no specified peak value and the signal level may in fact change in a random manner. The most common example is that of a speech signal, with different speakers using the same transmission facilities. The range of speech intensity may vary as much as 40 dB in going from the whisper of a quiet speaker to the bellowing tones of a powerful speaker. It is apparent that to cover this dynamic range effectively nonuniform quantisation-level spacing, or its equivalent, signal compression, must be used. If this is not done and equally spaced levels are chosen to cover the widest signal variation expected, the soft speakers will be penalised. The same problem obviously arises in the radar rainfall signals expected to cover a wide dynamic range.

The signal-to-quantisation noise ratio (SNR) can be utilised to represent the influence of noise on the signal. The effect of noise on the performance of a system depends on the amount of noise relative to the signal. In a speech system quantisation noise cackle, as heard by a listener, is only objectionable if it is noticeable compared to the signal intensity of the speaker. A given noise level is more objectionable when a quiet speaker is speaking than when a loud one is communicating. To overcome the problem caused by uniform quantisation, it is necessary to introduce a nonuniform quantisation. In practice it is simple to nonlinearly compress the signal such as with logarithmic processing and then apply uniform-level spacing to the compressed output signal. It has been shown that in this case, the variation of SNR can be greatly decreased when compared with uniform quantisation.

In the case of uniform quantisation, suppose the value range is [0 , V], quantisation level is M, so quantising step q will be:

$$q = V / M \tag{3,2}$$

Each value of the signal between (n- 1/2)q and (n+ 1/2)q is rounded to nq. With an input signal power of σ^2 we have as the signal-to-noise ratio

$$SNR = \sigma^2 / (q^2/12) \tag{3,3}$$

Since the quantisation noise is fixed, independent of σ^2 , in the case of uniformly spaced levels, the SNR is proportional to σ^2. For a signal at low intensity the SNR reduces correspondingly and the quantisation noise becomes that much more noticeable.

A typical nonuniform quantisation has a logarithmic form. There are two popular

schemes used presently: namely the μ law and the A law (see Proakis,J G 1989).

μ law:

$$y = \frac{\ln(1 + \mu x / V)}{\ln(1 + \mu)} \qquad 0 \le x \le V$$

Where, parameter μ can be varied to obtain a variety of characteristics. μ is usually set to 225.

A law:

$$y = \frac{1 + \ln Ax}{1 + \ln A} \qquad \frac{1}{A} \le x \le 1$$

$$y = \frac{Ax}{1 + \ln A^{-}} \qquad 0 \le x \le \frac{1}{A}$$

Parameter A controls the dynamic range increase and it represents V here. The A law characteristic is defined to be linear for small x and logarithmic for large x.

SNR has been found to be almost constant over the quantisation range in the nonuniform case. Uniform spacing thus favours the higher-amplitude signals at the expense of the lower-amplitude signals. Fig 3.2 (from Schwartz,1981) shows such characteristics clearly.

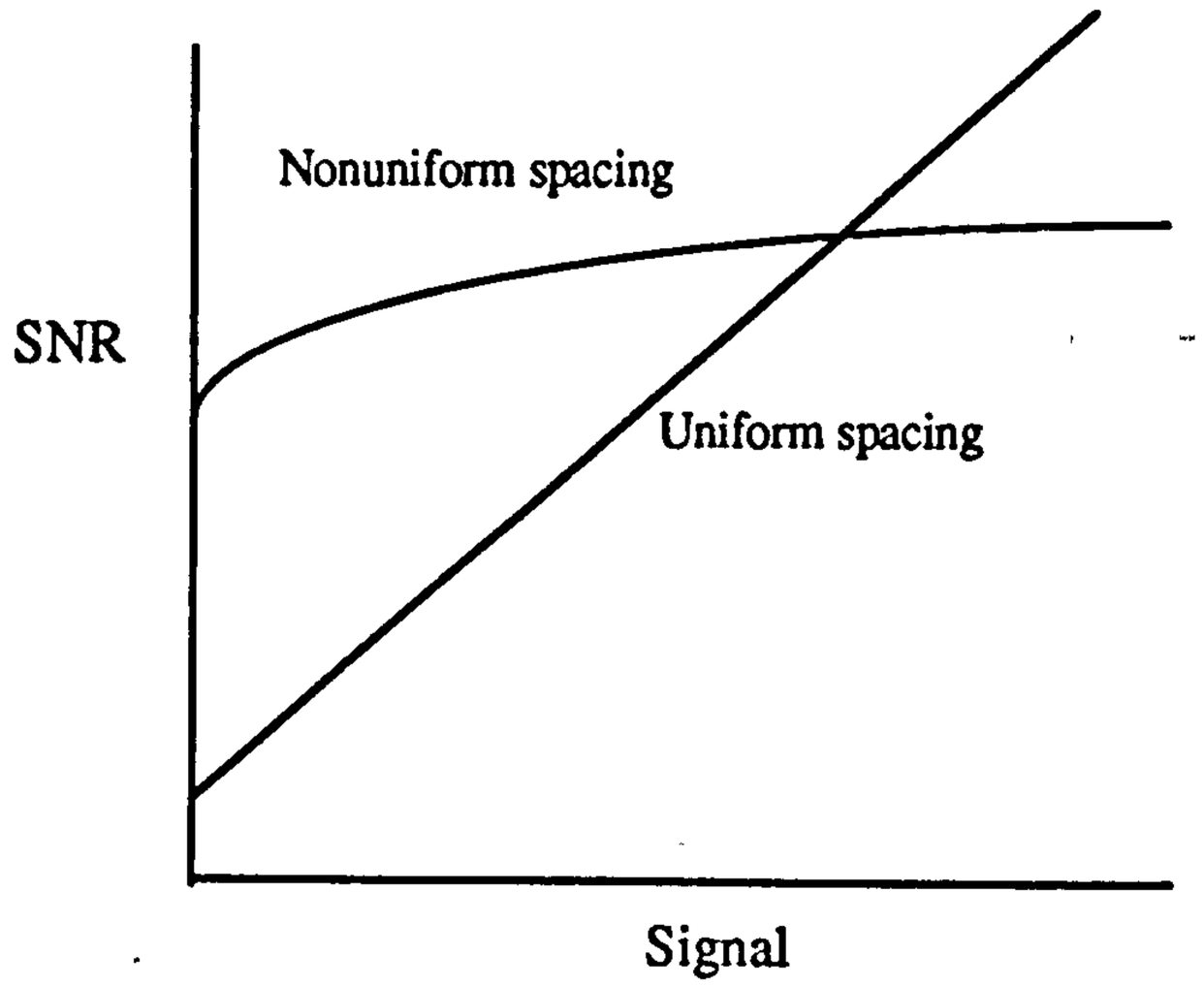

Figure 3.2 Signal-to-quantisation noise ratio (from Schwartz,1981)

3.3 Present Radar Data Quantisation Scheme

The rainfall intensity from the Meteorological Office consists of two types: 3 bit (8 level) and 8bit (208 levels). 3-bit data make use of the whole 3 bit to represent the data. The 8 bit scheme uses 208 levels out of the 256 available levels, the remaining levels are utilised for data transmission control and checking.

The two schemes are listed in the Table 3.1 and Table 3.2.

Table 3.1 3-bit Data

Intensity Level	Intensity Range (mm/hr)	3 - Bit Value(mm/hr)
1	< 0.125	0.0
2	0.125 - 1	0.56
3	1 - 4	2.5
4	4 - 8	6.0
5	8 - 16	12.0
6	16 - 32	24.0
7	32 - 126	79.0
8	> 126	319.0

The 8 bit data were divided into four groups according to the data value and their increments.

Table 3.2 8-bit Data

Segment Id	Intensity (mm/hr)	i Range	Intensity Range (mm/hr)
1	i / 32	i = Deci [0 , 63]-1	[0, 1.96875]
2	i / 32	i = Deci [64 , 252]-4	[2.0, 7.875]
3	i / 32	i = Deci [256, 1008]-16	[8.0, 31.5]
4	i / 32	i = Deci [1024 , 4032]-64	[32.0, 126.0]

Radar data are held in float notation. This allows numbers up to 4032 to be held in 8 bits. Units of 1/32 mm/hr are used, which allows rates of up to 126 mm/hr to be held. The two high order bits of the byte are the exponent and the other 6 bits are the mantissa. The value is interpreted as (2 to the power of twice the exponent) times the mantissa (see Banks C J et al. 1984, FAAG Report 108). For example, for a number of 01011111, it will be converted into $2^2*31=124$ and from Table 3.2 it can be found this number is in group two with the step of 4. To get the rainfall intensity, this number is substituted into the equation on the left and the result is 3.875 mm/hr.

3.4 Quantisation Error

To simplify the research and generate some common results, synthetic rainfall data was utilised to analyse the quantisation error so that the process can be reproduced and compared to other researchers' work. We suppose the rainfall rate obeys a normal distribution law since it follows some characteristic features of true rainfall data (Refer to Graham, 1988 for detailed analysis). As the rainfall rate can not be negative, the x value will distributed from $[0,+\infty]$. The ordinary normal distribution density is

$$f(x) = \frac{1}{\sigma\sqrt{2\pi}}\, e^{-(x-\mu)^2/2\sigma^2} \qquad (3,4)$$

$$x \in [-\infty, +\infty],\ \sigma > 0,\ \mu \in [-\infty, +\infty]$$

The modified normal distribution is given by the following:

$$f(x) = \frac{2}{\sigma\sqrt{2\pi}}\, e^{-x^2/2\sigma^2} \qquad (3,5)$$

$$x \in [0, +\infty],\ \sigma > 0$$

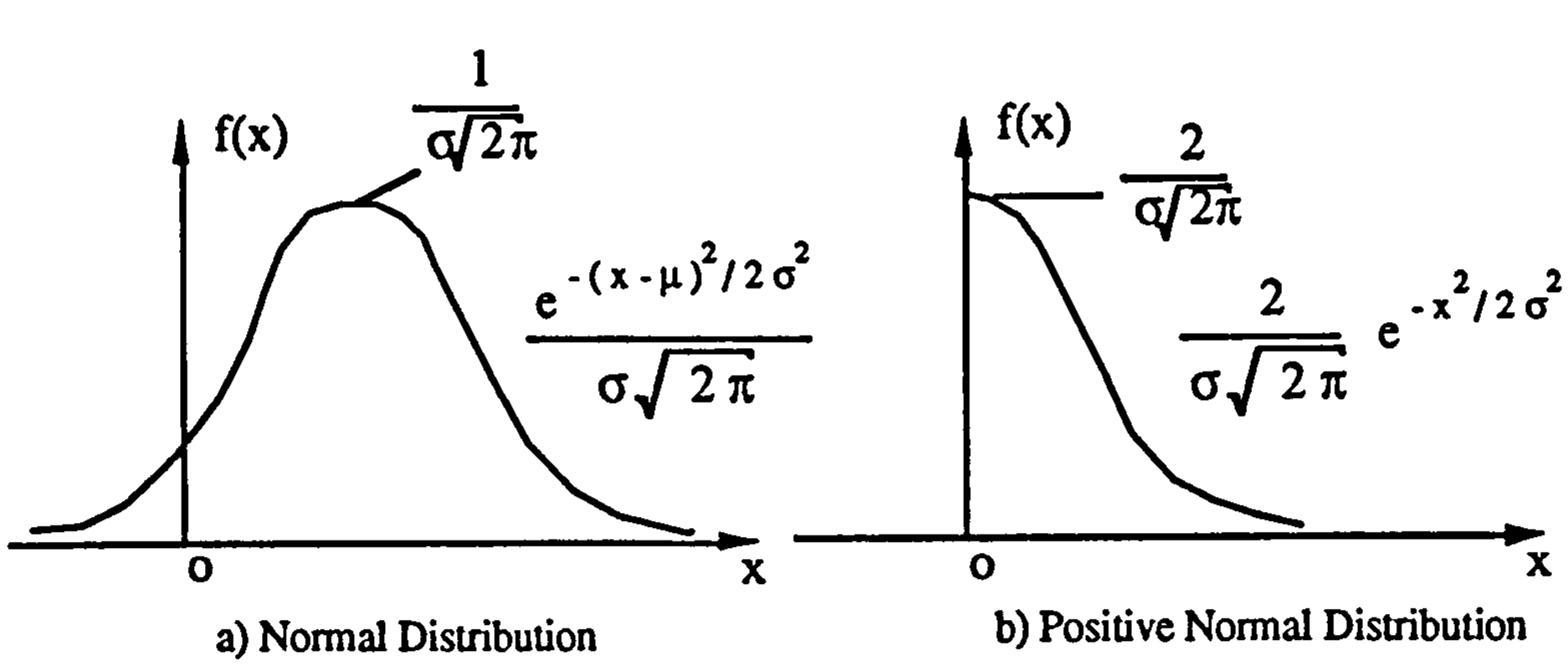

Figure 3.3 Probability Density Function

By changing the variance (σ), we can obtain different kinds of rainfall rate distribution. With larger σ, the average rainfall intensity tends to also be larger. With Figure 3.4 and Figure 3.5, the synthetic rainfall distribution curves are plotted according to the variance σ.

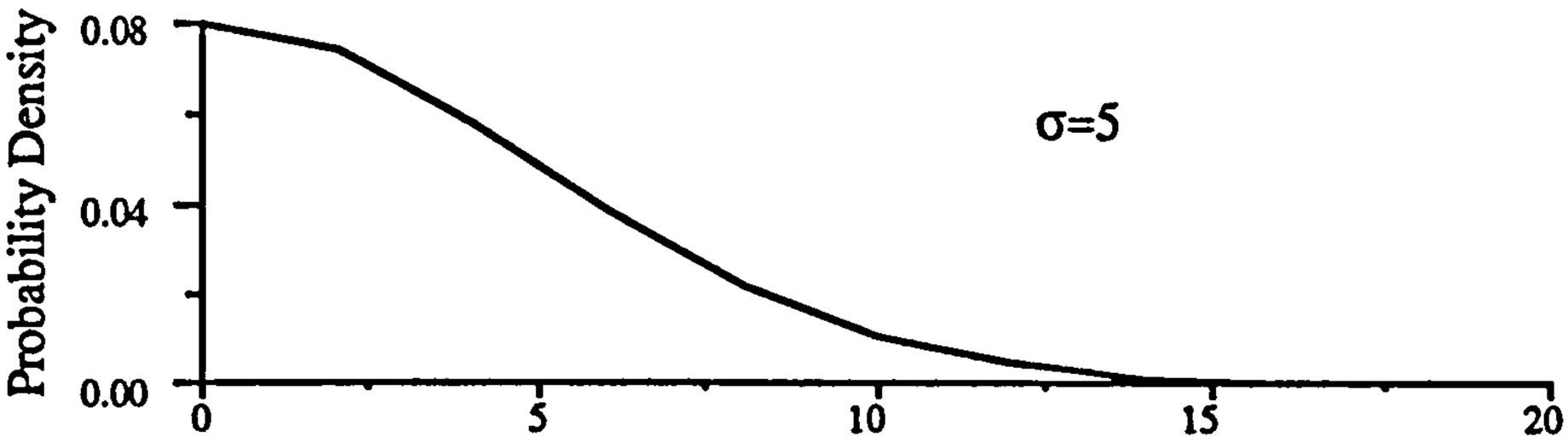

Figure 3.4 Synthetic Rainfall Distribution with σ = 5

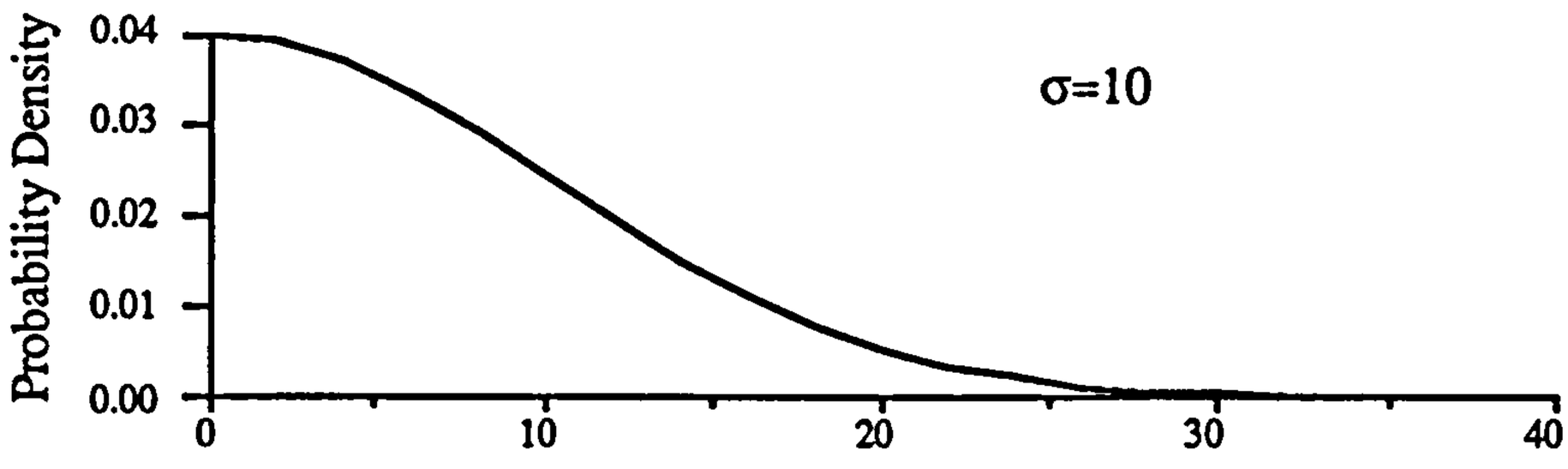

Figure 3.5 Synthetic Rainfall Distribution with σ = 10

The shapes of the rainfall data distribution are similar. Figure 3.6 - Figure 3.11 show two sets of rainfall data generated by changing the variance by 10 and 100. The effects of the 3 bit transformation are also shown in these Figures.

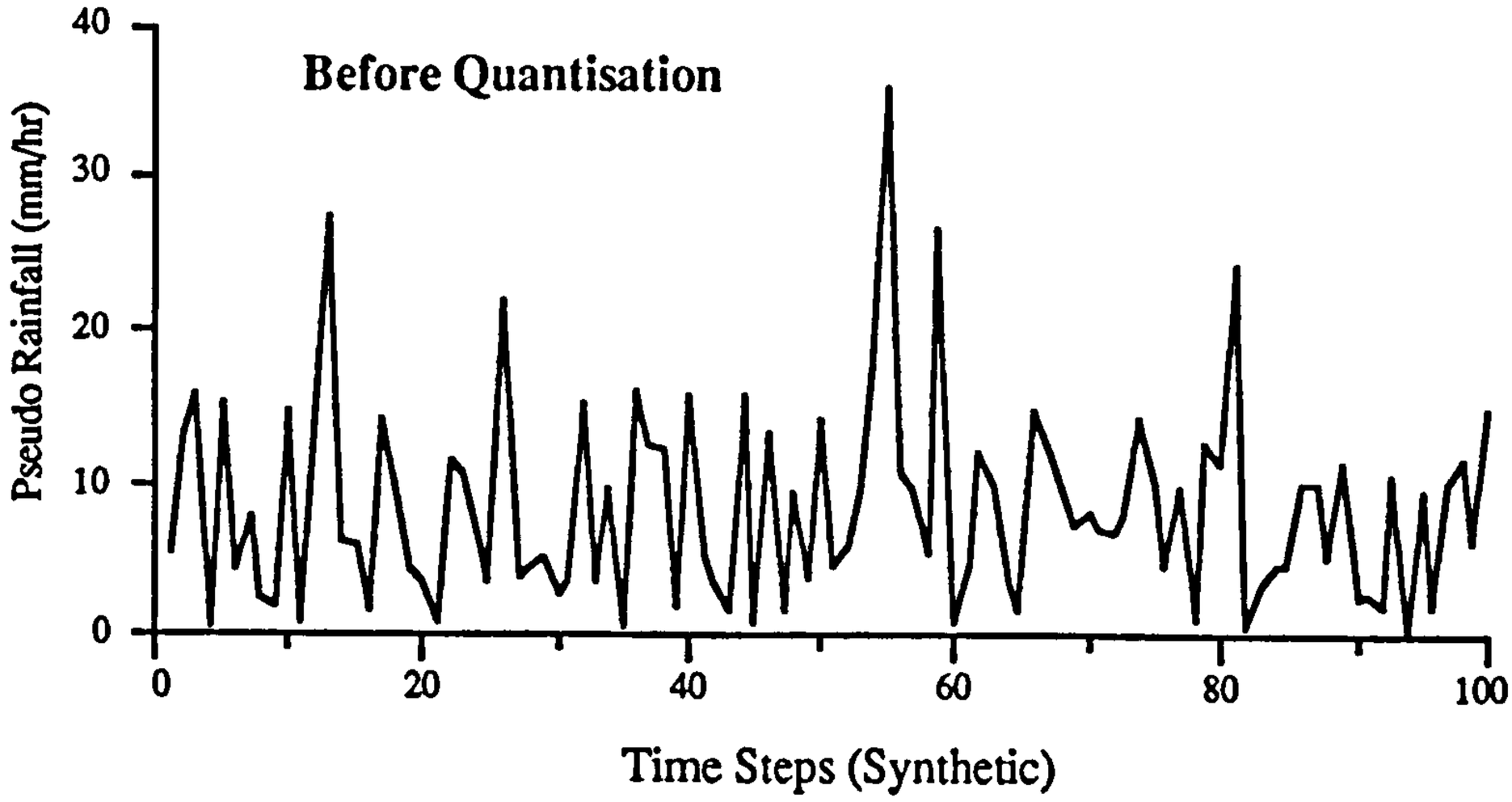

Figure 3.6 Synthetic Rainfall Data with σ = 10

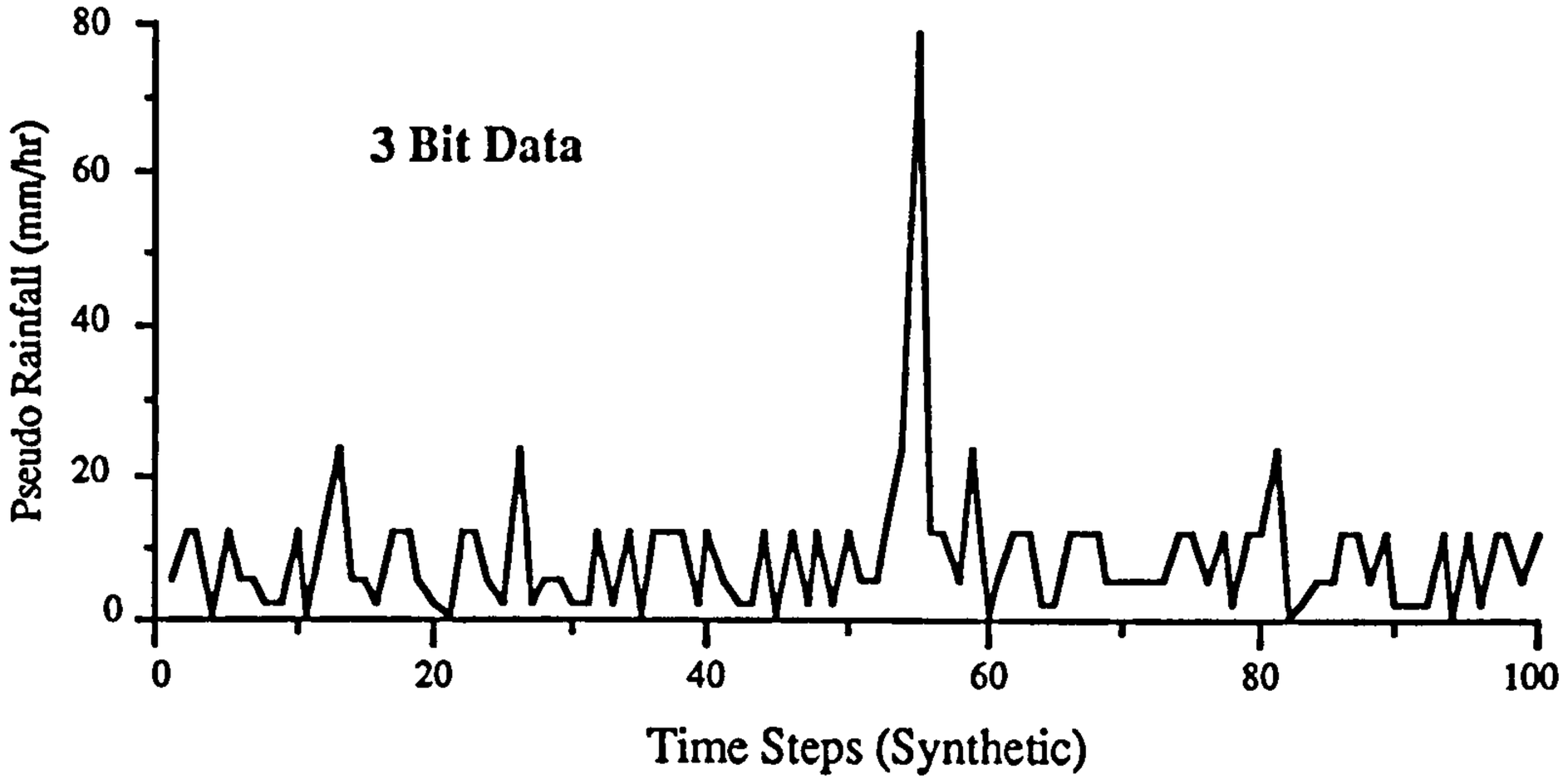

Figure 3.7 3-Bit Synthetic Rainfall Data with σ = 10

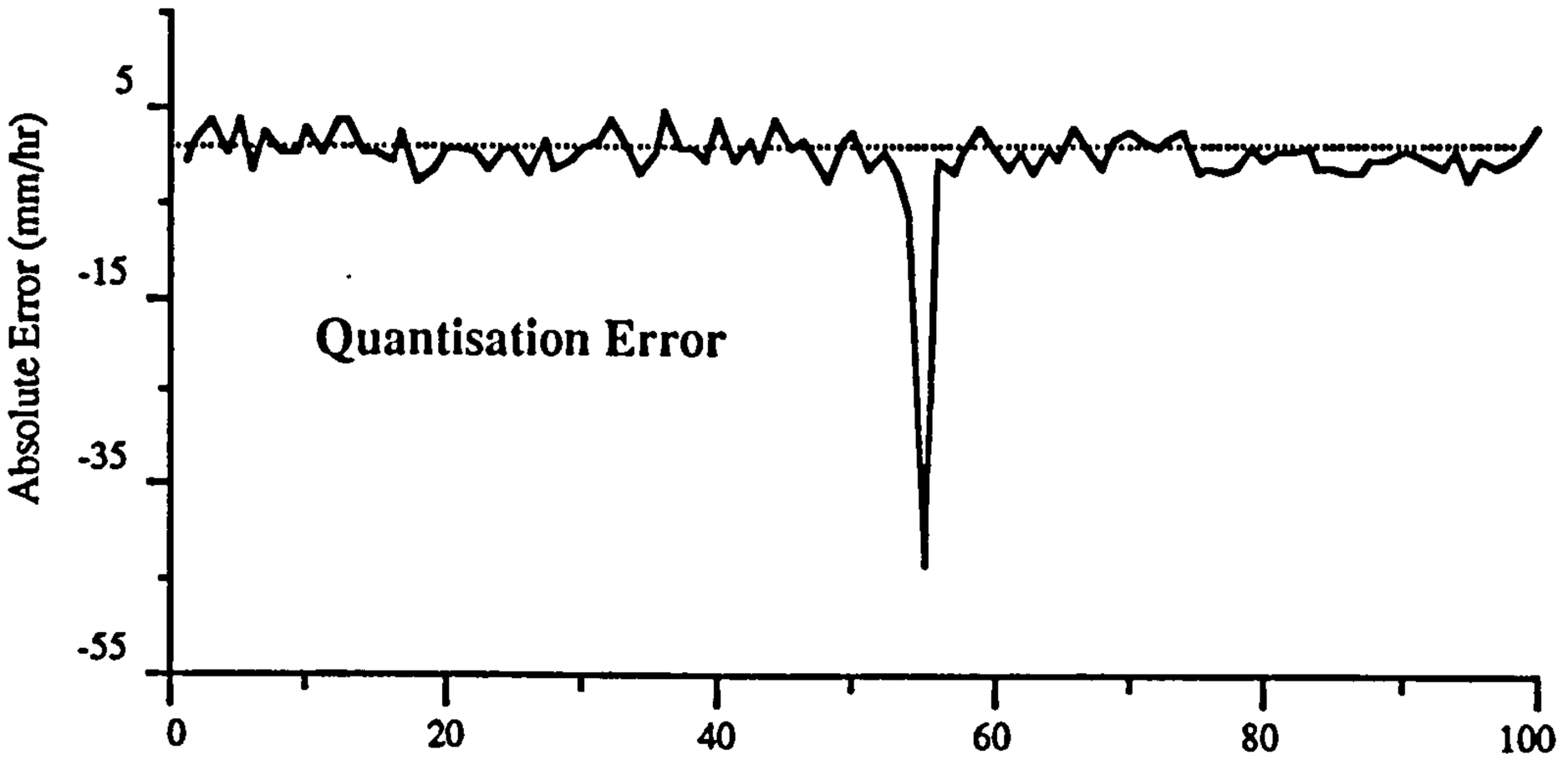

Figure 3.8 Error Caused by Quantisation with σ = 10

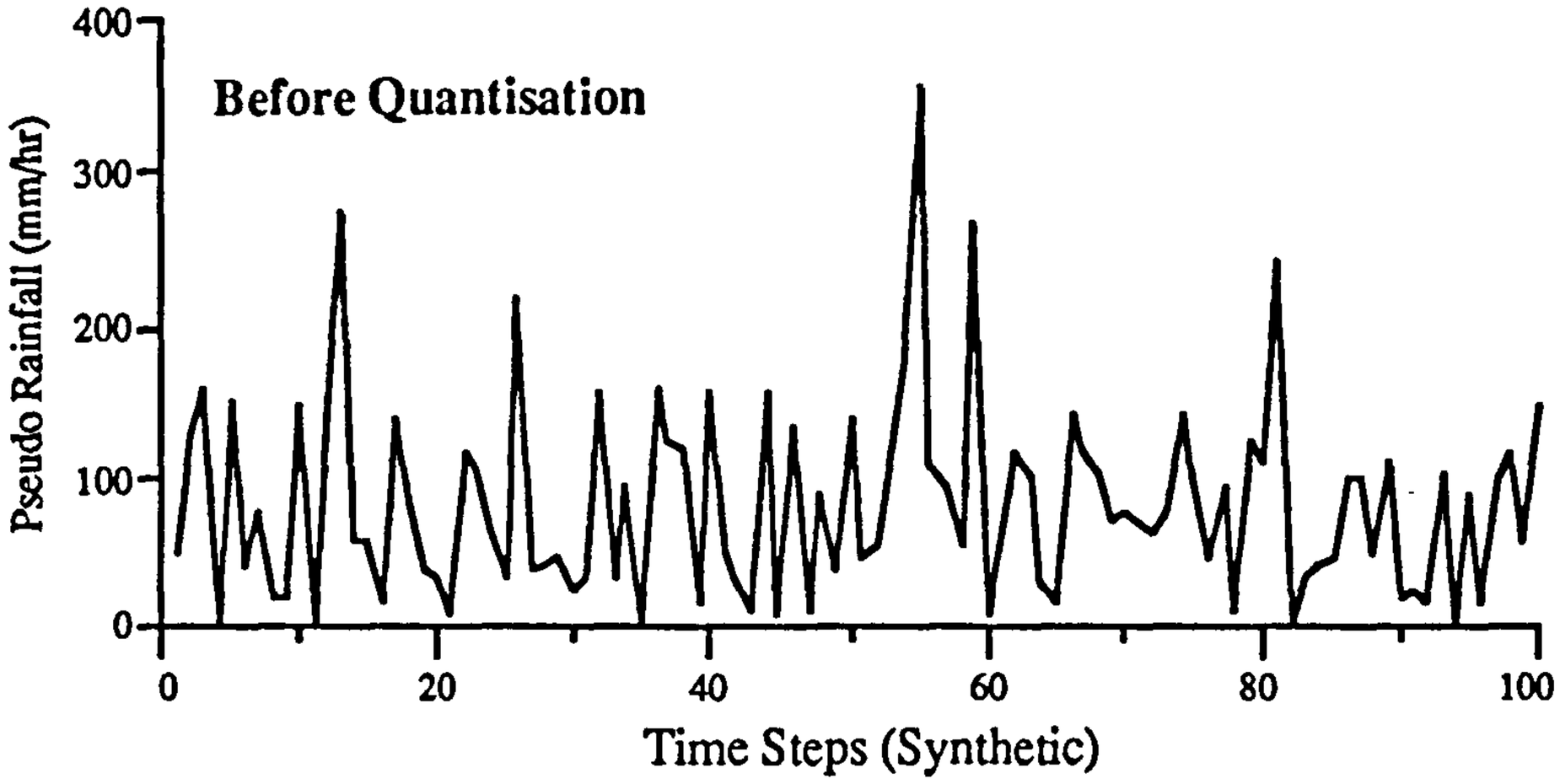

Figure 3.9 Synthetic Rainfall Data with σ = 100

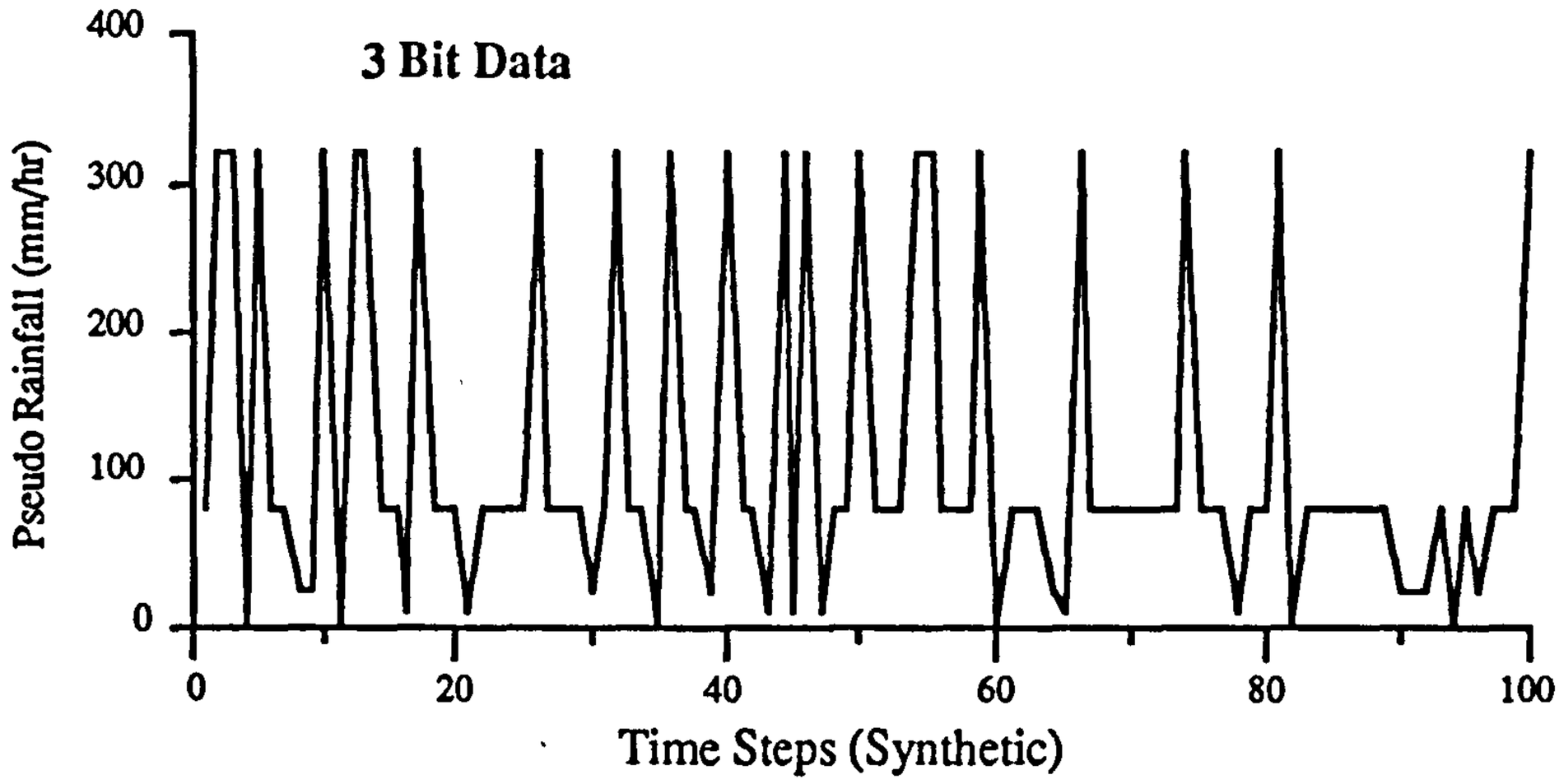

Figure 3.10 3-Bit Synthetic Rainfall Data with σ = 100

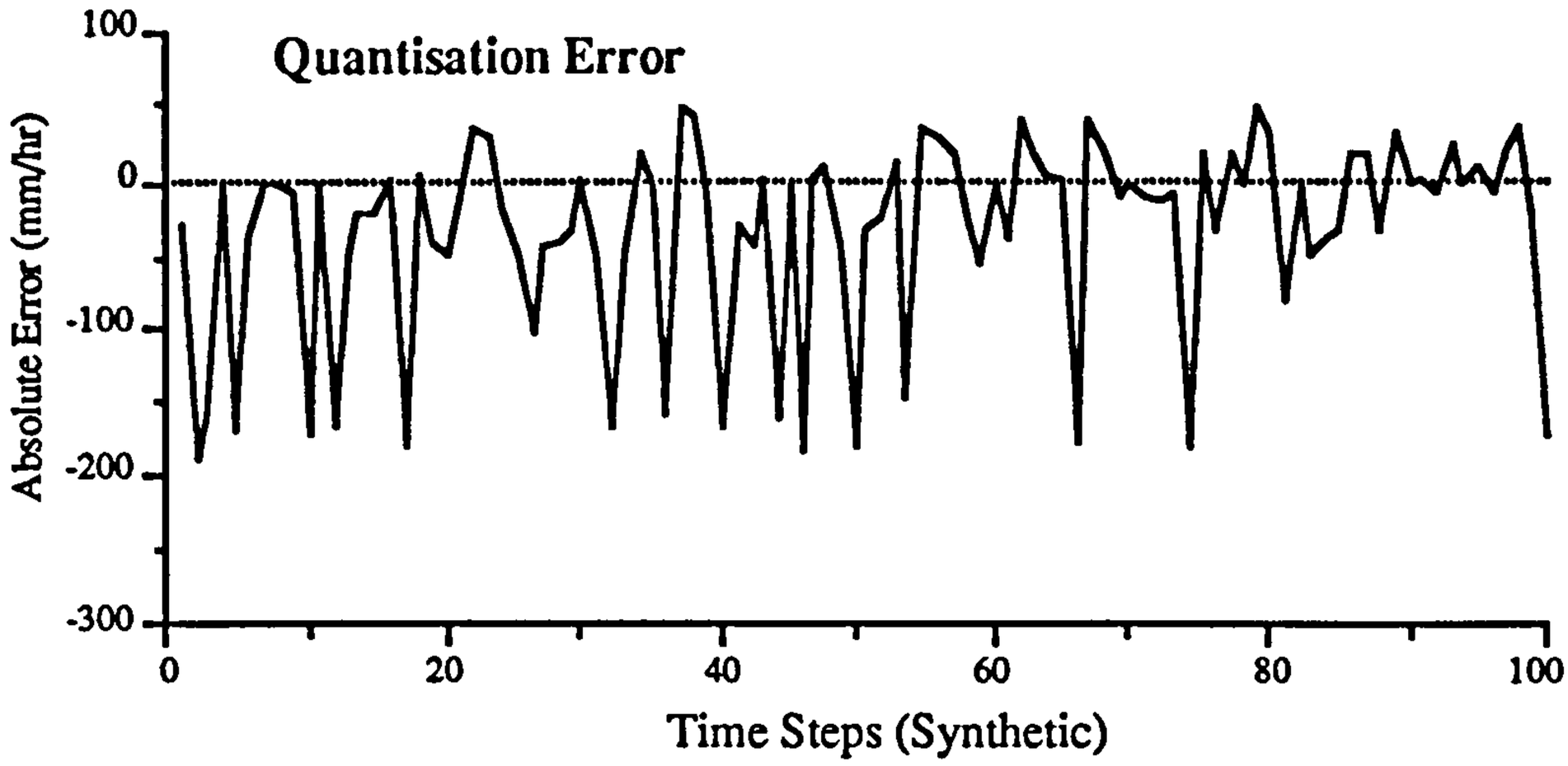

Figure 3.11 Error Caused by Quantisation with σ = 100

From the figures above, it can be found that errors caused by quantisation are around the zero line and increase with rainfall intensities. The distribution of errors is not uniform as more negative errors occurs than positive ones. This illustrates the potential of a better scheme based upon non-uniform procedures. To illustrate such effect, relationships between the average rainfall rate, signal power, signal noise ratio and the variance are drawn in the Figure 3.12 - Figure 3.14.

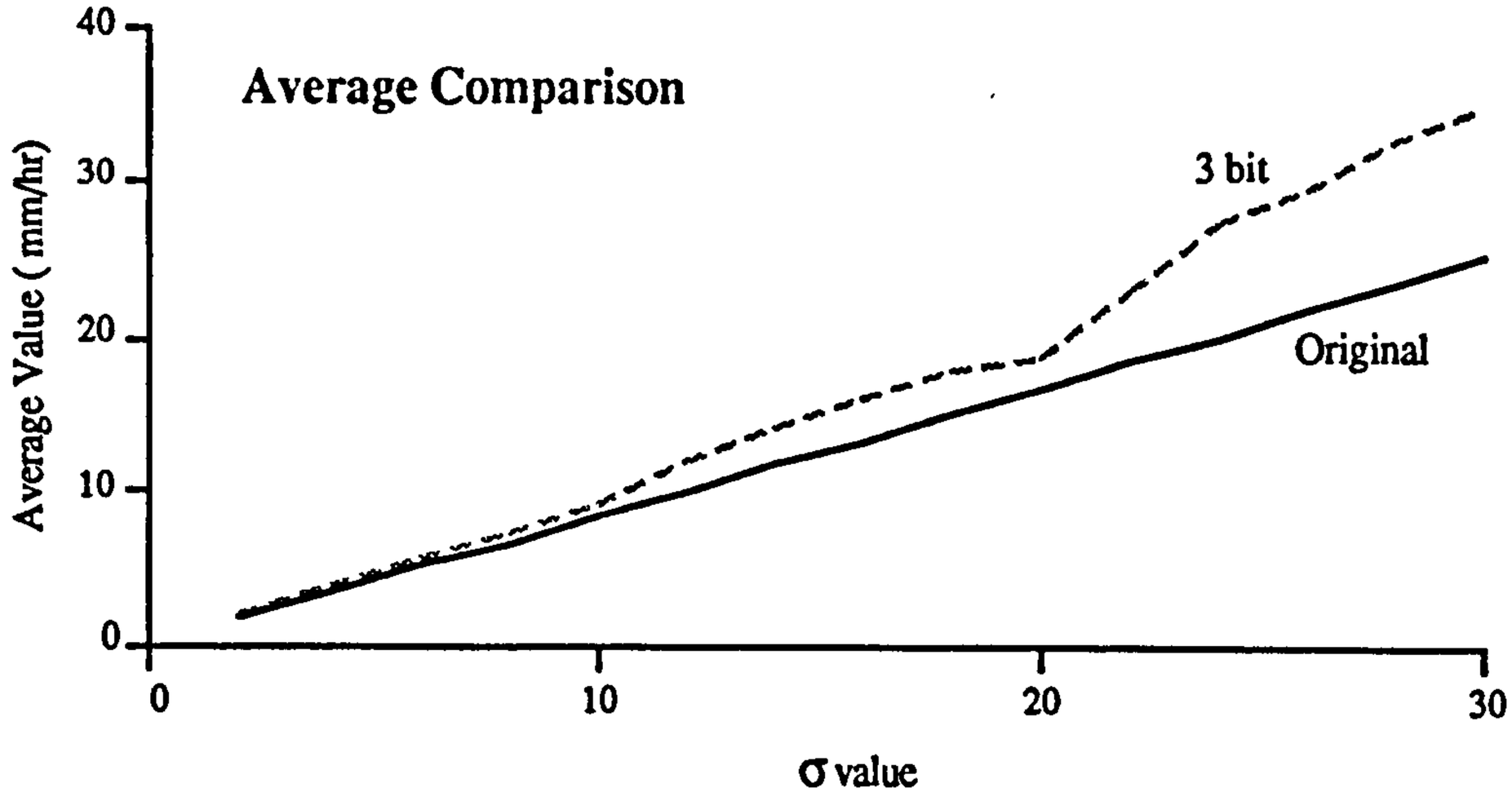

Figure 3.12 Average Comparison between Original and 3-Bit Data (σ≤30)

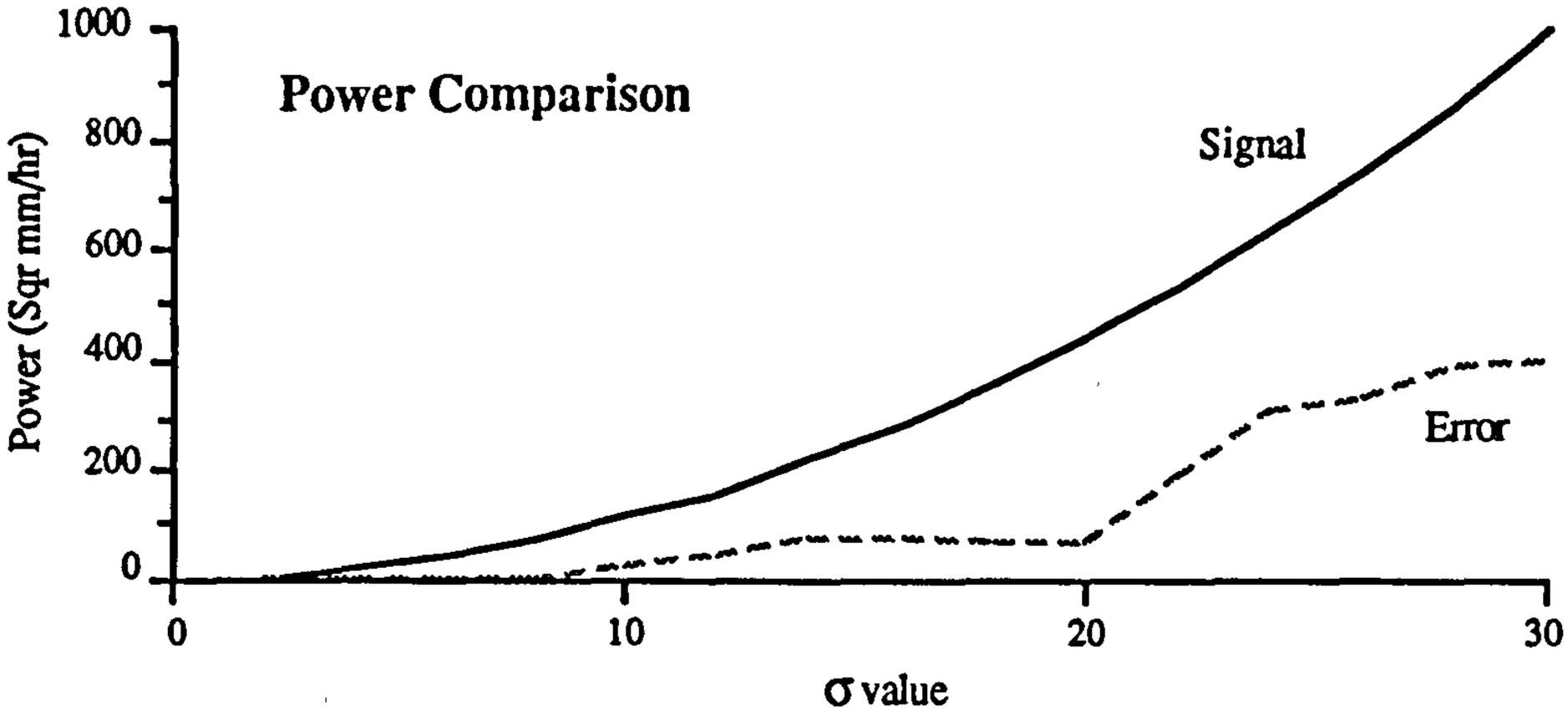

Figure 3.13 Signal Power Comparison between Original and 3-Bit Data (σ≤30)

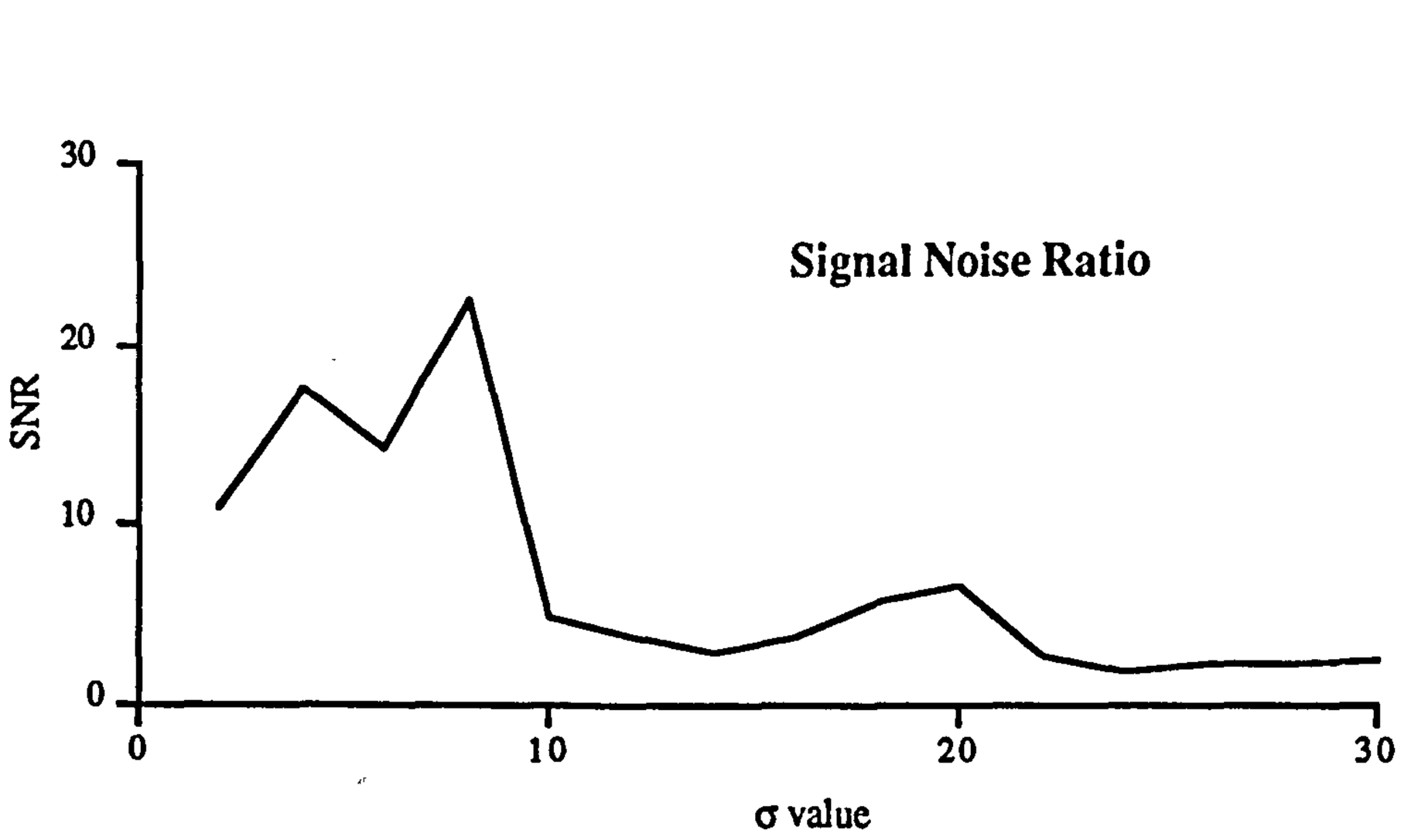

Figure 3.14 Signal Noise Ratio between Original and 3-Bit Data (σ≤30)

Here the average value is derived by

$$\bar{R} = \frac{1}{N} \sum_{i=1}^{N} R_i$$

and the power value is derived by

$$P = \frac{1}{N} \sum_{i=1}^{N} R_i^2$$

where R_i is the individual rainfall intensity and N is the number of data.

From the above figures we observe how the average value of the deviation increases with the variance. This means that the middle value in the quantisation scheme is not the same as that in the data. The quantisation error is increasing as σ increases. Before σ reaches 20, the quantisation error is reasonably small. To depict a larger range of rainfall intensities, Figure 3.15 - Figure 3.17 are plotted to the extend the range to σ=1000.

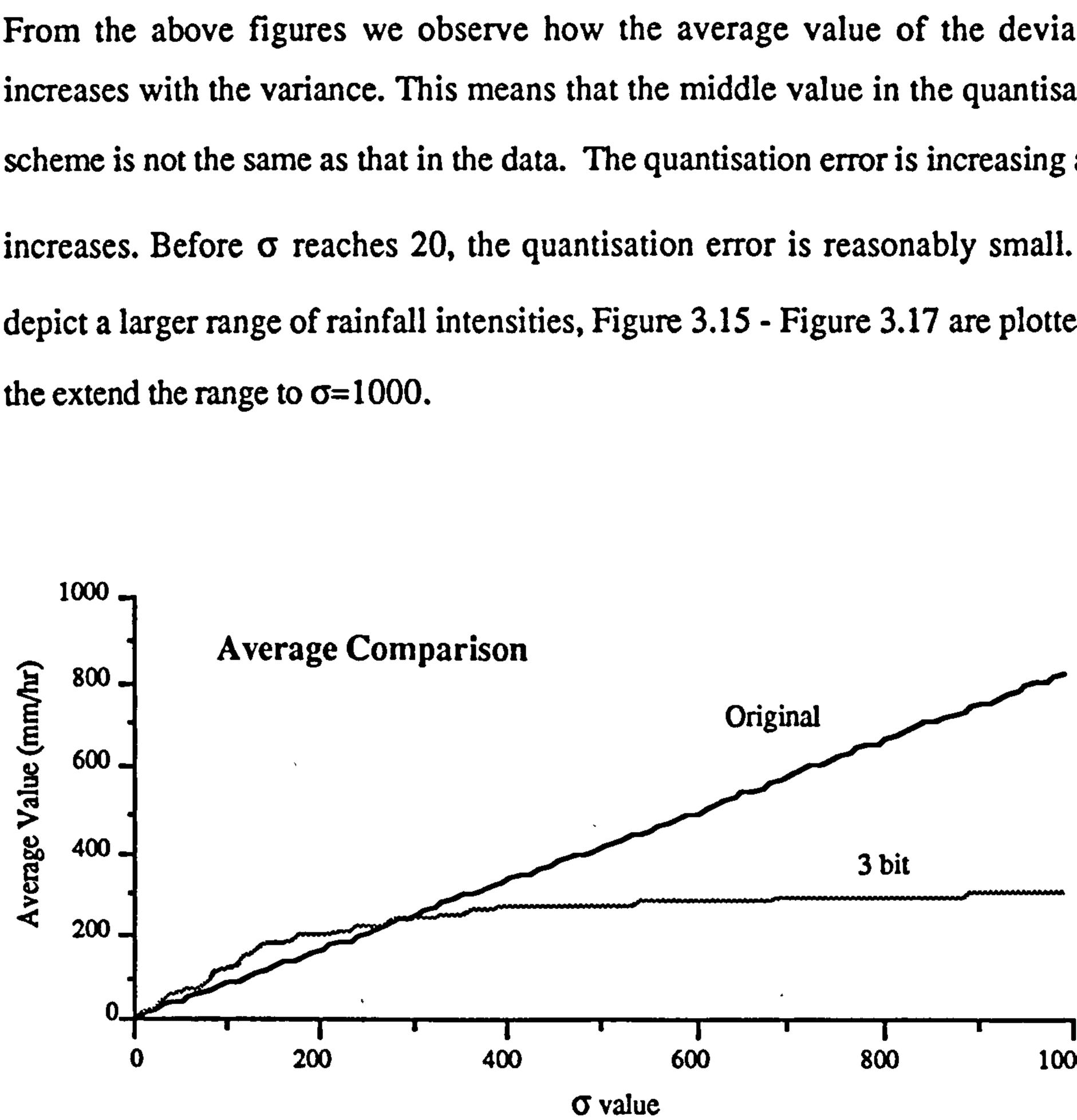

Figure 3.15 Average Comparison between Original and 3-Bit Data ($\sigma \leq 1000$)

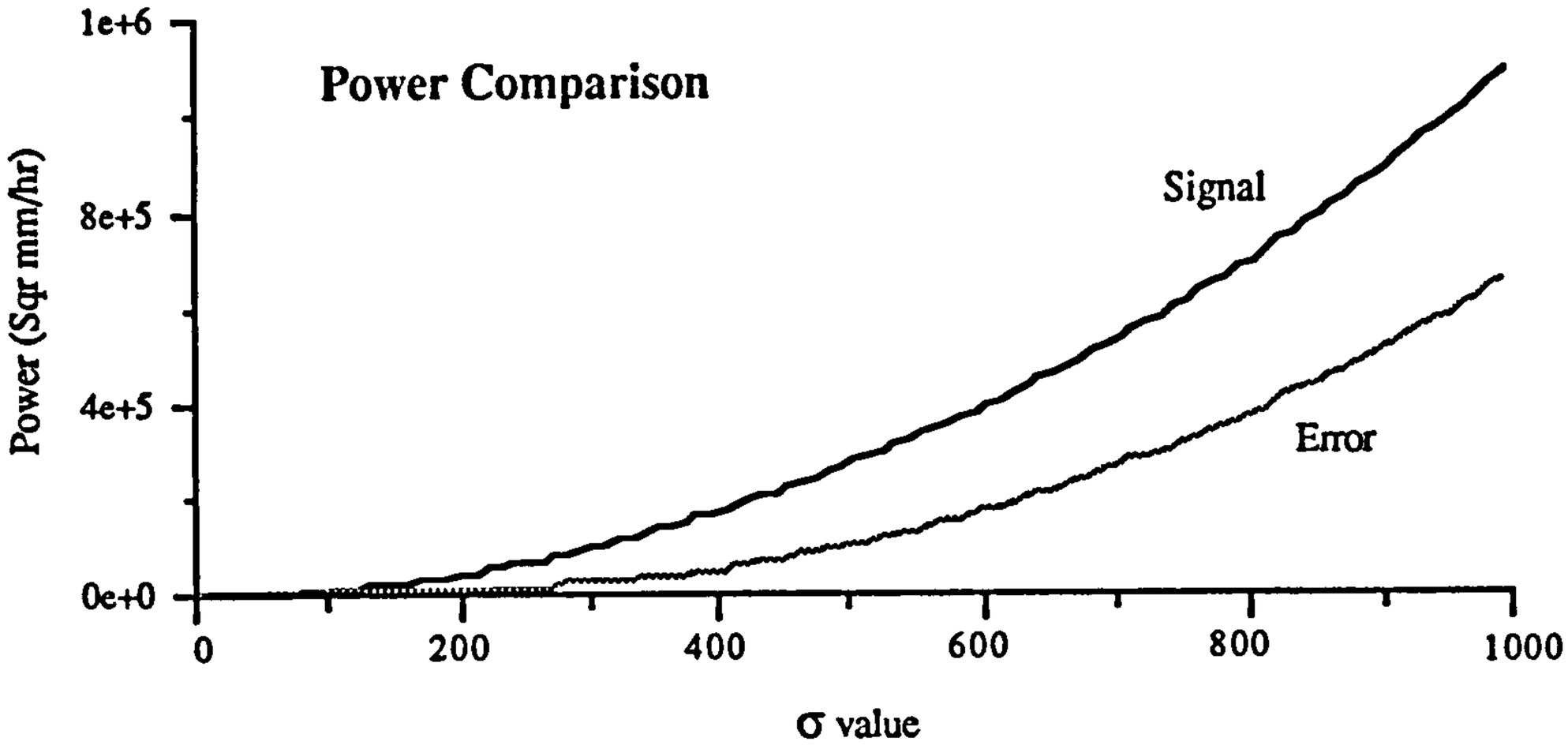

Figure 3.16 Signal Power Comparison between Original and 3-Bit Data ($\sigma \leq 1000$)

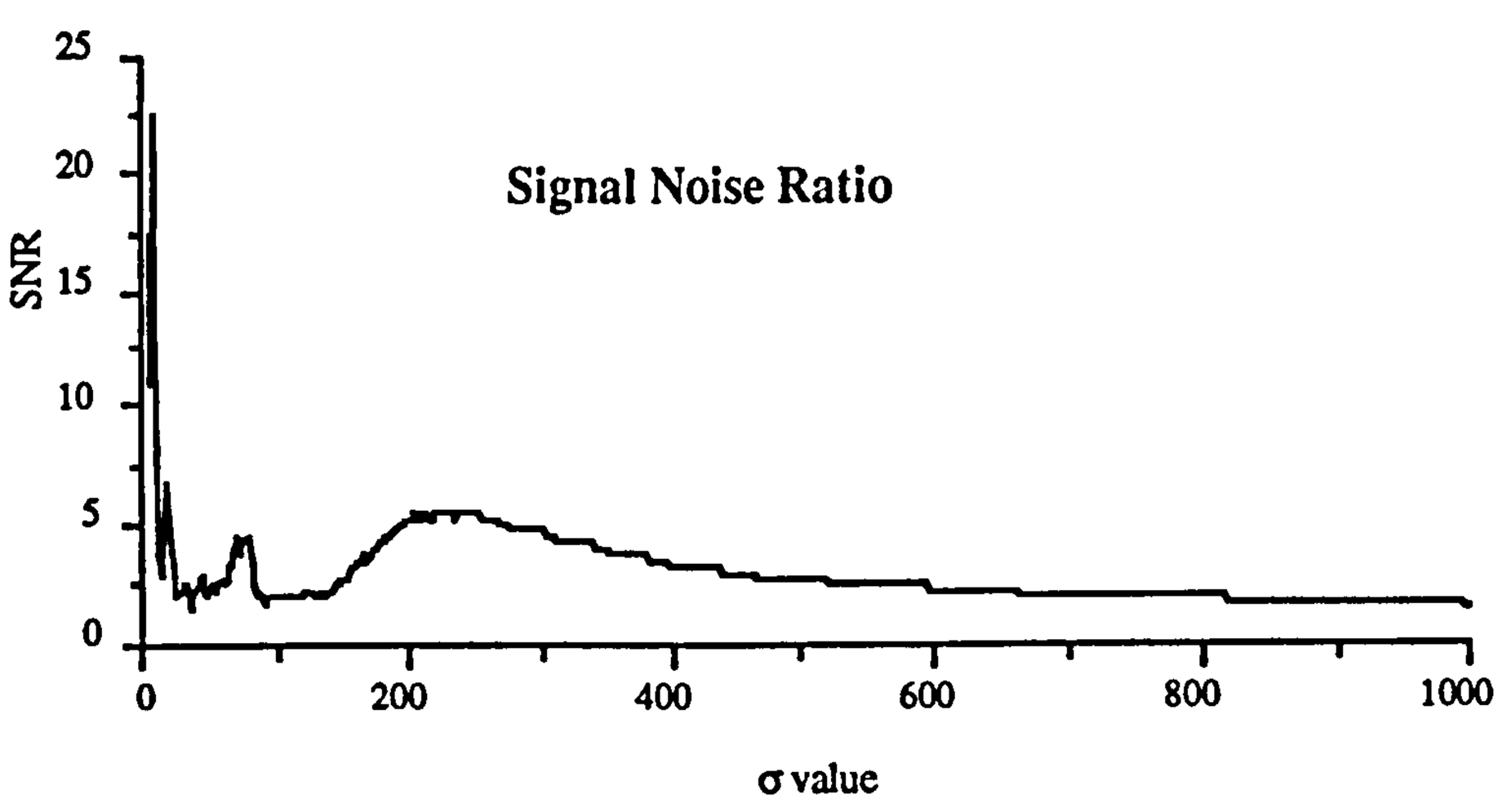

Figure 3.17 Signal Noise Ratio between Original and 3-Bit Data ($\sigma \leq 1000$)

When the σ reaches 150 (in standardised form), the average deviation begins to decrease and is zero at a variance value of 260. From that point on, the 3 bit average value is always below the original value. This is because at high rainfall intensity, a large portion of rainfall rate exceeds the 3 bit quantisation range and the high magnitude rainfall rate is suppressed. This shows that the dynamic range of

the quantisation scheme is very important and should be decided by analysing the actual rainfall data.

3.5 Radar Rainfall Distribution

It has been found that the statistical properties of the rainfall distribution will influence the quantisation scheme. In this section, some preliminary analyses are carried out to discuss the radar rainfall distribution. A test was undertaken by using some 5 minute Upavon Radar data to assess the basic features of the radar rainfall data distribution.

Radar data files from the Upavon Radar site which contain a relatively heavy rainfall rate are used for such a purpose. 2 km resolution data from node (18,18) to node (58,58) were used (given that the bottom left was (0,0)), that meant 400 2km x 2km nodes in each picture. Rainfall rates are distributed from 0,1,2,..., 150 mm/hr. Figure 3.18-Figure 3.21 provide analysis of the Upavon radar data.

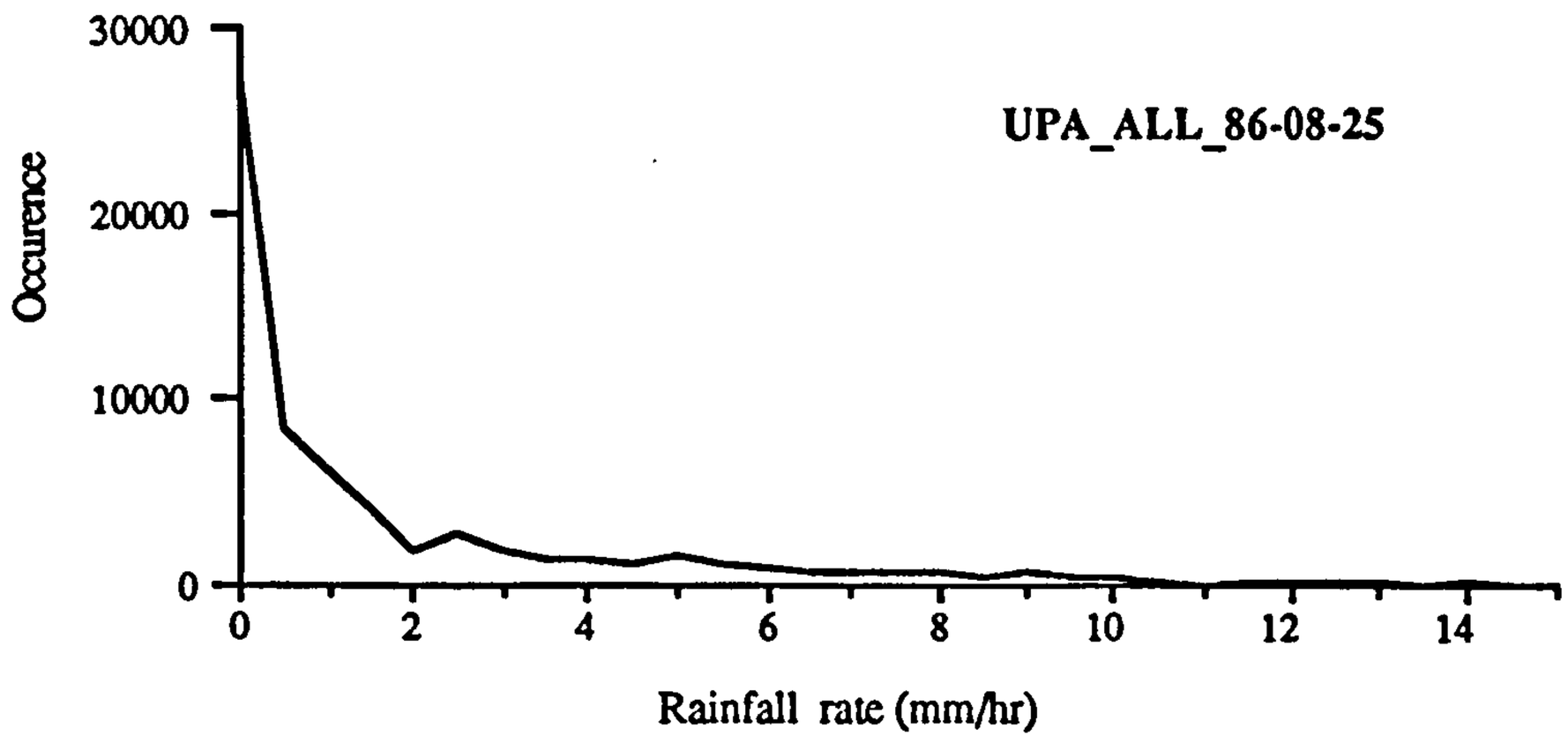

Figure 3.18 Radar Rainfall Data Distribution 1

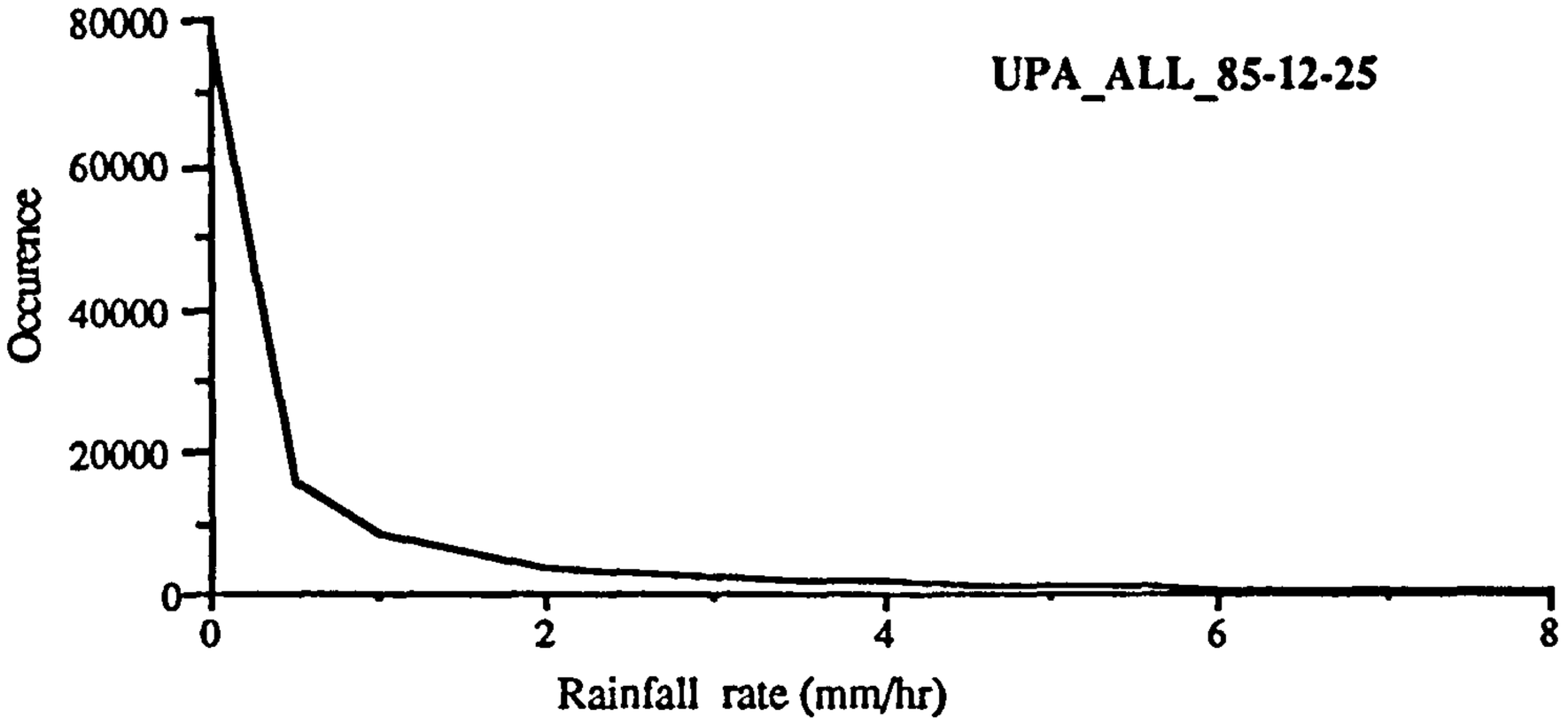

Figure 3.19 Radar Rainfall Data Distribution 2

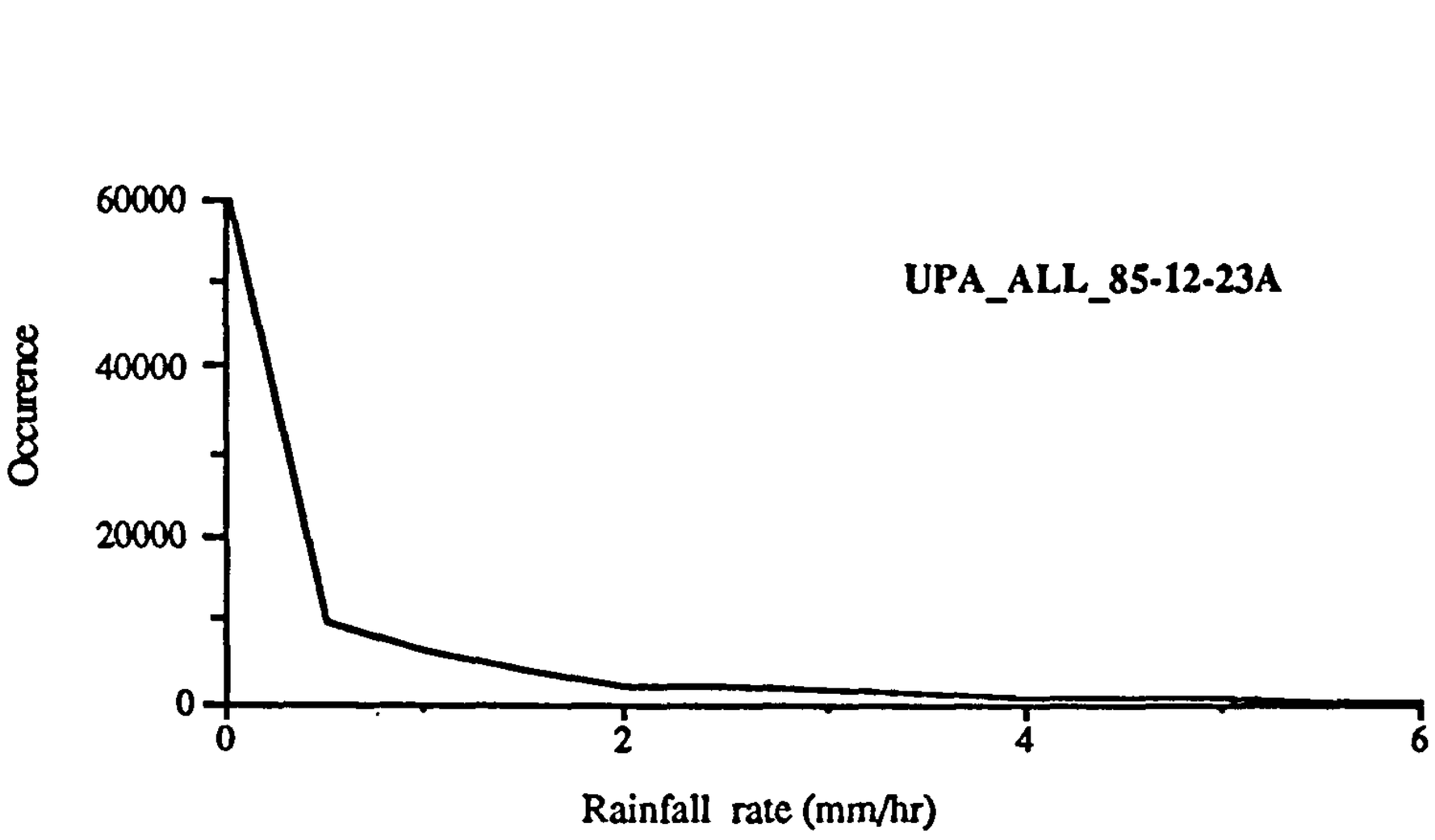

Figure 3.20 Radar Rainfall Data Distribution 3

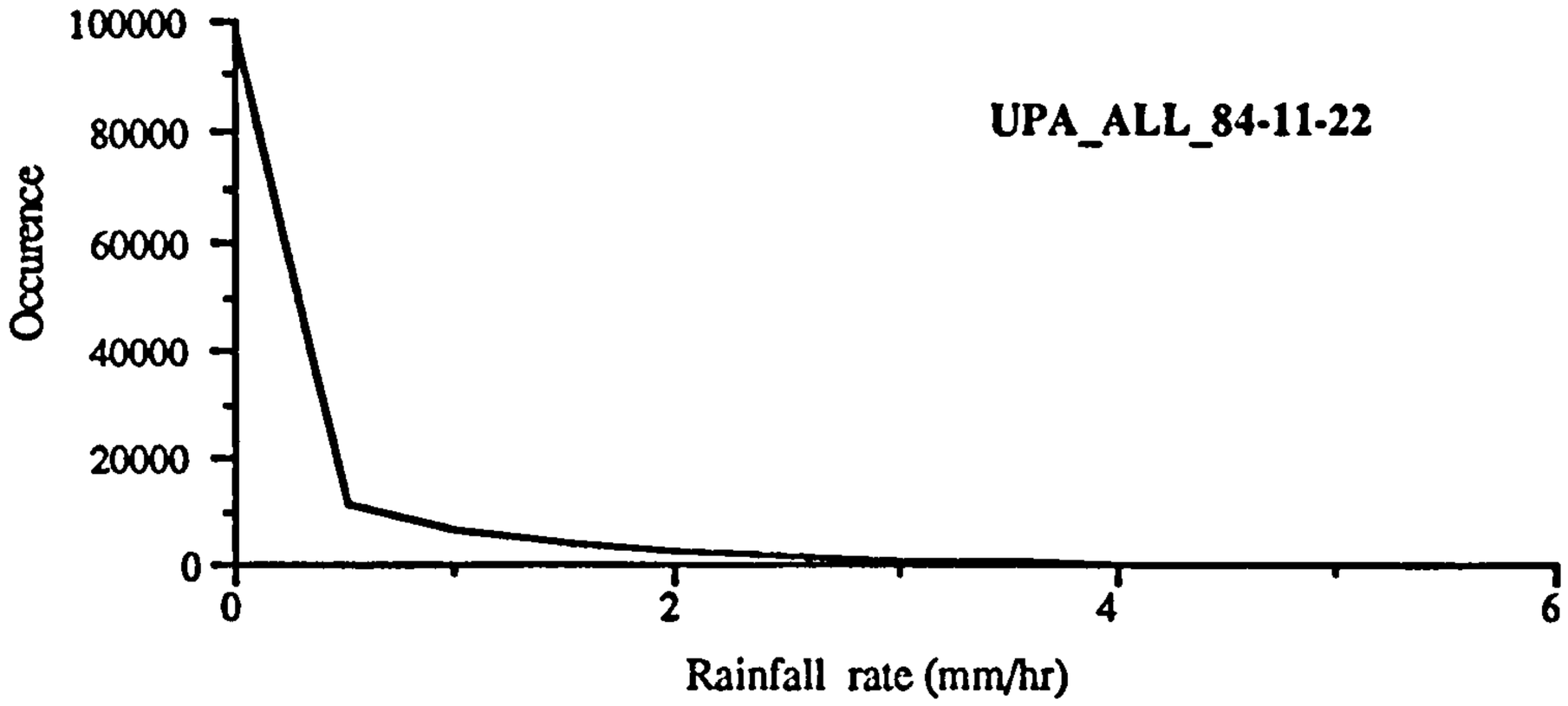

Figure 3.21 Radar Rainfall Data Distribution 4

Compared with the positive normal distribution, the radar rainfall rate sample distribution is similar except contained more lower level intensity data as in Figure 3.22. This portion is well below 0.5 mm/hr and depended on how many zeros were included in the sample data.

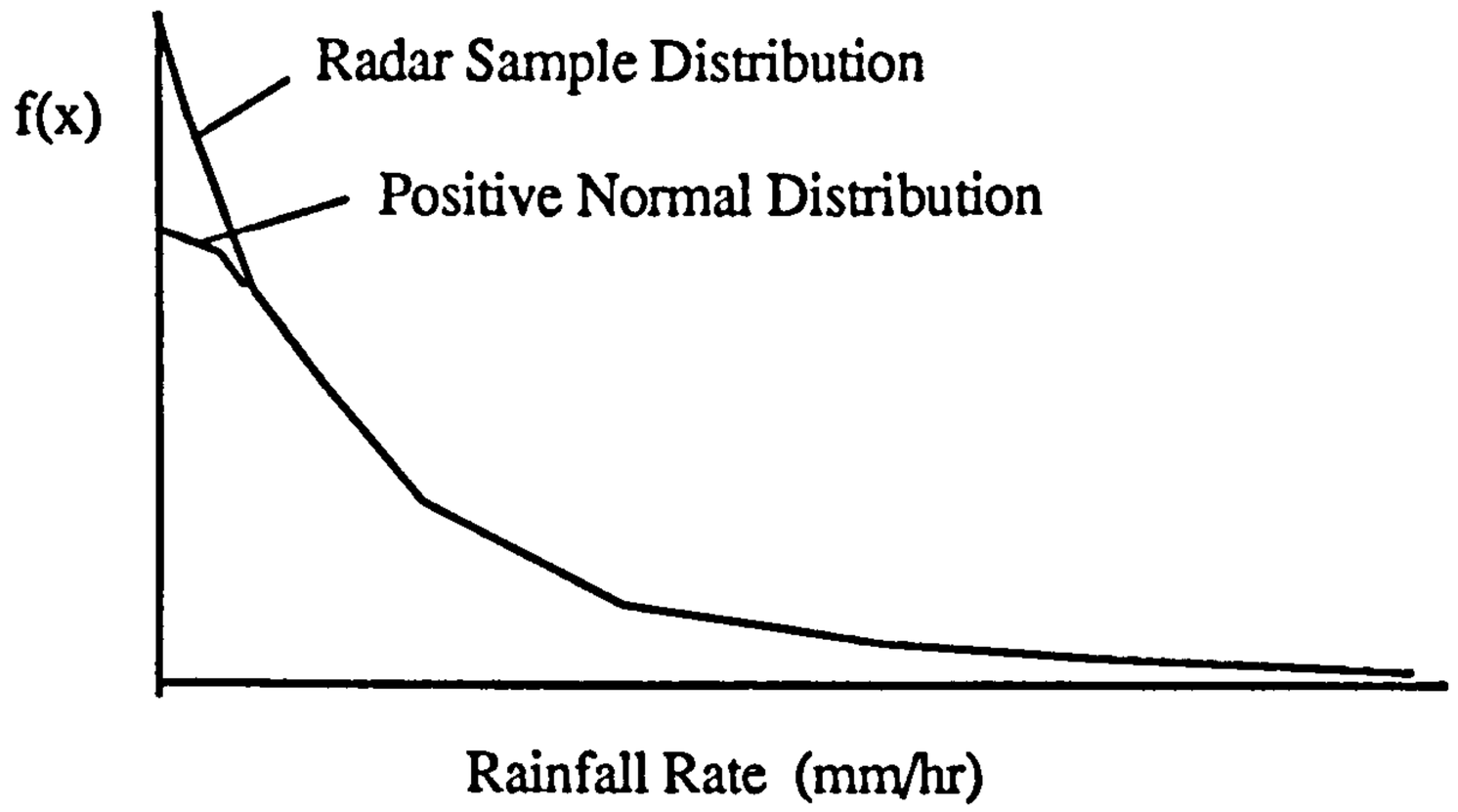

Figure 3.22 Comparison of Positive Normal and Radar Data sample

The rainfall data was obtained by scanning every 5 minutes. In hydrological processes usually hourly data are utilised for flood forecasting models and it is common to average 5 minutes data over one hour. It has been shown that the

longer the time length, the more the rainfall rate distribution approximates the normal distribution(Figure 3.23).

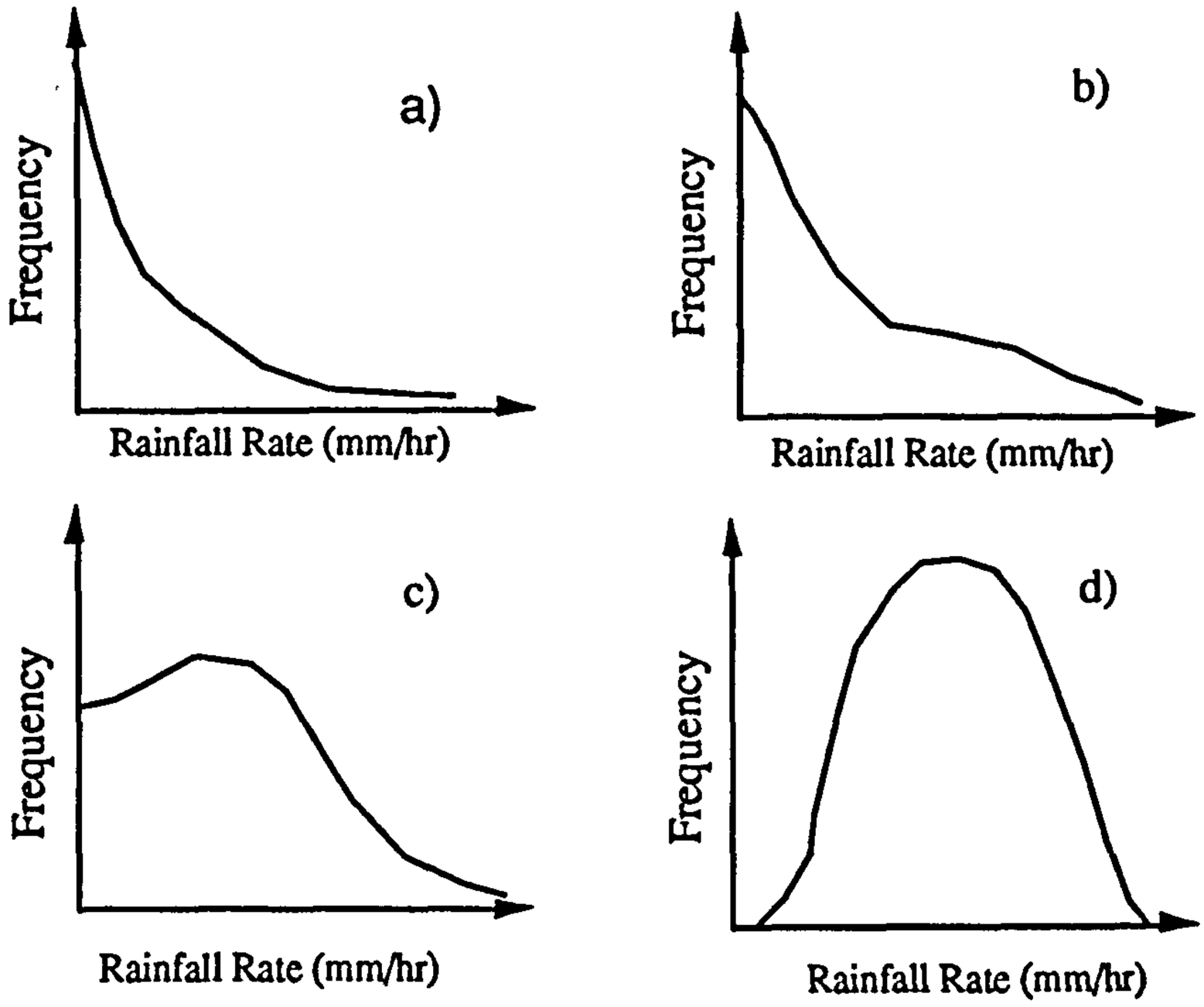

Figure 3.23 Schematic Rainfall Frequency Change with period length

Note : *a) Short Duration;*

b)Medium Duration;

c)Long Duration;

d)Very Long Duration.

This can also be explained by reference to the Limit Theorems from Probability Theory.

Suppose independent random variables X1, X2, ...Xn,,

$$E(X_k)=m_k,\ D(X_k)=\sigma_\kappa^{\,2}\ \ (k=1,2,...)$$

Let

$$B_n^2 = \sum_{k=1}^{n} \sigma_k^2$$

The probability distribution function $F_n(x)$ will be:

$$\lim_{n \to \infty} F_n(x) = \lim_{n \to \infty} P\left\{ \frac{\sum_{k=1}^{n} X_k - \sum_{k=1}^{n} m_k}{B_n} \leq x \right\}$$

$$= \int_{-\infty}^{x} \frac{1}{\sqrt{2\,p}} e^{-t^2/2} dt$$

When n is very large, Σx will approximate the normal distribution. For comparison, two events were chosen to demonstrate such effects and the results are shown in following figures.

Events Chosen: *UPA_ALL_86-08-25*

UPA_ALL_85-12-25

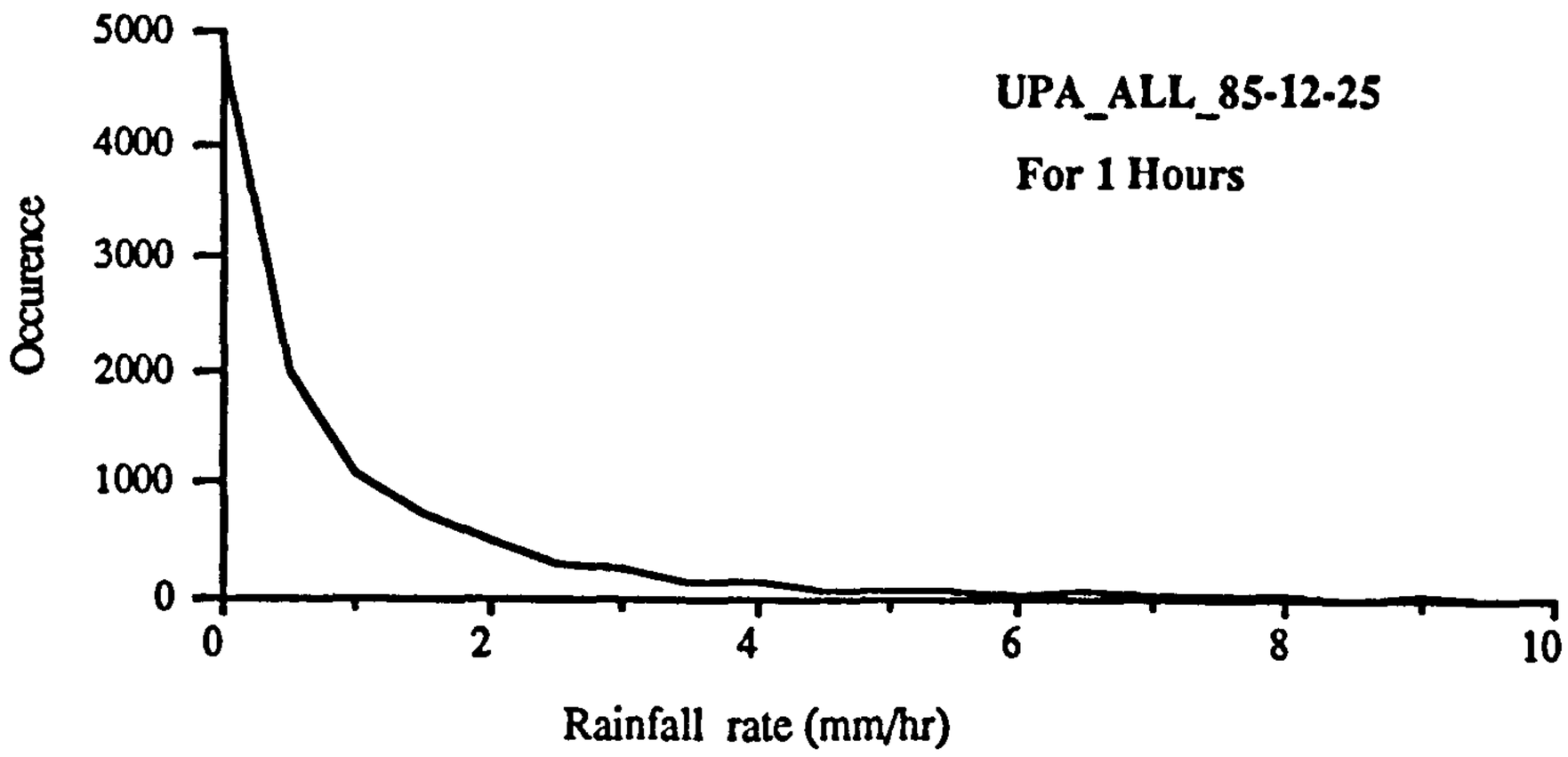

Figure 3.24 Rainfall Distribution with Different Duration 1

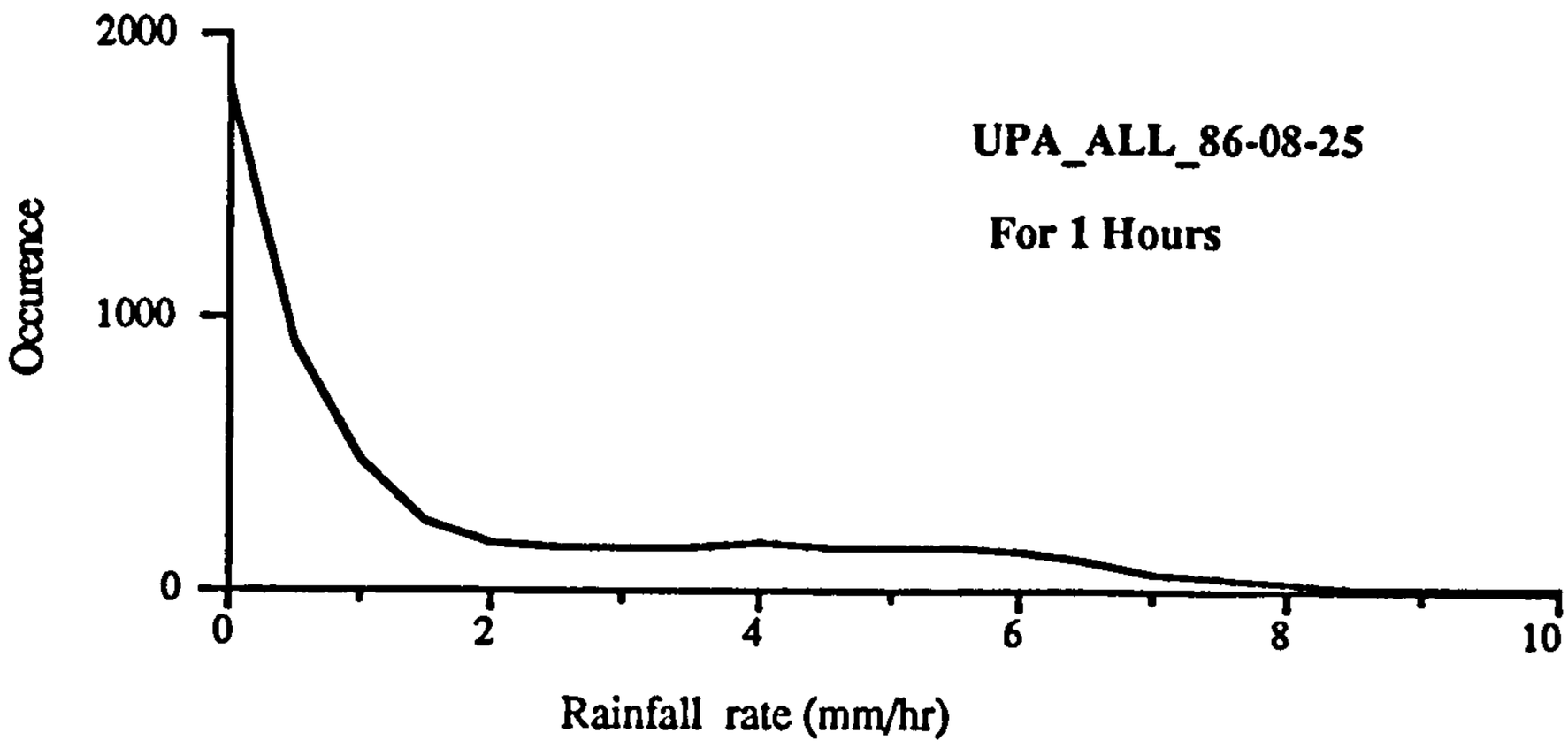

Figure 3.25 Rainfall Distribution with Different Duration 2

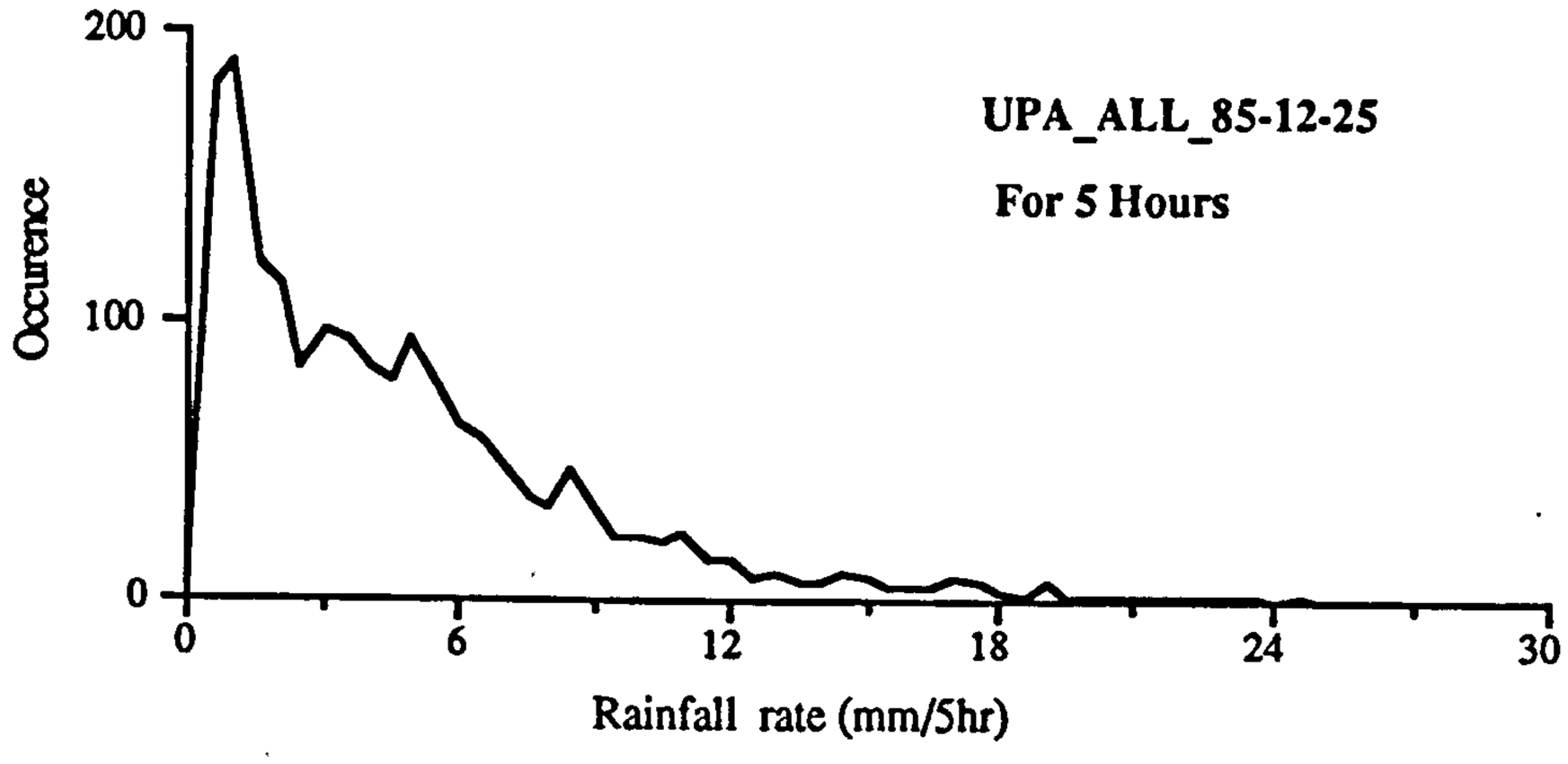

Figure 3.26 Rainfall Distribution with Different Duration 3

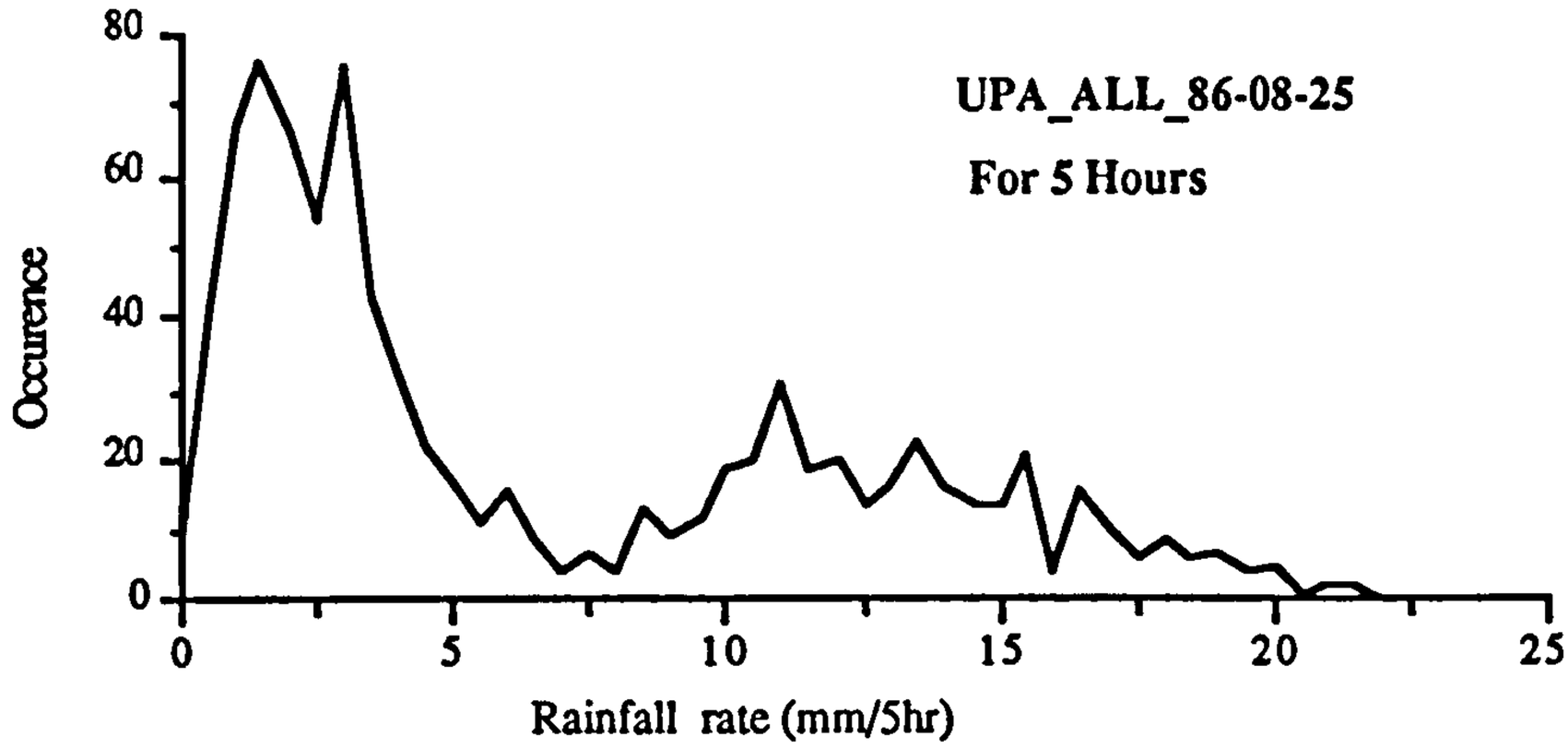

Figure 3.27 Rainfall Distribution with Different Duration 4

The computation show that when the averaging interval increases from 1 hour to 5 hours, the rainfall rate distribution behaves as the theorem described above defines. With hourly data, not much error will be introduced by using positive normal distributions to generate the synthetic data for the research. The results above show that a positive normal distribution is close to the true rainfall distribution and could be utilised to generate synthetic rainfall data for 1 hour periods.

3.6 Optimum Quantisation of Rainfall Data

Quantisation scheme is important issue and some further analysis is carried out to illustrate the statistic quantisation method. In the past sections, the influence of 3 bit quantisation has been discussed. Different quantisation levels can be utilised to represent the radar rainfall data. It is worth while to study which is the best quantisation scheme so the minimum distortion can be achieved by using the same number of bits (or code) to describe the same set of data. From the statistical point of view, the optimum quantisation method will depend on the statistical properties of the related radar data. In this section, some considerations will be given to reconsidering the optimum quantisation proposal for radar rainfall data.

In designing a quantisation scheme, statistical analysis of the data should be carried out. Suppose that the data sequence $\{x_i\}$ has a pdf (probability density function) p(x) and we want to use R bit to represent it (that is $L = 2^R$ levels). Then the average distortion resulting from quantisation of the signal amplitude is given:

$$D = \int_0^\infty f(x_q - x)\,p(x)\,dx \qquad (3,6)$$

where $f(x_q - x)$ denotes the desired function of the error. For the rainfall process, the minimum rainfall rate is zero. It is difficult to set the maximum rainfall rate so an infinity is used to represent the highest rainfall intensity.

The optimum quantiser can be obtained by minimising D. This optimisation problem has been considered by Lloyd (1982) and Max (1960). Let the output level be y_k when the input signal amplitude is in the range $x_{k-1} \le x < x_k$. For an L-level quantiser, the end points are $x_0=0$ and $x_l=\infty$. The resulting distortion is then given by:

$$D = \sum_{k=1}^{L} \int_{x_{k-1}}^{x_k} f(y_k - x)\,p(x)\,dx \qquad (3,7)$$

Which is now minimised by optimally selecting the $\{y_k\}$ and $\{x_k\}$.

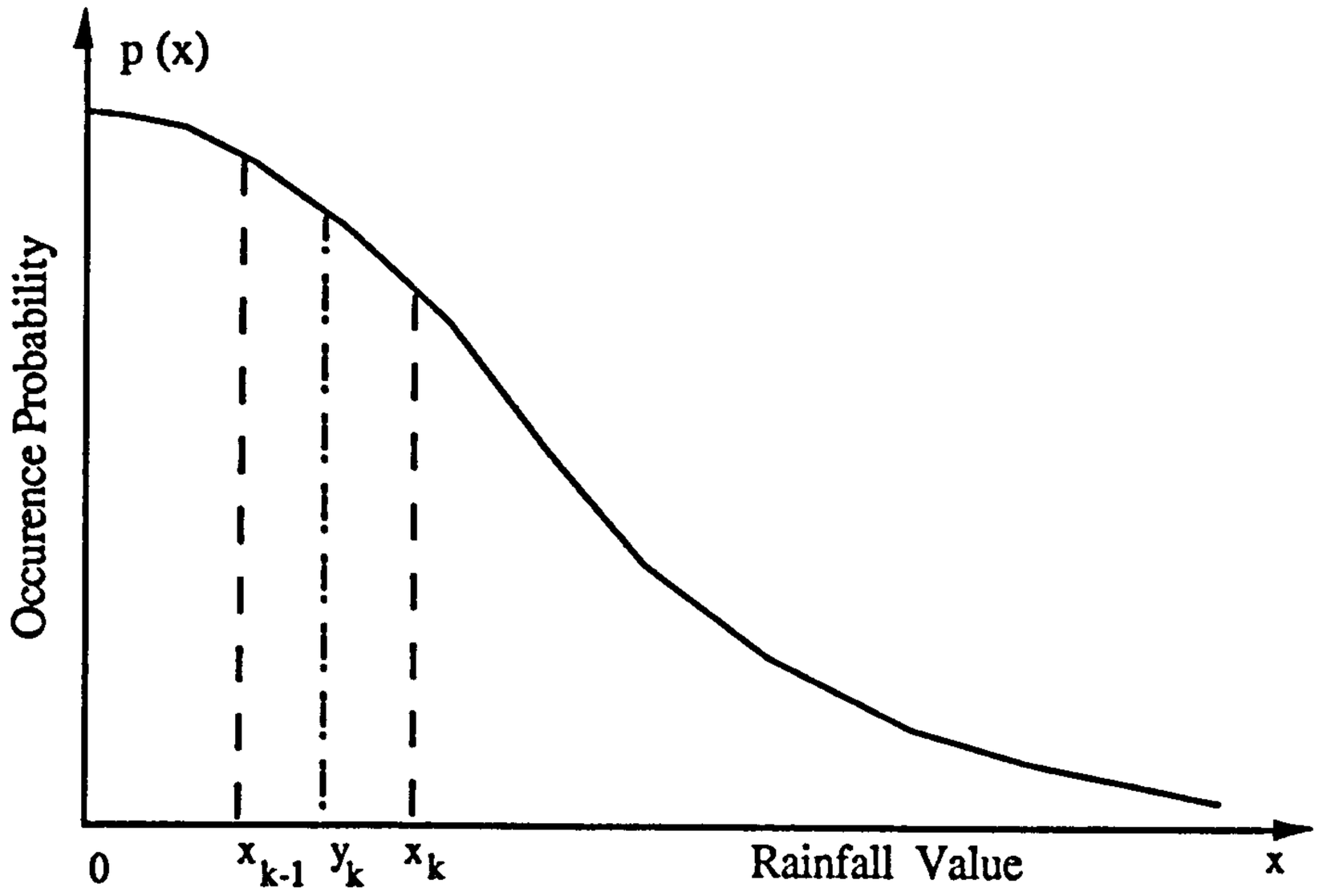

Figure 3.28 Quantisation and output level

The necessary conditions for a minimum distortion are obtained by differentiating D with respect to the $\{ x_k \}$ and $\{ y_k \}$. The result of this minimisation is the pair of equations

$$f (y_k - x_k) = f (y_{k+1} - x_k) \quad k = 1, 2, \ldots, L - 1 \tag{3,8}$$

$$\int_{x_{k1}}^{x_k} f' (y_k - x) p(x) dx = 0 \quad k = 1, 2, \ldots, L \tag{3,9}$$

As a special case, we consider minimising the mean square value of the distortion. In this case, $f(x)=x^2$ and hence,

$$x_k = \frac{y_k + y_{k-1}}{2} \qquad k = 1, 2, \ldots, L-1 \tag{3,10}$$

Which is the midpoint between y_k and y_{k-1}. The corresponding equations

determining { y_k } are

$$\int_{x_{k-1}}^{x_k} (y_k - x) \, p(x) \, dx = 0 \qquad k = 1, 2, \ldots, L \tag{3,11}$$

Thus, y_k is the centroid of the area of p(x) between x_{k-1} and x_k. These equations may be solved numerically for any given p(x).

With the procedure described above, we can obtain an optimum quantisation scheme and obtain an optimum output level under fixed quantisation intervals(such as in the case of using the 3 bit radar data product from the Met Office.) As a comparison, a computation is carried out to judge the effectiveness of the optimum quantisation procedure.

Table 3.3 Optimum Output Level for The Met Office Quantisation Scheme

Range (mm/h)	The Met Office	σ=5	σ=10	σ=20	σ=30	σ=40	Logarithmic Average
0 - 0.125	0	0.062	0.062	0.062	0.062	0.062	0
0.125 - 1	0.56	0.561	0.562	0.562	0.562	0.562	0.354
1 - 4	2.5	2.425	2.480	2.494	2.496	2.497	2.000
4 - 8	6.0	5.689	5.919	5.978	5.989	5.993	5.657
8 - 16	12.0	10.025	11.379	11.837	11.925	11.956	11.314
16 - 32	24.0	17.340	20.051	22.758	23.431	23.674	22.627
32 - 126	79.0	N/A	34.652	40.442	47.318	54.341	64
> 126	319.0	N/A	N/A	N/A	128.860	132.933	512

Note: N/A in the above table means the that probability of the rainfall rate data being in the related range is below 10^{-8} and should be considered as highly unlikly to happen in practical case.

Since it is difficult to analytically determine the result, a Monte Carlo method is utilised to compute the optimum output level from the Meteorological Office quantisation scheme. The results has been listed in the Table 3.3.

Comparison figures are presented to compare the different methods. It has been shown that the logarithmic (or harmonic) scheme performs better than the arithmetic and the optimum can be achieved by the use of the probabilistic approach.

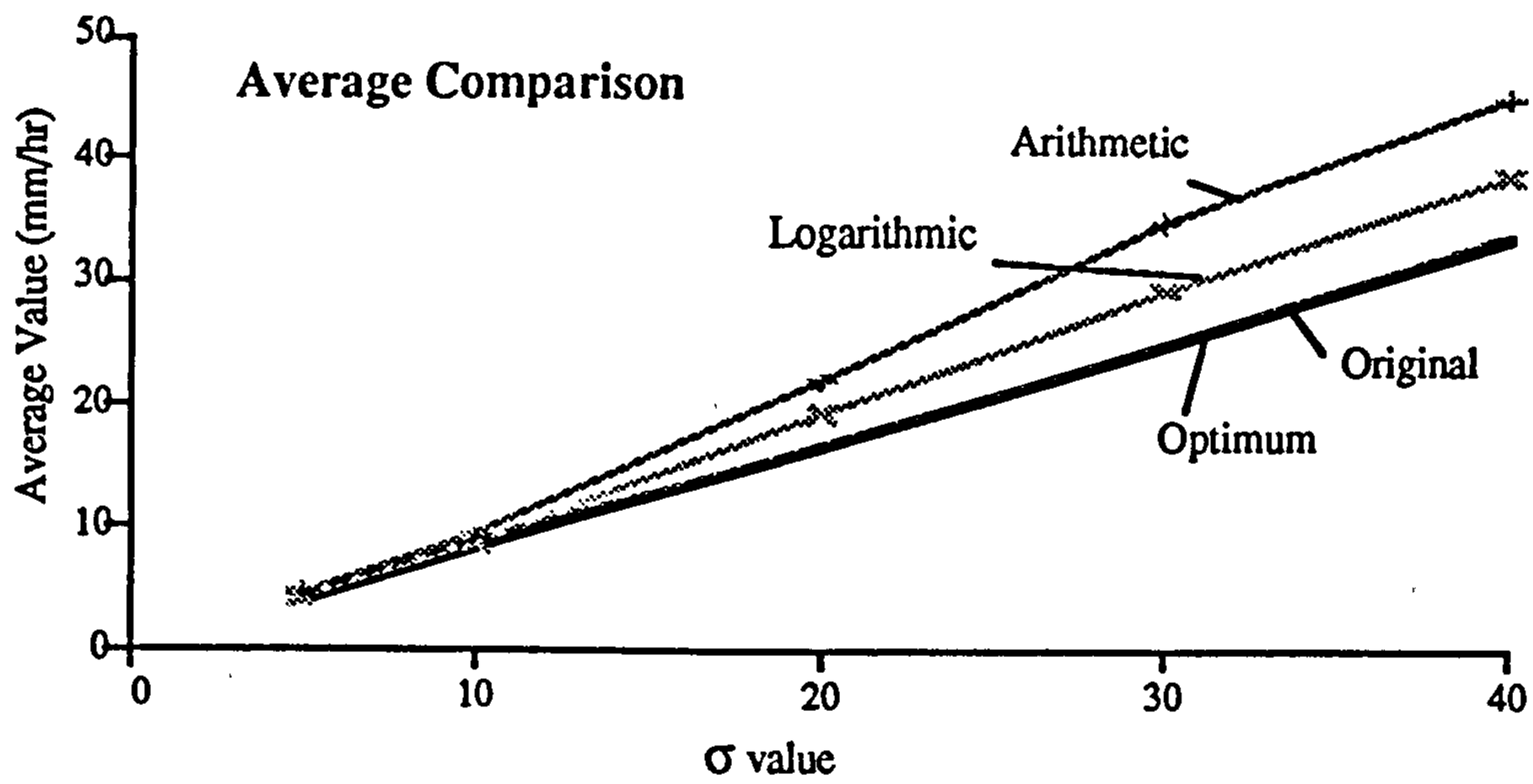

Figure 3.29 Average Value Comparison between Different Allocation Schemes

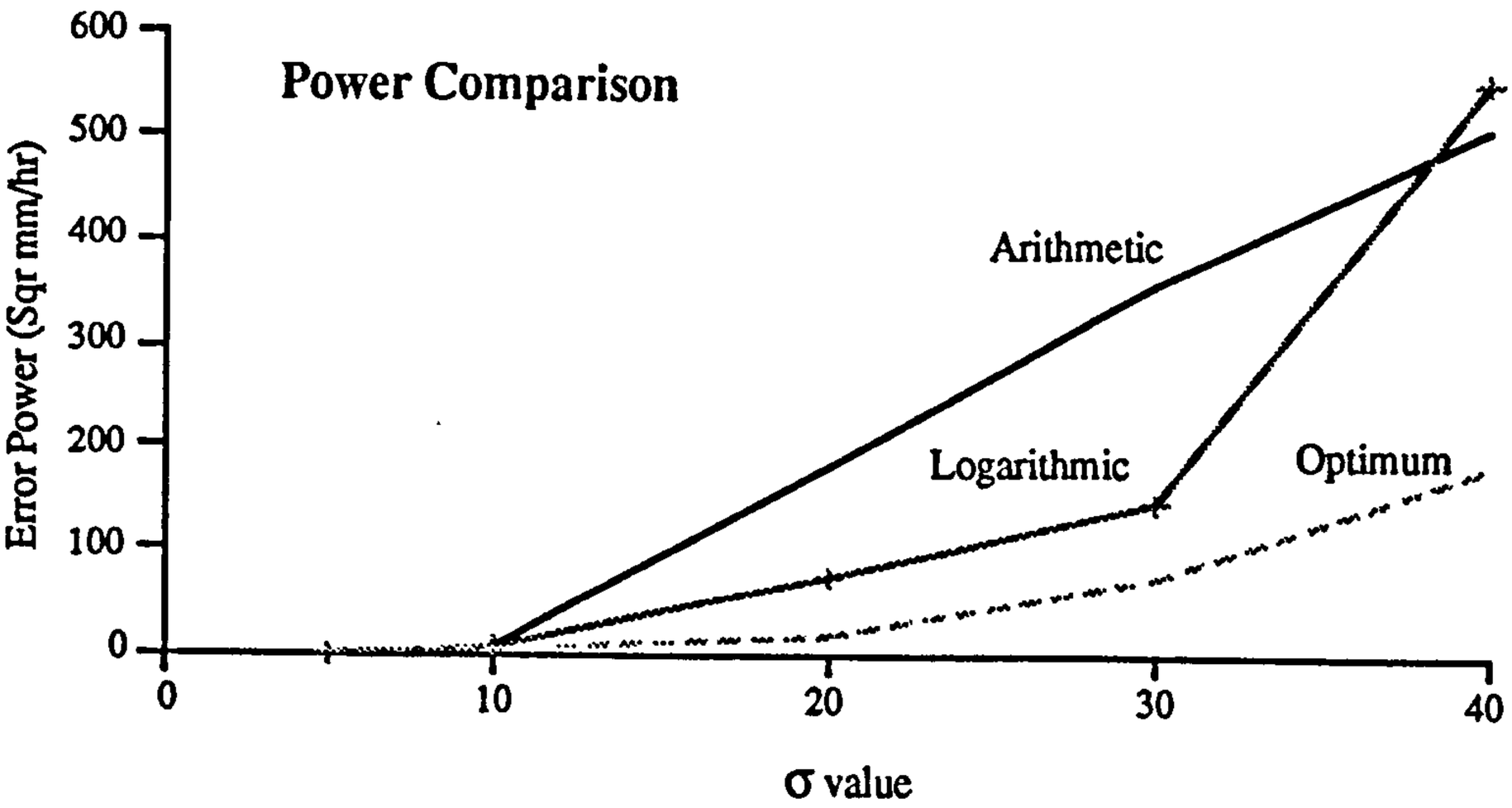

Figure 3.30 Error Power Comparison between Different Allocation Schemes

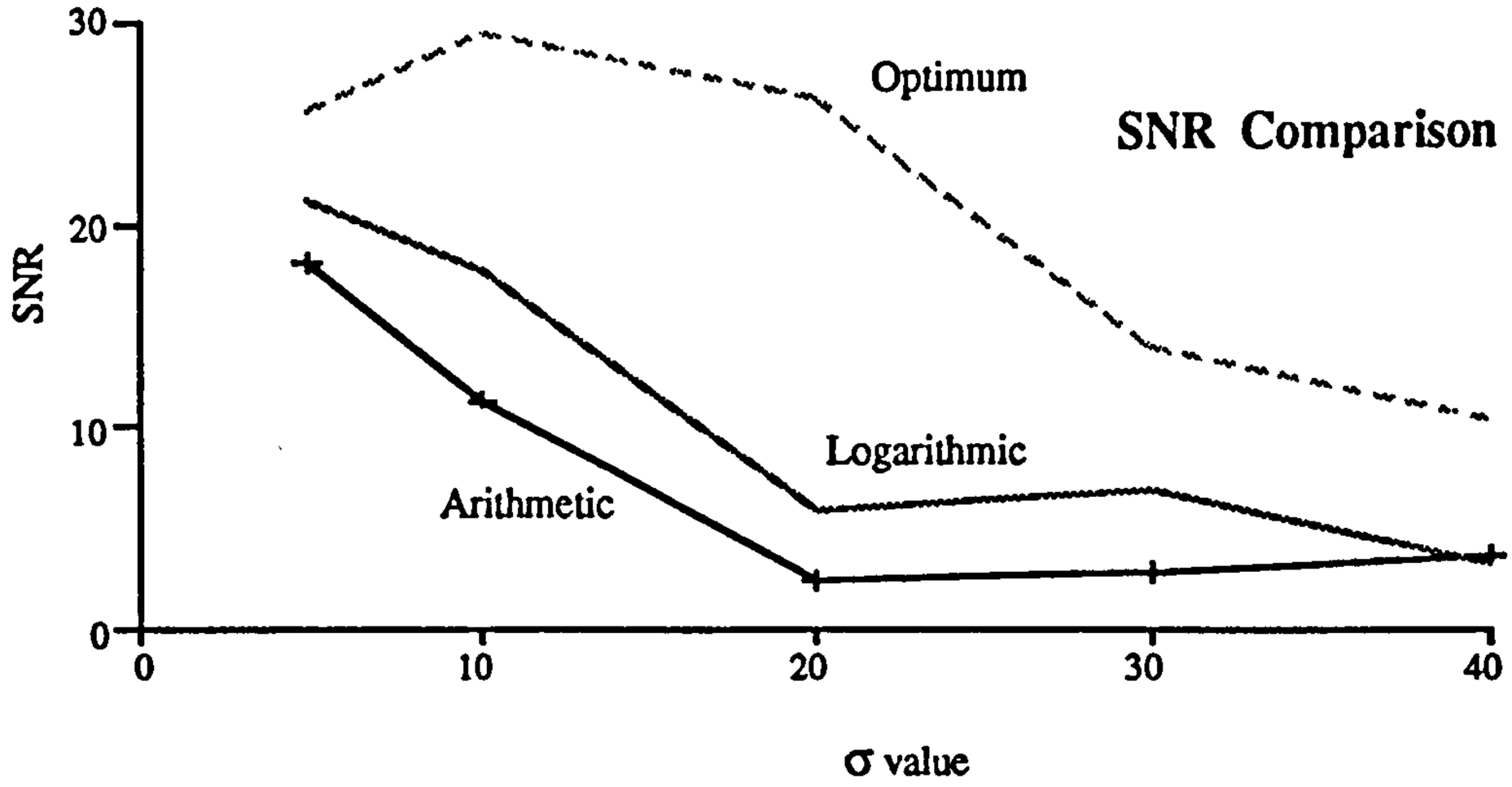

Figure 3.31 SNR Comparison between Different Allocation Schemes

The results show a remarkable improvement in quantitative data integrity for the optimum quantisation scheme compared with other schemes.

Information theory can also be utilised to achieve the optimum quantisation scheme. A scheme which can maximise the information contained in a quantised data set is then chosen as the optimum quantisation scheme.

Information theory is a branch of probability theory originating from two papers by C.E Shannon (1948). He provided the first consistent attempt towards the measurement of such difficult and abstract notions as information and uncertainty. The information measure is a logarithmic function that depends upon the uncertainty, or probability of occurrence, associated with the message symbol. Thus if a particular message symbol s_i was to occur with probability p_i, we would say that the self-information associated with this symbol is defined as :

$$S_i\,(s_i) = -\log_2 p_i \ \text{Bits}$$

The information content of a message symbol is the negative of the logarithm of the

probability that this symbol will be emitted from the source. The information content of an individual symbol is termed self-information, S_i. The choice of the logarithmic base determines the unit of information content. If the chosen base is two (which is the usual case) the unit is termed a *bit*. Thus the self-information content of a symbol from a binary source in which the symbols 0 and 1 occur with equal probability, is equal to $\log_2(2) = 1$ Bit. If the base chosen is 10 then the unit is termed a *hartley*; if the base chosen is the natural base the unit is termed a *nat*.

The average information of the whole symbol source is termed *Entropy* and it is an important quantity in Information Theory. Entropy is given by the following expression:

$$H(s) = \sum_i p_i \log_2 \left(\frac{1}{p_i}\right) \qquad (3,8)$$

Since any quantiser reduces a continuous amplitude source into a discrete amplitude source, we may treat the discrete amplitudes as symbols, say $S = \{s_k, 1 \le k \le M\}$, with associated probabilities $\{p_k\}$. By maximising the entropy, we can obtain the optimised quantisation intervals.

Considering that:

$$\sum_i p_i = 1$$

According to Information Theory, the maximum information content of a source having M elements is $\log_2 M$ Bit, and is achieved only when all elements have equal probability.

The entropy described is called Shannon's entropy. Underlining the importance of Shannon's entropy, it is necessary to notice at the same time that this formula gives us the measure of information as a function of the probabilities with which various events occur. There exist many fields dealing with random events where it is necessary to take into account both these probabilities and some qualitative characteristics of events. So a qualitative weight can be introduced into the computation of entropy and the information content will depend both on the probabilities of events and on qualitative weights of the possible events. This entropy is called the *weighted entropy*. It is defined as :

$$I(s) = \sum_i p_i w_i \log_2 \left(\frac{1}{p_i}\right) \qquad (3,9)$$

If $w_1 = w_2 = \ldots = w$, then $I(s) = H(s)$.

In hydrological processes different rainfall intensities can play different roles in flood forecasting. Proper selection of entropy weights is quite important in the quantisation scheme. Although large rainfall intensities should carry larger weight, in the U.K. it has been found that quite a number of floods are caused by relatively small rainfall intensities, presently an equal weight entropy is utilised in the analysis of the quantisation process.

The following table shows the entropy from the Met Office 3-bit quantisation scheme. From the point of view of Information Theory, the optimum entropy for 3 bit coding would be H = 3 Bit. That means each quantisation level contains 3 bit information. From the table, it is seen that when the data variance is 5, the entropy is 1.9 bit/per level. One bit of information is wasted compared with the optimum 2 bit quantisation scheme to achieve the same information content.

Table 3.4 Entropy Value For the Met Office 3 Bit Quantisation Method

Variance σ	5	10	20	30	40
Entropy	1.919	2.216	2.369	2.285	2.117

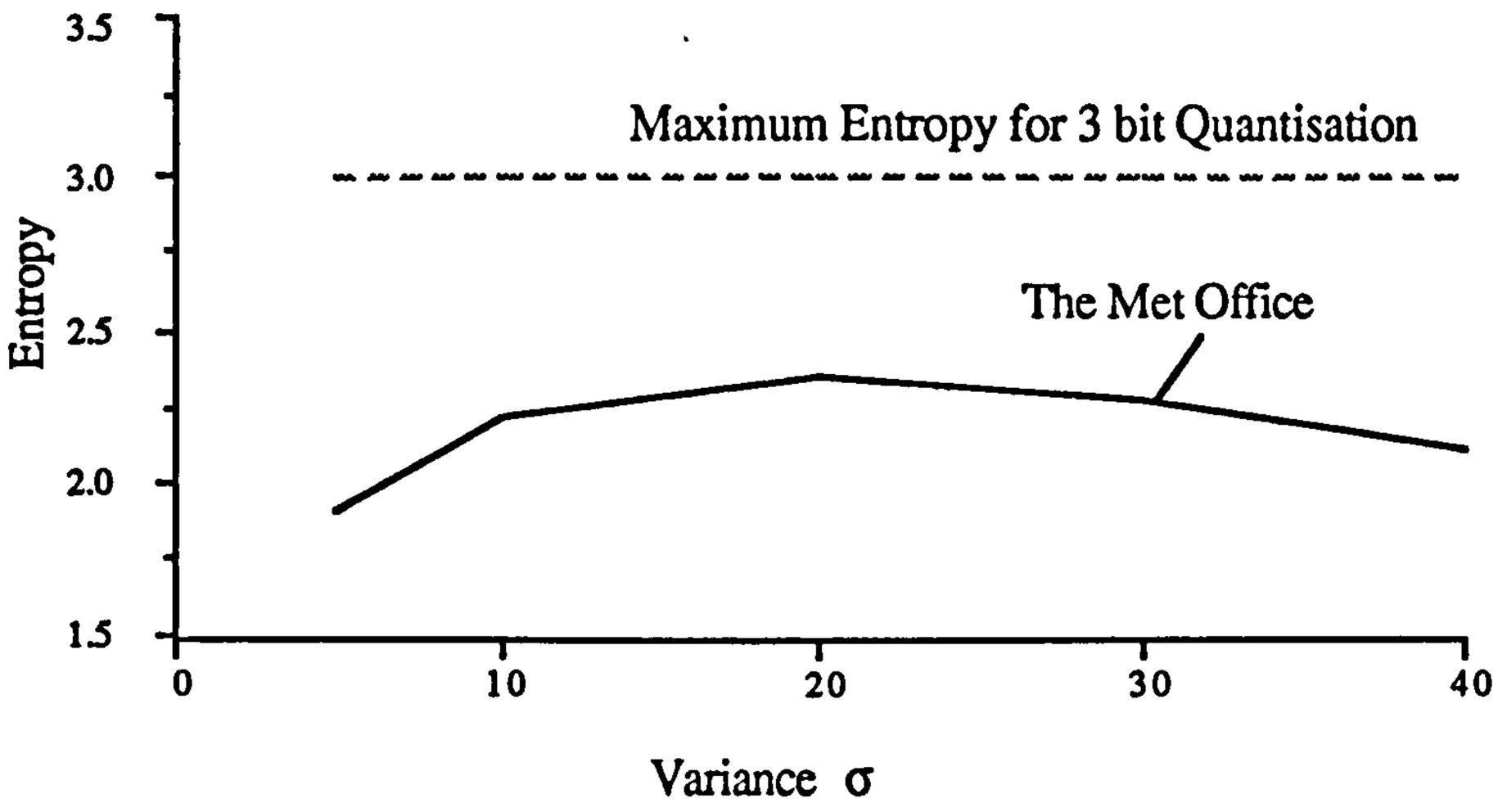

Figure 3.32 Entropy from the Met Office 3 Bit Quantisation Method

Table 3.5 Entropy Value For the Met Office 8 bit Quantisation Method

Variance σ	5	10	20	30	40
Entropy	6.967	7.011	7.128	7.094	7.063

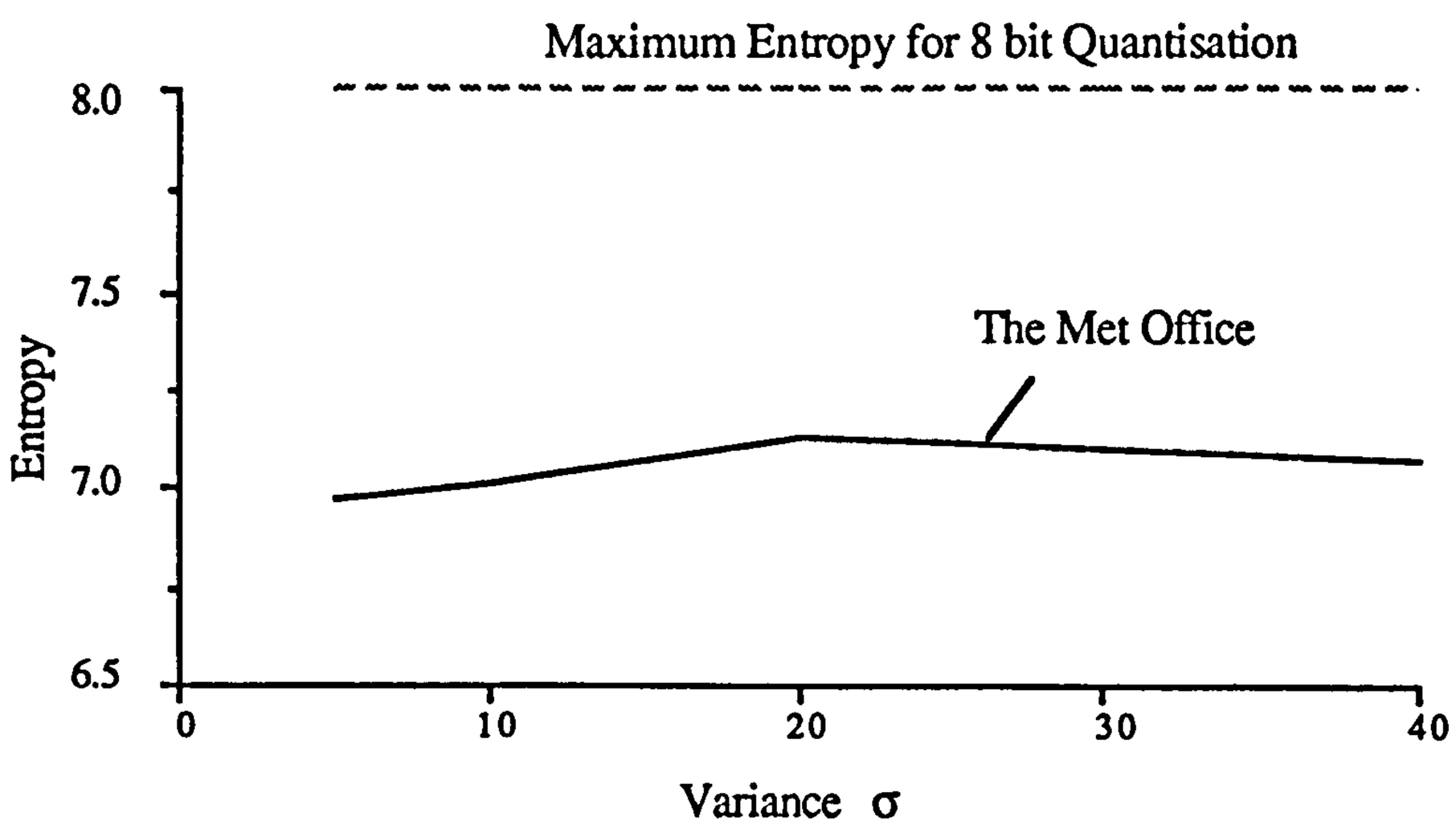

Figure 3.33 Entropy from the Met Office 8 bit Quantisation Method

These results indicate that further improvements can be expected by adopting an improved quantisation scheme.

3.7 Optimum Word Length for Radar Data Quantisation

Usually the more bits used to represent rainfall data, the more accurate the output data quality. But the cost will increase as we increase the word length to represent radar data, so there must be an optimum word length with which we can achieve both high quality of output data and low cost.

The choice of word length (or the number of quantisation levels) is a kind of decision process. Our target is to maximise the benefit of the scheme. The purpose of quantisation is to obtain the useful information and to decrease the cost of data management. When we select 3-bits or 8-bits as the word length, it is true that 8-bit data are much more accurate that 3-bit data. The question is to judge the cost and the benefit of the new information introduced by more accurate data. If the cost of the extra bits exceeds the benefit, then extra data accuracy is not required.

It has been found that the information content is related to the probability and the value of information is a very subject related concept which depends on the knowledge about the data. The same information may have great value for some applications, and no value for others. Thus, whenever we talk about the value of information, we must specify the purpose of the application.

The following figures illustrate the relationship between the quantisation word length and the quantisation noise.

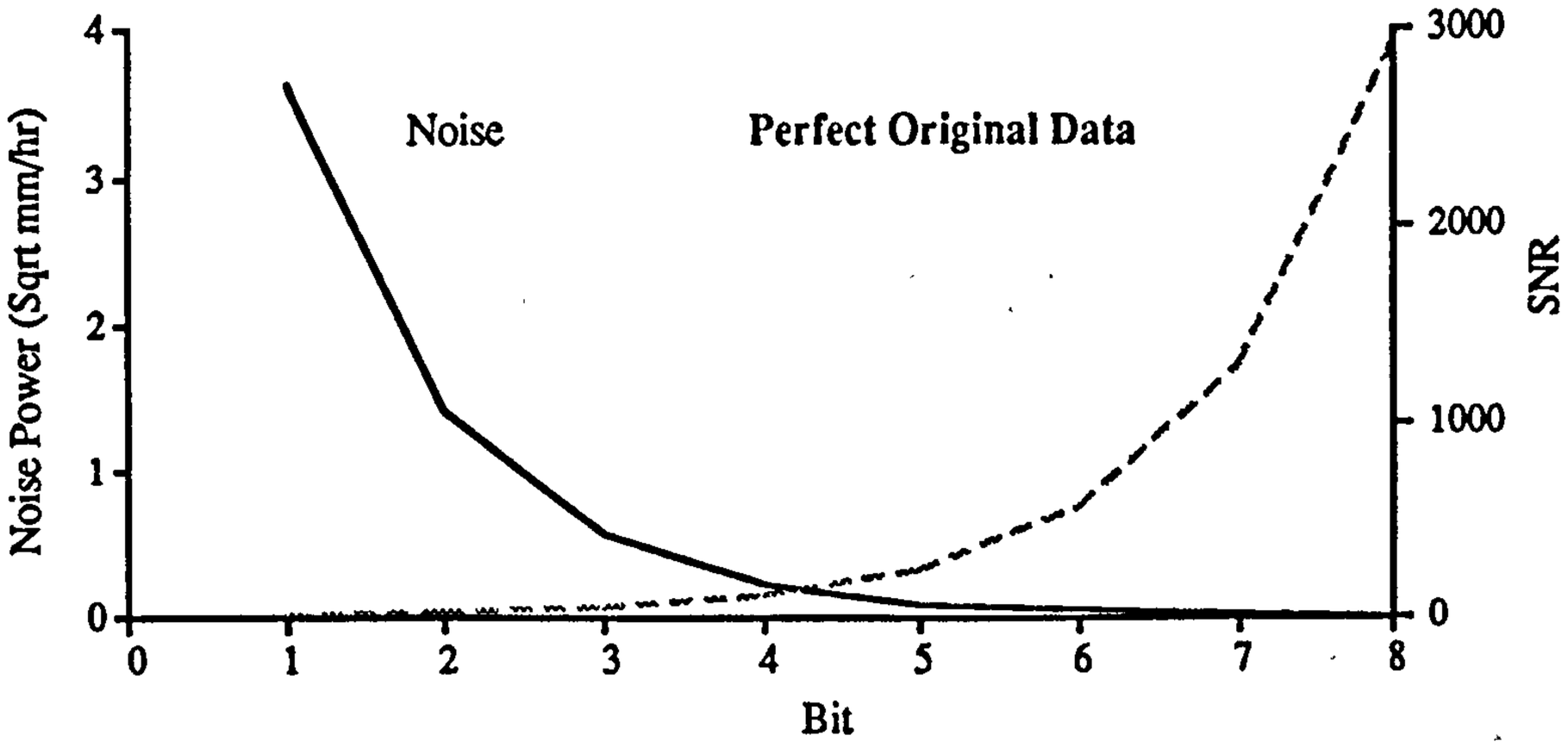

Figure 3.34 Influence of Quantisation Level to Noise Power and SNR 1

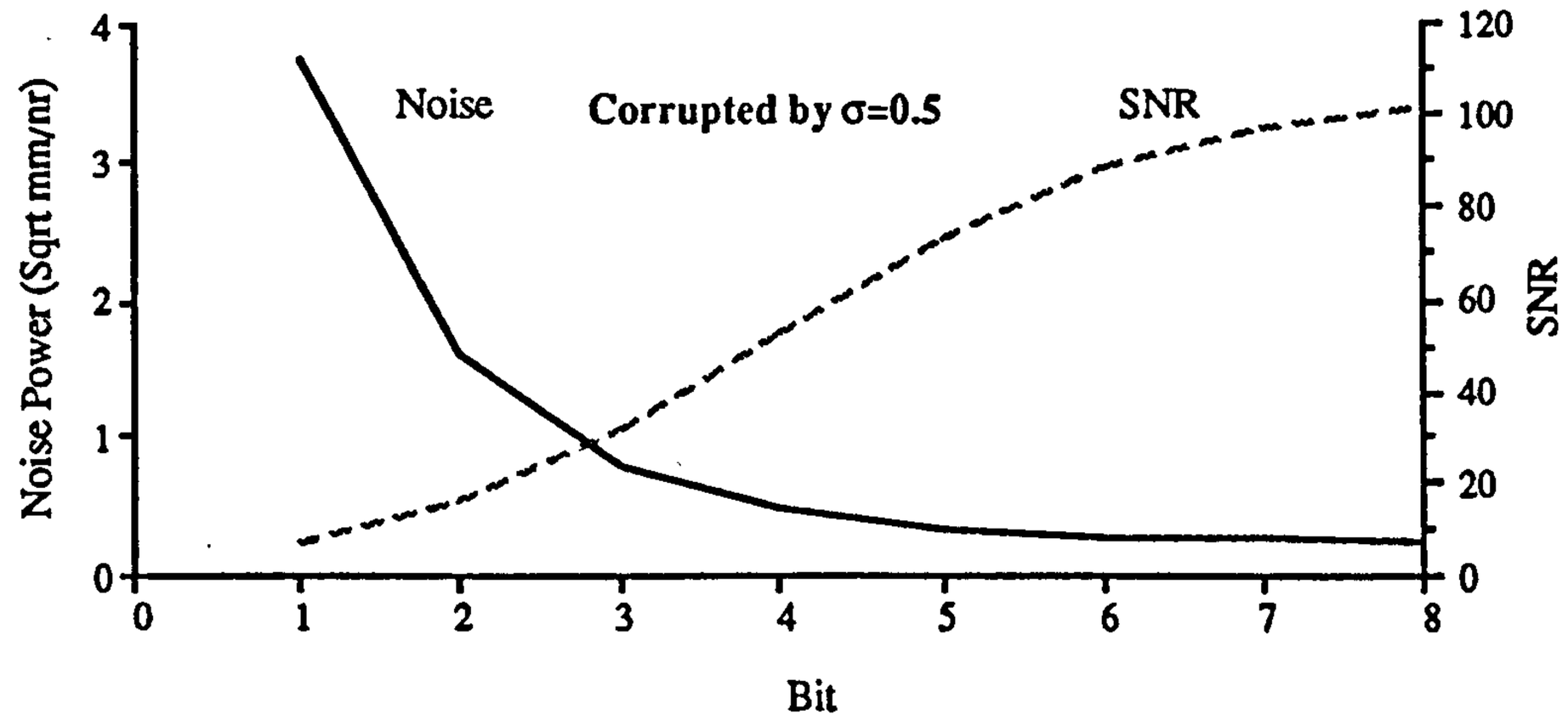

Figure 3.35 Influence of Quantisation Level to Noise Power and SNR 2

Figure 3.34 and Figure 3.35 show the influence of the word length on the quantisation noise and clearly indicate that in a noisy environment that 4-bit data probably proves optimal though 3-bit data is practically acceptable. 8-bit data would appear to contain extra information of relevance to the hydrologist at either the input or output side of the equation but at a consequent high cost in terms of a rather marginal return in additional information.

We can find from the above figures that the data quantisation accuracy will not be improved linearly with the increasing of the word length. This can be illustrated by Table 3.6 and 3.7 and Figures 3.36.

Table 3.6 Wordlengh Influence on Output Data Accuracy (Perfect Data)

Bit	1	2	3	4	5	6	7	8
Error Power	3.61	1.40	0.57	0.24	0.10	0.04	0.02	0.01
SNR	6.9	17.8	43	104	239	559	1257	2908
Accuracy %	61.9	76.3	84.8	90.2	93.5	95.8	97.2	98.1

Table 3.7 Wordlengh Influence on Output Data Accuracy (Contains 10% Error Power))

Bit	1	2	3	4	5	6	7	8
Error Power	3.79	1.61	0.80	0.48	0.34	0.28	0.26	0.24
SNR	6.5	15.4	31.2	52.0	73.2	88.1	96.9	97.1
Accuracy %	60.7	75.0	82.1	86.1	88.3	89.3	89.8	90.1

The accuracy is represented as

$$\text{Accuracy} = 100\left(1 - \frac{\sum_{i=1}^{N} | R_o - R_q |}{\sum_{i=1} R_o}\right)$$

Where R_o is the rainfall data before quantisation and R_q is the rainfall data after quantisation.

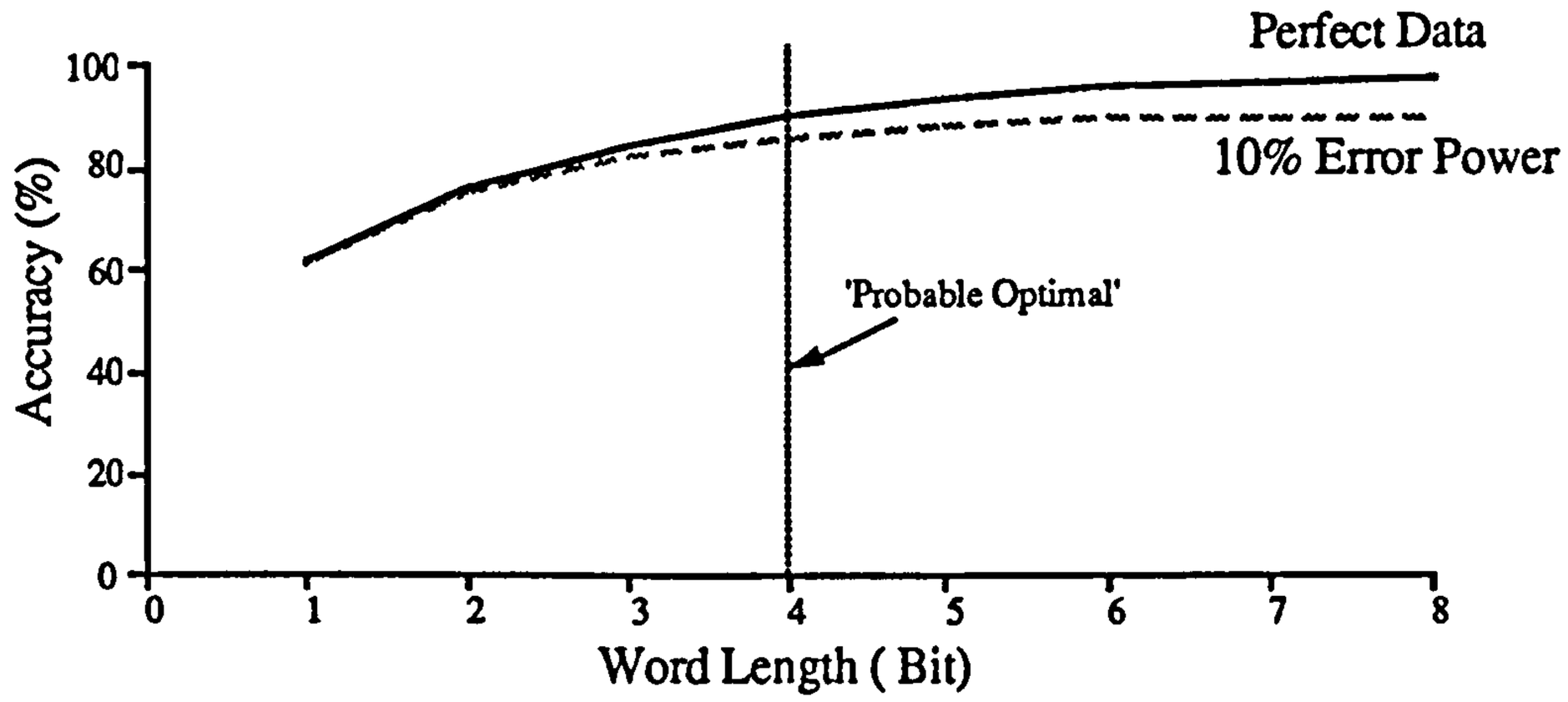

Figure 3.36 Quantisation accuracy and the wordlength

The assessment of quantisation levels is a complicated subject. From the computational results, we find that the quantisation accuracy is a nonlinear process and it is not numerically worthwhile to utilise long word length (i.e. like more than 8 bit) to represent the radar data. Another important conclusion is that the original radar data quality will influence the accuracy of the quantised radar data. With noise corrupted radar data (as shown in the above figures and tables) it is impossible to improve the accuracy even with a very long word length. A law of diminishing returns would seem to apply. Above all, for hydrological purposes, 4-bit data would seem to be more appropriate than other schemes and in some sense

represents the `optimal' choice from a `hydrological' and quantitative perspective.

3.7 Adaptive Quantisation of Radar Data

From the statistical point of view, the optimum quantisation method will depend on the statistical properties of the related radar data. As storm data keeps changing with time, the quantisation scheme should also change with time. Static quantisation schemes ignore the dynamic variation of the rainfall data and attempt to cover the whole range of rainfall data with a static scheme. The result is in most cases is that the quantisation works with low efficiency. To overcome such a drawback, some considerations have been given to construct an adaptive quantisation procedure for radar rainfall data. It is highly probable that similar arguments will pertain with other forms of remotely sensed precipitation including that which will eventually be obtained from satellite systems.

Adaptive quantisation means that the dynamic range of the quantisation scheme will change with the magnitude variation of the rainfall data. Regardless of the magnitude of the rainfall data, adaptive quantisation will always reflect the quantitative natural variation of the rainfall process and make full use of each quantisation level.

A unit quantisation skeleton with a dynamic range of 1.0 should be set up first. When a new radar frame comes, a computation is carried out utilising this frame to find the actual data range. The quantisation of this frame of radar data will be based on its data range. Suppose that the data sequence $\{xi\}$ has a dynamic range of M and we want use R bit to represent it (that is $l = 2^R$ levels).

The unit quantisation skeleton is :

Quantisation levels,

$$Q_l \quad \{ i= 1, 2, \ldots, l+1 \}$$

Quantisation output ,

$$U_l \quad \{ i = 1, 2, \ldots, l \}$$

With $Q_1=0$, $Q_{l+1}=1.0$ and $U_1=0$

Here U_i represent the rainfall data which fall in the range of $\{Q_i, Q_{i+1}\}$.

The actual quantisation will be as below

Quantisation levels ,

$$T_l=Q_l*M \quad \{ i= 1, 2, \ldots, l+1 \} \tag{3,10}$$

Quantisation output ,

$$O_i= U_l*M \quad \{ i= 1, 2, \ldots, l \} \tag{3,11}$$

With $T_1=0$, $T_{l+1}=M$ and $O_1=0$

The unit quantisation skeleton should be decided to reflect the radar data statistical properties. An optimum unit quantisation skeleton can be achieved upon the analysis of large number of radar frames. For simplicity and the data consistency, it is possible to build a procedure which is based on the existing quantisation

scheme.

Suppose the existing quantisation scheme is :

Quantisation levels ,

$$T_i \quad \{ i= 1, 2, \ldots, l+1 \}$$

Quantisation output ,

$$O_i \quad \{ i= 1, 2, \ldots, l \}$$

With $T_1=0$, $T_{l+1}=M$ and $O_1=0$

The derived unit quantisation skeleton will be

Quantisation levels ,

$$Q_i=T_i/M \qquad \{ i= 1, 2, \ldots, l+1 \} \tag{3,12}$$

Quantisation output ,

$$U_i = O_i/M \qquad \{ i= 1, 2, \ldots, l \} \tag{3,13}$$

With $Q_1=0$, $Q_{l+1}=1.0$ and $U_1=0$

The data range of each frame can be found by :

$$\text{Max } [x_i] \quad \{ i= 1, 2, \ldots, l \} \tag{3,14}$$

A case study by using Upavon radar data is presented here to illustrate the application of adaptive quantisation. The 3 bit quantisation scheme from the U.K. Met Office is used for comparison.

First a unit quantisation skeleton is set up. A logarithmic increment was used to level slice [0,1] and the arithmetic mean was chosen to represent each slice.

Table 3.8 Unit Quantisation Skele

Intensity Number	Data Range (mm/hr)	3 - bit Value (mm/hr)
1	0 - 0.00781	0.0
2	0.00781 - 0.0156	0.0117
3	0.0156 - 0.03125	0.0234
4	0.03125 - 0.0625	0.0469
5	0.0625 - 0.125	0.0938
6	0.125 - 0.25	0.1875
7	0.25 - 0.5	0.375
8	0.5 - 1.0	0.75

Now we can use this unit quantisation skeleton to quantise the radar data. The radar data range should be decided from each radar frame and it would be written into the data header for further decoding usage. Some computational results are given in figure 3.9.

The error is obtained by

$$\text{Error} = \frac{1}{N}\sum_{i=1}^{N}(R_o - R_q)^2$$

The error reduction is obtained by

$$\text{Error Reduction} = \frac{\text{Error2} - \text{Error1}}{\text{Error2}} \times 100$$

Where R_o is the rainfall data before quantisation and R_q is the rainfall data after

quantisation. Error2 is static error and Error1 is adaptive error. The unit of error is $(mm/hr)^2$.

Table 3.9 Event from Upavon 85-12-24

No.	Data Range (mm/hr)	Static Error	Adaptive Error	Error Reduction (%)
1	1.44	4.71	0.326	93.1
2	2.25	1.12	0.598	46.7
3	0.47	1.34	0.063	95.3
4	0.18	4.99	0.119	97.6
5	0.78	6.49	1.060	83.6

Table 3.10 Event from Upavon 86-01-10

No.	Data Range (mm/hr)	Static Error	Adaptive Error	Error Reduction (%)
1	4.62	6.71	1.27	81.1
2	5.25	7.51	1.41	81.2
3	2.62	8.45	0.75	91.1
4	3.12	6.67	0.64	90.0
5	5.25	1.33	0.26	80.3

Table 3.11 Event from Upavon 86-08-25

No.	Data Range (mm/hr)	Static Error	Adaptive Error	Error Reduction (%)
1	8.00	2.87	0.87	69.7
2	9.00	3.57	1.31	63.3
3	14.00	3.41	1.29	62.0
4	11.5	3.95	1.58	59.9
5	21.0	6.17	3.62	41.3

It can be seen that significant quantisation error reduction occurs and the radar data accuracy can be greatly improved without increasing quantisation word length. The information content of the data is thus maximised for a limited word length.

3.8 Quantisation Influence on Hydrological Model

3.8.1 Impact of Quantisation Noise on a TF Model

Consider quantisation noise e_q with prescribed spectral density $G_1(\omega)$ passing through a linear transfer function model with frequency transfer function $H(\omega)$. An output spectral density $G_2(\omega)$ is produced from the TF model.

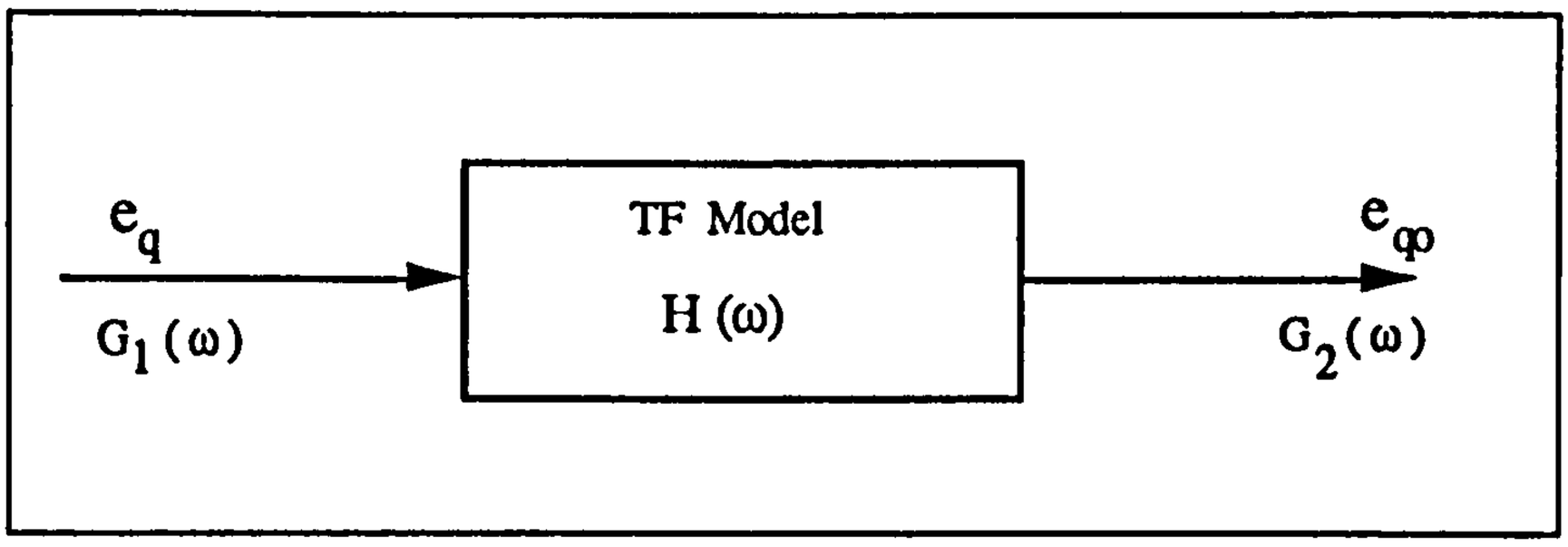

Fig 3.36 Quantisation Noise through a TF model

The effect of a linear TF model on the quantisation noise is described by the following relationship between input and output spectral densities:

$$G_2(\omega) = | H(\omega) |^2 G_1(\omega) \qquad (3,15)$$

In a hydrological application, the TF model acts as low-pass filter. The bandwidth of the TF is quite low so that most of the quantisation error will be filtered out and

consequently a relatively short word length will still preserve the primary information carried in the precipitation signal.

3.8.2 Prefiltering Data to Reduce Noise and Prevent Aliasing

Strictly, before we use radar rainfall data to predict river flow, some prefiltering process should be carried out. Usually a linear filter is utilised. The linear filter is a device which operates on the input $x_1(t)$ to give an output $x_2(t)$ according to

$$x_2(t) = \sum_{l=0}^{\infty} h_k x_1(t-k) \qquad (3,18)$$

Where h_k is the weighting function or impulse response function of the filter. Suppose that the input $x_1(t)=s(t) + z(t)$, where $s(t)$ is the signal or useful information and $z(t)$ is the noise or unwanted information. The optimal filter is then defined as the weight function which minimises the mean square of the error signal between the actual and desired outputs. The calculation of the optimal filter is made easier by working with the spectra of the signal $s(t)$ and the noise $z(t)$

Another important issue concerned with prefiltering the radar data is that the information at frequencies higher than the Nyquist is lost by model sampling (usually the model sampling interval is larger than the rainfall measurement sampling interval, this means lower frequency sampling). It is then important not to let the folding effect distort the interesting part of the spectrum below the Nyquist frequency. This is also achieved by a linear filter.

Suppose the highest frequency of the useful information in the signal is ω_N, then

the spectrum of the filtered output will be

$$Y(\omega) = | H(\omega) |^2 X(\omega) \qquad (3,19)$$

Ideally, $H(\omega)$ should have a characteristic such that

$$| H(\omega) | = 1, \quad \omega \leq | \omega_N |$$

$$| H(\omega) | = 0, \quad \omega > | \omega_N |$$

This can be realised only approximately. With an ideal filter we can achieve a sampled spectrum with no aliasing effects.

As the spectrum of the noise is more broadband that that of the signal. The prefilter then essentially cuts away the high-frequency noise contributions. This is a significant noise reduction if the noise spectrum has considerable energy above the Nyquist frequency.

Presently, a moving average filter is adopted in the research group which has equal weights in the window.

$$x_2(t) = \frac{1}{k} \sum_{l=0}^{k-1} x_1(t-k) \qquad (3,20)$$

Its frequency response for different averaging steps is shown in following figures.

The frequency are represented in the angle unit (the maximum value is π).

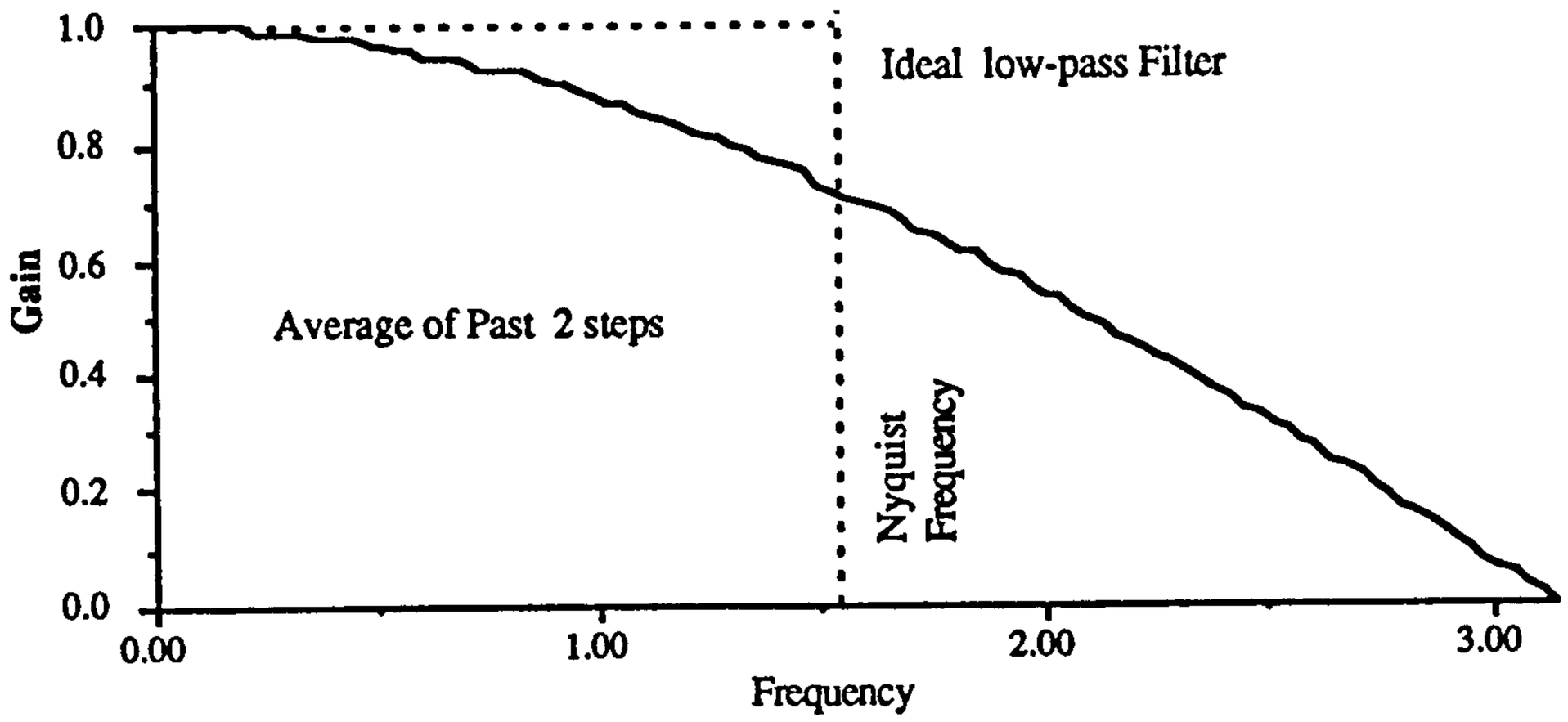

Figure 3.37 Frequency Response from 2 Average Steps

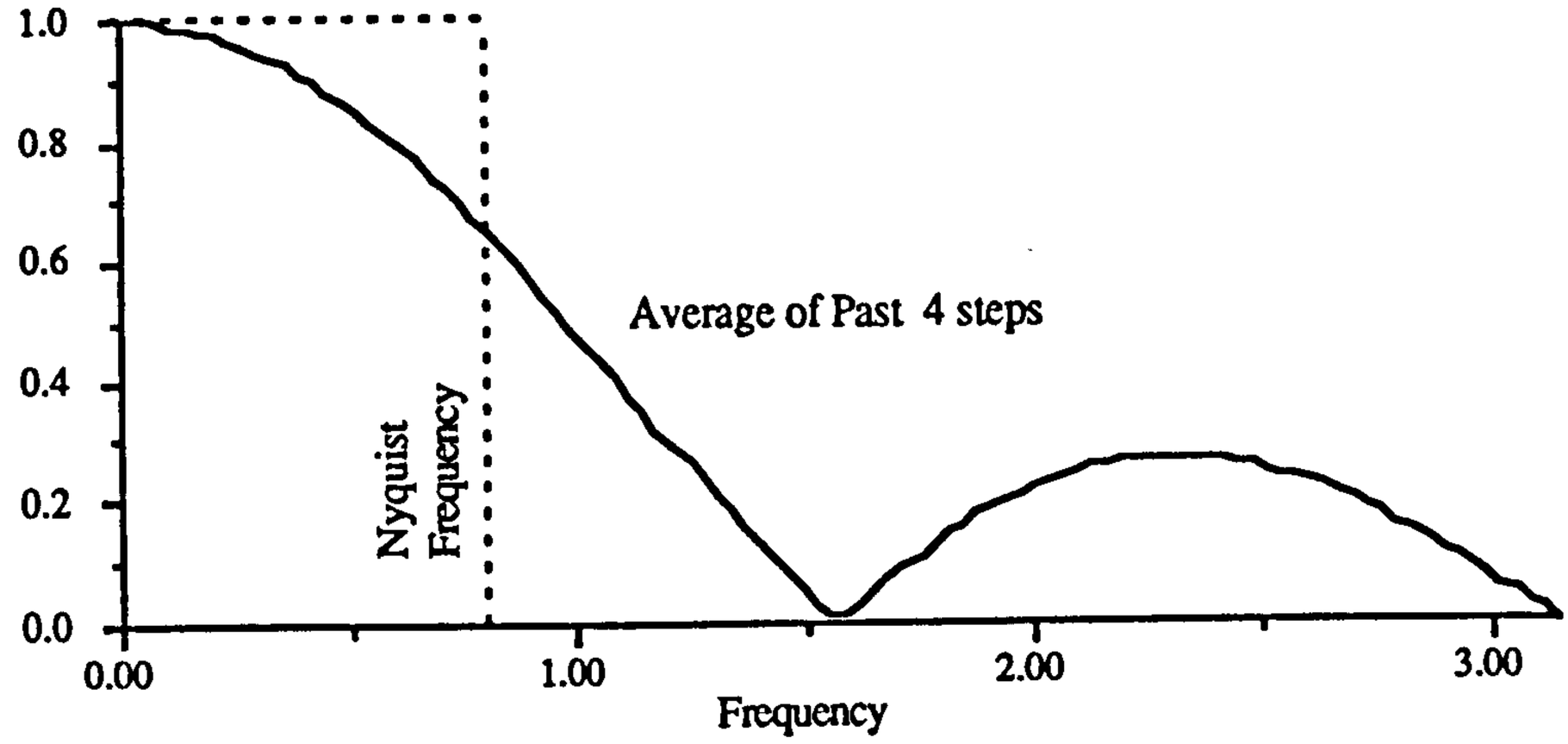

Figure 3.38 Frequency Response from 4 Average Steps

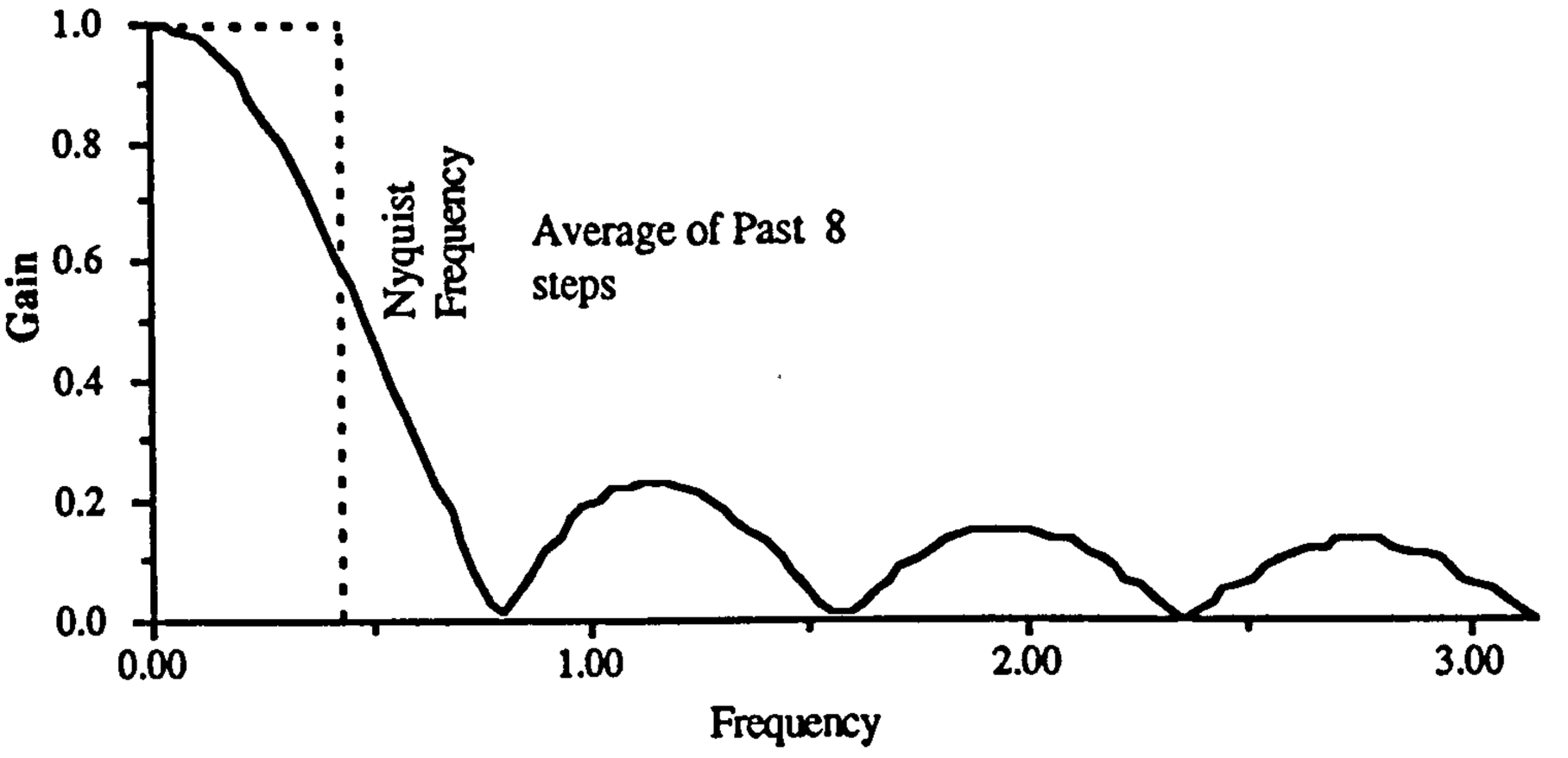

Figure 3.39 Frequency Response from 8 Average Steps

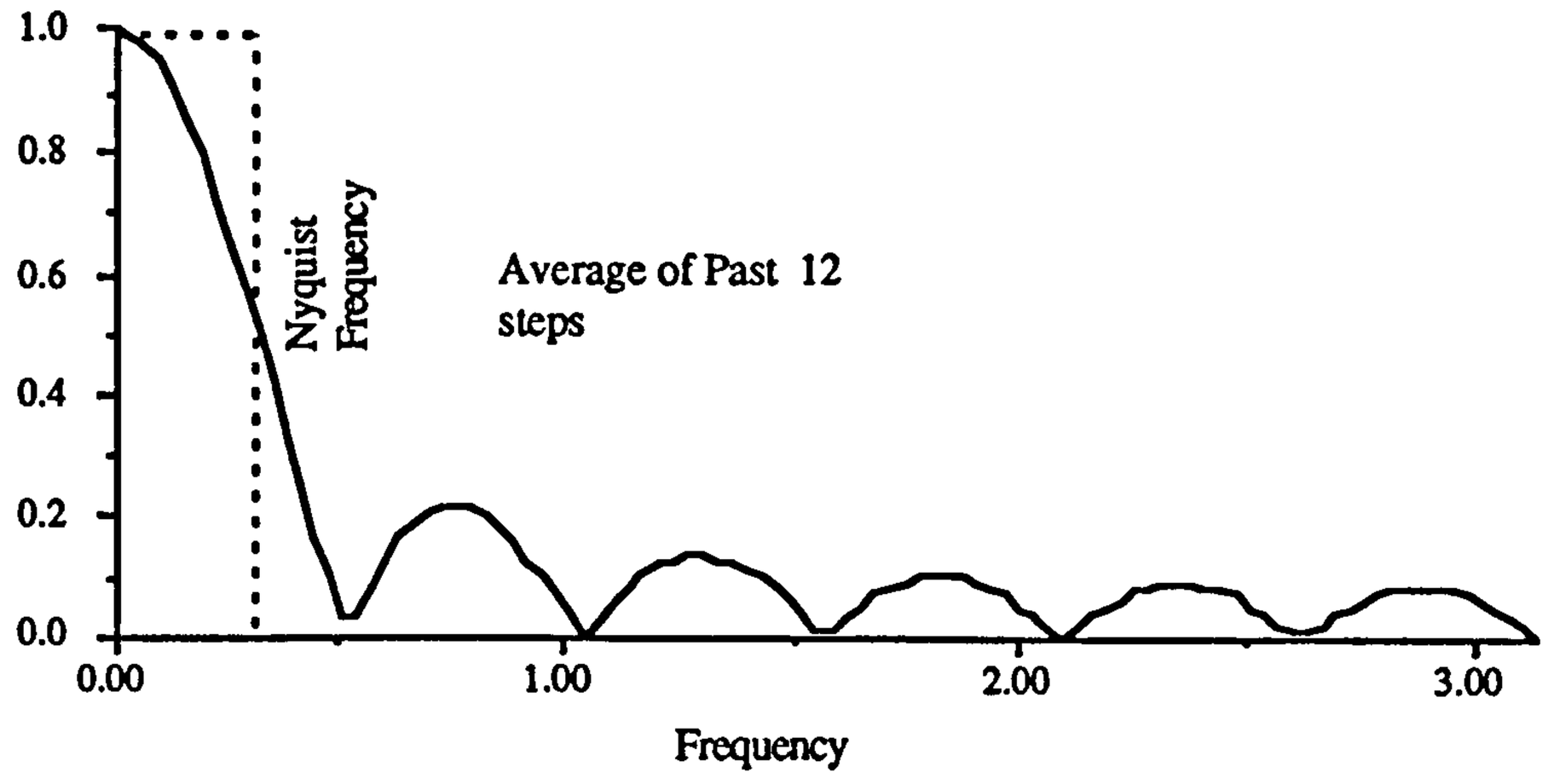

Figure 3.40 Frequency Response from 12 Average Steps

Figure 3.37 -- Figure 3.40 indicates the filter frequency response and it can be observed that the filter frequency response will be close to the ideal Nyquist frequency when the number of moving average steps are increased.

Figure 3.41-Figure 3.43 illustrate the influence of prefiltering on quantisation errors.

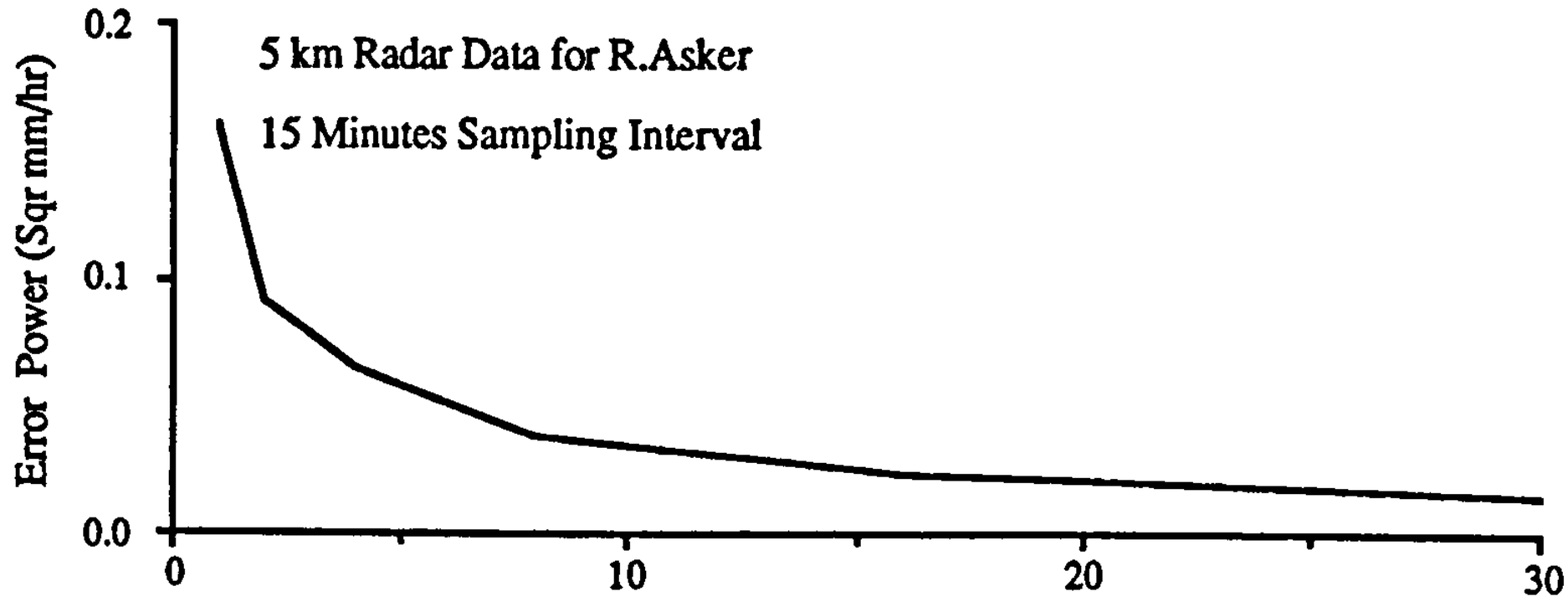

Figure 3.41 Quantisation Error Reduction by Prefiltering Radar Data 1

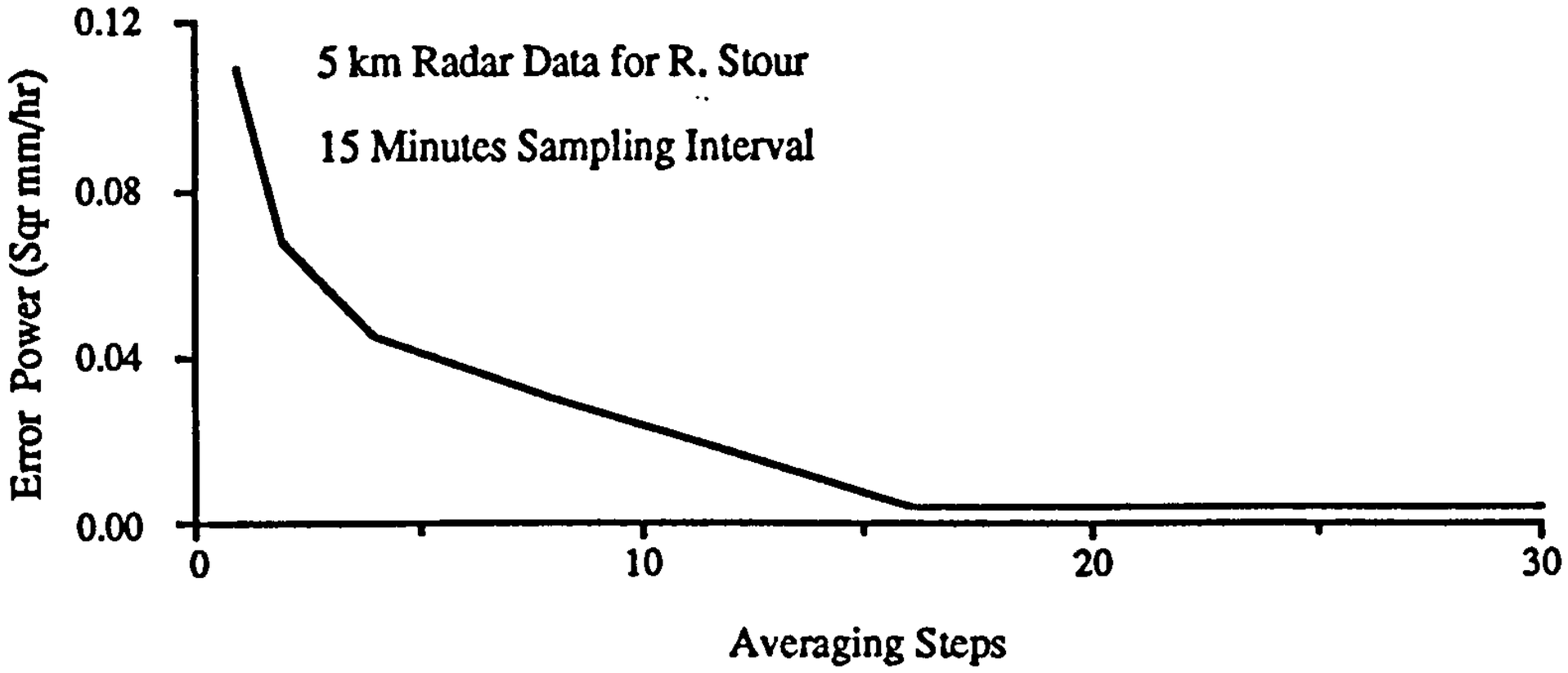

Figure 3.42 Quantisation Error Reduction by Prefiltering Radar Data 2

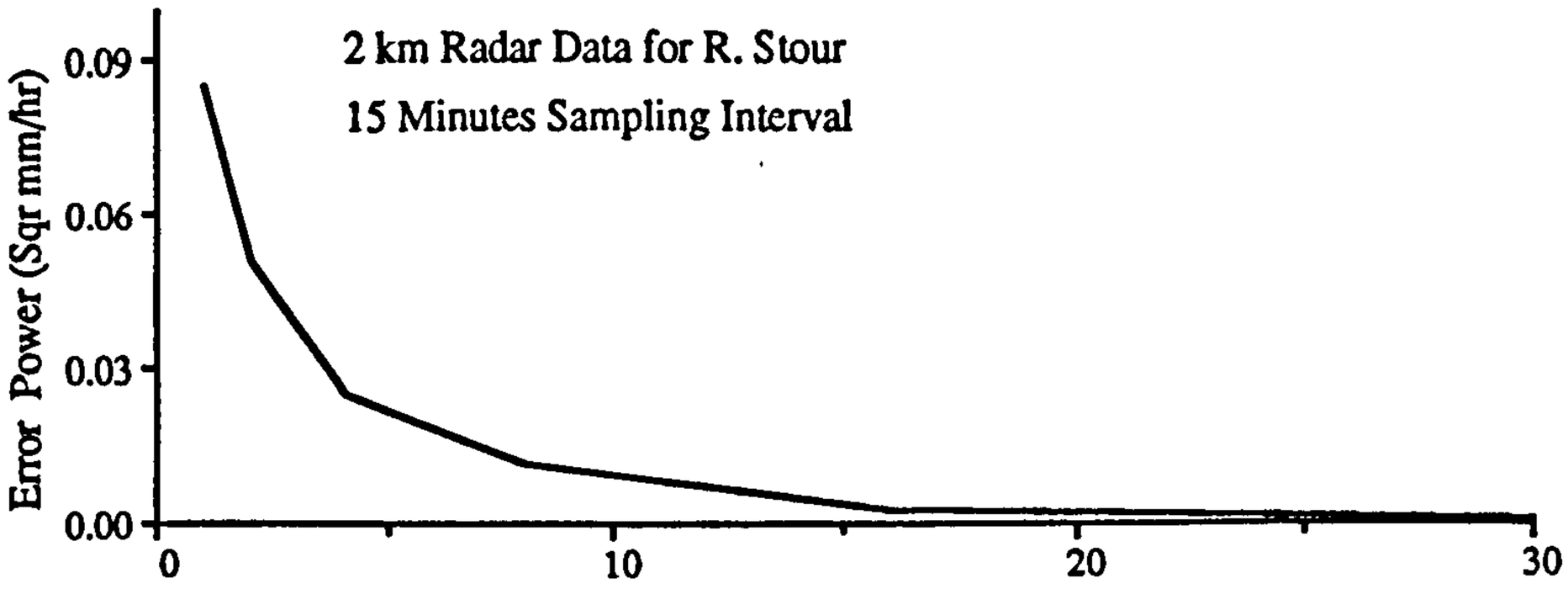

Figure 3.43 Quantisation Error Reduction by Prefiltering Radar data 3

The quantisation error could be greatly reduced by utilising 2 or 4 step moving average filtering.

3.8.3 Influence of Quantisation on Flood Forecasting

Some practical cases are considered to show the influence of quantisation of radar rainfall data on the flood forecasting process.

In this section the River Stour (at Hammoon) was utilised to carry out a case study. The TF model utilised was as below,

UPPER STOUR (at Hammoon) TF(2,4) Timestep = 5 hr

$$\mathbf{Flow_{t+1} = 0.9709\ Flow_t - 0.1716\ Flow_{t-1} + \Delta [1.1116\ Rain_t + 0.8092\ Rain_{t-1} + 2.0554\ Rain_{t-2} + 0.9915\ Rain_{t-3}\ )}$$

Δ is a model updating factor developed by Cluckie and Owens (see Cluckie and Owens, 1987) and will be further introduced in other sections of the thesis. For convenience, an hourly model of the River Stour was utilised and the computational results are presented in the following figures.

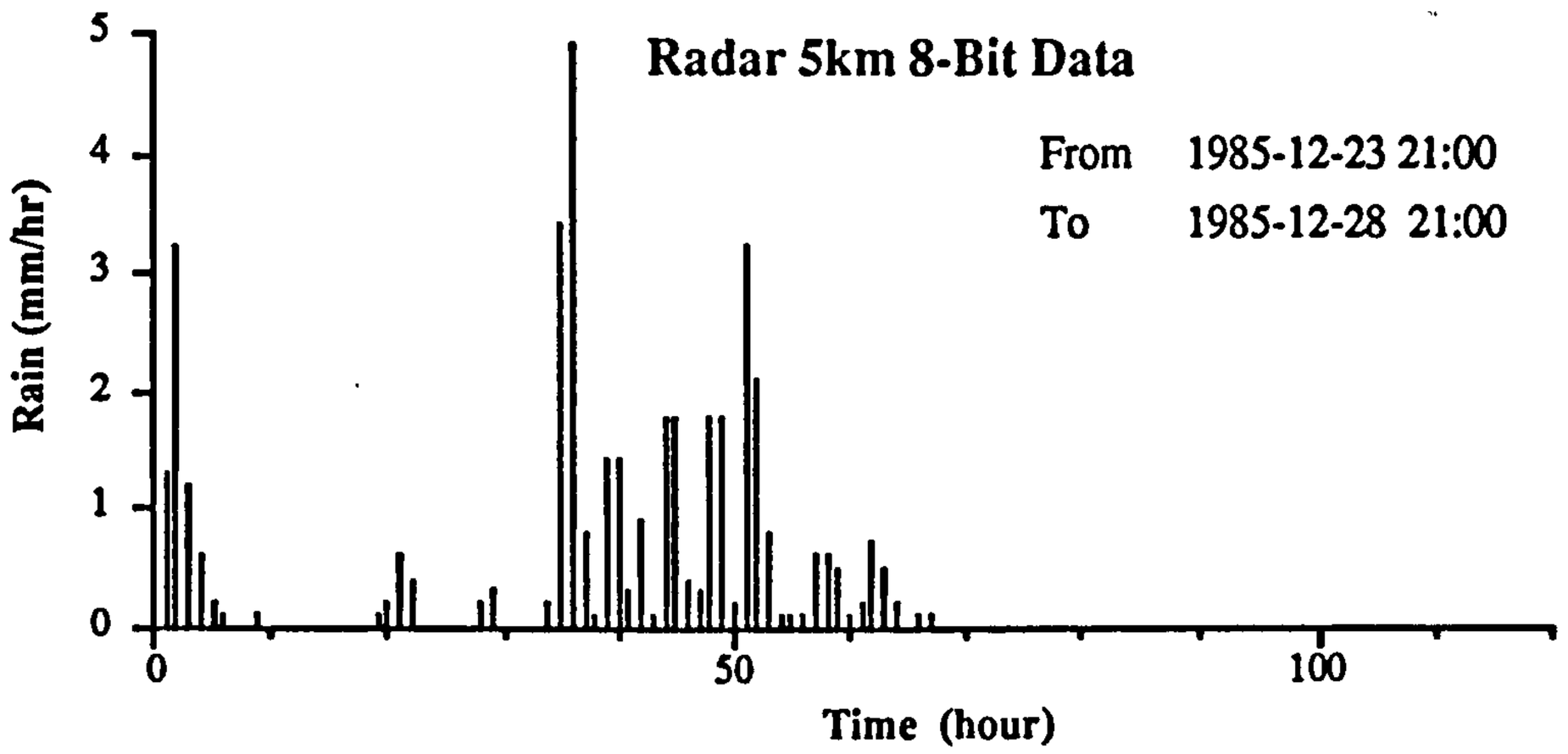

Figure 3.44 8-Bit Radar Rainfall Data

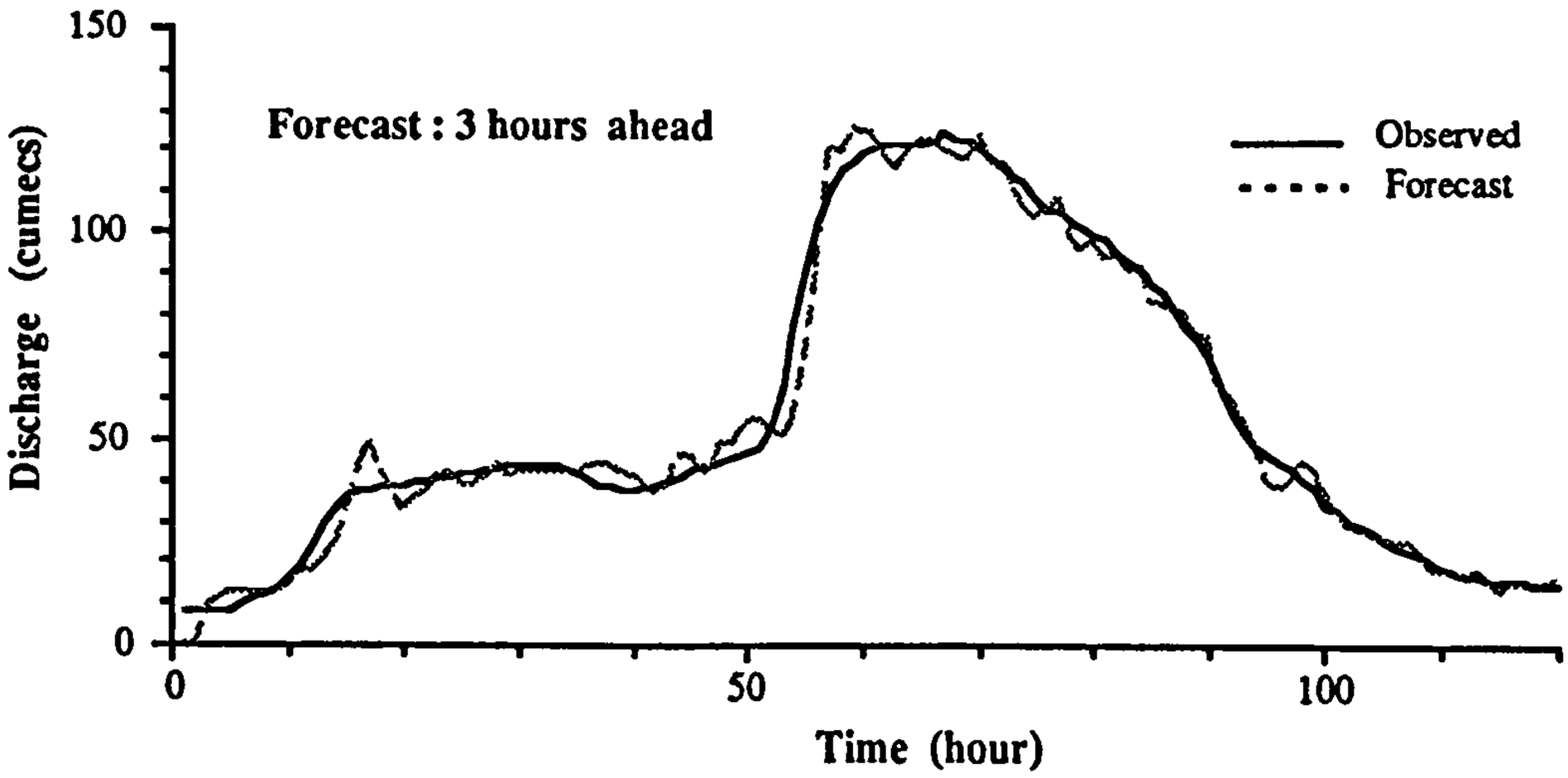

Figure 3.45 3 Step Forecasting by 8-Bit Data

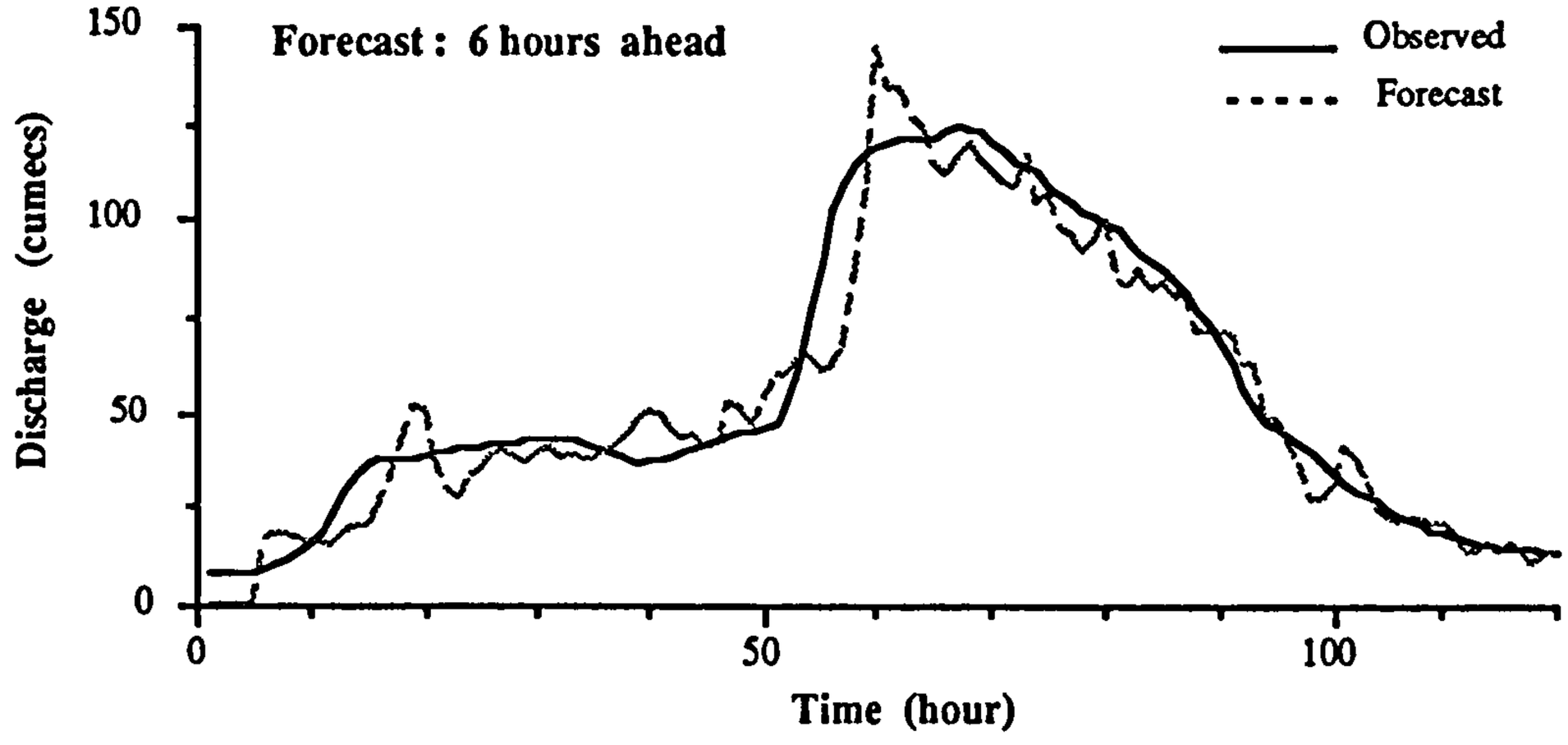

Figure 3.46 6 Step Forecasting by 8-Bit Data

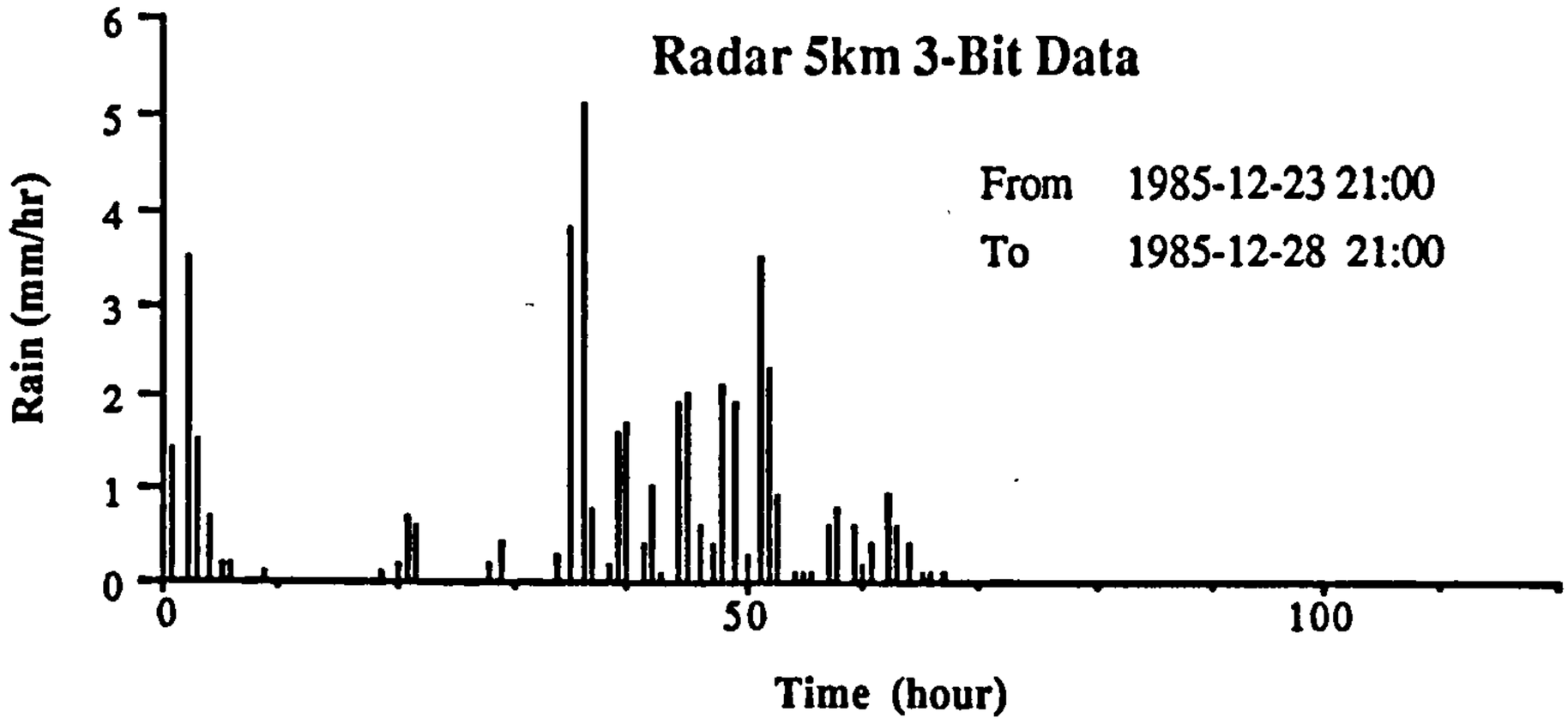

Figure 3.47 3-Bit Radar Rainfall Data

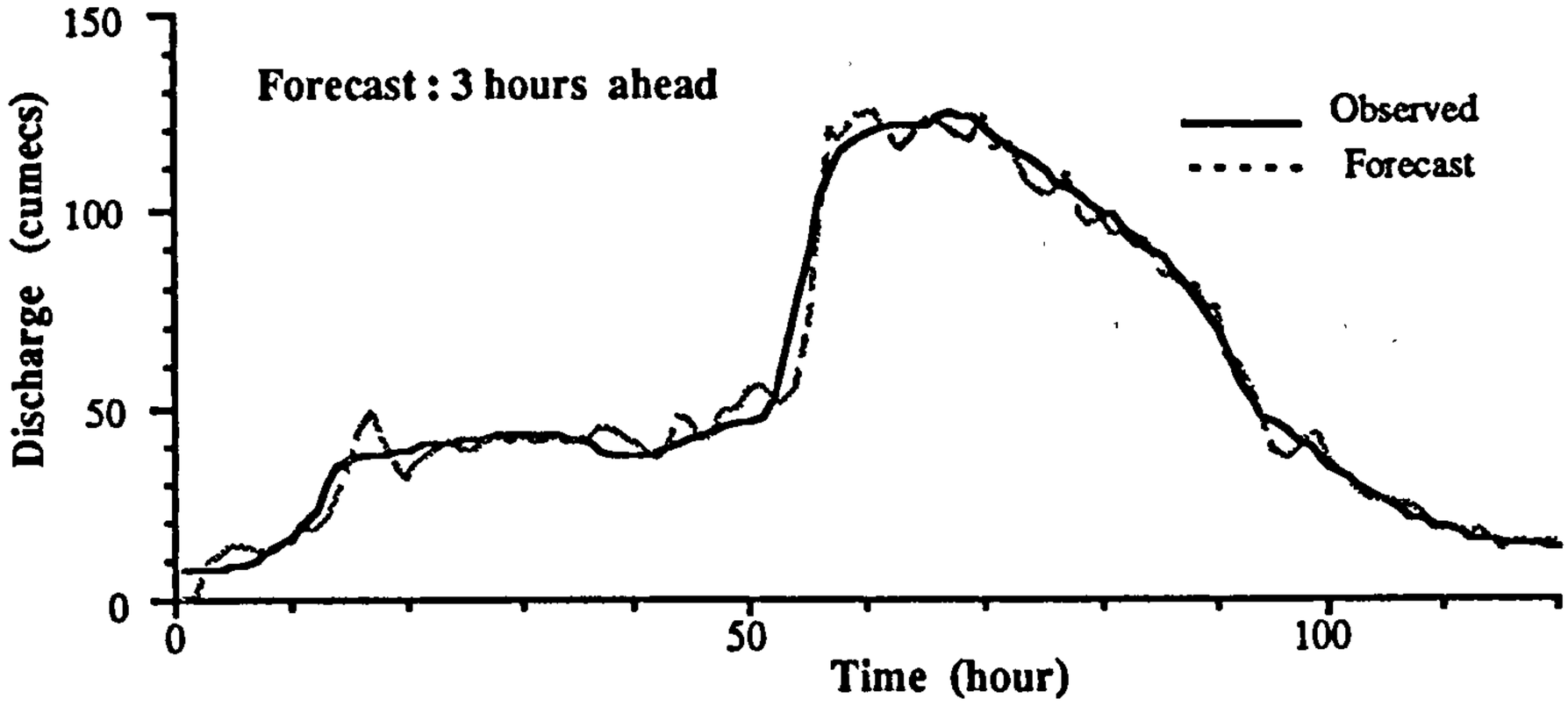

Figure 3.48 3 Step Forecasting by 3-Bit Data

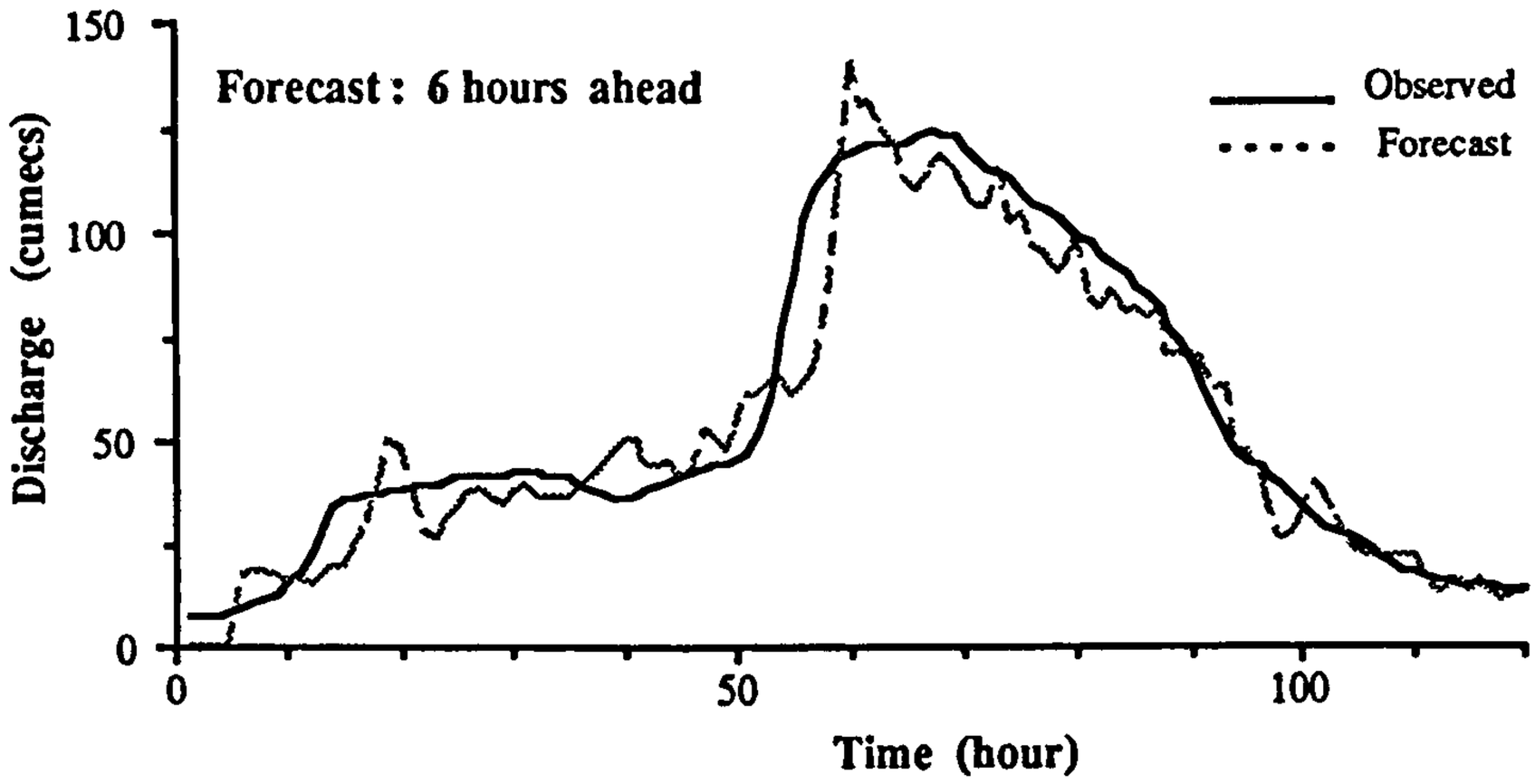

Figure 3.49 6 Step Forecasting by 3-Bit Data

It was found that 8-bit data produced no obvious benefit in real-time flood forecasting when compared with 3 bit data. This and other similar results (Cluckie & Tilford 1988, Cluckie, Tilford and Shepherd 1989) confirming the theoretical arguments developed in section 3.9.1.

3.9 Summary

Signal quantisation of radar rainfall measurements is an important issue in modelling the hydrological process. The quantisation noise can be decreased by choosing the quantum steps or level slicing schemes to be sufficiently fine to preserve the original information content of the data. A trade-off amongst accuracy, quantisation noise, and the number of quantisation levels is required. As few quantisation levels as possible are chosen consistent with the preservation of the information content of the signal process.

A practical radar data quantisation scheme will depend upon the statistical properties of the radar rainfall data. It has been found that the radar rainfall distribution varies with several factors.

The measurement noise contained in the original data set will affect the quantisation scheme. In this case (and it is always true in practice) , high resolution is not worthwhile because the accuracy of the data will not be improved. It has been found that there is a negligible difference between 4-bit and 8-bit data. Although the results indicate that 3-bit data can be utilised in flood forecasting models without causing significant errors. It would be more appropriate to use 4-bit data than the original 8-bit data. However, the difference between 4-bit and 3-bit is also negligible on almost all occasions.

Prefiltering of radar data removes a large percentage of the quantisation noise. By selecting a more optimal numerical filter, a further reduction of quantisation error can be achieved.

The TF forecast model acts as a low pass filter and the quantisation noise will be

reduced after the prefiltering of the quantised radar signal. A case study from the River Stour has been used to illustrate this aspect. Though other rivers have been studied in the Anglian and the Northwest regions to confirm the general conclusion.

Adaptive quantisation provides a very useful tool to improve the radar data quantitative precision without increasing the number of quantisation levels. Unlike static radar quantisation schemes, adaptive quantisation makes full use of almost all information contained in the incoming signal. The decoding of adaptively quantised data is almost the same as statically quantised data except that a data range indicator has to be available in the radar data header. This indicator is used to recover the quantised data from either in real-time or from an archive. With decreased data range, adaptive quantisation will tend towards the static quantisation scheme but is always better than it.

PART III RAINFALL RUNOFF MODEL

CHAPTER 4

TRANSFER FUNCTION MODEL ANALYSIS

4.1 Introduction

The notion of a mathematical model is fundamental to hydrology. A model is a very useful and compact way to summarise the knowledge about a process. As mentioned in Chapter 1, the TF (Transfer Function) model has been increasingly utilised in hydrology in recent years and it has been proven to be an effective model. However, several problems still exist in the application of TF models such as the difficulty in identification of the TF model and real-time robust parameter updating. In this chapter analysis is carried out to reveal the internal properties of the TF model and the development of a Physical Realisable Transfer Function (PRTF) model.

4.2 Z - Transform Process

The Z- transform provides the engineer with a powerful method for the analysis of linear time-invariant discrete systems. Consider the discrete-time sequence u(t), for t = 0, 1, 2,.... Since a causal sequence forms the basis of most physical systems, right-sided Z-transforms will be emphasised, that is, sequences for which the time index t is defined only for positive values. The Z-transform of this sequence is defined as (Refer to DeFatta, Lucas and Hodgkiss 1988) :

$$U(z) = Z[u(t)] = \sum_{t=0}^{\infty} u(t)\, z^{-t} \qquad (4,1)$$

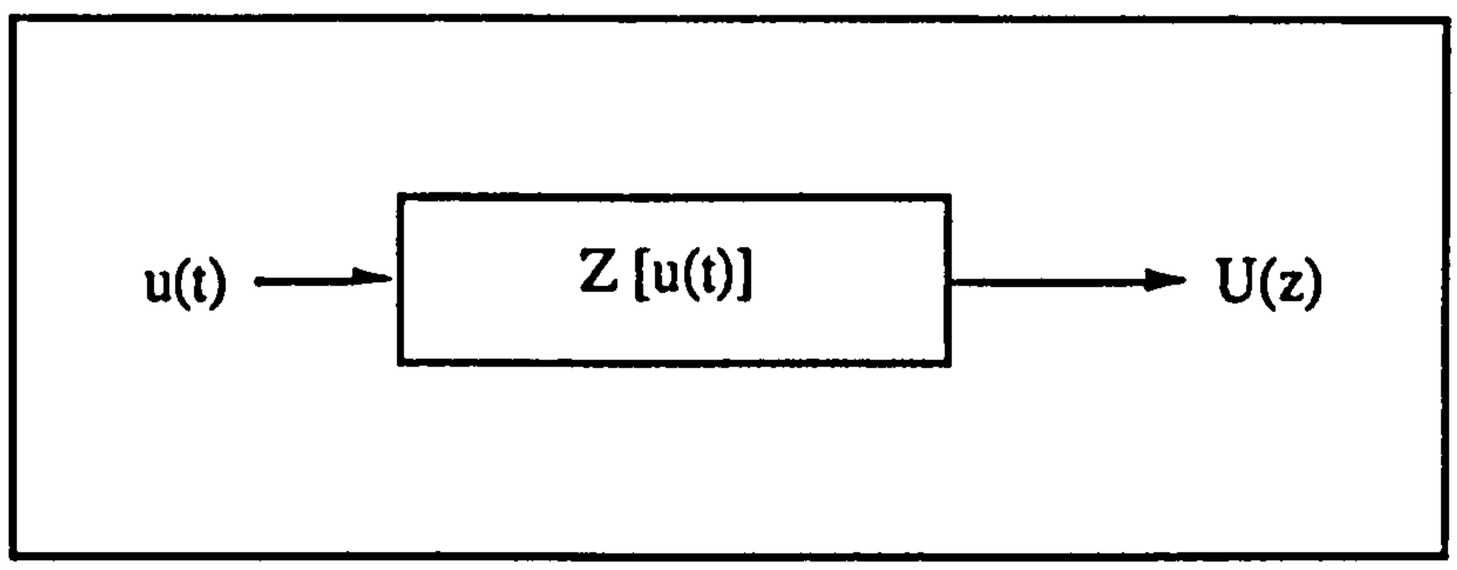

Figure 4.1 The Z-transform process

It is instructive to view the Z-transform as a transformation that maps an input sequence u(t) into a complex function U(z). Therefore, the Z-transform process is an operation on the input signal. This transformation to the z-domain allows the analysis of linear time-invariant discrete time systems to be performed with relative ease.

If u(t) is to have a z-transform, then the magnitude of U(z) must be finite. We now define the region of convergence (ROC) to be the set of all z in the complex z-plane for which the magnitude of U(z) is finite. Representing z in polar form, we require that

$$|U(z)| = \left| \sum_{t=0}^{\infty} u(t)\, z^{-t} \right| \leq \sum_{t=0}^{\infty} |u(t)|\, r^{-t} < \infty \qquad (4,2)$$

For the sums of Eq.(4,2) to be finite, we must satisfy the condition $|u(t)| \leq MR^t$ for $t \leq 0$. The series will converge outside a circle of radius R. On substituting these bounds into Eq.(4,2), we obtain

$$\sum_{t=0}^{\infty} | u(t)\, z^{-t} | \leq M \left[\sum_{t=0}^{\infty} R^t\, r^{-t} \right] \qquad (4,3)$$

We now observe that the sum in Eq.(4,3) is finite if and only if $R/r < 1$, that is, Eq4.1 converges absolutely for all z in the ring of convergence $R< |z|$.

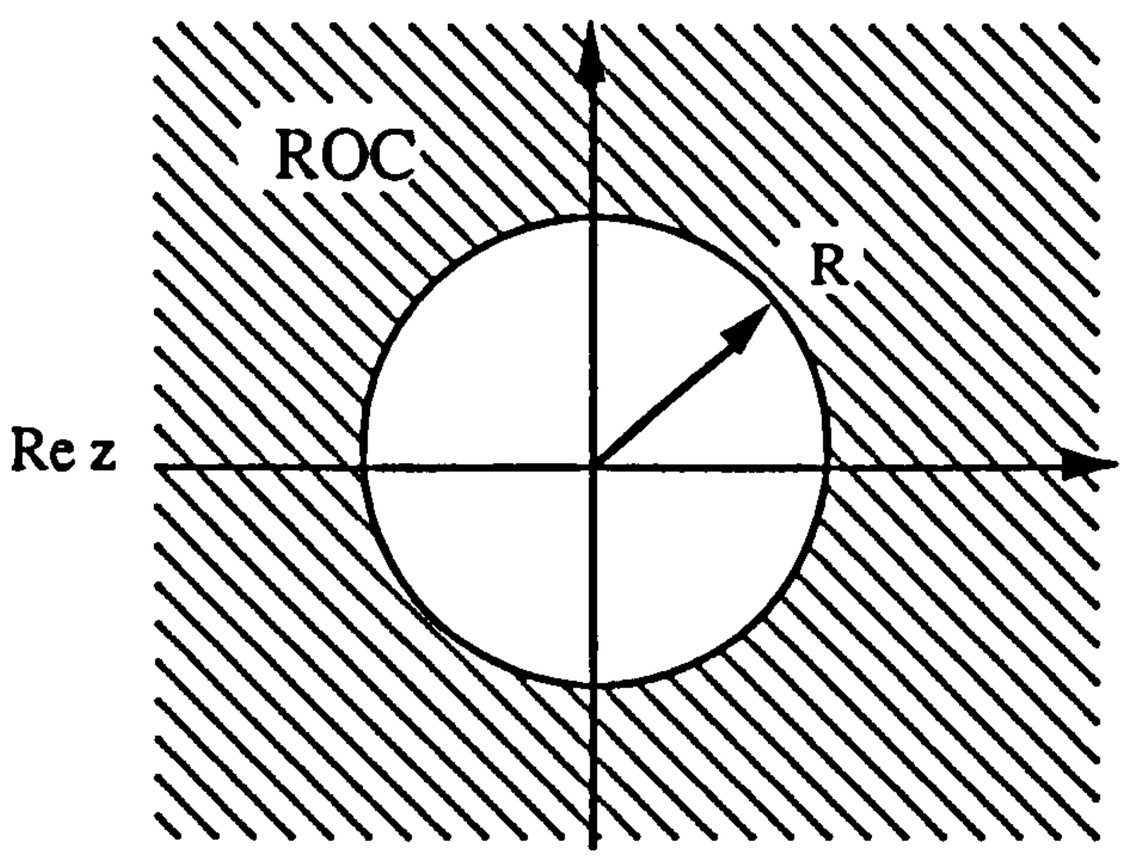

Figure 4.2 Region of convergence $|z| > R$

In summary, for causal sequences the ROC is exterior to a circle passing through the pole farthest from the origin in the z-plane. Also, no poles of U(z) can occur within the ROC since the Z-transform does not converge at a pole. If the sequence is also stable, then all poles lie inside the unit circle and the ROC includes the unit circle.

The time delay property of the Z-transform is very important to the interpretation of TF models. The delay theorem for causal sequences can be expressed as

$$Z[\,u(t-k)\,] = z^{-k}U(z) + z^{-k}\sum_{m=-k}^{-1} u(m)\,z^{-m}\quad,\quad k>=0 \qquad (4,4)$$

where k is an arbitrary delay integer.

This property is useful when considering a system with nonzero initial conditions. For the case when $u(t) = 0,\ t < 0$, that is, for zero initial conditions we obtain

$$Z\,[\,u(t-k)\,] = z^{-k}\,U(z) \qquad (4,5)\ .$$

This property is used extensively to transform difference equations to the z-domain when the initial conditions are zero.

From the definition of the unit-impulse function, we can write that

$$Z\,[\delta(t)] = 1 \qquad \text{ROC}\ :\ |z|>=0 \qquad (4,6)$$

Since $Z\,[\delta(t)]$ is independent of z, the ROC is the entire z-plane. It can be shown that since $Z[\delta(t)] = 1$, that is, $U(z)=1$, then the unit-impulse response of a discrete system can be obtained by finding the inverse Z-transform of the system transfer function. The three basic methods that can be employed to recover the original sequence from its Z-transform are :

1. Complex inversion integral.
2. Partial-fraction expansion.
3. Inversion by division.

Since the complex integration method is the most general method and essentially the same as the partial-fraction method, our analysis will focus on the application of the method of residues for the evaluation of the complex inversion integral to get the unit-impulse response of a TF model.

The Z-transform inversion integral can be derived from

$$U(z) = Z[u(t)] = \Sigma\, u(t)\, z^{-t}$$

and using the Cauchy integral theorem from the theory of complex variables. Multiplying both sides by z^{m-1} and then integrating around a closed contour in the z-plane, it follows that

$$\oint_c U(z)\, z^{m-1}\, dz = \oint_c \sum_{n=0}^{\infty} u(t)\, z^{m-t-1}\, dz \qquad (4,7)$$

According to the Cauchy integral theorem, if the integration path is within the ROC, and if the ROC includes the unit circle, the series u(t) is absolutely convergent. It is then valid to interchange the summation and integration, yielding

$$\oint_c U(z)\, z^{m-1}\, dz = \sum_{n=0}^{\infty} \oint_c u(t)\, z^{m-t-1}\, dz \qquad (4,8)$$

If the path of integration encloses the origin, then, according to the Cauchy integral

theorem, the integral on the right side is zero except for m = t, where for this case the integral reduces to $2\pi j$. We finally obtain the Z-transform inversion integral

$$u(t) = Z^{-1}[\,U(z)\,] = \frac{1}{2\pi j}\oint_c U(z)\, z^{t-1}\, dz \qquad (4,9)$$

Equation (4,9) represents a contour C, within which U(z) is analytic; That is, let the poles of the system, p_i, be inside the closed contour C. For rational Z-transforms, the contour integral given by Eq.(4,9) can be evaluated using Cauchy's residue theorem, which is a fundamental result obtained from complex variable theory. First define $U_0(z)$ as a rational function with the denominator expanded in a product of pole factors

$$U_0(z) = U(z)\, z^{t-1} = \frac{N(z)}{\prod_{i=1}^{N}(z - p_i)^{m_i}} \qquad (4,10)$$

where N is a positive integer representing the total number of poles and m_i is the pole order. Then by the residue theorem we obtain for poles inside the contour of integration.

$$u(t) = \sum_{i=1}^{N} \operatorname*{Res}_{z=p_i} [\,U_0(z)\,] \qquad t >= 0 \qquad (4,11)$$

where for simple poles, that is, m=1, the residue of $U_0(z)$ at p_i is given by

$$\operatorname*{Res}_{z=p_i} [\,U_0(z)\,] = \lim_{z \to p_i} [\,(z - p_i)\, U_0(z)\,] = (z - p_i)\, U_0(z)\,|_{z=p_i} \qquad (4,12)$$

For an *m*th-order pole, (m =2, 3,...) the residue is given by

$$\underset{z = p_l}{\text{Res}} \left[U_0 (z) = \frac{1}{(m - 1) !} \lim_{z \to p_l} \frac{d^{m-1}}{dz^{m-1}} \left[(z - p_l)^m \; U_0 (z) \right] \right.$$

$$= \frac{1}{(m - 1) !} \frac{d^{m-1}}{dz^{m-1}} \left[(z - p_l)^m \, U_0 (z) \right] \Big|_{z = p_l}$$

(4,13)

For the poles of $U_o(z)$ outside the contour of integration, the sum of the residues of $U_0(z)$ is given by

$$u(t) = - \sum_{l=1}^{N} \underset{z=p_l}{\text{Res}} \left[U_0(z) \right] \qquad t < 0$$

(4,14)

It should be noted that for the case where $U_o(z)$ has a simple pole at the origin when t = 0, u(0) is determined independently. We also note that the terms in the inverse Z-transform are determined by the poles of the transform function, with the zeros affecting only the magnitude of the terms.

4.3 Z-Transform Analysis of TF Model

A general form of TF model can be derived as

$$Y(t) = \sum_{i=1}^{N} a_i \, Y(t-i) \; + \sum_{j=0}^{M} b_j \, U(t-j)$$

(4,15)

Rearranging the above equation:

$$Y(t) - \left[\sum_{i=1}^{N} a_i \, Y(t-i) \right] = \sum_{j=0}^{M} b_j \, U(t-j) \qquad (4,16)$$

Employing the Z transform to both sides

$$Z[Y(t) - (a_1 \, Y(t-1) + a_2 Y(t-2) + \ldots + a_N Y(t-N)] =$$
$$Z[b_0 \, U(t) + b_1 \, U(t-1) + b_2 \, U(t-2) + \ldots \; b_M U(t-M)] \qquad (4,17)$$

We assume

$$A(z) \; Y(z) = B(z) \; U(z)$$

Where

$$A(z) = 1 - a_1 z^{-1} - a_2 z^{-2} - \ldots - a_N z^{-N}$$

$$B(z) = b_0 + b_1 z^{-1} + b_2 z^{-2} + \ldots + b_M z^{-M}$$

Let

$$H(z) = \frac{Y(z)}{U(z)} = \frac{B(z)}{A(z)} = \frac{\sum_{l=0}^{M} b_l \, z^{-l}}{1 - \sum_{l=1}^{N} a_l \, z^{-l}} \qquad (4,18)$$

$$Y(z) = H(z) \; U(z) \qquad (4,19)$$

H(z) is the transfer function of rainfall and runoff.

As an example case, a TF model from the River Asker in the Wessex region is used to illustrate the Z-transform analysis.

TF(2,3) for River Asker is as below

Flow(t) = 0.9709flow(t-1)-0.1716 flow(t-2) +

1.1116 rain(t-1) + 0.8092 rain(t-2)+2.0554 rain(t-3)+0.9915 rain(t-4)

To get

Flow(z) = H(z) Rain(z)

Applying the Z-transform to both sides, we get

$$A(z) = 1 - (0.9709\ z^{-1} - 0.1716\ z^{-2})$$

$$B(z) = 1.1116\ z^{-1} + 0.8092\ z^{-2} + 2.0554 z^{-3} + 0.9915 z^{-4}$$

So

$$H(z) = (1.1116\ z^{-1} + 0.8092\ z^{-2} + 2.0554 z^{-3} + 0.9915 z^{-4}) /$$

$$[1 - (0.9709\ z^{-1} - 0.1716\ z^{-2})].$$

The excitation of y(t) by a unit-impulse sequence yields the unit-impulse response h(t) of the system. Since H(z) is in the form of a rational function with real coefficients (ratio of polynomials), h(t) is of infinite duration.

Now to determine the inverse Z-transform of the function.

Let $C(z) = A(z)^{-1}$, then

$$C(z) = 1/(1- (0.9709\ z^{-1}-0.1716\ z^{-2}))$$

$$= 1/[S\ (z^{-1}-\beta 1)\ (z^{-1}-\beta 2)]$$

$$= z^2 / [\ S\ \beta_1\ \beta_2\ (\ z - 1/\beta_1)(\ z- 1/\beta_2)]$$

where β_1=4.304, β_2=1.354, S= 0.1716

$$B(z) = (1.1116\ z^3 + 0.8092\ z^2 + 2.0554z + 0.9915)/z^4$$

$$H(z) =(1.1116\ z^3 + 0.8092\ z^2 + 2.0554z + 0.9915)/$$

$$[z^2\ S\ \beta_1\ \beta_2\ (\ z - 1/\beta_1)(\ z- 1/\beta_2)]$$

H(z) has 3 poles (0, $1/\beta_1$, $1/\beta_2$). By the residue theorem,

$$h(t) = \operatorname*{Res}_{z=0} [H_0(z)] + \operatorname*{Res}_{z=\frac{1}{\beta_1}} [\ H_0(z)] + \operatorname*{Res}_{z=\frac{1}{\beta_2}} [H_0(z)]$$

The result is a complicated expression and is omitted here. The impulse response of the Asker model is shown in Figure 4.3. From the figure we can observe that the TF model for the river Asker is a stable and physical realisable model. The term physically realisable means a stable TF model with no negative or fluctuating impulse response. In the next section, we are going to discuss the situation where unsatisfactory TF models for the rainfall runoff process can be identified.

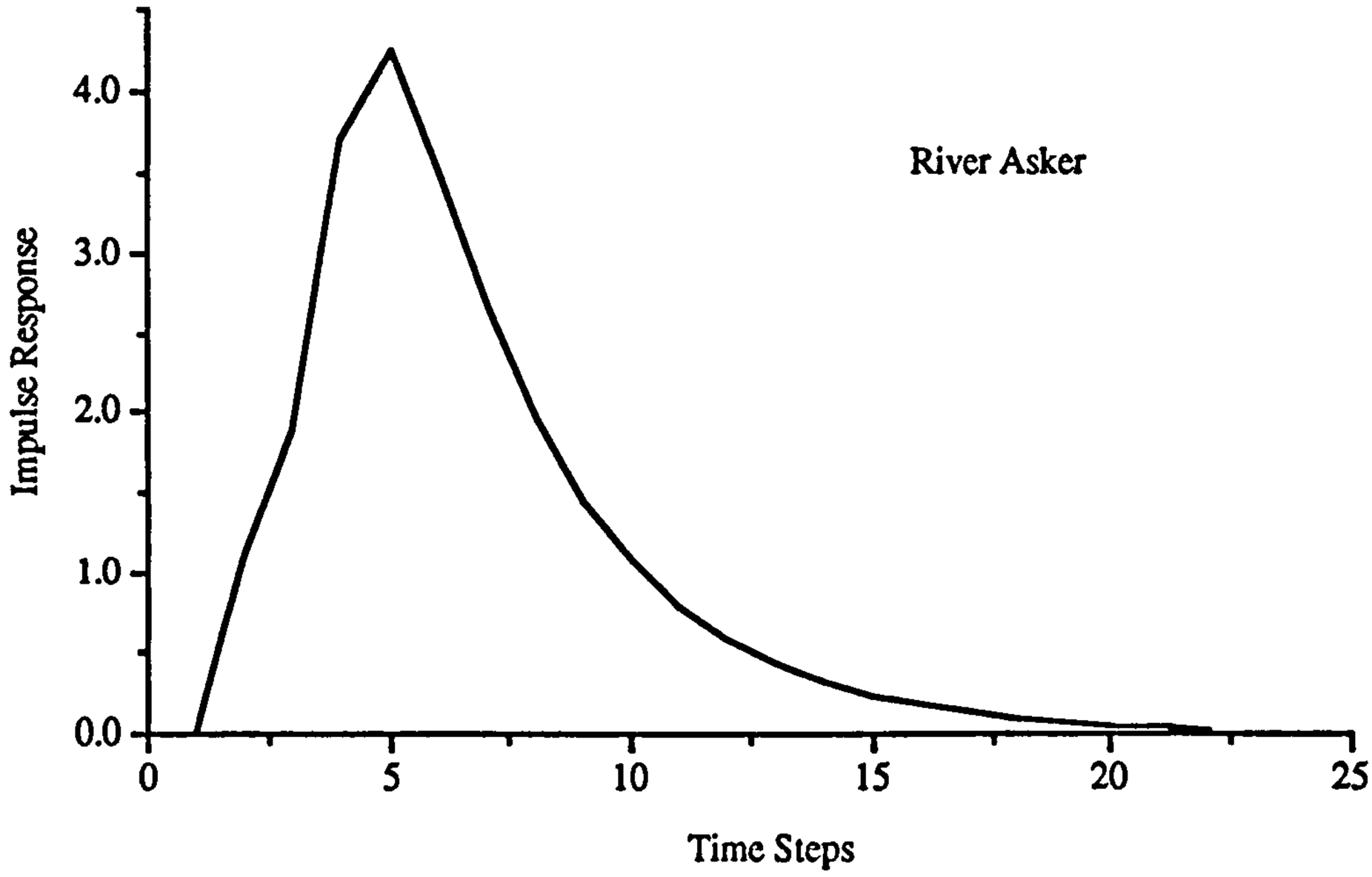

Figure 4.3 Impulse Response of River Asker

4.4 Unsatisfactory TF Model for Hydrology

The response of a linear system like the TF model is uniquely characterised by its impulse response function. If a system receives an input of unit amount applied instantaneously (a unit impulse) at time τ, the response of the system at a later time t is described by the unit impulse response function $u(t-\tau)$; $t-\tau$ is the time lag since the impulse was applied. In hydrology, the TF model is used for the simulation of the rainfall runoff process. This distinguishes the TF model in hydrology with one in other areas as the impulse response of a TF model should not only be stable but also non-negative. Three unsatisfactory cases for hydrological applications are discussed below: Unstable, Fluctuation and Negative Response.

4.4.1 Unstable

As we know, the unit- impulse response of a TF Model can be expressed as

$$h(t) = \sum_{i=1}^{N} \operatorname*{Res}_{z = p_i} [\ H(z)\ ]\ p_i^{n-1} \qquad (4,20)$$

where $p_i = r_i e^{\phi ij}$, that is , r_i and ϕ_i specify the magnitude and angular location of the poles inside the unit circle and N is the number of poles inside the unit circle. As a result, a necessary and sufficient condition that the foregoing summation converges is $|p_i| < 1$, for i = 1, 2, . . . N. Therefore, if the system is causal (i.e. $t \geq 0$), the system response will remain bounded if the poles of the transfer function are all inside the unit circle. Formally, we can state that a linear time-invariant discrete system with unit-impulse response h(t) is stable if and only if

$$\sum_{t=0}^{\infty} |\ h(t)\ | < \infty \qquad (4,21)$$

Finally, the *stability criterion* can be evaluated by finding the poles of the transfer function. Notice that since the poles of B(z) are all located at the origin in the z-plane, B(z) are always stable.

A basic model like

$$H(z) = \frac{(-\beta)}{(\ z^{-1} - \beta\ )} = \frac{z}{(\ z - \frac{1}{\beta})} \qquad (4,22)$$

$$H(z) = \frac{\beta_1 \beta_2}{(z^{-1} - \beta_1)(z^{-1} - \beta_2)} = \frac{z^2}{(z - \frac{1}{\beta_1})(z - \frac{1}{\beta_2})} \qquad (4,23)$$

The transfer function in Eq(4,22) has a real pole and the transfer function in Eq(4,23) has two poles which occurs in complex conjugate pairs. If β_1 and β_2 are both real, it will be illustrated in a later section that H(z) in Eq(4,23) can considered as a cascade form (or equivalently as a parallel form) of H(z) in Eq(4,22). As a result, if the characteristics of H(z) in Equation (4,22) and Equation(4,23) are known, it can greatly help us to understand other complex forms of transfer function.

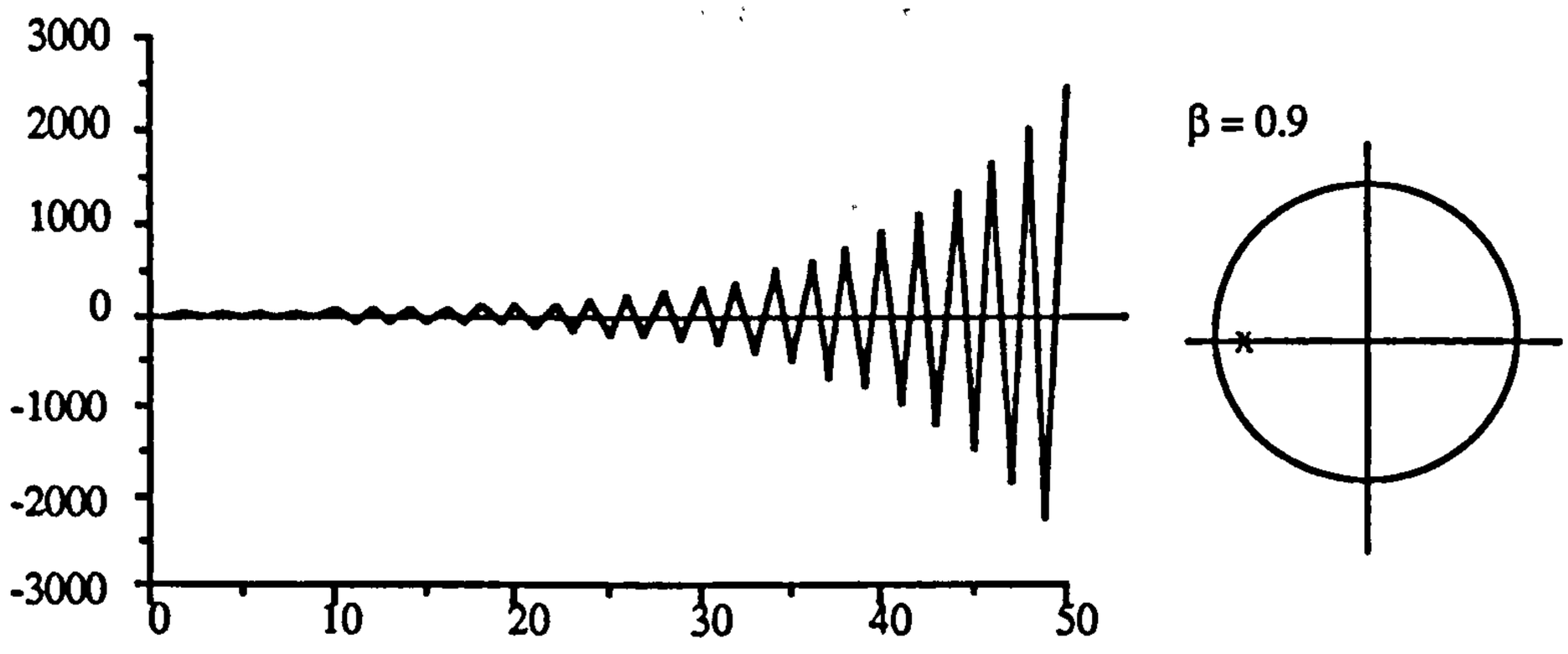

Figure 4.4 Unstable Impulse Response for Single Pole TF Model

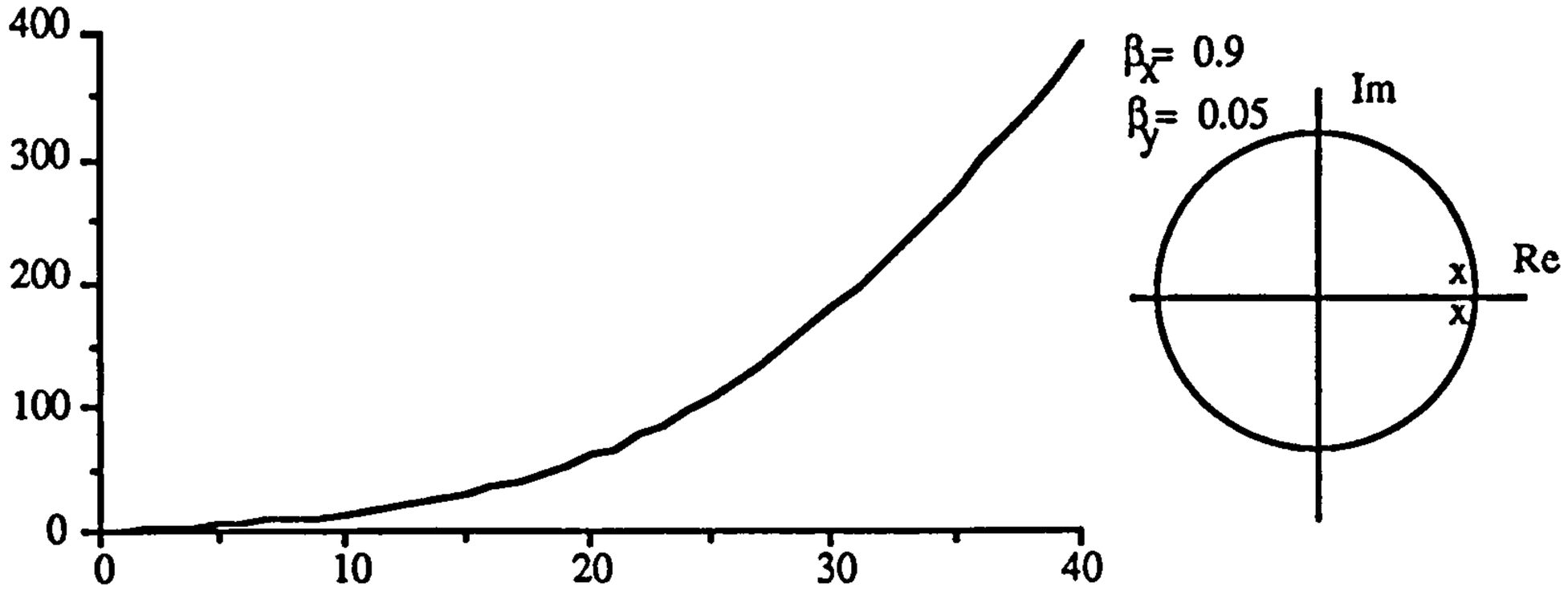

Figure 4.5 Unstable Impulse Response for Double Pole TF Model

Figure 4.4 and Figure 4.5 illustrate the unstable response from two TF Models. These results show failure examples of TF models not only in hydrology but in other areas as well.

4.4.2 Fluctuation

In the hydrological area, it is necessary to not only avoid unstable impulse responses but also to ensure that the impulse response is not oscillatory or fluctuating. In Figure 4.6 and 4.7, although pole β is outside of unit circle (or $1/\beta$ inside the unit circle) , resulting responses are not satisfactory for rainfall runoff simulation.

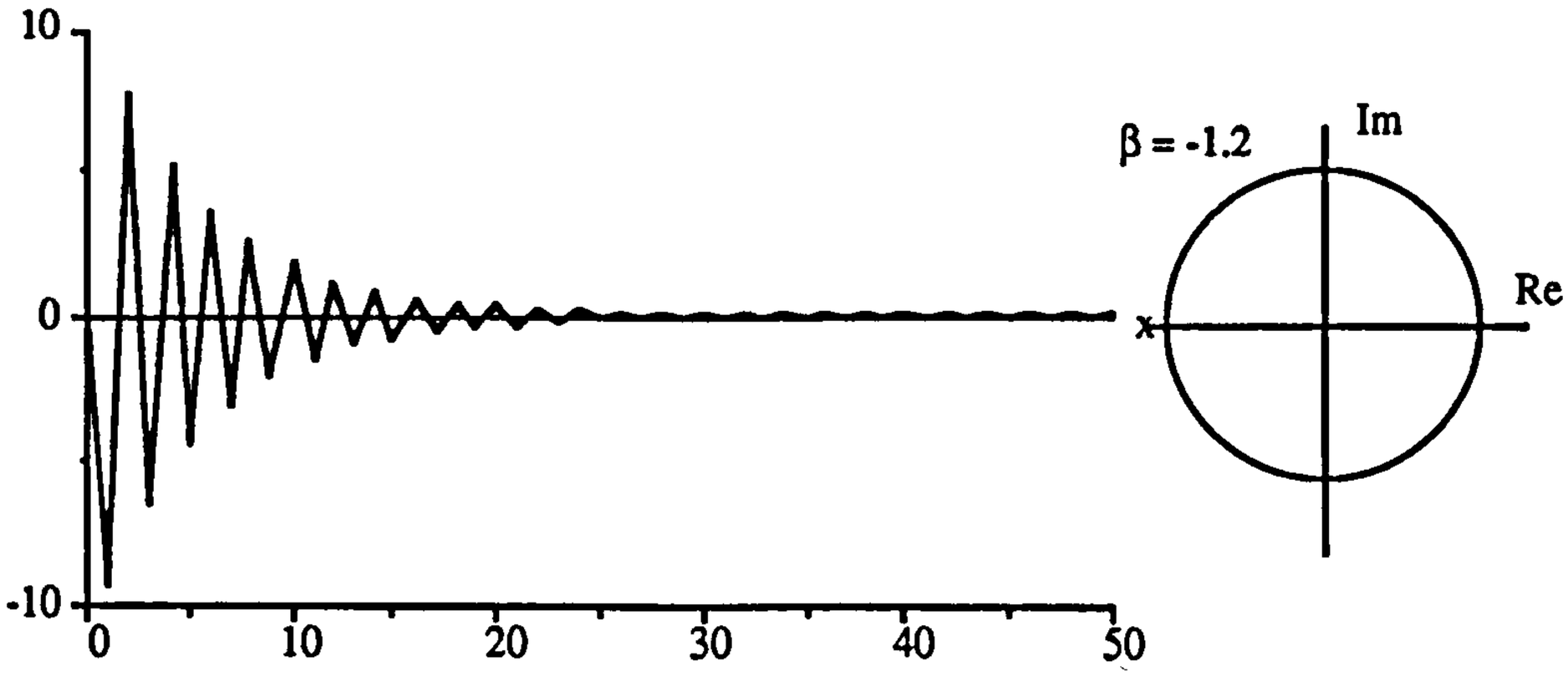

Figure 4.6 Stable But oscillatory Response for Single Pole TF Model

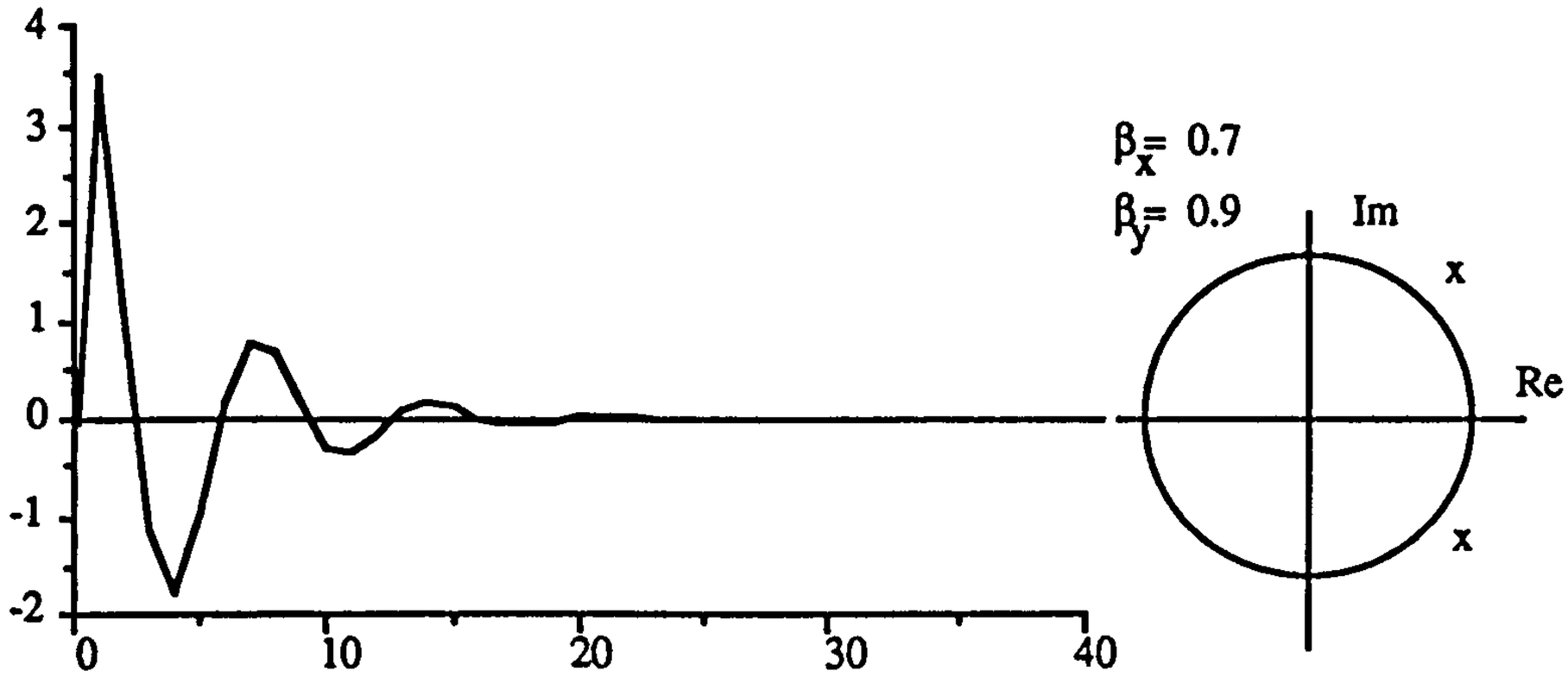

Figure 4.7 Stable But oscillatory Response for Double Pole TF Model

The reason for a stable but fluctuating response can be derived from the inverse Z-transformation.

For a single pole TF model

$$H_0(z) = H(z)\, z^{t-1} = \frac{z^t}{z - \frac{1}{\beta}} \tag{4,24}$$

$$h(t) = \operatorname*{Res}_{z=\frac{1}{\beta}} [\, H_0(z)] = \left(\frac{1}{\beta}\right)^t \quad , \quad t=1,\ 2,\ 3, \tag{4,25}$$

It can be seen that for $\beta < -1$ (or $1/\beta < 0$), we have

$$h(t) > 0 \quad \text{when} \quad t = 2i, \quad i = 1, 2, 3, \ldots$$

$$h(t) < 0 \quad \text{when} \quad t = 2i - 1, \quad i = 1, 2, 3, \ldots$$

h(t) will be sometimes larger than zero and other times smaller. If β is positive, there will be no fluctuating response function.

For a double pole TF model

$$H_0(z) = H(z)\, z^{t-1} = \frac{z^{t+1}}{\left(z - \frac{1}{\beta_1} \right) \left(z - \frac{1}{\beta_2} \right)}$$

Let $1/\beta_1 = a + jb$, and $1/\beta_2 = a - jb$. The impulse response is then

$$h(t) = \operatorname*{Res}_{z = a+jb} [\, H_0(z)] \; + \operatorname*{Res}_{z = a - jb} [\, H_0(z)]$$

$$= \frac{z^{t+1}}{z - a + jb} \Big|_{z = a + jb} + \frac{z^{t+1}}{z - a - jb} \Big|_{z = a - jb}$$

$$= \frac{1}{j2b} \left[(a+jb)^{t+1} - (a - jb)^{t+1} \right] \qquad (4,26)$$

Since

$$a \pm jb = r\, e^{\pm j\phi}$$

where

$$r^2 = a^2 + b^2 \;, \qquad \phi = \arctan \left(\frac{b}{a}\right)$$

we have

$$h(t) = \frac{r^t}{j2b} [\, r\, e^{j(t+1)\phi} - re^{-j(t+1)\phi} \,]$$

Finally, since $b = r \sin \phi$, we obtain

$$h(t) = \frac{r^t}{\sin \phi} \sin [\, (t+1)\, \phi \,] \qquad (4,27)$$

h(t) represents a damped sinusoid decaying exponentially to zero.

Figure 4.6 and Figure 4.7 illustrated the stable oscillatory response from two TF Models. To avoid a fluctuating response, the ϕ should be zero, that means there should be no complex poles for a stable and non-fluctuating TF model.

4.2.3 Negative Response

Negative response is a special case of the fluctuating type. It usually happens at the tail of the response function. Although it is very close to the physical realisable response, it is still not suitable for hydrological applications.

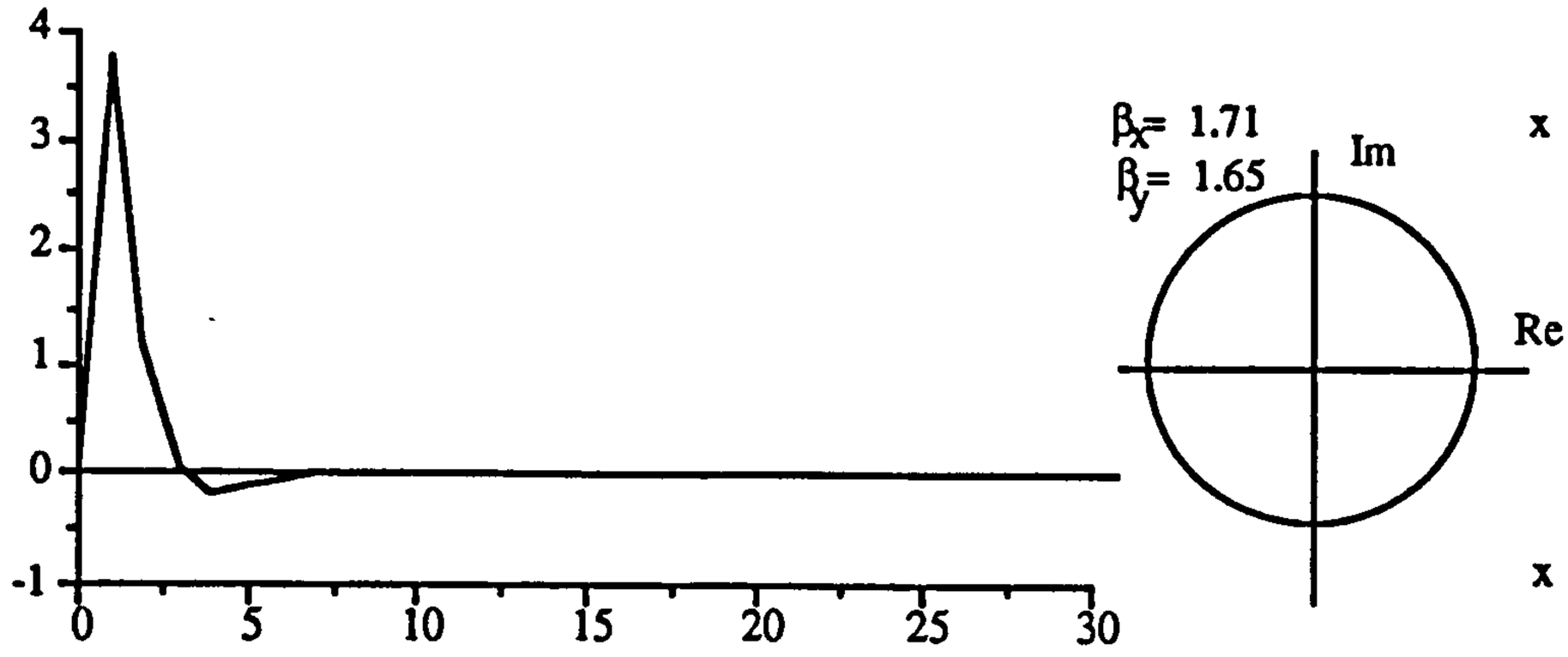

Figure 4.8 Stable But Negative Impulse Response at Tail for Double Pole TF Model

4.5 Physical Realisable TF Model (PRTF)

4.5.1 First and Second Order Pole's Constraints for PRTF

From the last section it was shown that to achieve a physical realisable first or second order TF model, the poles of the TF model must be constrained into the positive real axis and β is outside (or $1/\beta$ inside) the unit circle.

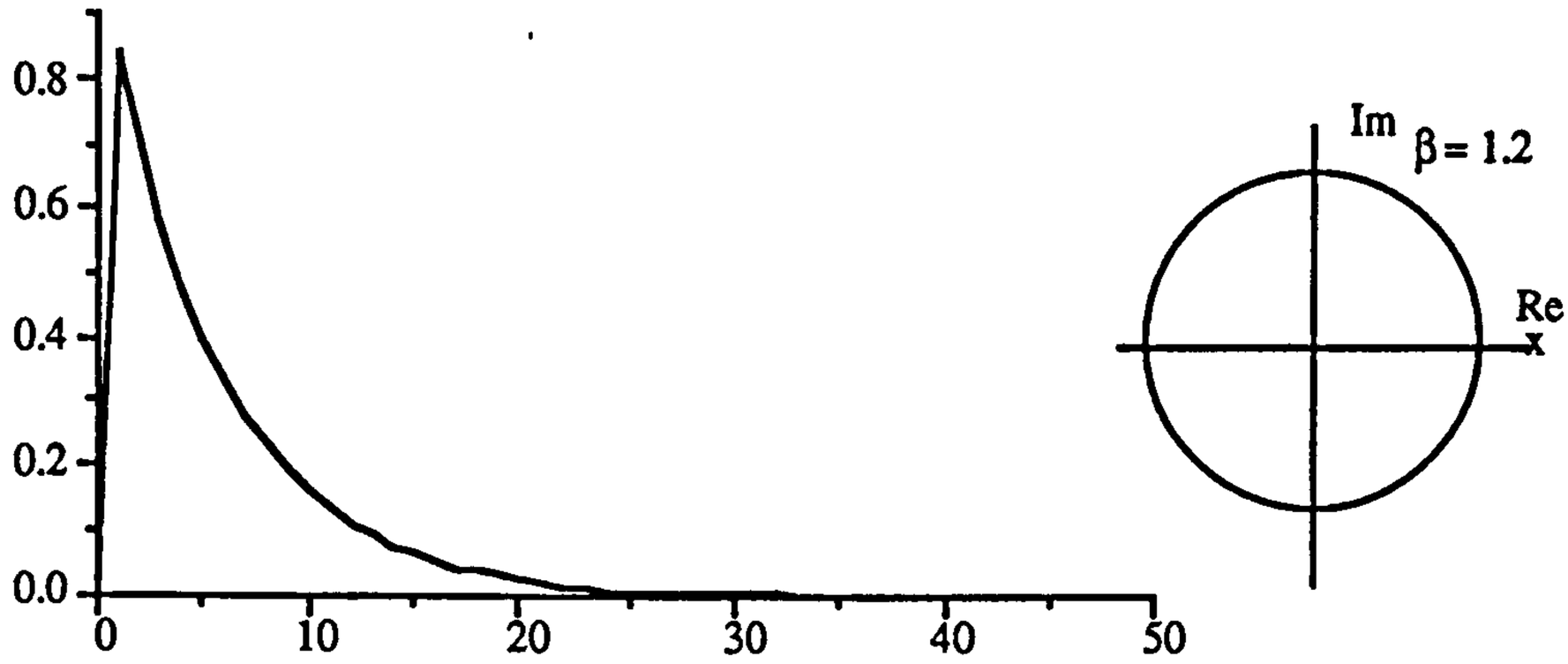

Figure 4.9 A Physical Realisable Response for Single Pole TF Model

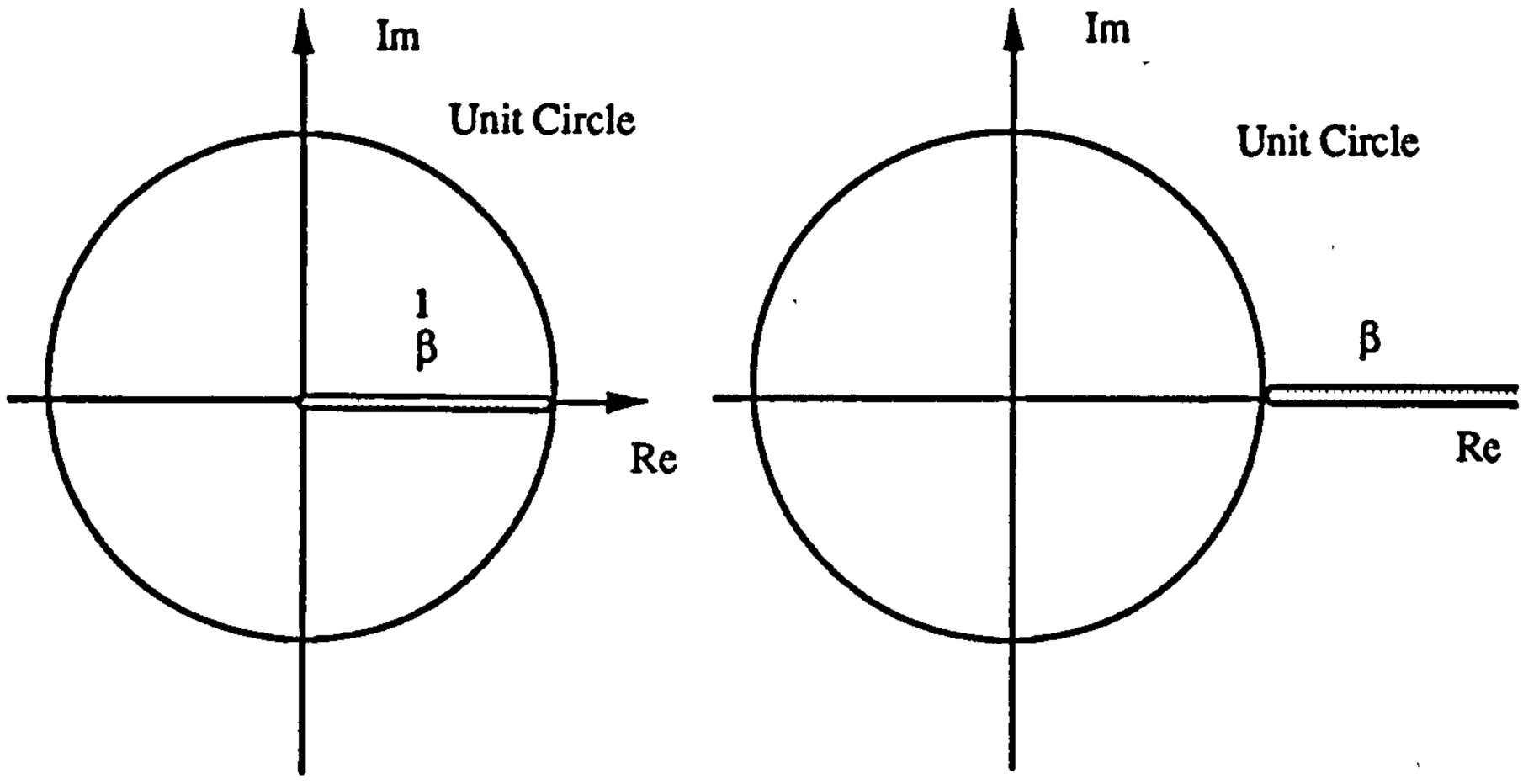

a) Requirment of PRTF Model for $1/\beta$ b) Requirment of PRTF Model for β

Figure 4.10 Pole's Location for PRTF Model

To understand other complex forms of TF model, it is necessary to analyse the cascade and parallel forms of the TF model. It can be shown that the realisation of any H(z) can be factored into the realisation of two transfer functions, that is

$$H(z) = H_D(z)\, H_N(z) = B(z)\left(\frac{1}{A(z)}\right)$$

$$= \sum_{l=0}^{M} b_l z^{-l} \left(\frac{1}{1 - \sum_{l=1}^{N} a_l z^{-l}}\right) \qquad (4,28)$$

Equation(4,28) gives H(z) as the product of the denominator portion of the transfer function, $H_D(z)$, with the numerator portion given by $H_N(z)$. This is referred to as a cascade factorisation of the transfer function into the feed-forward portion resulting from the zeros (the numerator) and the feedback portion resulting from the poles (the denominator).

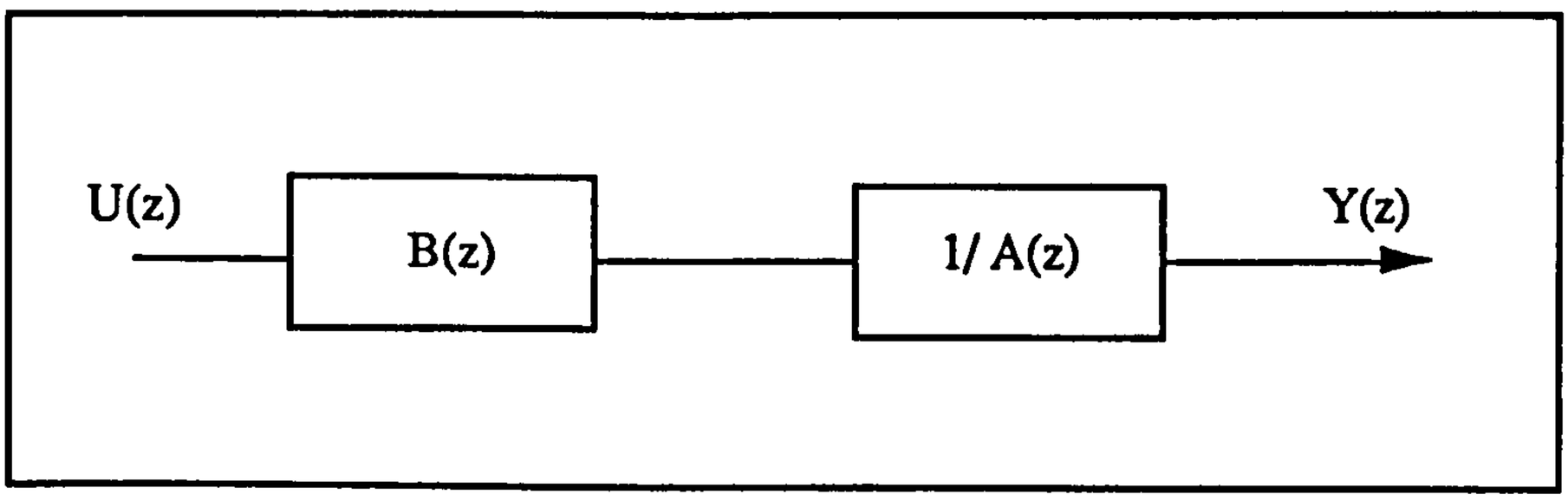

Figure 4.11 Cascade of TF Model

The impulse response function of the TF model can then be derived from two parts which are discussed separately.

4.5.2 B(z) Part

B(z) is a finite impulse response linear system. The shape of the impulse response is directly decided from the B(z) parameters. Since the poles of B(z) are all located at the origin in the z-plane, B(z) is always stable.

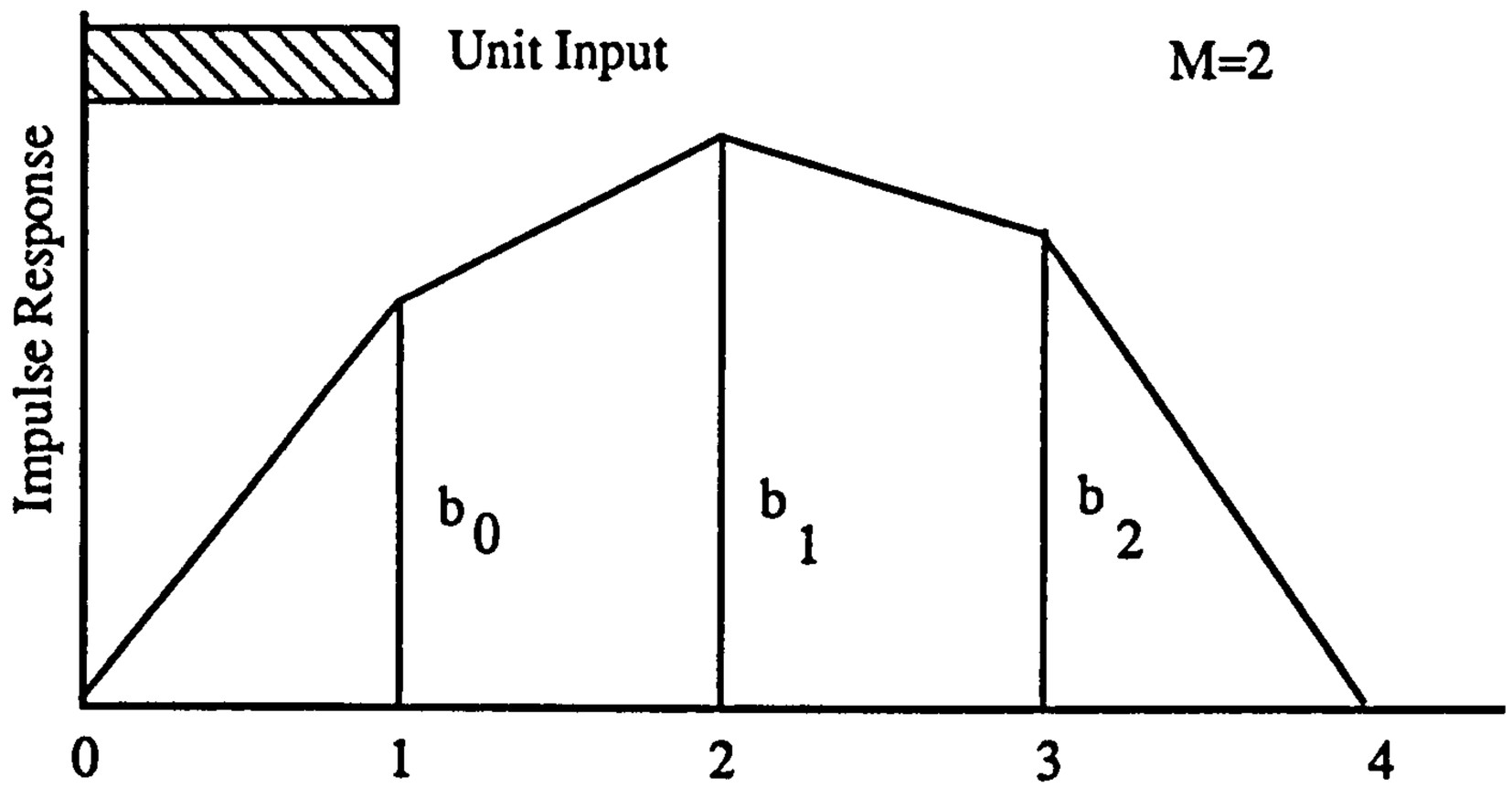

Figure 4.12 Impulse Response from B(z) part.

4.5.3 1/ A(z) Part

The 1/A(z) is a infinite impulse response linear system as illustrated in Figure 4.5.

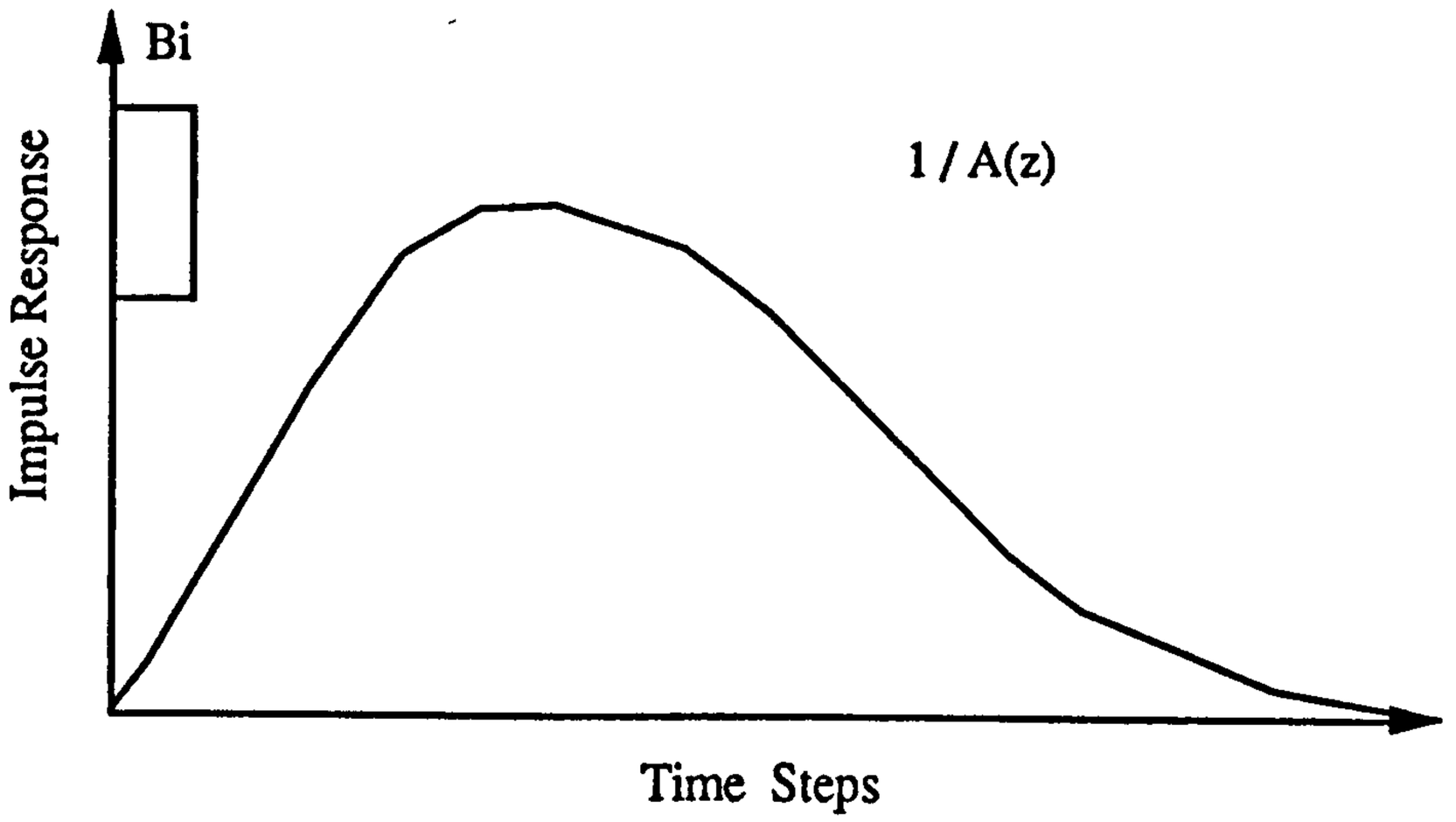

Figure 4.13 Impulse Response of 1/A(z)

If the impulse response of B(z) can be viewed as rainfall and 1/A(z) as the Unit hydrograph, the impulse response of H(z) can be viewed as the river flow. It is then straightforward to show that to achieve a physical realisable TF model , 1/A(z) must be a positive stable TF Model without fluctuation. And if parameters in B(z) are limited to positive, a physical realisable TF model can then be achieved by combining B(z) and 1/A(z).

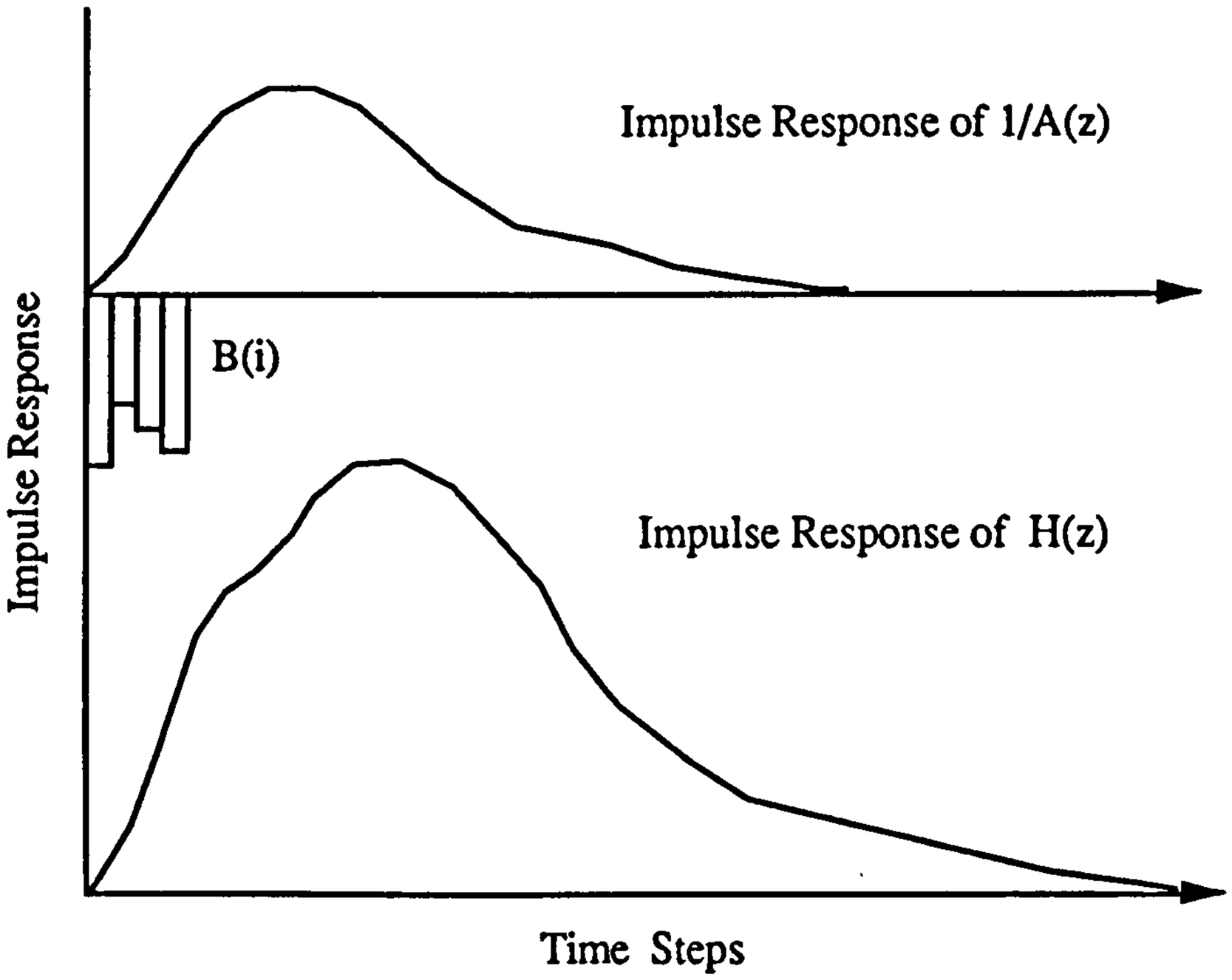

Figure 4.14 Impulse Response of H(z)

Transfer function 1/A(z) can then be transformed into a rational function

$$\frac{1}{A(z)} = \frac{(-1)^N p_1 p_2 \cdots p_N}{(z^{-1} - p_1)(z^{-1} - p_2) \cdots (z^{-1} - p_N)} \qquad (4,29)$$

Since the coefficients of the polynomial of H(z) are real, all the complex poles will

occur in complex conjugate pairs, where p_i are the non-repeat poles of the rational function.

For distinct poles the function C(z)= 1/A(z) is expanded in the form

$$C(z) = \frac{C_1}{z^{-1} - p_1} + \frac{C_2}{z^{-1} - p_2} + \ldots + \frac{C_{N-1}}{z^{-1} - p_n} \qquad (4,30)$$

In this sense, the transfer function of C(z) is given by the parallel form of a summation of transfer functions.

$$C(z) = \sum_{i=1}^{N} C_i(z) \qquad (4,31)$$

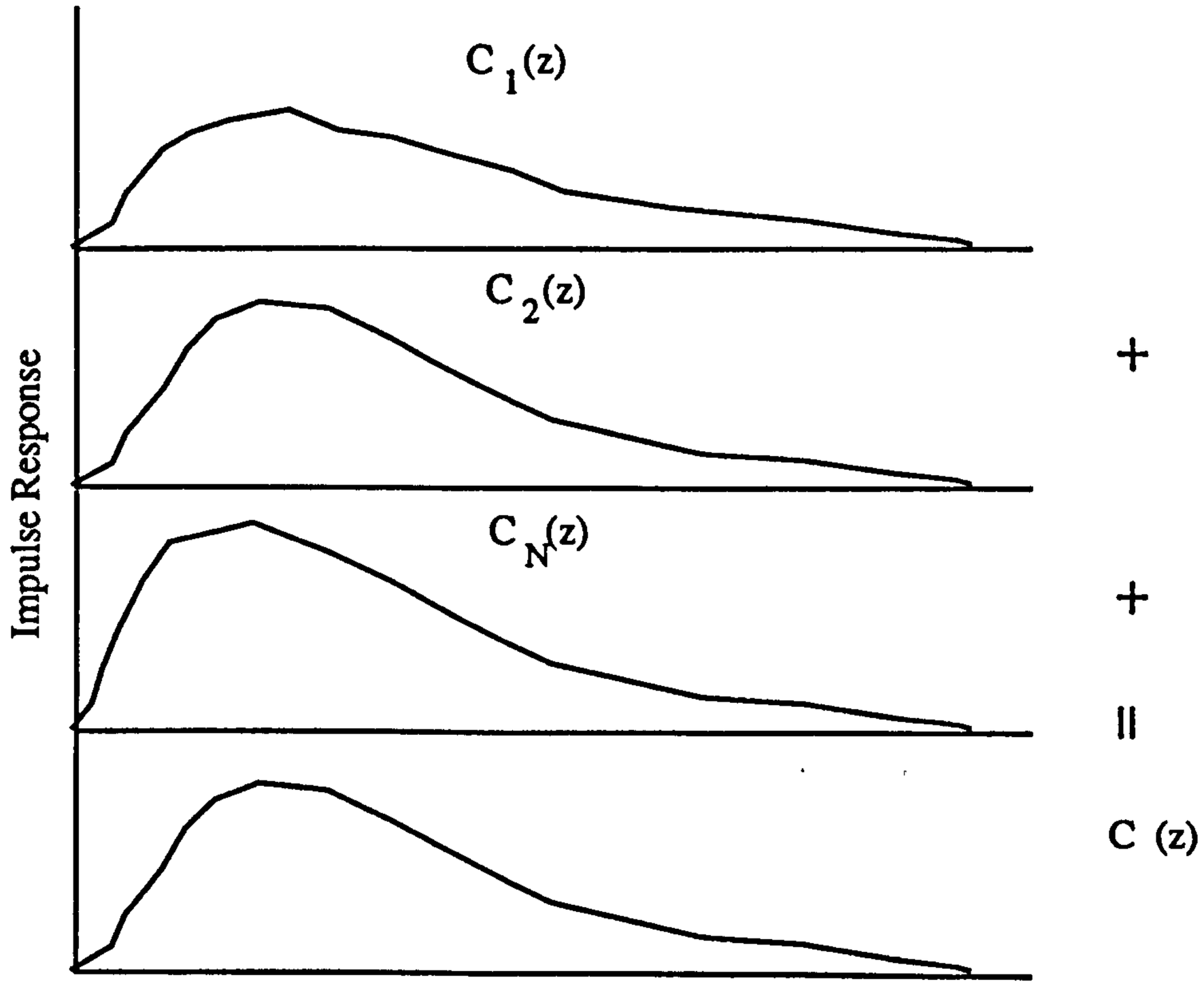

Figure 4.15 Parallel Form of H(z) components

From figure 4.15, if any of the components in the parallel transfer function is not stable then the resulting C(z) will highly likely be unstable or fluctuating. This result also hold true when C(z) has repeat poles.

This result can also be extended from first and second order TF models to more complex TF models and a general PRTF model can be derived as :

$$H(z) = \frac{\sum_{l=0}^{M} b_l z^{-l}}{S \prod_{l=1}^{N} (z^{-1} - \beta_l)^{m_l}} \qquad (4,32)$$

$$\beta_l \in \Re \quad \text{and} \quad \forall \beta, \quad \beta_l > 1.0$$

$$b_i \geq 0 \qquad i=0,\ 1,\ 2,\ \ldots\ M$$

And

$$S = \frac{1}{\prod_{l=1}^{N} (-\beta_l)^{m_l}} \qquad (4.33)$$

where N is a positive integer representing the total number of poles and m_i is the pole order. As all the poles are in the unit circle and real, the transfer function represented in Eq (4,33) are always stable, non-negative and non-fluctuating.

Although the PRTF from Eq.(4,32) and Eq.(4,33) are always stable with no fluctuation and negative value, it is not straightforward to estimate the model parameters and it is difficult to adjust the model impulse response. A simplified model form is used in the following chapters to build a model and to utilise it in the following computer simulations.

$$H(z) = \frac{\sum_{l=0}^{M} b_l z^{-l}}{S\ (z^{-1} - \beta)^N} \qquad (4,34)$$

$$\beta_i \in \Re \quad \text{and} \quad \forall \beta, \quad \beta_i > 1.0$$

and

$$S = \frac{1}{(-\beta)^N} \qquad (4,35)$$

Here, only one pole is used and the experience from the following chapters shows that N= 3 is suitable for most catchments. The limitation for all $b_i \geq 0$ has been removed as it was found in the following work that in the practical situation it will usually not affect the physical relisability of the model and the negative b_i can be helpful to the adaptivity of the PRTF model.

As $(z^{-1}-\beta)^N$ can be written as

$$(z^{-1} - \beta)^N = (z^{-1})^N + N (z^{-1})^{N-1} (-\beta) + \frac{N(N-1)}{2!} (z^{-1})^{N-2} (-\beta)^2 +$$

$$+ \frac{N(N-1)(N-2)}{3!} (z^{-1})^{N-3} (-\beta)^3 + \ldots +$$

$$+ \frac{N(N-1) \ldots [N-(k-1)]}{k!} (z^{-1})^{N-k} (-\beta)^k + \ldots + (-\beta)^N \qquad (4,36)$$

and

$$C_N^k = \frac{N(N-1)\ (N-2)\ \ldots\ [\ N - (k-1)\ ]}{k!}$$

So a PRTF can be written as

$$y(t) = \sum_{i=1}^{N} a_i\ y(t-i) + \sum_{i=0}^{M} b_i\ u(t-i) \qquad (4,37)$$

$$a_i = -S\ C_N^{N-i}\ (-\beta)^{N-i} = -\ C_N^{N-i}\ (-\beta)^{-i}$$

$$\beta_i \in \Re \quad \text{and} \quad \forall \beta, \quad \beta_i > 1.0$$

Eq (4,37) is written in common TF model format and is easy to appliy in practice.

4.6 Features of PRTF

PRTF has common features just as the general TF model. As its poles are constrained some new features are very useful for the model identification and flood simulation.

The pole locations of a TF model can influence the stability of the TF model. The behaviour of a simple PRTF model can be analysed when its pole changes. In the following figures, the influence of the pole's locus on the TF behaviour is illustrated.

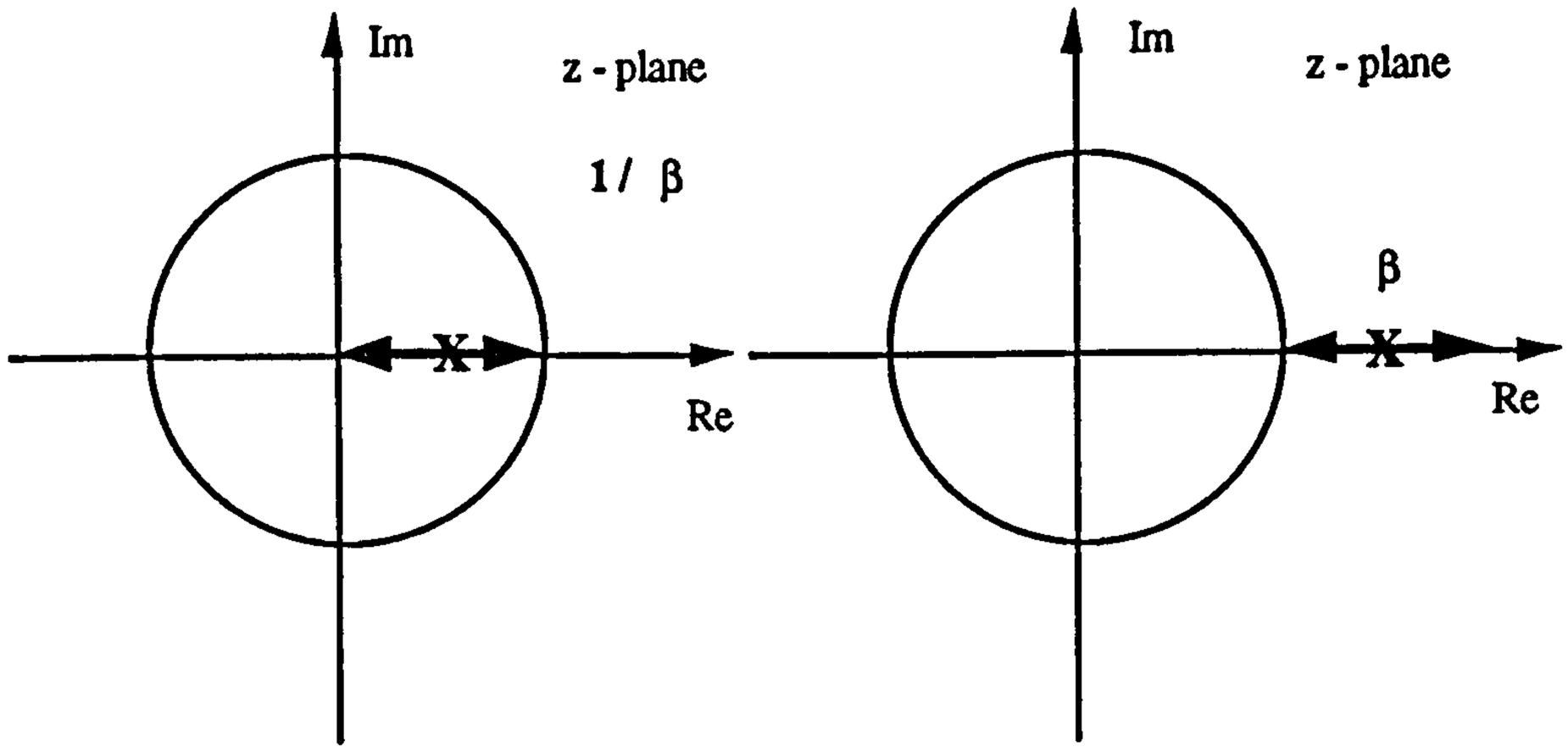

Figure 4.16 Moving Range of Poles for PRTF

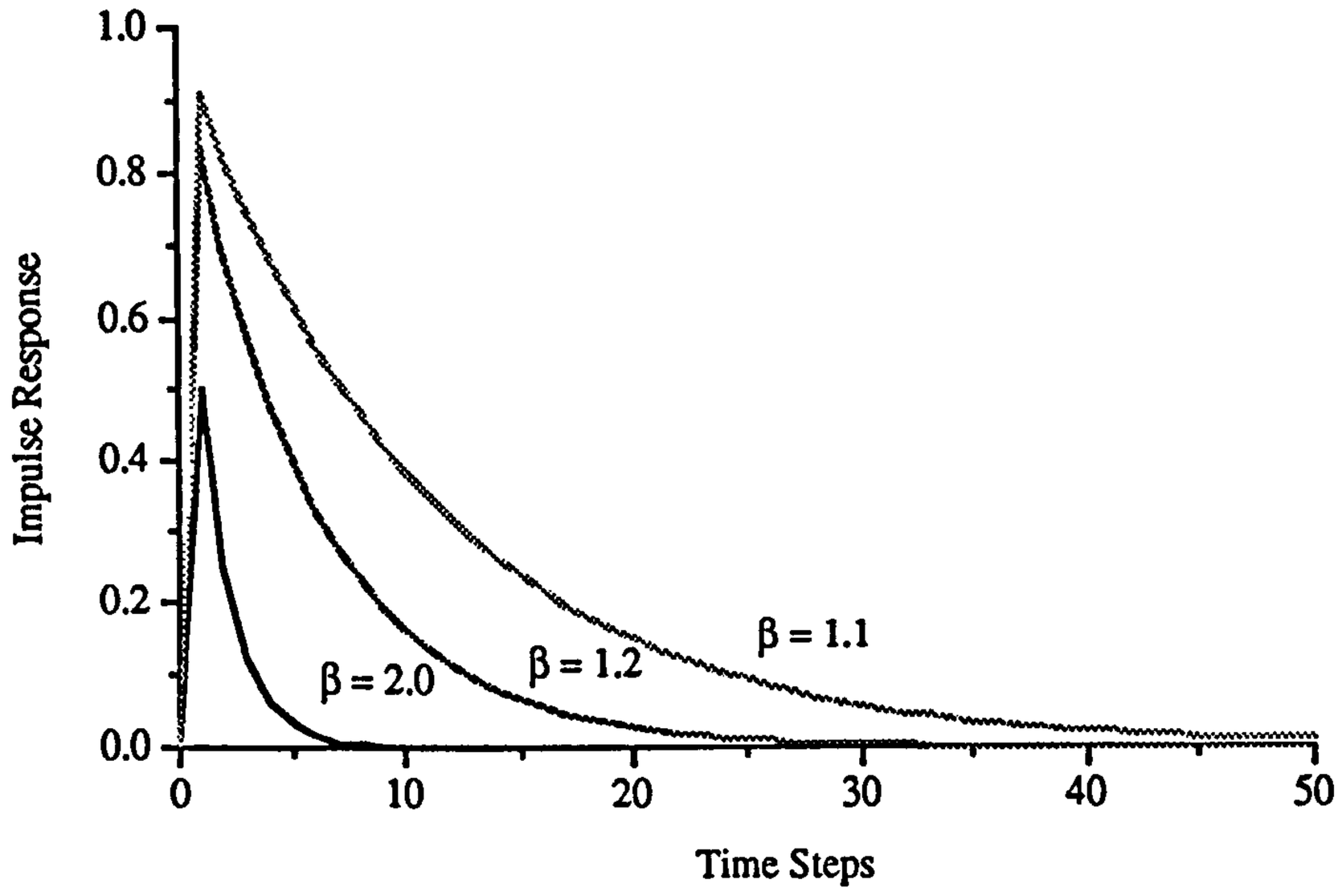

Figure 4.17 Impulse Response from Single Pole PRTF

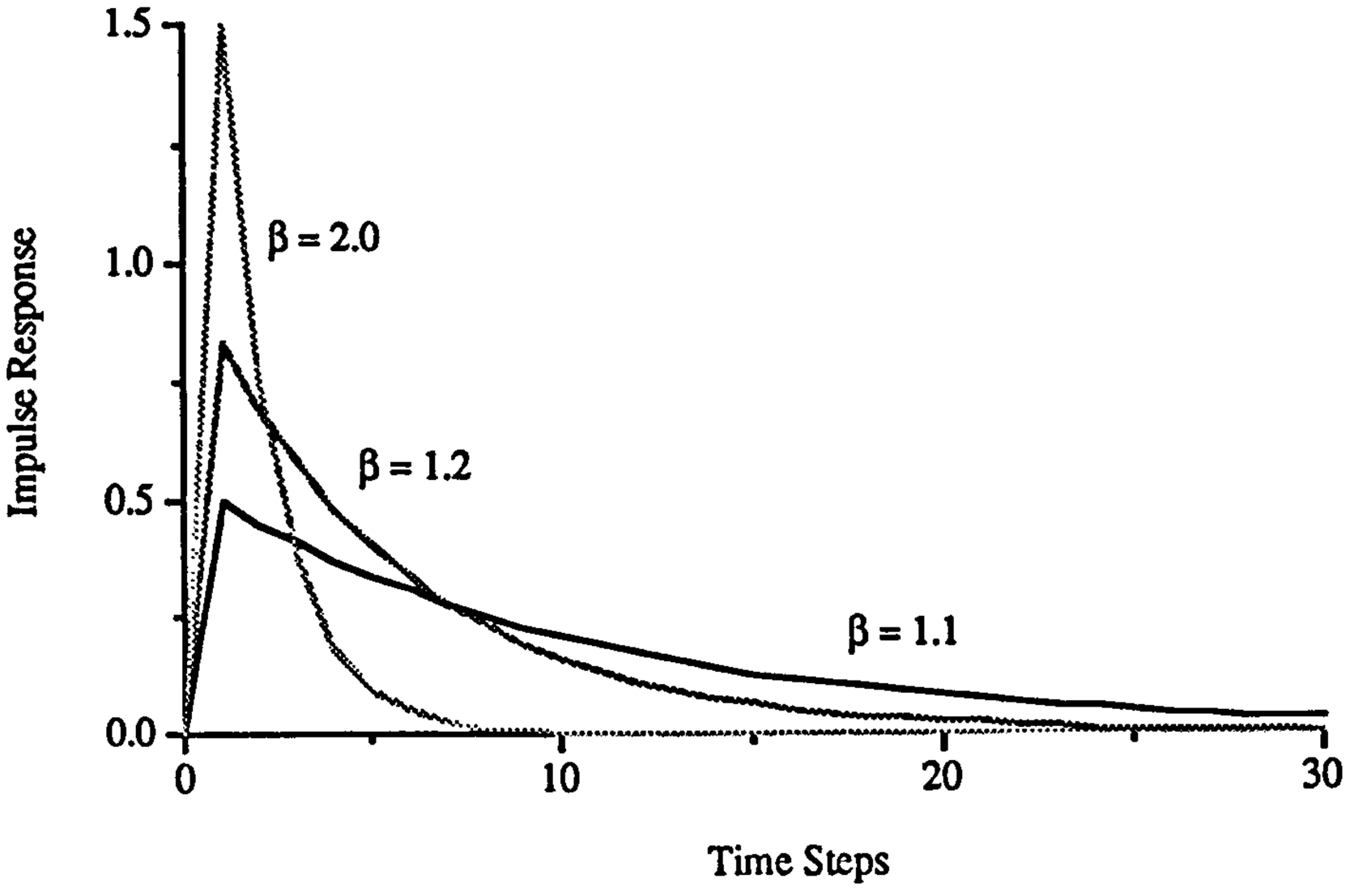

Figure 4.18 Impulse Response from Single Pole PRTF with Constant Area

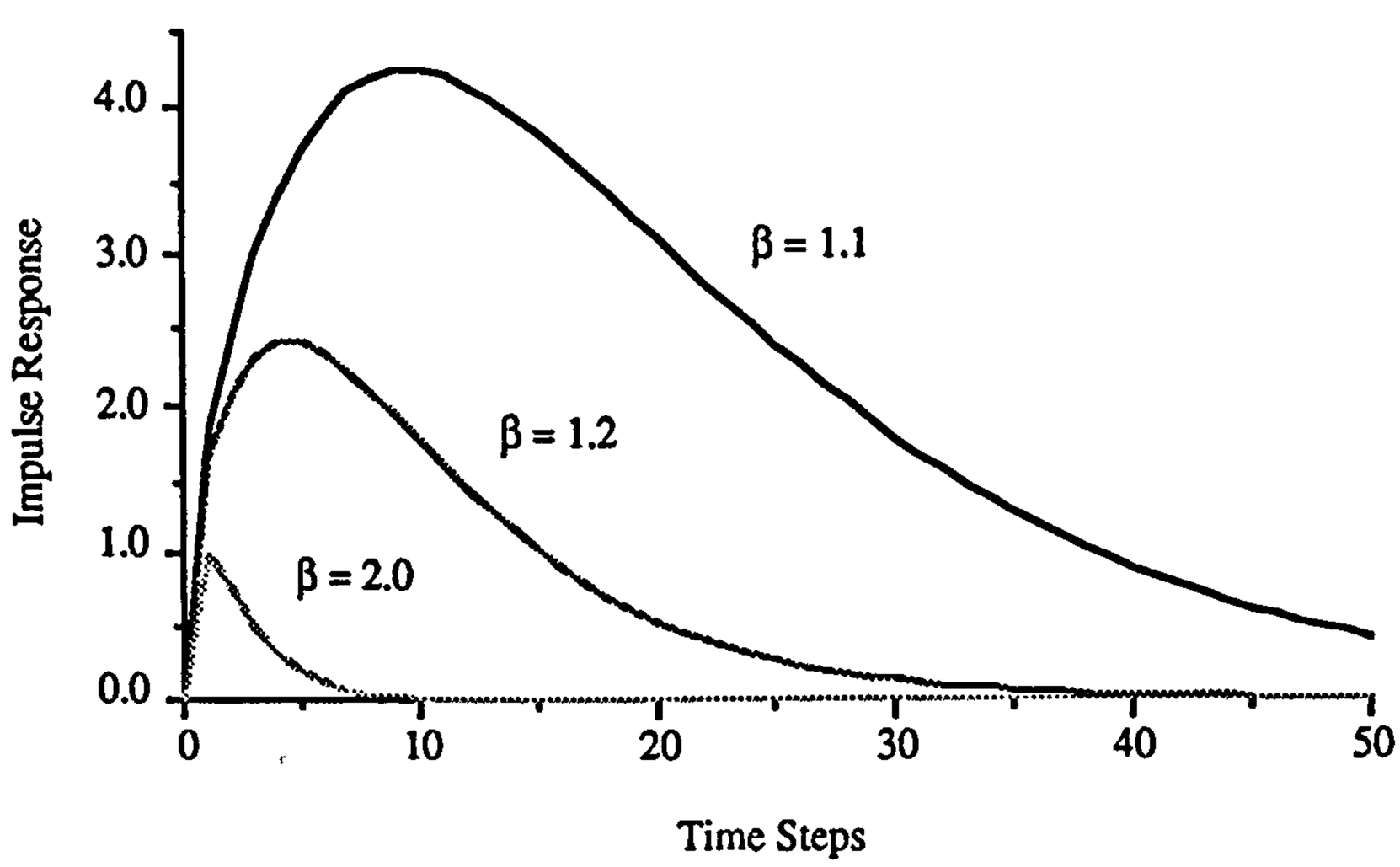

Figure 4.19 Impulse Response from Double Pole PRTF

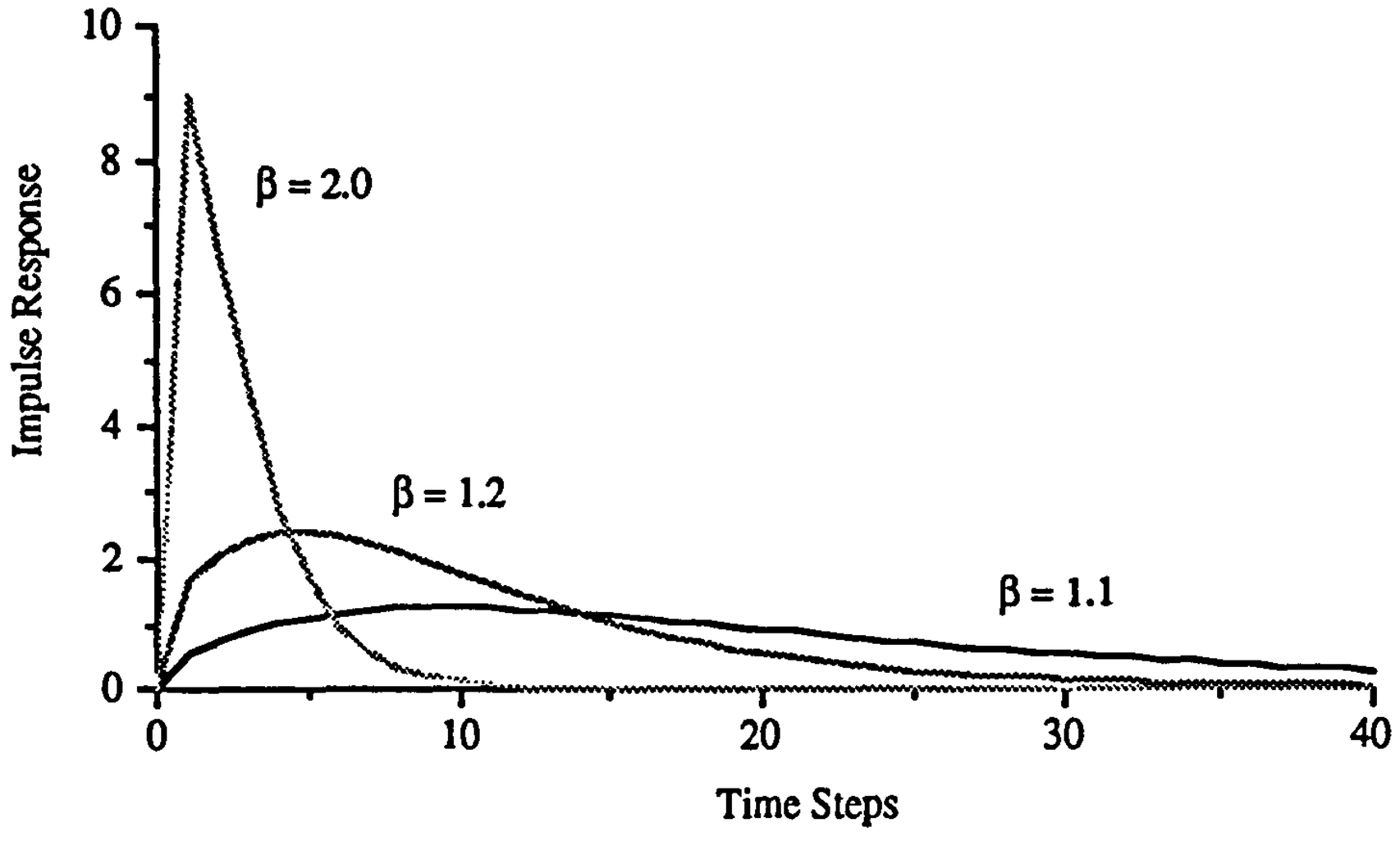

Figure 4.20 Impulse Response from Double Pole PRTF with Constant Area

Figure 4.21 Impulse Response from Triple Pole PRTF

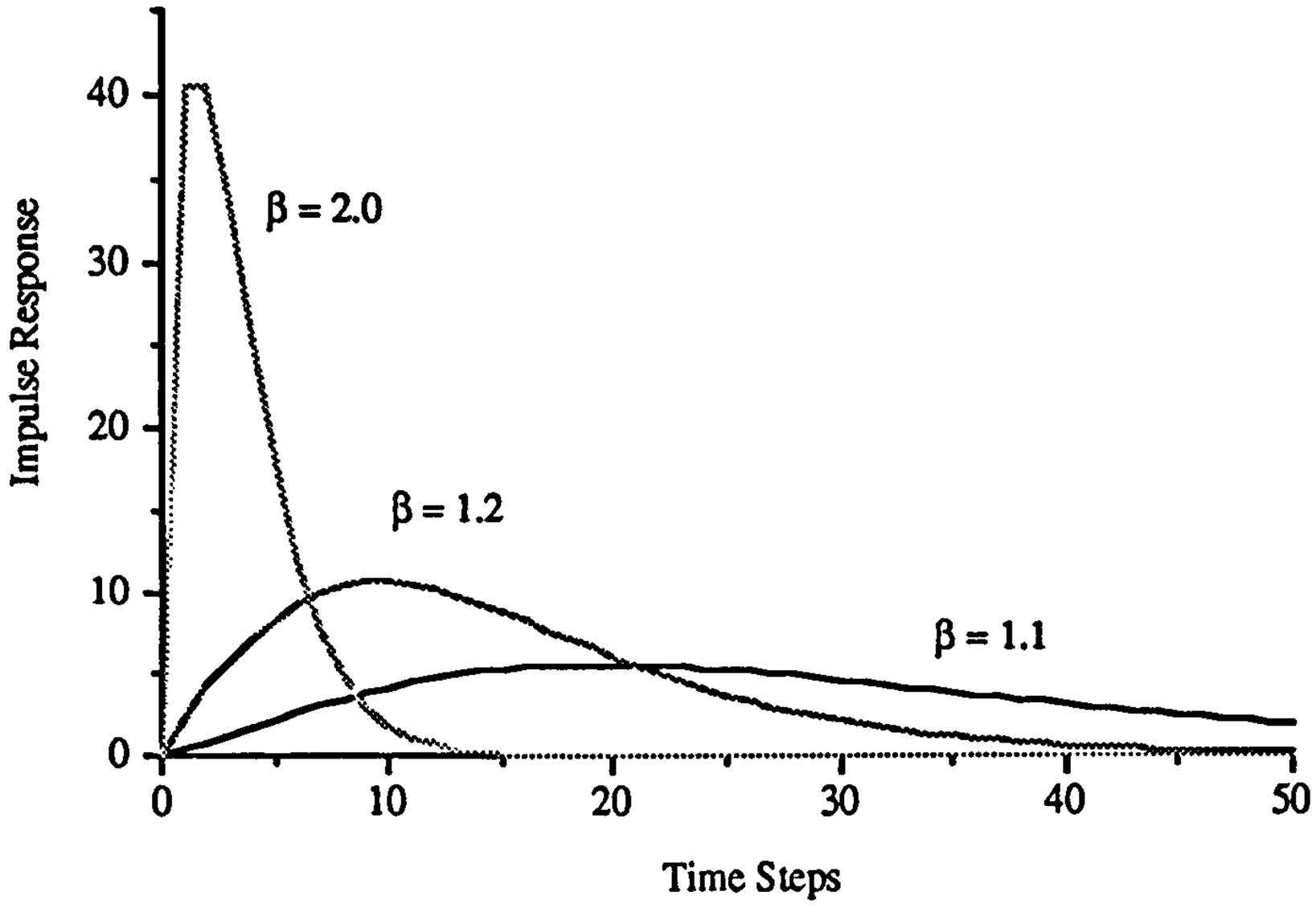

Figure 4.22 Impulse Response from Triple Pole PRTF with Constant Area

From the figures above, it was found that the pole's position can dramatically influence the impulse response of TF model. This feature is very important for PRTF model updating in real-time flood forecasting. From chapter 6, it can be found that the impulse response of 1/A(z) is

For N = 1

$$h(t) = \left(\frac{1}{\beta}\right)^t \qquad (4,26a)$$

where $t = 1, 2, \ldots,$

For $N \geq 2$

$$h(t) = \frac{(N-1+t)\,(N-2+t)\ldots(1+t)}{(N-1)!}\left(\frac{1}{\beta}\right)^t \qquad (4,26b)$$

where $t = 1, 2, \ldots,$

For special cases, if N = 2

$$h\,(t) = (\,1+t)\,(\frac{1}{\beta}\,)^t \qquad (4,27)$$

If N= 3 then

$$h\,(\,t\,) = \frac{(2+t)\;(1+t)}{2}\;\;(\frac{1}{\beta}\,)^t \qquad (4,28)$$

Let

$$k(t) = (\,\frac{1}{\beta}\,)^t \qquad (4,29)$$

and

$$P\,(t) \;\; = \frac{(N-1+t)\;(N-2+t)\;.\;.\;.\;(1+t)}{(N-1)\;!} \qquad (4,30)$$

where K(t) is a kernel function and P(t) is a polynomial function.

So the PRTF model consists of

$$h(t) \;\; = \; P(t)\;\; K(t) \qquad (4,31)$$

The impulse response of a PRTF was found to be composed of a kernel function K(t) and a polynomial function P(t). K(t) is a monotonic decreasing function and P(t) is a monotonic increasing function. The following figures show that both K(t) and P(t) are changeable with the poles position and order. It is illustrated that the kernel function K(t) is only influenced by the model's pole position while the polynomial function P(t) is only influenced by the model pole's order.

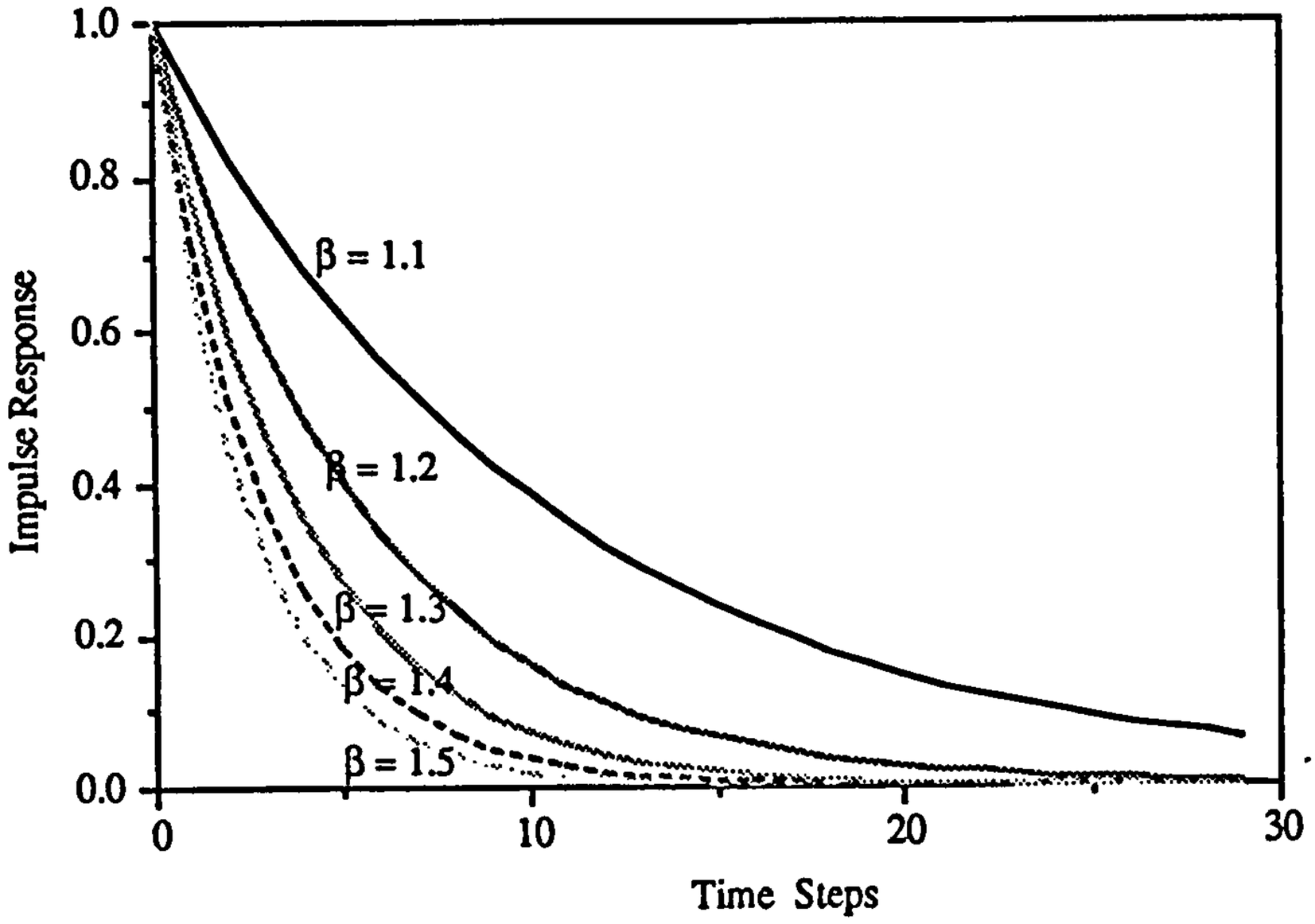

Figure 4.23 Kernel Function K(t) Change with Pole's Position

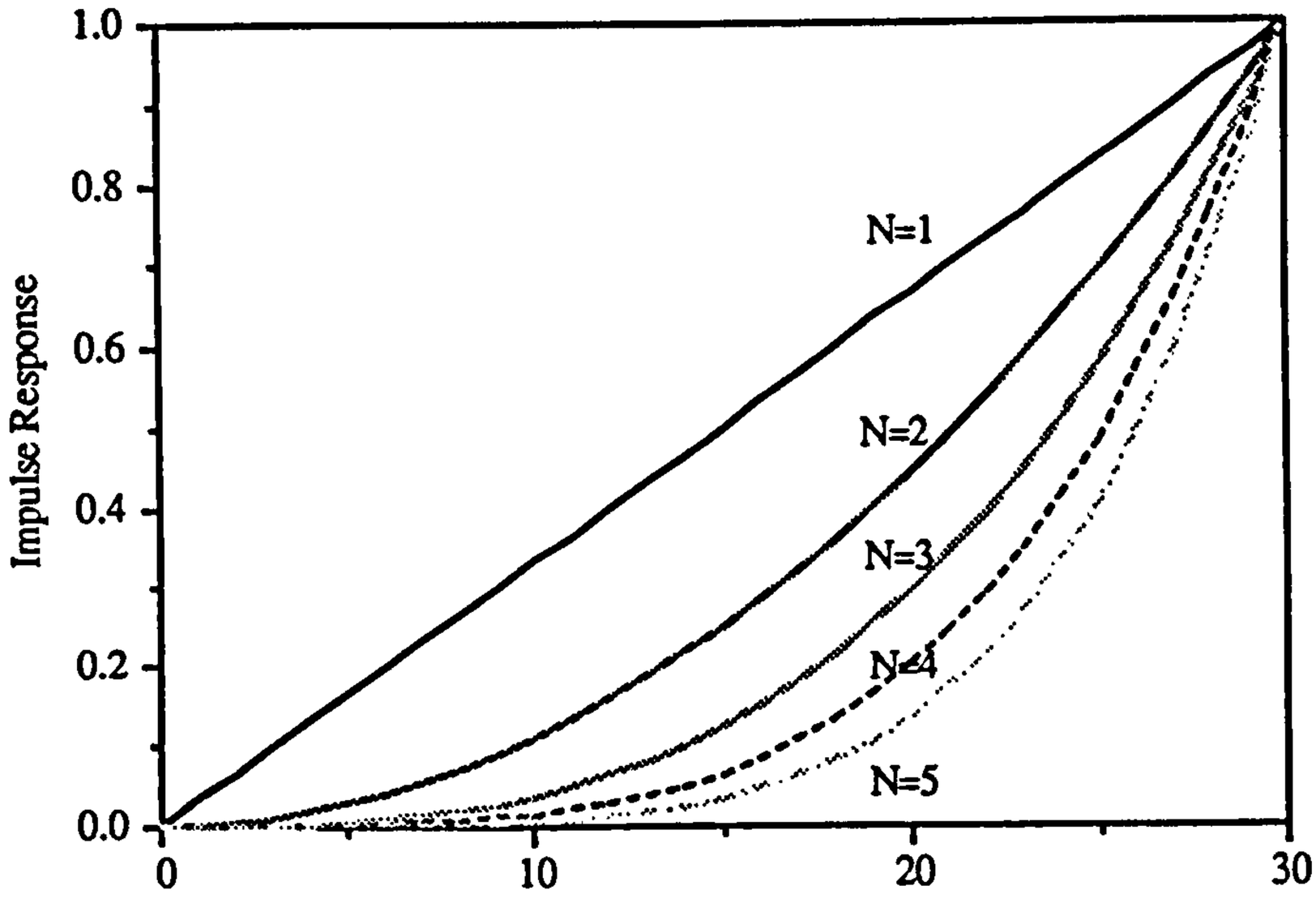

Figure 4.24 Polynomial Function P(t) Change with Pole's Order

The values in the above figures have been standardised such that they have the

same maximum value. Results show that the kernel function K(t) and the polynomial function P(t) have a very similar appearance except in opposite directions.

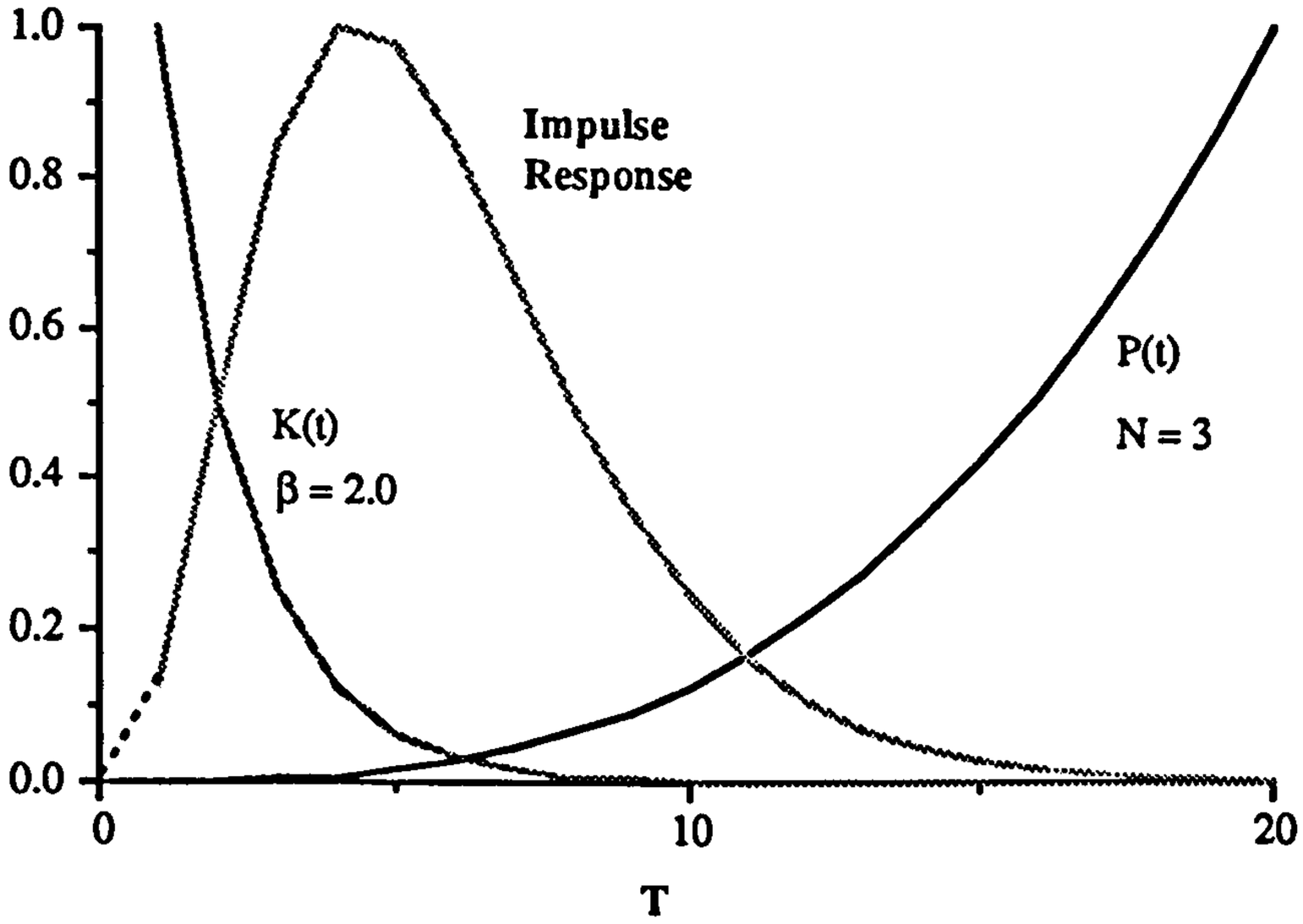

Figure 4.25 Impulse Response with Pole's Position (β = 2.0)

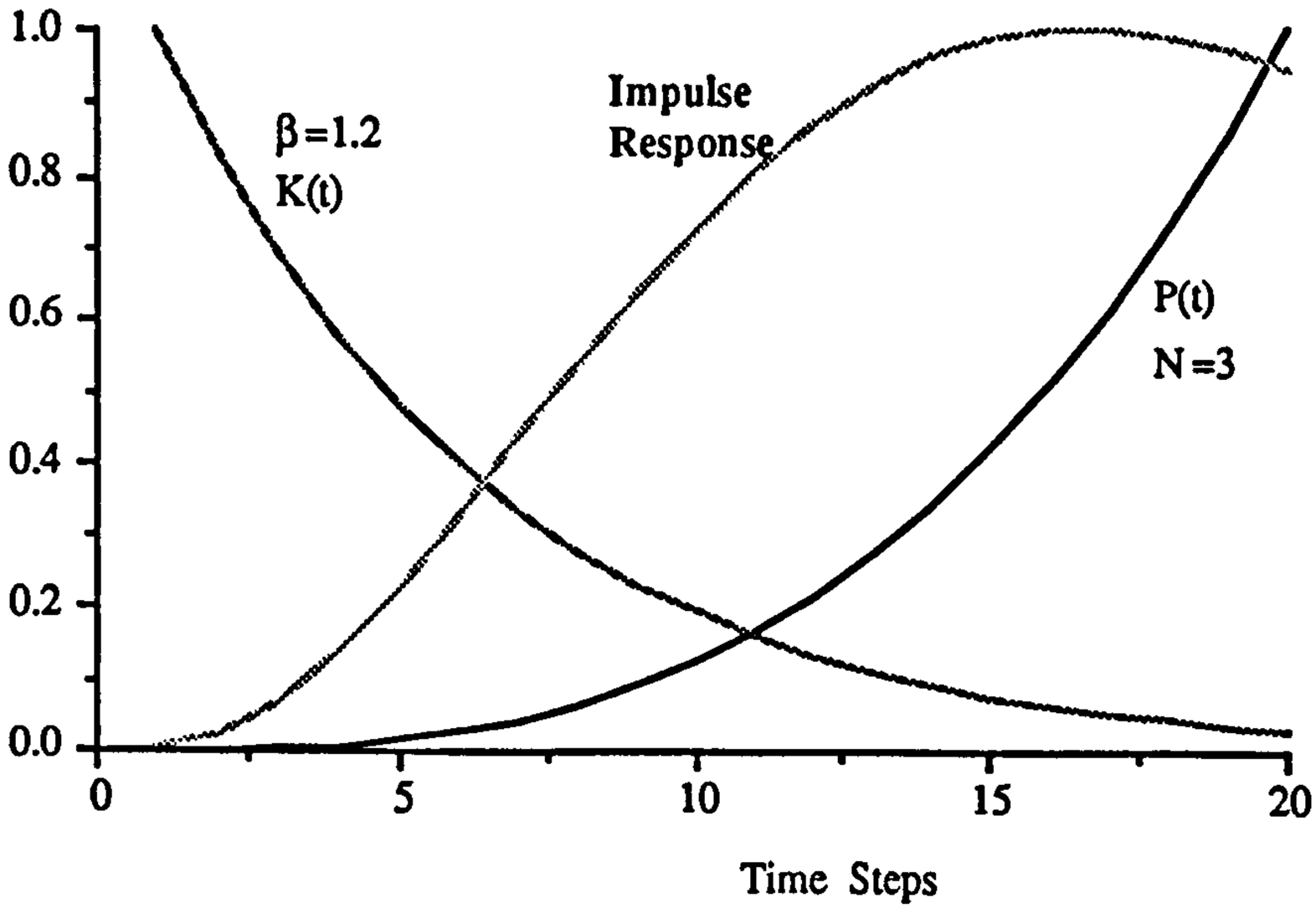

Figure 4.26 Impulse Response with Pole's Position (β = 1.2)

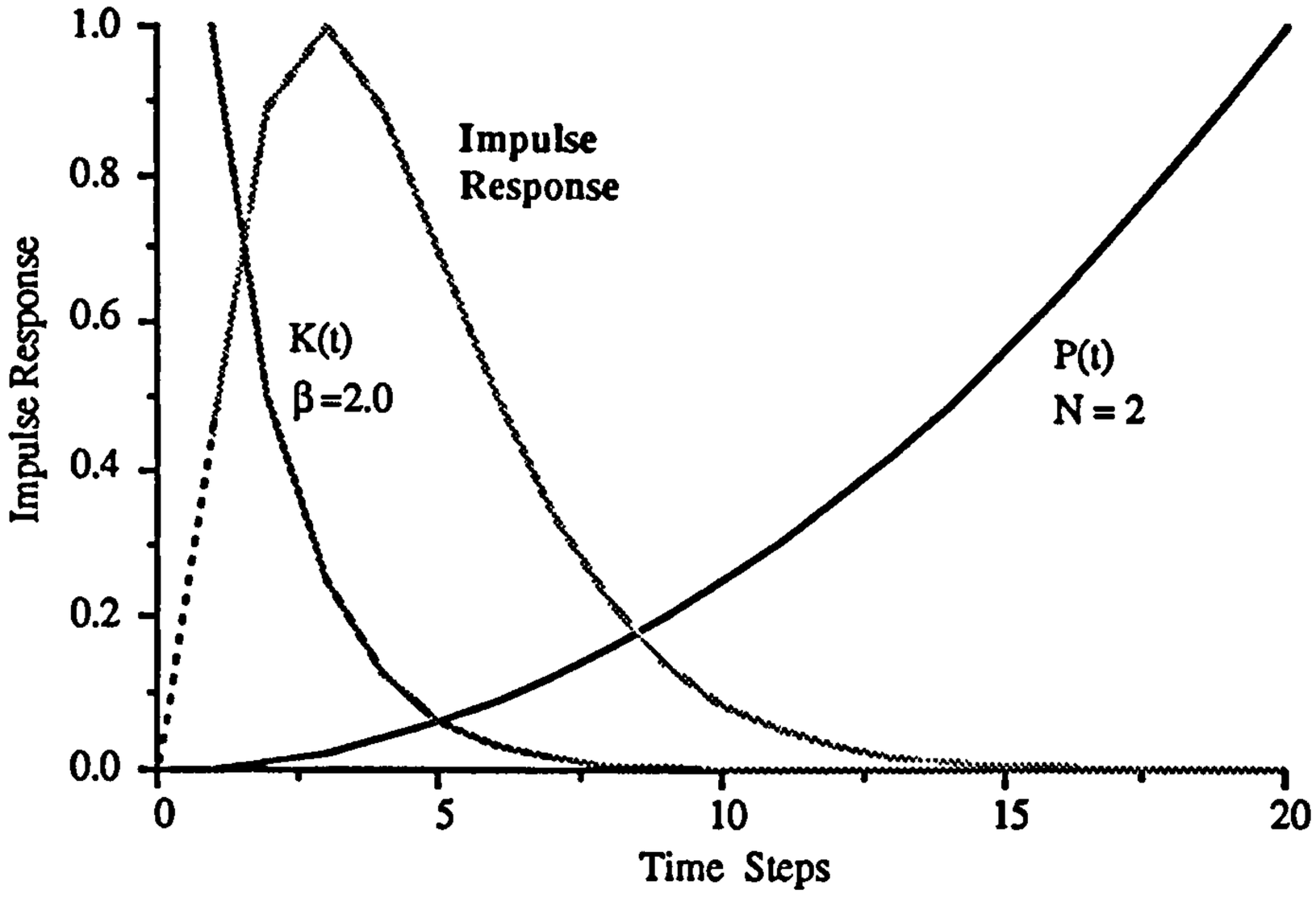

Figure 4.27 Impulse Response by Small Pole's Order

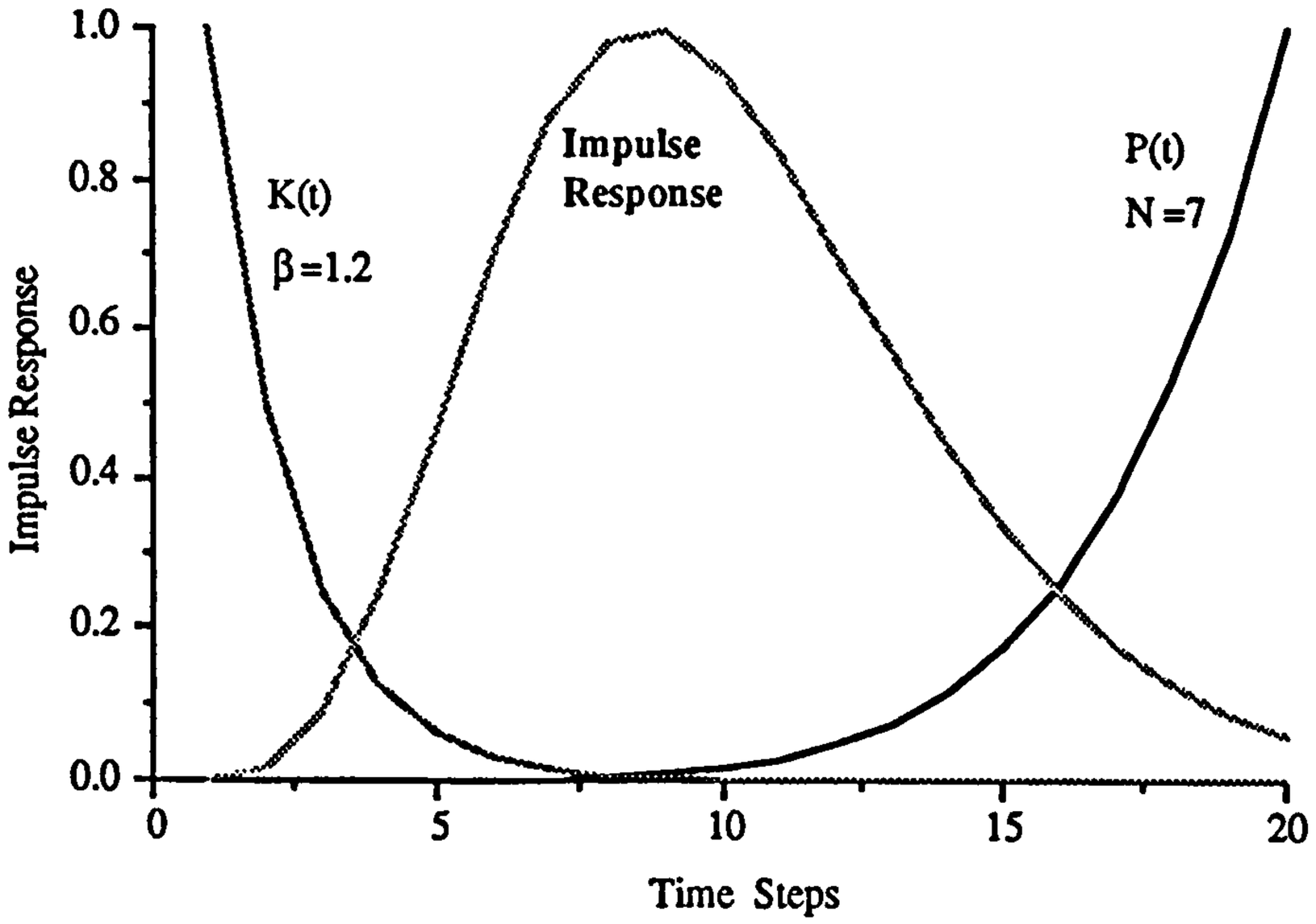

Figure 4.28 Impulse Response by Large Pole's Order

It can be observed that when the model pole's order is fixed, the shape of the TF model will change with the pole's position. The peak location of a TF model impulse response will increase when $1/\beta$ increases. The same result can be found when the model pole's position is fixed, the peak location of the TF model impulse response will increase when the model pole's order N increases. As the impulse response function h(t) is the product of the kernel function K(t) and the polynomial function P(t), it can be seen that the shape of a TF model impulse response can be changed either by altering the model pole's position or by altering the model pole's order.

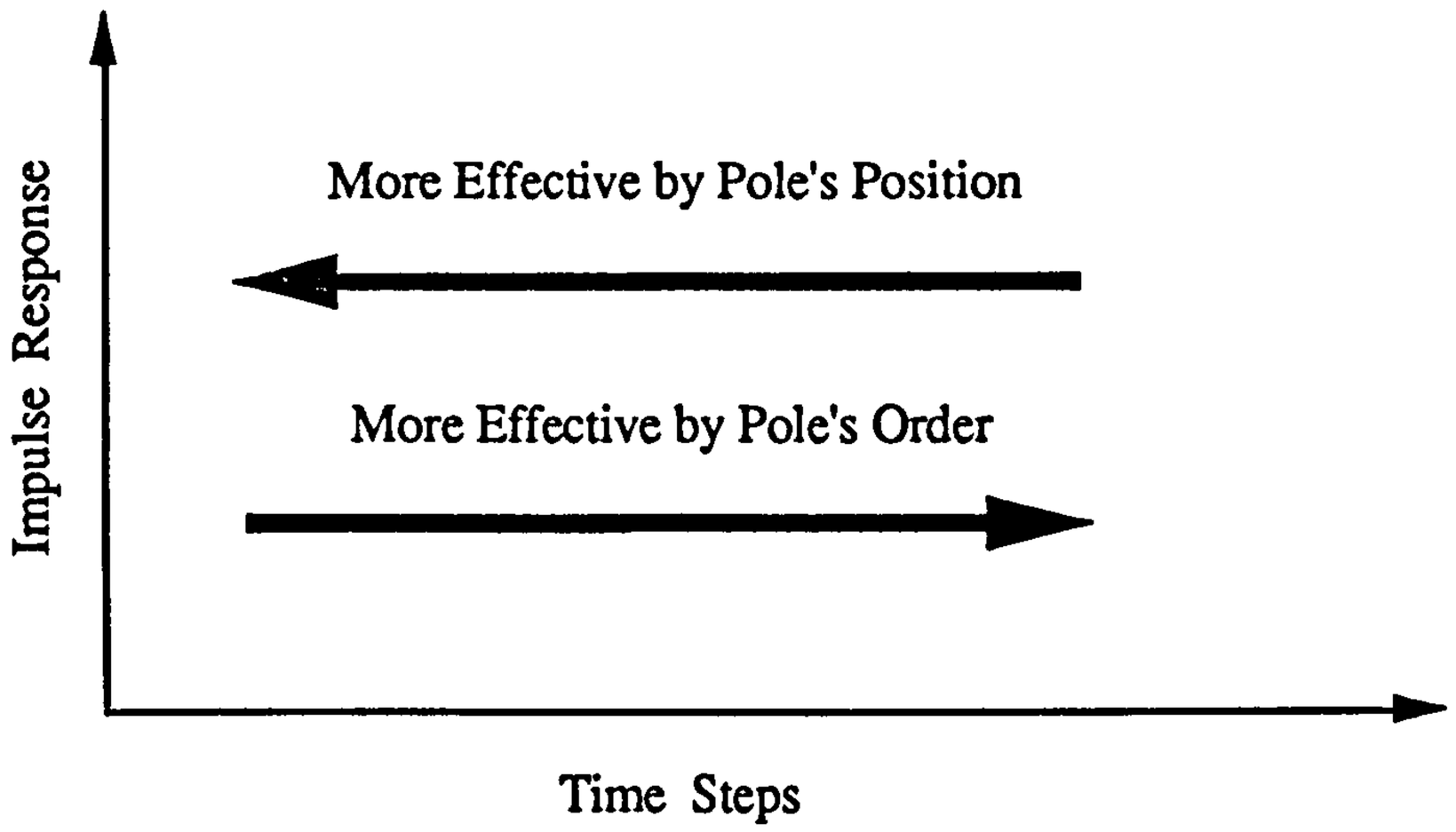

Figure 4.29 Impulse Response Sensitivity by Model Pole

Since the kernel function k(t) has more shape influence on smaller time steps, it is very effective for changing the peak of the model impulse response in this area. As the peak of the model moves to the right, it become less effective to adjust the impulse response by the kernel role. The model pole's order plays an opposite function. As the change of TF model pole's order is not a continuous process and must be integer 1, 2, . . ., etc and also the large pole's order is not reasonable for

N > 10 (this means that there is more than ten parameters for the A(z) part), the adjustment of the TF model shape by the pole's position is more practical. To achieve a desirable result, the pole's order should be kept at a reasonable low order (experience shows that N = 3 was on the low and not unreasonable side).

4.7 Summary

This chapter describes the basic theory of the Z-transform process and utilises related mathematical tools to analyse the TF model. It showed that instability, fluctuation and negative impulse response are due to incorrect pole positions. A new TF model structure (PRTF) is proposed such that all unsatifactory impulse response forms can be avoided. The resulting model is easy to identify and always in a physical realisable form.

An important feature of the PRTF is that its impulse response shape can be adjusted by directly altering the model pole's position and model pole's order. It was found that adjusting the model pole's position was more practical than adjusting the model pole's order. The identification of a PRTF will be discussed in the next chapter.

CHAPTER 5

IDENTIFICATION OF PRTF MODEL

5.1 Introduction

Identification is the process of constructing a mathematical model of a dynamic system from observation and prior knowledge. System identification includes the following

Experimental planning (Hydrological data selection)

Selection of model structure (The order of TF model)

Parameter estimation (Least square principle)

Validation (Simulation of process by the model)

This chapter concentrates on the selection of model structure and model parameter estimation.

5.2 Least Square Estimation

The identification of a TF model from the rainfall and runoff data is to estimate the model structure and parameters. The least-squares method has been used successfully in the identification of a linear system model for decades. In the present research it was found that the direct application of the least square criterion

to the TF model can yield unstable and fluctuating impulse response function which are physically unrealisable. This may be due to the nature of the historical rainfall and runoff records, which may not be accurate or long enough to provide a representative sample population, and all the information essential for satisfactory identification.

To be satisfactory, a system identification method should yield a robust result, in the sense that the computed TF model not only can reproduce historical flood hydrographs and provide a good prediction of future hydrographs from storm rainfall, but also be easy to identify.

According to Gauss (1809) the principle of least squares is that the unknown parameters of a model should be chosen in such a way that *the sum of the squares of the differences between the actually observed and computed values multiplied by numbers that measure the degree of precision is a minimum.* To be able to give an analytic solution, the computed values must be linear functions of the unknown parameters.

In the general least-square problem, the model utilised relates an observed variable y_t, the regressand, to p explanatory variables, the regressors u_{1t} to u_{pt}, all known in advance or observed. In dynamic models like the TF model the sample-index variable t is time. The model has one unknown coefficient θ_i per explanatory variable. If the u's for one sample and θ's are collected into p-vectors such that :

$$ut = [\, u_{1t},\ u_{2t},\ \ldots\ u_{pt}]^T \qquad (5,1)$$

$$\theta = [\, \theta_1,\ \theta_2,\ \ldots\ \theta p]^T$$

then the model is given by :

$$yt=f(u_t,\theta) + e_t, \quad t= 1, 2, 3, \ldots, N \tag{5,2}$$

where e_t accounts for observation error (measurement noise) and modelling error, since even without observation error few models are perfect. We aim to find the value Θ of θ which minimises

$$S \triangleq \sum_{t=1}^{N} e_t^2 = \sum_{t=1}^{N} (y_t - f (u_t , \theta))^2 \tag{5,3}$$

for the practically useful case where f(. , .) is linear in the unknown coefficients making up θ. That is

$$y_t = u_t^T \theta + e_t, \qquad t = 1, 2, 3, \ldots, N \tag{5,4}$$

To make the algebra tidy, collect all the samples y_1 to y_N into a N-vector **y**, all the u_t vectors into an Nxp matrix U and e_1 to e_N into **e**, giving

$$y = U\theta + e$$

and

$$S = e^Te = (y^T - \theta^TU^T)(y-U\theta)$$

The θ that makes the gradient of S zero is therefore

$$\Theta = [\, U^T U]^{-1}\, U^T\, y \qquad (5,5)$$

Such a process is a batch algorithm that processes all the observations of y and u simultaneously and produces a single estimate of the parameter vector. By contrast, the recursive methods process the observations one sampling instant at a time and update the parameter estimates each time. Batch algorithms are suitable only when estimates are required once and for all or at long intervals, or when computing is cheap, since they process the entire record every time. Most real-time applications are better met by recursive algorithms since time and computing power are strictly limited. In this thesis, the recursive least square algorithm is adopted to estimate the TF model parameters.

The recursive least square algorithm for the ordinary TF model is given by :

$$y_t = a_1\, y_{t-1} + a_2 y_{t-2} + \cdots a_N y_{t-N} + b_0\, u_t + b_1 u_{t-1} + \cdots + b_M u_{t-M} \qquad (5,6)$$

$$\hat{\Theta}_{t+1} = \hat{\Theta}_t + K_{t+1}\,[\, y_{t+1} - X_{t+1}^T\, \hat{\Theta}_t\,] \qquad (5,7)$$

where

$$K_{t+1} = P_t\, X_{t+1}\,[\, X_{t+1}^T\, P_t\, X_{t+1} + 1\,]^{-1}$$

$$P_{t+1} = [\, I - K_{t+1}\, X_{t+1}^T\,]\, P_t$$

$$\hat{\Theta}_t = \begin{bmatrix} a_1 \\ a_2 \\ \vdots \\ a_N \\ b_0 \\ b_1 \\ \vdots \\ b_M \end{bmatrix} \qquad X_t = \begin{bmatrix} y_{t-1} \\ y_{t-2} \\ \vdots \\ y_{t-N} \\ u_t \\ u_{t-1} \\ \vdots \\ u_{t-M} \end{bmatrix}$$

The general least square method can't directly be applied to the identification of the PRTF model. Some modification had to be made to utilise the idea.

5.3 Identification of PRTF

Estimating the parameters of a PRTF is not a linear parameter estimation problem and modification is needed to utilise the least square estimation procedure. As the parameters for y are controlled by the A(z) part, a two step procedure was adopted to estimate the A(z) and B(z) separately.

5.3.1 Parameter Estimation for A(z)

The parameters for A(z) are controlled by the root value of A(z) and the correct choice of pole locations β and the pole order is important. From the last chapter it was shown that the shape of the impulse response of 1/A(z) can be described as

For N = 1

$$h(t) = \left(\frac{1}{\beta}\right)^t \qquad (5,5a)$$

where $t = 1, 2, \ldots,$

For $N \geq 2$

$$h(t) = \frac{(N-1+t)\,(N-2+t)\,\ldots\,(1+t)}{(N-1)\,!}\,\left(\frac{1}{\beta}\right)^{t} \qquad (5,5b)$$

where $t = 1, 2, \ldots,$

The pole order and pole location can both influence the behaviour of the TF model. A pole order N of 2 or 3 or more is desirable for the adjustability of the PRTF model. But in practice, a TF model will have too long a memory and not be parametrically concise. It was found that with the same peak location a large pole order N can produced a narrow impulse response function as in Figure 5.1.

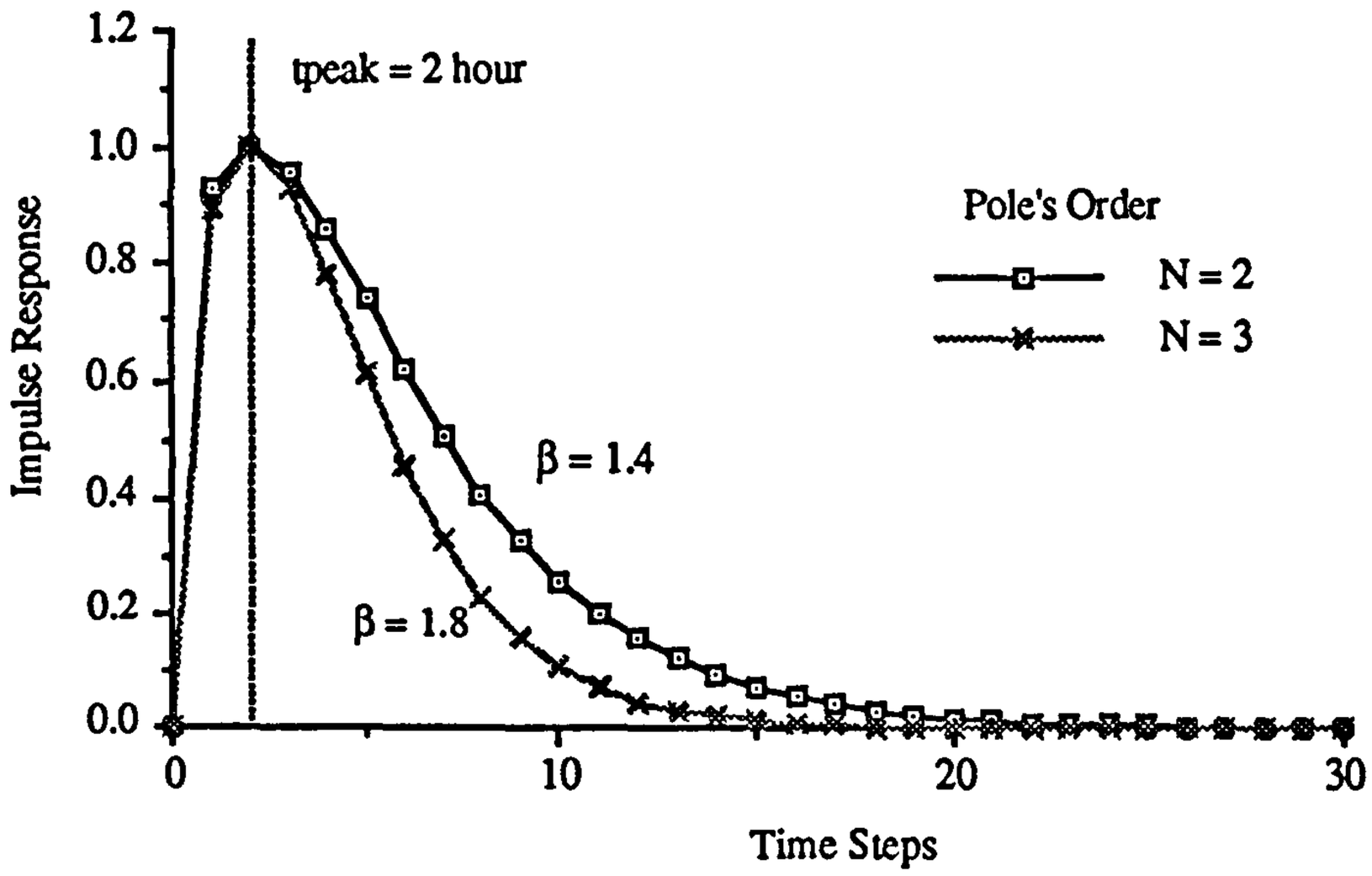

Figure 5.1 A Narrowing Effect by Pole's Order Increasing in Low Peak Time

The effect is more obvious when the pole location β becomes large. A narrow impulse response function can accommodate more cases than a broad one. Another

interesting fact is that a pole order will not influence the rising limb as much as the recession limb. This can explain the situation that some TF models can simulate the rising limb very well but the recession limb very poorly.

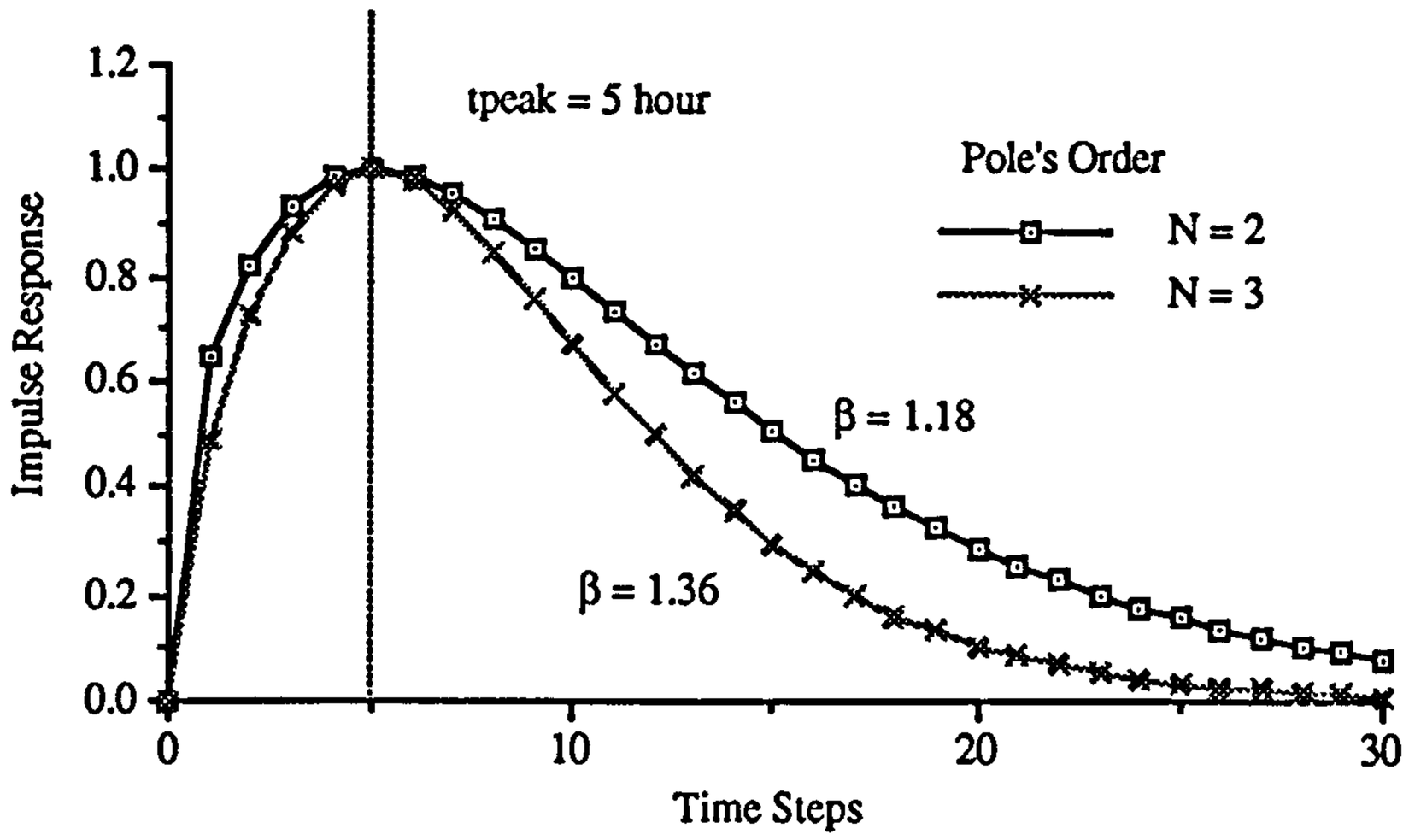

Figure 5.2 A Narrowing Effect by Pole's Order Increasing in High Peak Time

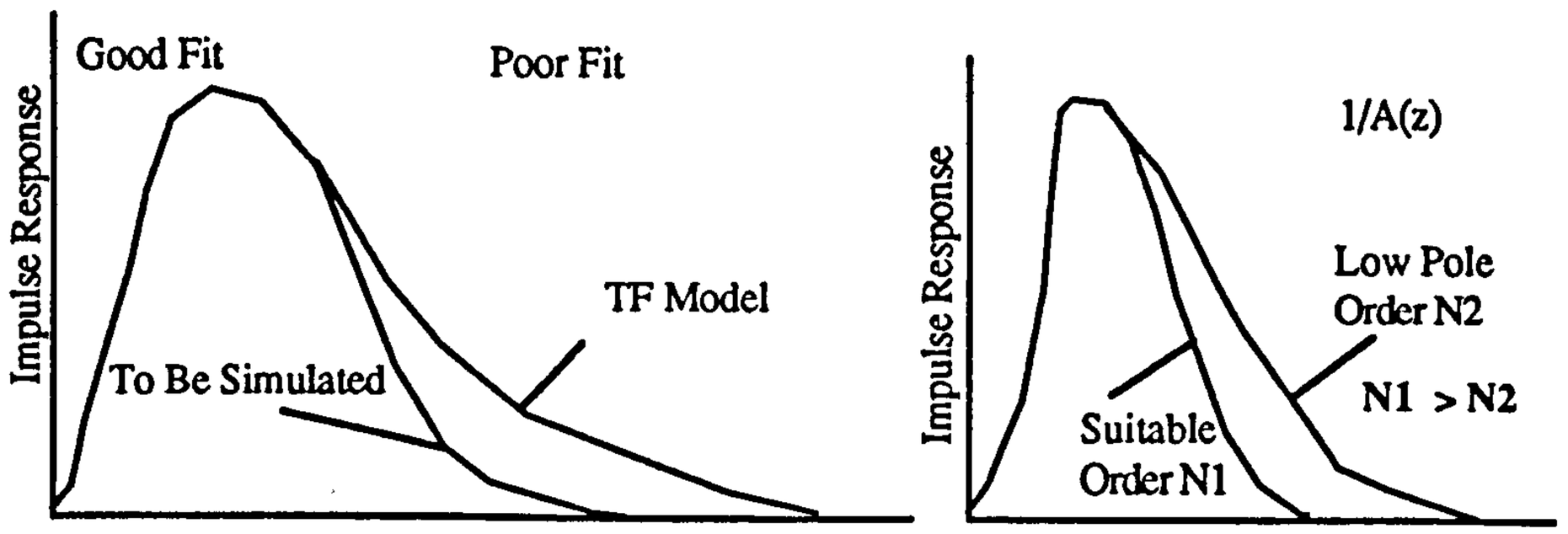

Figure 5.3 A Typical Phenomenon For TF Model With Low Pole Order

The solution to the overshooting recession limb is to select a narrow impulse

response of 1/A(z) compared with the hydrological system to be simulated. This is not meant that a higher pole order must be selected. In fact there are two solutions which can be adopted. One is to select a high order; Another is to use negative b_i parameters to force the the recession limb down. As a high pole order is not easy to be handled as mentioned before ($N \approx 3$ is suggested in this thesis), the negativity of b_i parameters is more practical. This is why the PRTF b_i positive condition in chaper 4 was removed in the course of practice.

As the shape change of impulse response is not linear with the β value and also the root value β is very abstract so that it is not convenient to adjust the β value. In Chapter 6,a relationship has been found such that the peak time t_{peak} of the impulse response from 1/A(z) is closely related to the root value β. For commonly used second and third order A(z) PRTF, we have derived a relationship :

For N = 2

$$t_{peak} = \frac{1}{\ln \beta} - 1 \tag{5,8}$$

$$\beta = e^{\frac{1}{(t_{peak}+1)}} \tag{5,9}$$

For N = 3

$$t_{peak} = \frac{\frac{2}{\ln \beta} - 3 + \sqrt{(3 - \frac{2}{\ln \beta})^2 - 4(2 - \frac{3}{\ln \beta})}}{2} \tag{5,10}$$

$$\beta = e^{\frac{2t_{peak}+3}{(t_{peak}^2 + 3t_{peak} + 2)}}$$

When the right t_{peak} is known, A(z) parameters can be easily computed from

$$a_i = - C_N^{N-i} \ (- \beta)^{-i} \qquad (5,11)$$

where $i = 1, 2, \ldots N$

At initialisation, t_{peak} can be roughly estimated as

$$t_{peak} = C_t - M \qquad (5,12)$$

where

C_t ----- Estimated Catchment Response Time

M ---- The Number B(z) parameters

If there is no idea about the catchment response time, a zero value can used as an initial t_{peak} estimate. That is :

$$t_{peak} \ |_{k=1} = 0 \qquad (5,13)$$

An optimisation technique is needed here to achieve an optimum (or least error) t_{peak} value.

A TF model from the River Tone at Greenham in the Wessex Region is used to illustrate the influence of t_{peak} on the PRTF model.

Rainfall is generated from pseudo random generator and is represented in Figure 5.4.

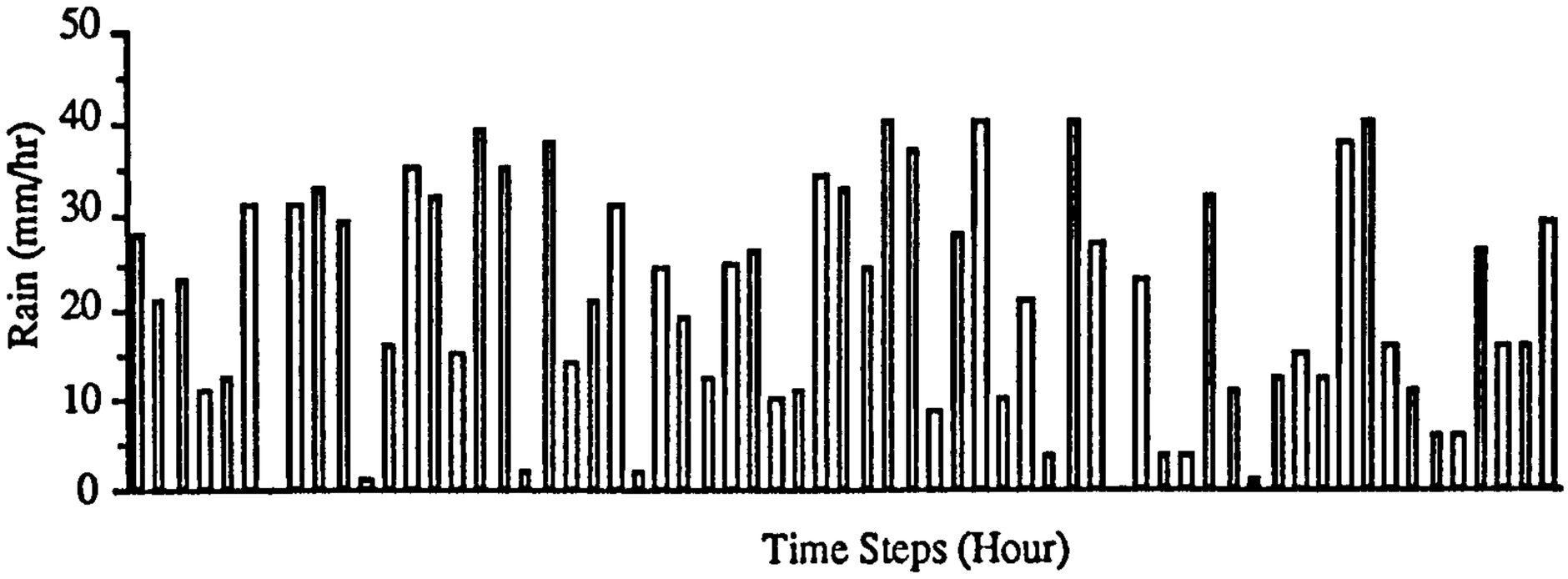

Figure 5.4 Rainfall Data for River Tone

From Eq(5,6) - Eq(5,9), a relation between t_{peak} and β can be illustrated in Figure 5.5. It is found that a nonlinear reletionship exists between t_{peak} and β. t_{peak} approaches zero when β is increasing and will increase infinitely when β is close to 1.0. This is the reason that β is not easily adjusted compared with t_{peak}.

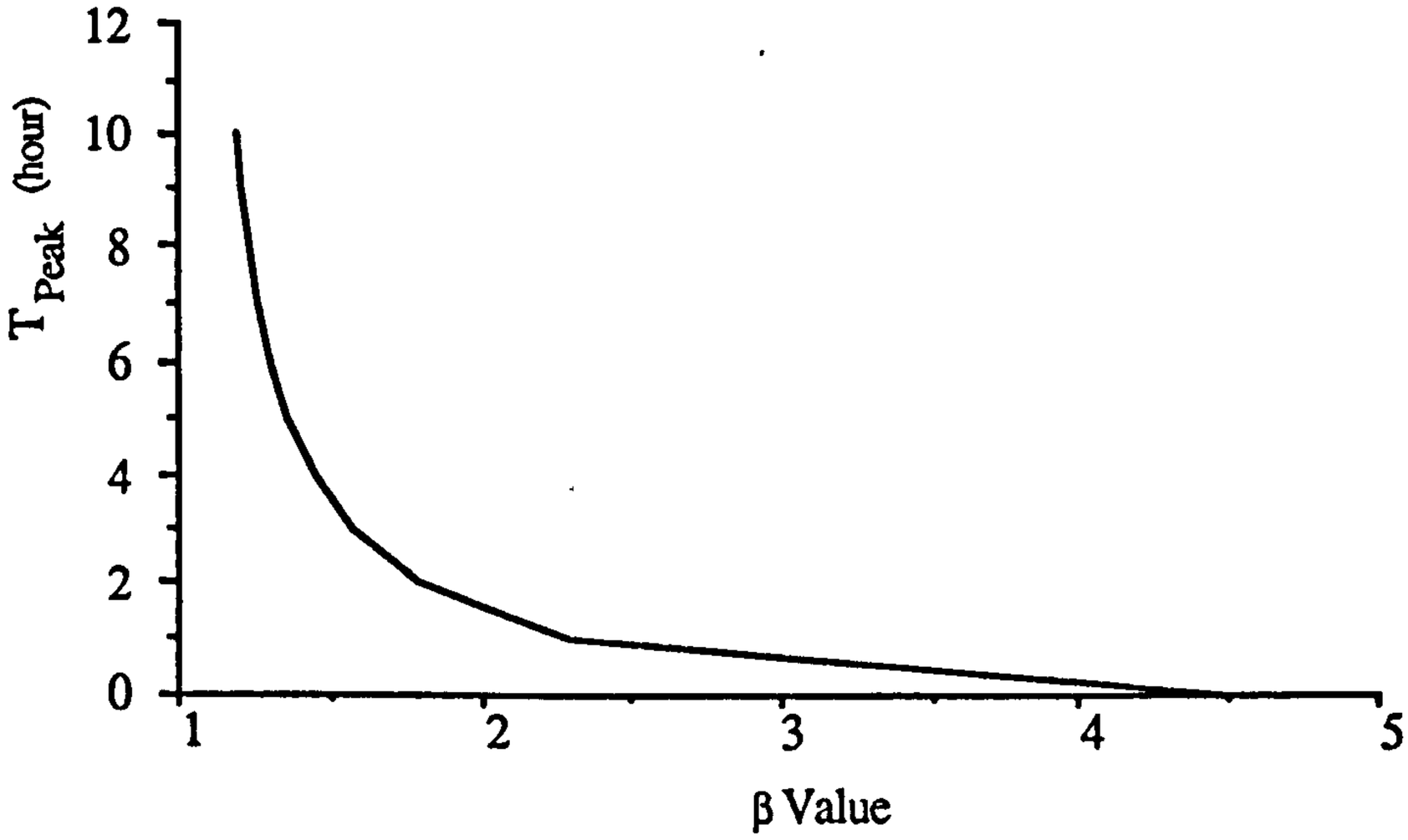

Figure 5.5 Relation between β and T_{peak}

River flow data is convoluted with the unit hydrograph model to give measured

flow.

UH peak flow PO = 20 cumecs; (Refer to page 145 for the detail)

UH time to peak TO = 5 Hrs;

UH duration of steep recession WO = 8 Hrs;

UH duration of shallow recession BO = 24 Hrs;

To identify a suitable t_{peak} for the River Tone model, 11 t_{peak} values were chosen to depict the influence of t_{peak} on the goodness of fit . From Figure 5.6 it can be seen that there is a distinct minimum error location and this makes it easy to identify the correct t_{peak}. Finally $t_{peak} = 3.7$ was selected as the model parameter.

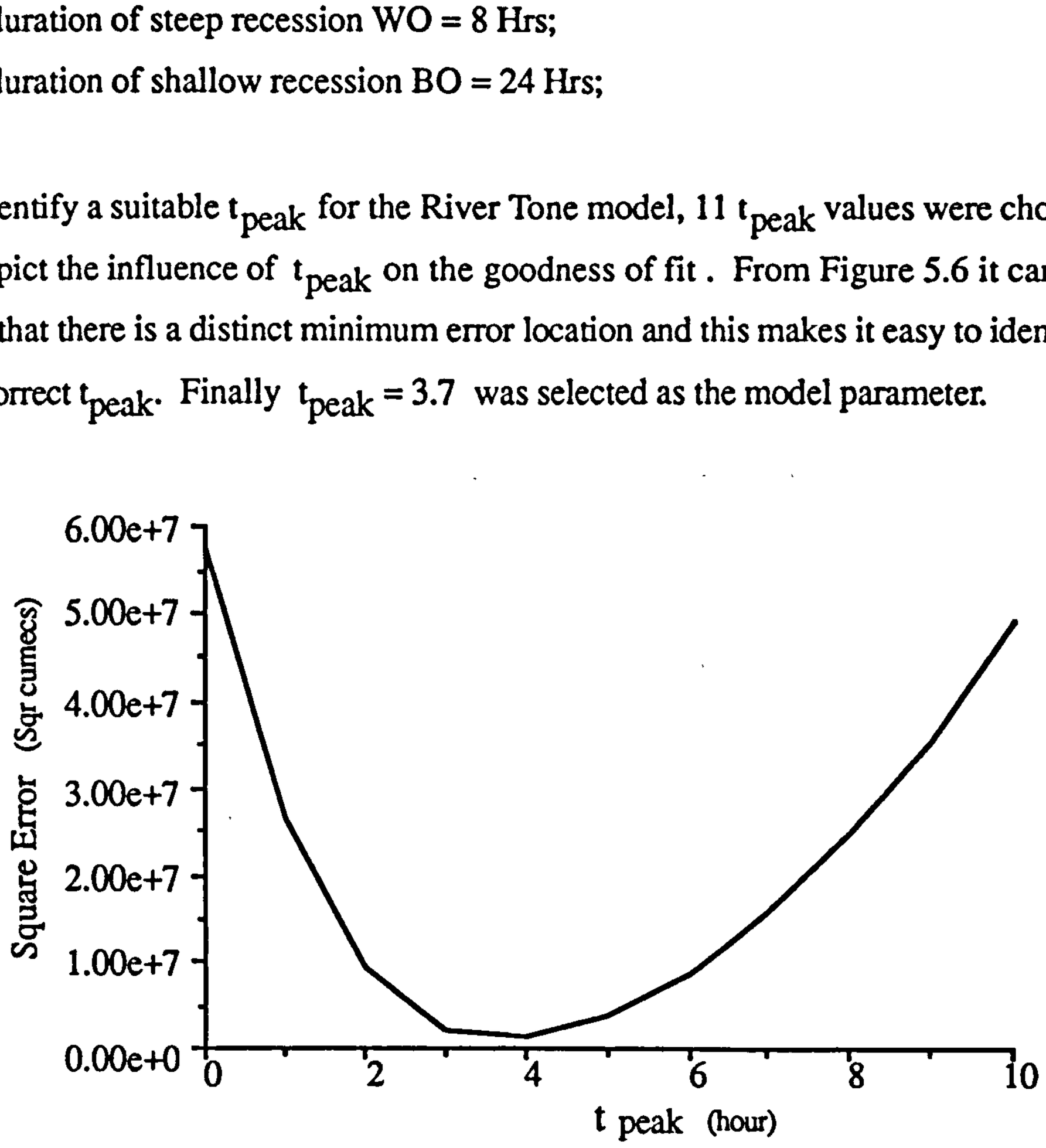

Figure 5.6 Influence of t_{peak} on the Goodness of Fit of TF Model

The square error is derived by

$$\text{Square Error} = \sum_{i=1}^{N} (F_m - F_p)^2$$

Where F_m is measured flow and F_p is predicted flow.

The simulated flow is illustrated in Figure 5.7.

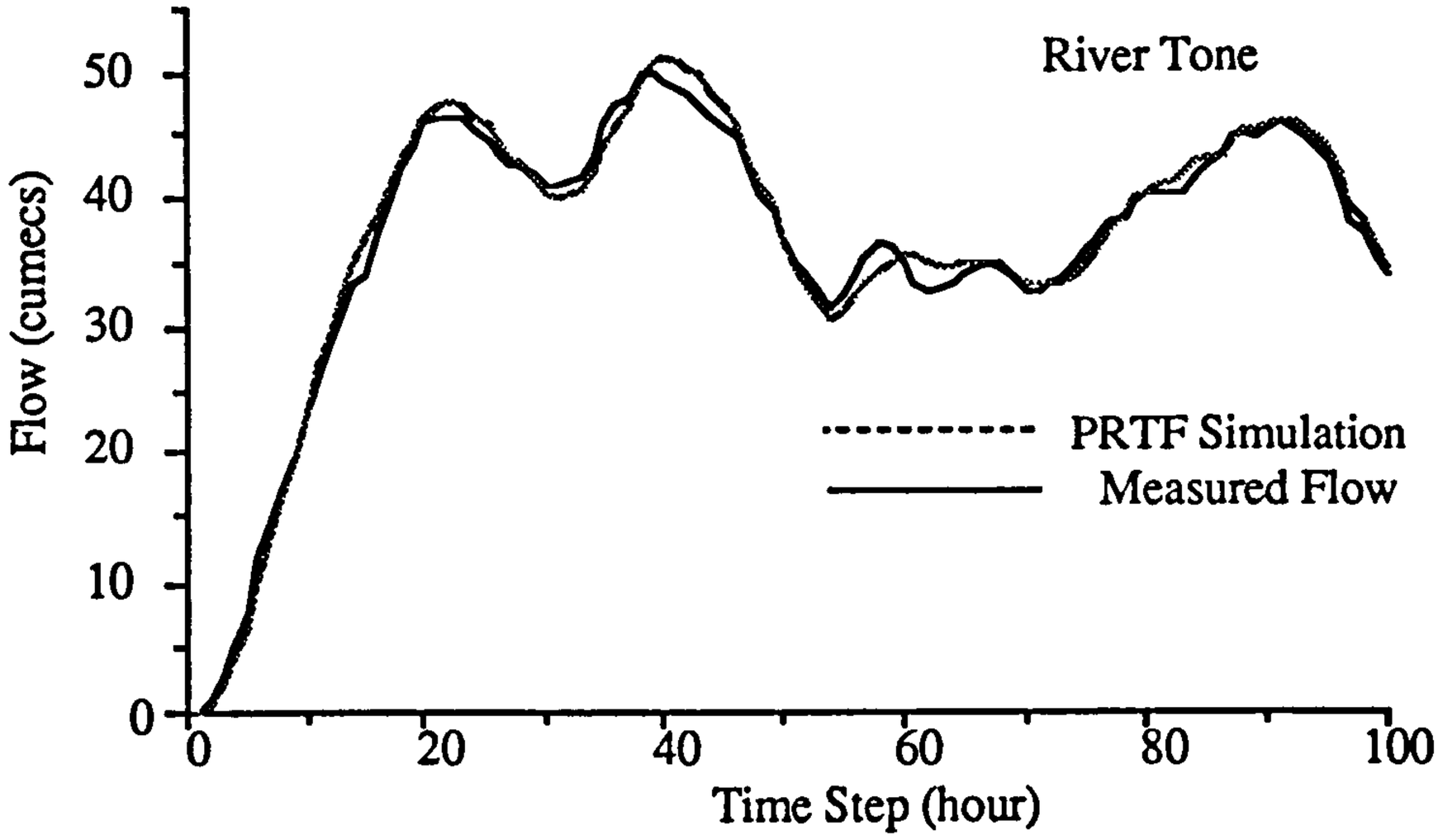

Figure 5.7 River flow for River Tone

The identified model parameters are :

(3,5) model with T_{peak} =3.7, β= 1.474

b(0)=3.2194; b(1)= 0.5330; b(2) = -0.2407; b(3)=2.3829; b(4)=0.8012

5.3.2 Parameter Estimation for B(z)

When the A(z) parameters are selected, according to the least square principle, the procedure to identify B(z) can be derived as below.

To simplify the equation, a new variable ζ is introduced to replace the original y.

$$\zeta_t = y_t - \sum_{i=1}^{N} a_i \, y_{t-i} \tag{5.14}$$

$$a_i = - C_N^{N-i} \, (- \beta)^{-i}$$

The identified system can be expressed as

$$\zeta = X\Theta + e \tag{5,15}$$

or $$\zeta_t = b_0 \, u_t + b_1 u_{t-1} + \ldots + b_M u_{t-M}$$

Parameters for B(z) can be estimated as

$$\hat{\Theta}_{t+1} = \hat{\Theta}_t + K_{t+1} [\zeta_{t+1} - X_{t+1}^T \hat{\Theta}_t] \tag{5,16}$$

where

$$K_{t+1} = P_t \, X_{t+1} [X_{t+1}^T \, P_t \, X_{t+1} + 1]^{-1}$$

$$P_{t+1} = [I - K_{t+1} \, X_{t+1}^T] \, P_t$$

$$\hat{\Theta}_t = \begin{bmatrix} b_0 \\ b_1 \\ b_2 \\ \cdot \\ \cdot \\ \cdot \\ b_M \end{bmatrix} \qquad X_t = \begin{bmatrix} u_t \\ u_{t-1} \\ u_{t-2} \\ \\ \\ \\ u_{t-M} \end{bmatrix}$$

Computation Process:

$$P_t \rightarrow K_{t+1} \rightarrow \hat{\Theta}_{t+1} \rightarrow P_{t+1}$$

Initialisation:

$$t = 1 , \qquad P_1 = 1000\ I$$

$$\hat{\Theta}_1 = \begin{bmatrix} 0 \\ 0 \\ 0 \\ \cdot \\ \cdot \\ \cdot \\ 0 \end{bmatrix}$$

Kt, P_t and Θ_t are updated with the addition of each rainfall and runoff event.

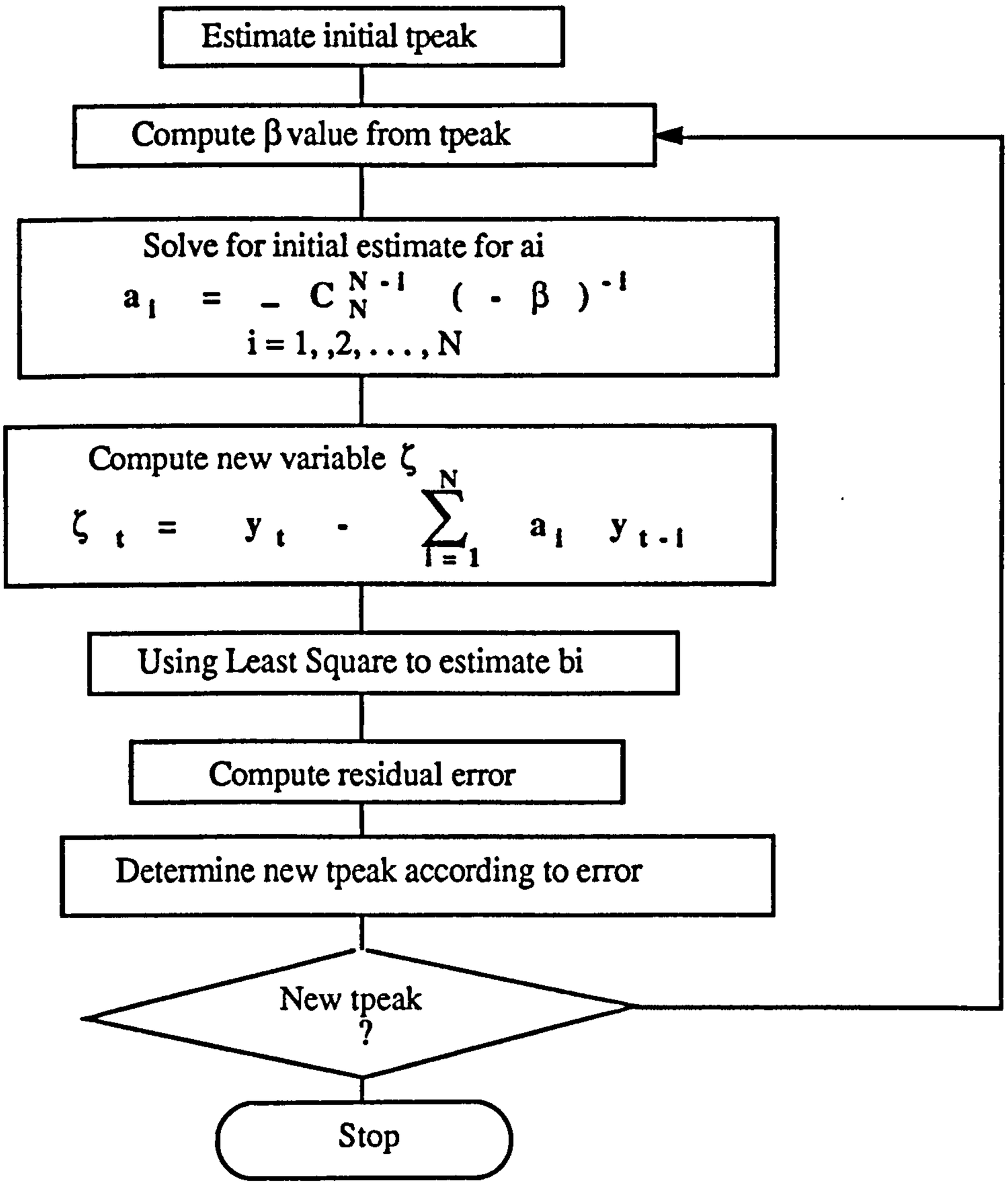

Figure 5.8 Flowchart for PRTF Identification

A flowchart for the PRTF model estimation is presented in Figure 5.8.

5.4 Transformation of TF Model into PRTF Model

Many TF models exist in the water industry which need to be transferred into PRTF form before using them for real-time robust updating. In principle, PRTF and the

ordinary TF model are in the same family except that the PRTF should follow a specific law as described in Chapter 4. To identify the PRTF from the ordinary TF model, flow data are generated from the TF model by inputing pseudo random rainfall data. A modified least square scheme described in last section is then used to identify the PRTF model. A case study to transfer TF models from the River Asker and River Stour into PRTF models and examination of the differences between two types of TF models is presented below.

The relationship between sampled rainfall data and flow data are illustrated in Figure 5.9. River flow data are instanuously sampled while the radar rainfall data are averaged over the last hour.

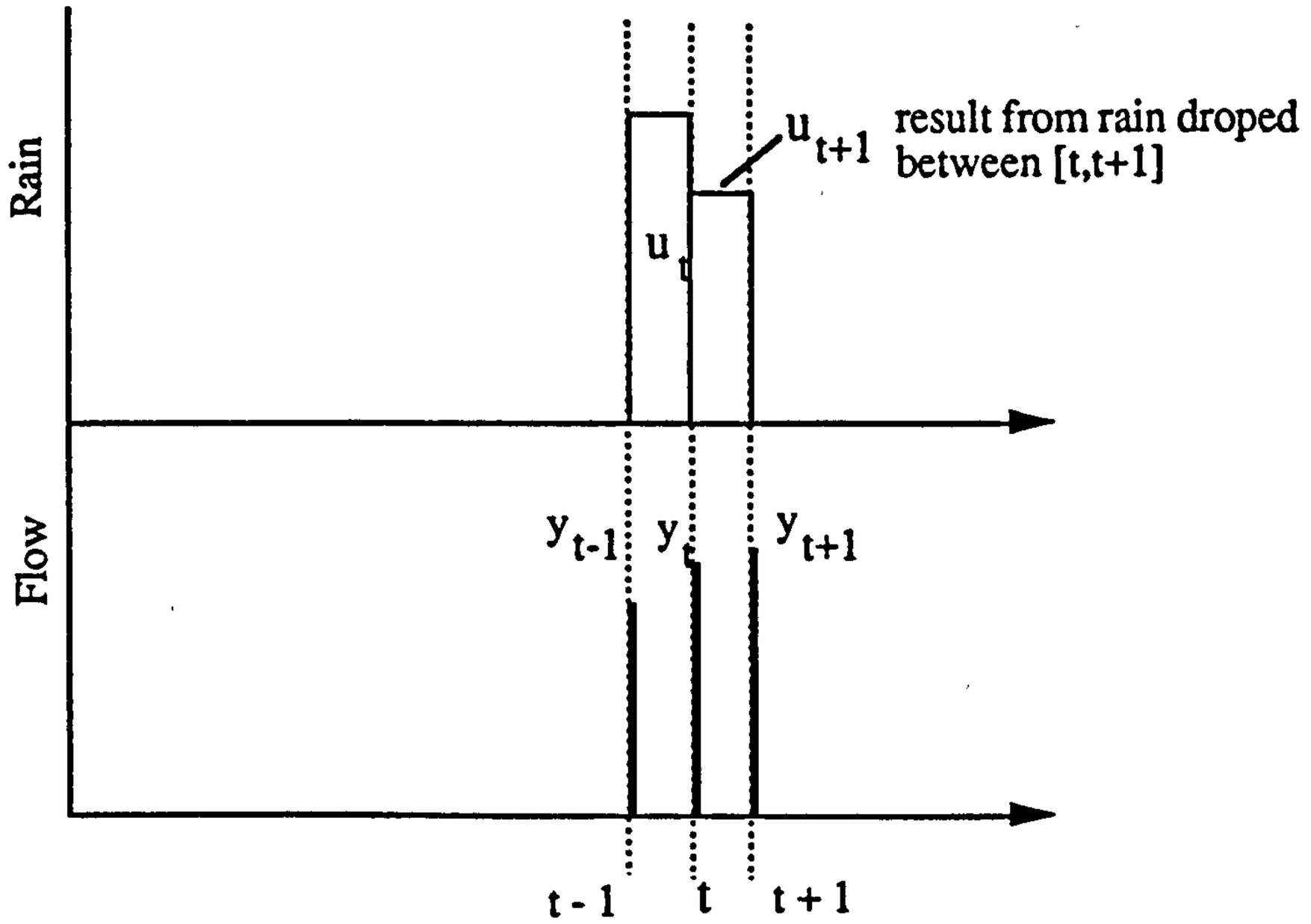

Figure 5.9 Relation between Sampled Rain and Flow Data

The time lag influence on the TF model impulse response is presented in Figure 5.10.

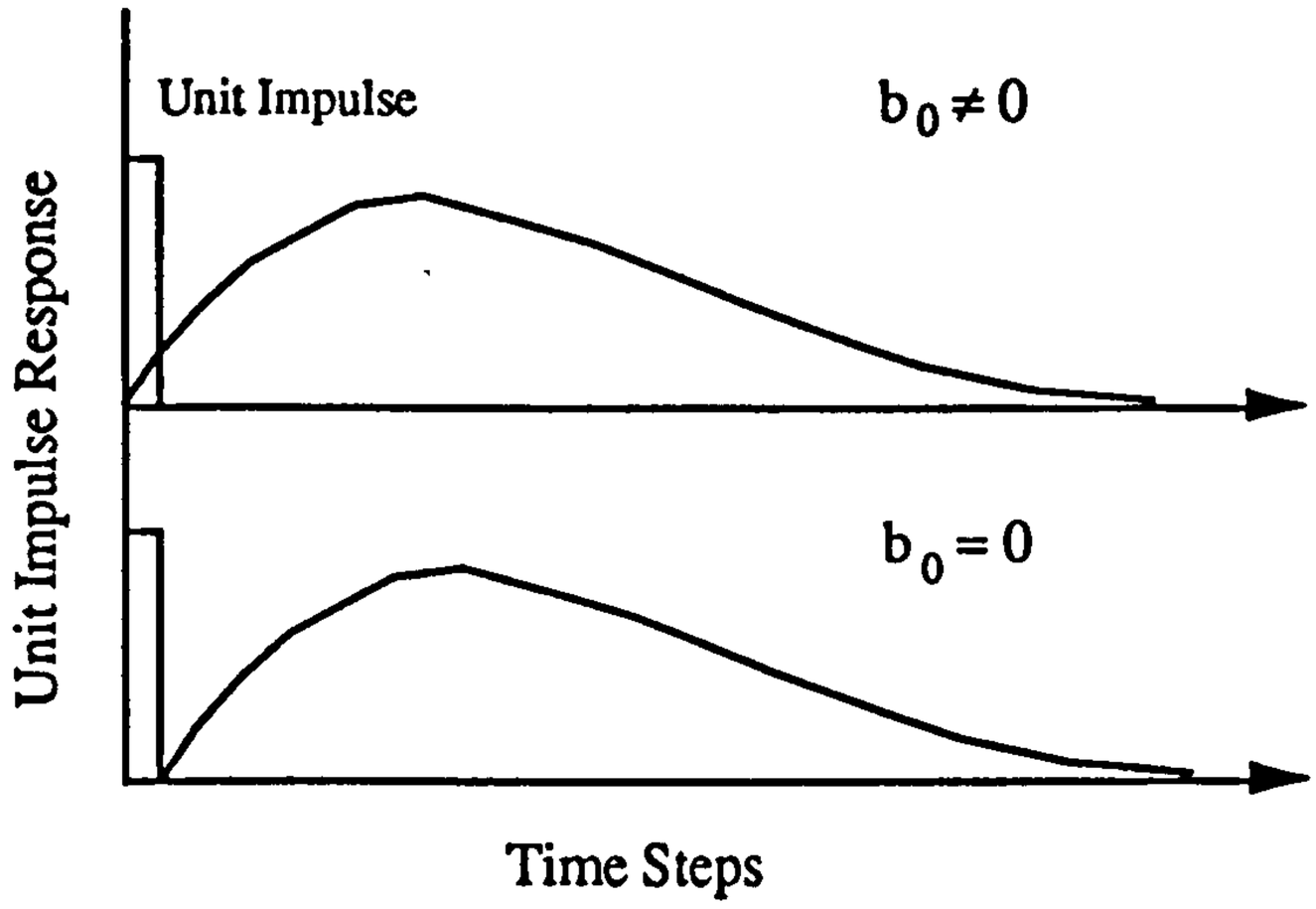

Figure 5.10 Effect of Time Lag on Impulse Response of TF Model

River Asker (at Bridport) TF (3,3) Timestep = 1 hr

$$yt+1 = 1.3756y_t - 0.7086y_{t-1} + 0.2094y_{t-2} + 0.1183u_t + 0.1358u_{t-1} + 0.1139u_{t-2}$$

This model has a 1 step time lag. For PRTF identification, there is usually no time lag in the model structure because the selected storm for the catchment should be evenly distributed. During real time forecasting, the time lag of the PRTF will be variable according to the situation.

First the t_{peak} is to be estimated. From Figure 5.11 it can be found that t_{peak} = 1.5 is suitable.

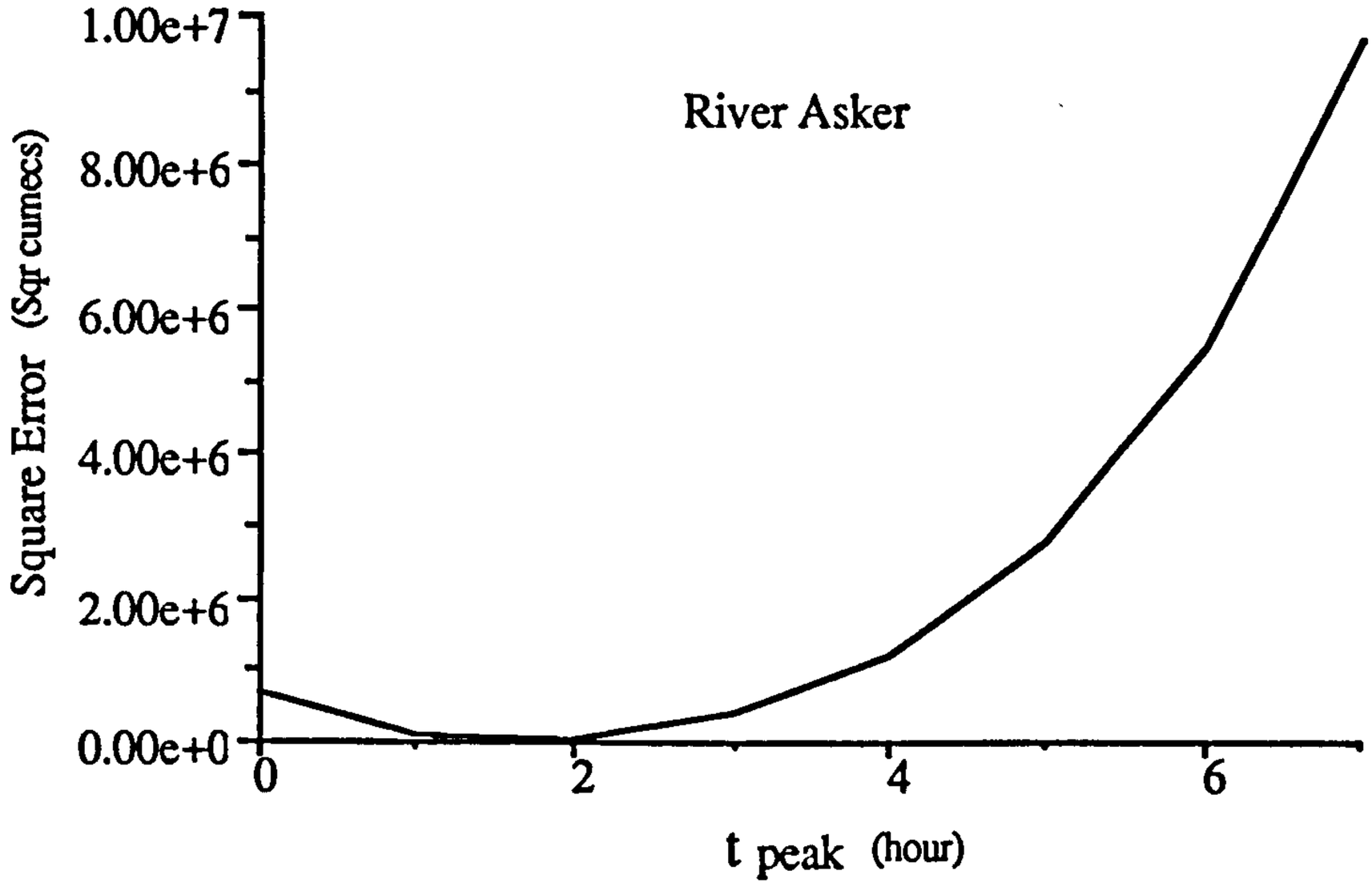

Figure 5.11 Selection of tpeak Value for River Asker

The impulse response of the River Asker Model is represented in Figure 5.12.

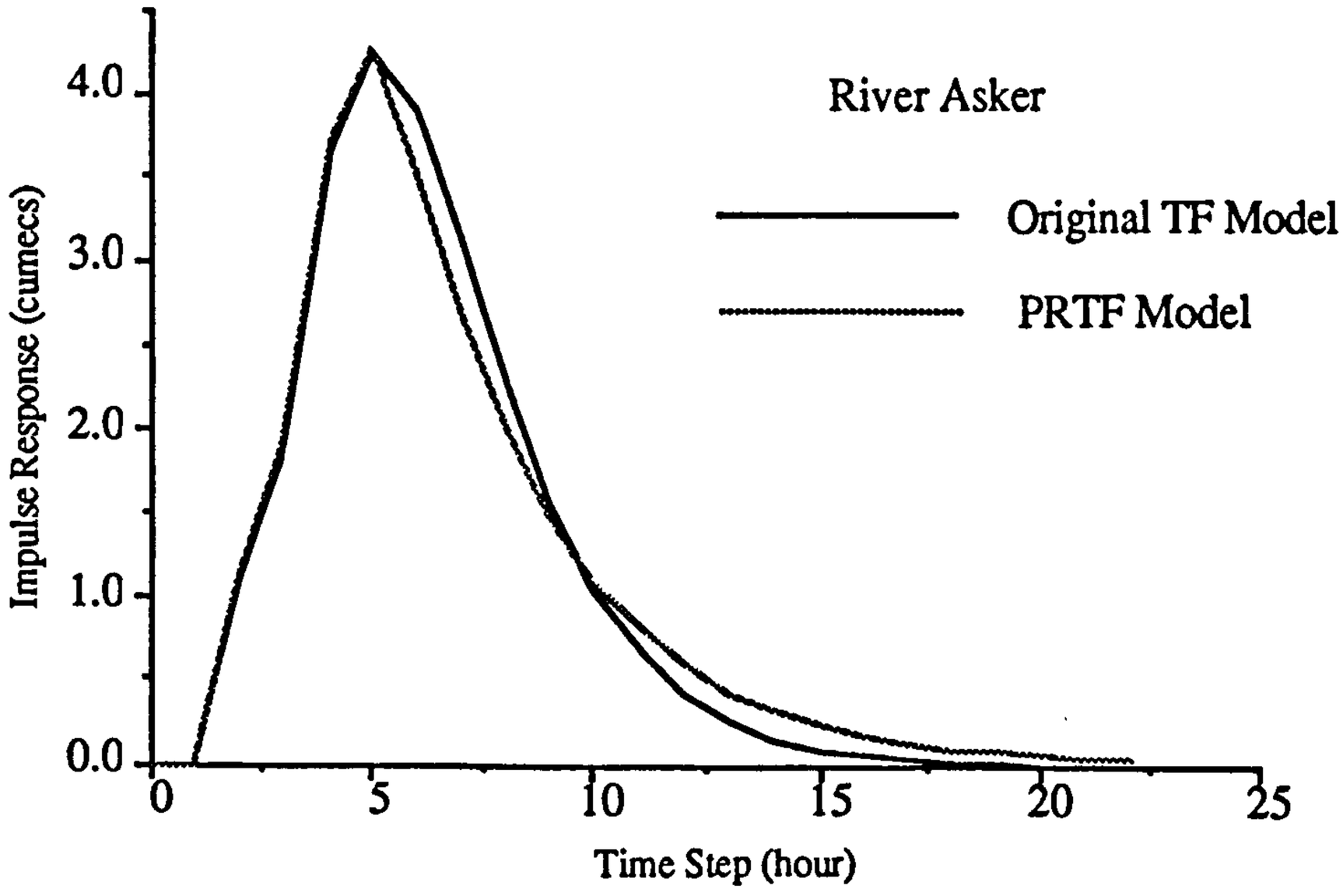

Figure 5.12 Impulse Responses of Two Types of TF Model for River Asker

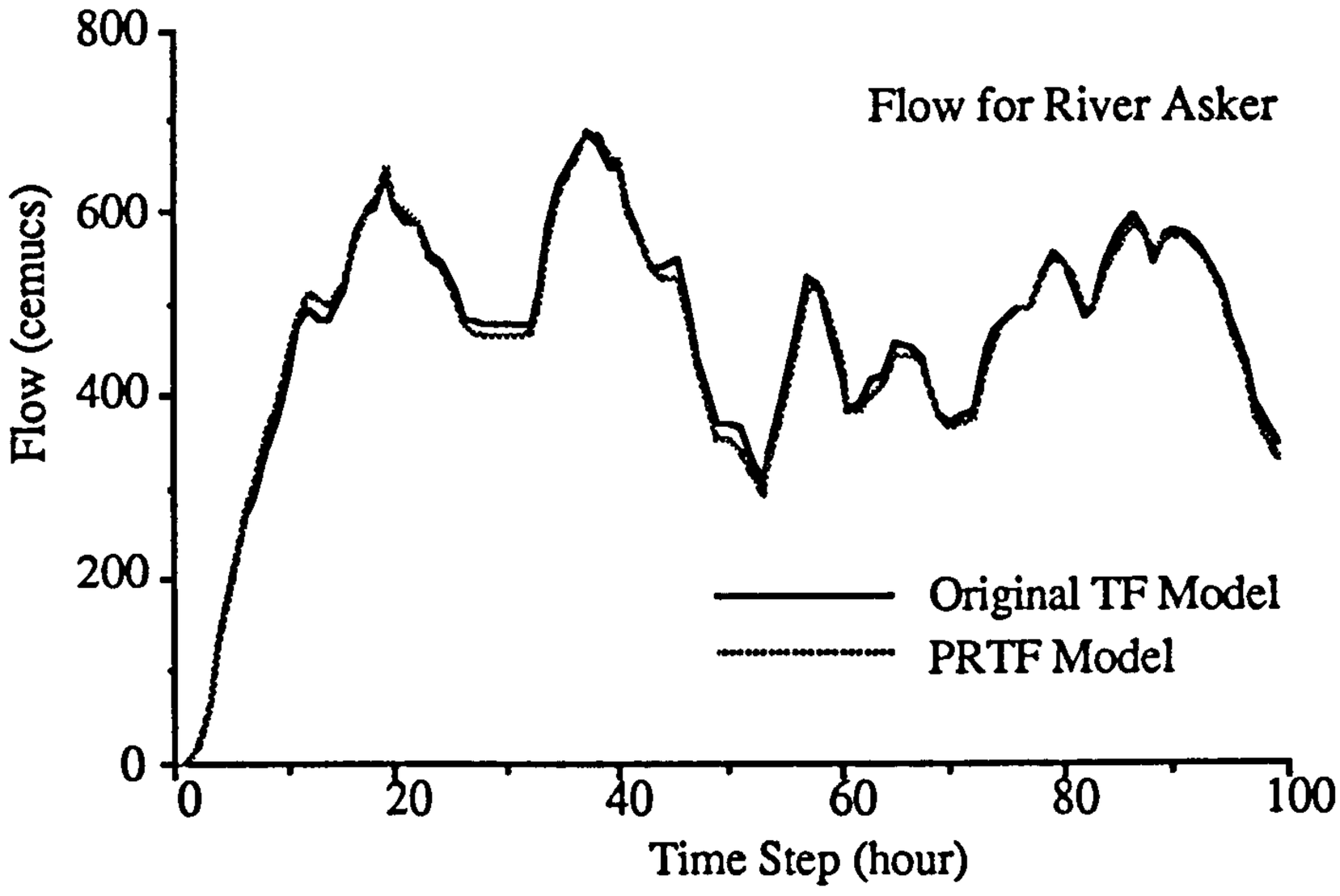

Figure 5.13 Simulated River Flow from Two Types of TF Models for River Asker

The identified PRTF for the River Asker is

Tpeak =1.5, β = 1.985

a(1) = 1.5112

a(2) = - 0.761

a(3) = 0.128

b(1) = 1.1105

b(2) = 0.1318

b(3) = 1.7423

The identification results indicate that a good simulation can be achieved by the PRTF model. Both the impulse response function and the river flow simulation are very close.

The PRTF model for the River Stour can be derived in the same way. From Figure

5.14, t_{peak} can be found as 2.2 steps.

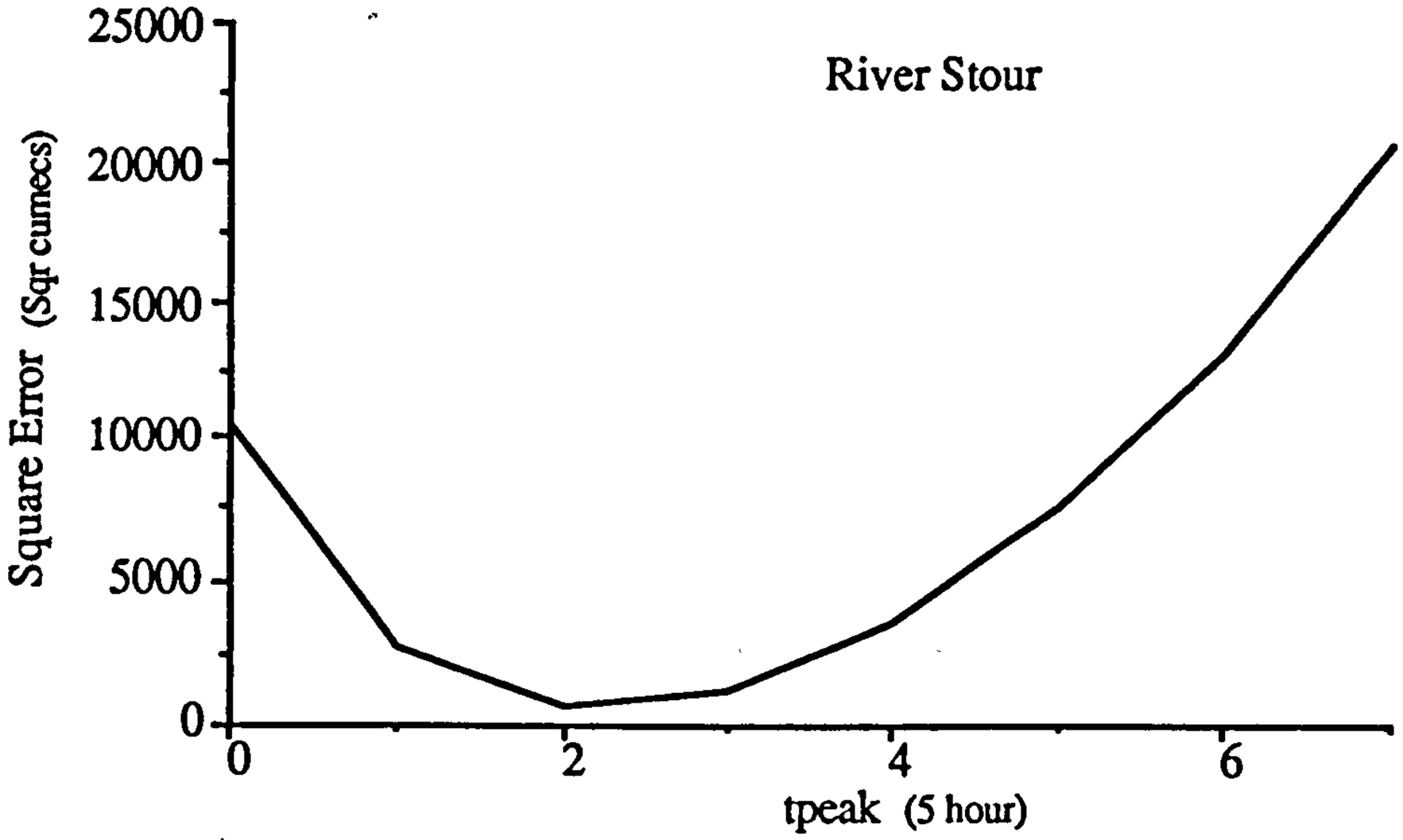

Figure 5.14 Selection of tpeak Value for River Stour

Impulse response of River Stour model is represented in Figure 5.15.

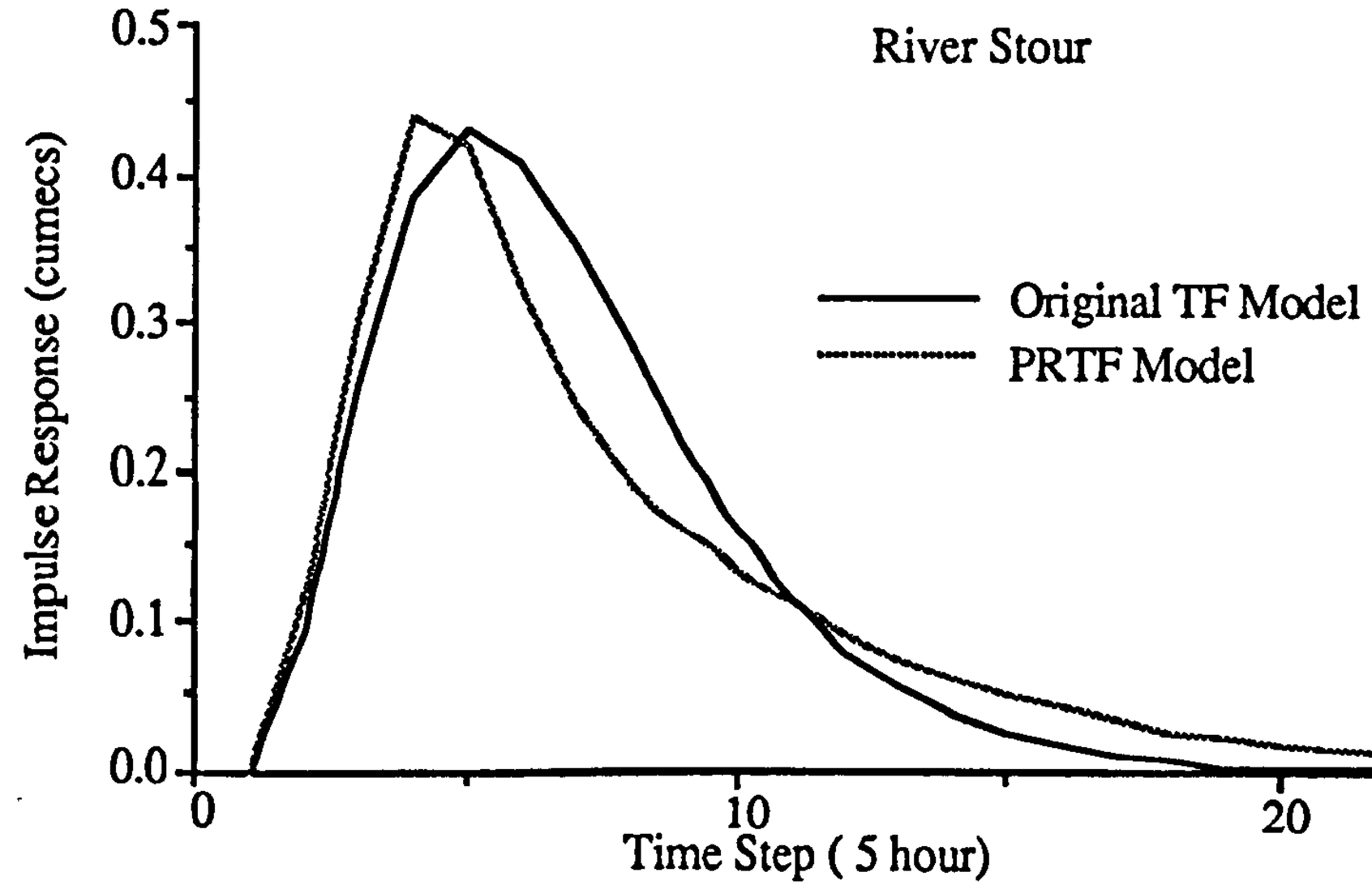

Figure 5.15 Impulse Responses of Two Types of TF Model for River Stour

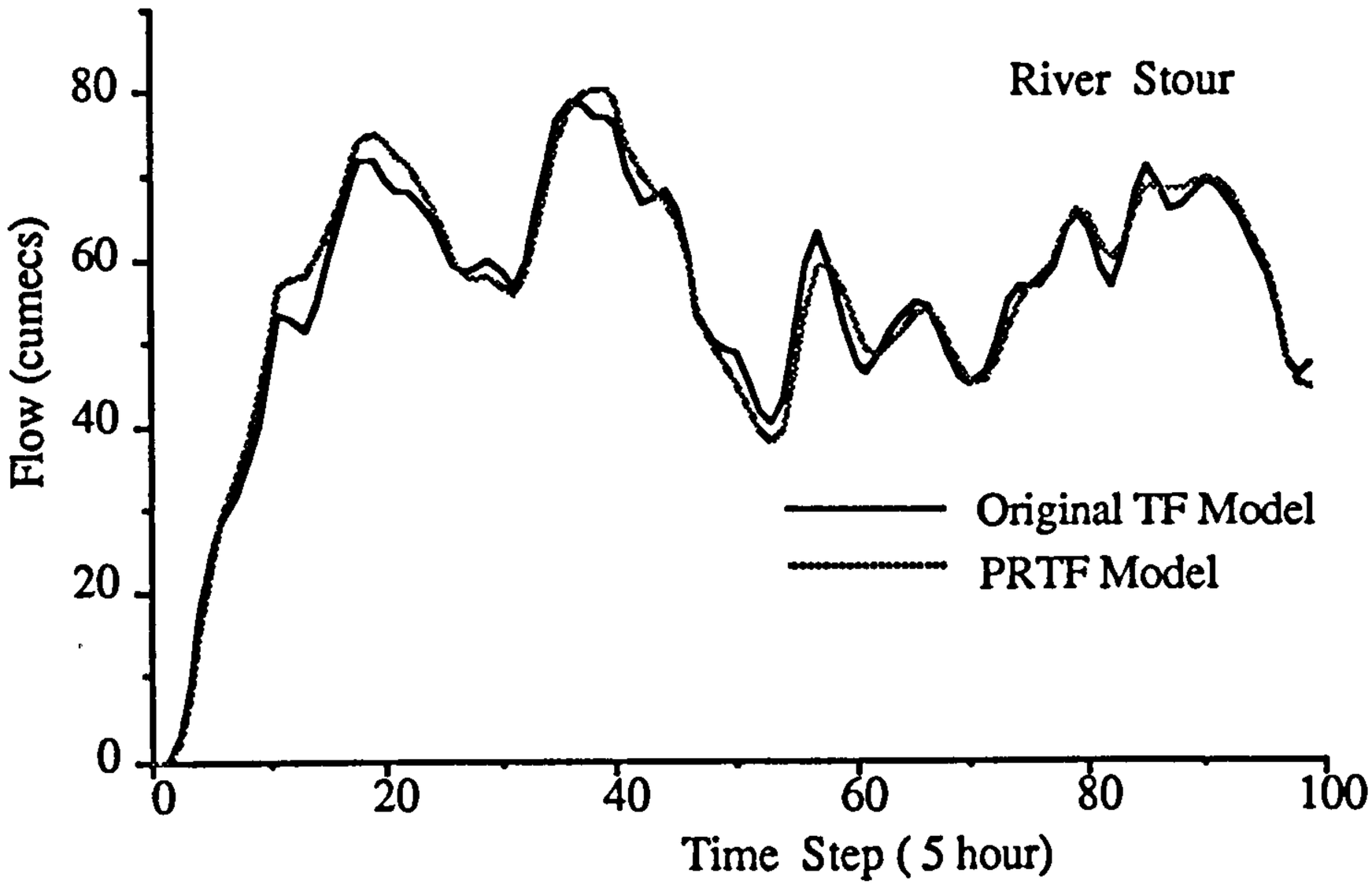

Figure 5.16 Simulated River Flow from Two Types of TF Models for River Stour

The identified PRTF for the River Stour is

Model (3,3) with Tpeak =2.2, β = 1.73

a(1) = 1.730

a(2) = - 0.997

a(3) = 0.192

b(1) = 0.0951

b(2) = 0.0903

b(3) = 0.0397

For the River Stour, the impulse response functions of the TF and the PRTF are as close as for the River Asker, and the river flow simulations are very close from both models.

5.5 Transformation of UH Model into PRTF

The unit hydrograph is a popular technique widely used in the water industry and is the unit pulse response function of a linear hydrological system. First proposed by Sherman (1932), the unit hydrograph (originally named unit-graph) of a watershed is defined as a direct runoff hydrograph (DRH) resulting from 1 in (usually taken as 1cm in SI units) of excess rainfall generated uniformly over the drainage area at a constant rate for an effective duration. The unit hydrograph is a simple linear model that can be used to derive the hydrograph resulting from any amount of excess rainfall.

The principles of linear system analysis form the basis of the unit hydrograph method. In hydrology, the unit pulse response function in a linear system sense corresponds to the unit hydrograph.

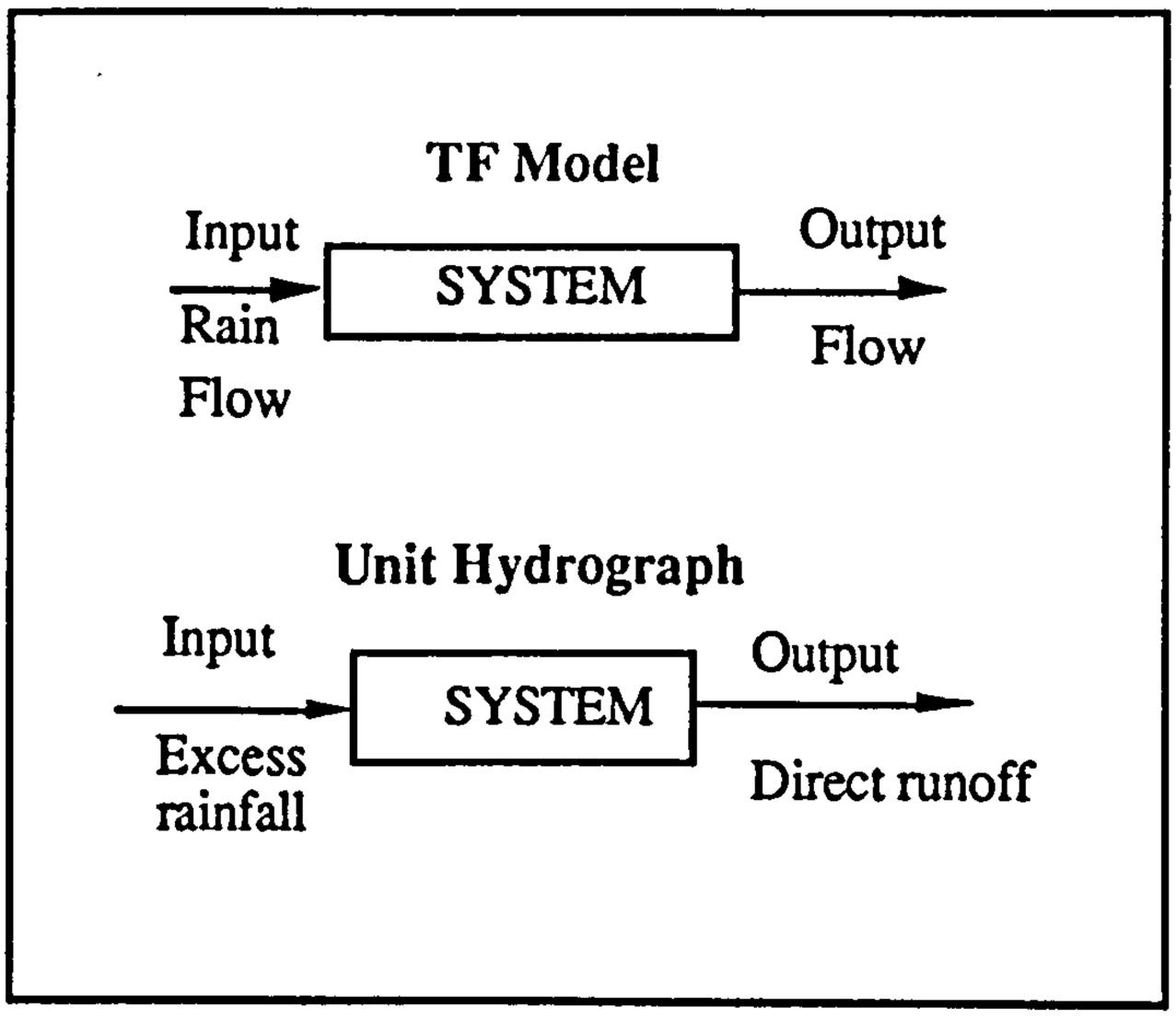

Figure 5.17 Data Flow in UH and TF

As the unit hydrograph is widely used, it would make full use of current resource if the transfer function model can be generated from the existing unit hydrograph model. As mentioned above, there exists a close similarity between the transfer function (which is based on the linear system) and unit hydrograph model as illustrated in Figure 5.18. This will forms the basis of the model transformation.

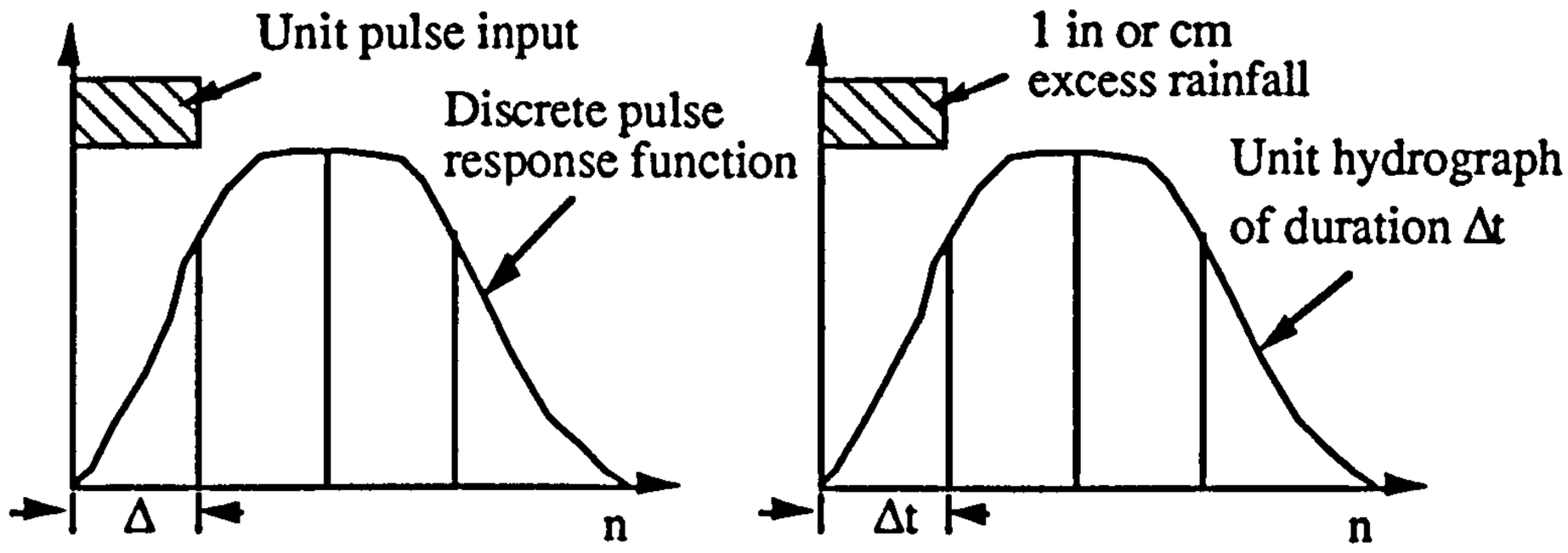

Figure 5.18 Reponse Function of TF and UH

In NRA Wessex region, the shape and timing of the UH were principally defined by 4 model parameters as follows

PO	=	UH peak flow
TO	=	UH time-to-peak
WO	=	UH duration of steep recession
BO	=	UH duration of shallow recession

These parameters are illustrated in Figure 5.19.

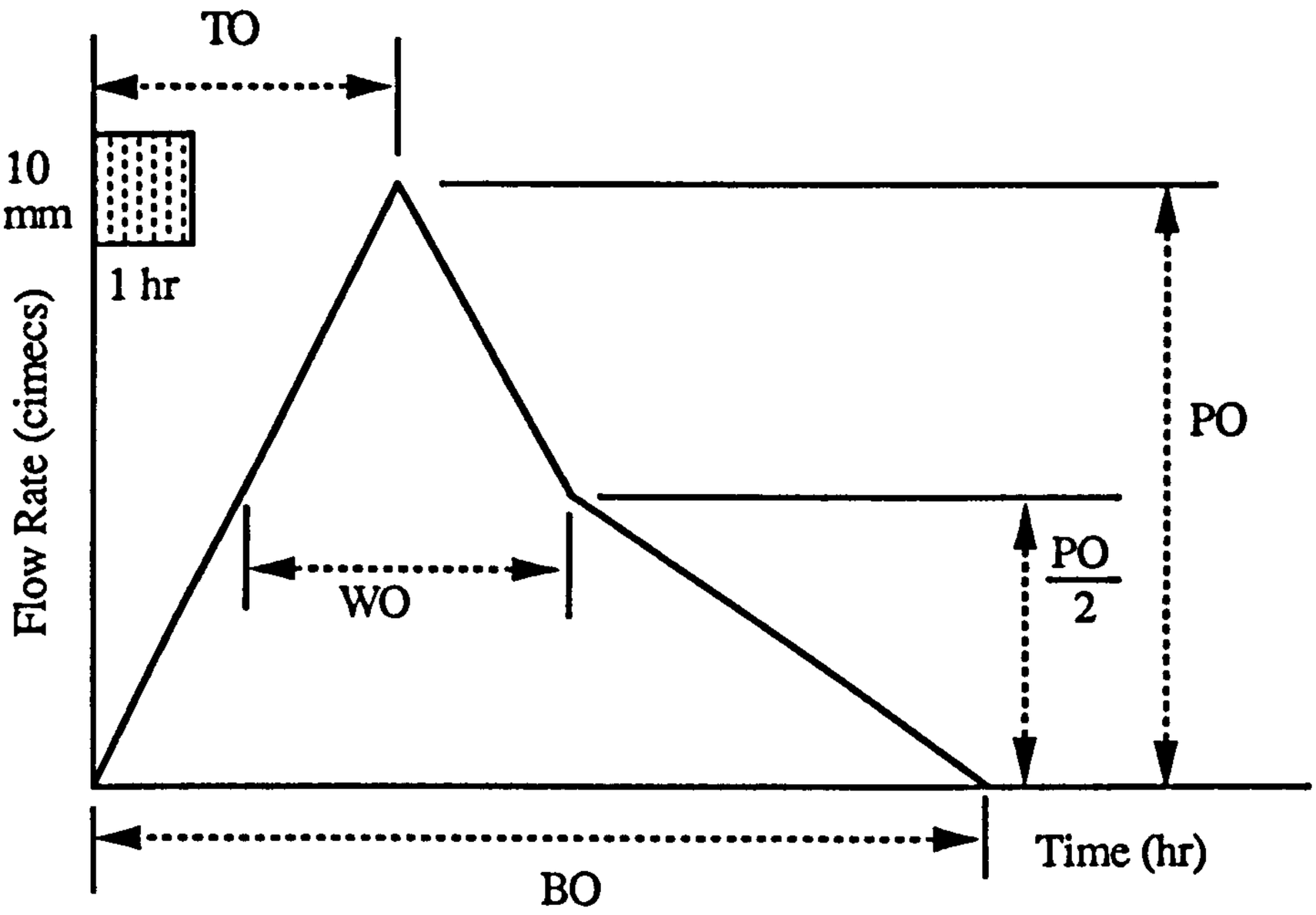

Figure 5.19 Unit Hydrograph Definition Sketch

The Unit Hydrograph ordinates are synthesised from these parameters, which have the following values for the existing model:

	PO	TO	WO	BO
	cumecs	hr	hr	hr
Lovington	40	10	10	26
Halsewater	22	7	10	30
Chisleborough	20	10	12	25
Bishops Hull	50	10	12	33
Greenham	20	5	8	24
Pen Mill	53	11	11	38

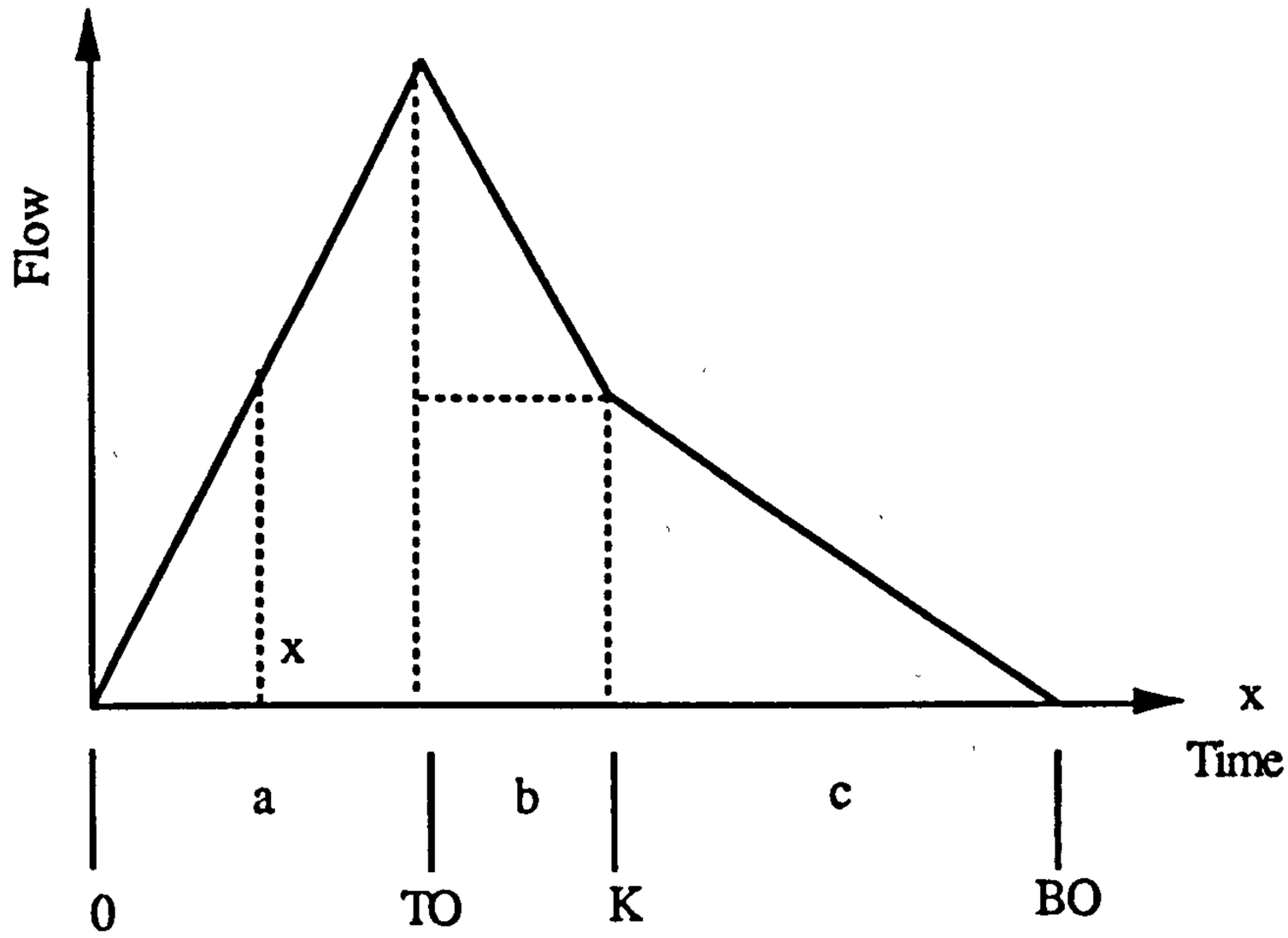

Figure 5.20 Ordinates Computation from Unit Hydrograph

From Figure 5.20, U(x) can be derived as

Let $K = TO/2 + WO$

If $x \leq TO$ then

$$U(x) = x / TO * PO \qquad (5,17a)$$

if $TO < x \leq K$ then

$$U(x) = PO - (x - TO)/ (K - TO)*PO/2 \qquad (5,17b)$$

If $x > K$ then

$$U(x) = PO/2 - (x - K)/(BO - K)* PO/2 \qquad (5,17c)$$

The identified results are (Refer to SOM Division 1973 for the details of the catchments),

Lovington tpeak=6.5, β=1.285, a (1)=2.3341, a(2)= - 1.8160, a(3) = 0.4710
b(1)=4.3925, b(2)= 0.2849, b(3) = - 0.5251, b(4)=0.9885,
b(5) = -0.0789, model time interval= 1 hour.

Halsewater tpeak=6.5, β=1.285, a (1)=2.3341, a(2)= - 1.8160, a(3) = 0.4710
b(1)=3.0610, b(2)= - 1.0536, b(3) = 0.3184, b(4)=1.4623,
b(5) = - 0.8030, model time interval= 1 hour.

Chisleborough tpeak=6.5, β=1.285, a (1)=2.3341, a(2)= - 1.8160, a(3) = 0.4710
b(1)=2.1604, b(2)= 0.0161, b(3) = 0.0166, b(4)=0.4938,
b(5) = 0.0094, model time interval= 1 hour.

Bishops Hull tpeak=8.1, β=1.232, a (1)=2.4344, a(2)= - 1.9755, a(3) = 0.5344
b(1)=5.5638, b(2)= -0.1791, b(3) = -1.0869, b(4)= 0.9240,
b(5) = - 0.4000, model time interval= 1 hour.

Greenham tpeak=3.7, β=1.474, a (1)=2.0348, a(2)= - 1.3802, a(3) = 0.3120
b(1)=3.2194, b(2)= 0.5330, b(3) = - 0.2407, b(4)=2.3829,
b(5) = 0.8012, model time interval= 1 hour.

Pen Mill tpeak=8.0, β=1.235, a (1)=2.4291, a(2)= - 1.9668, a(3) = 0.5308
b(1)=3.2271, b(2)= -1.222 4, b(3) = 2.6083, b(4)=-0.1618,
b(5) = 0.8990, model time interval= 1 hour.

The following figures are used to illustrate three of the models identified by the PRTF model.

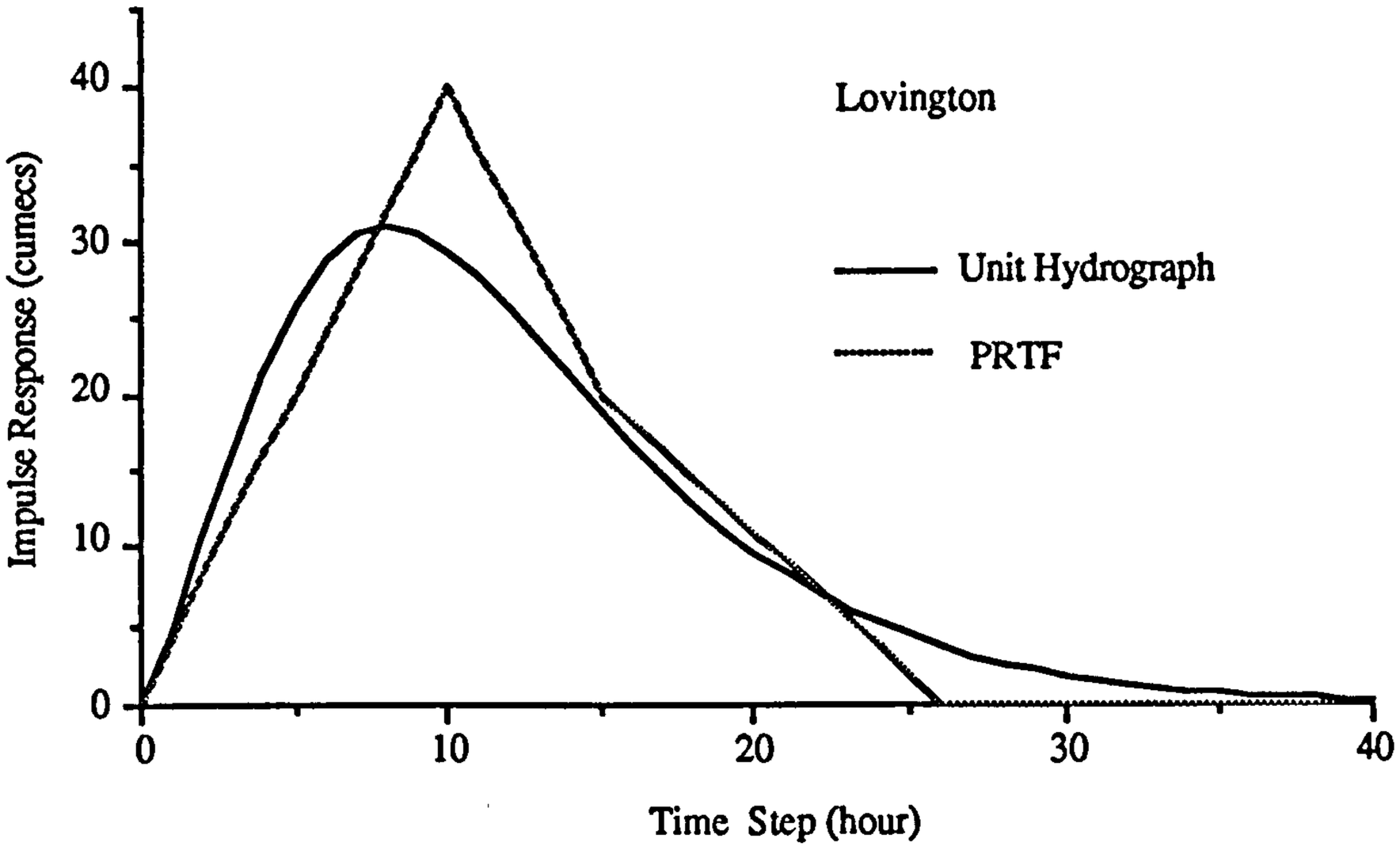

Figure 5.21 Impulse Response by PRTF 1

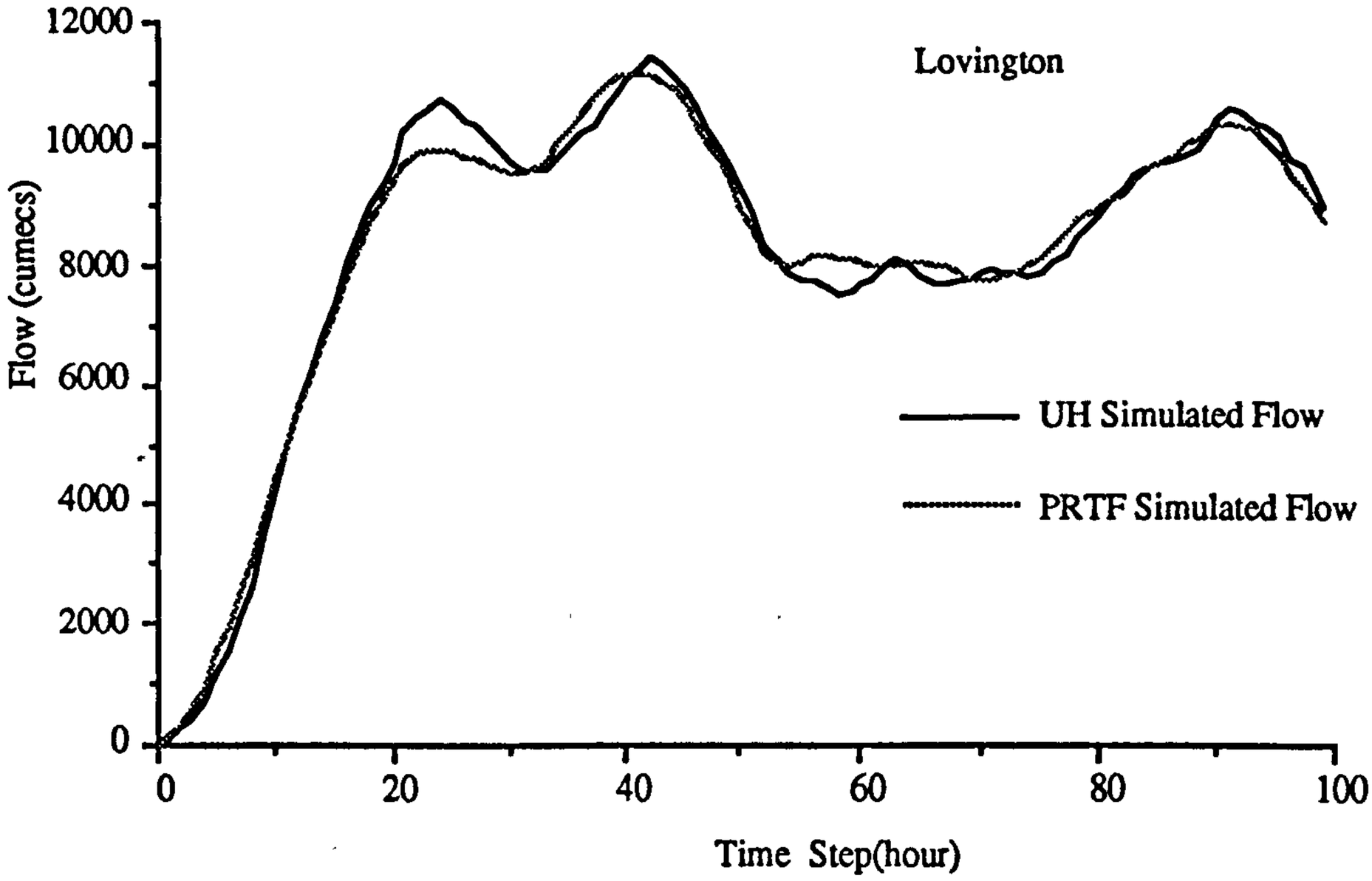

Figure 5.22 Flow Simulation by PRTF 1

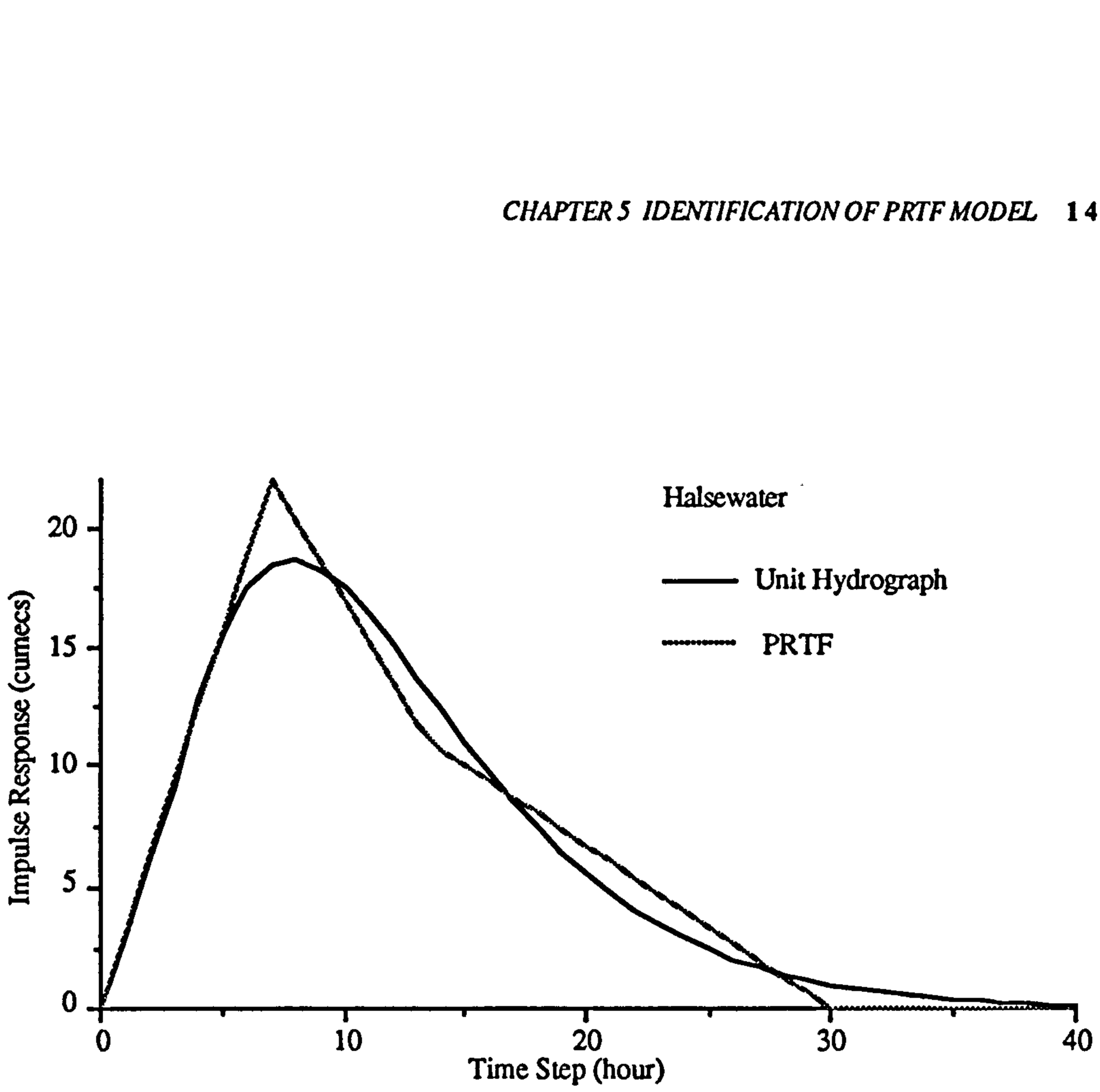

Figure 5.23 Impulse Response by PRTF 2

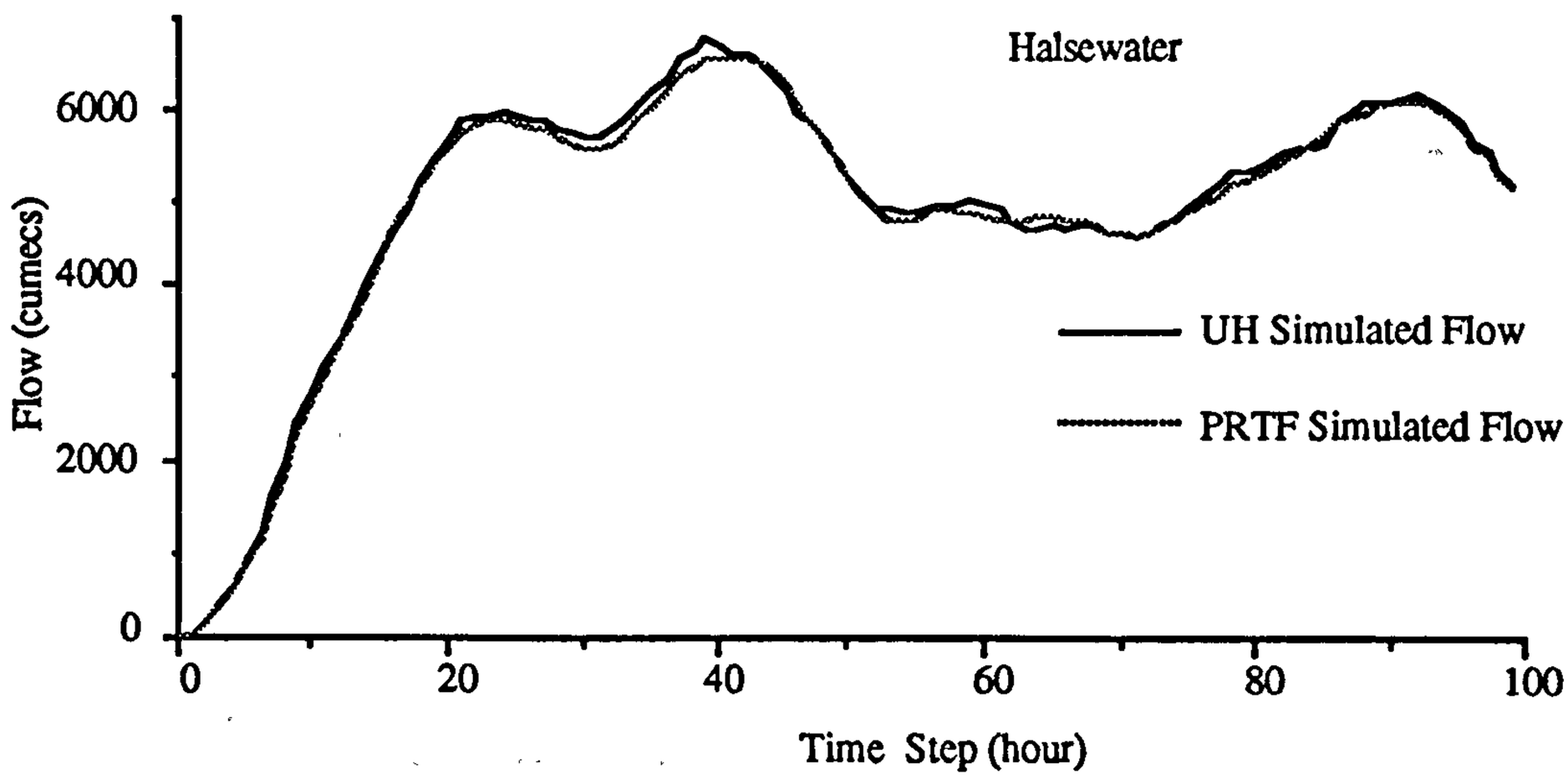

Figure 5.24 Flow Simulation by PRTF 2

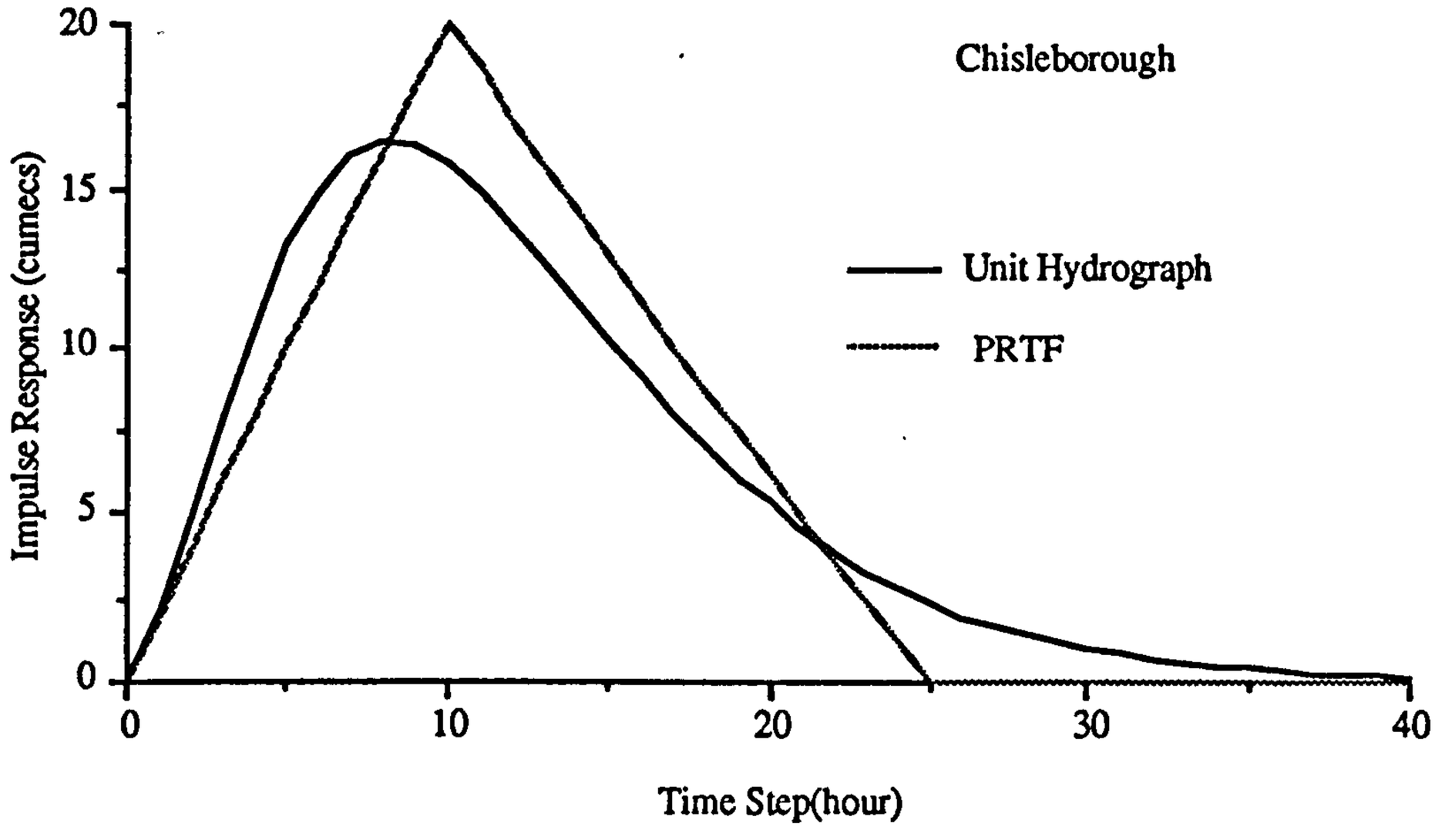

Figure 5.25 Impulse Response by PRTF 3

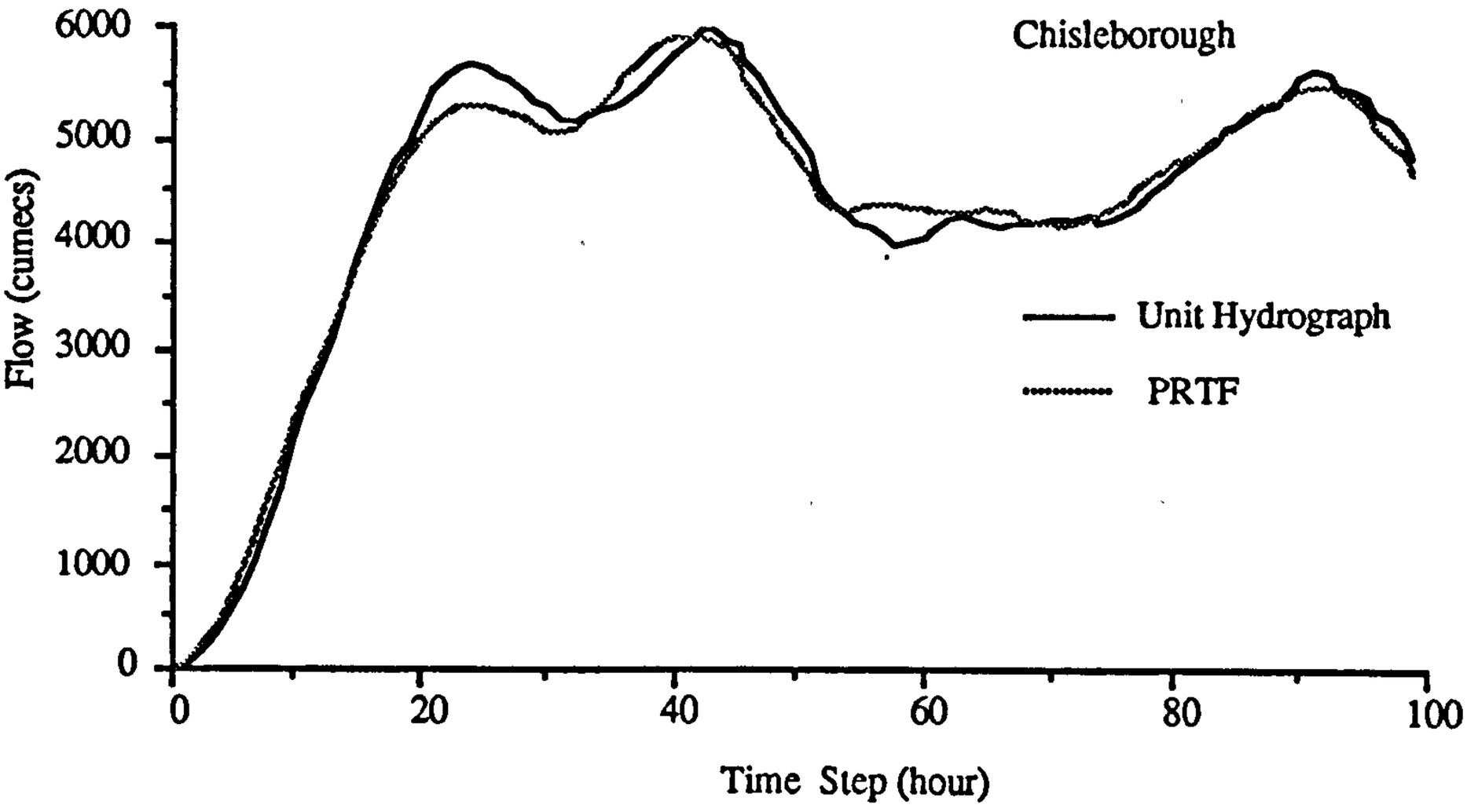

Figure 5.26 Flow Simulation by PRTF 3

The above figures show some examples from Somerset. It can be observed that the PRTF can effectively simulate the UH model process. Although the UH is composed of a broken line approximation, the impulse response from the PRTF can smoothly simulate the the UH response. As the effective rainfall data are input into UH, adjustment is needed when utilising the PRTF derived from the UH in flood forecasting.

5.5 Summary

The identification of the PRTF model is addressed in this chapter. The order of the model is an important item. A higher pole order can produce a narrow shape of impulse response from 1/A(z) and can adapt to more situations than a lower order one. But a longer memory will be resulted and a compromise has to be made to achieve the best result without using a highter order. Another solution is to remove the restriction of positive b_i parameters in the PRTF.

A modified least square estimation technique has been proposed. Two iterative steps are needed to estimate the PRTF model parameters. As there is no worry about unstable and fluctuating response characteristics, the identification of the PRTF is much easier than for the ordinary TF model.

Since many TF models and UH models currently exist in the water industry, case studies are provided to illustrate transformation of TF and UH models into PRTF models. It was found that the PRTF can successfully replace the TF model and the UH model.

CHAPTER 6

ADJUSTABILITY OF PRTF MODEL

6.1 Introduction

The impulse response of the TF is critical to the accuracy of the model forecasting. As the rainfall runoff is nonlinear and time variant, it is necessary that the impulse response of the forecasting model should reflect the current situation in the catchment. In this chapter, equations have been derived to introduce 3 new adjustment factors which can alter the shape, volume and time of the model. With the new adjustment factors, the TF model potentially can perform better than a model with a static impulse response as illustrated in chapter 7. The detailed considerations apply to both conventional TF models as to the PRTF model which this chapter primarily concentrates upon.

6.2 Main Error Sources from TF Model

A major problem in the real-time operation of a hydrological model is that the simulated runoff generally deviates from the measured runoff at the time of forecast. In order to obtain optimal benefit from the real-time runoff measurements in the forecasts, some sort of updating of the hydrological model is required before the forecast is made.

There are several ways of updating model forecasts, including the following :

a) Error prediction. This most obvious method approaches the problem by accepting that a discrepancy exists between the model forecasts and the flow observations and trys to anticipate how this is likely to develop in the near future. The procedure generally works well in the case where the error has the same trend in the near future as the past. It is not very effective in the case of a timing error.

b) State Update. The catchment runoff (or some other observable quantity) acts as a state variable so that a telemetered observation can be used to update the state of the model directly. The formulation of the TF model makes this method very easy to apply. Telemetered flows are inserted in place of previously forecast values as soon as they become available.

c) Parameter Update. The parameters in the model are adaptive to recent model performance. The Kalman filtering technique has been generally utilised in many areas for adaptive updating. The kalman filter has the capacity for dealing with a non-stationary process and a simple scalar kalman filter can be described as below:

$$X(n+1) = aX(n) + k(n+1)\,(y(n+1) - c\,aX(n))$$

$$k(n+1) = \frac{p_1(n+1)\,c}{c^2 p_1(n+1) + \sigma_v}$$

$$p_1(n+1) = a^2\,p(n) + \sigma_g$$

$$p(n) = (1-k(n)\,c)\,p_1(n)$$

Where k is the Kalman gain. The scalar kalman filter can only handle the first order Markov model (ie a (1,0) TF noise Model). In practice a vector Kalman filter is more applicable when the process can be described as a ARMA type process. When a Kalman filter is to be utilised in parameter updating, the model paramters can be described as a simple random walk process.

$$\theta(k+1) = \theta(k) + w(k)$$

Here the parameters are allowed to vary in accordance with probabilitic laws governing the noise process w(k). The problem with the Kalman filter is that it requires explicit knowledge of the environment in the form of correlation functions, state space models or possibly even probability density functions. In many situations such functions are unknown and/or time-varying. An adaptive filter is a means of realising an optimal estimator in some of these situations. The explicit knowledge' is replaced with a requirement for a second input sequence, known as a training or desired input. Three commonly utilised adaptive filters are Recursive least squares, Stochastic gradient methods andSelf-orthogonalising algorithms.

Cluckie and Harpin (1982) investigated many adaptive schemes and found it was very difficult to apply them to flood forecasting models as there was not enough time updating steps available for the models. A simple approach was proposed by Cluckie and Smith (1980) and further developed by Cluckie and Owens (1987) as described below.

This approach aims at updating the percentage run-off represented by the model. A real-time correction factor, delta, scales the rainfall parameters of the model to match the model's steady-state gain with the event percentage run off in the following manner:

$$Y_{t+1} = a_1 y_t + a_2 y_{t-1} + \ldots + a_p y_{t-p} + \Delta_t (b_0 U_{t+1} + b_1 u_t + b_2 u_{t-1} + \ldots b_q u_{t-q})$$

Where

$$\Delta_t = \mu \Delta_t + (1-\mu) \frac{y_t - (a_1 y_{t-1} + a_2 y_{t-2} + \ldots + a_p y_{t-p})}{b_1 u_{t-1} + b_2 u_{t-2} + \ldots + b_q u_{t-q}}$$

$0 \leq \mu \leq 1$ is a smoothing factor.

Such a procedure performs quite well in some applications and the initial delta is important which depends on the hydrologist's experience. Usually it can set to 1.0 if the catchment conditions are unknown. It has been found in some cases, that the delta utilised to update the percentage runoff has a detrimental effect. This is because the delta is effectively used to modify the MA part of the model. In some cases, the MA parameters are quite small even equal to zero or become negative which prohibit the usage of delta in such situation.

It is not easy to say which approach should be adopted in the real time flood forecasting in general terms. As the TF model is primarily used in this thesis, we only analyse how to update the model to correct the forecast deviation.

The TF model is a linear time-invariant system, while rainfall runoff is a class of nonlinear and nonstationary system. There are many factors which influence the catchment response. It has been shown that the parameters governing the transfer function will thus differ for various magnitudes of input and different time steps. The following figure shows that in the same catchment there exists many unit impulse response functions.

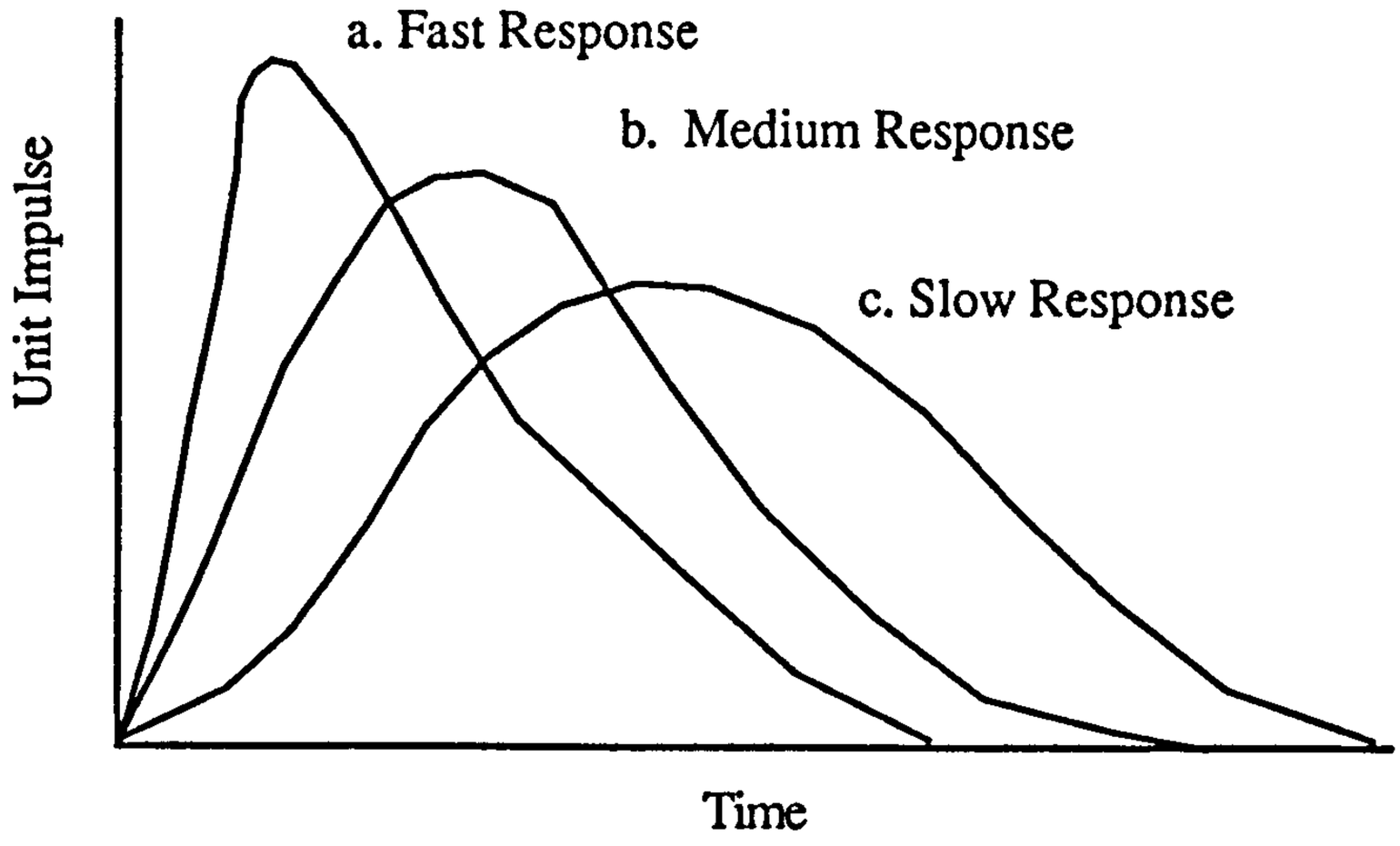

Figure 6.1 Differences of Catchment Unit Impulse Response Shapes

Figure 6.1 shows the catchment responses are different with different storm type and catchment condition. Sometimes it is fast while sometimes slow.

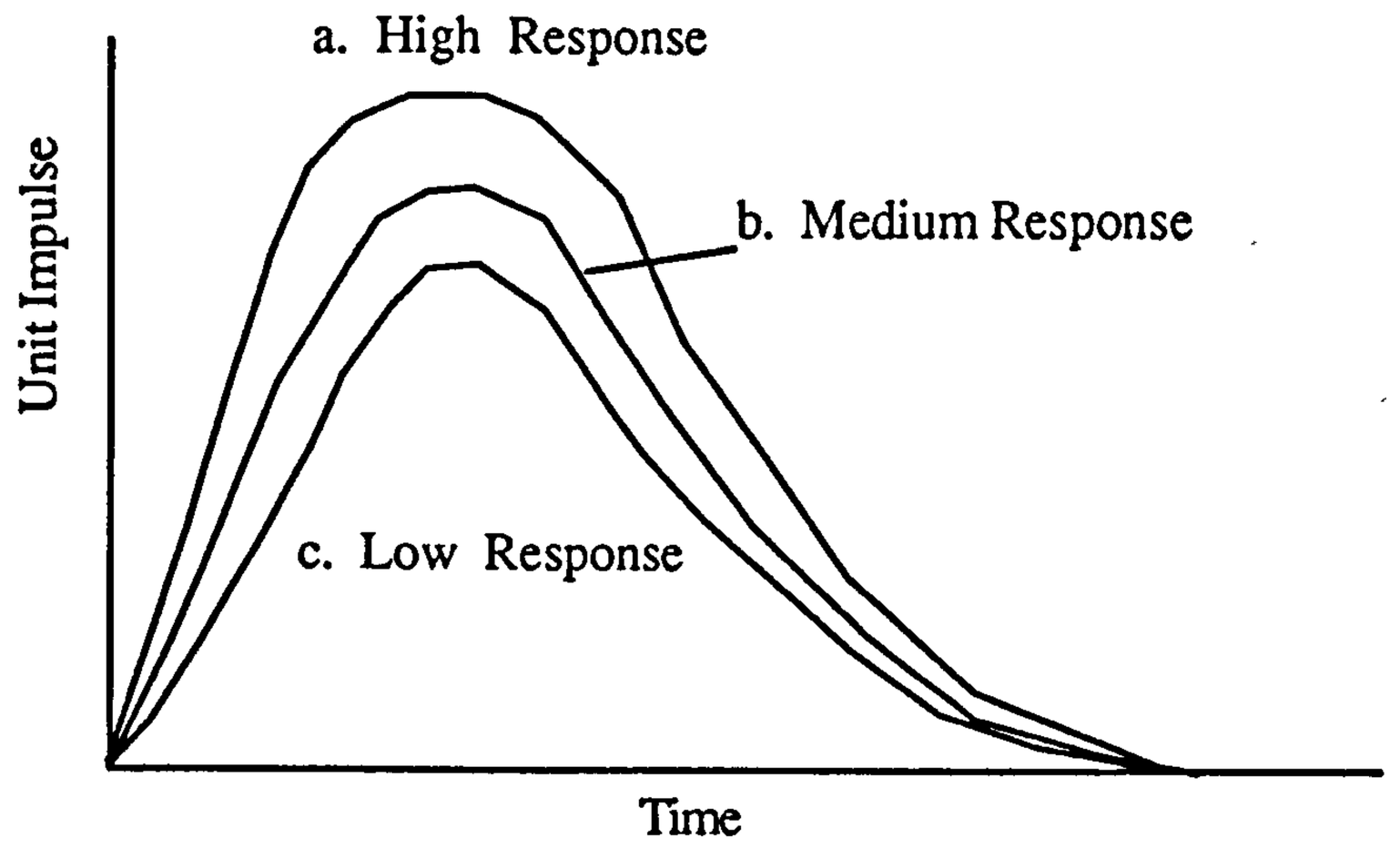

Figure 6.2 Differences of Catchment Unit Impulse Response Volumes

Figure 6.2 shows the catchment responses have different volume responses. If the catchment is very wet, there will be more production of river flow and vice verse.

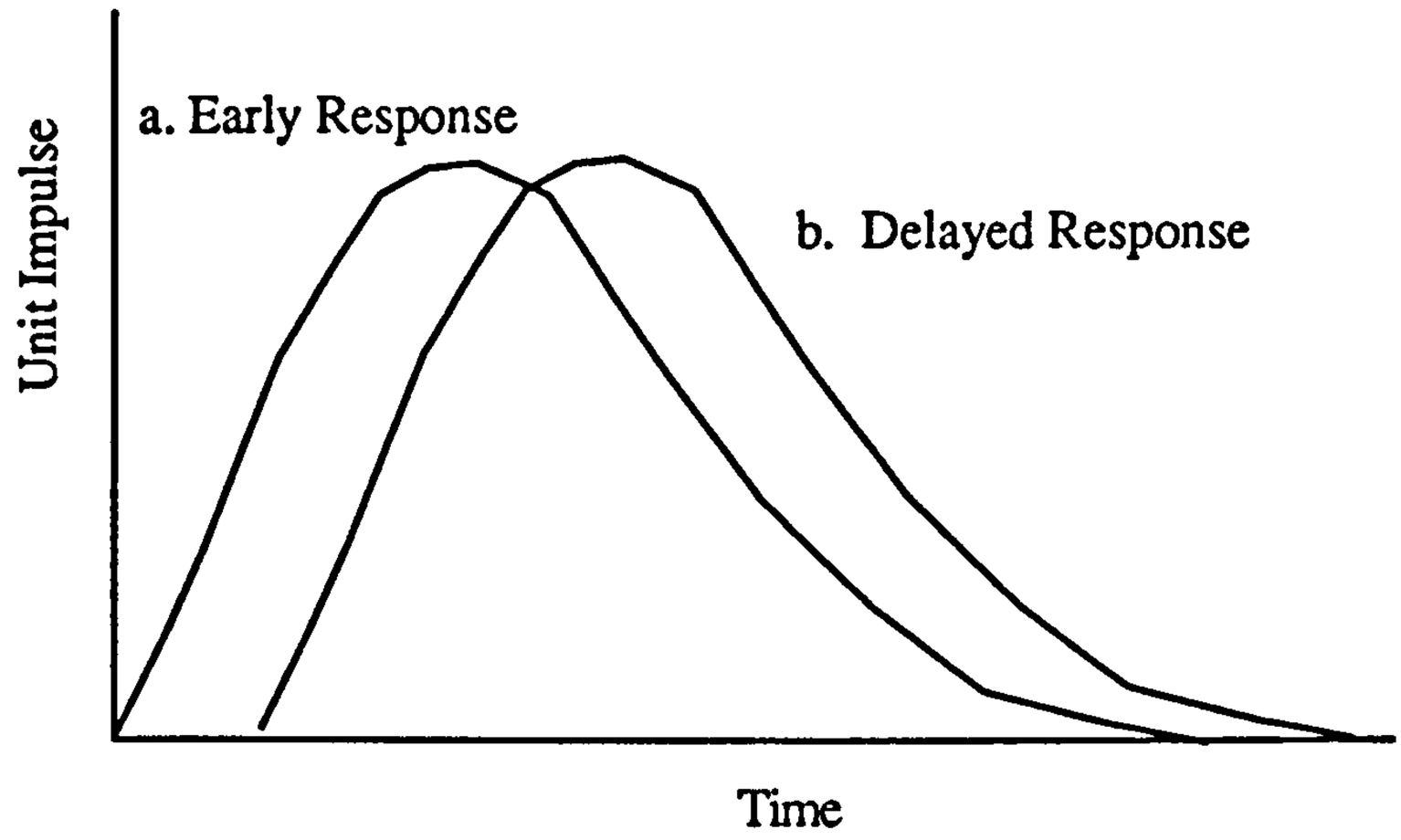

Figure 6.3 Differences of Catchment Unit Impulse Response Times

Figure 6.3 shows the catchment responses have different timing variations. If the storm is located on the up per part of the catchment, the response will be delayed.

The main error source from a model is that a static model can only simulate one type of catchment response and the forecast can only work well if a similar event as the model calibration event happens. The error caused by three types of impulse response can be illustrated in the following figures.

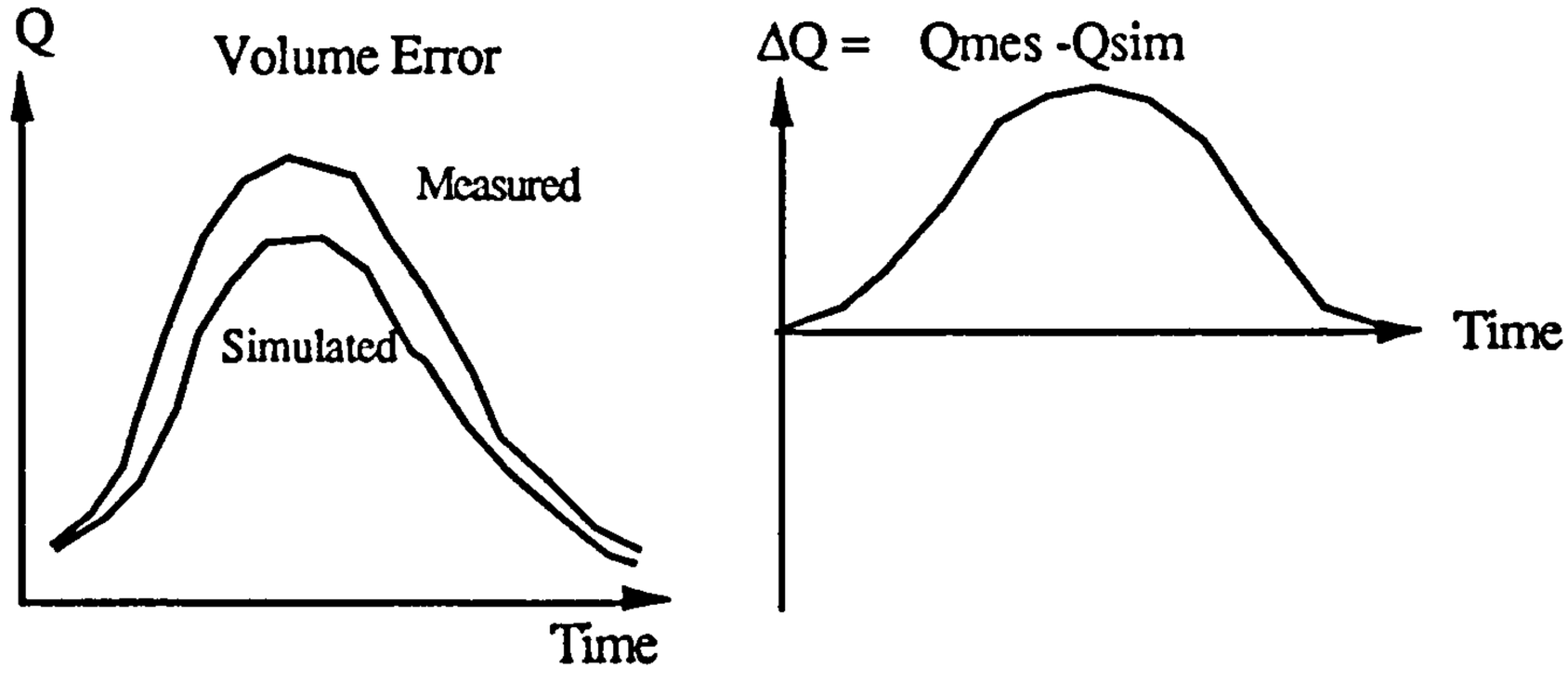

Figure 6.4 TF Simulation Error by Incorrect Impulse Response Volume

The forecasting error caused by incorrect impulse response volume has a convex curve if the catchment is very wet or has a concave curve if the catchment is very dry.

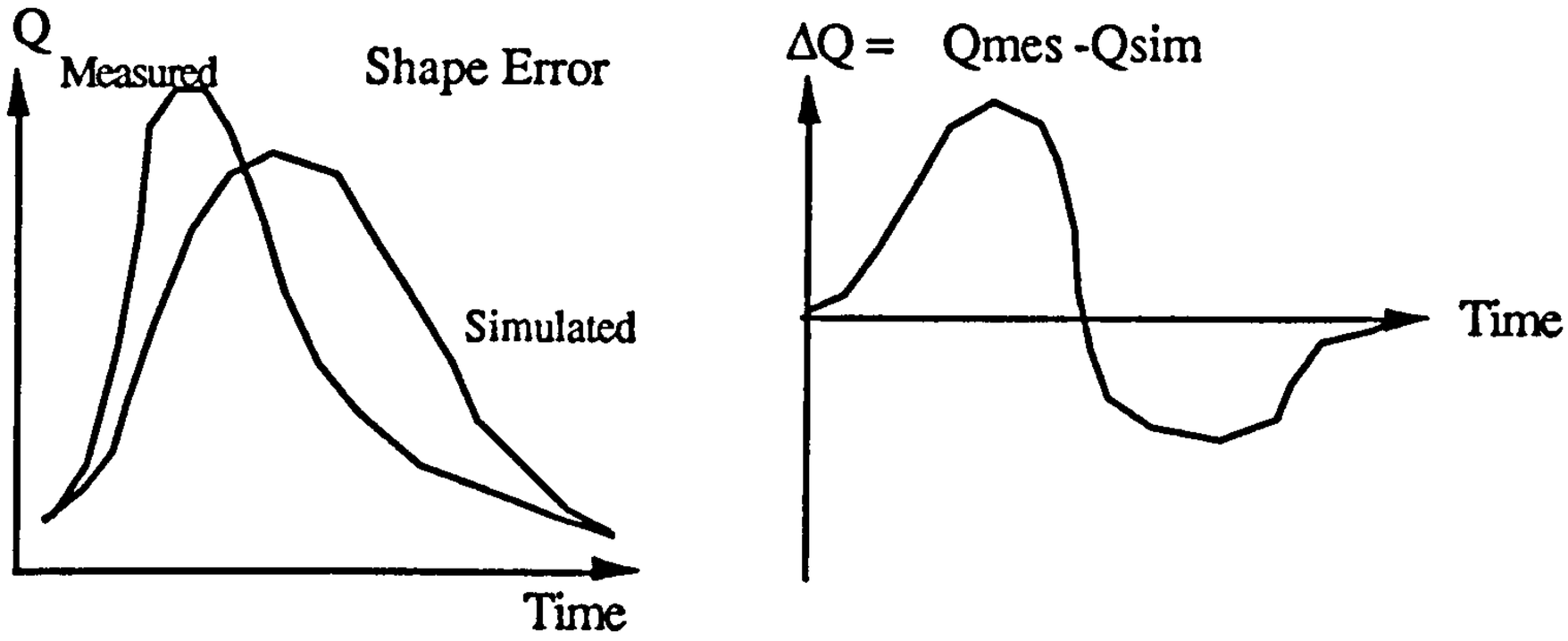

Figure 6.5 TF Simulation Error by Incorrect Impulse Response Shape

The forecasting error caused by incorrect impulse response shape has a similar shape as the sine curve.

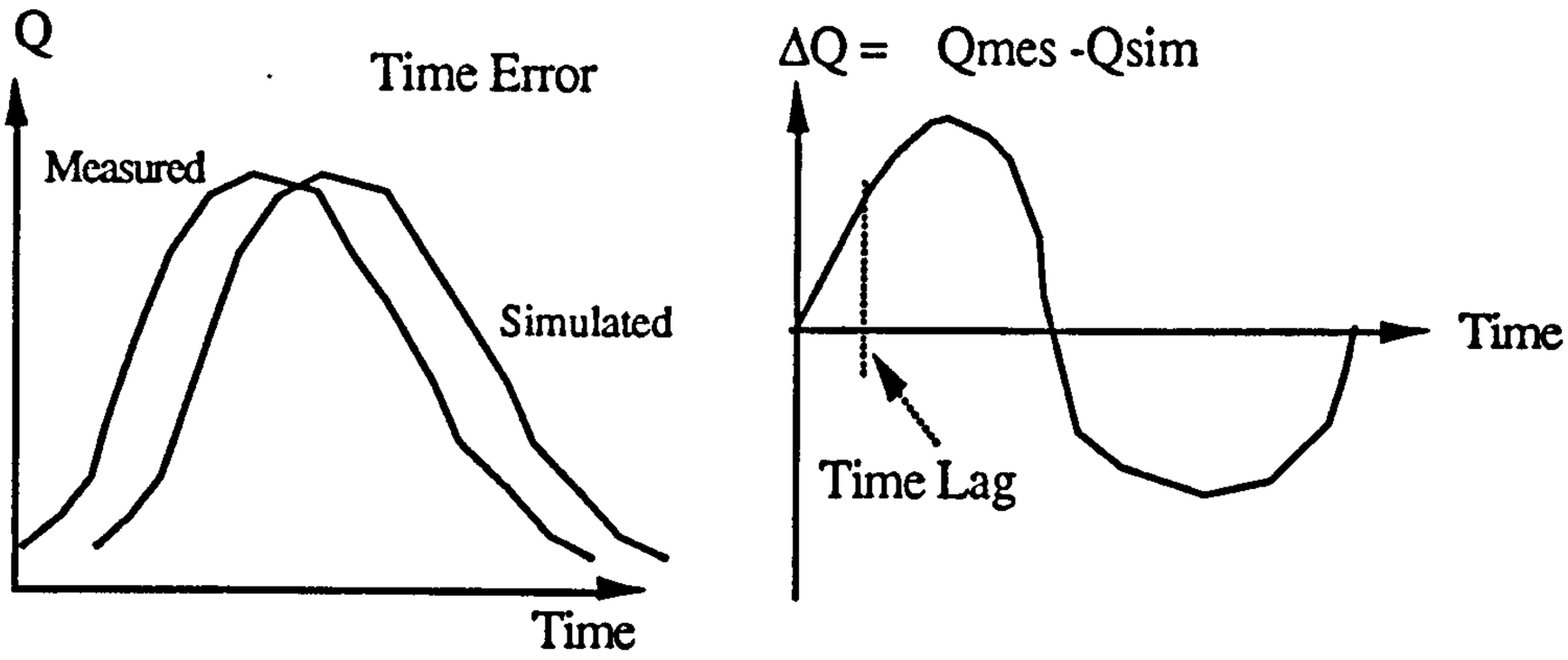

Figure 6.6 TF Simulation Error by Incorrect Impulse Response Time

The forecasting error caused by incorrect impulse response time also has a similar shape as the sine curve.

During real-time forecasting

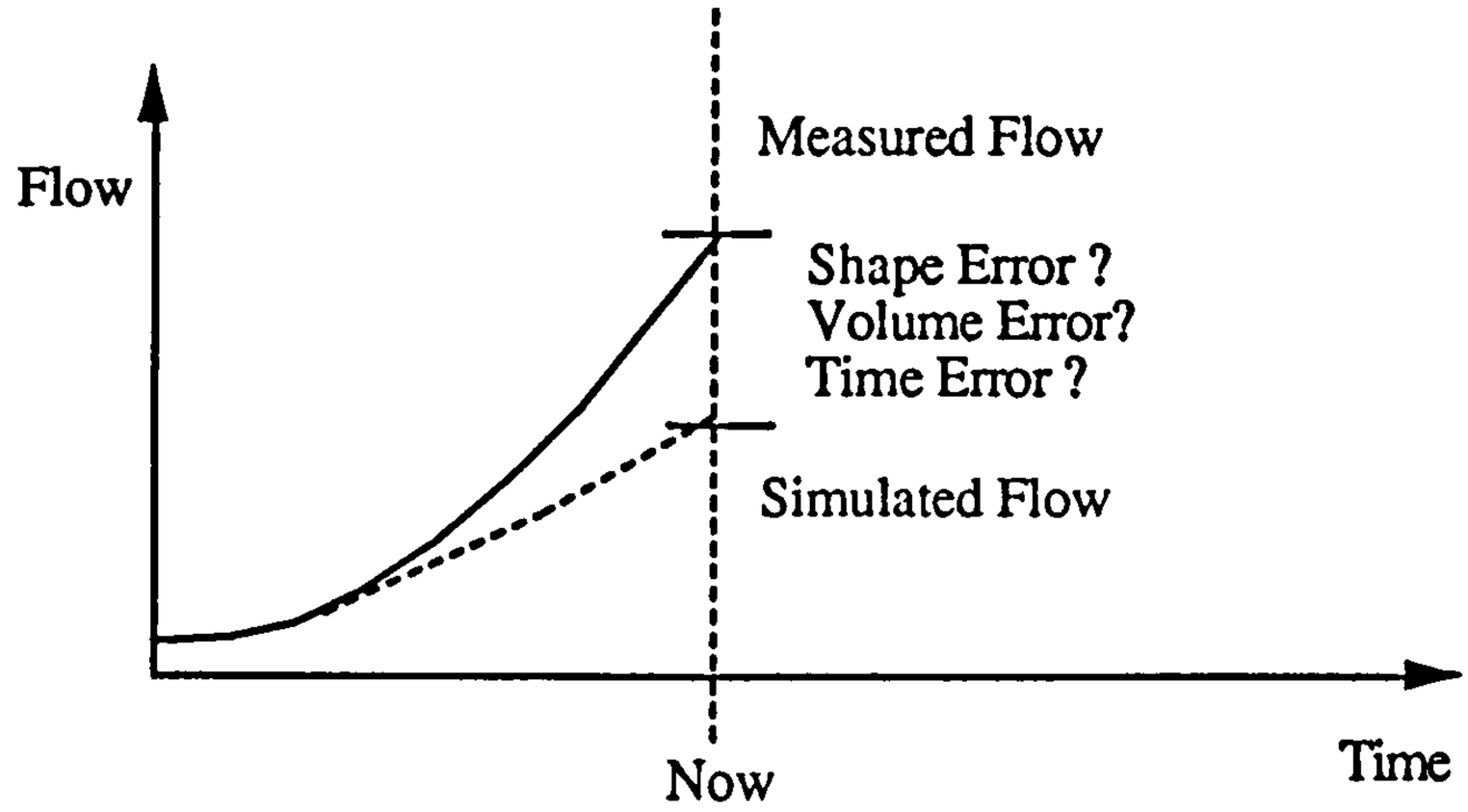

Figure 6.7 Real Time Forecasting Error

The task of updating flood flood forecasting system is to select the right unit impulse function for the actual event. This means that the parameters of the model must be able to change. The next chapter will the deal with error sources illustrated in Figure 6.7.

6.3 Adjusting PRTF Model Impulse Response

Many researchers have investigated ways of updating the parameters in the TF model. The commonly used way is to use real-time filter theories to estimate new parameters from the recent observations. Cluckie and Harpin (1982) investigated many adaptive schemes including Kalman filters and found it was very difficult to apply them in real time flood forecasting system as there was not enough time steps and hence information to update the model parameters and it was likely that the system would become unstable or fluctuating.

With the PRTF model in porticular, it is possible to derive an adaptive TF model which is easy to update and can be updated robustly. Generally speaking, the impulse response H(z) from an adaptive transfer function can be written as :

$$H(z)=F(\alpha,\beta,\tau,z) \qquad (6,1)$$

where

α -- Volume factor

γ -- Shape factor

τ -- Time factor

Each factor can only influence one aspect of the TF model. One of them can cause the TF model to become unstable or fluctuating. By adjusting these three factors, it is possible to make the TF model more accurate than the static TF model.

The general identified PRTF is

$$y(t) = \sum_{i=1}^{N} a_i\ y(t-i) + \sum_{i=0}^{M} b_i\ u(t-i) \qquad (6,2)$$

$$a_i = -S\ C_N^{N-i}\ (-\beta)^{N-i} = -C_N^{N-i}\ (-\beta)^{-i}$$

$$\beta \in \Re \text{ (Real)} \quad \text{and} \quad \beta > 1.0$$

In real-time forecasting, it would be convenient to use the forecasting form of the TF model where the model parameters will change with catchment conditions and storm type. The forecasting form of the TF model is as :

$$y(t) = \sum_{i=1}^{N} A_i\ y(t-i) + \sum_{i=0}^{M} B_i\ u(t-i) \qquad (6,3)$$

$$A_i = a_i \qquad i=1,\ 2,\ \ldots\ N$$

$$B_i = b_i \qquad i=0,\ 1,\ 2,\ \ldots\ M$$

$$a_i = -S\ C_N^{N-1}\ (-\beta)^{N-1} = -C_N^{N-1}\ (-\beta)^{-1}$$

$$\beta \in \Re \text{ and } \beta > 1.0$$

It is noted that the model parameters a_i and b_i have been replaced by A_i and B_i as the forecasting model will keep changing is parameters. The identification form of the PRTF is the basis for the forecasting form of the PRTF and the parameters change will occur around the identification form of the PRTF.

The following procedures are used to derive the PRTF with adjustment factors.

6.3.1 Volume Adjust Factor α

The impulse response of TF model is

$$H(z)=B(z)/A(z)$$

A straightforward way to change the impulse response volume is to multiply all the b_i with a constant factor $(1+\alpha)$, α here is the percentage of volume change. A volume adjustable PRTF would be as follows:

$$y(t) = \sum_{i=1}^{N} A_i\ y(t-i) + \sum_{i=0}^{M} B_i\ u(t-i) \qquad (6,3)$$

$$A_i = a_i \qquad i=1,\ 2,\ \ldots\ N$$

$$B_i = (1 + \alpha)\ b_i \qquad i = 0, 1, 2, \ldots M$$

$$a_i = -S\ C_N^{N-i}\ (-\beta)^{N-i} = -C_N^{N-i}\ (-\beta)^{-i}$$

$$\beta \in \Re \text{ and } \beta > 1.0$$

Two TF models from Somerset are used here to test the effectiveness of factors.

The Yeo Model is a (3,5) TF model (River Yeo at Pen Mill in Wessex Region) with identification model form as ($\beta = 1.235$) is used to illustrate the effects of α factor

b(0)= 3.2271

b(1)= - 1.2224

b(2)= 2.6083

b(3)= - 0.1618

b(4)= 0.8990 with model time interval of 1 hour

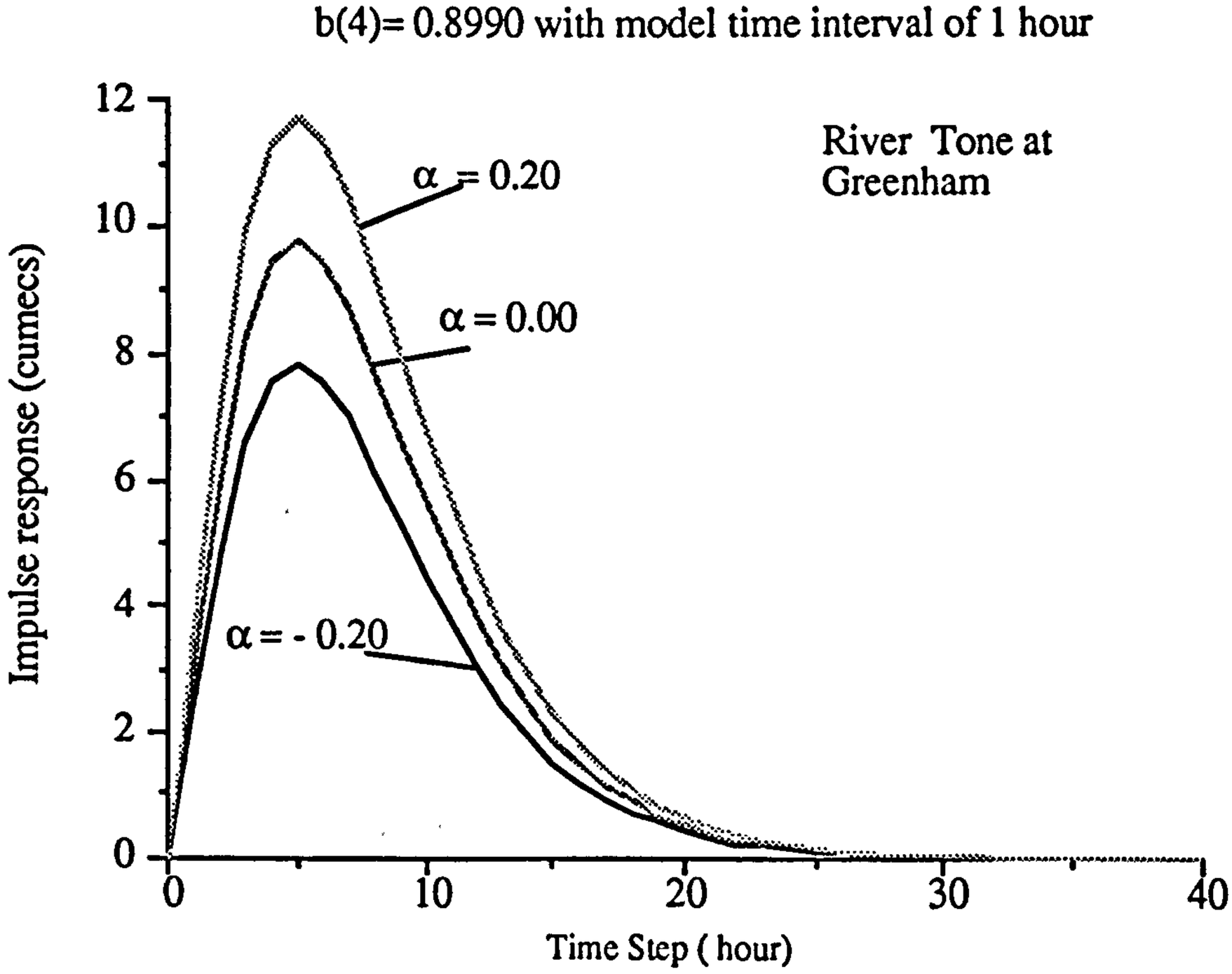

Figure 6.8 Effect of α on Impulse Response of Yeo Model

Tone Model is a (3,5) TF model (River Tone at Greenham in Wessex Region) with identification model form as (β = 1.474) is used to illustrate the effects of α factor.

b(0)= 3.2194

b(1)= - 0.5330

b(2)= -0.2407

b(3)= -2.3829

b(4)= 0.8012 with model time interval of 1 hour

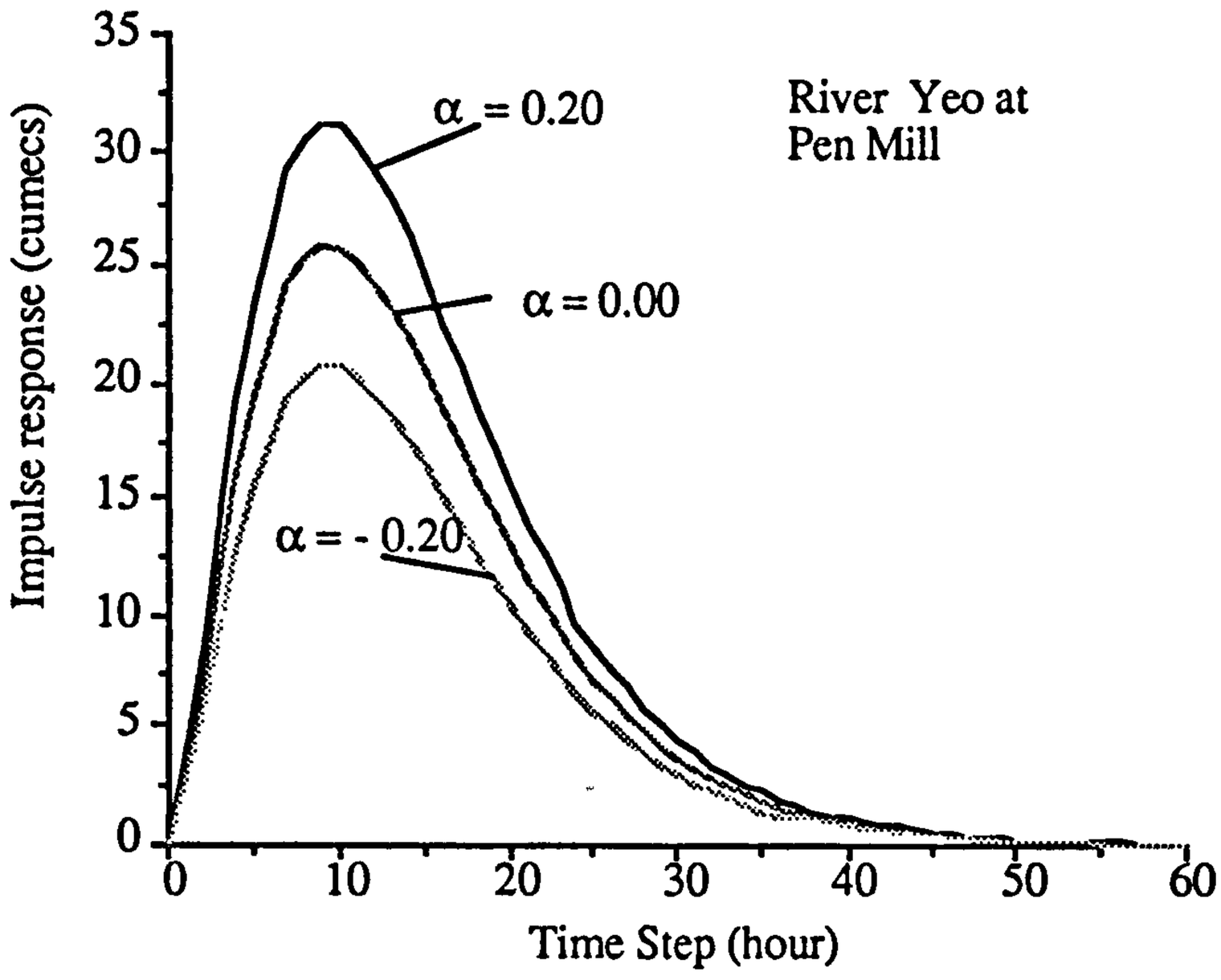

Figure 6.9 Effect of α on Impulse response of Tone Model

Results show from Figure 6.8 and Figure 6.9 that the volume adjust factor can effectively alter the volume of the TF model impulse response without distorting the response shape and time. This indicates that the α factor has been set correctly.

6.3.2 Shape Adjust Factor γ

The shape of a TF model is influenced by the A(z) part. To control the shape of the impulse response, an index is needed to identify the degree of the shape. The shape adjust factor γ is used to illustrate the peak location deviation between the forecasting form of the PRTF and the identification form of the PRTF. The unit of γ is the time step of the model and it can be a real number as distinct from integer.

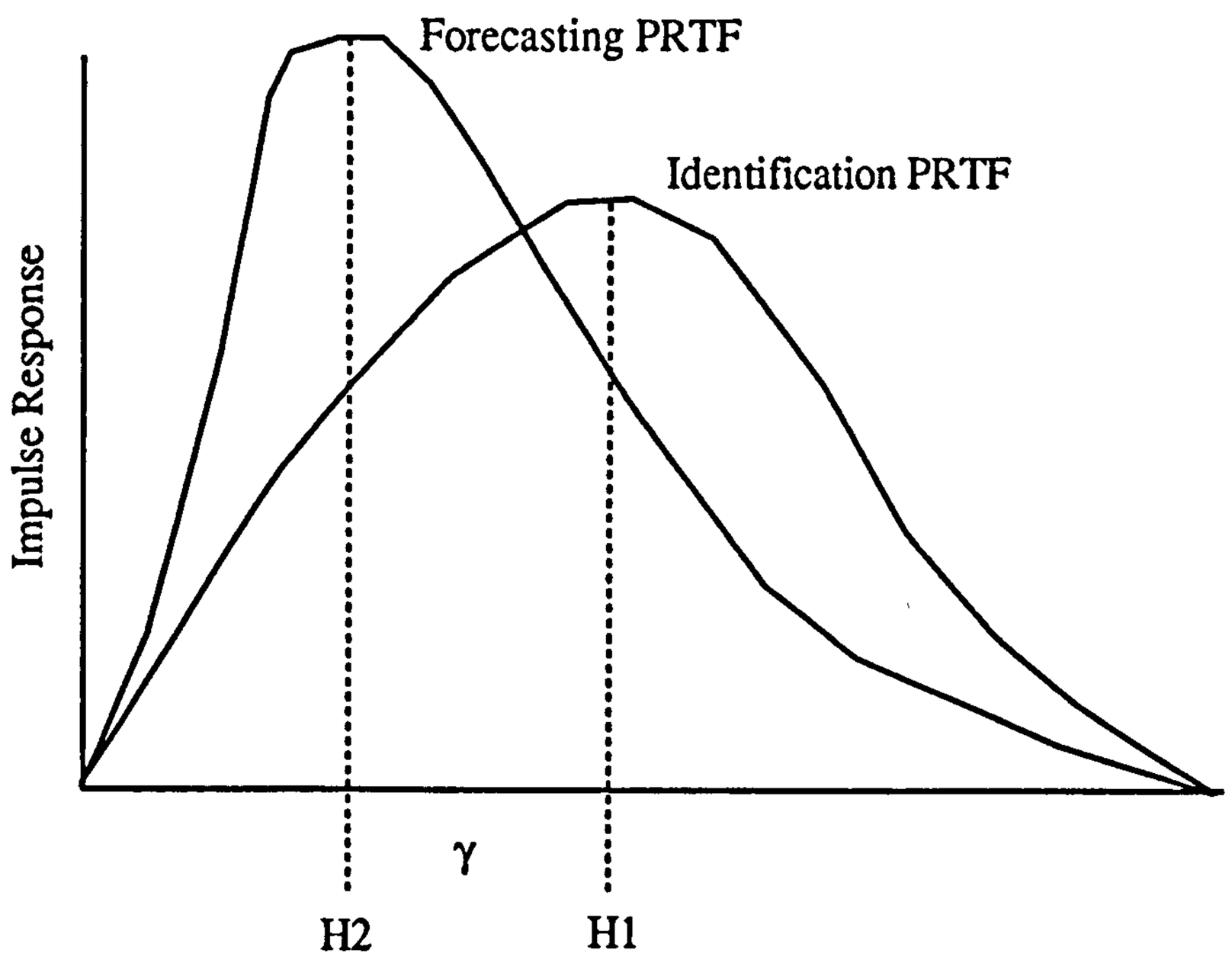

Figure 6.10 γ Factor and Peak Location of PRTF 1/A(z) Part Impulse Response

From Figure 6.10, γ factor can be derived from peak location H1 and H2.

$$\gamma = \mathbf{H2 - H1} \tag{6,5}$$

As we know that the roots of A(z) (or poles of 1/A(z)) will control the shape of the PRTF, the peak location of 1/A(z) can be derived from the poles of 1/A(z), i.e.

$$\gamma = f\ (\beta) \tag{6,6}$$

The impulse response of 1/A(z) is

$$A(z) = S\ (\ z^{-1} - \beta\ )^N \tag{6,7}$$

$$S = \frac{1}{(\ -\beta\ )^N}$$

It has an Nth order pole and according to the residue theorem, the impulse response can be derived.

First define $A_0(z)$ as a rational function with the denominator expanded in a product of pole factors

$$A_0\ (\ z) = A(z)\ z^{t-1} = \frac{(-\beta)^N\ z^{t-1}}{(z^{-1} - \beta)^N} \tag{6,8}$$

$$= \frac{z^N\ z^{t-1}}{(\ z - \frac{1}{\beta}\ )^N}$$

where N is the pole order at point $1/\beta$

where for simple poles, that is, N = 1,

$$A_0(z) = \frac{z^t}{\left(z - \frac{1}{\beta}\right)}$$

The residue of $A_0(z)$ is given by

$$\operatorname*{Res}_{z=\frac{1}{\beta}} [A_0(z)] = \lim_{z \to \frac{1}{\beta}} \left[\left(z - \frac{1}{\beta}\right) A_0(z)\right]$$

$$= z^t \Big|_{z=\frac{1}{\beta}} = \left(\frac{1}{\beta}\right)^t$$

For a Nth-order pole, (N = 2, 3, . . .) the residue is given by

$$\operatorname*{Res}_{z=\frac{1}{\beta}} [A_0(z)] = \frac{1}{(N-1)!} \lim_{z \to \frac{1}{\beta}} \frac{d^{N-1}}{dz^{N-1}} \left[\left(z - \frac{1}{\beta}\right)^N A_0(z)\right]$$

$$= \frac{1}{(N-1)!} \frac{d^{N-1}}{dz^{N-1}} \left[\left(z - \frac{1}{\beta}\right)^N \frac{z^N z^{t-1}}{\left(z - \frac{1}{\beta}\right)^N}\right] \Big|_{z=\frac{1}{\beta}}$$

$$= \frac{1}{(N-1)!} \frac{d^{N-1}}{dz^{N-1}} \left[z^{N-1+t} \right] \Big|_{z=\frac{1}{\beta}}$$

As

$$\frac{d(z^k)}{dz} = k\, z^{k-1}$$

So

$$\underset{z=\frac{1}{b}}{\text{Res}} [A_0(z)] = \frac{(N-1+t)(N-2+t)\ldots(1+t)\, z^t}{(N-1)!} \Big|_{z=\frac{1}{\beta}}$$

$$= \frac{(N-1+t)(N-2+t)\ldots(1+t)}{(N-1)!} \left(\frac{1}{\beta}\right)^t \qquad (6,9)$$

where $t = 2, \ldots$ and $N \geq 2$

The impulse response function of 1/A(z) will be

$$h(t) = \left(\frac{1}{\beta}\right)^t \qquad (6,10a)$$

where $t = 1, 2, \ldots, N = 1$

$$h(t) = \frac{(N-1+t)(N-2+t)\ldots(1+t)}{(N-1)!} \left(\frac{1}{\beta}\right)^t \qquad (6,10b)$$

where $t = 1, 2, \ldots, N \geq 2$

if N= 2 then

$$h\ (t) = (\ 1+t)\ (\ \frac{1}{\beta}\ )^{t} \qquad (6,11)$$

if N= 3 then

$$h\ (\ t\ ) = \frac{(2+t)\ \ (1+t)}{2}\ \ (\frac{1}{\beta}\ )^{t} \qquad (6,11)$$

Take h(t) as a continuous function, the peak of h(t) can be derived as

$$\frac{dh(t)}{dt}\ = 0 \qquad (6,12)$$

for N=2

$$1+\ (1+t)\ \ln\ (\frac{1}{\beta}) = 0$$

$$t = \frac{1}{\ln\ \beta}\ \ -1$$

So given a β value, the peak time will be (for N=2)

$$t_{peak} = \frac{1}{\ln\ \beta}\ \ -\ \ 1 \qquad (6,13)$$

If the peak time is given, a desirable β will be

$$\beta = e^{\frac{1}{(\ t_{peak}\ \ +1\ )}} \qquad (6,14)$$

for N=3

$$\frac{d}{dt}\left[\frac{(2+t)\ (1+t)}{2}\ \left(\frac{1}{\beta}\right)^t\ \right] = 0$$

$$(2+t)\ (1+t)\ \ln\left(\frac{1}{\beta}\right) + 2t + 3 = 0$$

$$t^2 + \left(3 - \frac{2}{\ln\beta}\right) t + 2 - \frac{3}{\ln\beta} = 0$$

Solving the equation ,we get :

$$t = \frac{\frac{2}{\ln\beta} - 3 \pm \sqrt{\left(3 - \frac{2}{\ln\beta}\right)^2 - 4\left(2 - \frac{3}{\ln\beta}\right)}}{2}$$

As the impulse response is a single peak curve, the positive sign is selected from the root result. Given the β value, the peak time will be (for N=3)

$$t_{peak} = \frac{\frac{2}{\ln\beta} - 3 + \sqrt{\left(3 - \frac{2}{\ln\beta}\right)^2 - 4\left(2 - \frac{3}{\ln\beta}\right)}}{2} \qquad (6,15)$$

It also possible to derive β from t_{peak} and here

$$\ln \beta = \frac{2t + 3}{t^2 + 3t + 2}$$

So a desirable β will be

$$\beta = e^{\frac{2t_{peak} + 3}{(t_{peak}^2 + 3t_{peak} + 2)}} \qquad (6,16)$$

With the equation derived above, it is possible to derive the shape adjust factor γ.

For N=2, the new root corresponding to H2 is β_{new}.

$$H_2 = \frac{1}{\ln \beta_{new}} - 1 \qquad (6,17)$$

So

$$\gamma = H_2 - H_1 = \frac{1}{\ln \beta_{new}} - \frac{1}{\ln \beta} \qquad (6,18)$$

$$\beta_{new} = e^{\frac{1}{\gamma + \frac{1}{\ln \beta}}} \qquad (6,19)$$

New a_i value will

$$a_i = -C_N^{N-i} (-\beta_{new})^{-i} = -C_N^{N-i} \left(-e^{\frac{1}{(\gamma + \frac{1}{\ln \beta})}}\right)^{-i} \qquad (6,20)$$

$$\beta \in \Re, \quad \beta > 1.0 \text{ and } \gamma > \; - \frac{1}{\ln \beta}$$

where i =1, 2, . . . N

For N=3, the new root corresponding to H2 is β_{new},

$$H_2 = \frac{\frac{2}{\ln \beta_{new}} - 3 + \sqrt{\left(3 - \frac{2}{\ln \beta_{new}} \right)^2 - 4 \left(2 - \frac{3}{\ln \beta_{new}} \right)}}{2} \tag{6,21}$$

So

$$\gamma = H_2 - H_1 \tag{6,22}$$

$$= \frac{\frac{2}{\ln \beta_{new}} - 3 + \sqrt{\left(3 - \frac{2}{\ln \beta_{new}} \right)^2 - 4 \left(2 - \frac{3}{\ln \beta_{new}} \right)}}{2} -$$

$$\frac{\frac{2}{\ln \beta} - 3 + \sqrt{\left(3 - \frac{2}{\ln \beta} \right)^2 - 4 \left(2 - \frac{3}{\ln \beta} \right)}}{2}$$

It can be derived as

$$\ln \beta_{new} = \frac{2\psi + 3}{\psi^2 + 3\psi + 2}$$

where

$$\psi = \gamma + \frac{\frac{2}{\ln \beta} - 3 + \sqrt{\left(3 - \frac{2}{\ln \beta}\right)^2 - 4\left(2 - \frac{3}{\ln \beta}\right)}}{2}$$

So finally

$$\beta_{new} = e^{\frac{2\psi + 3}{(\psi^2 + 3\psi + 2)}} \tag{6,23}$$

New a_i value will

$$a_l = -C_N^{N-l}\,(-\beta_{new})^{-l} \tag{6,24}$$

$$\beta_{new} = e^{\frac{2\psi + 3}{(\psi^2 + 3\psi + 2)}}$$

$$\psi = \gamma + \frac{\frac{2}{\ln \beta} - 3 + \sqrt{\left(3 - \frac{2}{\ln \beta}\right)^2 - 4\left(2 - \frac{3}{\ln \beta}\right)}}{2}$$

$$\beta \in \Re, \quad \beta > 1.0$$

$$\gamma > -\frac{\frac{2}{\ln \beta} - 3 + \sqrt{\left(3 - \frac{2}{\ln \beta}\right)^2 - 4\left(2 - \frac{3}{\ln \beta}\right)}}{2}$$

Now, the Yeo Model is used to illustrate the effect of the γ factor.

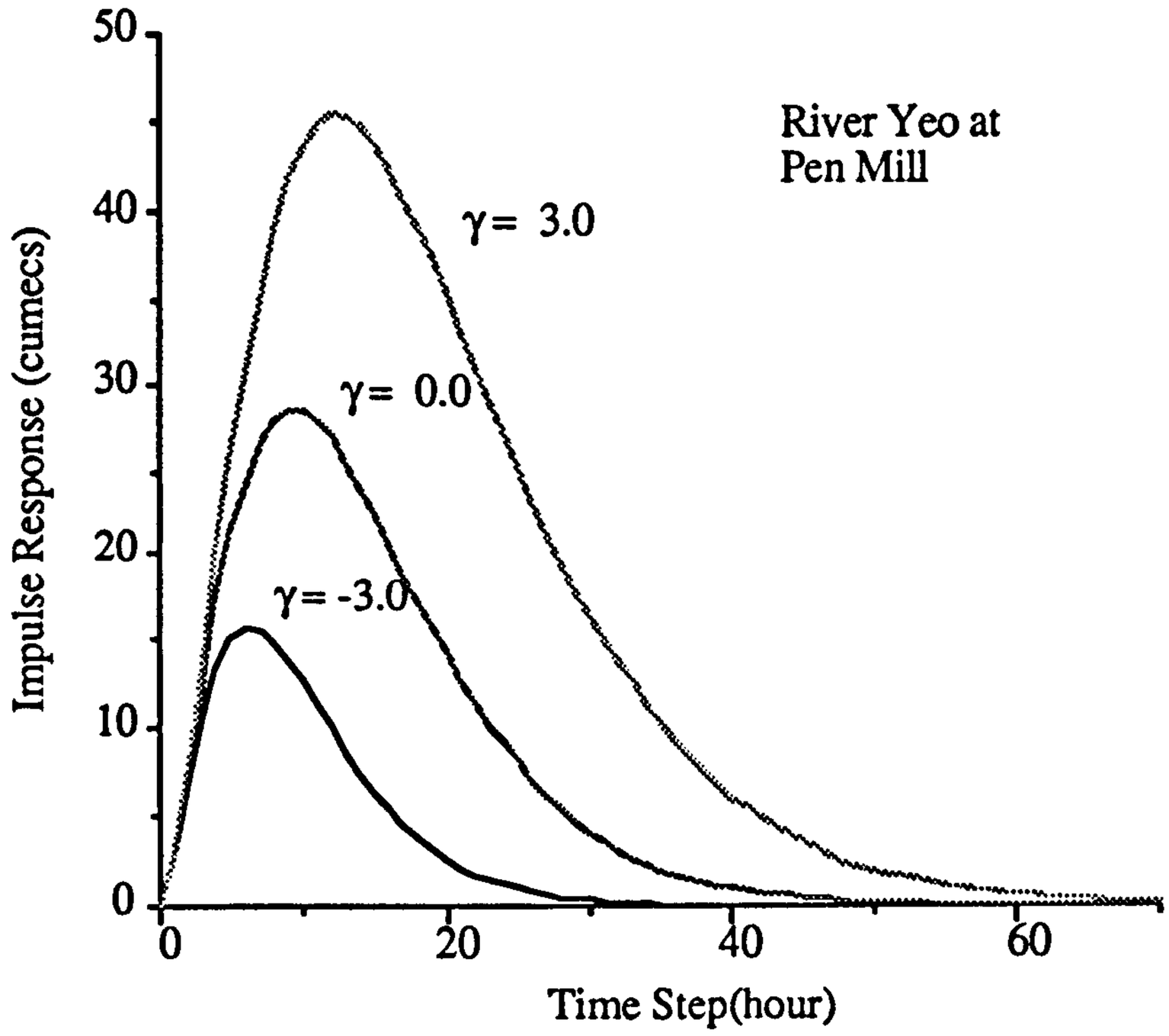

Figure 6.11 Effect of γ factor on Impulse Response of Yeo Model

As we found in Figure 6.11, the peak of the impulse response can be adjusted by the γ factor. One problem here is that the γ factor also alters the volume of the impulse response and conflicts with the α factor. To overcome the impulse area change, it is necessary to modify B_i parameters at the same time in order to preserve the orginal impulse area and hence the mass balance of the system.

$$\mathbf{AREA_1} = \frac{1}{\left(1 - \frac{1}{\beta}\right)^N} \qquad (6,25)$$

$$\mathbf{AREA_2} = \frac{1}{\left(1 - \frac{1}{\beta_{new}}\right)^N}$$

The B_i in Eq (6,3) will be

$$B_i = (1 + \alpha) \frac{AREA_1}{AREA_2} \; b_i \qquad i = 0, 1, 2, \ldots M$$

$$= (1 + \alpha) \left[\frac{1 - \frac{1}{\beta}}{1 - \frac{1}{\beta_{new}}} \right]^N b_i \qquad (6,26)$$

Or it can be simplified as

$$B_i = \frac{\beta_{new}^N (\beta - 1)^N}{\beta^N (\beta_{new} - 1)^N} \; (1 + \alpha) \; b_i \qquad i = 0, 1, 2, \ldots M \qquad (6,27)$$

For N = 2 the shape and volume adjustable forecasting PRTF will be

$$y(t) = \sum_{i=1}^{N} A_i \; y(t-i) + \sum_{i=0}^{M} B_i \; u(t-i) \qquad (6,28)$$

$$A_i = a_i \qquad i=1, 2, \ldots N$$

$$B_i = \frac{\beta_{new}^N (\beta - 1)^N}{\beta^N (\beta_{new} - 1)^N} \; (1 + \alpha) \; b_i \qquad i = 0, 1, 2, \ldots M$$

$$a_i = - C_N^{N-i} (- \beta_{new})^{-i} = - C_N^{N-i} \left(- e^{\frac{1}{(\gamma + \frac{1}{\ln \beta})}} \right)^{-i}$$

$$\beta_{new} = e^{\frac{1}{\gamma + \frac{1}{\ln \beta}}}$$

$$\beta \in \Re, \quad \beta > 1.0 \text{ and } \gamma > -\frac{1}{\ln \beta}$$

For N = 3 the shape and volume adjustable forecasting PRTF will be

$$y(t) = \sum_{i=1}^{N} A_i \, y(t-i) + \sum_{i=0}^{M} B_i \, u(t-i) \qquad (6,29)$$

$$A_i = a_i \qquad i=1,\ 2,\ \ldots\ N$$

$$B_i = \frac{\beta_{new}^{N} (\beta - 1)^{N}}{\beta^{N} (\beta_{new} - 1)^{N}} (1 + \alpha) b_i \qquad i = 0,\ 1,\ 2,\ \ldots\ M$$

$$a_i = - C_N^{N-i} (- \beta_{new})^{-i} \qquad (6,24)$$

$$\beta_{new} = e^{\frac{2\psi + 3}{(\psi^2 + 3\psi + 2)}}$$

$$\psi = \gamma + \frac{\frac{2}{\ln \beta} - 3 + \sqrt{(3 - \frac{2}{\ln \beta})^2 - 4 (2 - \frac{3}{\ln \beta})}}{2}$$

$$\beta \in \Re, \quad \beta > 1.0$$

$$\gamma > - \frac{\frac{2}{\ln \beta} - 3 + \sqrt{(3 - \frac{2}{\ln \beta})^2 - 4 (2 - \frac{3}{\ln \beta})}}{2}$$

Two models from the River Yeo and the River Tone are chosen to illustrate the γ factor.

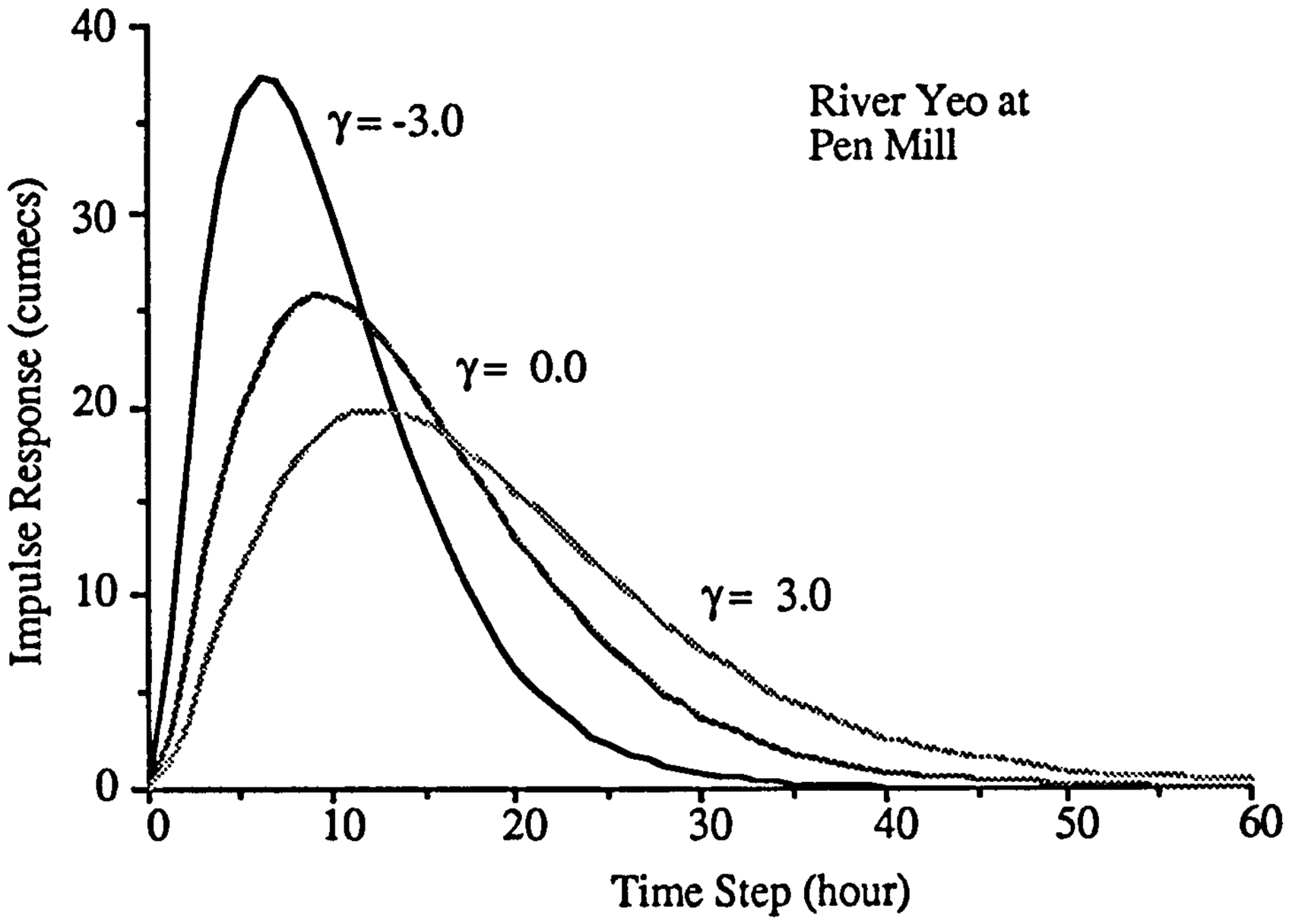

Figure 6.13 Effect of γ factor on Impulse Response of Yeo Model

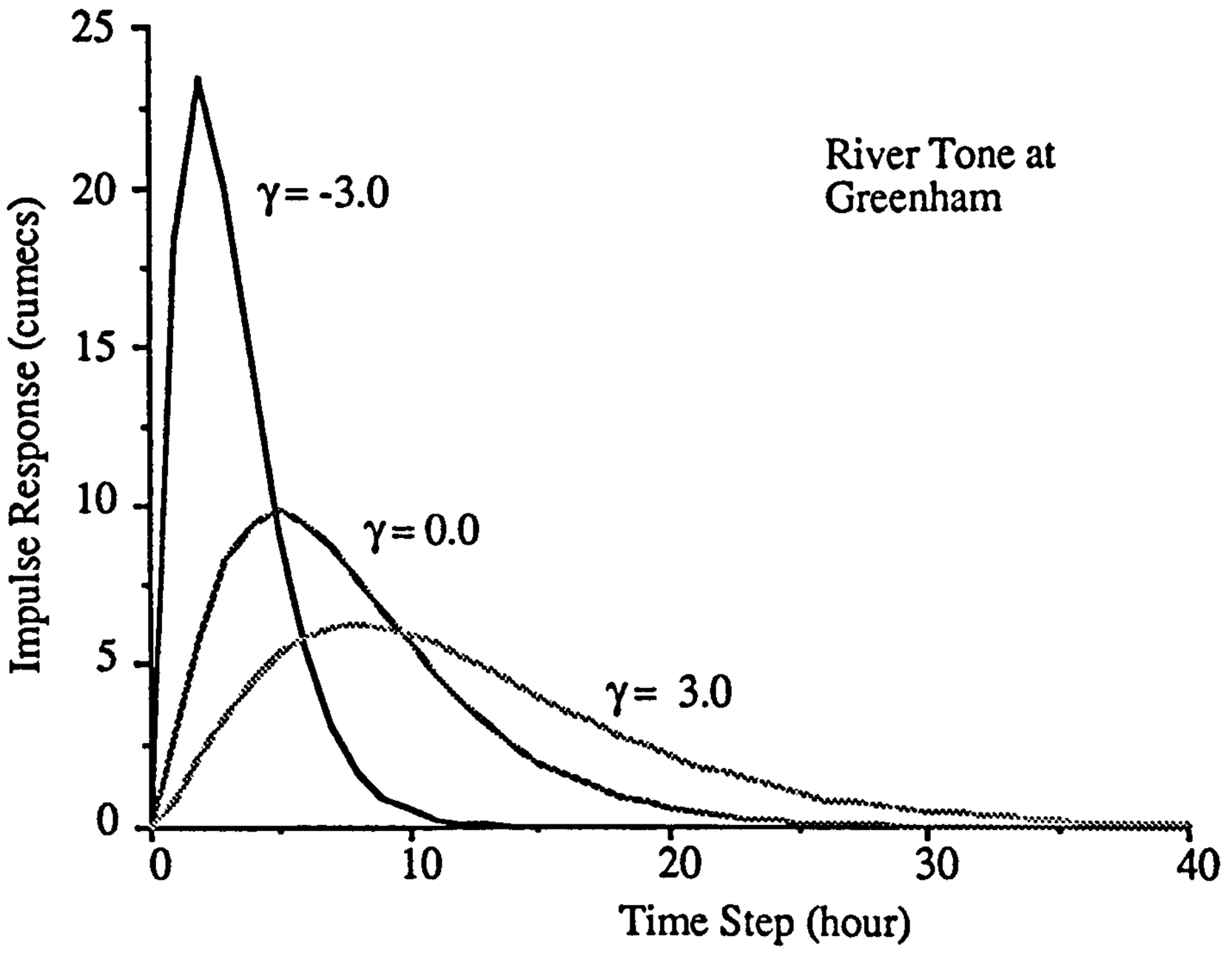

Figure 6.14 Effect of γ factor on Impulse Response of Tone Model

The results show from Figure 6.12 and Figure 6.13 that the Shape adjust factor γ can effectively alter the shape of the TF model impulse response without changing the response volume and time. This proves that the shape adjustment factor γ is correctly derived.

6.3.3 Time Adjust Factor τ

The impulse response time of a PRTF can be adjusted by a time shift operator applied to the rainfall terms.

$$y(t) = \sum_{i=1}^{N} A_i \; y(t-i) + \sum_{i=0}^{M} B_i \; u(t-\tau-i) \qquad (6,26a)$$

or in another form to shift B_i parameters as

$$y(t) = \sum_{i=1}^{N} A_i \; y(t-i) + \sum_{i=\tau}^{M+\tau} B_{i-\tau} \; u(t-i) \qquad (6,26b)$$

where $\tau = 0,1,2, \ldots$

Two models from the River Yeo and the River Tone were chosen to illustrate the τ factor.

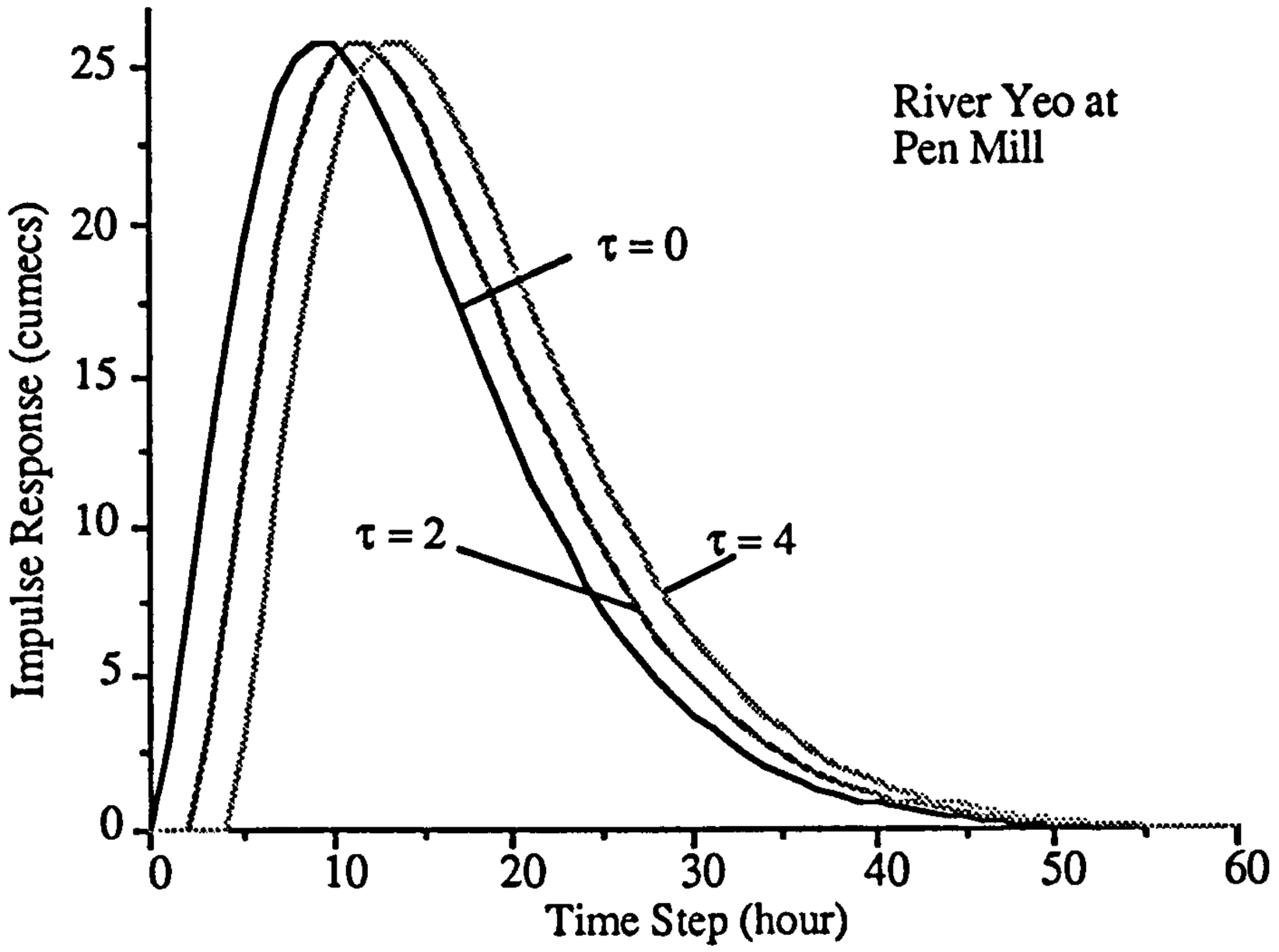

Figure 6.15 Effect of τ factor on Impulse Response of Yeo Model

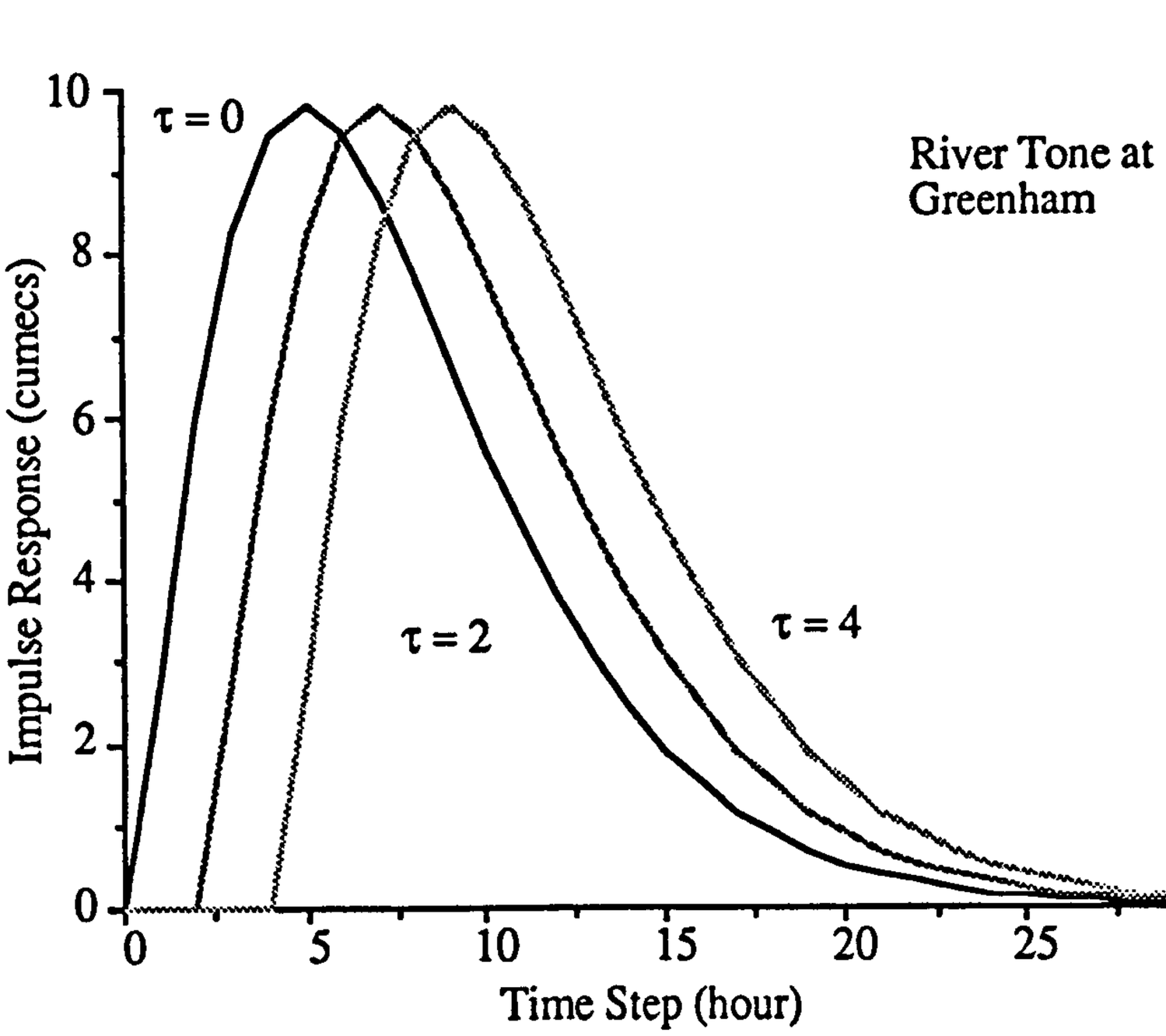

Figure 6.16 Effect of τ factor on Impulse Response of Tone Model

The results show from Figure 6.14 and Figure 6.15 that the time adjust

factor τ can effectively alter the time of the TF model impulse response without distorting the response shape and volume. This justifies the selection of the τ factor.

6.4 Forecasting Form of PRTF Model

The final form of the adjustable PRTF will be :

$$y(t) = \sum_{i=1}^{N} A_i \; y(t-i) + \sum_{i=0}^{M} B_i \; u(t - \tau - i \;) \qquad (6,27)$$

or as

$$y(t) = \sum_{i=1}^{N} A_i \; y(t-i) + \sum_{i=\tau}^{M+\tau} B_{i-\tau} \; u(t - i \;)$$

$$A_i = a_i \qquad i=1,\ 2,\ \ldots\ N$$

$$B_i = \frac{\beta_{new}^{N} \; (\beta - 1)^{N}}{\beta^{N} \; (\beta_{new} - 1)^{N}} \; (1 + \alpha) \; b_i \qquad i = 0,\ 1,\ 2,\ \ldots\ M$$

$$a_i = - C_N^{N-i} \; (- \beta_{new})^{-i}$$

$$\beta \in \Re, \quad \beta > 1.0$$

where $\tau = 0,1,2, \ldots$

For special cases, if $N = 2$

$$\beta_{new} = e^{\gamma + \frac{1}{\ln \beta}}$$

$$\gamma > -\frac{1}{\ln \beta}$$

If $N = 3$

$$\beta_{new} = e^{\frac{2\psi + 3}{(\psi^2 + 3\psi + 2)}}$$

$$\psi = \gamma + \frac{\frac{2}{\ln \beta} - 3 + \sqrt{(3 - \frac{2}{\ln \beta})^2 - 4(2 - \frac{3}{\ln \beta})}}{2}$$

$$\gamma > -\frac{\frac{2}{\ln \beta} - 3 + \sqrt{(3 - \frac{2}{\ln \beta})^2 - 4(2 - \frac{3}{\ln \beta})}}{2}$$

Some mathematical combinations are :

for $N = 2$

$$a_1 = - C_2^1 (-\beta)^{-1} = \frac{2}{\beta}$$

$$a_2 = - C_2^2 (-\beta)^{-2} = - \frac{1}{\beta^2}$$

For N = 3

$$a_1 = - C_3^1 (-\beta)^{-1} = \frac{3}{\beta}$$

$$a_2 = - C_3^2 (-\beta)^{-2} = - \frac{3}{\beta^2}$$

$$a_3 = - C_3^3 (- \beta)^{-3} = \frac{1}{\beta^3}$$

6.5 Summary

The impulse response of a TF is critical to the accuracy of the model forecasting. In this chapter, 3 adjustment factors are introduced into the PRTF model. Each factor is developed to only influence one aspect of the TF model. None of them can cause the TF model to become unstable or fluctuating. Computational results were satisfactory. These features are important for river flow forecasting and may be used as tools for Artificial Intelligence applications in real-time flood forecasting systems.

CHAPTER 7

CATCHMENT RESPONSE AND FLOOD FORECASTING

7.1 Introduction

The rainfall runoff process is a nonlinear and time variant process. To achieve better flood forecasting, the impulse response of the TF model should change with catchment conditions and storm type. In this chapter, analysis is concentrated on the catchment response to the storm type and the adaptivity of the PRTF model. Firstly, a distributed kinematic wave model is used to generate runoff according to various types of storms and research is carried out to analyse the behaviour of the catchment response. Some case studies are used to illustrate how the PRTF can cope with the catchment response changing. A RST (Rainfall Separation Tank) model is also developed to improve the river flow simulation process.

7.2 Kinematic Wave Model Computation

The St Venant Equation (Refer to Chow, Maidment and Mays 1988 for the detail) is used to model the unsteady flow in open channels, it has the form :

Continuity:

$$\frac{\partial A}{\partial t} + \frac{\partial Q}{\partial x} = q \qquad (7,1)$$

Momentum:

$$\frac{\partial V}{\partial t} + V\frac{\partial V}{\partial x} + \frac{g}{A}\frac{\partial(\dot{y}A)}{\partial x} + \frac{Vq}{A} = g\,(S - S_f) \qquad (7,2)$$

where V - flow speed

x - distance along the channel

Q - channel flow

A - channel cross section area

t - time

q - distributed flow along the side of the channel

g - gravity acceleration

S - gravity slope

S_f - friction slope

The Saint-Venant equations have various simplified forms, each defining a one dimensional distributed routing model. The simplest distributed model is the kinematic wave model, which neglects the local acceleration, convective acceleration, and pressure terms in the momentum equation; that is, it assumes S = S_f and the friction and gravity forces balance each other.

The kinematic wave model is defined by the following equations.

Continuity (The same as the original form):

$$\frac{\partial Q}{\partial x} + \frac{\partial A}{\partial t} = q \qquad (7,3)$$

Momentum:

$$S = S_f \tag{7,4}$$

The momentum equation can also be expressed in the form

$$A = \alpha Q^{\beta} \tag{7,5}$$

where

α & β are coefficients.

The kinematic wave method has been applied to describe flow over planes, as a model of the rainfall-runoff process. In this application the lateral flow is equal to the difference between the rates of rainfall and infiltration, and the channel flow is taken to be flow per unit width of plane.

The kinematic wave model of the rainfall-runoff process offers advantages over the unit hydrograph method in that it is a solution of the physical equations governing the surface flow, but the solution is only for one-dimensional flow, whereas the actual watershed surface flow is two-dimensional as the water follows the land surface contours. As a consequence, the kinematic wave parameters, such as Manning's roughness coefficient, must be adjusted to produce a realistic outflow hydrograph. Eagleson(1970), Overton and Meadows(1976), and Stephenson and Meadows(1986) present detailed information on kinematic wave models for the rainfall-runoff process.

The Saint-Venant equations for distributed routing are not amenable to analytical solution except in a few special simple cases. They are partial differential equations that, in general, must be solved using numerical methods. There are two popular methods: finite difference (FD) and finite element methods (FEM). Finite

difference methods are found to be discrete techniques wherein the domain of interest is represented by a set of points or nodes and information between these points is commonly obtained using Taylor series expansions. In contrast, the finite element method employs piecewise continuous polynomials to interpolate between nodal points. Although points or nodes play a role in finite element theory, the emphasis is directed more toward the interpolation functions. The FEM possesses considerable advantages when used to solve highly spatially dependent problems and is less efficient in solving time dominated problems. Conversely, the FD method only approximates complex spatial boundaries but excels in solving essentially time dependent problems. The finite difference method is adopted here to solve the partial equation.

The fundamental concept encountered in this form of approximation theory is that the domain of solution of the given partial differential equation is first subdivided by a net with a finite number of mesh points. The derivative at each point is then replaced by a finite difference approximation. Alternatively, one can visualise this discretisation procedure as the replacement of the solution of the partial differential equation with a polynomial and the differentiation of this polynomial.

The finite-difference form of Eq(7,3) can be expressed as

$$\frac{Q_{i+1}^{j+1} - Q_i^{j+1}}{\Delta x} + \frac{A_{i+1}^{j+1} - A_{i+1}^{j}}{\Delta t} = \frac{q_{i+1}^{j+1} + q_{i+1}^{j}}{2} \qquad (7,5)$$

Eq(7,4) can be expressed as

$$A_{i+1}^{j+1} = \alpha \left(Q_{i+1}^{j+1} \right)^{\beta}$$
$$A_{i+1}^{j} = \alpha \left(Q_{i+1}^{j} \right)^{\beta} \qquad (7,6)$$

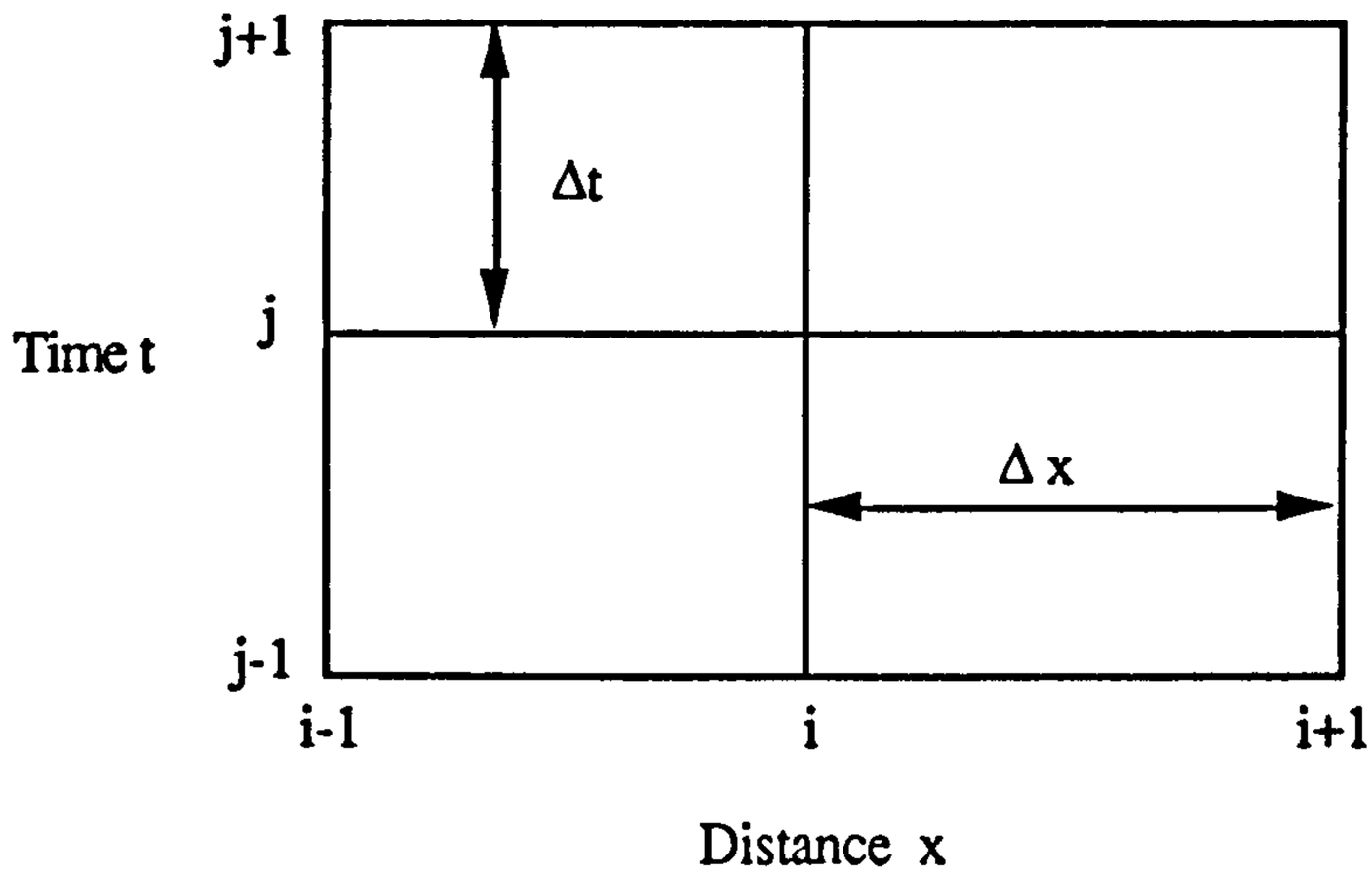

Figure 7.1 The Grid used for Numerical Solution by Finite Differences

Eqs (7,6) is substituted into (7,5) to obtain, after rearranging,

$$\frac{\Delta t}{\Delta x} Q_{i+1}^{j+1} + \alpha (Q_{i+1}^{j+1})^{\beta} = \frac{\Delta t}{\Delta x} Q_{i}^{j+1} + \alpha (Q_{i+1}^{j})^{\beta} + \Delta t \left(\frac{q_{i+1}^{j+1} + q_{i+1}^{j}}{2} \right) \qquad (7,7)$$

This equation has been arranged so that the unknown discharge is on the left-hand side, and all the unknown quantities are on the right-hand side. It is a nonlinear equation, so a numerical solution scheme such as Newton's method will be required.

The known right-hand side at each finite-difference grid point is

$$C = \frac{\Delta t}{\Delta x} Q_{i}^{j+1} + \alpha (Q_{i+1}^{j})^{\beta} + \Delta t \left(\frac{q_{i+1}^{j+1} + q_{i+1}^{j}}{2} \right) \qquad (7,8)$$

From which a residual error is defined as

$$f(Q_{i+1}^{j+1}) = \frac{\Delta t}{\Delta x} Q_{i+1}^{j+1} + \alpha (Q_{i+1}^{j+1})^{\beta} - C \qquad (7,9)$$

The first derivative of error is

$$f'(Q_{i+1}^{j+1}) = \frac{\Delta t}{\Delta x} + \alpha\beta \, (Q_{i+1}^{j+1})^{\beta-1} \qquad (7,10)$$

Using Newton's method(Chow, Maidment and Mays 1988) with iterations k = 1, 2, . . .

$$(Q_{i+1}^{j+1})_{k+1} = (Q_{i+1}^{j+1})_{k} - \frac{f(Q_{i+1}^{j+1})_{k}}{f'(Q_{i+1}^{j+1})_{k}} \qquad (7,11)$$

The convergence criterion for the iterative process is

$$| f (Q_{i+1}^{j+1})_{k+1} | \leq \varepsilon \qquad (7,12)$$

where ε is an error criterion.

7.3 Impulse Response from Different Types of Storms

As the kinematic wave model can be used to simulate the rainfall runoff process, the relationship between storm type and the catchment impulse response was analysed here.

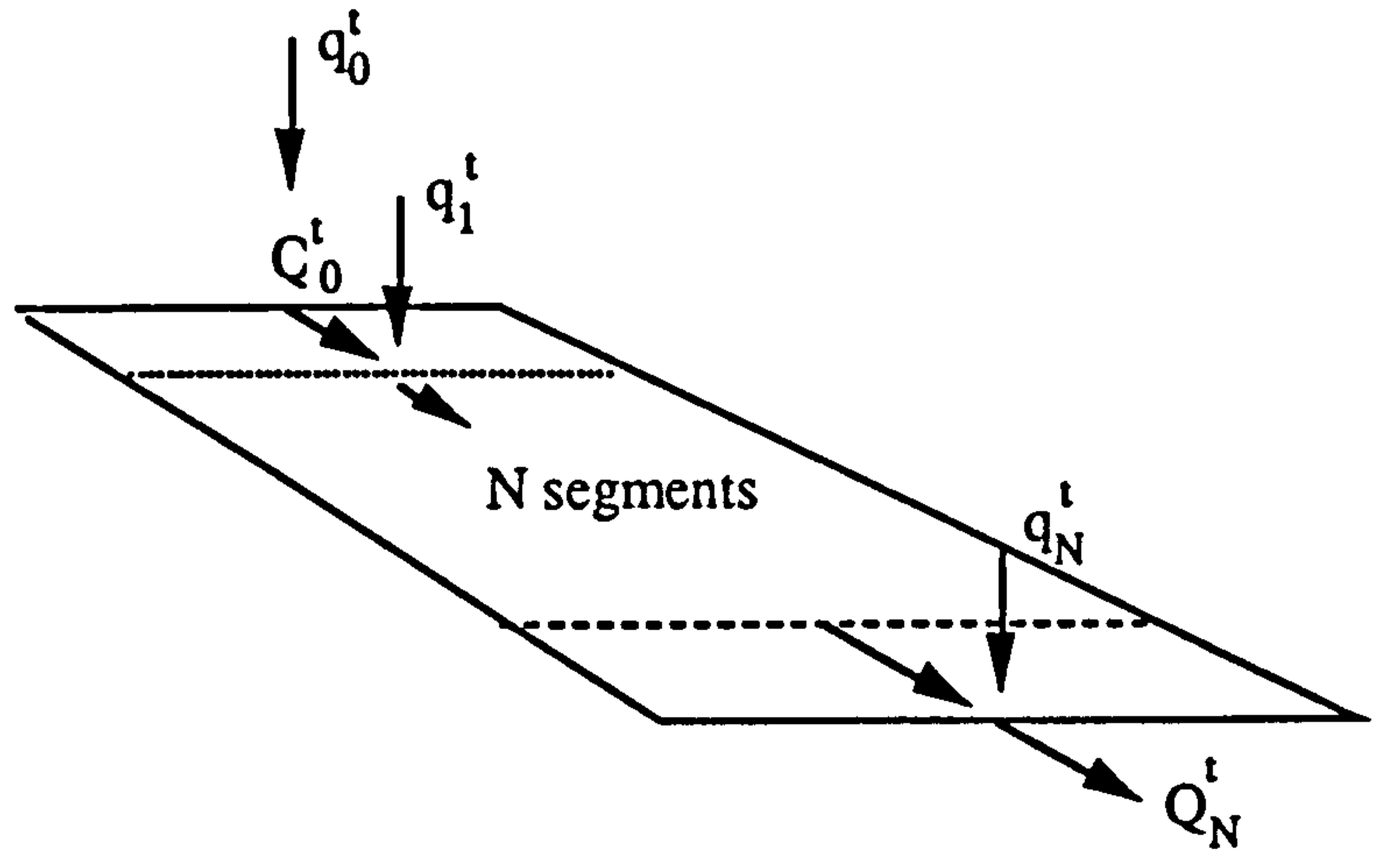

Figure 7.2 Simulated Catchment by Kinematic Wave Model

The parameters are selected as follows.

A 0.5 km wide catchment is 5 km long, has a bed slope of 10 percent, and a Manning's roughness factor of 0.035. Boundary value and initial value are

$$Q_i^j \mid_{j=0} = Q_0 \quad \text{(i)}$$

$$Q_i^j \mid_{i=0} = 0 \quad \text{(Start of Catchment flow)}$$

Manning's equation with $P \approx B$, $S_0 = S_f$, and channel width B is written

$$Q = \frac{S_0^{1/2} A^{5/3}}{n P^{2/3}} \tag{7,13}$$

which can be solved for A as

$$A = \left(\frac{n P^{2/3}}{\sqrt{S_0}} \right)^{3/5} Q^{3/5} \qquad (7,14)$$

So $\beta = 0.6$

and

$$\alpha = \left(\frac{n P^{2/3}}{\sqrt{S_0}} \right)^{0.6} \qquad (7,15)$$

here

$$\alpha = \left(\frac{0.035 \cdot 500^{2/3}}{\sqrt{0.1}} \right)^{0.6}$$

$$= 3.2$$

To identify a PRTF model from the kinematic wave model, evenly distributed random rainfall data was input into the model. The solution is as below.

PRTF (3,3) model with $t_{peak} = 4.0$,

b(0)=187.1

b(1)=28.45

b(2) = -85.9

Model time interval is 3 minutes.

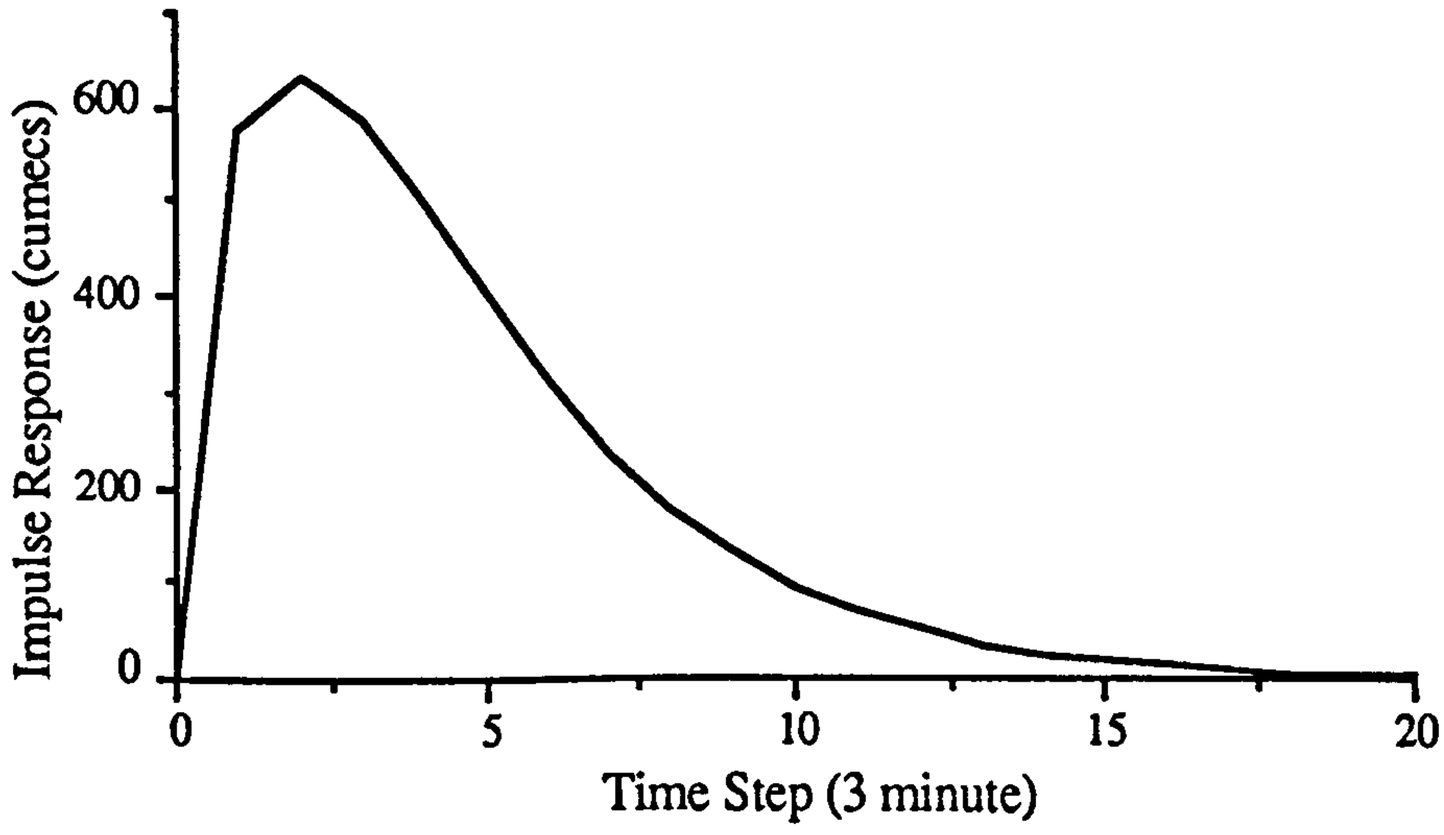

Figure 7.3 Impulse Response from Kinematic Wave Model

7.3.1 Influence of Rainfall Intensity

To analyse the catchment response to different rainfall intensity, ten storms were generated with 10 different intensities. It can be imagined that the catchment will respond to the storm intensity as illustrated in Figure 7.3.

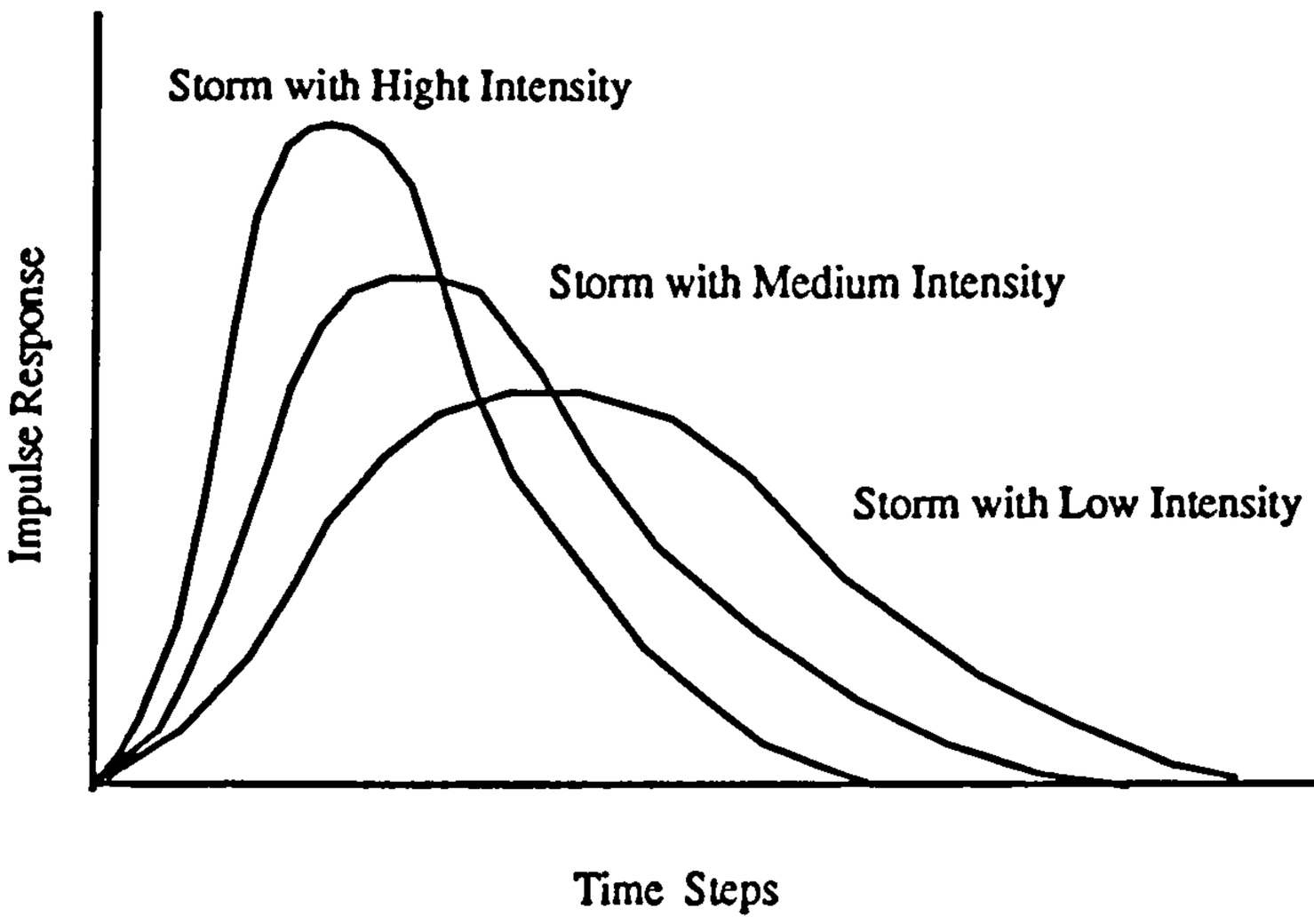

Figure 7.3 Influence of Storm Intensity on Catchment Response

It is known that a high intensity storm will generate fast response and a lower intensity one will generate slow response. As we know, the t_{peak} parameter in the PRTF controls the shape of the impulse response of the TF model, a relationship can be therefore derived between the storm intensity and tpeak.

As flow speed is related to the flow discharge

$$v = k\, Q^{\beta}$$

where k - equation parameter related with catchment

t_{peak} should be a inverse of flow speed v, so

$$t_{peak} = \frac{L}{k\, Q^{\beta}} \qquad (7,16)$$

where k, L is parameters related with catchment.

Catchment discharge comes from storm rainfall and directly relates to storm intensity when the storm is evenly distributed. We assume that

$$Q = a\, I \qquad (7,17)$$

where a = constant parameter related to the catchment.

Substitute Equation (7,17) into Equation(7,16), we have

$$t_{peak} = \left(\frac{c}{I}\right)^{\beta} \qquad (7,18)$$

Where c,β ------ Equation Parameters

I ------ Storm Average Intensity

Eq(7,18) assumes for the same catchment with a uniform storm distribution, there exists a unique relationship between storm intensity and the response shape of the catchment. A diagram is plotted in Figure 7.4 to represent the relationship between t_{peak} and storm intensities derived from Eq(7,18).

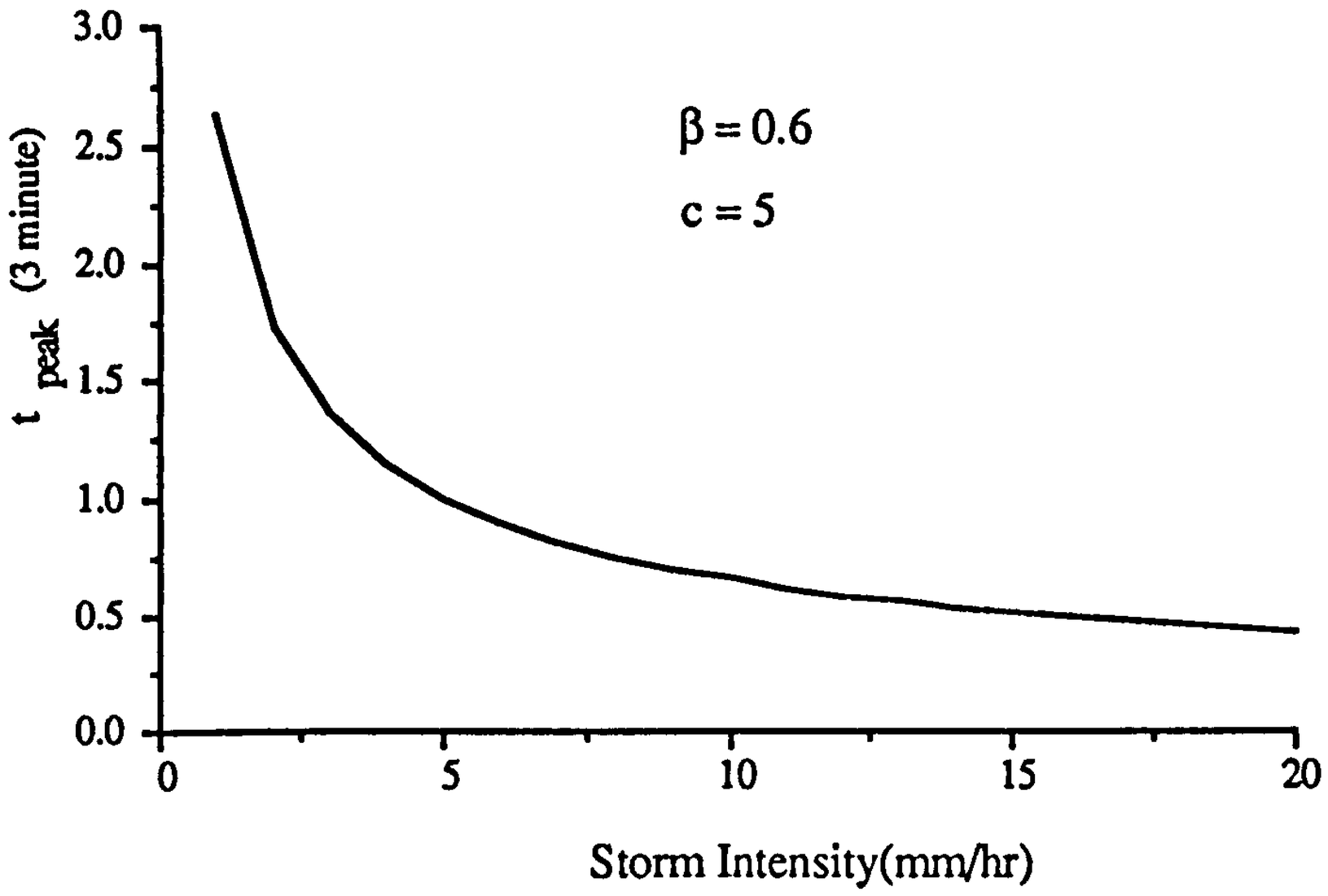

Figure 7.4 Idealised Relationship between Storm Intensity and t_{peak}

To verify the correctness of Equation (7,18), several intensities were tested to estimate parameters c & β and their relationship with tpeak. The result is shown in Figure 7.5.

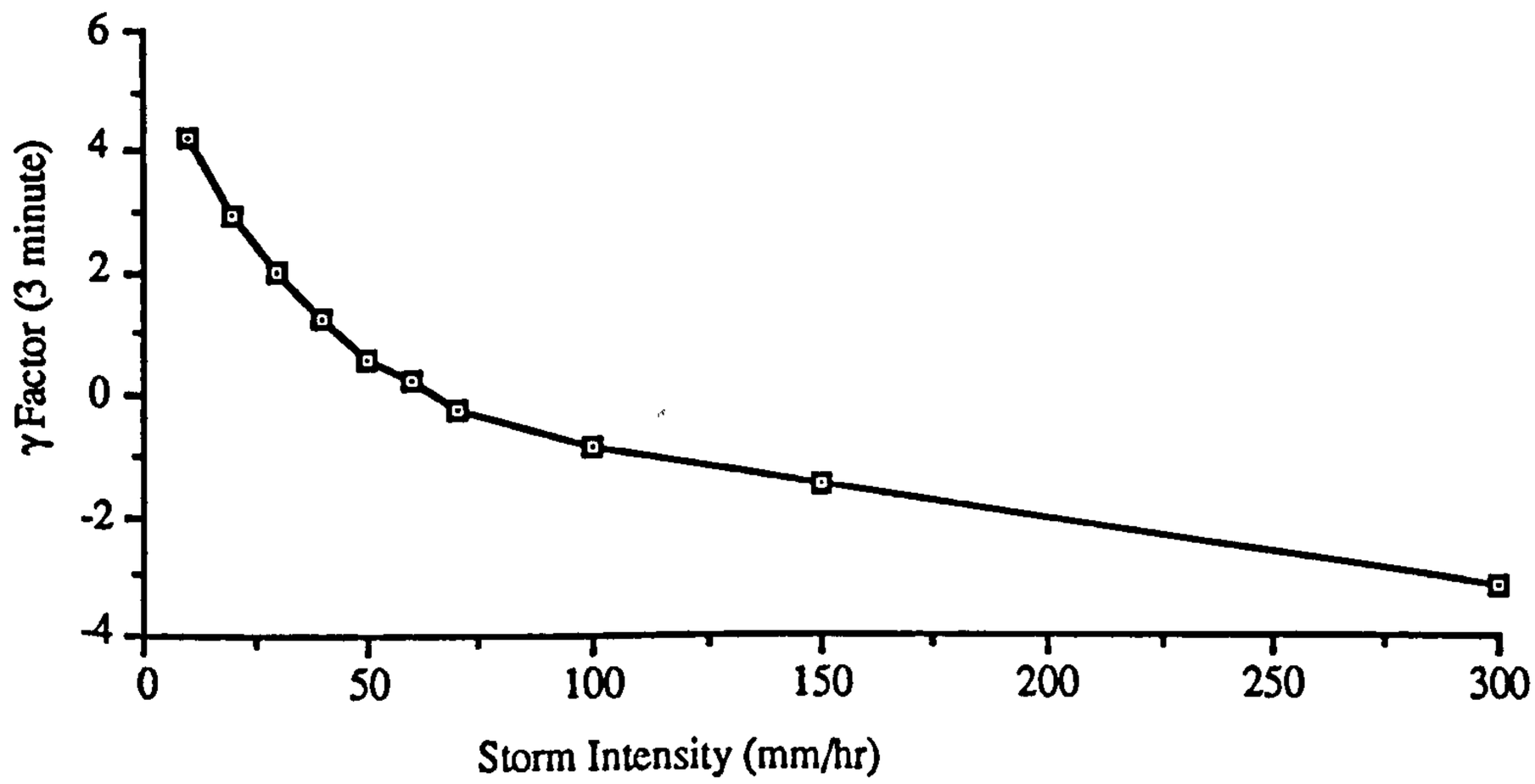

Figure 7.5 γ Factor and Storm Intensity

From Figure 7.5, it is found that the curve is similar to figure 7.4 and the derived equation for tpeak (which is related to the γ factor) is correct. Some examples of impulse responses influenced by storm intensities are given below.

In Figure 7.6-7.7, a comparison is made between the PRTF simulation with and without changing the impulse response of the model. It can be seen that an observable improvement after altering the impulse response of the PRTF model results.

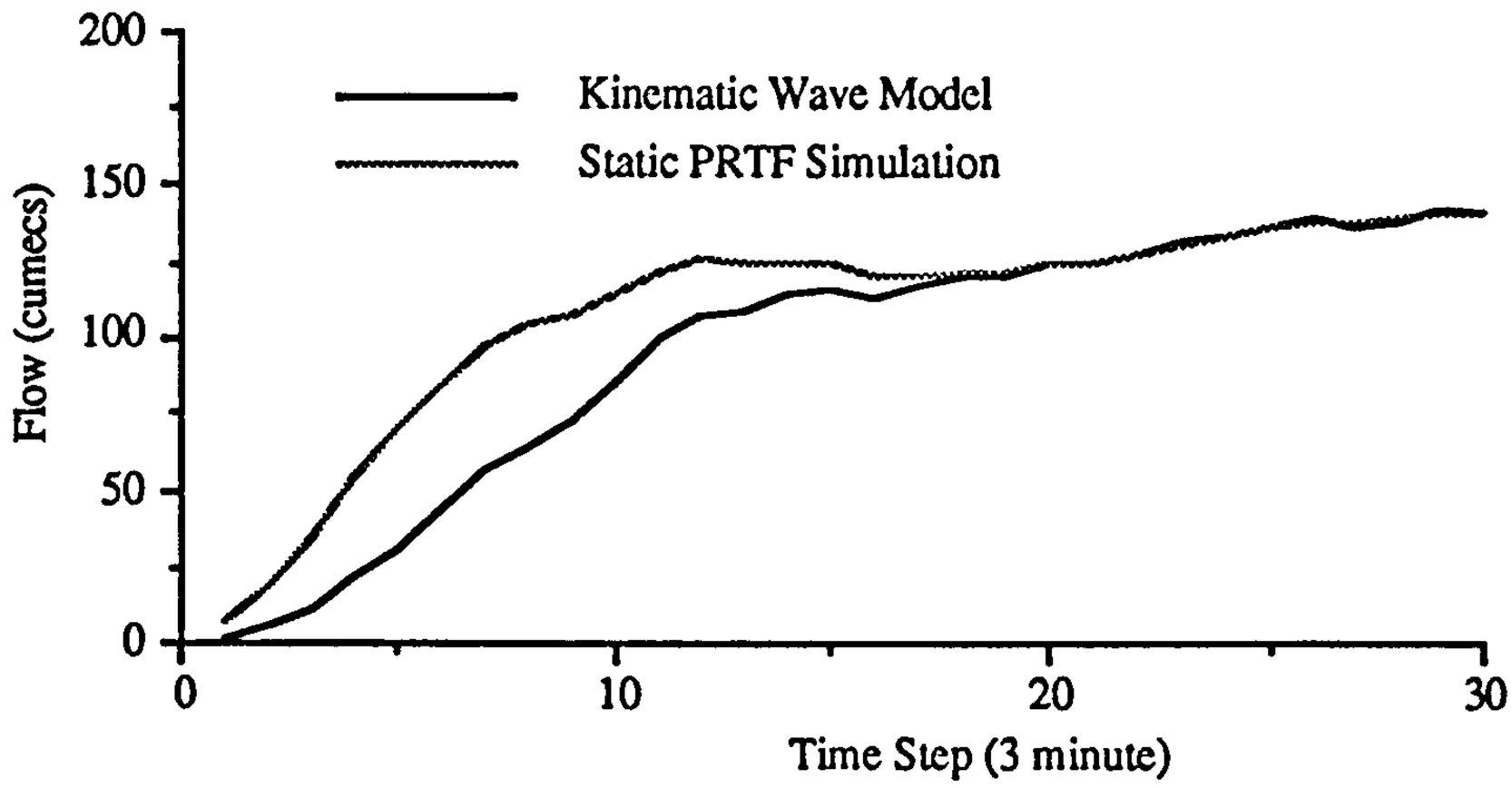

Figure 7.6 Static PRTF Simulation in 20 and 50 mm/hr Storm

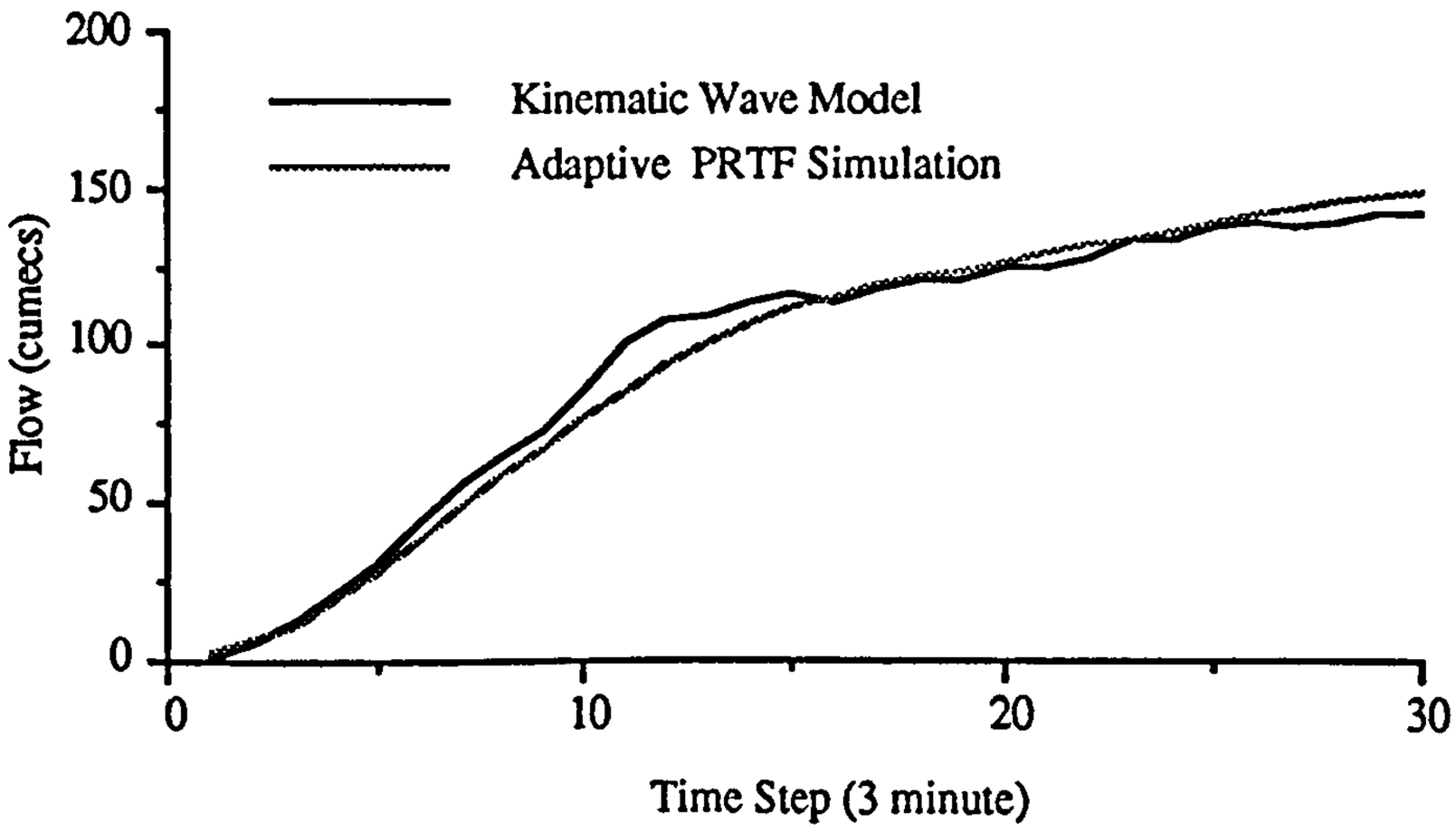

Figure 7.7 Adaptive PRTF Simulation in 20 and 50 mm/hr Storm

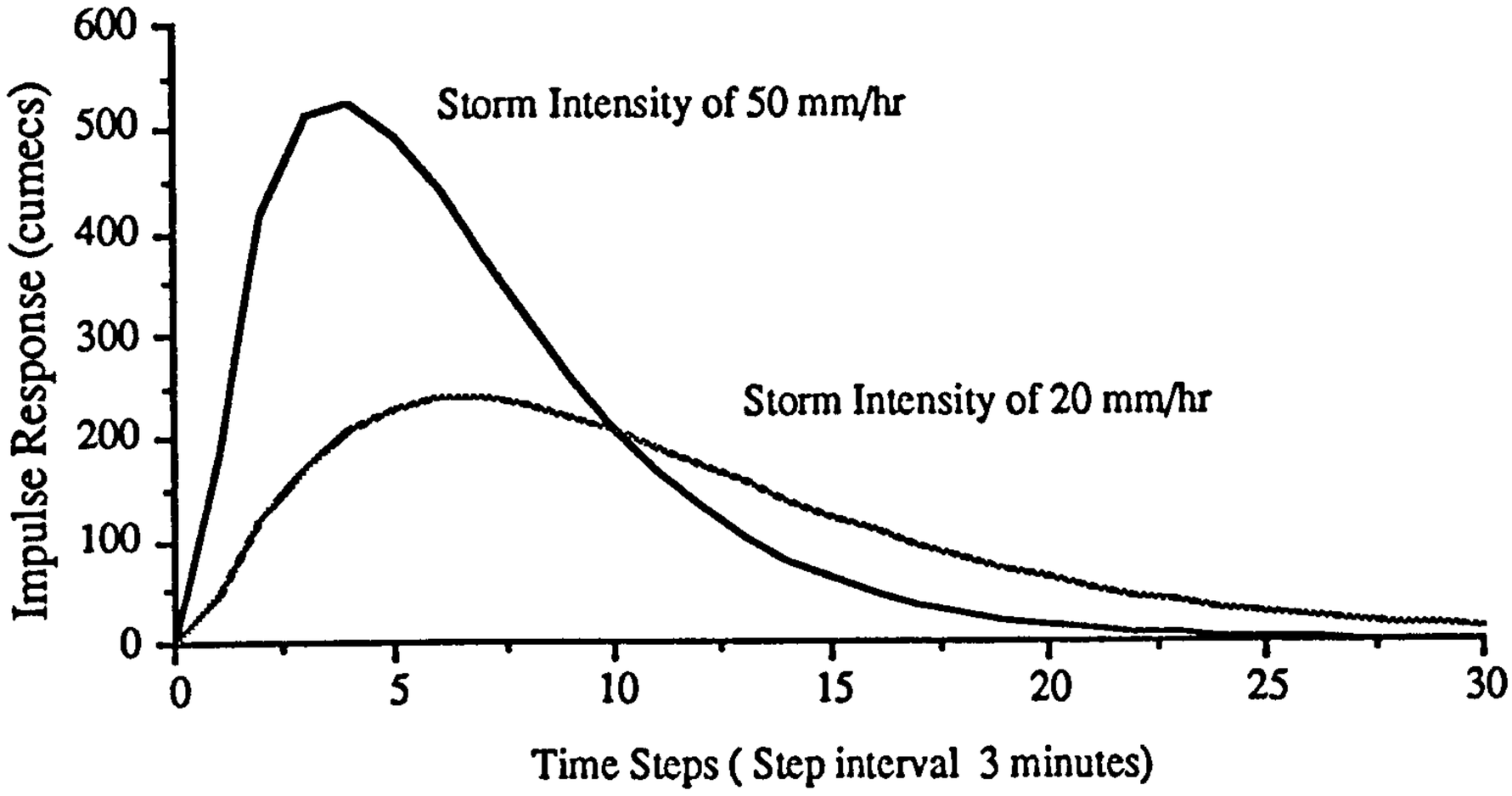

Figure 7.8 Catchment Response Function in Storm 20 and 50 mm/hr

It can be seen that the impulse response for 20 mm/hr is flatter than the 50 mm/hr rate and the peak is delayed.

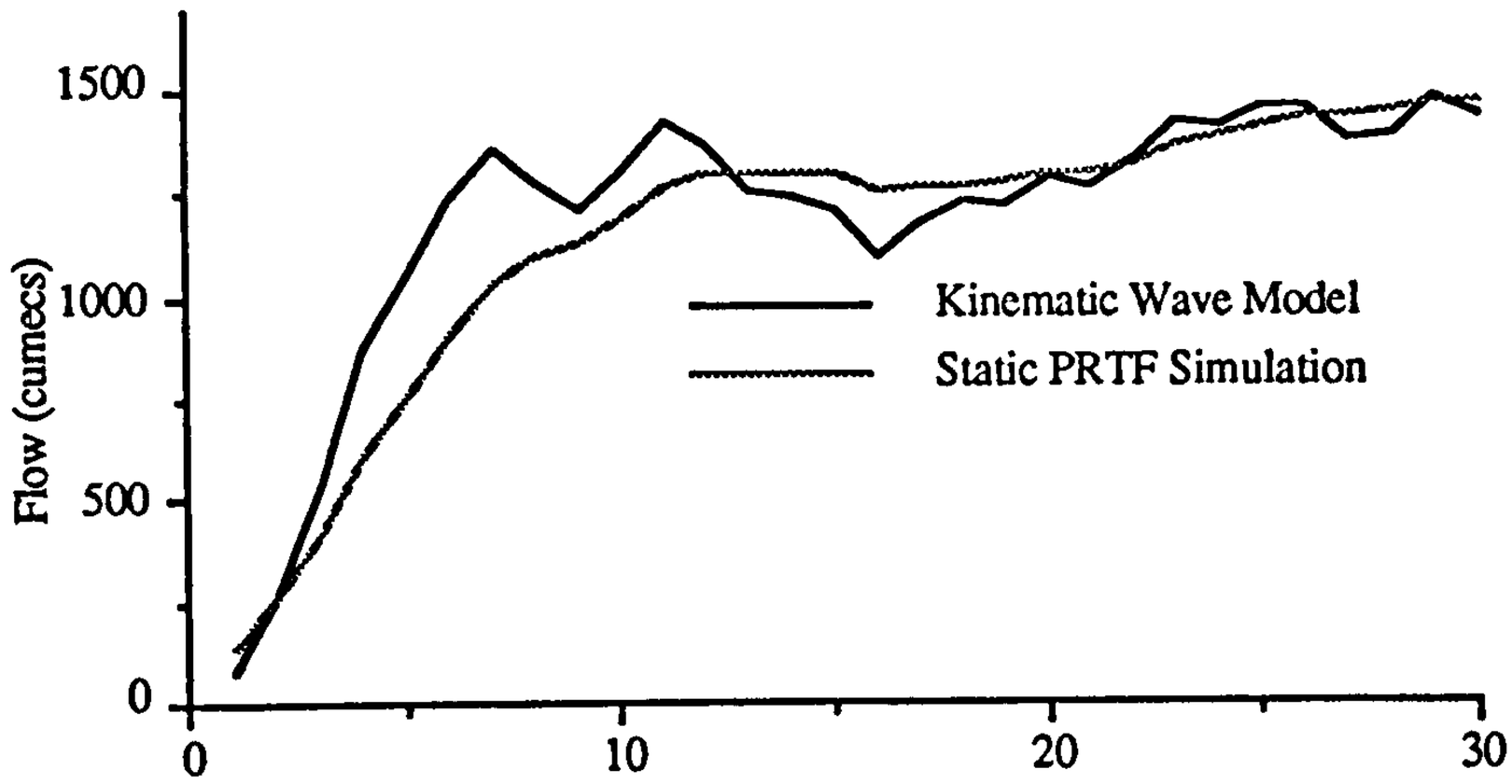

Figure 7.9 Static PRTF Simulation in 150 and 50 mm/hr Storm

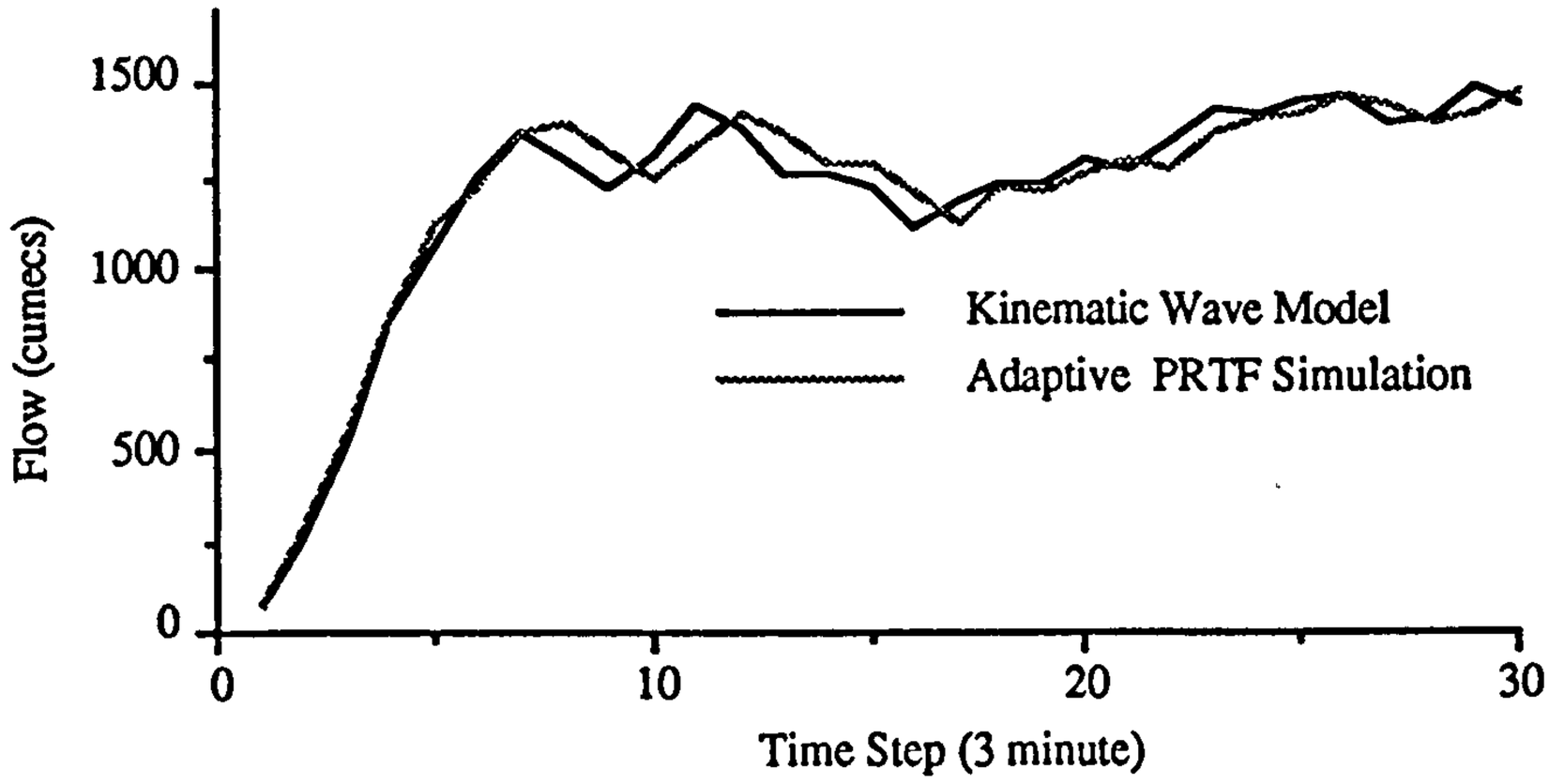

Figure 7.10 Adaptive PRTF Simulation in 150 and 50 mm/hr Storm

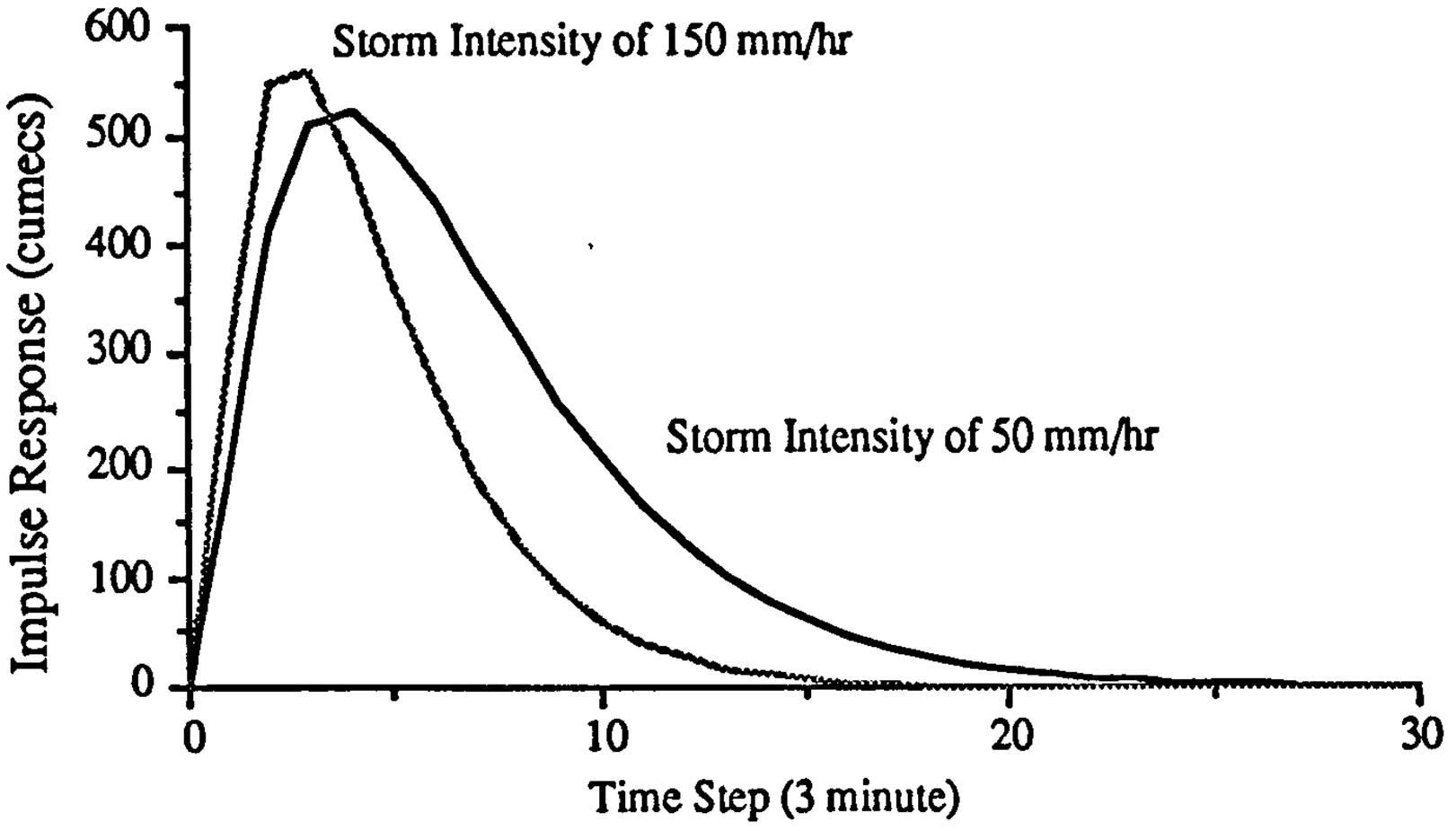

Figure 7.11 Catchment Response Function in Storm 150 and 50 mm/hr

It can be found the impulse response of 150 mm/hr is steeper than 50 mm/hr and the peak is advanced.

7.3.2 Influence of Rainfall Location

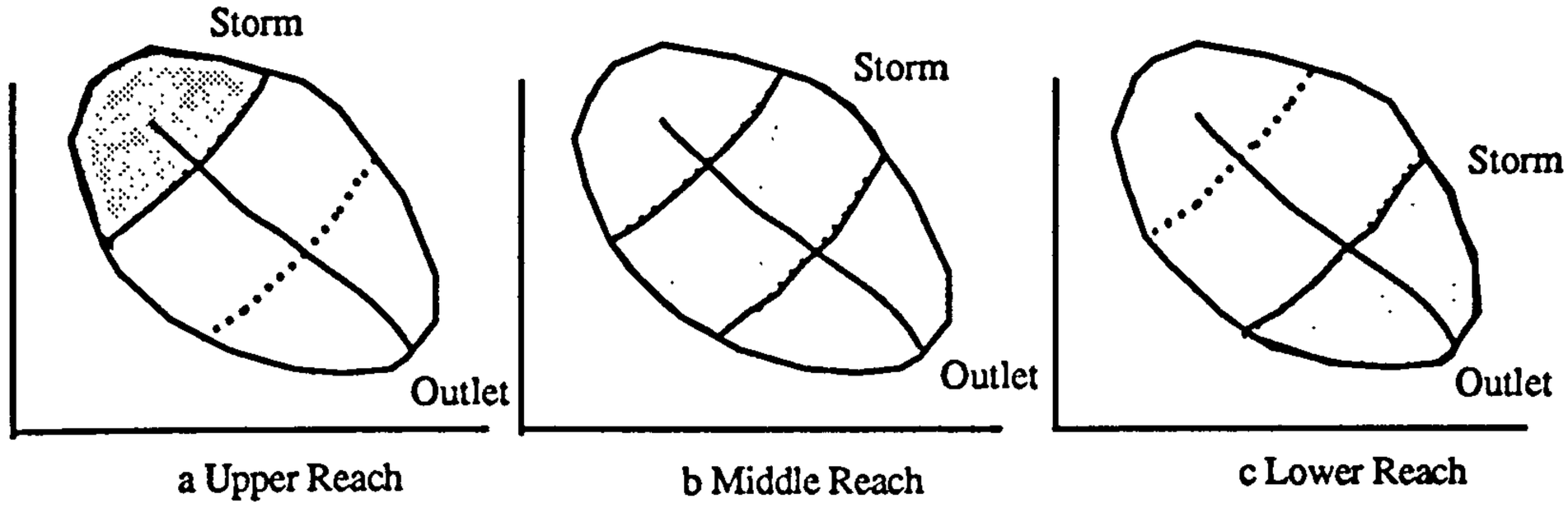

Figure 7.12 Storm Location on Catchment

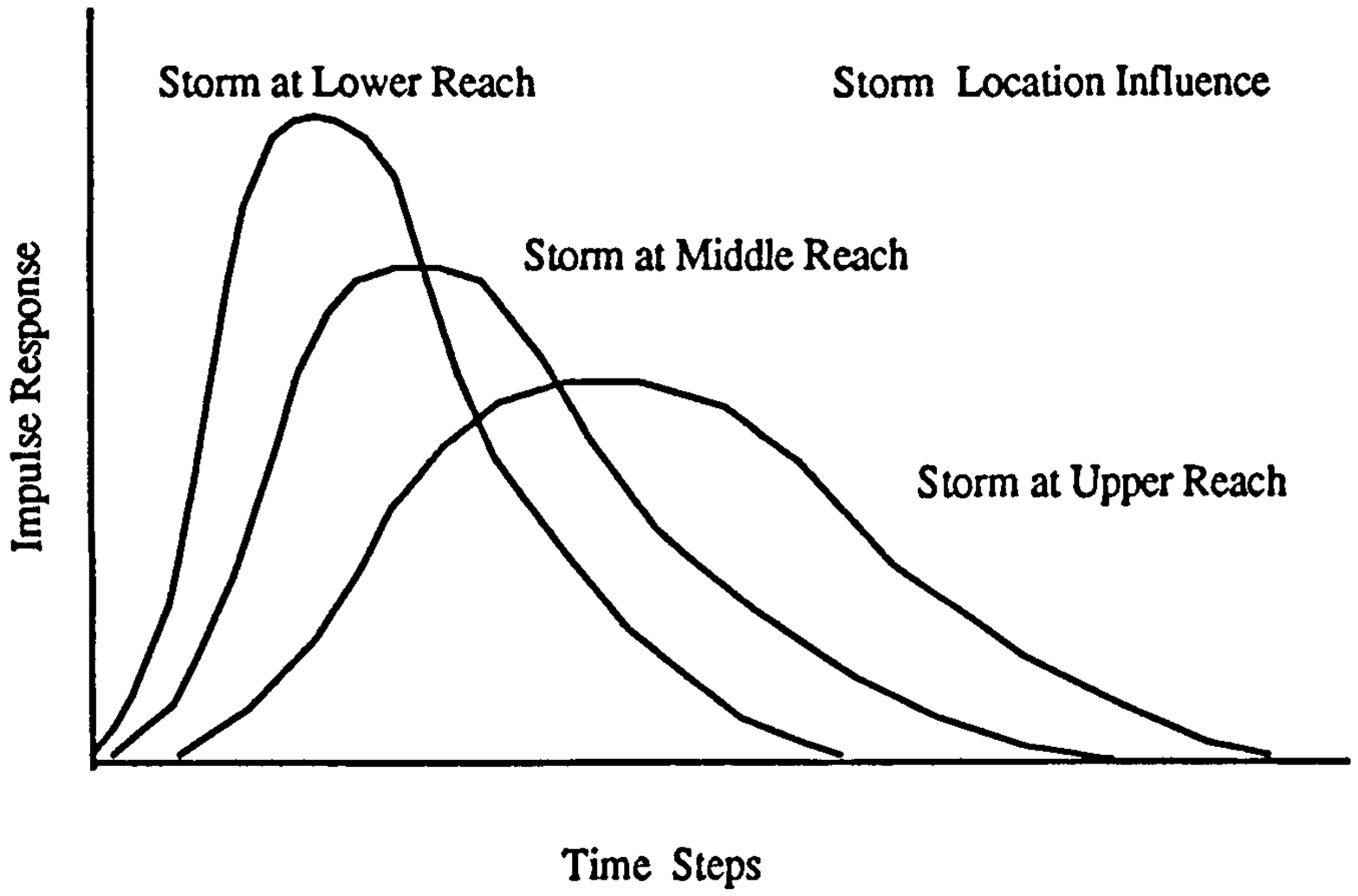

Figure 7.13 Influence of Storm Location on Catchment Response

The storm location will influence the catchment response as in Figure 7.12 and Figure 7.13. Storm centres over the lower rpart of the catchment will generate fast response and over the upper reaches a slow response. Two parameters need to be modified which are t_{peak} and time delay τ. It can be considered as a two step

process (1) Transposition of the impulse response time by time τ. (2) Reshape the impulse response by t_{peak}.

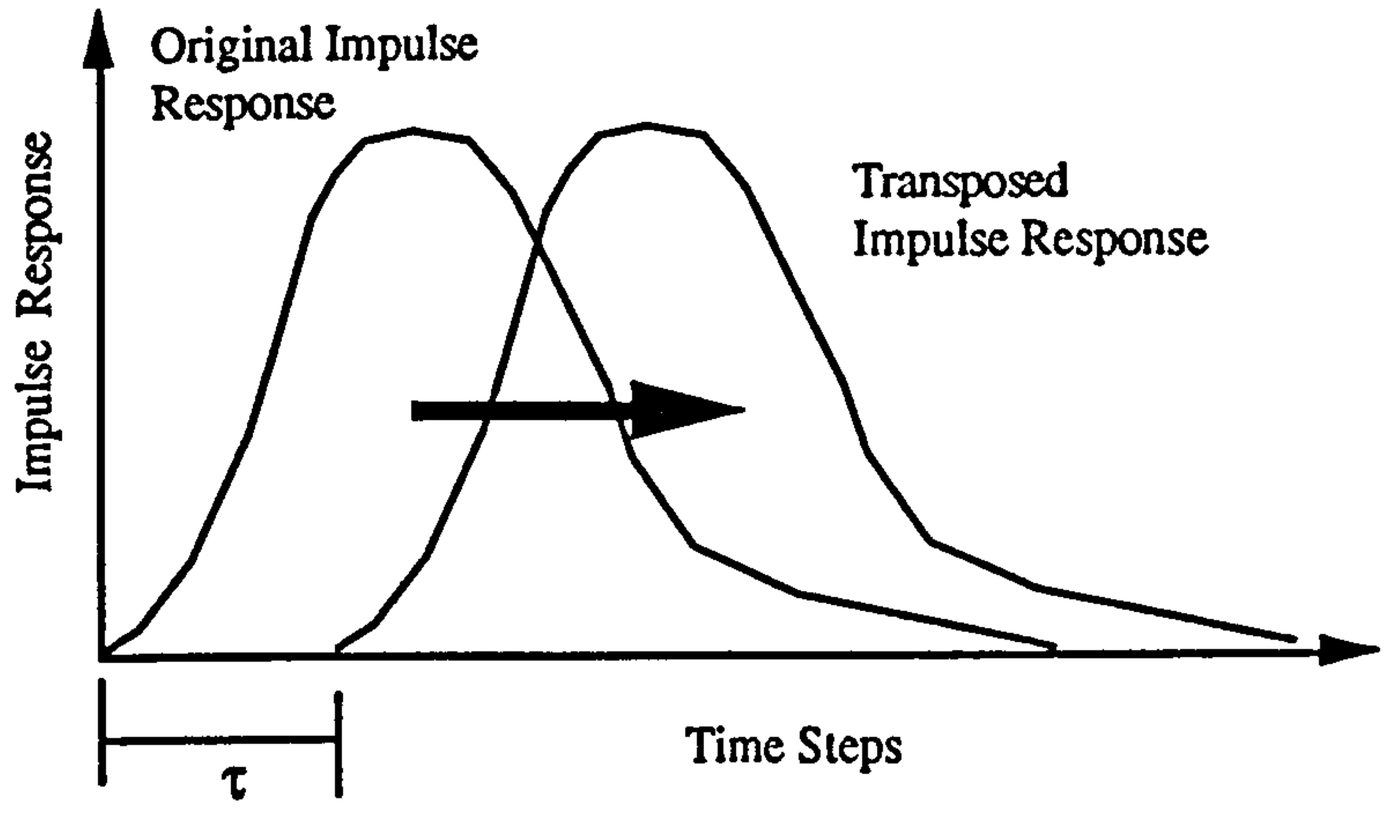

Figure 7.14 Transposition of PRTF from the Influence of Storm Location

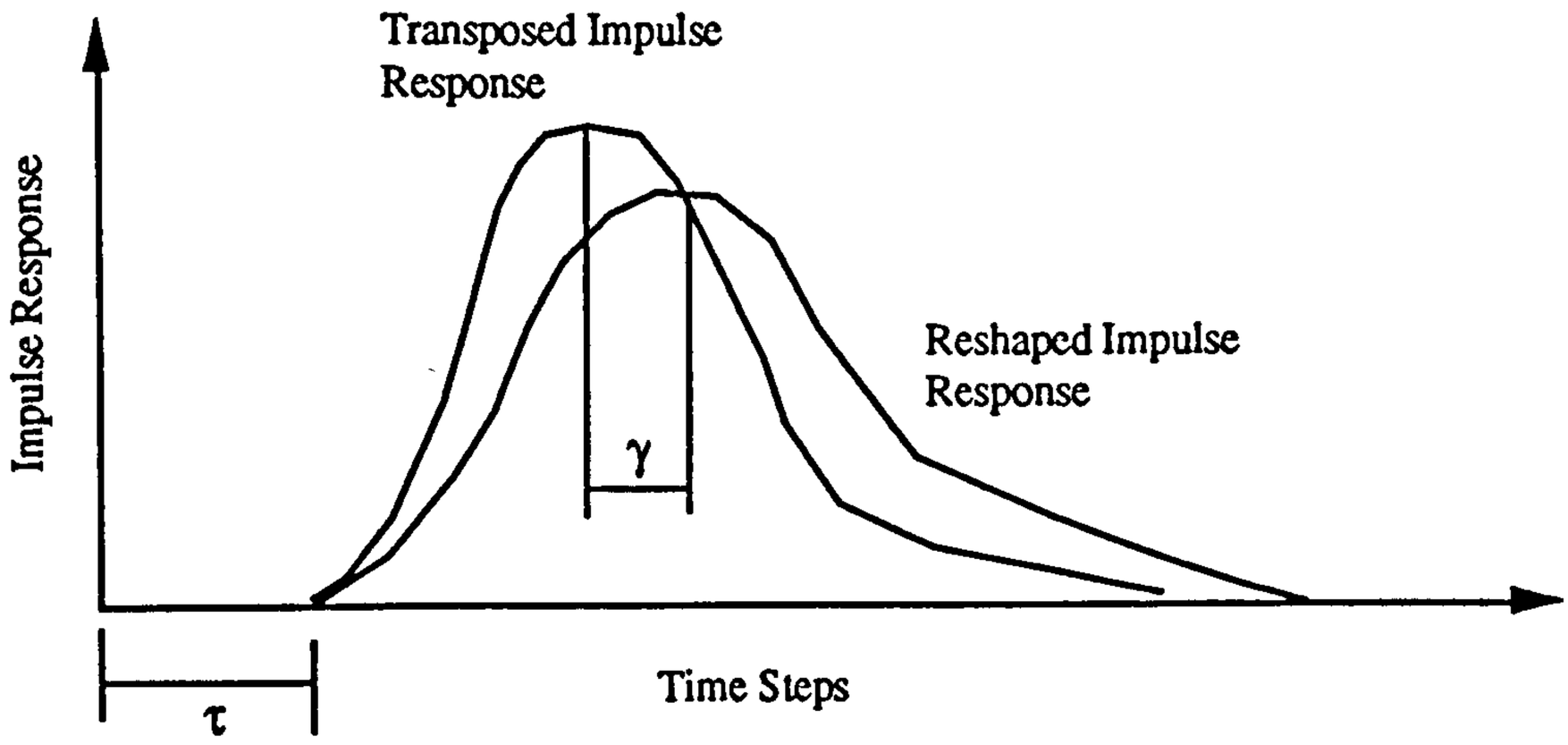

Figure 7.15 Reshape of PRTF from the Influence of Storm Location

The delay time τ is related to the location of storm, so

$$\tau = a_{loc} L_{loc} \tag{7.19}$$

where a_{loc} is parameter from catchment.

Parameter γ has not got a simple linear relationship with the storm location L_{loc}.

We assume :

$$\gamma = b_{loc} L_{loc}^{f} \qquad (7,20)$$

The following figures show that the assumption above is true during the kinematic wave simulation.

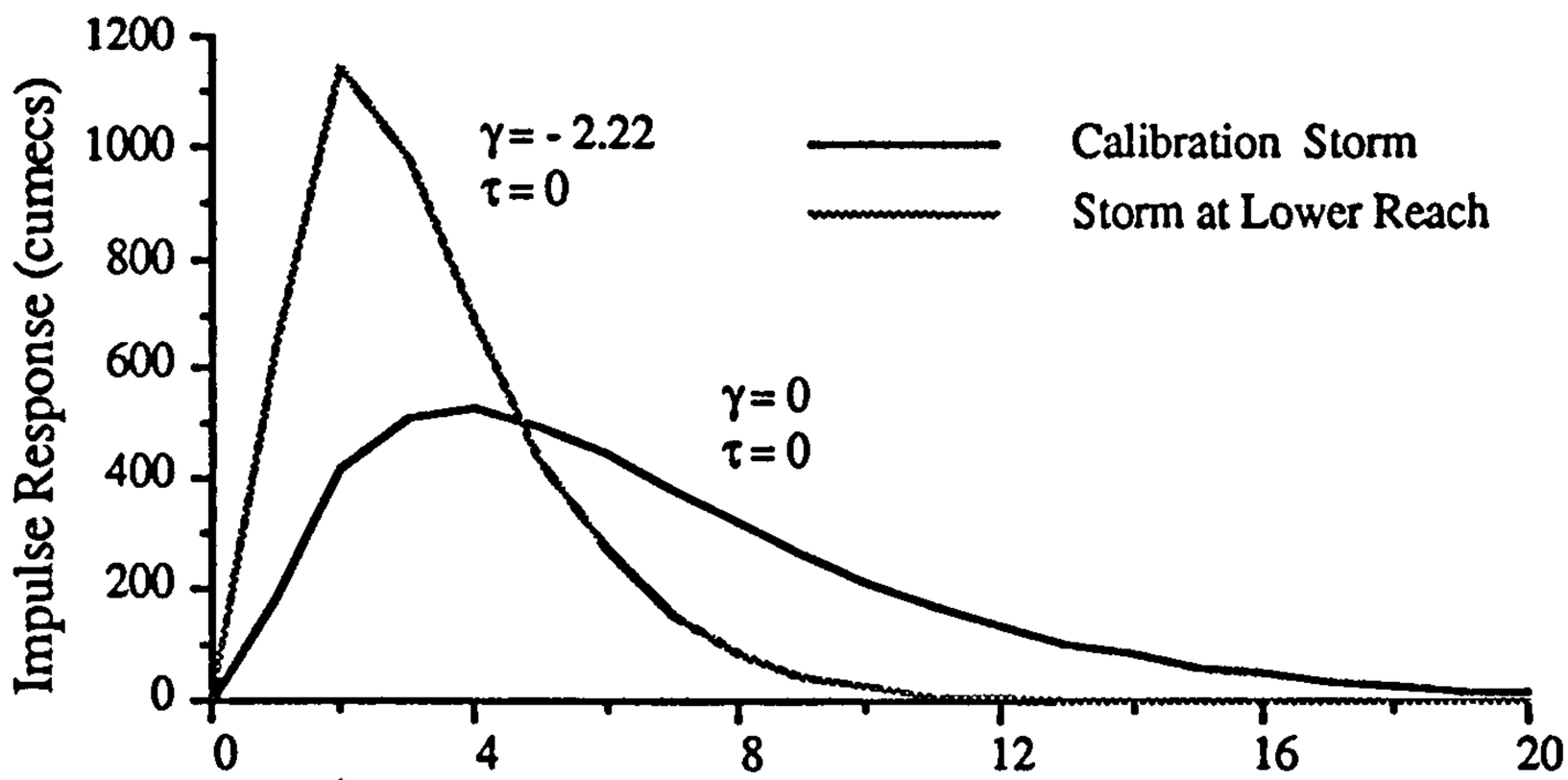

Figure 7.16 Impulse Response of Storm over Lower Catchment

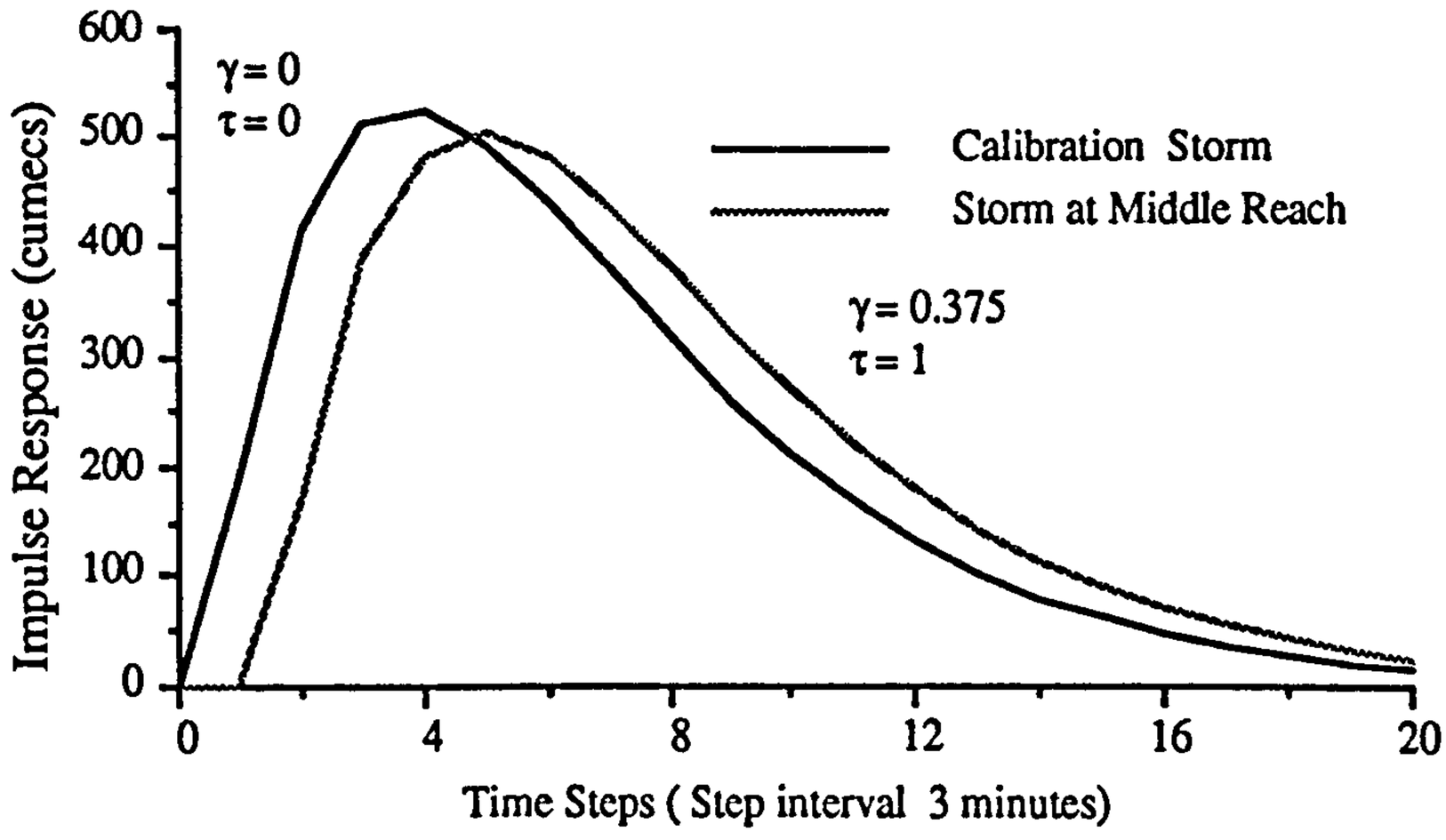

Figure 7.17 Impulse Response of Storm over Middle Catchment

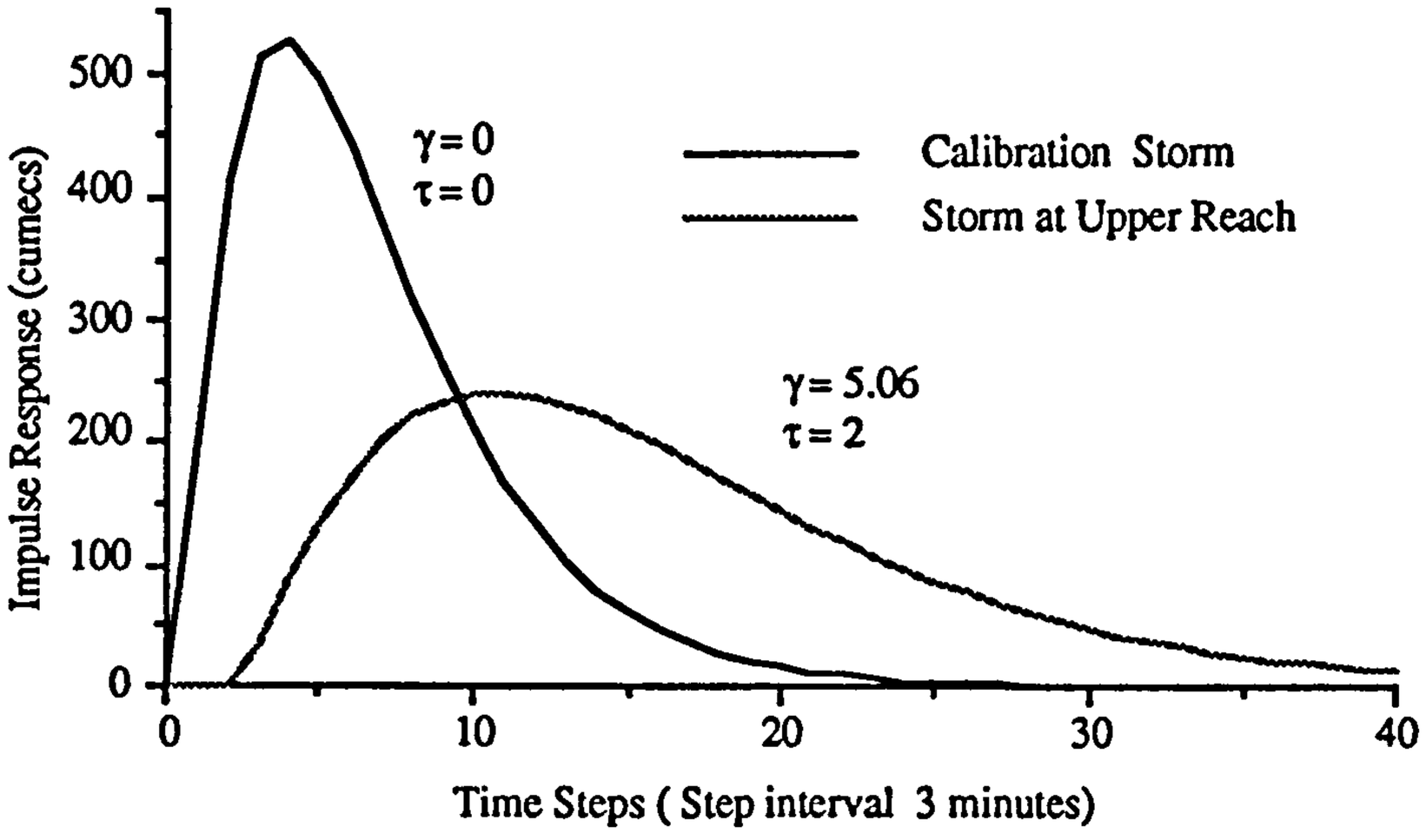

Figure 7.18 Impulse Response of Storm over Upper Catchment

7.3.3 Influence of Rainfall Movement

Storm movements were also very influential in relation to the catchment response. Here two storms were generated by the computer to simulate the movement of storms on the catchment with one moving up and another down the general alignment.

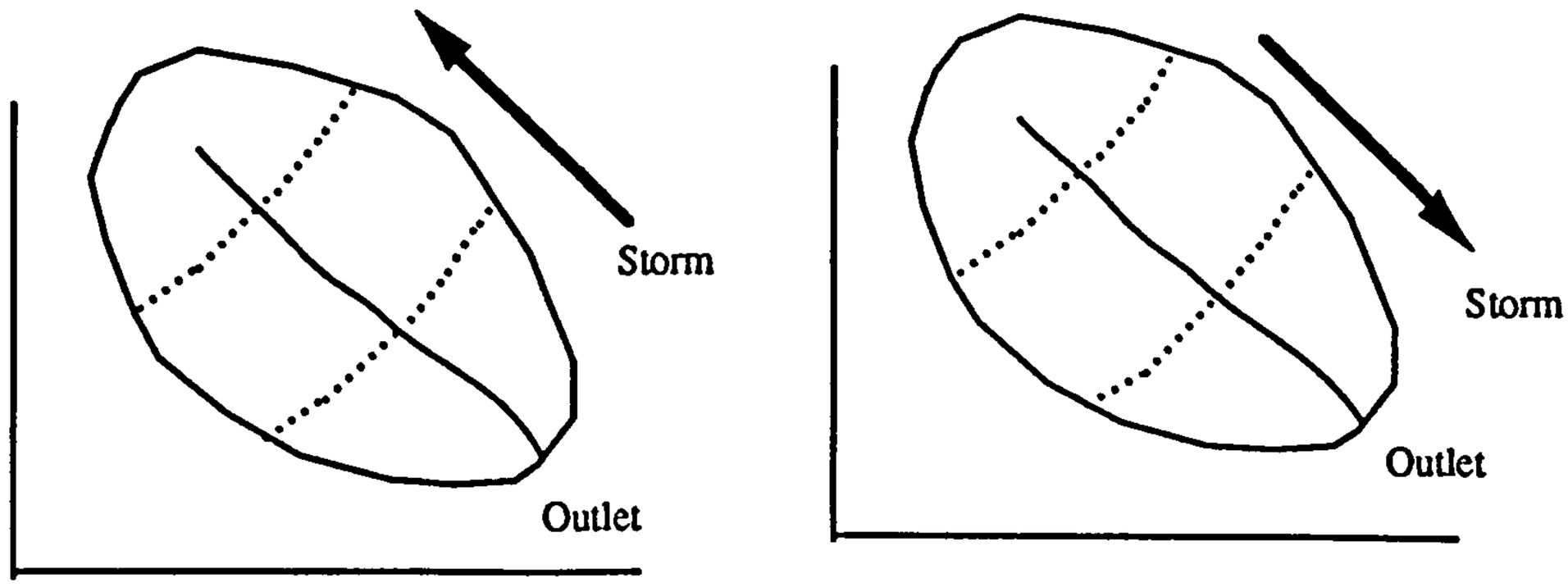

a Storm Movement from Lower Stream to Upper Stream

b Storm Movement from Upper Stream to Lower Stream

Figure 7.19 Storm Movement on the Catchment

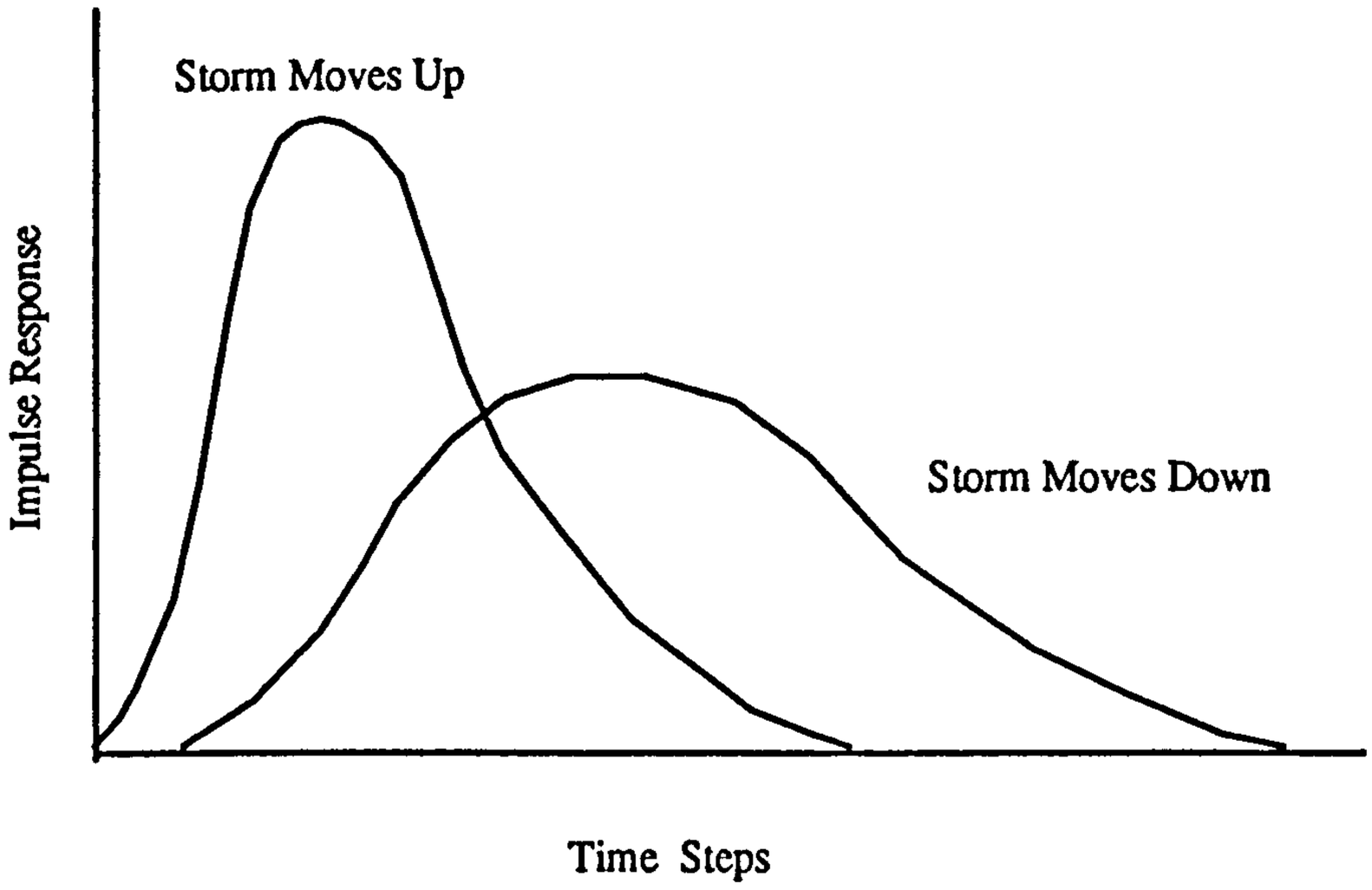

Figure 7.20 Assumed Influence of Storm Movement on Catchment Response

It can be understandable that a storm may occur close to the outlet of a catchment and will have an immediate and `peaky' impulse response and a storm that occurs close to the top end of a catchment will be delayed and produce a more attenuated impulse response. The computer simulation indicates that only half of this assumption is true.

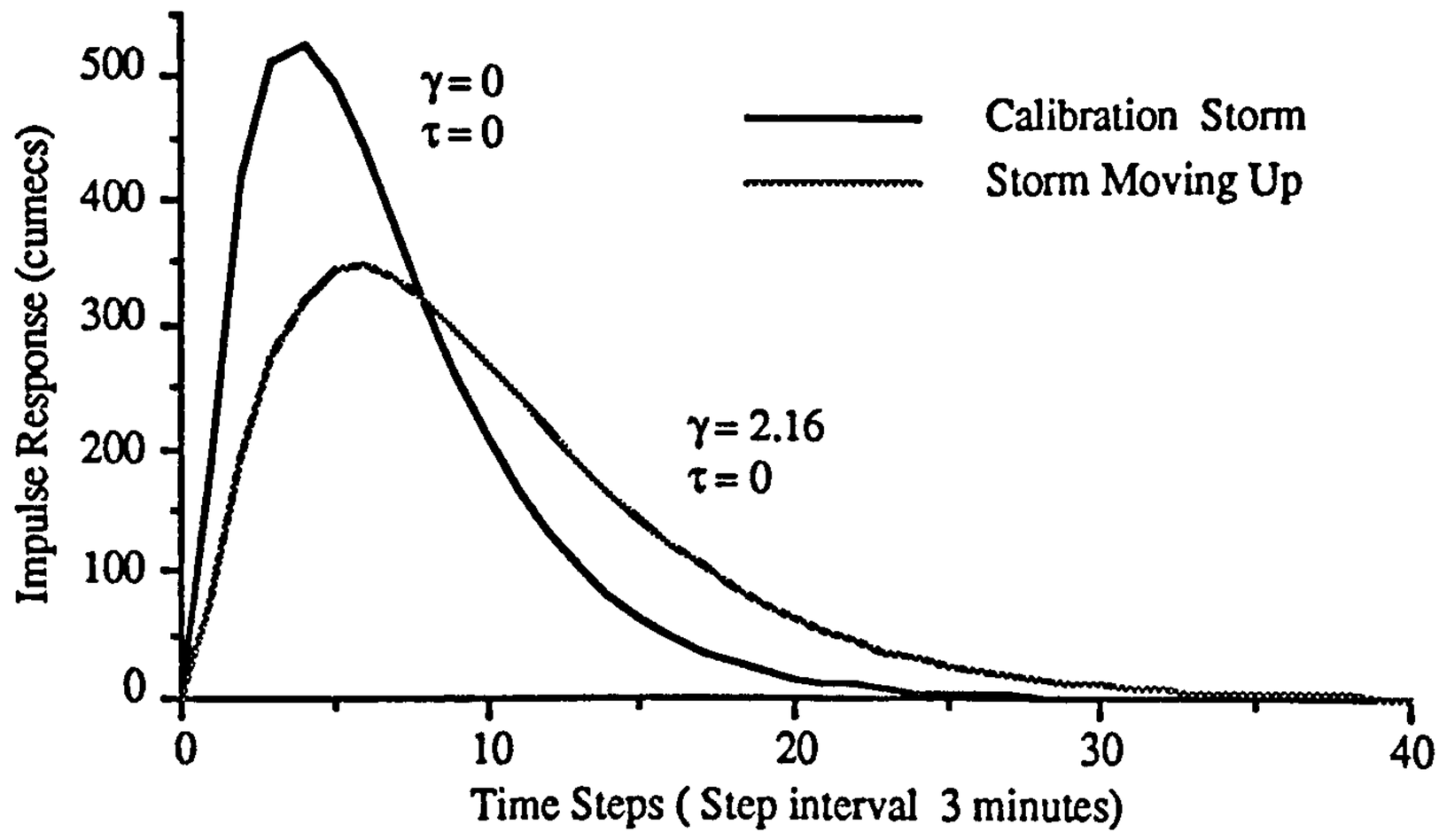

Figure 7.21 Storm Moving Up

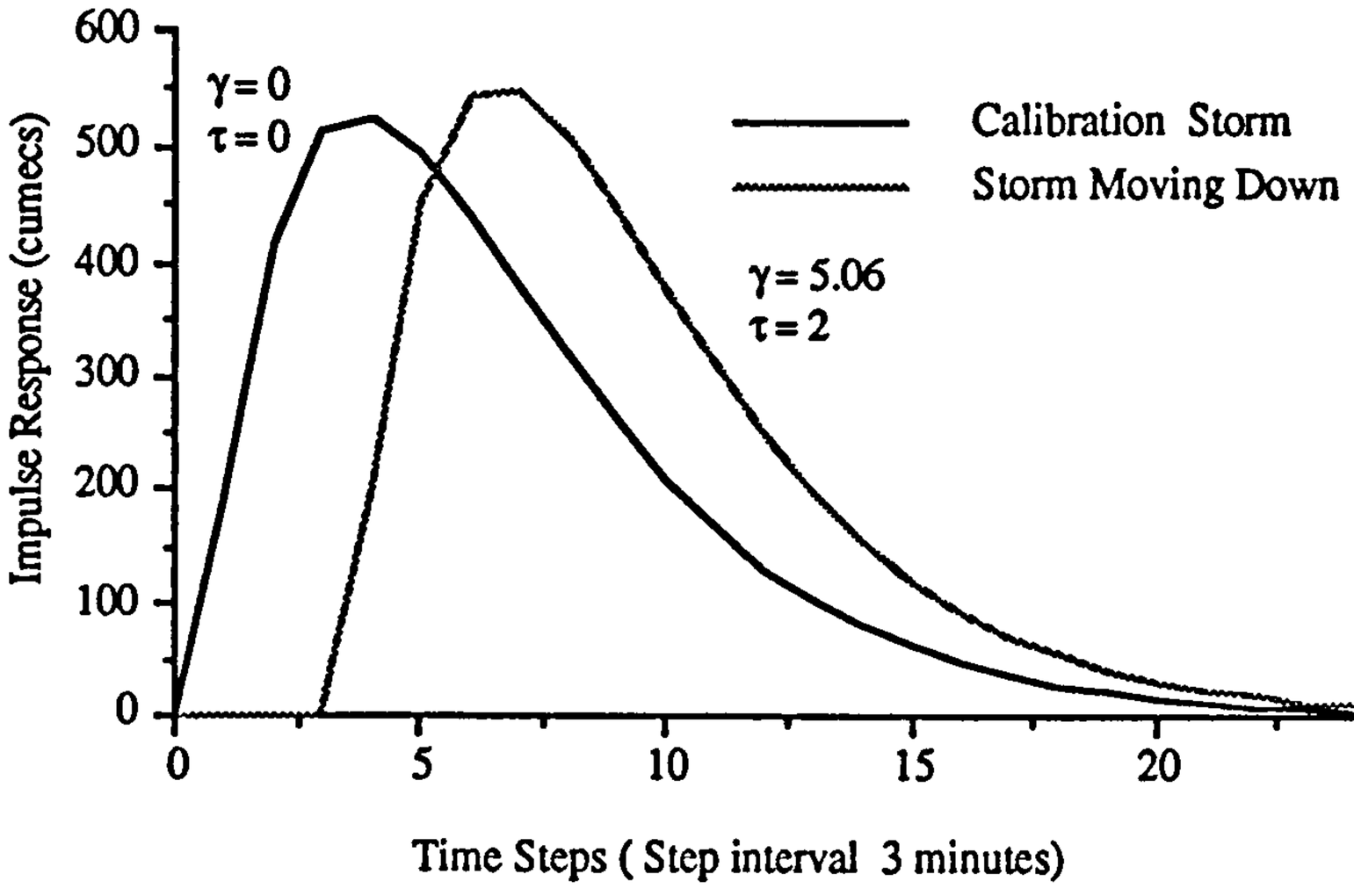

Figure 7.22 Storm Moving Down

The computation results show that a storm moving down the catchment can produce a `peaky' impulse response though it is delayed. This confirms that the storm moving speed as well as storm direction is also an important factor in the assessment of storm movement.

7.4 Flow Simulation from PRTF

The last section illustrated that the catchment behaves differently with different storm characteristics. The impulse response of a TF model should be adaptive with the storm changing. The effectiveness of the PRTF in adapting to the different storm situation was assessed by some case studies.

Rainfall and flow data are from Blackford Bridge in the Northwest region. Model calibration was carried out using data from 18 Dec 1982. By using the identification scheme introduced in Chapter 4, a calibrated PRTF is as below

(3,3) model with t_{peak}=14.7 hour

b(0)=0.015, b(1) = 0.1895, b(2) = - 0.0786, model time interval is 1 hour;

Three storm events are chosen to illustrate the PRTF runoff simulations.

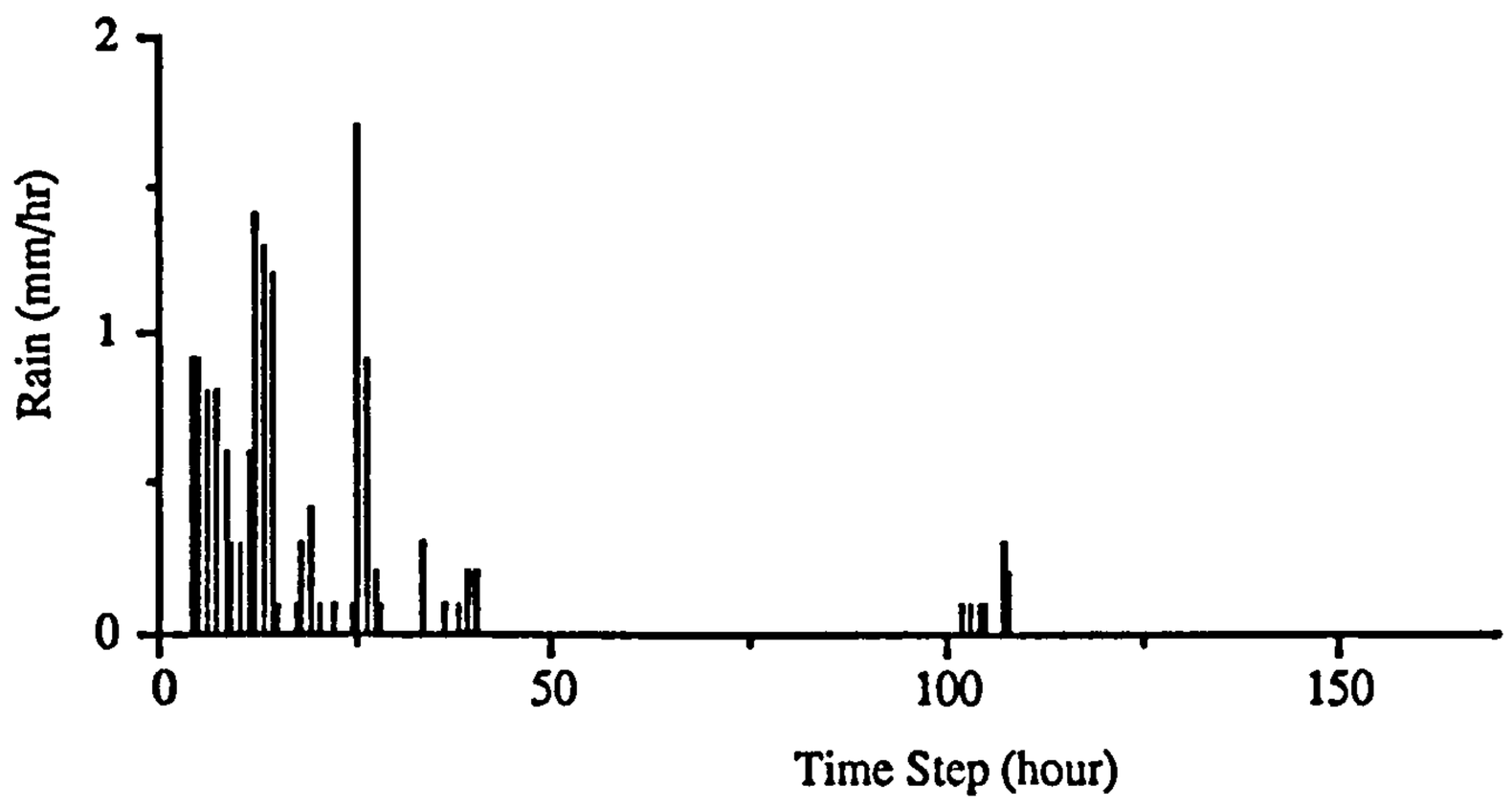

Figure 7.23 Storm Data Event 1

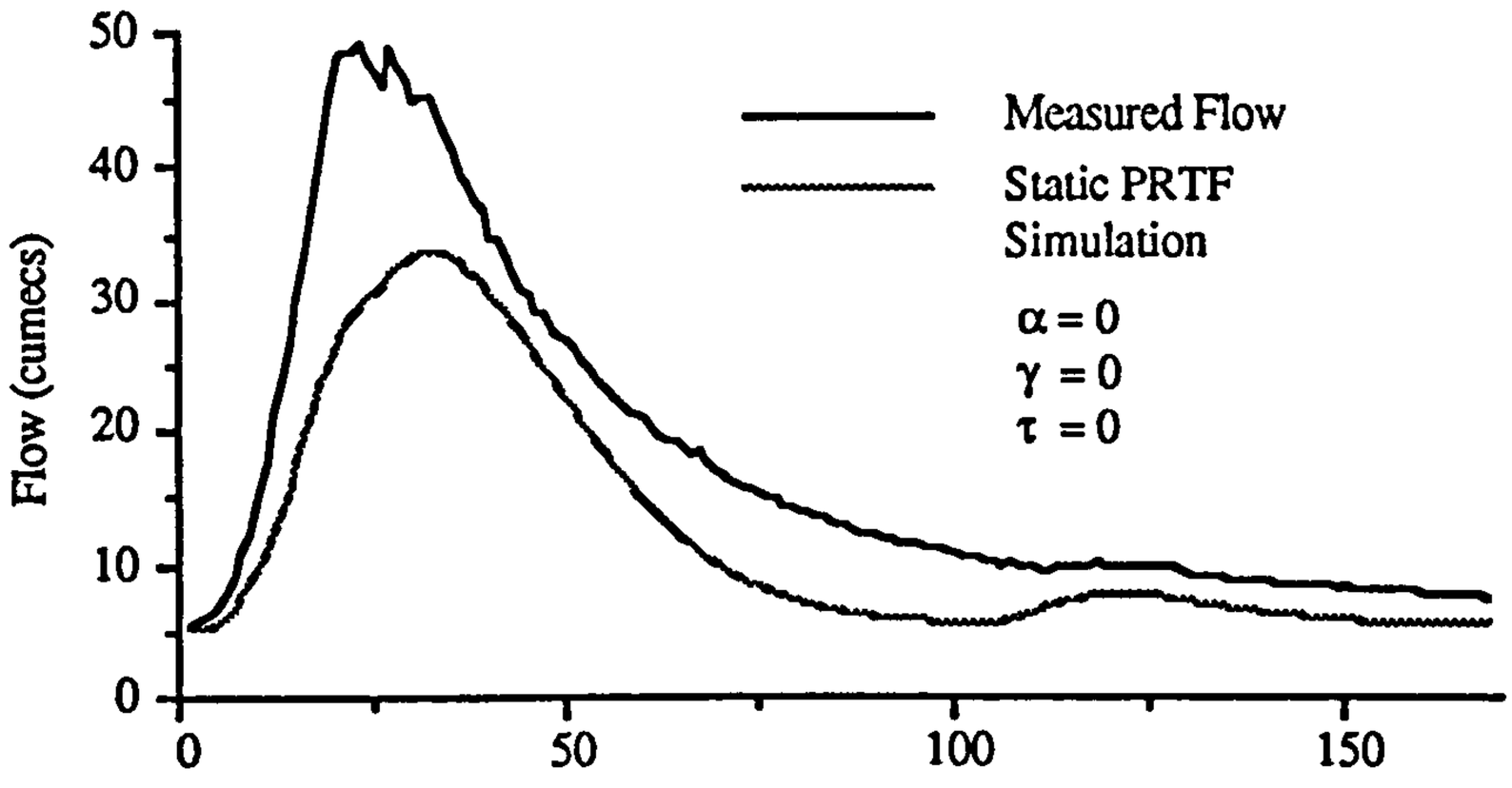

Figure 7.24 Flow Simulation by Static PRTF for Event 1

Figure 7.24 shows a PRTF simulation of the runoff process. It can be observed that a large difference exits between the measured flow and the simulated flow.

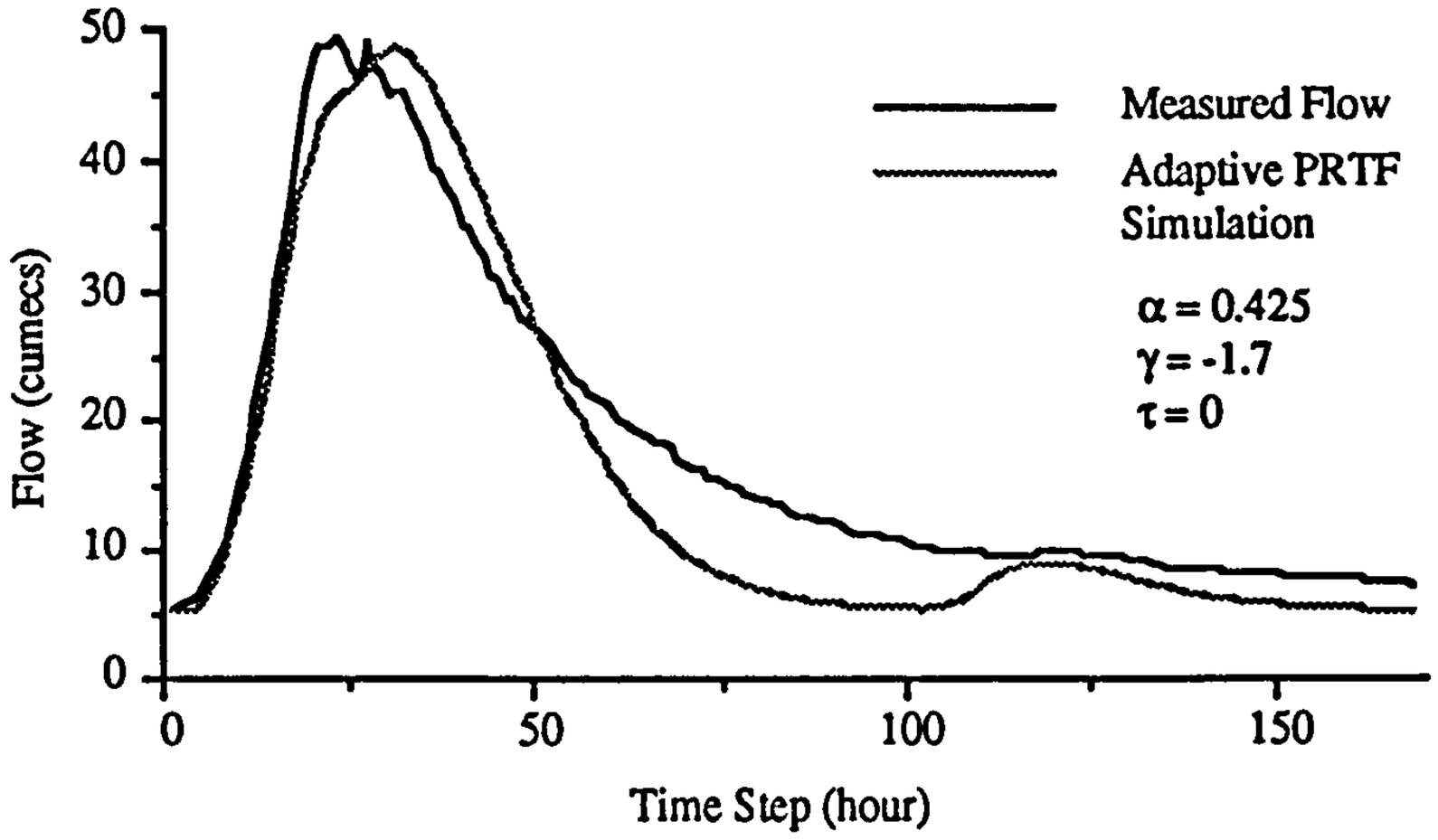

Figure 7.25 Flow Simulation by Adaptive PRTF for Event 1

Great improvement can be found in Figure 7.25 in the PRTF runoff simulation. The impulse response function is changed according to Figure 7.26.

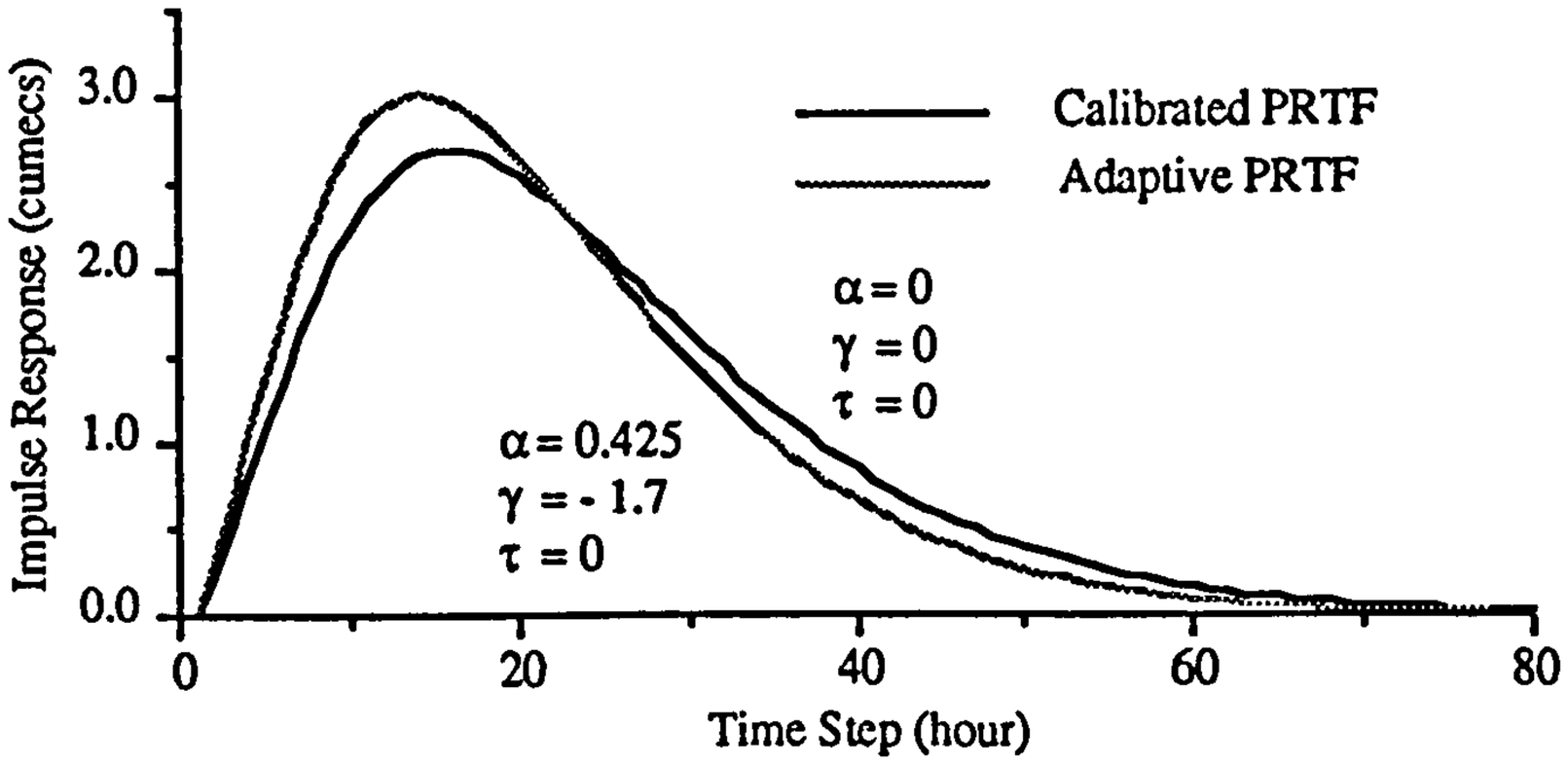

Figure 7.26 Adaptive Impulse Response for Event 1

Event 1 above comes from 12 Dec, 1985 (Internal Code A3).

Square Error by static PRTF simulation = 8292 Sqr cumecs

Square Error by static PRTF simulation = 2819 Sqr cumecs, with $\alpha = 0.425$, $\gamma = -1.7$ hour, $\tau = 0$ hour.

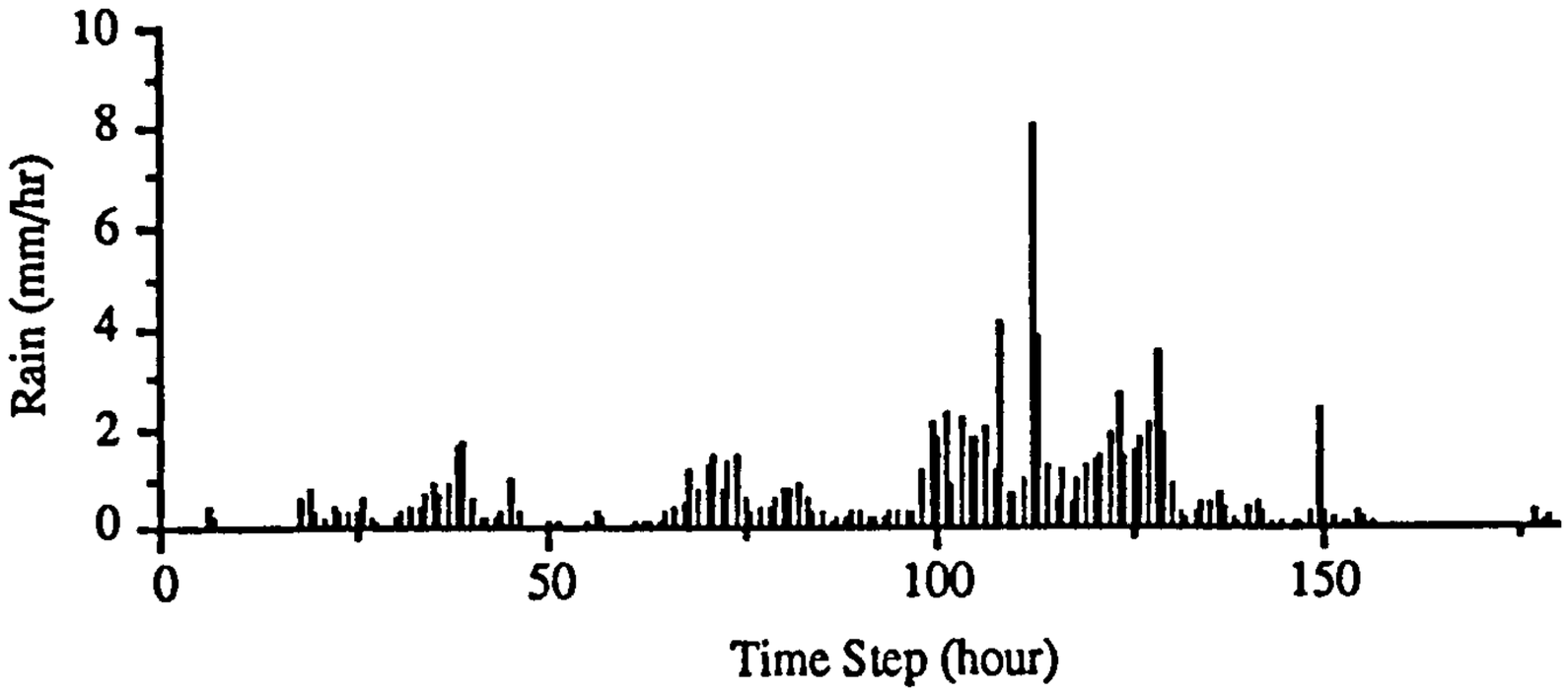

Figure 7.27 Storm Data Event 2

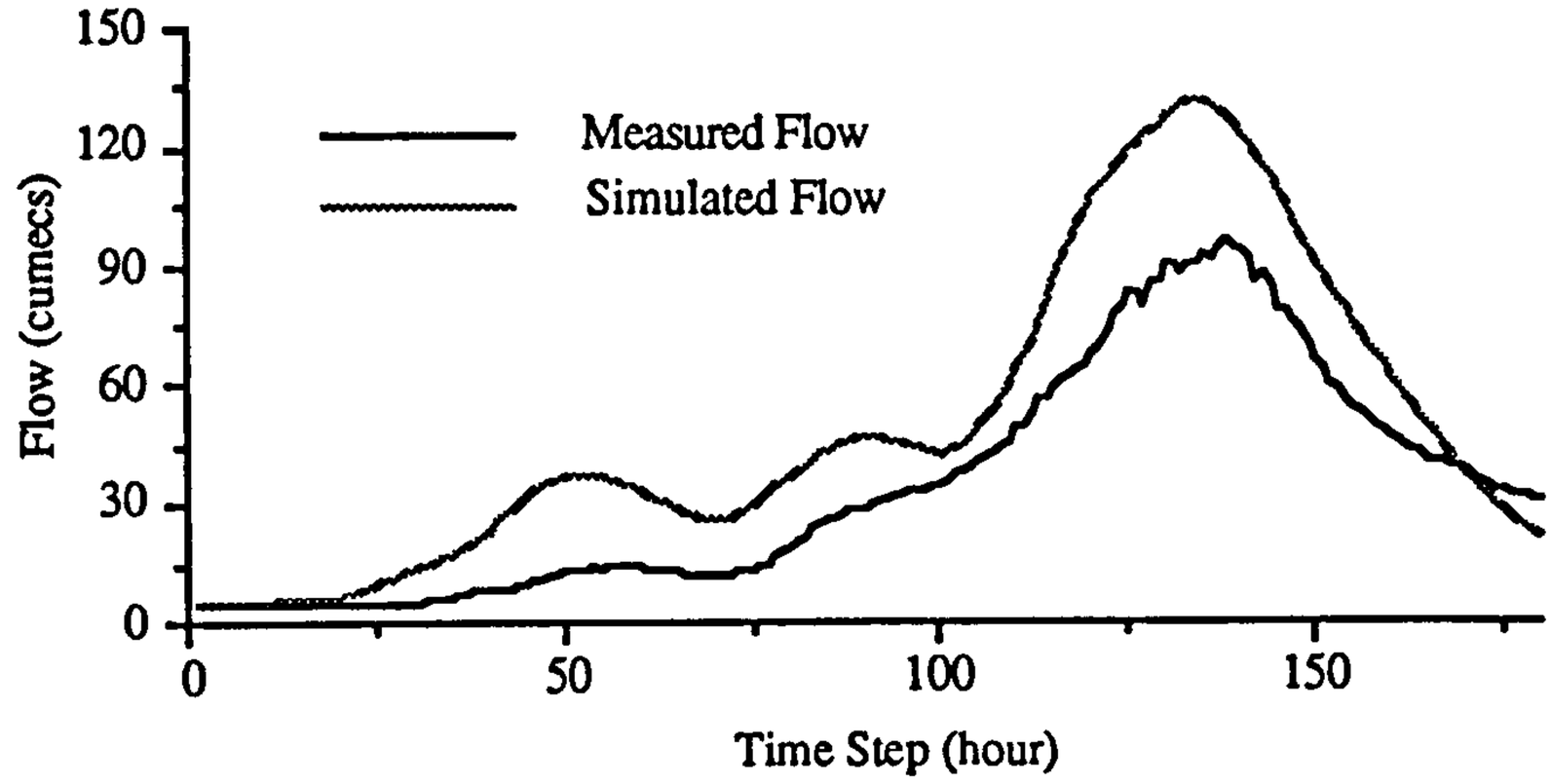

Figure 7.28 Flow Simulation by Adaptive PRTF for Event 2

Figure 7.28 shows a PRTF simulation of the runoff process from storm event 2. It can also be observed that a large difference exits between the measured flow and simulated flow.

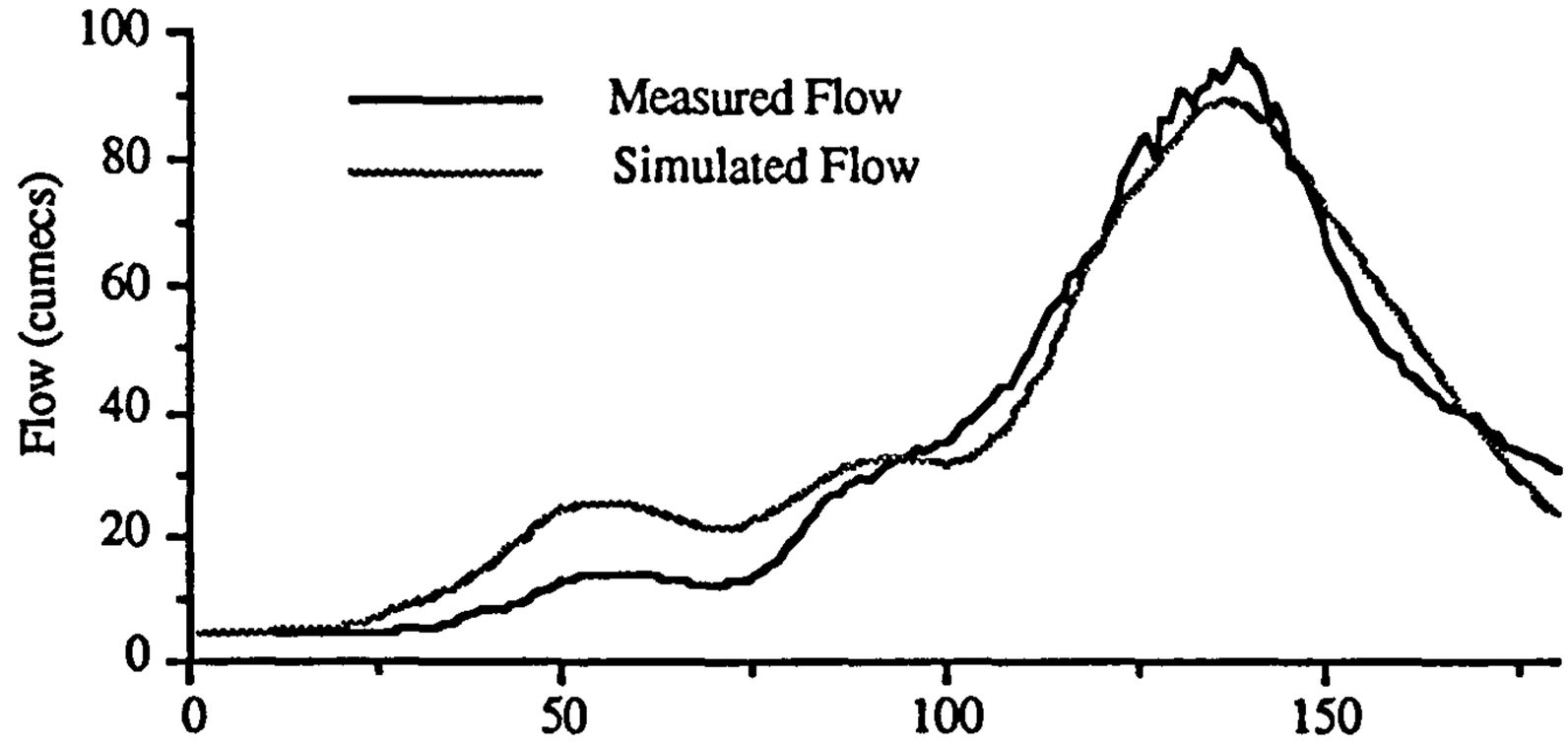

Figure 7.29 Flow Simulation by Static PRTF for Event 2

Great improvement can be found in Figure 7.29 in the PRTF runoff simulation. The impulse response function is changed according to Figure 7.30.

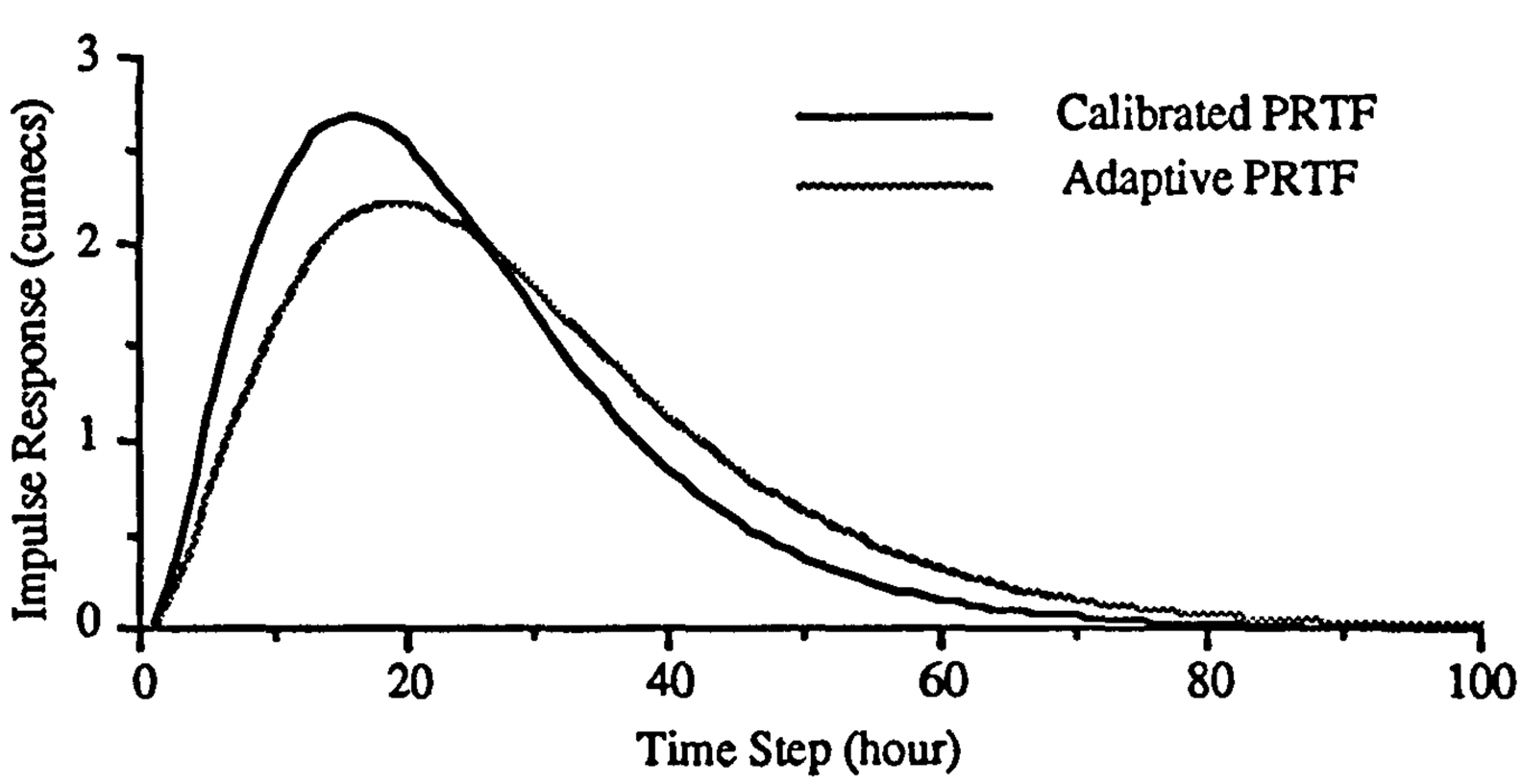

Figure 7.30 Adaptive Impulse Response for Event 2

Event 2 above comes from 8 Nov, 1983 (Internal Code B3).

Square Error by static PRTF simulation = 8292 Sqr cimucs

Square Error by static PRTF simulation = 2819 Sqr cumecs, with $\alpha = 0.425$, $\gamma = -1.7$ hour, $\tau = 0$ hour.

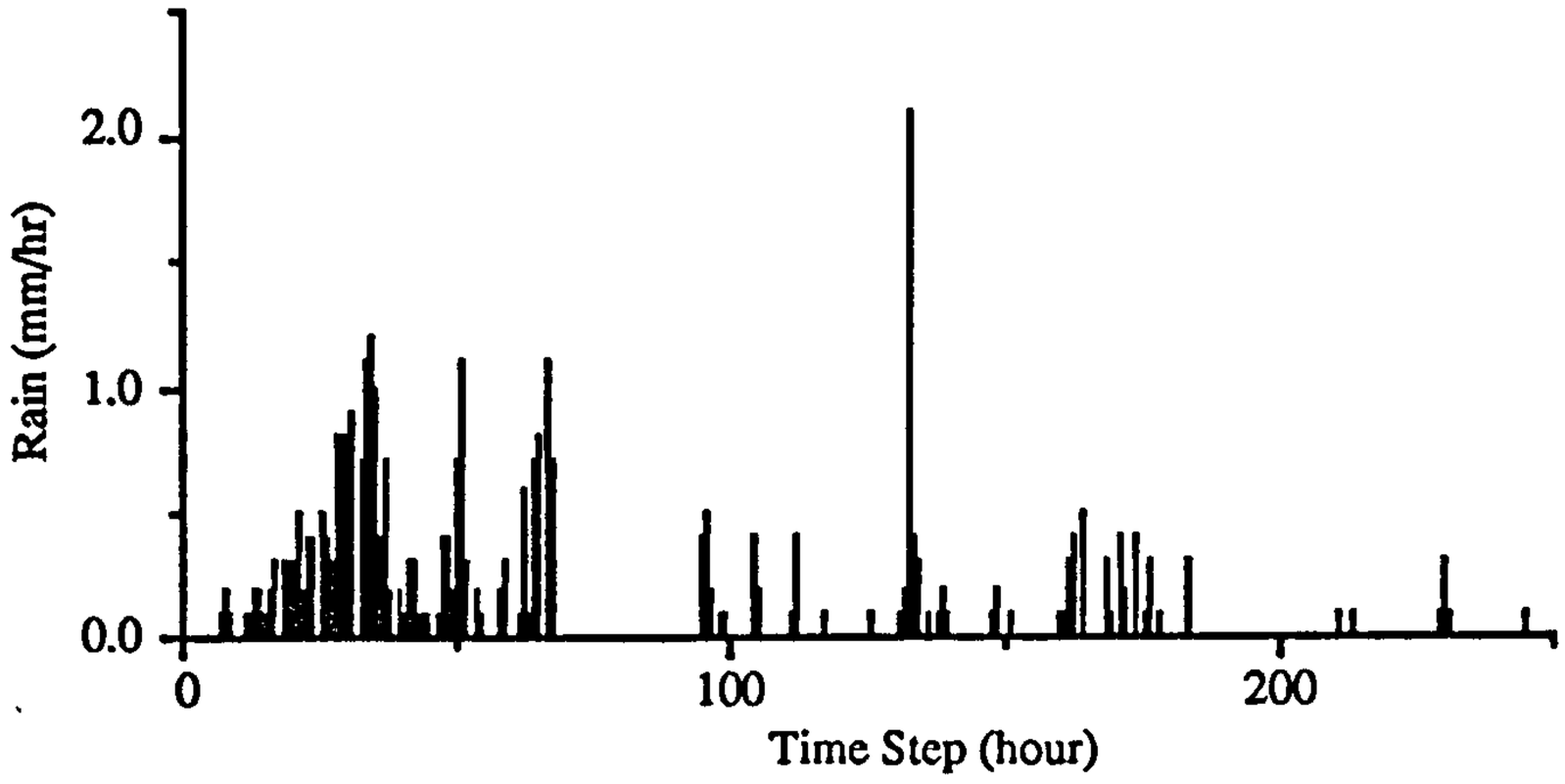

Figure 7.31 Storm Data Event 3

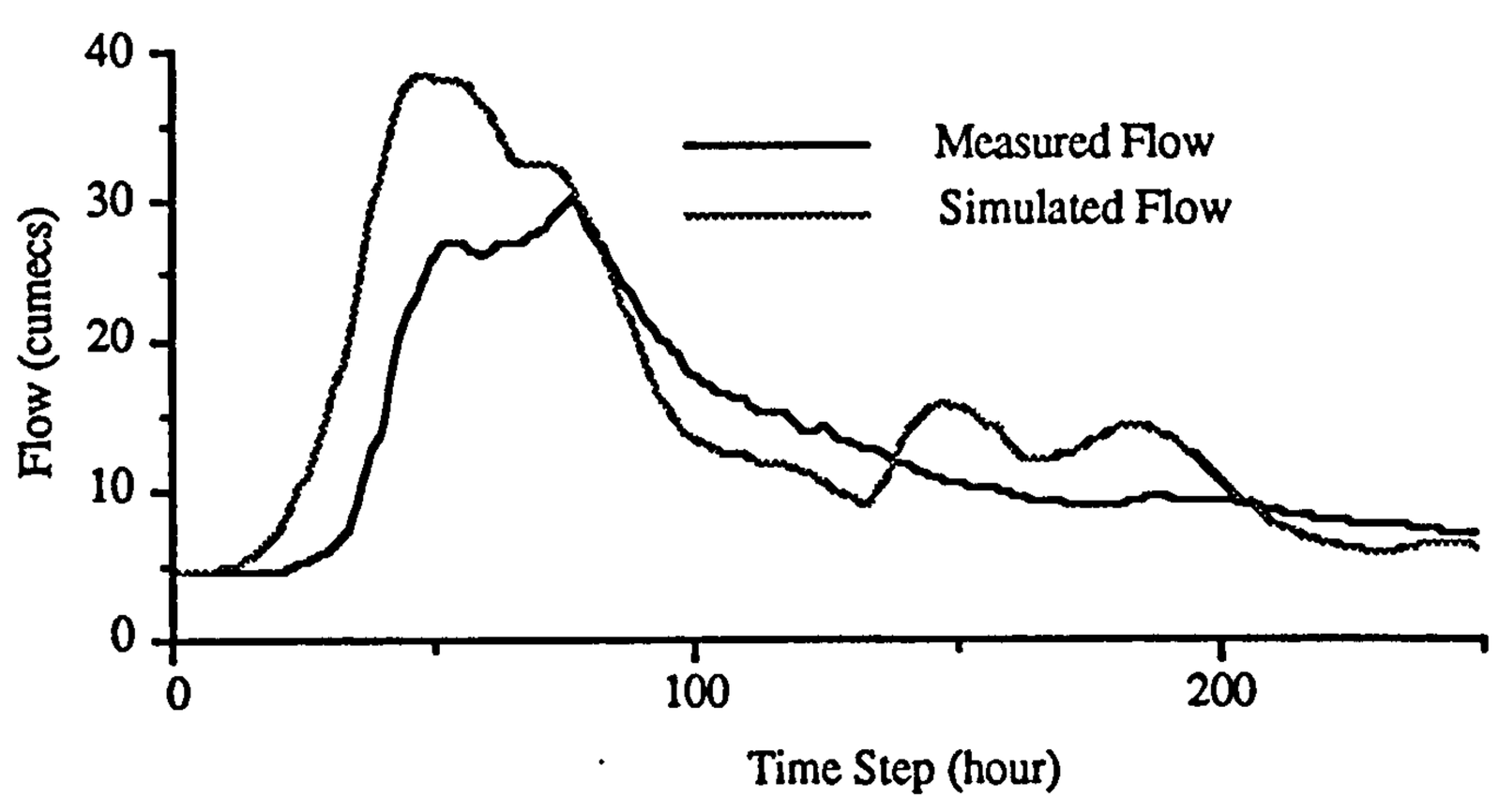

Figure 7.32 Flow Simulation by Static PRTF for Event 3

Figure 7.32 shows a PRTF simulation of runoff process from storm event 3. It can also be observed that a large difference exits between the measured flow and simulated flow.

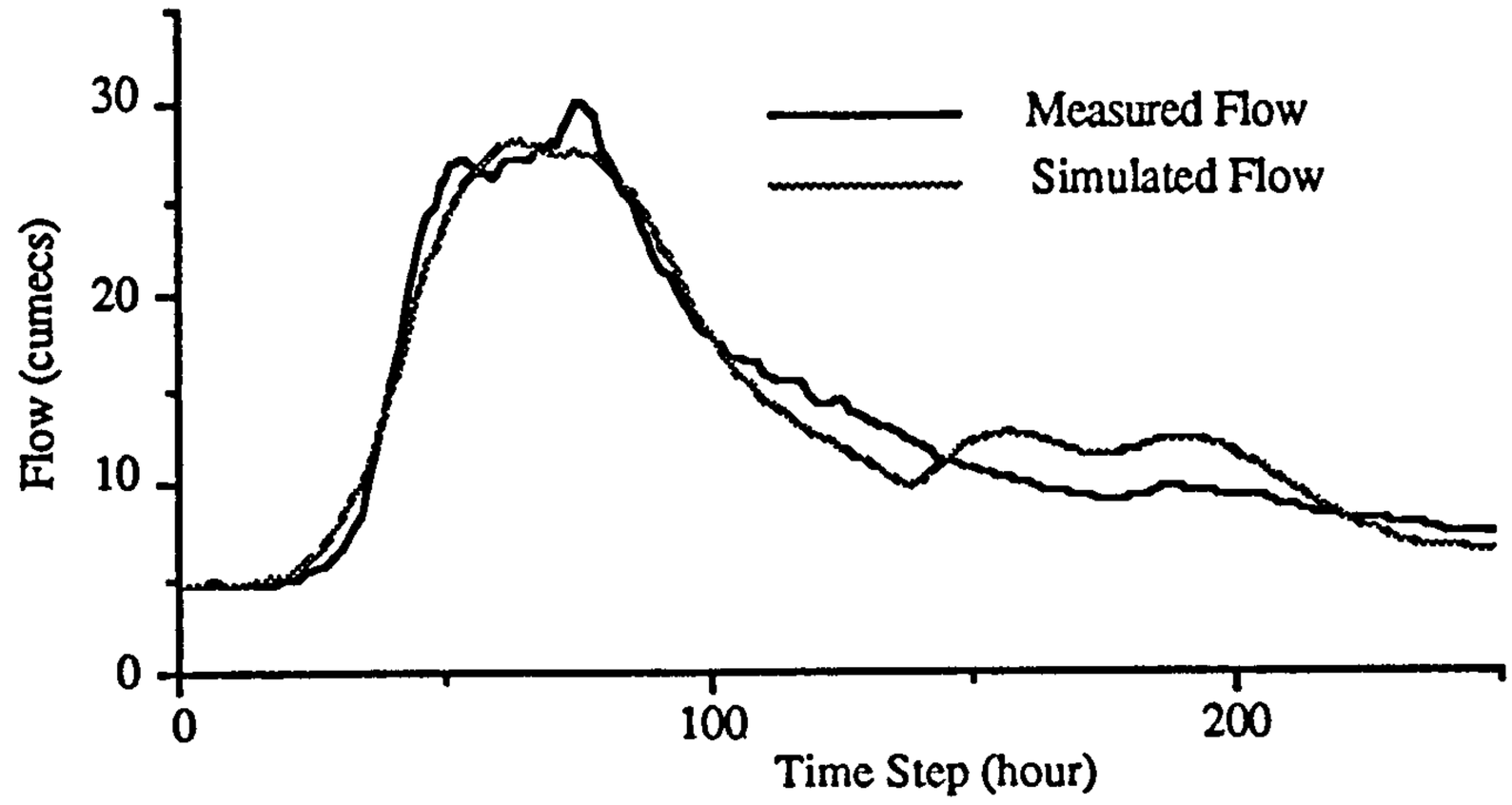

Figure 7.33 Flow Simulation by Adaptive PRTF for Event 3

Great improvement can be found in Figure 7.32 in the PRTF runoff simulation. The impulse response function is changed according to Figure 7.34.

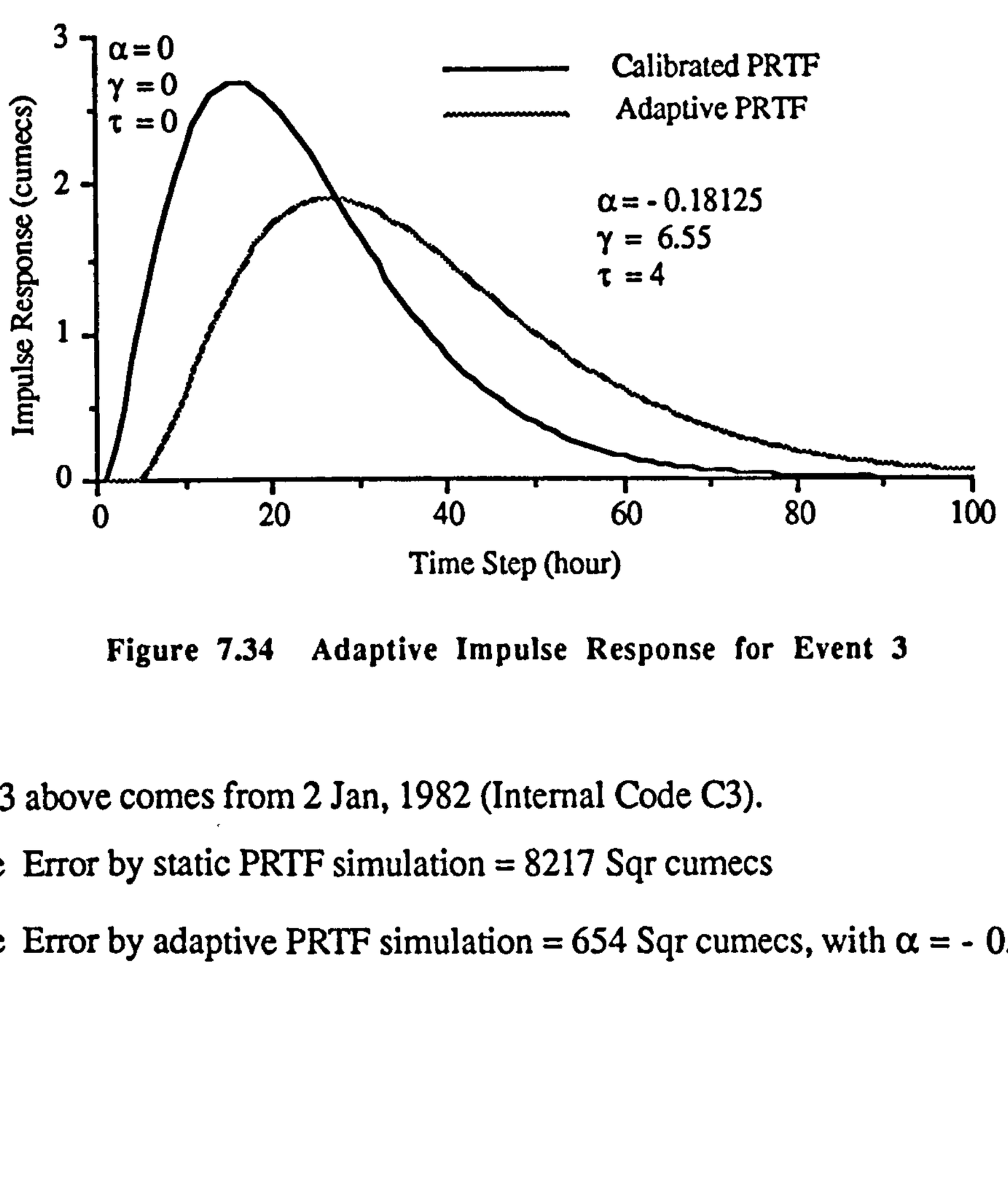

Figure 7.34 Adaptive Impulse Response for Event 3

Event 3 above comes from 2 Jan, 1982 (Internal Code C3).

Square Error by static PRTF simulation = 8217 Sqr cumecs

Square Error by adaptive PRTF simulation = 654 Sqr cumecs, with α = - 0.18,

γ = 6.66 hour, τ =4 hour.

Results show that the model simulation can be greatly improved by adapting the model impulse response to the catchment conditions. By adjusting 3 parameters of the model, it was found that the PRTF can easily adapt to the new situation without causing system instability and fluctuation. Although the PRTF can adapt to the different catchment condition and storm type, some factors can decrease its ability to adapt. In next section, a rainfall loss analysis is carried out to enhance the performance of the PRTF when significant initial rainfall losses occur.

7.5 RST (Rainfall Separation Tank) to Improve the PRTF Simulation

It has been found that the PRTF can perform satisfactorily with different storm types and catchment conditions. As the total rainfall instead of net rainfall is used in the simulation, it can be illustrated that sometimes this can reduce the performance of the PRTF. When the rainfall runoff percentage is different, PRTF will adapt itself by adjusting its α factor as in Figure 7.34.

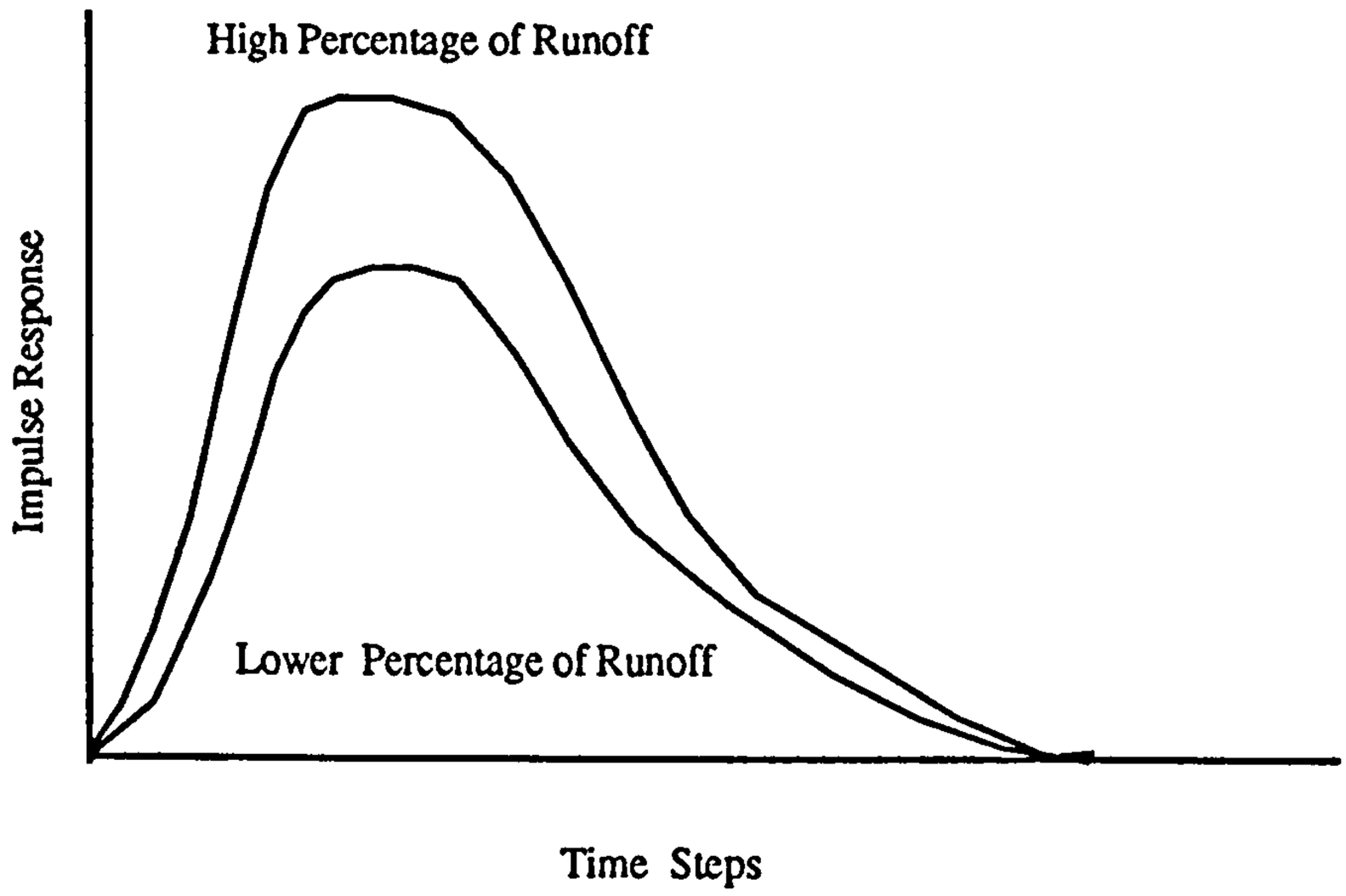

Figure 7.34 Influence of Percentage of Runoff on Catchment Response

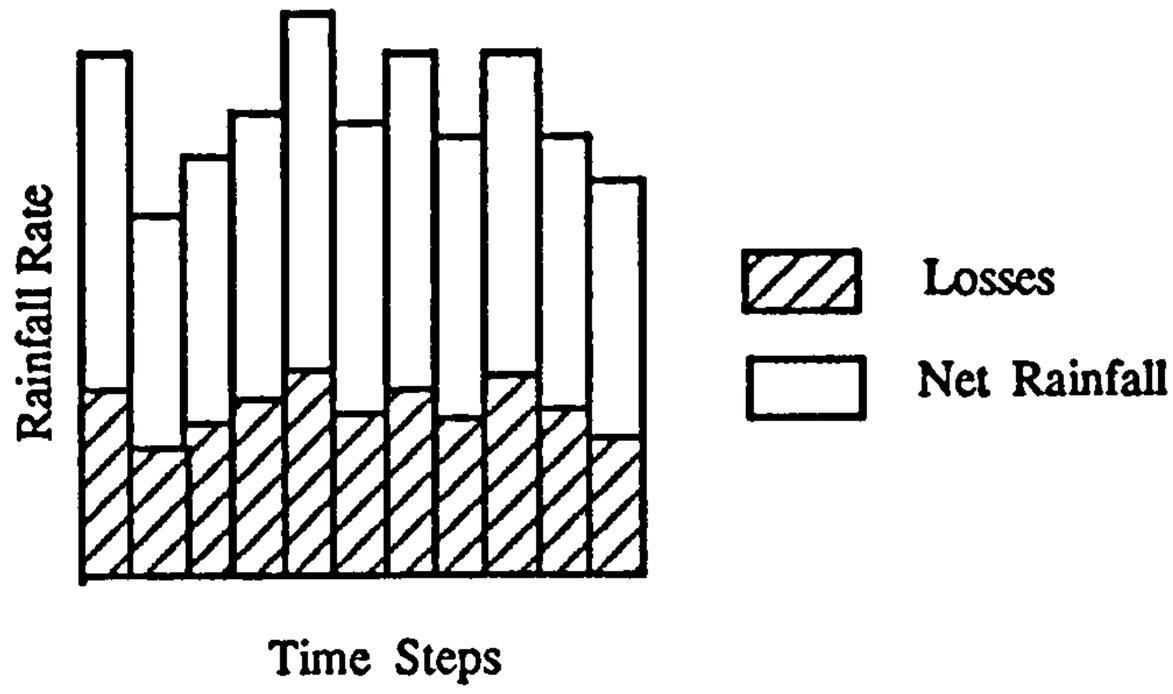

Figure 7.35 Rainfall Separation Proportional Loss Method

In this case, a proportion of the rainfall loss is assumed as in Figure 7.35. In reality, the percentage of runoff is closely related to soil conditions , vegetation conditions and weather conditions. The net storm rain (that portion of the total precipitation which will appear as direct surface flow) can be obtained from consideration of the phenomena of retention, infiltration and overland flow. Essentially, in terms of watershed yield (surface runoff), one may write a simple continuity equation (see Gray 1970):

$$\text{Precipitation} = \text{Depressional Storage} + \text{Evaporation} + \text{Infiltration} + \text{Interception} + \text{Surface Runoff}$$

In other words, runoff is the residual of precipitation after accounting for the various component losses. In practice, the most frequently considered techniques are loss rate methods: e.g. the fixed loss rate (ϕ - index) method and Horton's method. The variable loss rate concept is based on the theory of a limited capacity for a given soil type to absorb water by infiltration, the capacity decreasing as the soil moisture content rises. Although such threshold effects are clearly important on small homogeneous areas, the loss rate approach is less relevant at catchment scale. It could be assumed to be constant throughout the storm (Φ index) as

illustrated in Figure 7.36a. to consist of an initial loss and a continuing loss rate(Figure7.36b), or to change in the form of a curve(Figure 7.36c). The latter may prove to be more appropriate if the curve can be defined. The concept of the loss rate curve is the applied hydrologist's extension of the infiltration curve (Figure 7.36d), originally due to Horton (1940)

$$f_t = f_c + (f_o - f_c) e^{-kt} \qquad (7,21)$$

where f_t = infiltration rate at time t, f_o = initial infiltration rate, f_c = final constant infiltration rate.

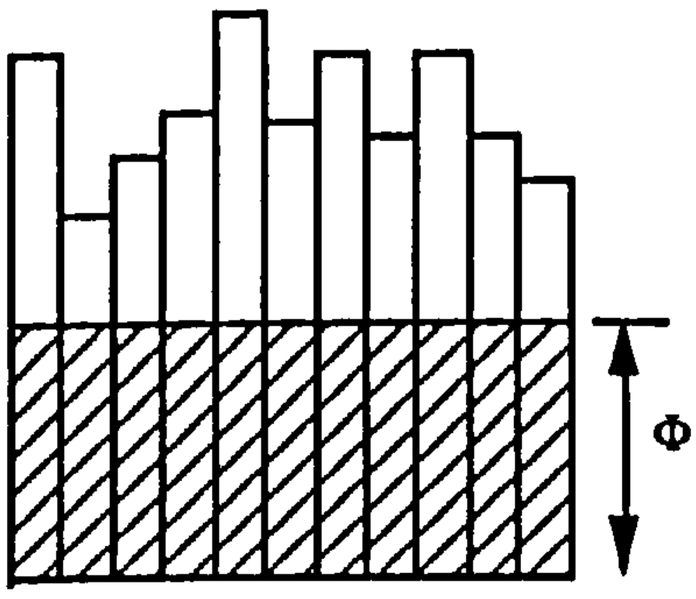

(a) Constant loss rate, Φ index

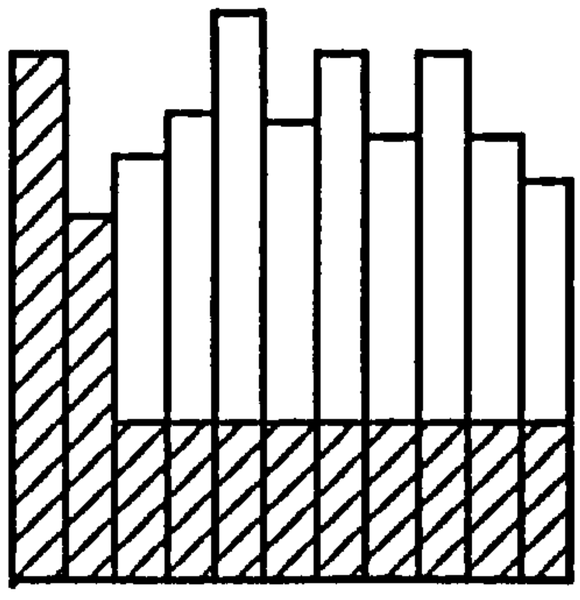

(b) Initial loss plus continuing loss

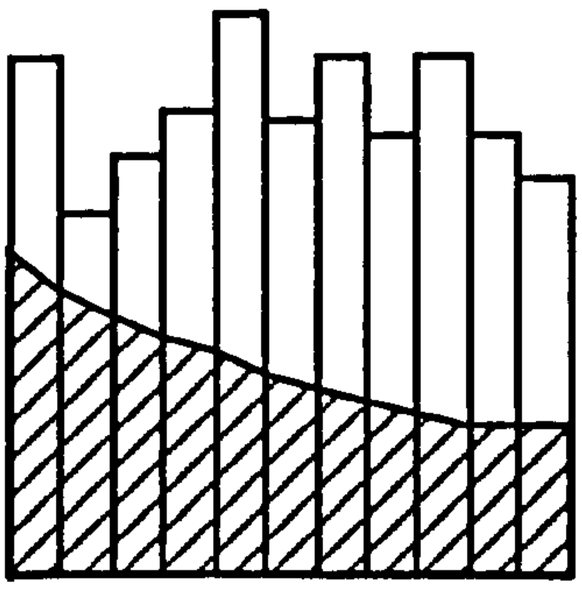

(c) Loss rate curve

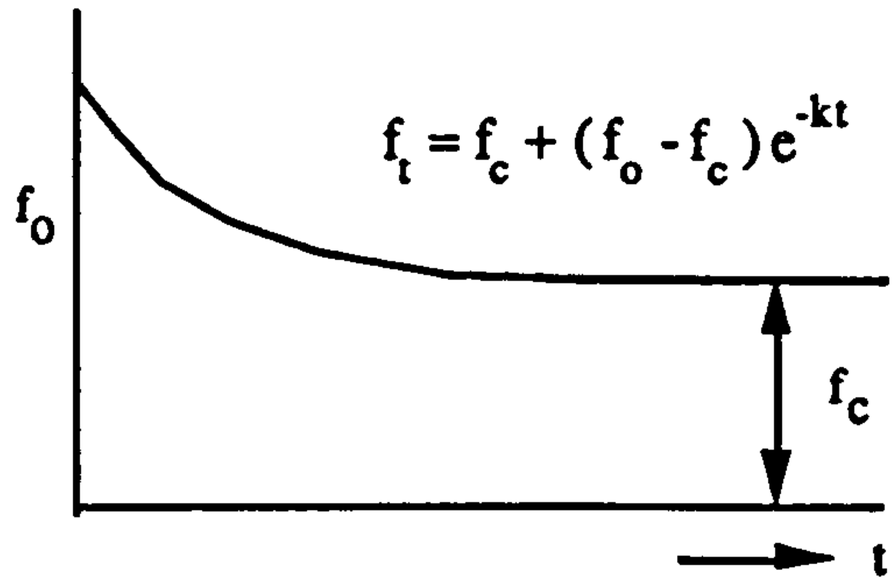

(d) Exponential decay curve of infiltration due to Horton

Figure 7.36 Variation of the Loss Rate Concept (NERC, 1975)

The loss rate curve is assumed to include the effects of all forms of loss in addition to infiltration.

For the convenience of the rainfall loss computation, a three parameter RST (Rainfall Separation Tank) is proposed here to modelling the rainfall separation as illustrated below,

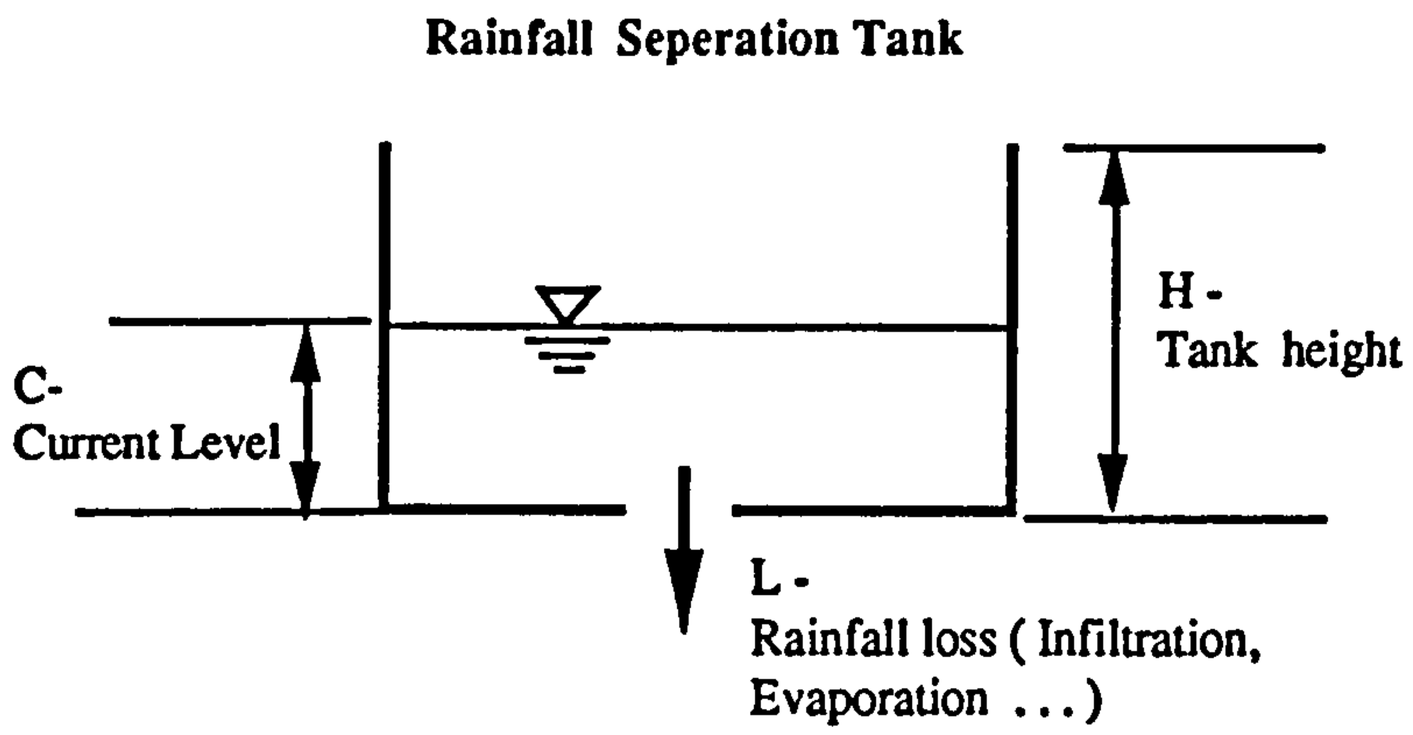

Figure 7.37 Initial Condition of RST

The tank height H represents the capacity of the catchment in absorbing rainfall. Rainfall loss L is a constant which includes all losses to rainfall data. L will be influenced by soil type and weather condition. Tank current level C represents the current catchment condition. When the catchment is dry , C will be small, otherwise C will be large.

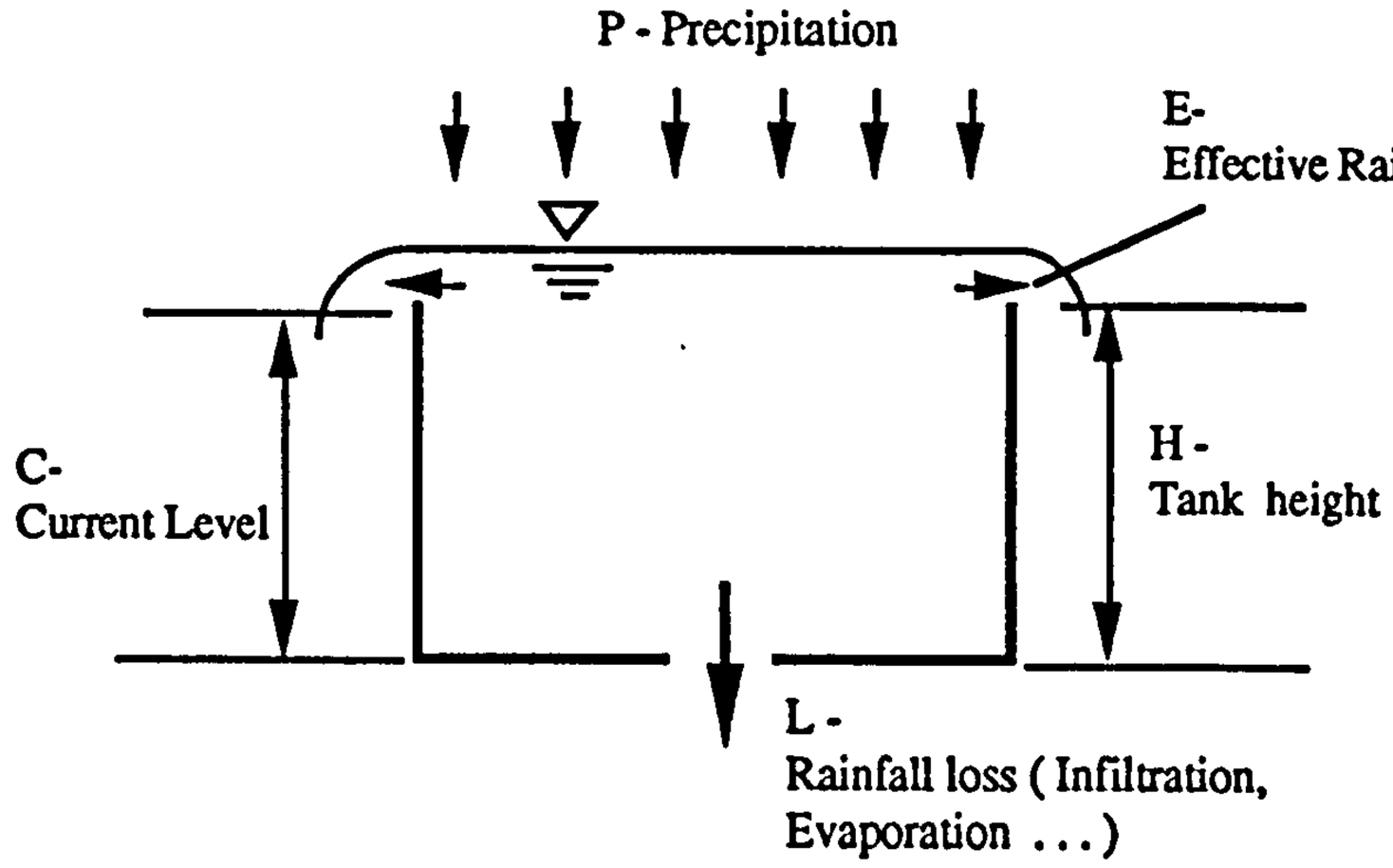

Figure 7.38 Effective Rainfall Production Procedure from RST

When precipitation occurs, the production procedure of effective rainfall can be illustrated by figure 7.38. If the precipitation is larger than the loss L, the tank level will rise and when the tank height is reached , effective rainfall is generated. If the precipitation is smaller than the loss L, the tank level will decrease and can become zero if the duration of such storm is long. In reality, rainfall intensity varies with time and the tank can simulate the situation by changing its level and effective over flow.

The advantage of the RST model is that it is easy to understand and convenient to use in practice. In real-time flood forecasting, the RST will replace the α factor to counter the influence of rainfall losses.

Basic RST Equation is

$C = 0$; Empty tank

$C = H$; Tank full;

So constraint is

$$0 \leq C \leq H, E(t) \geq 0$$

Computation procedure is

$$C(t) = C(t\text{-}1) + P(t) - L \quad (\text{when } P(t) - L \leq H) \qquad (7,20)$$

$$C(t) = H \quad (\text{when } C(t\text{-}1) + P(t) - L > H)$$

$$E(t) = C(t\text{-}1) + P(t) - L - H \quad (\text{when } P(t) - L > H)$$

$$E(t) = 0 \quad (\text{when } P(t) - L \leq H)$$

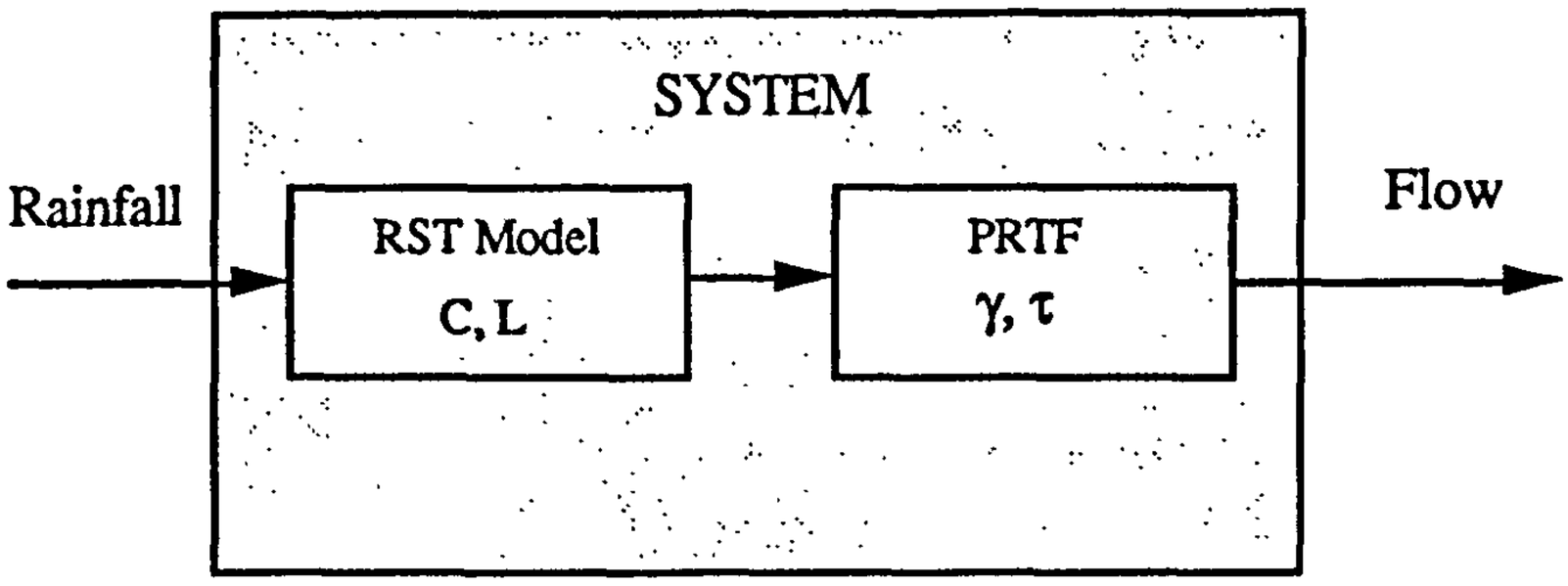

Figure 7.39 System Composed of RST & PRTF

Event 4 below comes from 5 Feb, 1984 (Internal Code C6).

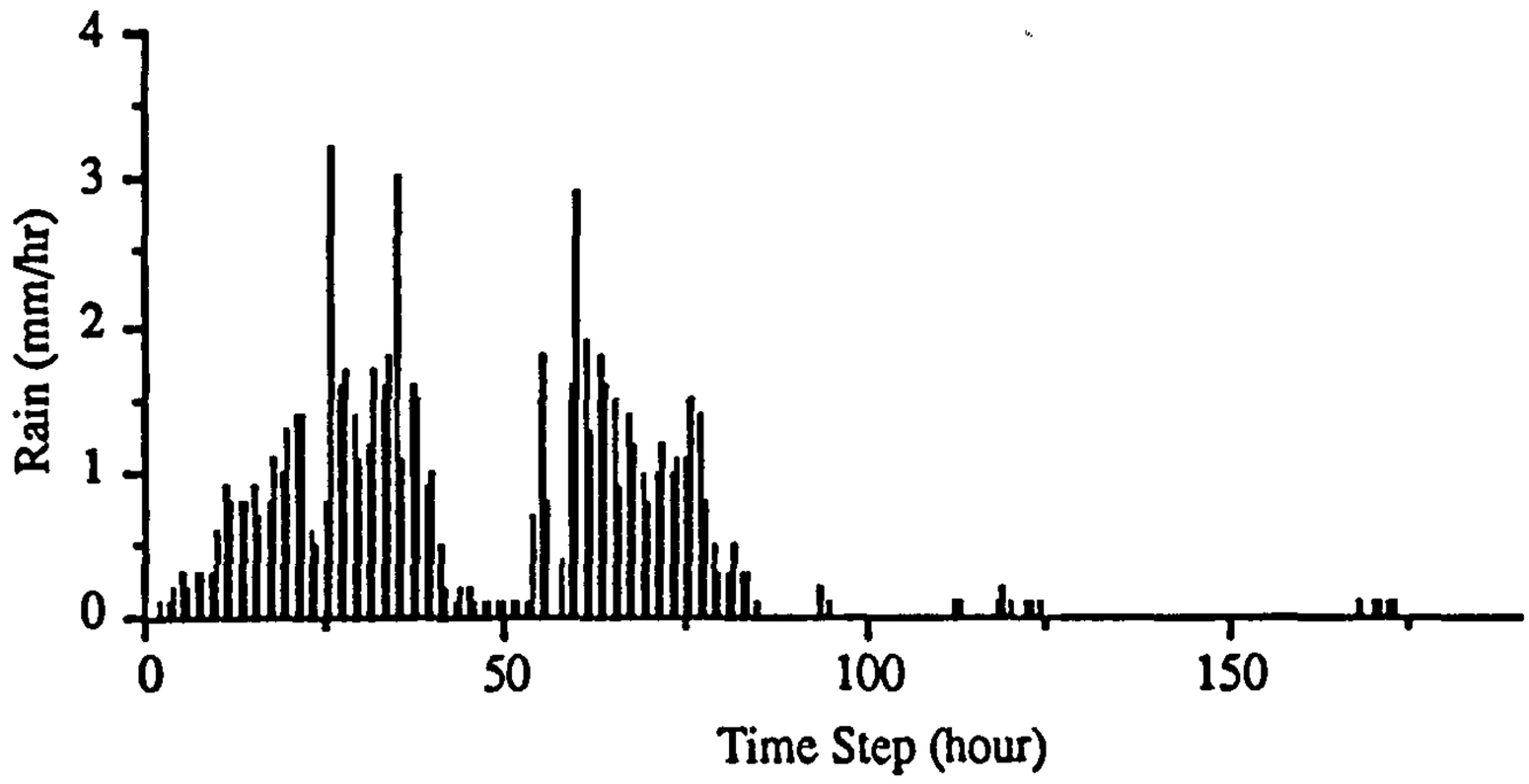

Figure 7.40 Storm Data for Event 4

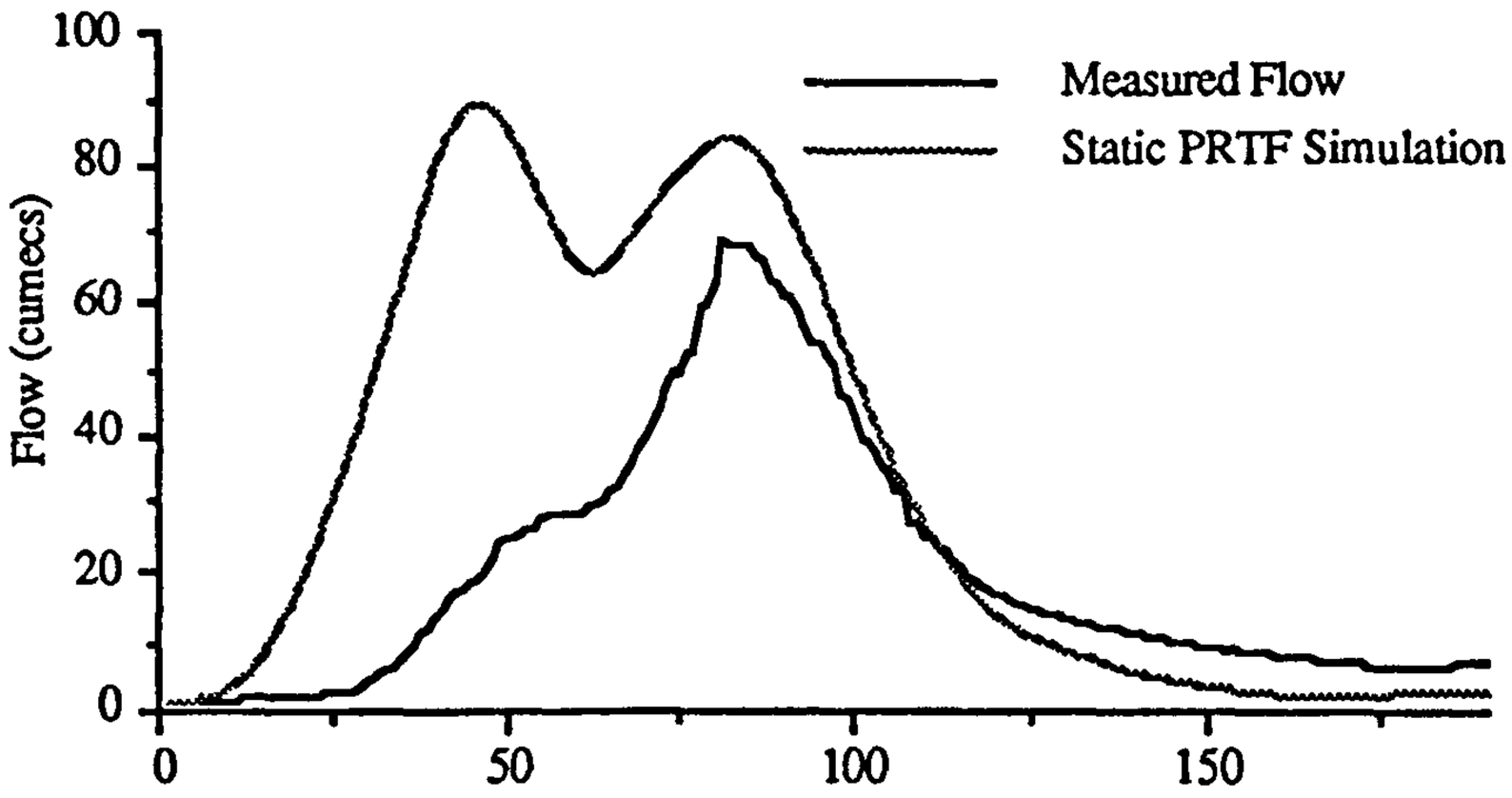

Figure 7.41 Static PRTF Simulation

An example is provided in Fig. 7.41 of a very poor rainfall runoff simulation by a static PRTF model. This was because the catchment was very dry before the storm arrived and a large portion of the rainfall had no contribution to the flow production.

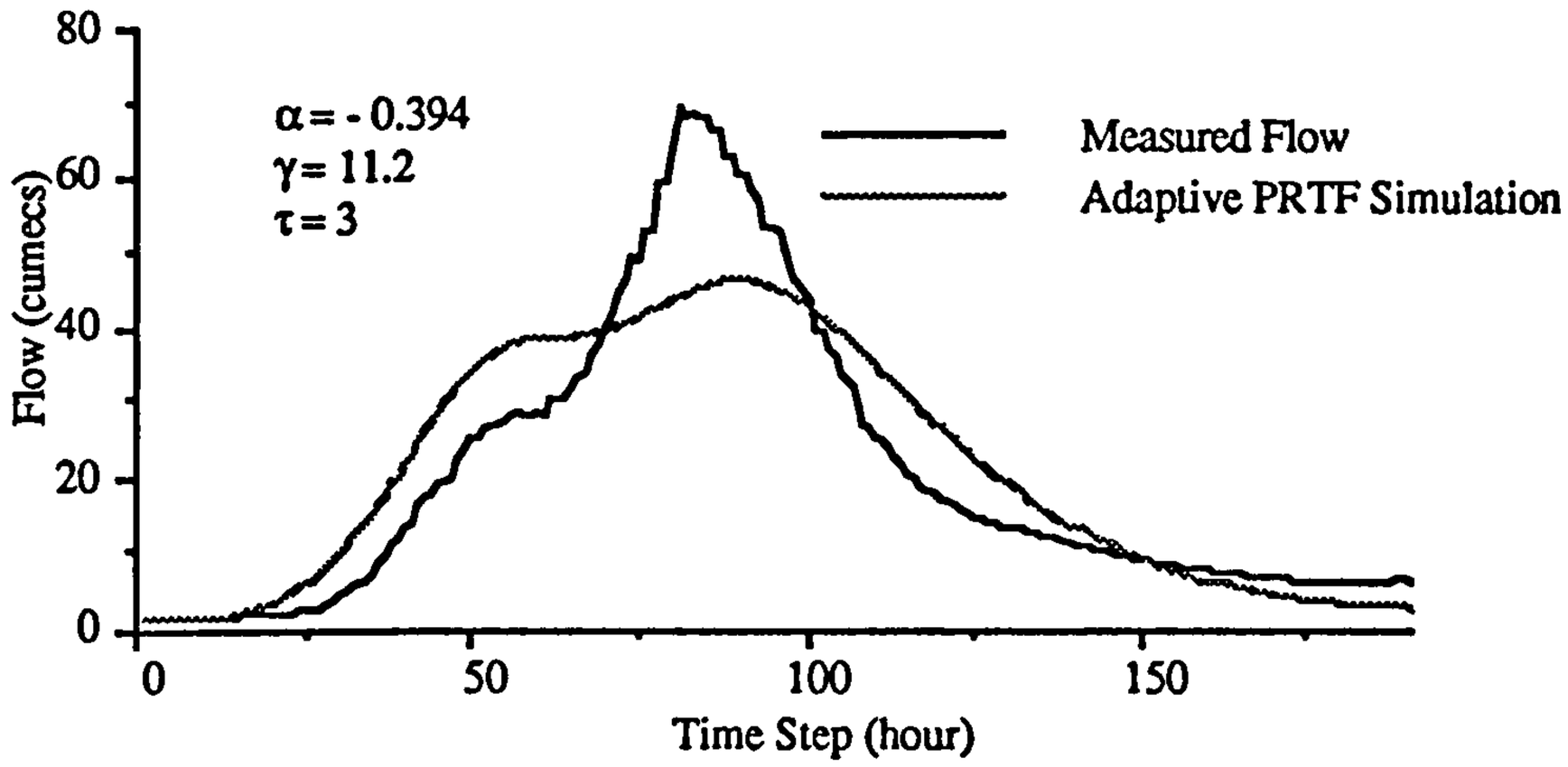

Figure 7.42 Adaptive PRTF Simulation

By adjusting the model impulse response, the flow simulation is greately improved, but the result is still not satisfactory. This illustrates that the volume adjustment factor α is not always effective in compensating the percentage of runoff changing.

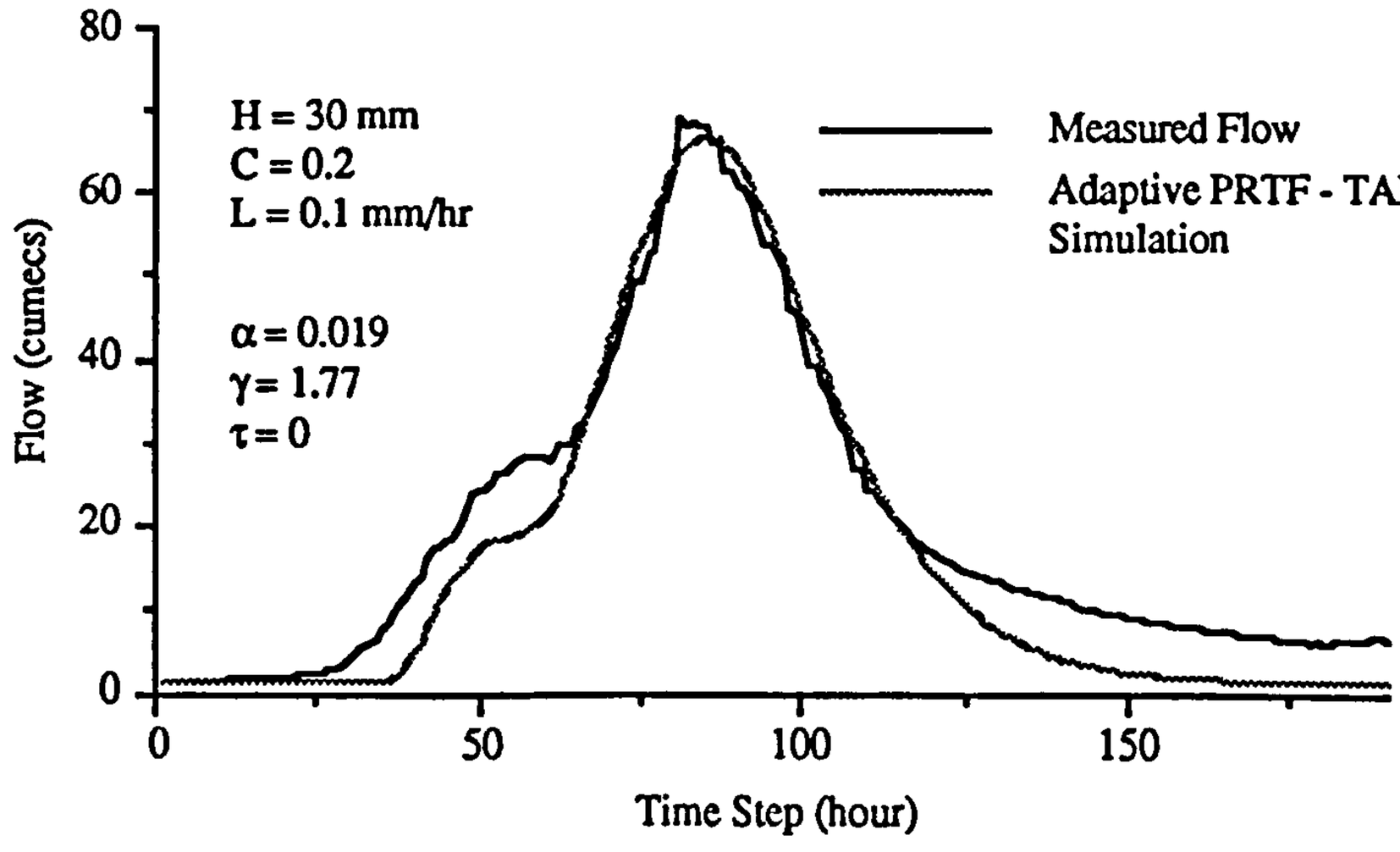

Figure 7.43 Adaptive PRTF - TANK Simulation of Event 4

In Figure 7.43, a RST+PRTF model can simulate the runoff process very effectively. This indicates that the RST can perform better that the volume adjustment factor α on its own. The following figures show the rainfall data by separating them into rainfall loss and effective rainfall.

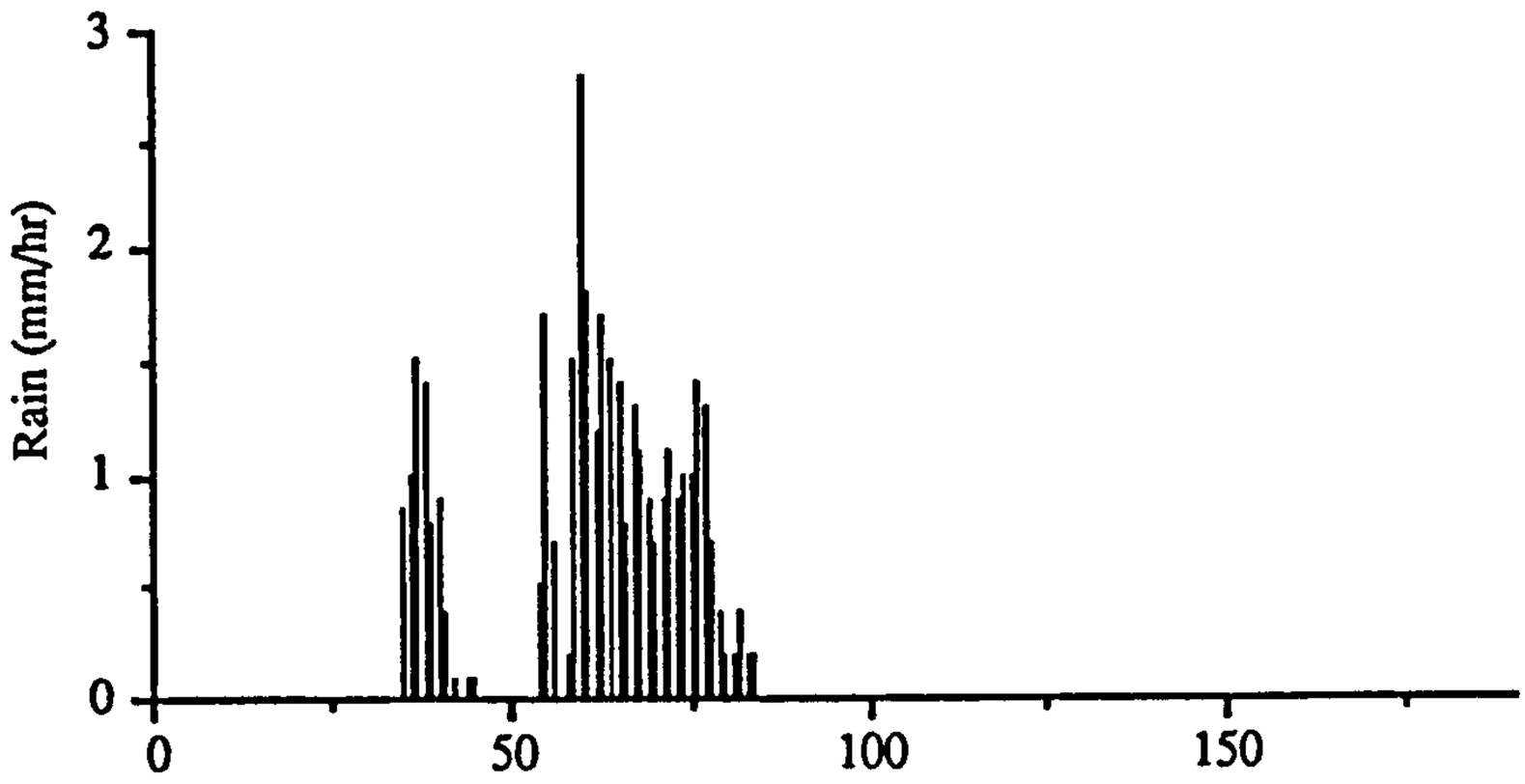

Figure 7.44 Net Rainfall from TANK model

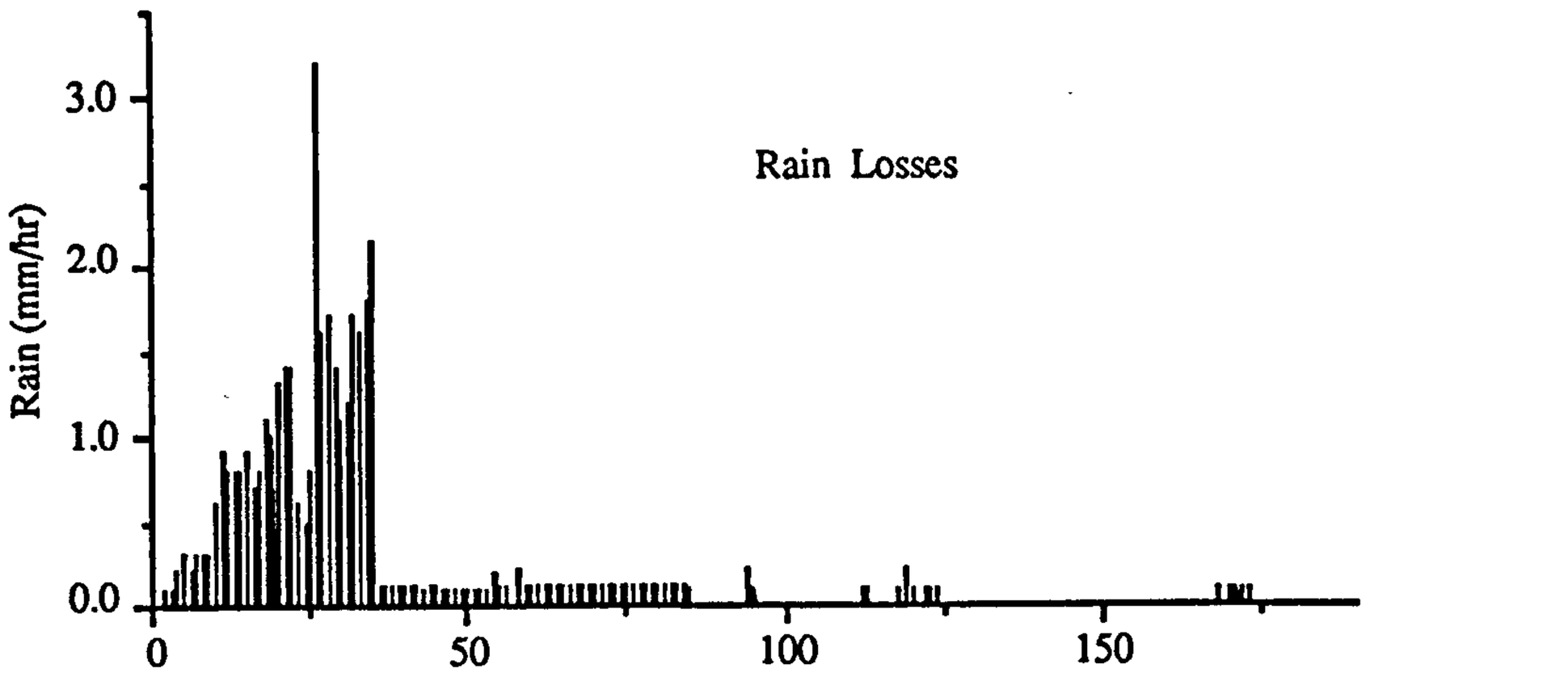

Figure 7.45 Rainfall Deduction from TANK model

If the α factor is kept constant as zero it was found that its effect can be replaced by the RST model as illustrated in Figure 7.46.

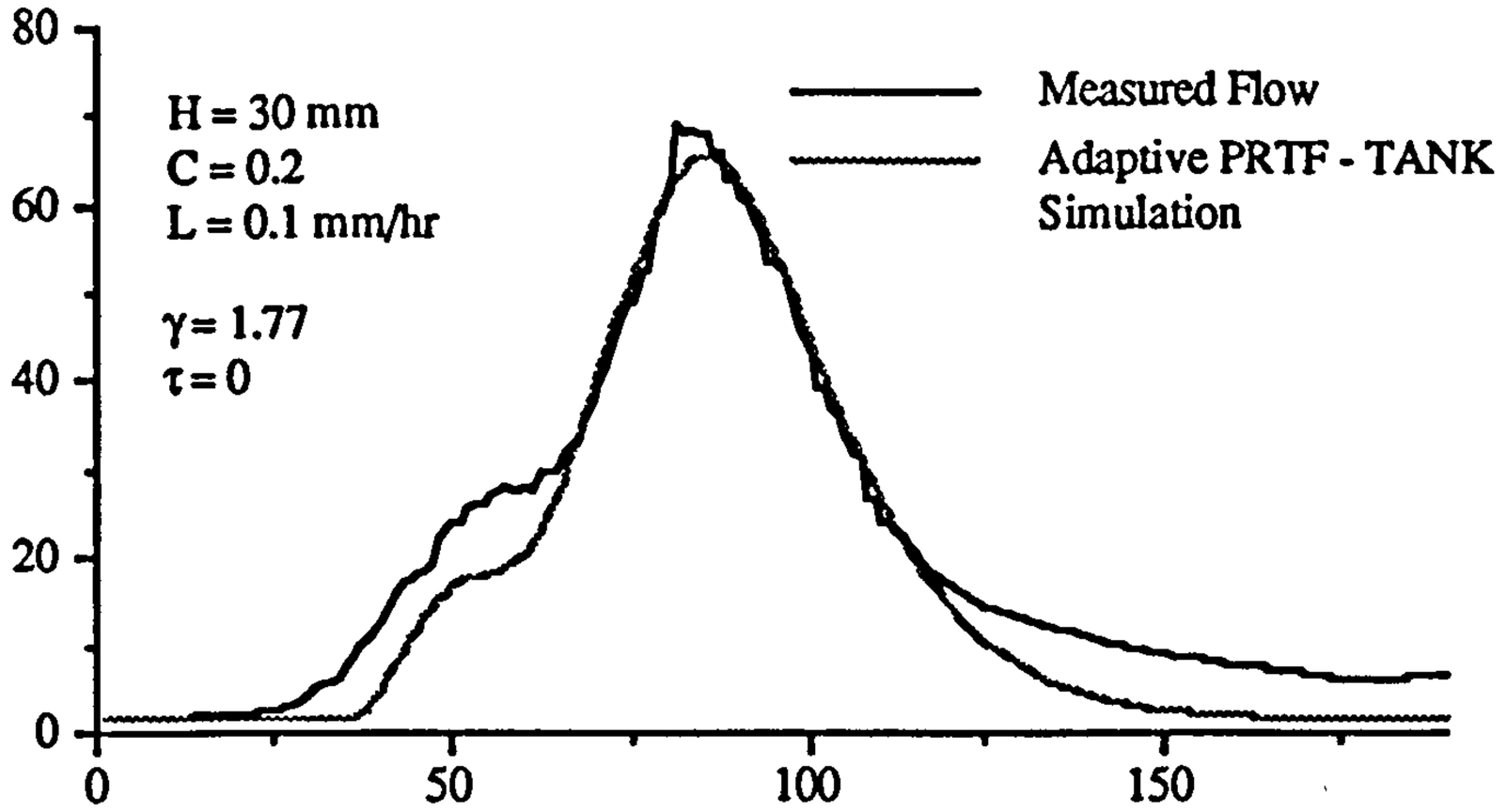

Figure 7.46 Adaptive PRTF - TANK Simulation of Event 4 without α factor

Computational results show that the RST+PRTF was an effective model system. Effective rainfall is computed from the RST model and was input into the PRTF model.

It was found that the square error from the static PRTF simulation = 1134291 Sqr cumecs, and the square error from the adaptive PRTF simulation = 11856 Sqr cumecs, with α = - 0.394, γ = 11.2 hour, τ =3 hour. When the PRTF was combined with the RST model, the square error from the adaptive PRTF simulation = 4274 Sqr cumecs, with α = 0.019, γ = 1.77 hour, τ = 0 hour and tank parameters as H =30 mm, C = 0.2 mm, L = 0.1 mm/hr. It is obvious that the RST+PRTF was the best simulation among them. Square error from the Adaptive PRTF simulation without the α factor was 4277 Sqr cumecs with γ= 1.77 hour and τ =0 hour. This shows that the RST can effectively replace the α factor.

7.6 Summary

In this chapter a distributed kinematic wave model was used to illustrate the catchment response to different kind of storm type. The catchment response behaves differently with storm characteristics. A more intense storm can produce fast catchment response compared with less intense storms. The distribution of the storm is also important in terms of affecting the catchment response. Results show that there exist some general characteristics in the catchment response. This could be further implemented in the expert system which can adjust the flood forecasting system from the past information, the current catchment conditions and storm type.

Through the simulation of the kinematic wave model and the data from Blackford Bridge, the PRTF has shown the ability to adapt to the variability of the catchment response and the result was promising.

A RST (rainfall separation Tank) was developed which can overcome some shortcomings of the pure PRTF and results show a great improvement in the case study described.

PART IV WRIP SYSTEM

CHAPTER 8

WEATHER RADAR INFORMATION PROCESSOR (WRIP) SYSTEM DESIGN

8.1 Introduction

WRIP (Stand for Weather Radar Information Processor) is an information system which can process the real-time radar information, monitor the catchment condition and model the storm and river flow behaviour. The system design is the process of creating the specification, or blueprint, used to implement an information system.

8.2 Components of WRIP

Commonly an information system integrates five components - people, procedure, data, software, and hardware - to produce information by accessing and processing data. The five component model of an information system is represented graphically in Figure 8.1. The components in the figure are arranged symmetrically to denote their equal importance in the system development process.

Notice that the two left-hand components concern people and the two right-hand components concern computers. Both hardware and people are actors - sources of activity. Both software and procedures are sets of instructions; software instructs hardware, whereas procedures instruct people. Data is the central component of the

WRIP information system. It is information that is entered, stored, and accessed to answer questions. People enter data, which is stored on hardware. This stored data is accessed and processed to generate reports, messages, and displays.

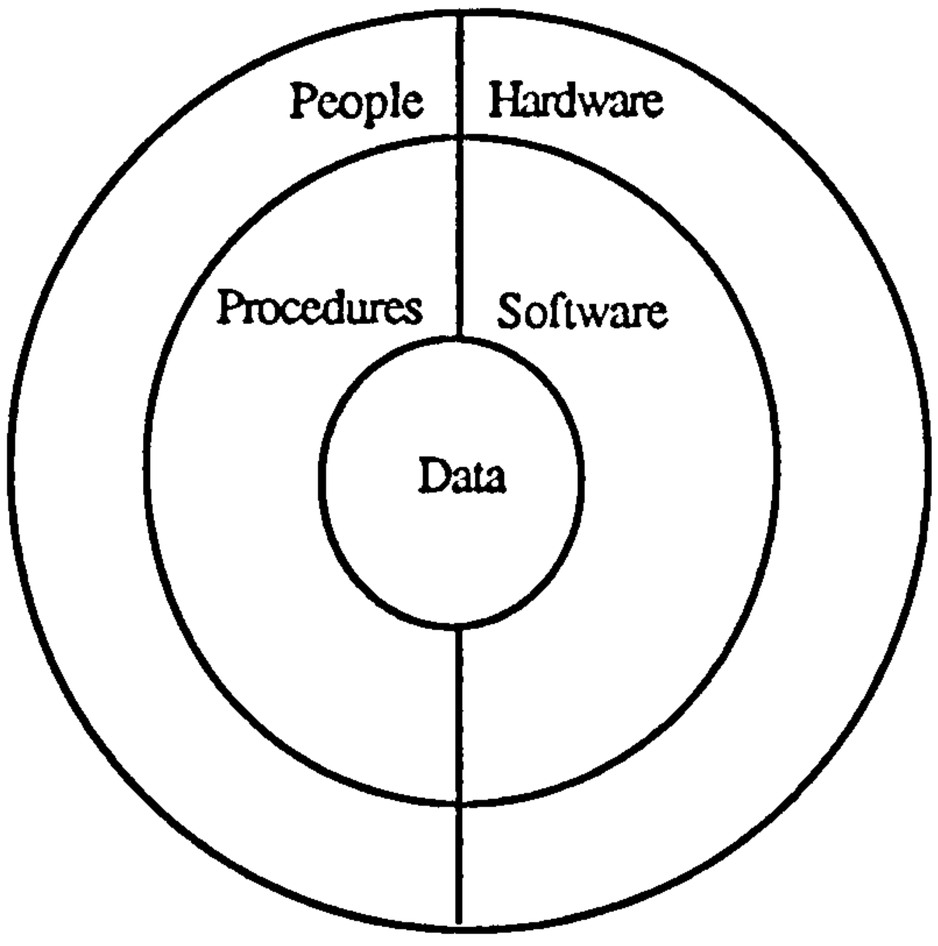

Figure 8.1 The Five Component Model of An Information System(Eleanor W. Jordan 1990)

The three types of data are

* input data - data received by hardware
* data stores - data stored in hardware
* output data - data generated by hardware

The design of the system involves the making full use of the database to provide as much information as possible to the users. Data sources for the WRIP system are represented in Figure 8.2. the WRIP database contains all the information provided by weather radar , telemetry raingauges, river flow stations, other weather information and materials input by the users (or hydrologists). The system should make it easy to allow all components to communicate with each other and avoid communication conflict.

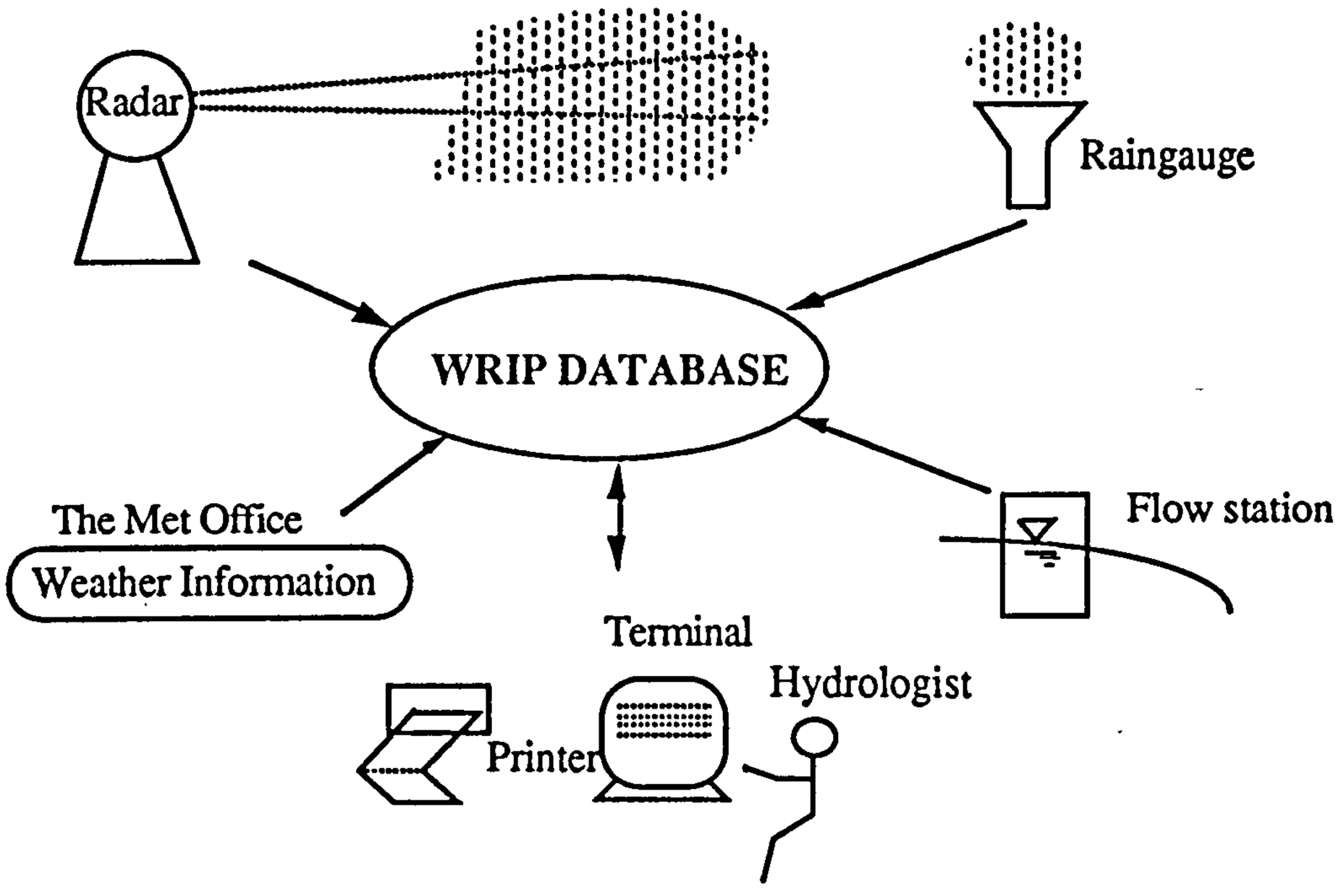

Figure 8.2 WRIP Data Source

The system design principles will be described in following sections.

8.3 User Interface Design

The user interface design is to specify how the system will appear to the users through its reports, screen, menus, and other control mechanisms. Because the user accesses the system via the interface, designing an effective user interface is crucial to meeting the ease-of-use and ease-of-learning objectives of the system quality.

Window-based user interfaces are becoming a common feature of most computer systems, and as a result, users have come to expect all applications to have polished user-friendly interfaces. Unfortunately, a user interface that is easy to use is seldom easy to build. Some experts estimate that as much as 90 percent of the total

effort required to develop a typical window and mouse-based application goes into the user interface (graphical user interface or GUI). The X Window system (Jones 1988) provides a standard window platform that allows application programmers to spend more time improving their Programs and less time porting to new computer systems as illustrated in Figure 8.3.

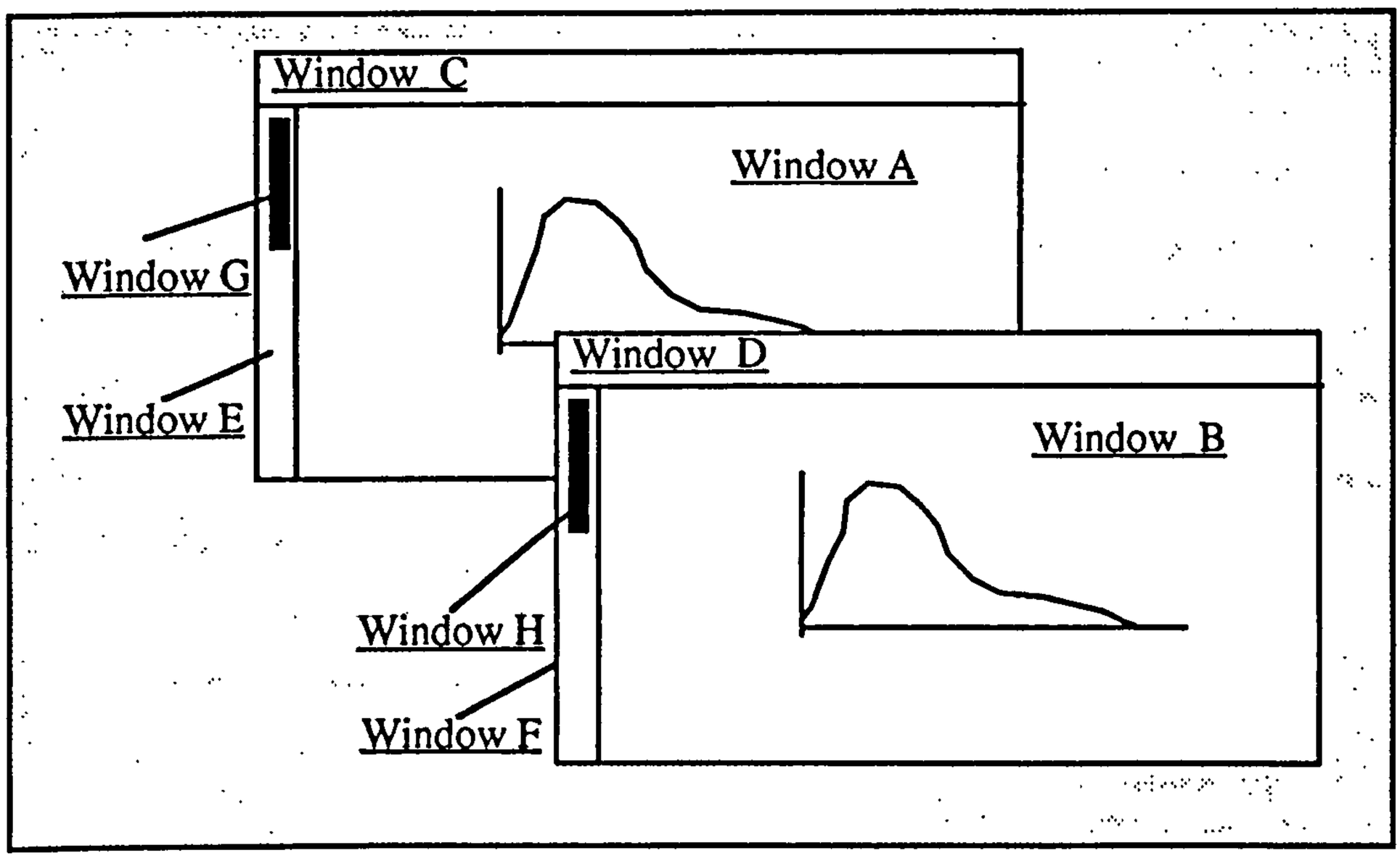

Figure 8.3 A Window Hierarchy in WRIP

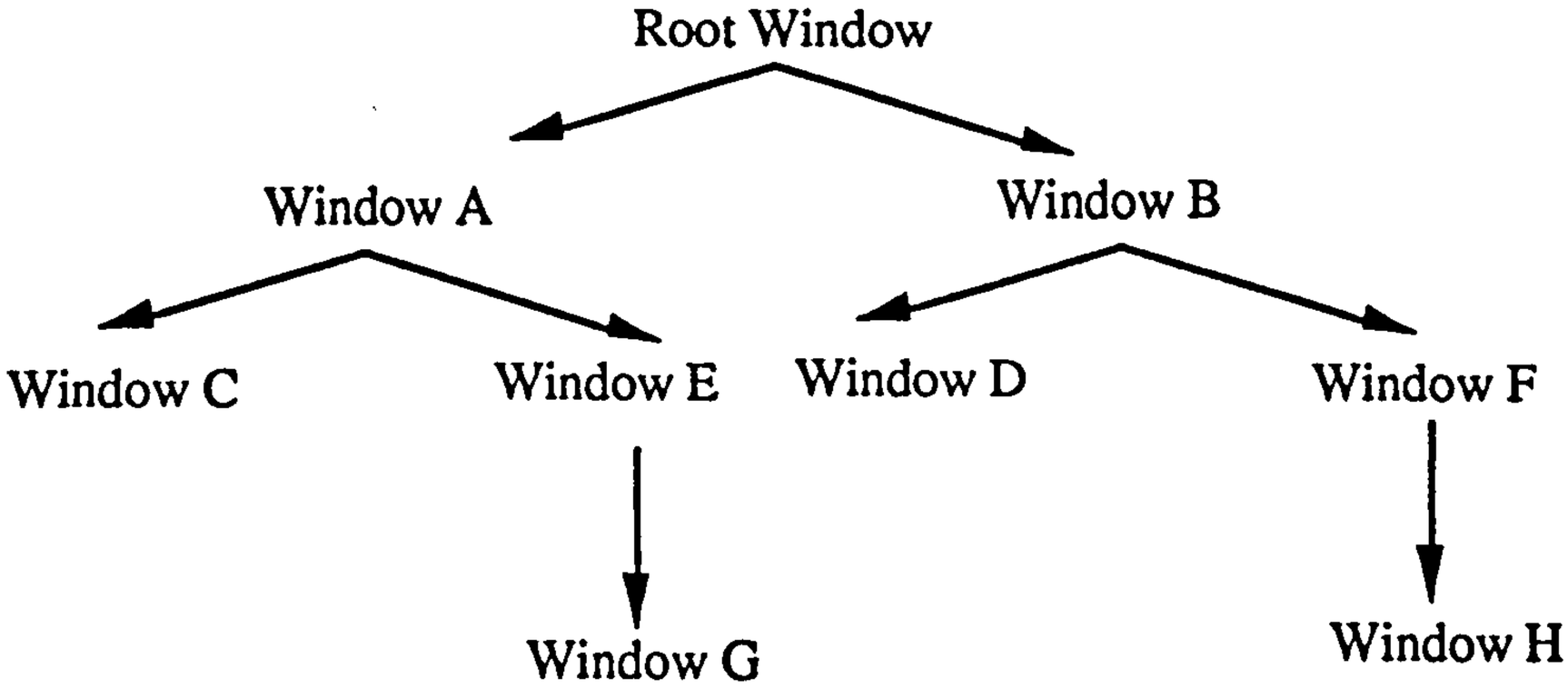

Figure 8.4 Window Tree for Fig. 8.3

X organises windows as a hierarchy, referred to as the window tree. The WRIP window hierarchy is represented in Figure 8.3 and Figure 8.4. The top window in this window tree is known as the root window. The root window occupies an entire physical screen, and can not be moved or resized. Every window except the root window has a parent window (also known as an ancestor) and can also have children (also known as descendants or subwindows). Windows that share the same parent are known as siblings.

The root window of WRIP shows a control panel and a real-time clock as illustrated in Figure 8.5. Most of the screen is left blank for further opening of application windows. The control panel is composed of a label widget, menu widget and push button widget. The most important functions in WRIP are classified into five parts: Radar Data, Raingauge data, Flow data, Modelling and File management.

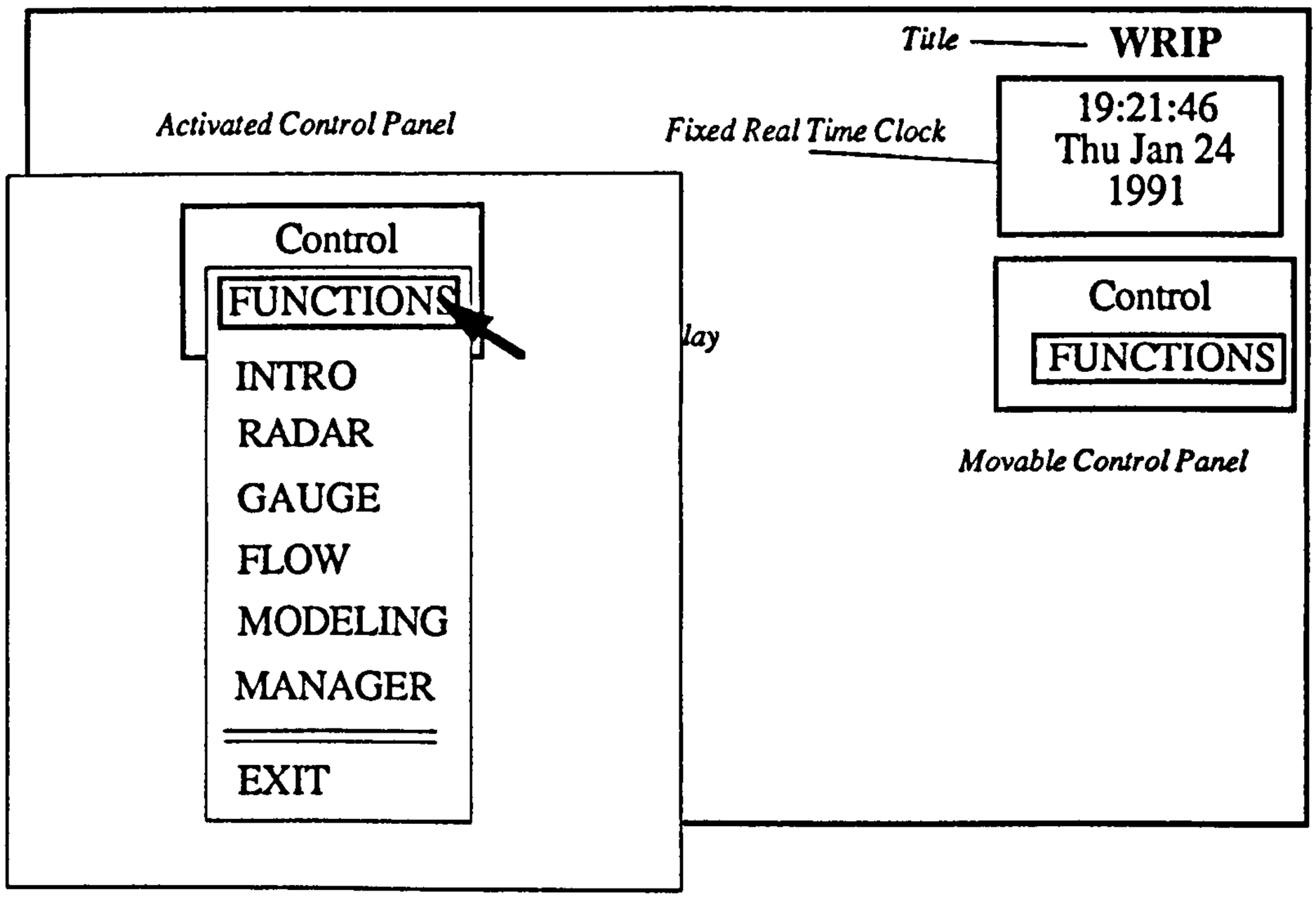

Figure 8.5 Root WRIP Window

By clicking a selected button from a control panel, a child of the WRIP root window will appear. The user can easily manoeuvre in any window. As the children of the WRIP root window support the primary functions, they are connected directed with the WRIP root window without crossing each other as represented in Figure 8.6.

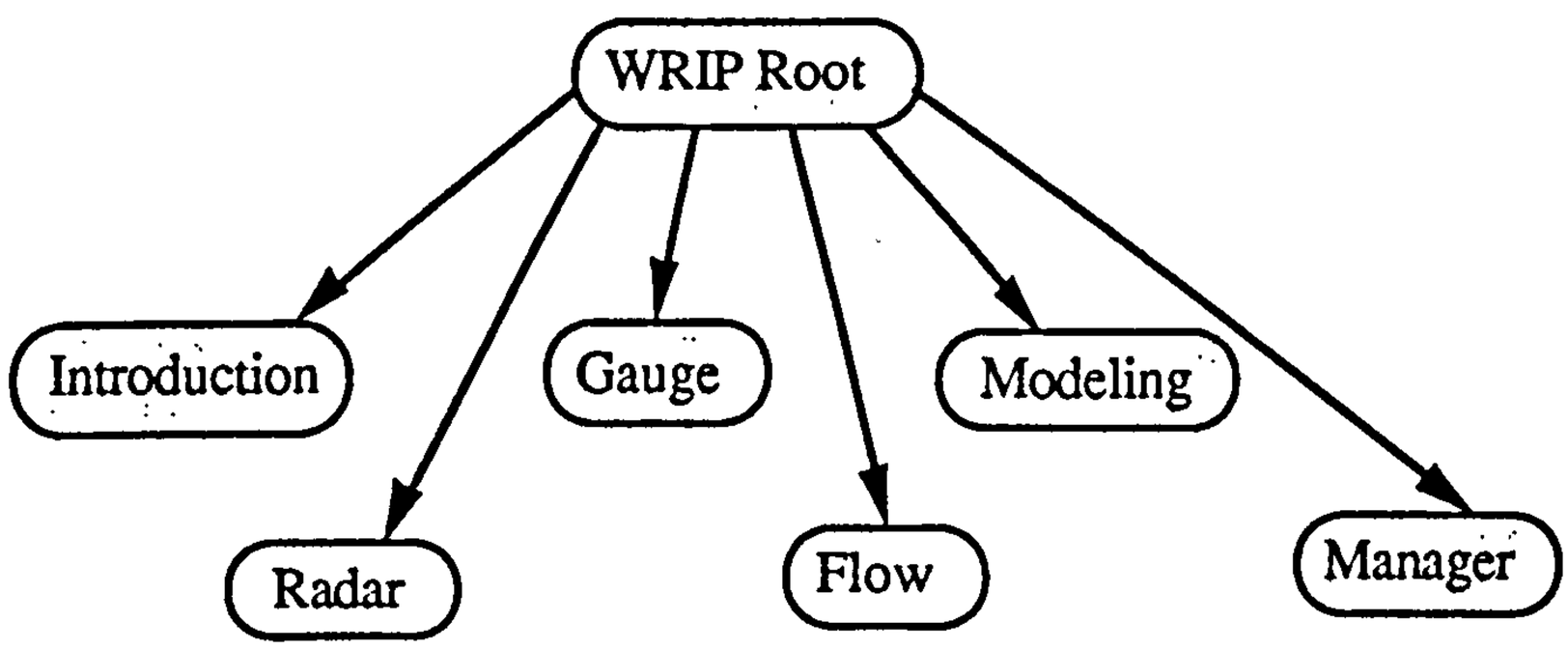

Figure 8.6 Children Window of WRIP Root

For the next level of windows, as some space is needed for graphics, menus are placed on the left of each window and space on the right is left for graphics.

8.4 Database Design

Database design is the process of specifying how the data requirements for a system will be implemented as a data base. Your objectives as you design a database are to ensure that it satisfies the data requirements of the users and the system quality criteria of functionality, maintainability, and flexibility. Transforming a data model into a database is a complex process.

Figure 8.7 shows the inputs and outputs of database design. Database design can be viewed as a three-step process. The first step, conceptual data model modelling.

The second step, logical database design, transforms the conceptual data model into a logical description of data used by a database management system (DBMS). The third step, physical database design, transforms the logical description into a physical model that describes how the database will be organised and accessed on secondary storage devices.

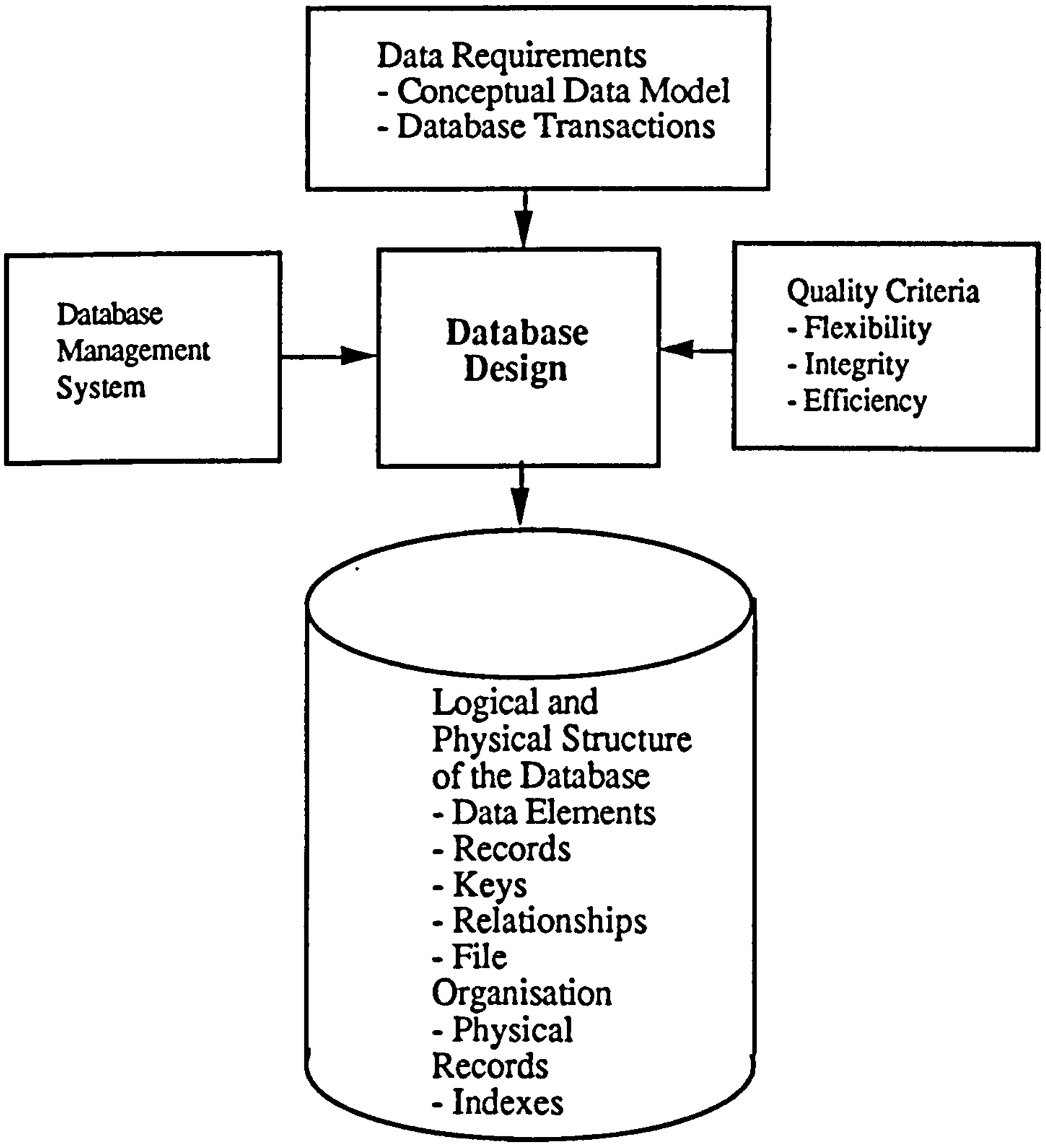

Figure 8.7 Database Design(Eleanor W. Jordan 1990)

At the first step in database design, a conceptual data model is to be set up. Conceptual data modelling is a technique for analysing and describing the data

needed by the users of a system. In analysing the data, the focus is on understanding the conceptual structure of the data.

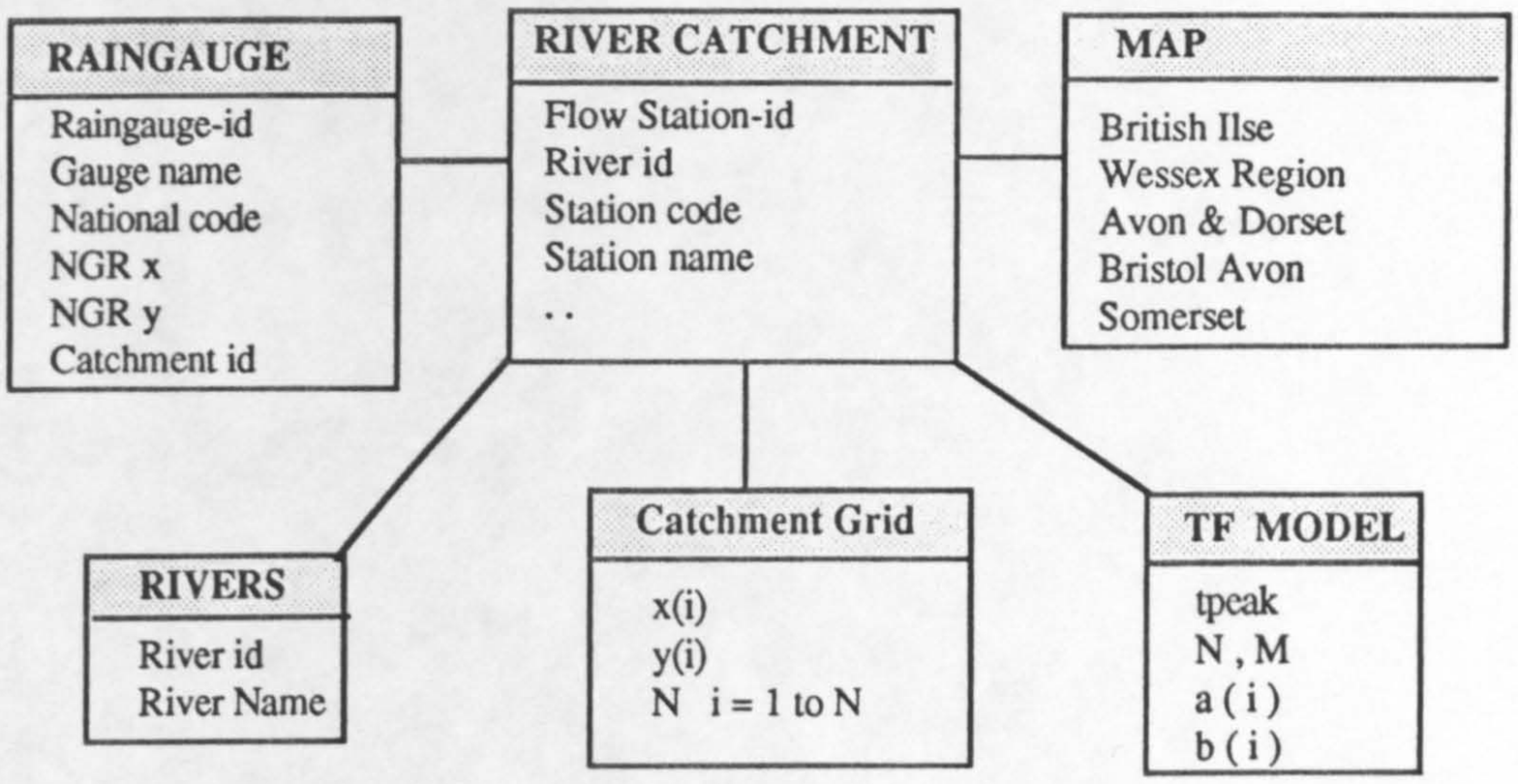

Figure 8.8 Conceptual Model for WRIP Permanent Database

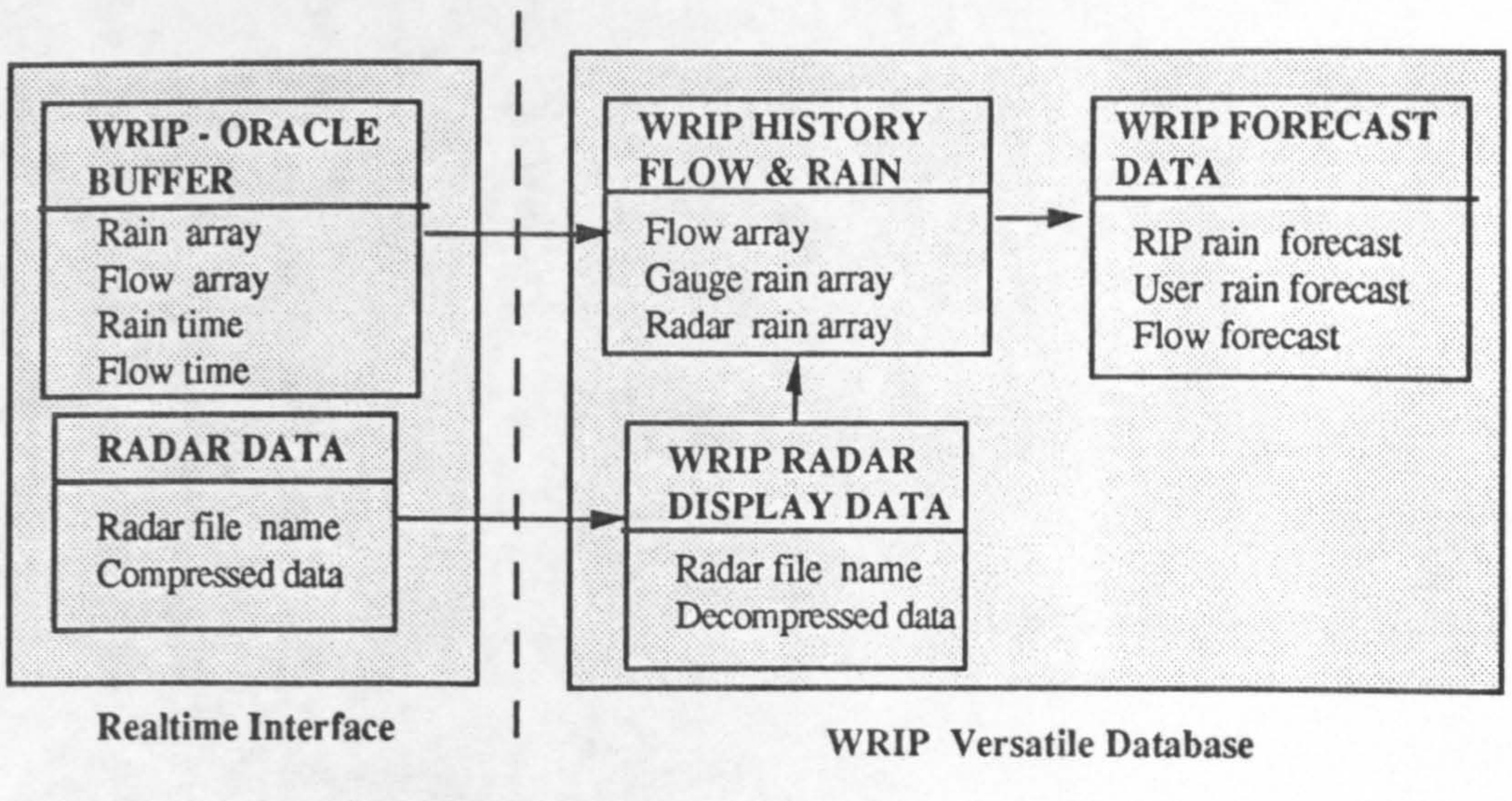

Figure 8.9 Conceptual Model in WRIP Versatile Database

The conceptual data model is built for WRIP as in Figure 8.8 and Figure 8.9. the next step was to translate the conceptual data model into a logical data structure that

conforms to the rules of the network DBMS used to implement the database. During this step, entities are transformed into records, attributes are transformed into data elements, identifiers are transformed into keys, and relationships between entities are transformed into relationships between records. After the logical and physical structures have been specified, they are described in a scheme written in the data description language of the DBMS.

Logical database design constructs describe the logical and physical data structures of a database. Four constructs make up a logical data structure: (1) data elements; (2) logical records, (3) keys, and (4) relationships.

A name within a box denotes a data element. A data element represents the smallest unit of information defined for data. Data elements, often called fields, correspond to attributes, derived attributes, or identifiers in a conceptual data model. A box with a label denotes a record. A record is a named group of data elements. A logical record corresponds to an entity or to a collection of attributes from one or many entities. An underlined data element denotes a key. A key uniquely identifies an instance of a record. A relationship is a correspondence between records.

8.5 Program Design

Program design is the process of packaging the interface, procedure, and database specifications into specifications for Programs. The objective during program design is to specify programs that are adaptable and easy to maintain.

8.5.1 Object-Oriented Programming

The emergence of object-oriented programming in the late 1980s is one of the most significant steps in the history of computing. The ideas behind object-oriented computing are now having a profound impact on the areas such as languages, databases and artificial intelligence. The recognition of object-oriented computing

is a classic example of overnight success after 20 years of painstaking research. It was only around 1986 that interest in object-oriented computing became significantly more widespread. Since 1986, the renewed interest in object-oriented computing has filtered down from research and development to practical exploitation. It is now commonplace for industry and commerce to adopt object-oriented solutions to their problems. Tools such as Objective-C [Cox86], C++ [Stroustrup86], CLOS [DeMichiel87], MacApp[Schmucker86] and Iris [Fishman87] are now in widespread use.

The first principle of object-oriented computing is that of data abstraction. The essence of data abstraction is that the programmer is presented with a higher level of abstraction over both the data and the algorithms required to manipulate. On closer examination, data abstraction actually encompasses two separate but closely related concepts :

i) modularisation, and
ii) information hiding.

Modularisation is concerned with the breaking down of complex systems into a number of self-contained entities (or modules). All information relating to a particular entity in the system is held within that module. Thus a module is self-contained and complete description of a part of the overall system structure. In terms of computing, this means that a module will contain all the data structures and algorithms required to implement that part of the system. This is beneficial as it means that there is an obvious place to go to if changes have to be made or problems occur. More fundamentally, Modularisation enforces a particular design approach whereby the programmer breaks down the problem domain into a number of recognisable conceptual entities. This design approach forms the essence of object-oriented computing.

Information hiding takes the level of abstraction one stage further by hiding the implementation details of a module from the user. With information hiding, users must access an object through a protected interface. This interface normally consists of a number of operations which, as mentioned above, collectively define the behaviour of an entity. The user is thus not allowed to see internal details such as local procedures or data structures. This is a major tool in handling complexity as it allows the user to abstract over a level of detail in the system. Information hiding also supports the development of more reliable Programs by strictly controlling the entry points to a module.

The modules in WRIP are designed according to object-oriented programing as in Figure 8.10.

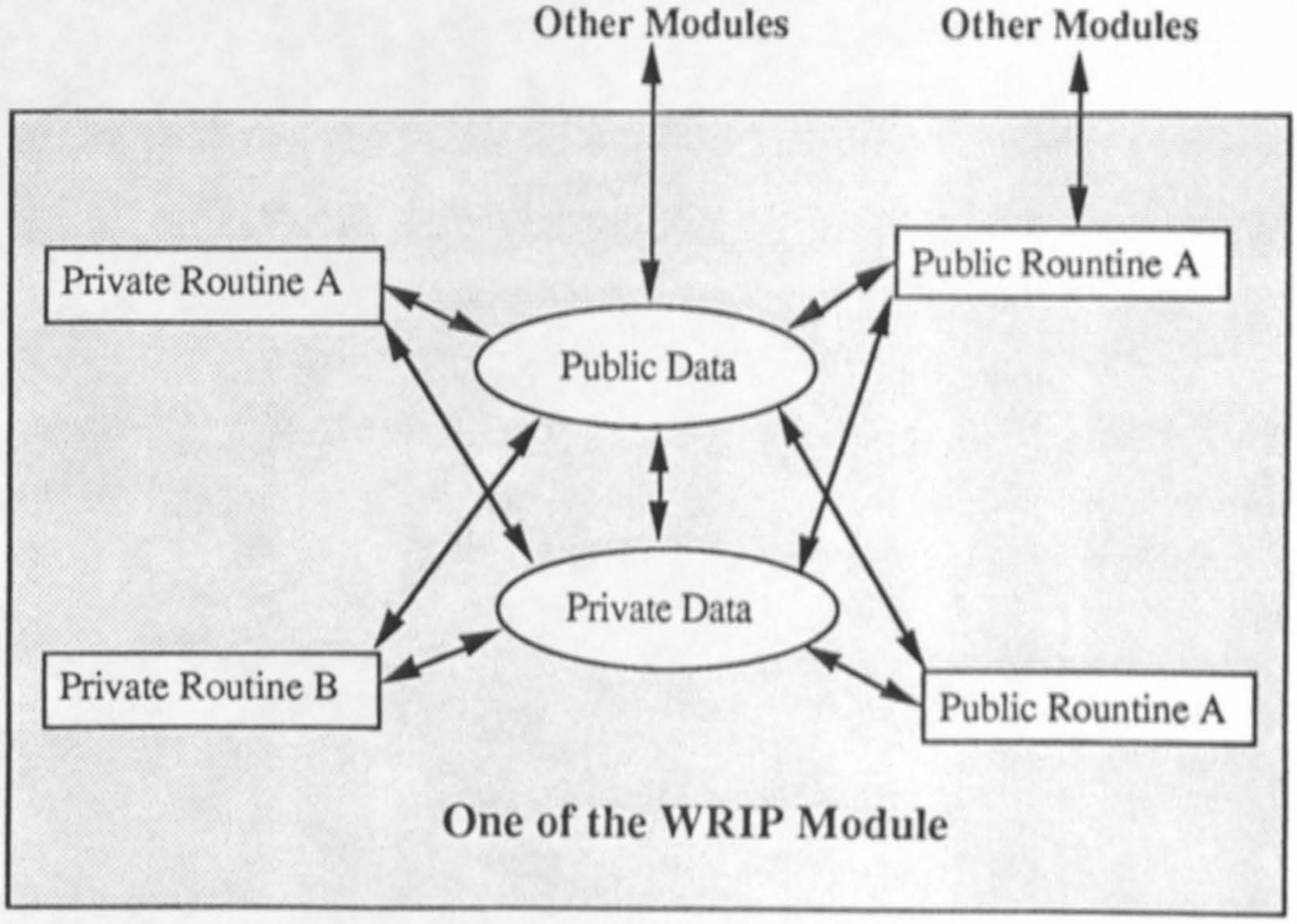

Figure 8.10 Object-Oriented WRIP Module

The public data items in WRIP are sharable to all modules (or Objects) and they

are kept in minimum numbers to prevent interference between different objects. The private data items are used by the internal private routines which control the data access, management and display. If any other module wants to access the private data items, it can only do so by asking the public routines in this module to carry out the specific function. In this way, the WRIP system became easier to code and convenient to maintain in the future.

8.5.2 Structure of WRIP Program

As WRIP is a window oriented system, the application software is based on the X-Window system. Although programmers can use Xlib to build applications, this library can be tedious and difficult to use correctly. Just handling the window manager conventions can require hundreds of lines of code.

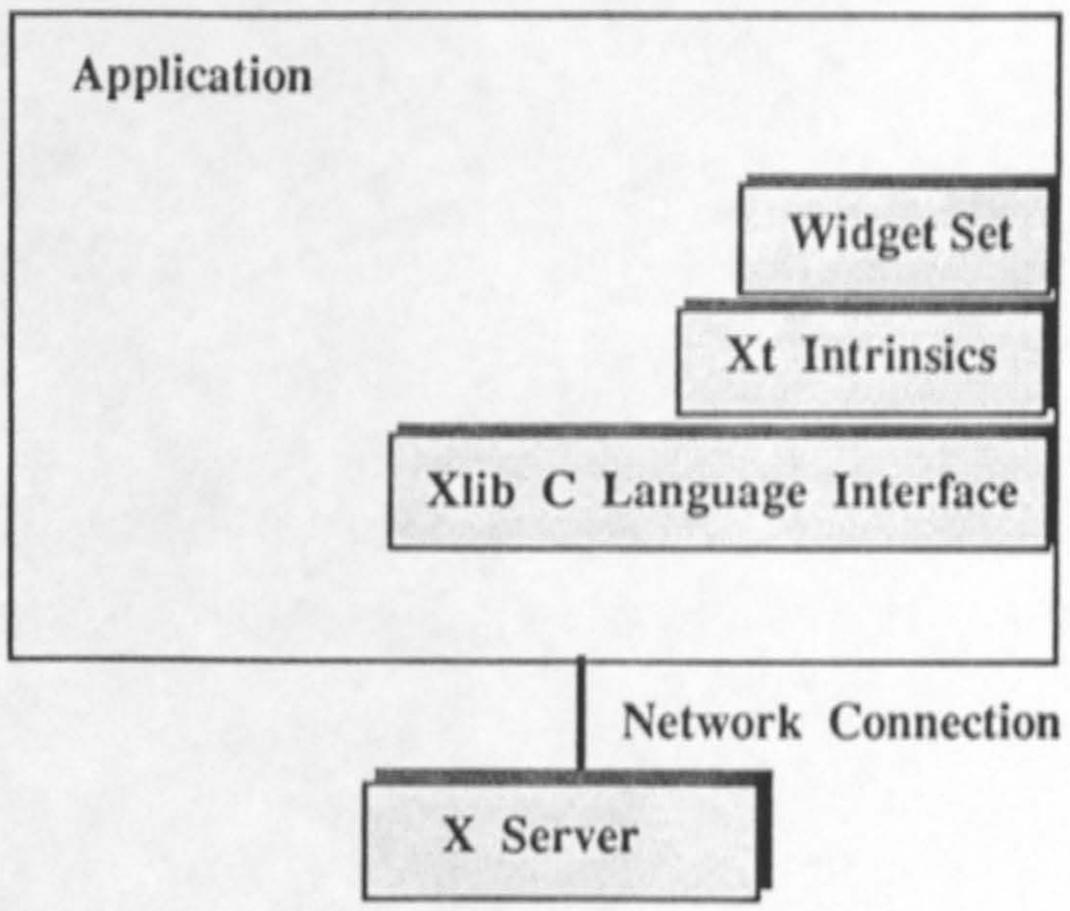

Figure 8.11 Programmer's View of the Complete X Window System

To ease the utilisation of X-Window, the C-language is adopted to use the both high level and low level X-Window utilities in graphics as illustrated in Figure 8.11. The start screen of WRIP is an input menu interface. The user controls the system

performance by selecting a desirable button in the menu. The control module is the central part of the system. It is used to manage all the main functions in WRIP.

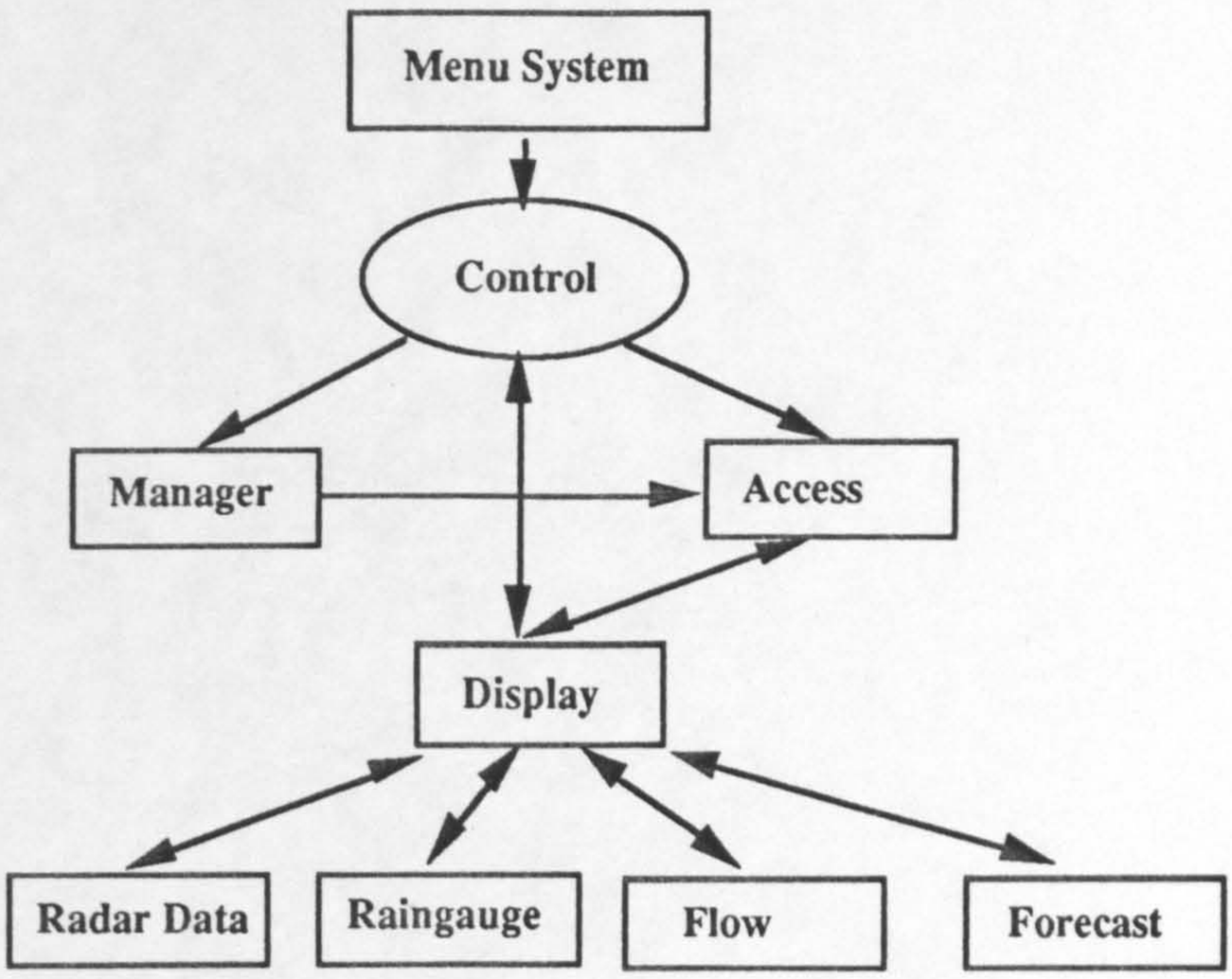

Figure 8.12 WRIP Structure

WRIP can not run in real-time without the WRIP server providing a data source for it. Figure 8.13 illustates the communication between WRIP and the WRIP server.

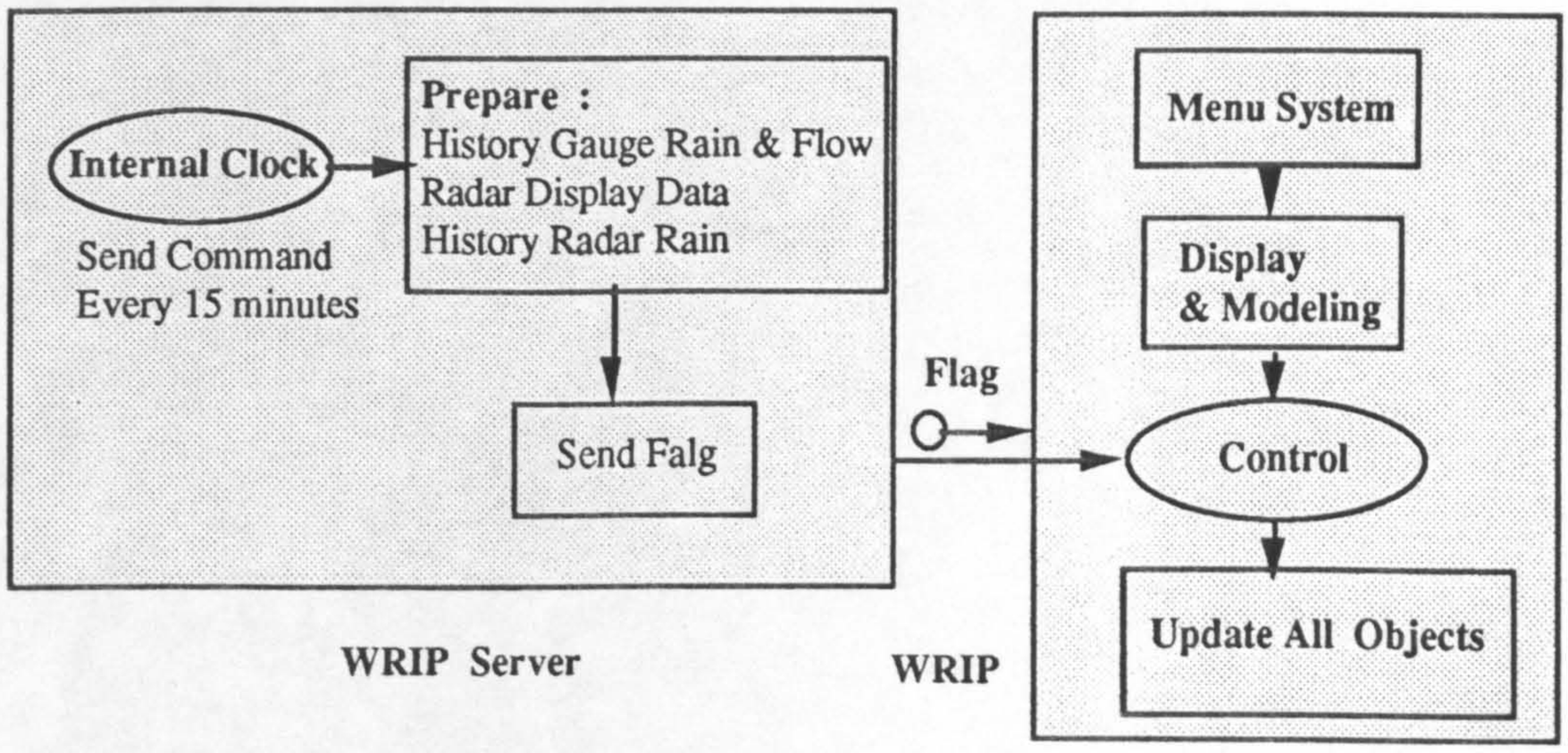

Figure 8.13 Data Synchronisation System for WRIP

The event flag is sent by the WRIP server to inform WRIP that the WRIP database has been updated. WRIP takes the event flag, updates its system and then clears the event flag for the next step.

8.5 Summary

WRIP is a real-time information system. which is used to process weather radar information and provide quantitative flood forecasting. A well designed system structure, user interface, database and program is crucial for a successful system. In this chapter, the system design principle of WRIP is described. A window-based user interface is adopted to convenience the using of WRIP. As the system is complicated and there is a large amount of data to be processed, an object-oriented computing concept was utilised in the WRIP program design. This has been found to be a significant improvement to the system development.

CHAPTER 9

APPLICATION OF WRIP IN NRA WESSEX REGION

9.1 Introduction

The Wessex region is characterised by infrequent heavy rainfalls and has produced many of the record British rainfall totals in addition to some of the more infamous floods. The continual development of modern telemetry systems and the concurrent application of flood forecasting procedures have led to the current system being evolved which will be based upon the real-time quantitative use of the composite radar network data for modelling purposes. This chapter describes the WRIP working environment in NRA Wessex Region and some specific technical issues in this region.

9.2 The Wessex Region

The Wessex region consists of three river basins each with its own hydrological regime varying from relatively rapid response catchments in Exmoor to the more sedate Bristol Avon. The increased availability of computers in the mid 1970's led to the development of the first predictive models based upon unit hydrograph convolution and flood routing. These models are still in use and rely on the precipitation input derived from representative telemetered raingauges in the catchments.

The region is characterised by infrequent heavy rainfalls. Indeed, many of the top falls appearing in the United Kingdom record books have occurred in the Wessex region: Martinstown, 275 mm in 1955, Lynmouth, 225 mm in 1952, Cannington, 225 mm in 1924 and Bruton, 225 mm in 1917. In all cases the spatial distribution of intense rainfall was small and were it not for the location of gauges within these storm cells the true precipitation would never have been known. The commissioning of the weather radar at Upavon in 1979 provided the opportunity to record these intense rainfall cells. The storm in May 1979, again centred near Bruton, was an early example of the value of weather radar with precipitation measurements from raingauges underestimating the true fall.

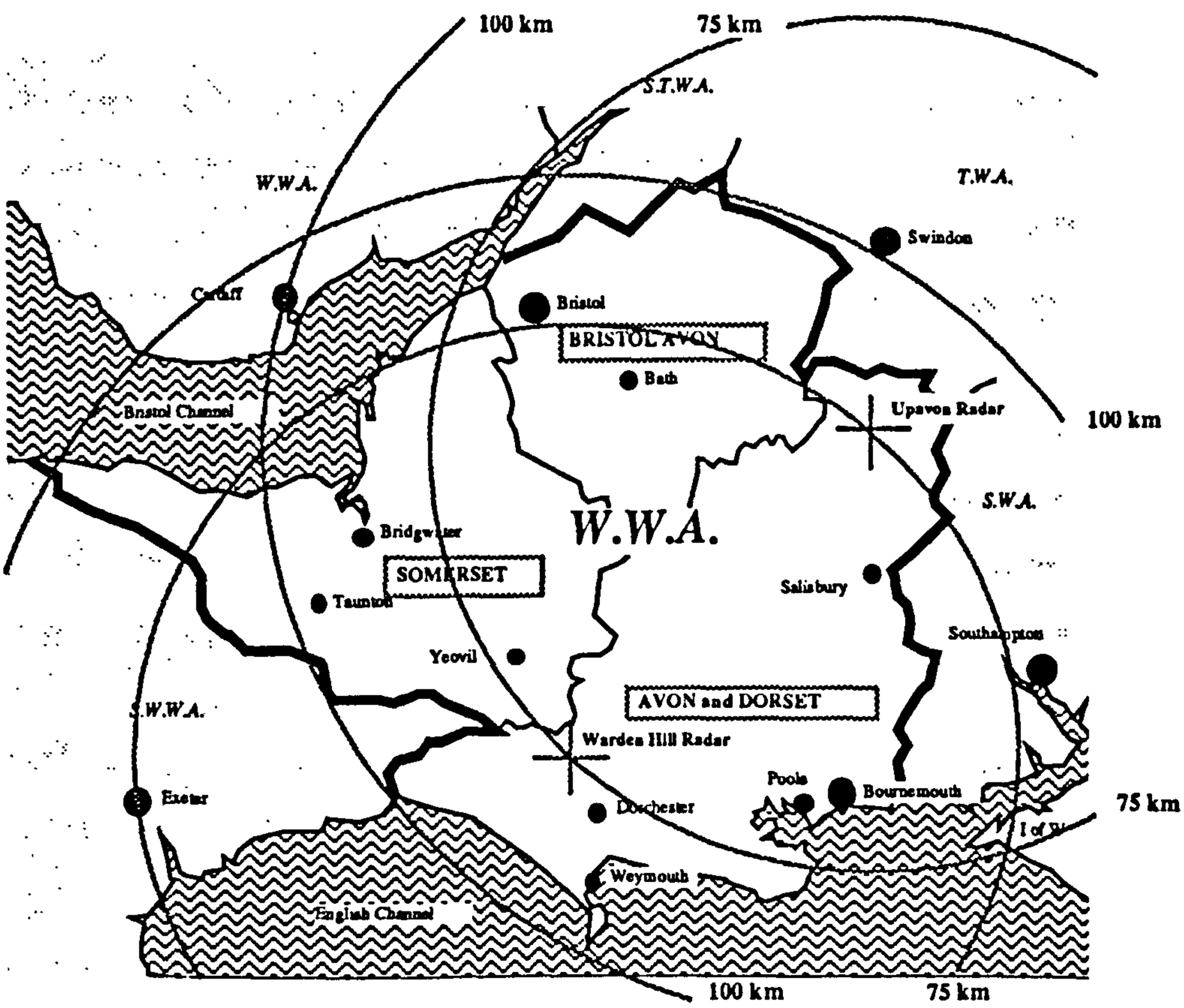

Figure 9.1 Wessex Region and Weather Radar Coverage

The gradual introduction of weather radars and the availability of the network picture prompted a review in recent years of the existing models. Associated with

the availability of increased computing power, the possibility of developing a regional model utilising weather radar as the primary precipitation input was explored. In 1984, the Wessex Water Authority was embarking on an Information Technology(IT) strategy based on integrated river basin management. Wessex already had a comprehensive telemetry system for the utility functions of supply and sewage treatment, digital maps of the assets and rivers, computer based flood models and the network radar product, all accessed within one 24 hour regional Control Room at Bristol.

This strategy was to produce an integrated Water Management System (WMS) allowing access to all functions through one computer screen using windows and including the facility to extract data from one source (window) and combine with data from another (window). Specifically, weather radar quantitative information was to be passed into real-time flood models and the forecast products disseminated through internal communication networks. Development of the WMS pilot concentrated on the Man-Machine Interface and was in association with Software Sciences Ltd.

Privatisation of the industry and the creation of a National Rivers Authority required the dismantling of river basin management integration and as a consequence, the IT strategy based on WMS had no future. However, the flood forecasting aspects; weather radar and flood models, and the development of the MMI; are proceeding in cooperation with the Water Resources Research Group at the University of Salford.

As previously described the Wessex region consists of three catchment based divisions each with its own particular hydrological regime (see Fig 9.1). The region is characterised by infrequent heavy rainfalls and an analysis of the extreme rainfall records for the British Isles produces a table of falls that concentrate on and around the Wessex region. This phenomenon was publicised by Bootman and

Willis(1979) which prompted further research into its cause. Such was the concern that the Institution of Civil Engineers Manual for Reservoir Design advises that local rainfall analysis should be applied rather than the regional analysis recommended elsewhere in the United Kingdom.

The hydrometeorology results from the interaction of warm moist northerly moving thunder cells with the jet stream meeting over the South West of England leading to both rapid rain cell development and negligible movement. The impact on flood forecasting has been to ensure that any models adopted can recognise and cope with intense localised rainfalls.

9.2.1 BRISTOL AVON

The ***Bristol Avon catchment*** (see Fig. 9.2) is bordered by the Cotswolds to the north, Salisbury Plain to the east and the Mendip Hills to the south.

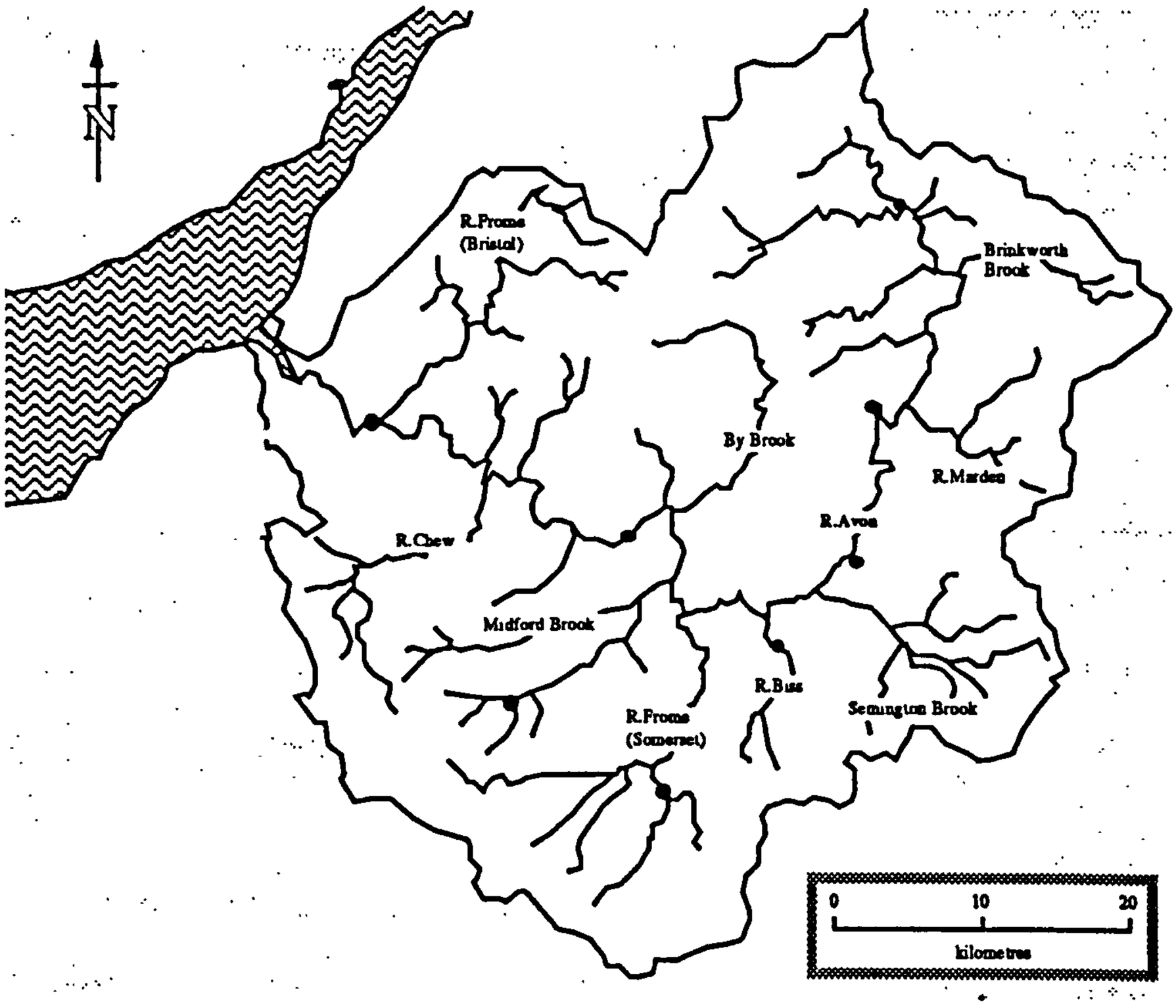

Figure 9.2 Bristol Avon Rivers

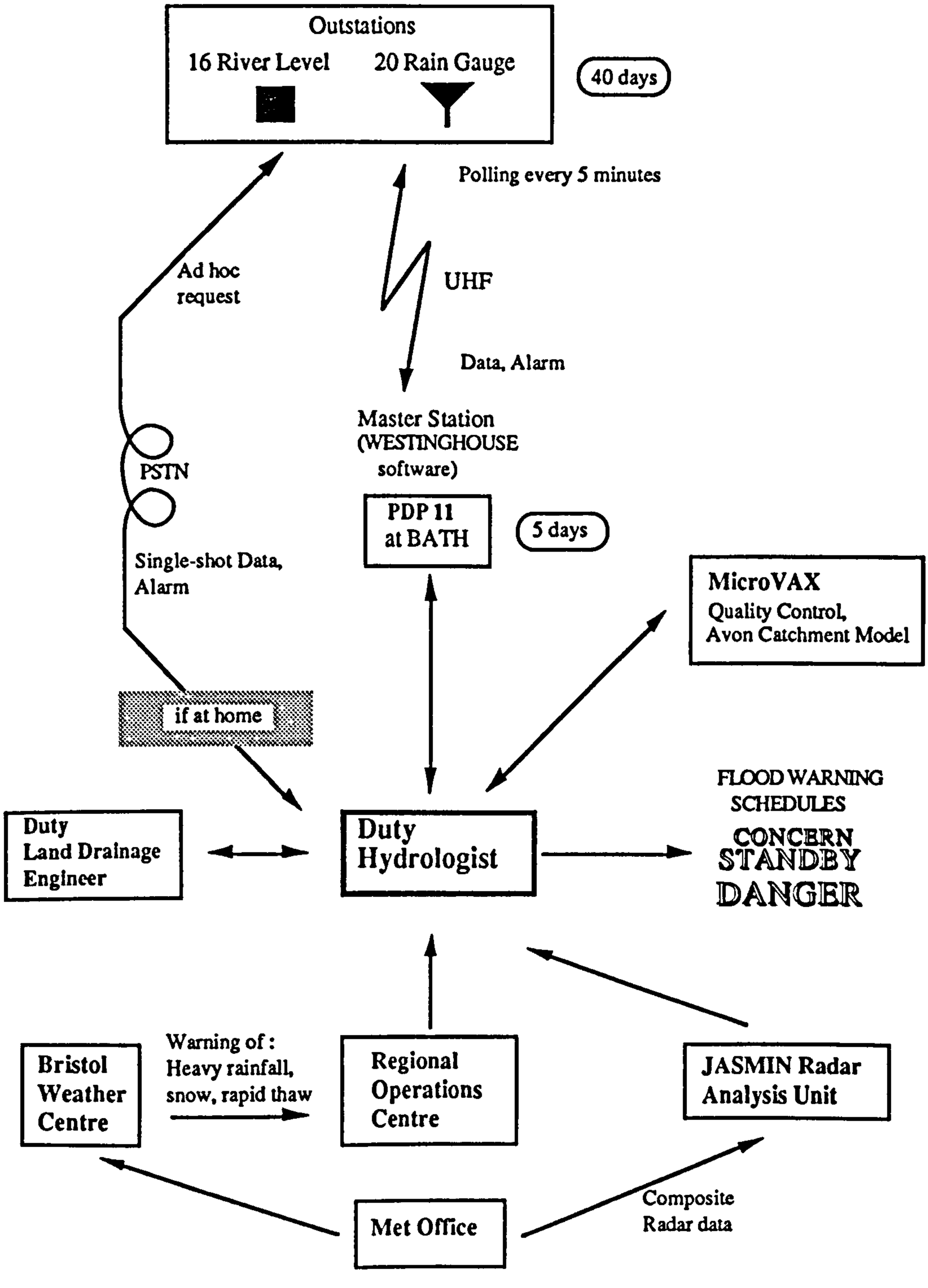

Figure 9.3 Existing Data Flow Within Bristol Avon Division

The River Avon itself rises in the Cotswolds and drains southward picking up tributaries from Salisbury Plain then turning westward, collecting tributaries from

the Mendips and draining to the sea through the Avon Gorge west of Bristol.

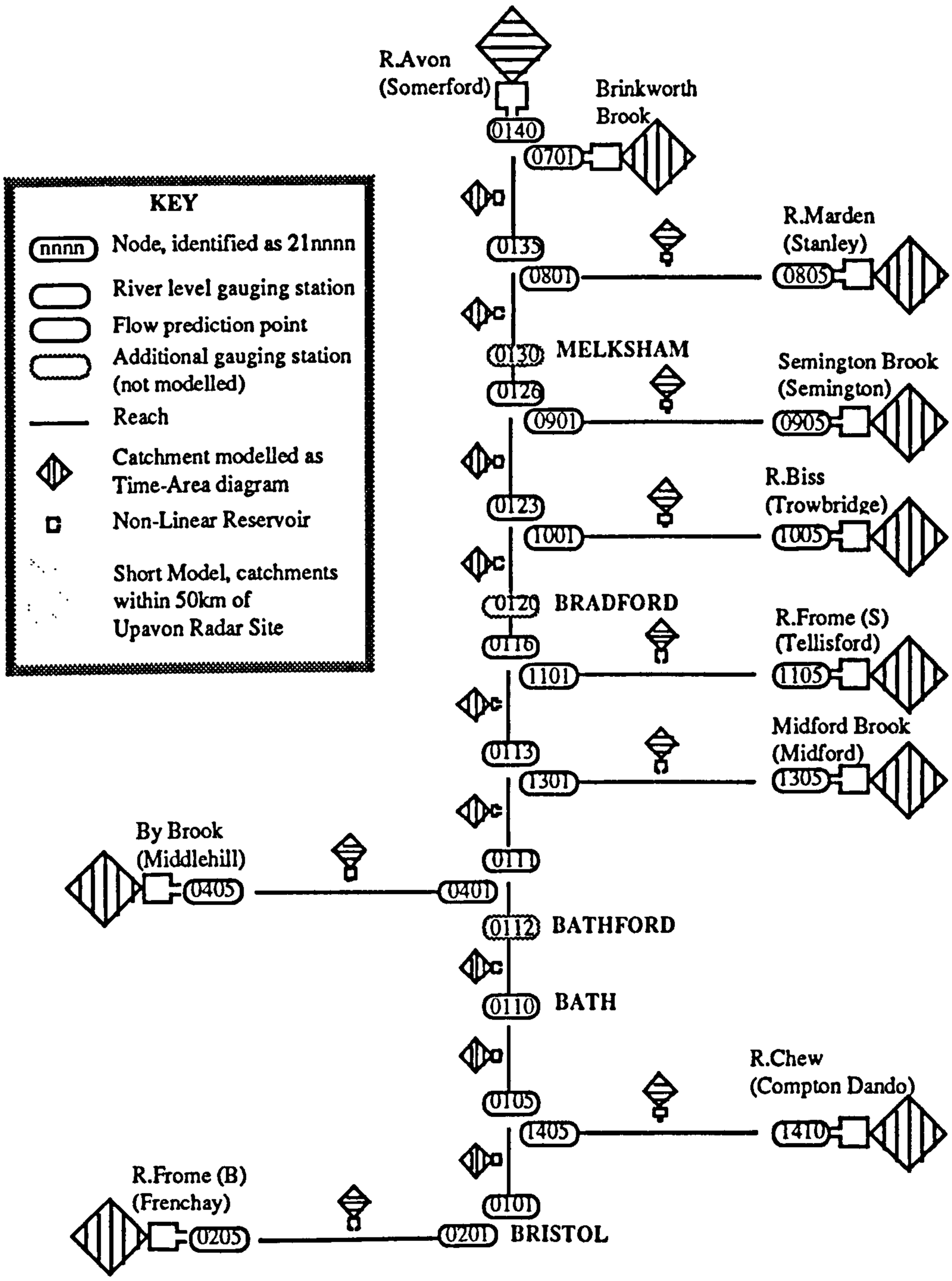

Figure 9.4 Schematic of Avon Catchment Model Network

The current flood forecasting model was developed for the Bristol Avon catchment

by Grimshaw and Wong(1975) and is shown in schematic form in Figure 9.4. The drainage system is modelled as a network of nodes connecting various subcatchment elements and open channel reaches. Discharging into the head of each reach is the flow either from a subcatchment or from another reach. Each reach has in addition a subcatchment element discharging into its mid-point, representing the lateral inflow. Each subcatchment is modelled using a non-linear reservoir lag-and-route rainfall/run-off model, and each reach a Muskingham river-routing model. Data collection is by a DEC VS2000 scanning 20 raingauges and 19 river level outstations as in Figure 9.3. The models have recently been re-written to operate on the same Vax VS2000 workstation.

9.2.2 AVON AND DORSET

The ***Avon and Dorset catchment*** (see Fig. 9.5) has two distinct areas.

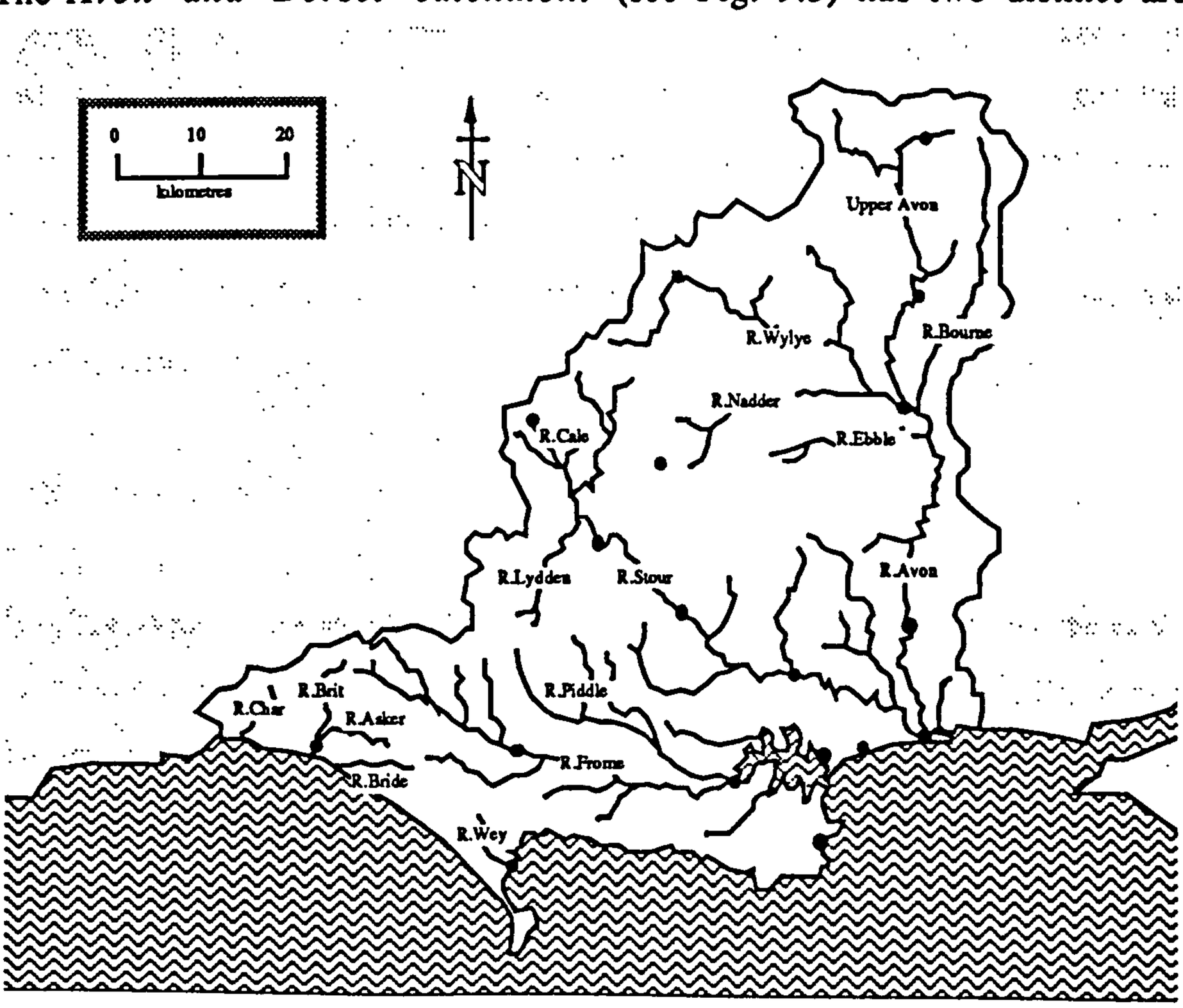

Figure 9.5 Avon and Dorset Rivers

To the east is the Hampshire Avon draining southwards from Salisbury Plain and the Stour draining south eastwards. To the west are the Dorset rivers, draining south from the Dorset Downs typically fast response chalk catchments. It is in one of these catchments where Martinstown is situated where the highest British daily rainfall of 275 mm was recorded in July 1955.

The models adopted for the Avon and Dorset rivers have been the subject of several research exercises. Initially developed as unit hydrograph models the current versions were developed as transfer-function models with elements of correlation for forecasting downstream levels (see Final Report on Flood Forecasting Project For Wessex Water Authority - Avon and Dorset Division, 1980 and Cluckie, Yu and Tilford, 1989). Bliss (1981) refined the models for real-time updating, but manual updating is the current practice.

Data collection is by a Texas dedicated computer scanning 18 raingauges and 33 river level outstations. This data collection system was part of the water industry's Experimental and Demonstration Facility (EDF). The models have operated on a portable Hewlett Packard programmable calculator during the period of system development.

9.2.3 SOMERSET

The ***Somerset catchment*** (see Fig. 9.6) is also divided into distinct regions. To the west are the catchments draining Exmoor and the Brendon Hills, very fast responding catchments adjacent to the River Lyn scene of the disastrous Lynmouth floods of August 1952. Central Somerset is drained through several rivers flowing through land below high tide level and reaching the sea near Burnham-on-Sea. North Somerset, now in the county of Avon, has a number of small rivers draining the Mendip Hills and flowing westwards.

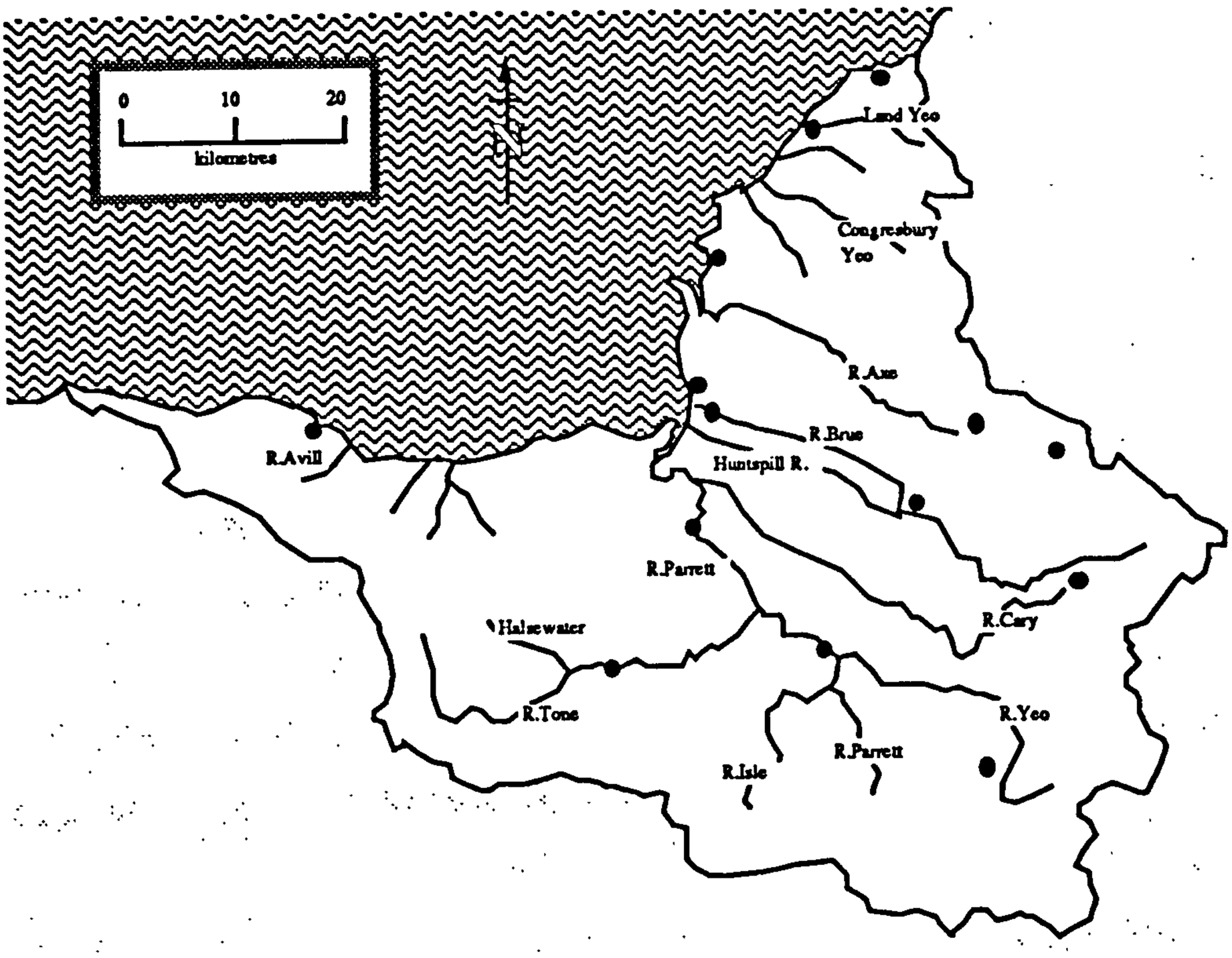

Figure 9.6 Somerset Rivers

The original flood forecasting models for the Somerset division were developed by Bootman(1978) based on unit hydrographs and level correlations. Rainfall input was derived by a surface fitting algorithm described by English(1978) to allow for missing data and to represent areal catchment totals. Biggs(1980) developed a system based upon transfer functions and applied a recursive least squares recalibration routine. The current models were reconverted to unit hydrographs by Bootman and Willis(1979) in order to operate on an Apple II microcomputer. Later modifications were added to the models by applying the transfer function approach to the embanked watercourses flowing through the central Somerset levels. The models have recently been converted to run on a Toshiba T5100 lap-top. The

current data collection from 13 raingauges and 8 river level sites is through Datacall outstations polled by a fixed Apple IIe masterstation, or by polling Telegen equipment as required from the Toshiba T5100.

9.3 WRIP Working Environment

9.3.1 Regional Computer and Telemetry System

The occurrence of intense rainfalls resulting in disastrous flooding in the summer months in the recent past; Martinstown, 275 mm in 1955, Lynmouth, 225 mm in 1952; and prolonged winter floods in October 1960: prompted the newly created River Authorities to embark on the development of flood forecasting procedures. At this time, techniques were graphical relying on manual observation of rainfall being telephoned to the Authority Offices.

The advent of teletone raingauges and computers in the late sixties established the basis for applying better methods of flood forecasting. The requirements to install rainfall and river gauges, and training in current metering, to identify water resources potential indirectly produced the database of flood records for model calibration. Significantly, the floods of July 1968, strengthened the case for prepared emergency procedures, including flood forecasting, in the Wessex region.

The increasing availability of computers in the 1970's, and the associated development of better modelling techniques allowed each division to install its own forecasting methodology, suited to the catchment, the resources and the staff expertise then available.

Wessex Rivers inherited three entirely different stand-alone telemetry systems. The flood forecasting models in use depended entirely upon manual input data gleaned from the telemetry systems and other observational data. Prior to the creation of

Wessex Rivers in preparation for the formation of the National Rivers Authority, the decision to replace the Bristol Avon telemetry with a system based on a DEC VAX 3600 computer had already been taken. Proposals were already in hand to replace the Somerset telemetry system and the decision was made to use a DEC VAX 3600 as the master station for a new Wessex Rivers Regional Telemetry System.

The computer receives information via the Public Switched Telephone Network (PSTN) and also by private wires from over 150 outstations collecting data from rain gauges, gauging stations, river level sites, pumping stations, sluices, etc. Not all are used for flood warning purposes directly but many are used to monitor operational situations throughout the river network. Figure 6 shows the general outline of the system.

The computer master station interrogates outstations to obtain present values and logged data as well as maintaining a database of the entire system. The information is presented from the database on a local monitor which includes graphic facilities. The computer is also capable of all archiving required. Information from the database is sent to remote PSTN terminal equipment in response to requests from those sources and carries out validation of all data received. Information from this new telemetry system continues to be manually fed into two of the flood forecasting models and this will continue until the new models are commissioned.

The Bristol Avon flood forecasting model has been rewritten to run on a DEC MicroVax II (MVII) computer which is linked in a cluster with the VAX 3600. As part of the enhancement of the Bristol Avon system, development of software to pass information from the primary database to the MVII is in hand. The two computers provide the core of the telemetry flood forecasting system and ultimately the MVII will be used to run all flood forecasting models. At that time, a further DEC VAX2000 workstation currently being configured by the Water Resources

Research Group at the University of Salford will provide the primary access to the system. Additionally, the MVII will be capable of running the telemetry in the event of a failure of the VAX 3600.

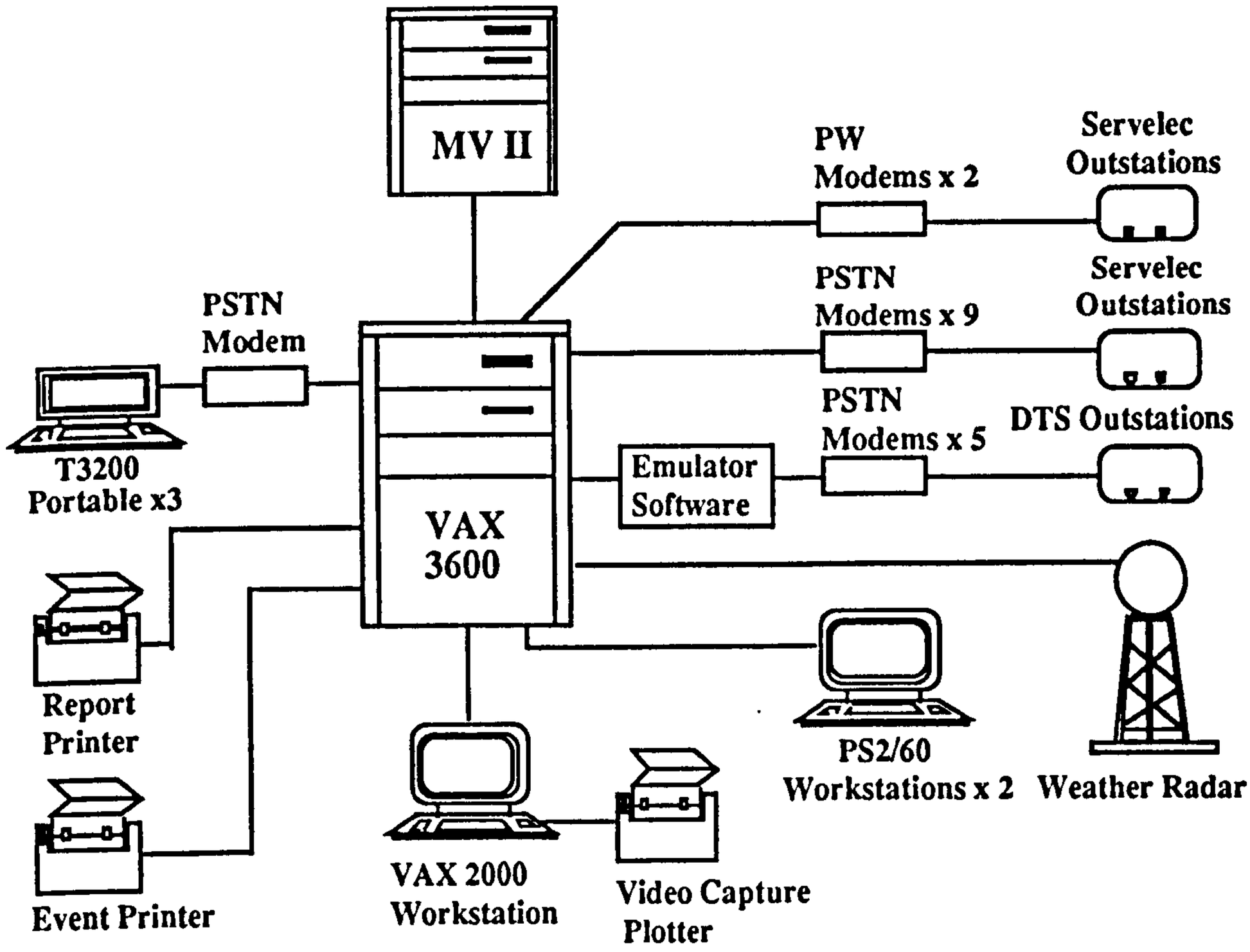

Figure 9.7 Computer Network in Wessex Region

Access to the VAX 3600 is via networked personal computers. The Area offices and the Regional Headquarters are to be linked using a megastream system and within the Area offices and the Regional Headquarters, all PC's will be networked at each location using Ethernet. It will thus be possible to obtain data held on the telemetry computers at any Area office as required.

106 new outstations are being provided serving 30 rain gauges, 40 flow gauging stations and river level sites, 22 combined rain gauge and flow sites, and 14

pumping station sites. These will cover the Bristol Avon and Somerset areas. Although the detail of each type of outstation is slightly different, all are capable of accepting digital and analogue inputs, displaying present values, dialling out to the master station if four high or four low level alarm set points are transgressed and retrieving logged data. The amount of logged data varies from 500 events for rain gauge outstations to 40 days of 15 minute data for flow gauge outstations. Outstations are capable of programming for PSTN setting up from the master station or from on site. Mains and standby batteries are provided on all sites.

In addition, these Servelec outstations are considered to be "intelligent" as logic controllers are incorporated in them to control activities on site. At operational sites (e.g. pumping stations and sluices) some will be used to control pumping and gate control. In addition, consideration is being given to the remote control from a Control Room of certain activities on some of these sites. At these locations, outstations will be linked to the master station by private wires rented from British Telecom whereas all other sites will rely on PSTN.

The Avon and Dorset area outstations are a relatively new design with similar, "unintelligent" capabilities to Servelec outstations and will be retained. However, as these are of Delta Technical Services (DTS) manufacture, emulator software is being provided on the DEC VAX 3600 to deal with these as if they were Servelec outstations.

The availability of weather radar was looked at enthusiastically by the Wessex region as providing the means to track and monitor intense rainfall cells and to provide objective answers to the quantitative precipitation forecasting problem. Although most of Wessex lay beyond the quantitative limit of the Upavon (Wiltshire) radar, the subjective coverage extended to the western boundary of the region. The commissioning of additional radars at Camborne (Cornwall) and Clee Hill (Shropshire) showed that most of Wessex had some coverage and thus the

region became one of the first users of the composite radar product. The availability of the composite, and the products ability to infill the unreliable Upavon radar area prompted Wessex to embark on a regional based flood forecasting system using radar as the primary precipitation data source.

The technology had advanced sufficiently to make a regional approach feasible. The radar images were available on a variety of data access and presentation devices from a number of different manufacturers. Stand-alone workstations were also appearing on the market. Offerings by Apollo, Sun and DEC allowed multi-tasking and high definition graphics through windowing, icons, menus and pop-ups (WIMPs). Latterly, the availability of high power lap-top machines from Toshiba and Compaq in particular have allowed the processing to go home with the duty hydrologist or forecaster for operational convenience.

The weather radar at Upavon has reached the end of its useful life and a new weather radar has finished construction at Warden Hill in Dorset which has provided quantitative cover for the whole of the Wessex Region. It is intended that the data from this site will be fed into the national network and the networked data will be received at the Bridgwater Headquarters directly by the DEC VAX 3600 computer. This will allow access to radar data on any of the networked PC's although it is intended that in normal circumstances one PC will be dedicated to the display of radar data.

As part of the development of the Regional Flood Forecasting System, access to radar data in places other than Regional Headquarters and Area offices is being provided. This is being achieved using a Toshiba T3200 portable PC which will also be able to access telemetry data and ultimately flood predictions via the DEC VAX 3600 (see Fig. 9.7). This will allow Duty Hydrologists to access all required information via one lap-top computer via any PSTN line allowing far more flexibility than is currently the case. This is particularly vital as the Area's manning

levels do not allow for the provision of a Duty Hydrologist in each area which has been the practice in the past. One Duty Hydrologist will cover the whole Region providing predictions and information to operational staff in all areas.

The T3200 portable PC is currently only available with a monochrome screen. It has therefore been necessary to develop a portable radar display system to allow for eight display levels of rainfall and this has resulted in the development of the **STORM** (**S**ystem **T**o **O**btain **R**adar Rainfall **M**easurements) system (see Fig 9.8) as part of project of WRIP. Ultimately once they are available, it is proposed to move towards the use of colour screens on the lap-top PC's and the portable displays will also provide direct communication with the real-time forecast models.

The provision of adequate quantitative radar data throughout the Wessex Rivers Area has made the use of radar for direct input into Flood Forecasting Models a viable proposition. It is still intended that a weather radar be commissioned in Devon which will also cover a significant part of the Wessex Region and the security provided by this overlap of coverage will be important. However, the models being developed will allow for radar and telemetry information to be automatically fed into the models and for predictions to be made. There will continue to be a facility to allow for manual editing and input as appropriate. These developments will allow for more timely flood warnings to be provided, particularly to those areas which are the subject of intense local heavy rainfall where the catchments are often very steep with short times of concentration. This will allow the provision of flood warnings to areas which currently cannot receive any warnings because of the lack of adequate lead time between rainfall and a flood occurring.

9.3.2 WRIP System Connection

The WRIP system connection is shown in figure 9.8. The weather radar data, telemetry raingauge and flow data are collected in the water authority office. The data can either be accessed by the terminal in the office or a portable system which can be operated at home or event on a trip by a car.

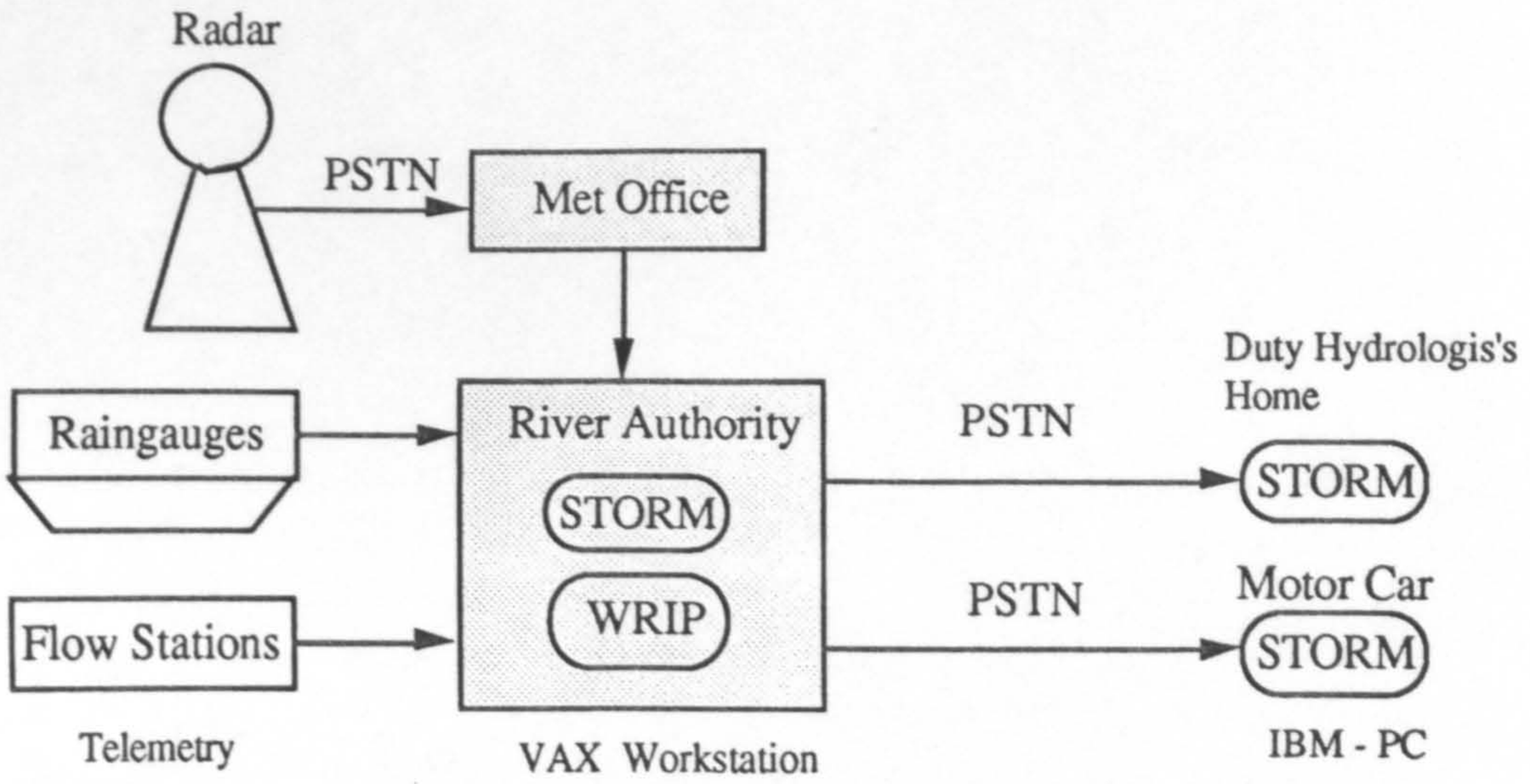

Figure 9.8 WRIP System Connection

As the telemetry system is archived by ORACLE software and radar data are collected by a radar rainfall data collection software, WRIP server will process data from both databases into WRIP database. A WRIP communication process can be illustrated in figure 9.10.

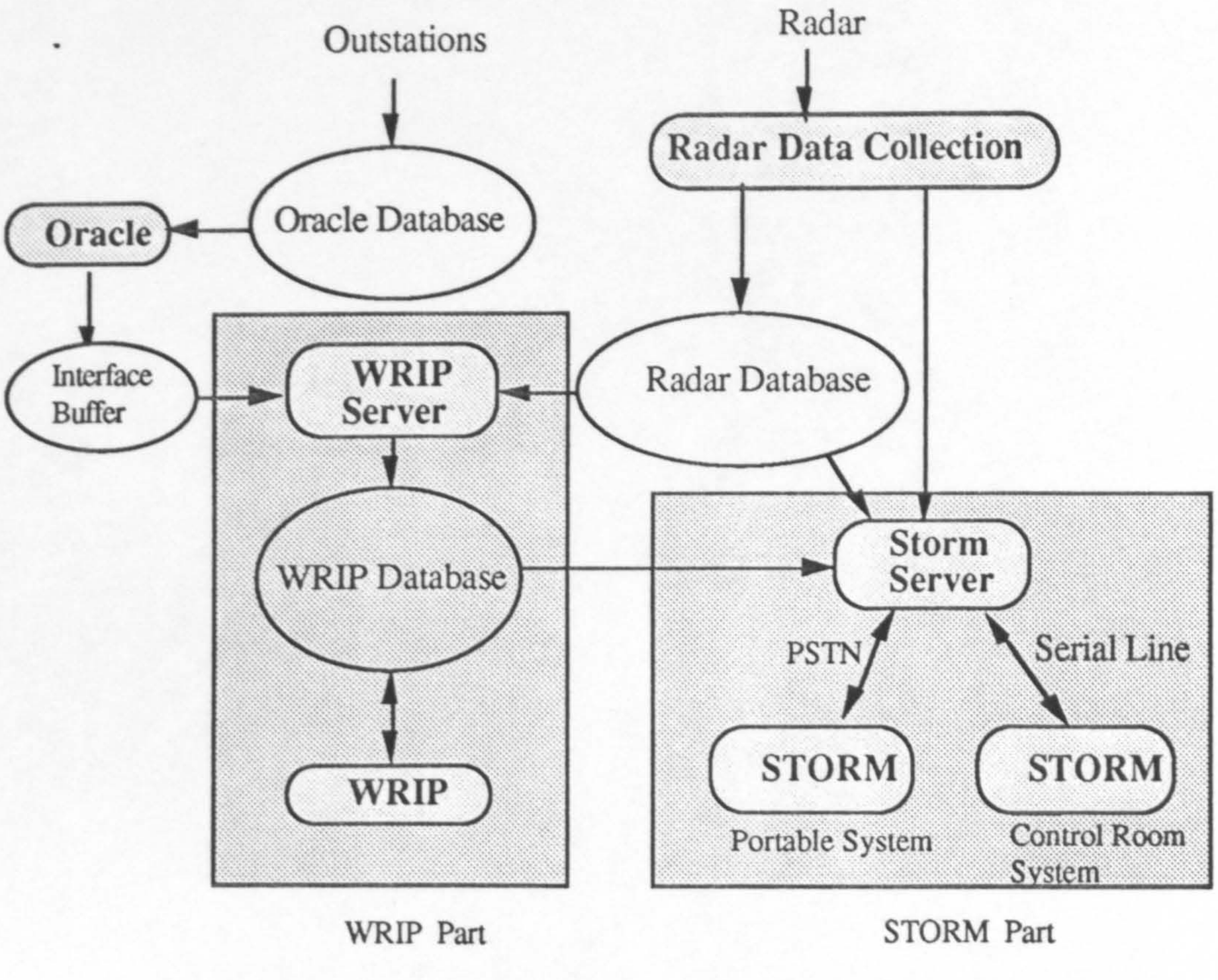

Figure 9.10 Communication Process in WRIP System

Outstation data are processed by ORACLE into a ORACLE database. Currently, raingauge data and river flow data are needed by WRIP, the output data from ORACLE is arranged as a direct access file with each gauge and flow station as one record. To ease the access and retrieve of data item, the raingauges and flow stations are identified by a unique id code as in figure 9.11.

Avon & Dorset	Bristol Avon	Somerset
101 Raingauge 1	201 Raingauge 1	301 Raingauge 1
102 Raingauge 2	202 Raingauge 2	302 Raingauge 1
⋮	⋮	⋮
1xx Raingauge xx	2xx Raingauge xx	3xx Raingauge xx

Figure 9.11 Identification Code for Raingauges in Wessex Region

9.5 Storm Forecasting in Wessex Region

The storm forecasting in WRIP is based on the pattern recognition technique. Firstly the storm movement is traced by pattern recognition and then a linear extrapolation is used to generate the forecasts.

Pattern recognition is regarded as a basic attribute of a human being, as well as other living organisms (Tou and Gonzalez 1974). According to the nature of the pattern recognised, we may divide the acts of recognition into two major types: the recognition of concrete items (like visual and aural pattern) and the recognition of abstract items(like an old argument, or solution to a problem). Storm tracking is within the first type of pattern recognition.

The design of an automatic pattern recognition system generally involves several major problem areas. The first one is concerned with the representation of input data which can be measured from the objects to be recognised. This is the sensing problem. Each measured quantity describes a characteristic of the pattern or object. The storm data measured by weather radar is in the form of a 2-dimensional digital array. This forms the basis of the storm pattern recognition.

The second problem in pattern recognition concerns the selection of design concept. The design concept for automatic pattern recognition are motivated by the way in which pattern classes are characterised and defined. Our experience suggests several basic possibilities. When a pattern class is characterised by a roster of its members, the design of a pattern recognition system may be based on the membership-roster concept. When a pattern class is characterised by common properties shared by all its members, the design may be based on the common-

property concept. When a pattern class exhibits clustering properties in the pattern space, the design may be based on the clustering concept. These basic design concepts are described in the following paragraphs (Tou and Gonzalez 1974).

1) Membership-roster concept

Characterisation of a pattern class by a roster of its members suggests automatic pattern recognition by template matching. Then sets of patterns belonging to the same pattern class is stormed in the pattern recognition system. When an unknown pattern is shown to the system, it is compared with the stored patterns one by one. The pattern recognition system classifies this input pattern as a member of a pattern class if it matches one of the stored patterns belonging to that pattern class.

2) Common-property concept

Characterisation of a pattern class by common properties shared by all of its members suggests automatic pattern recognition via the detection and processing of similar features. The basic assumption in this method is that patterns belonging to the same class possess certain common properties or attributes which reflect similarities among these patterns.

3) Clustering concept

When the pattern of a class are vectors whose components are real numbers, a pattern class can be characterised by its clustering properties in the pattern space. The design of a pattern recognition system based on this general concept is guided by the relative geometrical arrangement of the various pattern clusters.

For the storm movement tracking, the simplest membership-roster concept is adapted in the WRIP. Usually a cross correlation can be used to test the matching

patterns (Collier, 1989).

Currently, WRIP is using 3 bit Network 128x128 radar data. It format is shown in Figure 9.12.

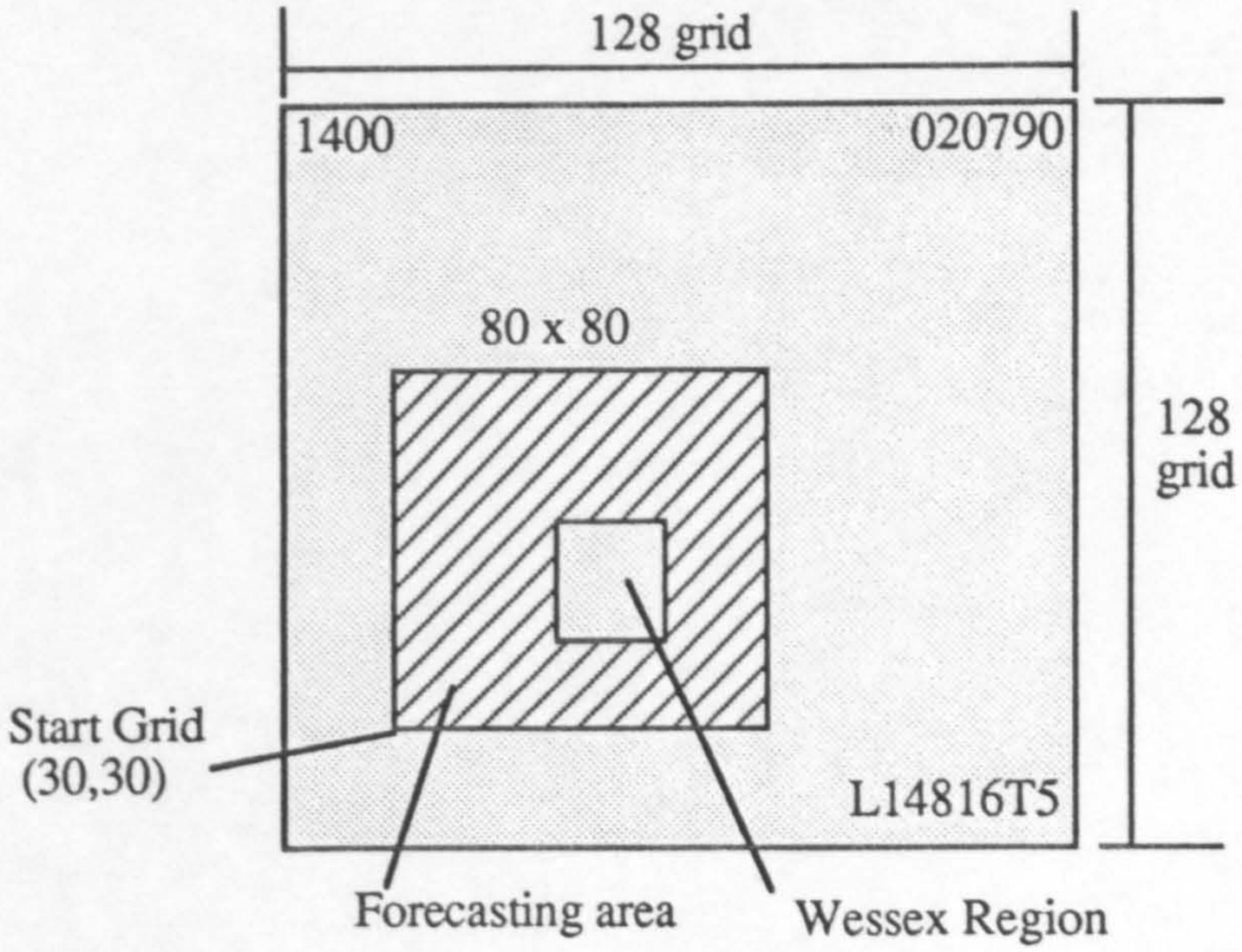

Figure 9.12 Cross Correlation Area for Wessex Region

The forecasting is up to 6 hours. The speed, direction and volume change are derived from maximising the correlation between two radar data fields for successive time frames through an appropriate displacement in space. Forecasting is based on linear extrapolation forecasting. A given pair of velocity components in an easterly and northerly direction are used to shift the rainfall field in space.

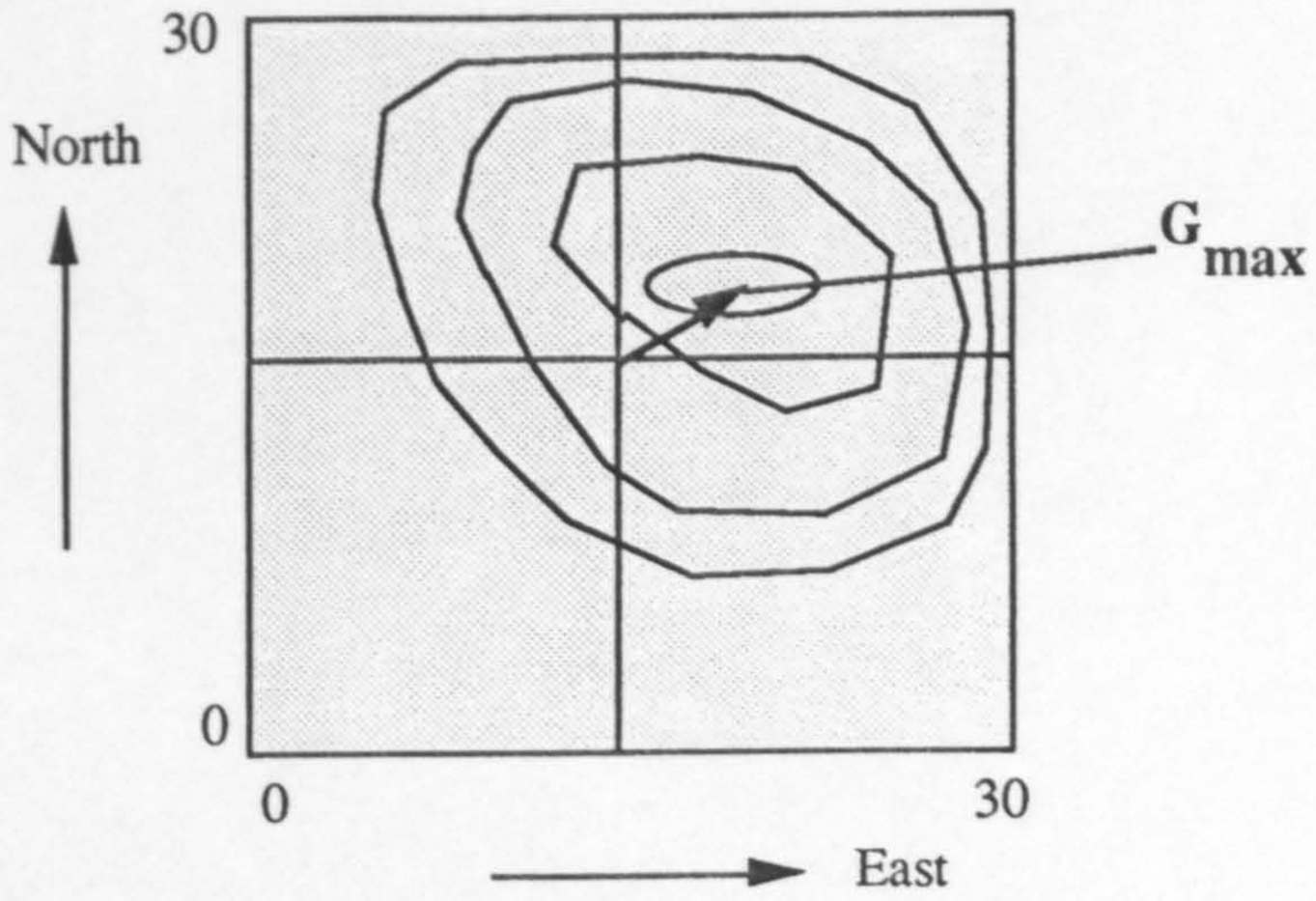

Figure 9.13 Correlation Surface of Wessex Region

Let x,y represent the two radar frames. The radar data will be denoted by $(x_{11},y_{11}),(x_{12},y_{12}),(x_{13},y_{13}),\ldots$

The correlation coefficient is given by

$$r = \frac{\sum(x_{ij} - \dot{x})\,(y_{ij} - \dot{y})}{\sqrt{[\sum(x_{ij} - \dot{x})^2 \sum(y_{ij} - \dot{y})^2]}} \qquad (9,1)$$

where

$$\dot{x} = \sum_i \sum_j x_{ij} / (N-1)$$

$$\dot{y} = \sum_i \sum_j y_{ij} / (N-1)$$

As the computed maximum point is in a grid scale, it can be more accurately estimated by polynomial approximation.

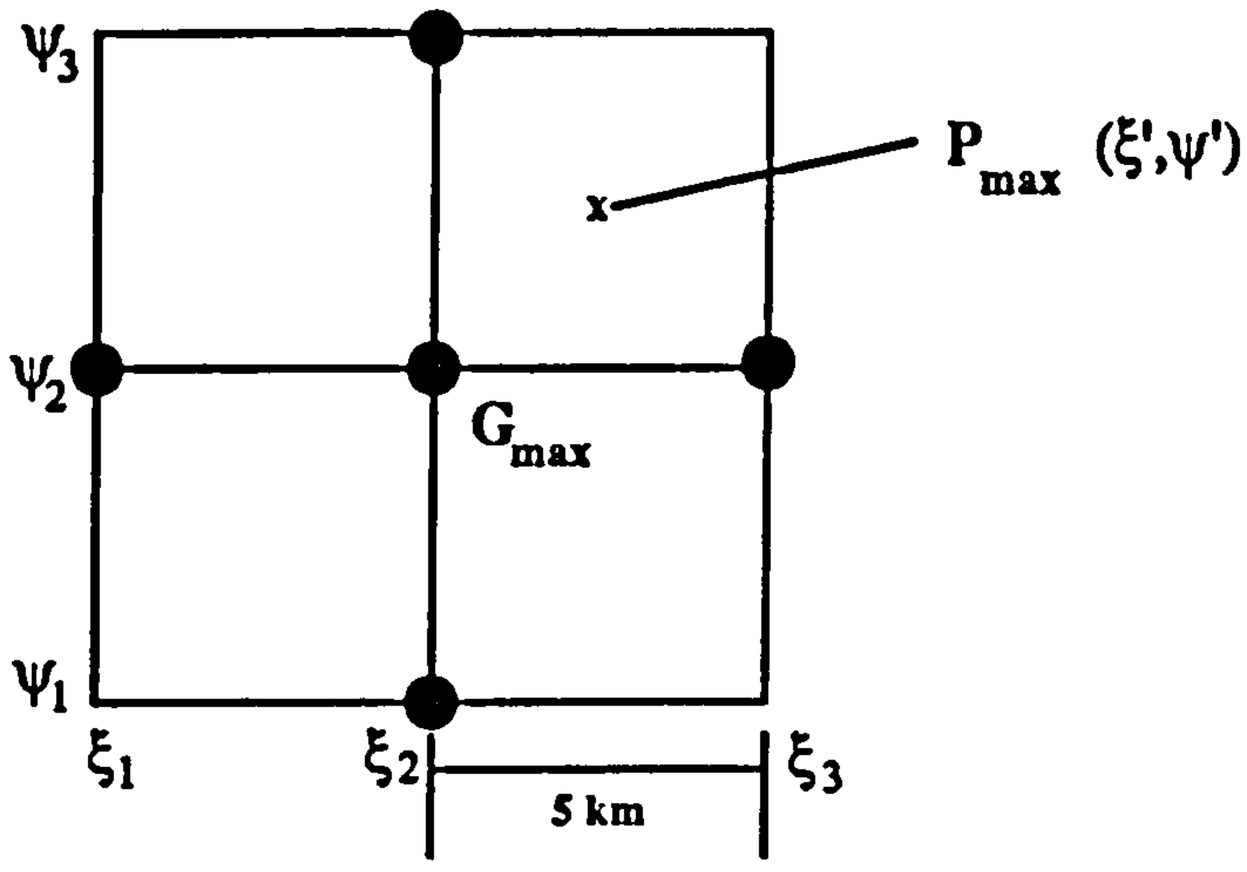

Figure 9.14 Maximum Point Grids

When Gmax point is found, 4 points around Gmax are also selected to compute the maximum point location Pmax as illustrated in Figure 9.14. A parabola curve is used to fit three point data in each direction in Figure 9.15.

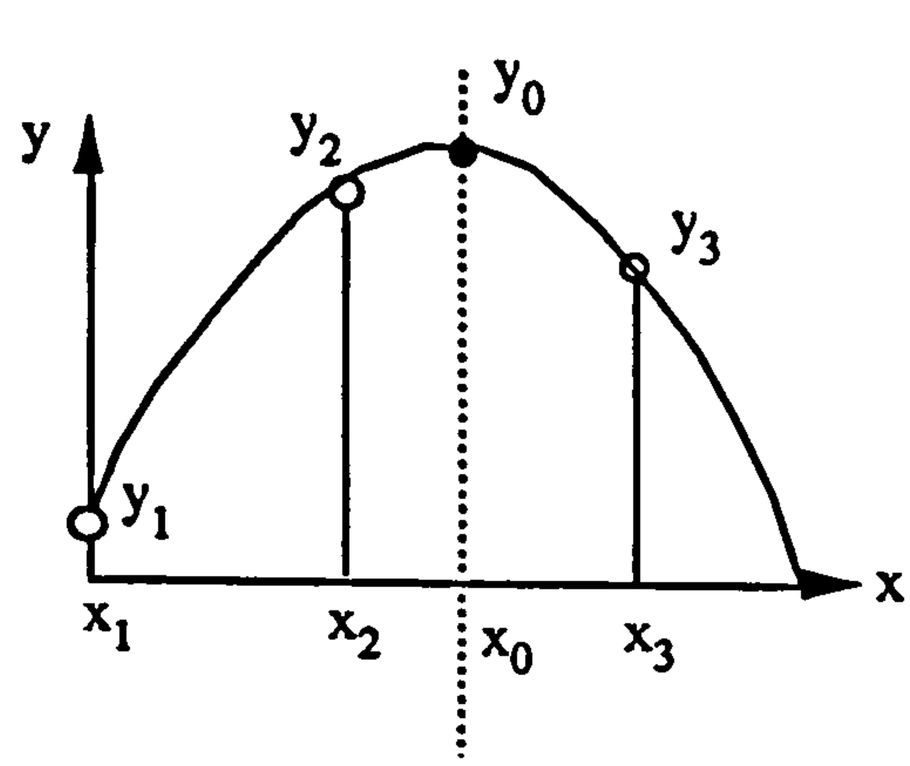

Figure 9.15 Parabola Curve Fitting for Pmax

The curve function can be described as

$$y - y_0 = a (x - x_0)^2 \qquad (9,2)$$

where x_0, y_0 and a are parameters of parabola curve function. x_0 is the maximum correlation point in this direction. Three parameters can be estimated from three

data points $(x_1,y_1),(x_2,y_2),(x_3,y_3)$ with following equations.

$$\begin{cases} y_1 - y_0 = a\,(x_1 - x_0)^2 \\ y_2 - y_0 = a\,(x_2 - x_0)^2 \\ y_3 - y_0 = a\,(x_3 - x_0)^2 \end{cases} \qquad (9,3)$$

To simplify the derivation, a few conditions are substituted into Eq (9,3). As we know that the spacing between three points is the same and equals to 5 km, the point location can be described as an integer times the 5km distance.

$$x_1 = (j-1)*5$$
$$x_2 = j*5$$
$$x_3 = (j+1)*5$$
where $j = 0, 1, 2, \ldots$

The final form of the maximum point location is (when $y_1 \neq y_3$)

$$x_0 = 5\left[j - \frac{1}{2\left(1 - 2\frac{(y_1 - y_2)}{(y_1 - y_3)}\right)}\right] \qquad (9,4)$$

or

$$x_0 = x_2 - \frac{5}{2\left(1 - 2\frac{(y_1 - y_2)}{(y_1 - y_3)}\right)} \qquad (9,5)$$

and when $y_1 = y_3$,

$$x_0 = x_2 \qquad (9,6)$$

When Pmax is found, three results can be derived from the equations above .

Speed (km/hr) $S = Sqrt (Sqr Sx + Sqr Sy)*4$

Direction (degree) $D = ATAN (Sy / Sx)$

Volume Change (%)

V =(New volume -Old Volume)/Old Volume

where Sx and Sy are the coordinates of Pmax.

The short term storm forecasting can be made by moving the current storm with S speed D direction and V volume change.

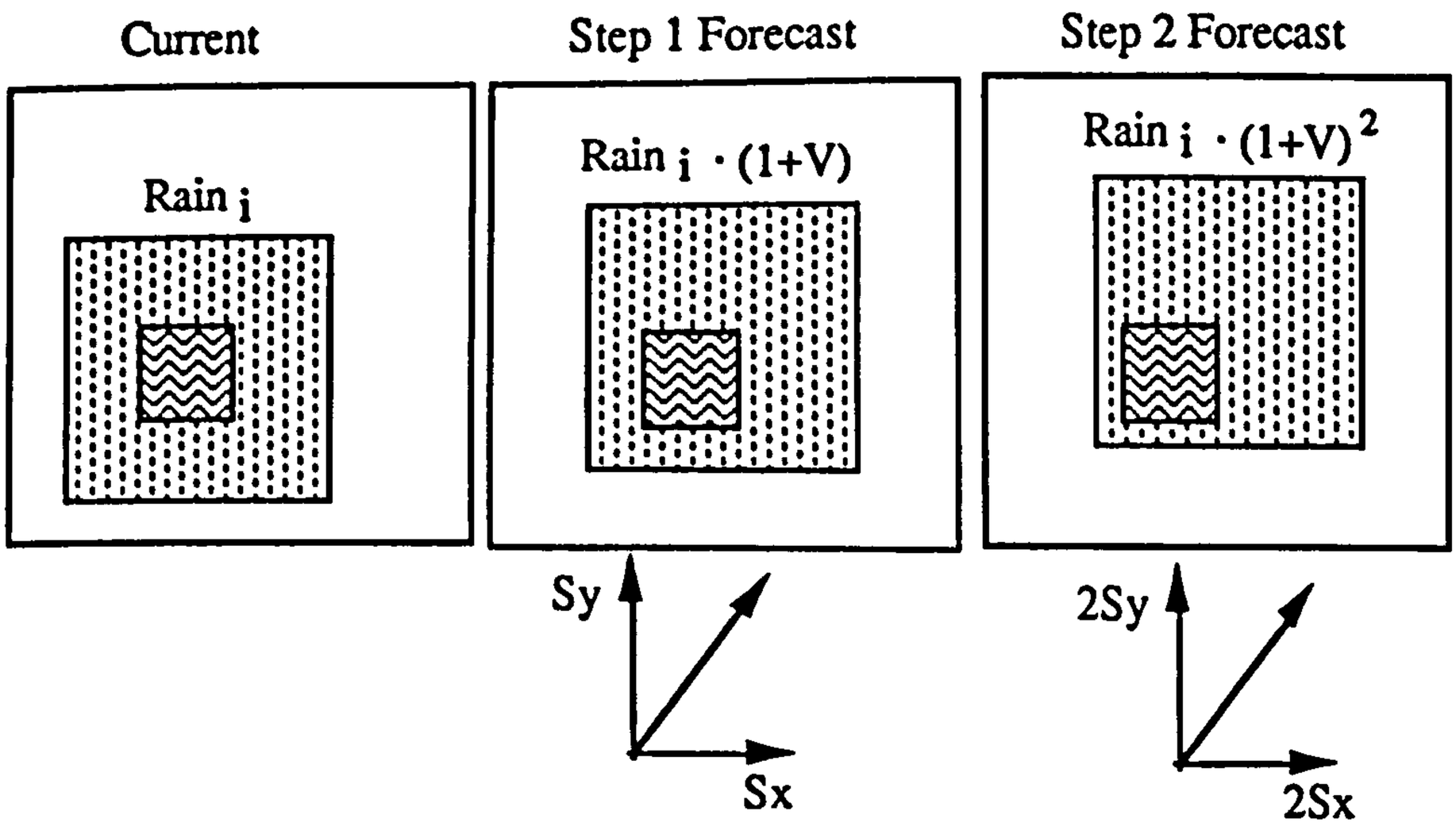

Figure 9.16 Storm Forecasting Steps

With a fast moving storm, it is possible that the current storm may move out of the Wessex Region. In this case, radar network data is more appropriate over a larger scale.

9.5 Flow Forecasting in Wessex Region

The main forecasting window is shown in figure 9.17. This window will be automatically updated every 15 minutes to coordinate with network radar data and

telemetry outstation data.

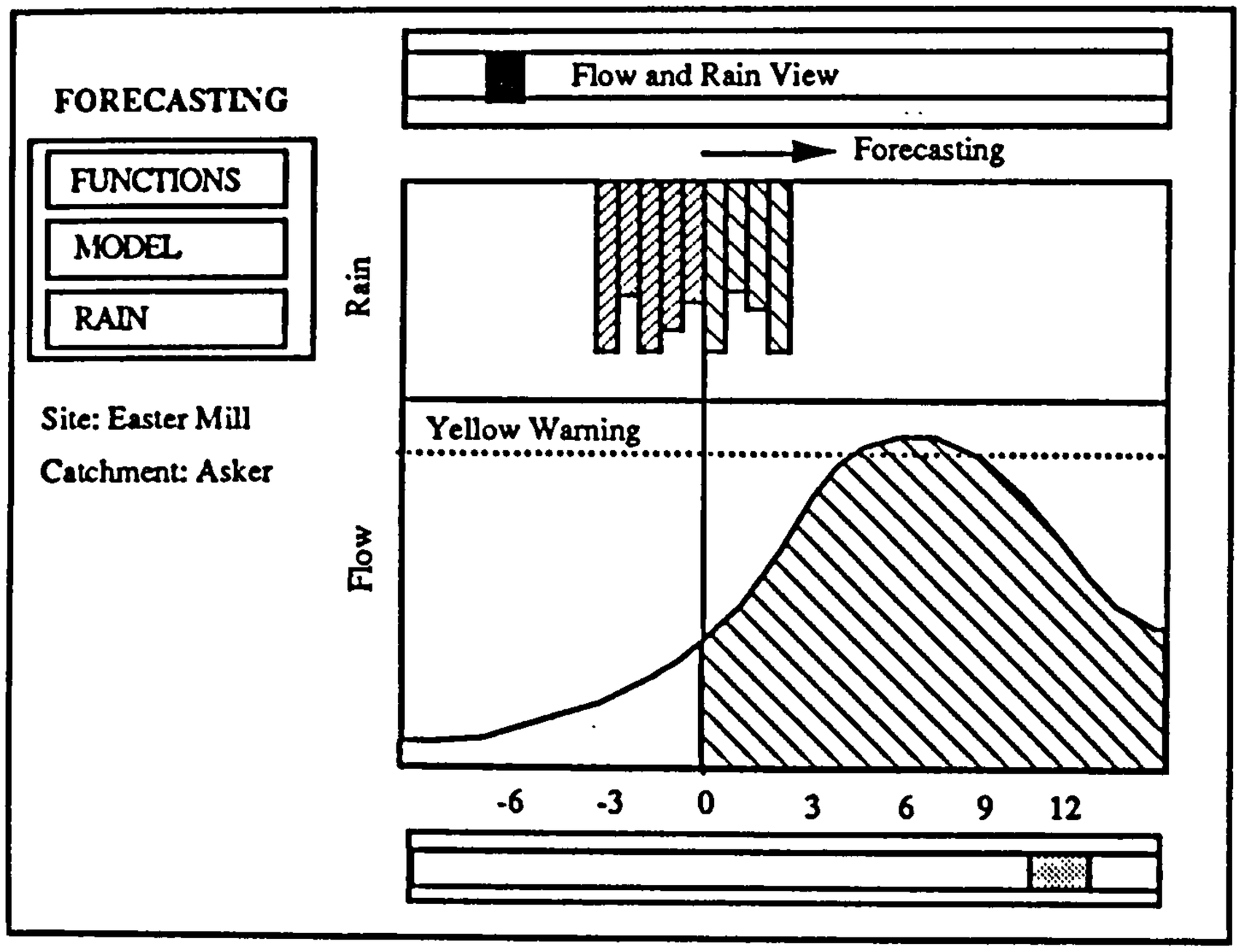

Figure 9.17 Forecasting Main Window

There exist several options for storm forecasting. Currently WRIP storm forecasting is used as default storm scenario. Users have options to select other storm scenario to view the different aspects of storm influence. The manually input storm given the user the flexibility to test all kinds of interesting storm profiles.

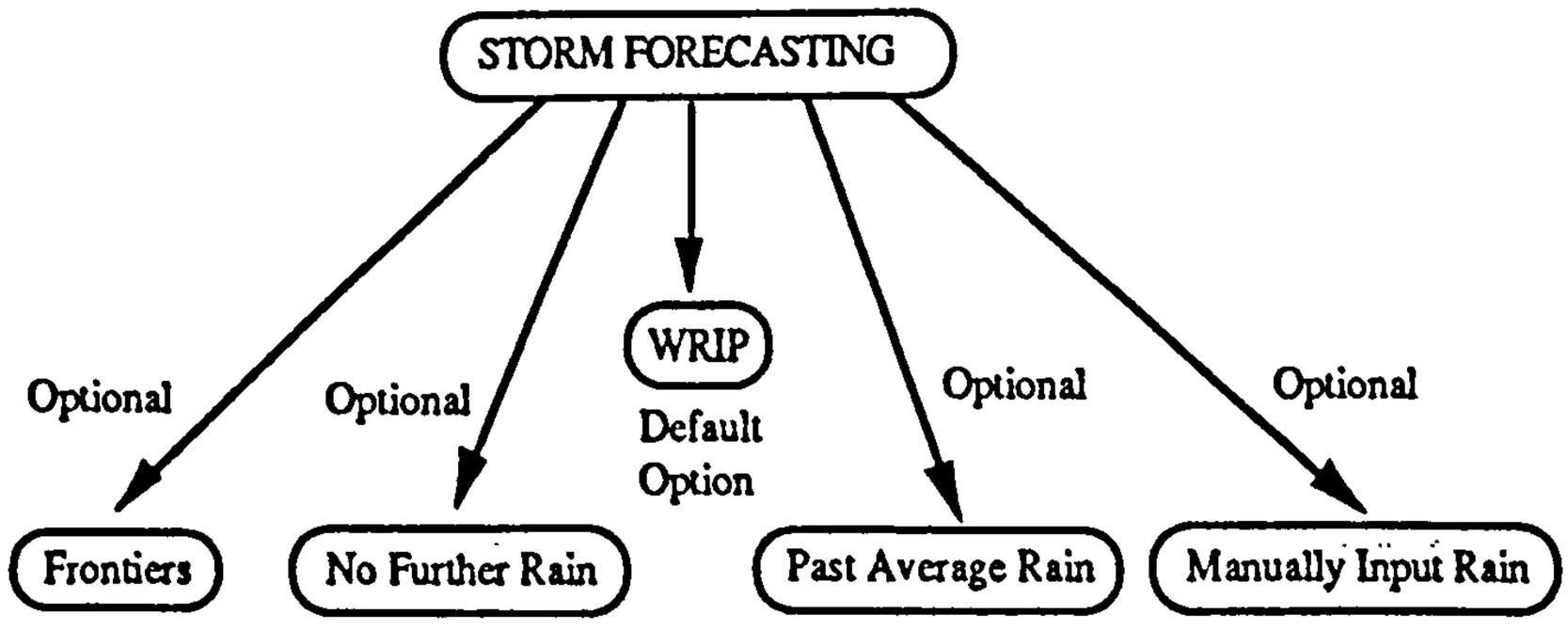

Figure 9.18 Storm Forecasting Selection

For the historic rain data, the default selection is radar derived data. In the case of radar network failure, the raingauge data will be used as backup data as in Figure 9.18.

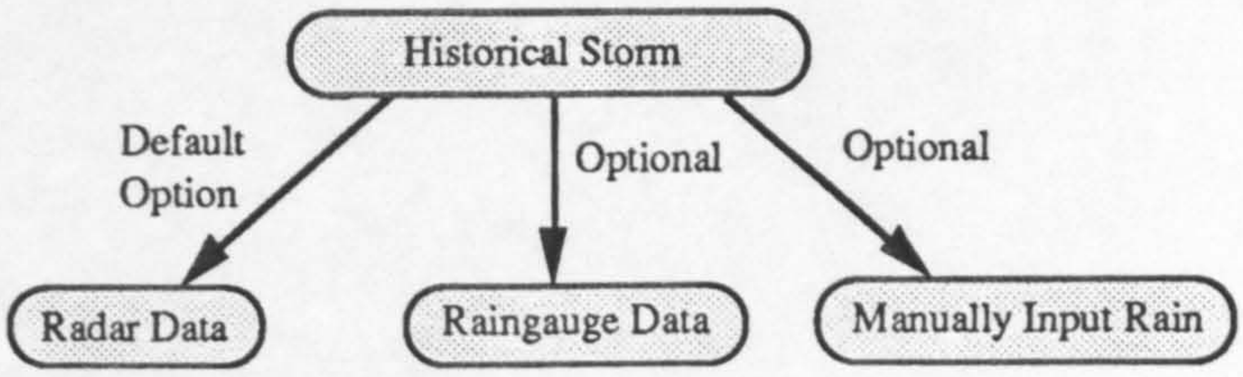

Figure 9.19 Historical Storm Selection

The flood forecasting model can be of variety forms. The current WRIP utilises the TF model as a forecasting tool. The parameter adjustment of the TF model has been addressed in previous chapters. Figure 9.20 illustrates a model adjustment window for the PRTF model. Users can explore the different parameter's influence on the flow forecasting ability in real-time. The flow feedback and storm type should be considered in adjusting model parameters. Experience in practical operation will help hydrologist select suitable parameters for the model.

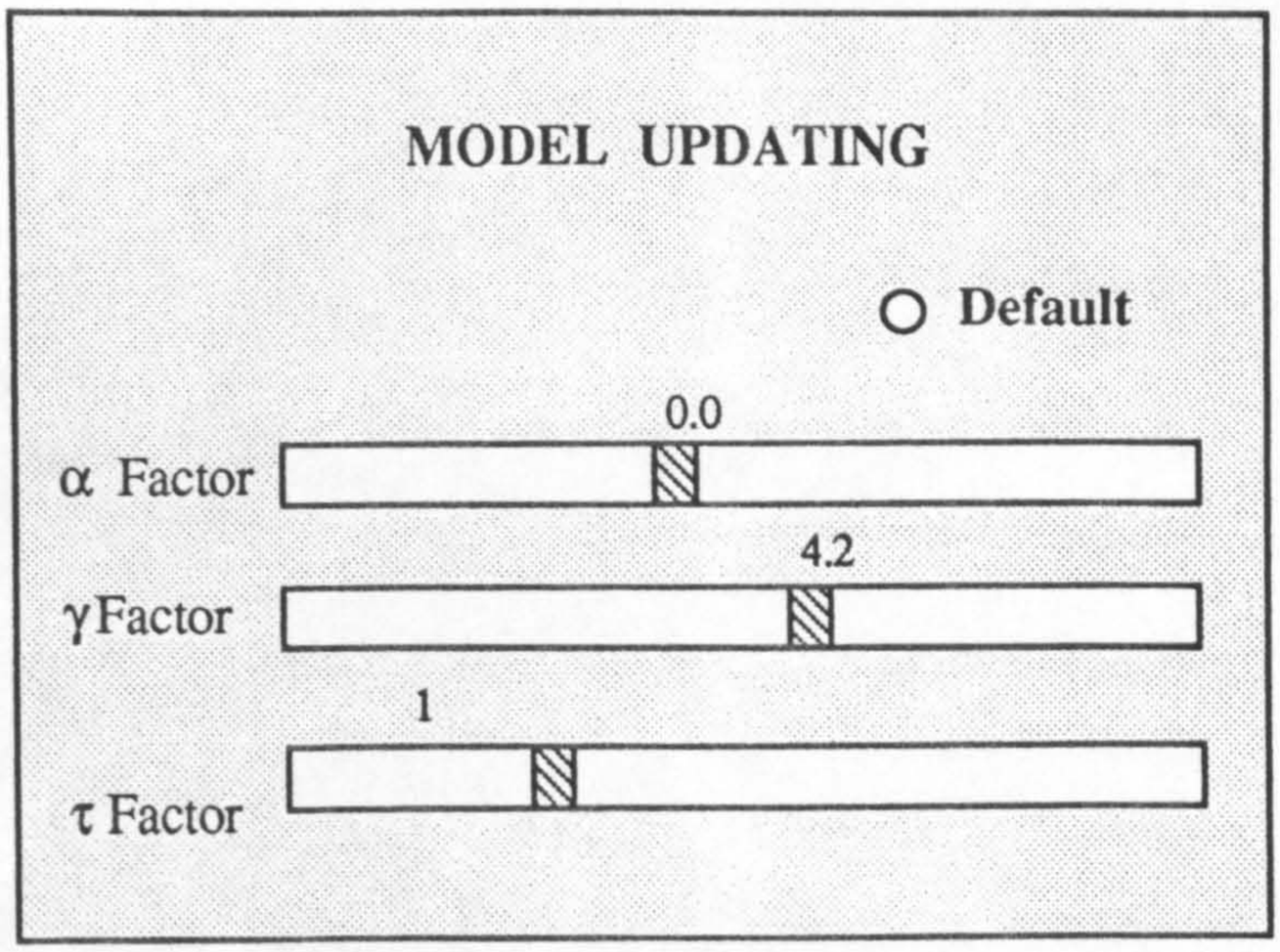

Figure 9.20 Model Adjustment Window

9.6 Summary

Application of WRIP in NRA Wessex region has been described in this chapter. A well organised computer and telemetry system has provided an appropriate environment for the WRIP system. The U.K. network 128x128 radar is utilised as a main rainfall data source. The storm forecasting scheme is based on a cross correlation surface with parabola curve fitting and a linear forecasting scheme is applied for the Wessex region. In the future this will be extended by access to the Met Office FRONTIERS system. For the flood forecasting, a default setting for the system is decided in the customisation of WRIP. The user has other options to choose which enable hydrologists to explore the catchments response to various kinds of storm type.

PART V CONCLUSIONS

CHAPTER 10

CONCLUSIONS AND RECOMMENDATIONS

10.1 Conclusions

Studies have been carried out to analyse weather radar data processing and to develop a real-time flood forecasting system. Some concluding comments are as below,

10.1.1 Radar Data Processing

a) Quantisation

• Signal quantisation of radar rainfall measurements is a important issue in the hydrological process. The quantisation noise can be decreased by choosing the quantum steps or level slicing schemes to be sufficiently fine to preserve the original information content of the data. A trade-off amongst accuracy, quantisation noise, and the number of quantisation levels is required. As few quantisation levels as possible are chosen consistent with the preservation of the information content of the signal process.

• A practical radar data quantisation scheme will depend on the statistical properties of radar rainfall data.

• The measurement noise contained in the original data set will affect the quantisation scheme. In this case (and it is always true in practice) , high resolution may not be worthwhile because the accuracy of the data will not be improved after some level. It has been found that there is insignificant difference between 4 bit and 8 bit data. The results from this thesis show that 3 bit data can be utilised in flood forecasting modelling without causing large error, though it would be more appropriate to use 4bit data to replace the original 8 bit data were this to become a future possibility.

• Adaptive quantisation provides a very useful tool to improve the radar data precision without increasing the quantisation levels. Unlike static radar quantisation scheme, adaptive quantisation will make full use of every bit of information in the quantisation scheme. The decoding of quantised data is almost the same except a data range indicator has to be placed in the radar data header and this indicator is used to recover the quantised data It should be seriously considered as a part of any future updates of at-site radar processing software in order to enhance the quantisation nature of the rainfall signal.

b) Sampling

• Temporal and spatial sampling have been discussed. The measurement sampling should be fast enough that the process is well damped above the Nyquist frequency. Although hourly radar data are used in the forecasting model, it has been shown that no more than 15 minute measurement sampling is necessary for

rural flood forecasting problems. A prefilter should be utilised when the radar rainfall data is to be input into flood forecasting model. At minimum this should consist of a moving average processor simulator.

- Spatial sampling is quite an important issue for fully distributed forecasting models. It will not affect the lumped TF model providing the sampling area is equal or smaller than the catchment size. Larger catchments can tolerate larger spatial sampling intervals. But low spatial sampling rate will cause some trouble for radar data calibration procedure, since it will be difficult to apply the pattern recognition technique to identify storm type and much difference will occur between the calibration raingauge data (point measurement) and radar data (spatial average measurement).

- Spatial averaging is a low pass filter process and will reduce some proportion of the quantisation noise.

c) Influence on Flood Forecasting

- For model identification, though a short sampling interval will contain as much information as possible , it will cause trouble for model parameter estimates owing to the presence of partial linear dependencies. If the sampling interval is too long in time or too long in space, residual autocorrelation will result and parameter estimates will be biased. An optimum model data interval should be chosen based upon the system response characteristics.

- Prefiltering of radar data removes a the large percentage of quantisation noise.

By selecting a more optimal numerical filter, a further reduction of quantisation error can be achieved.

• The TF forecast model acts as a low pass filter and the quantisation noise will be reduced after the prefiltering of the quantised radar signal. Some case studies have been used to illustrate this aspect.

10.1.2 Flood Forecasting Model

• The TF (Transfer Function) model has been widely utilised in hydrology and has been proven an effective model. However, several problems still exist in the application of the TF model such as the difficulty in identification of the model and real-time robust updating. A PRTF (Physical Realisable Transfer Function) model has been developed to overcome these shortcomings in ordinary TF models.

• An important feature of the PRTF is that its impulse response shape can be adjusted by altering the model pole's position and model pole's order. It is found that adjusting the model pole's position is more practical than adjusting the model pole's order.

• A modified least square estimation technique has been proposed. Two iterative steps are needed to estimate the PRTF model parameters. As there is no worry about instablility and fluctuations, the identification of a PRTF is much easier than for the ordinary TF model.

• Since many TF models and UH models exist in water industry, case studies were provided to illustrate the transformation of TF and UH models into PRTF model. It was found that the PRTF can successfully simulate the TF model and UH model.

• The impulse response of the TF is critical to the accuracy of model forecasting.

Three adjustment factors were introduced into the PRTF model. Each factor was constrained to influence one aspect of the TF model. None of them can cause the TF model to become unstable or fluctuating. Computational results were satisfactory.

- A distributed kinematic wave model was used to analyse the catchment response to different kinds of storm type. Results show that there exists some general characteristics in the catchment response. This can be further implemented in an Artificial Intelligent system which could adjust the flood forecasting system from the past information, the current catchment conditions and storm type. It is important that this approach to dealing with the variety of the catchment response is developed as a means of obtaining a comprehensive solution.

- Through the simulation of the kinematic wave model and the data from Blackford Bridge in the Northwest Region, PRTF has shown the ability to adapt to the variability of the catchment response and the result was promising.

- A RST (rainfall separation Tank) was developed which can overcome some shortcomings of pure PRTF models. Results showed a great improvement in many cases.

10.1.3 Development of WRIP System

- A well designed system structure, user interface, database and program is crucial for a successful system.

- A window-based graphical user interface (GUI) is adopted to ensure convenience

in using WRIP. As the system is complicated and there is large amount of data to be processed, an object-oriented computing concept was utilised in the WRIP program design. It has been found to be a significant improvement to system development and has resulted a major advance in real-time flood forecasting system utility.

- Storm forecasting is based upon pattern recognition techniques. It has been found that the membership-roster concept can be applied in the simple storm tracking system. A cross correlation with parabola curve fitting can closely locate the maximum cross correlation point. Future developments will embrace the Meteorological Office FRONTIERS system.

- The Wessex region is characterised by infrequent heavy rainfalls and has produced many of the record British rainfall totals in addition to some of the more infamous floods. A computerised WRIP system has made flood monitoring and forecasting much more productive and has provided the United Kingdom first integrated radar based flood forecasting system when it was commissioned during 1990 and early 1991.

10.2 Recommendations

- The data resolution (Sampling and quantisation) influence the operational cost and the application usage. More Statistical analysis should be carried out to assess the radar data processing scheme and its influence on the distributed catchments..

- PRTF and RST have been proven as a much improved model structure. More research is needed to fully apply it in real-time flood forecasting systems, however, it appears to offer considerable advantages over more conventional approaches.

- The application of Artificial Intelligent systems in realtime flood forecasting is likely to be very promising in the future. With more understanding about the hydrological process, it is more likely that an operational expert system will appear in the near future.

REFERENCES

A&D Division (1973) **Avon & Dorset Local Land Drainage District - Land Drainage Survey Report, Water Act 1973 Section 24(5).** Avon & Dorset Division, Wessex Water Authority

BA Division (1981) **Radio Telemetry Flood Warning Scheme.** Document PD 048/01, Bristol Avon Division, Wessex Water Authority.

BA Division (1973) **Bristol Avon Local Land Drainage District - Land Drainage Survey Report, Water Act 1973 Section 24(5).** Bristol Avon Division, Wessex Water Authority

Banks C J et al. (1984) **Communications and Data Formats.** FAAG Report 108

Battan, L J (1973) **Radar Observations of Atmosphere.** The University of Chicago Press

Bellanger,M (1989) **Digital Processing of Signals.** John Wiley

Biggs, K.L (1980) **Flood Warning User Manual, Somerset Division, Wessex Water** Authority

Bliss, J.C (1981) **A Study of the Forecasting Ability of a Real-Time Rainfall-Runoff Model for the River Asker, South West Dorset,** unpublished M.Sc. Thesis, Department of Civil Engineering, University of Birmingham

Birks, C, Bootman, A, Cluckie, I D and Han, D(1989) **Wessex Flood Forecasting System.**

Int. Symp. on Hydr. Appl. on Weather Radar, University of Salford, U.K.

Bootman, A.P. and Willis, A (1980) **The Benefit of Local Rainfall Analyses**, Paper 4, Flood Studies Report, Institution of Civil Engineers, 22 - 24 July

Bootman, A.P (1978) **Flood Warning User Manual**, Somerset Division, Wessex Water Authority

Box,G E Jenkins,G M (1976) **Time Series Analysis.** Revised Edition, Holden-Day

Brown, R G (1963) **Smoothing, Forecasting & Prediction.** Prentice-Hall, Inc.

Chatfield,C (1984) **The Analysis of Time Series: An Introduction.** Chapman and Hall

Chow, V T, Maidment, D and Mays, L (1988) **Applied Hydrology.** McGraw-Hill International Edition, McGraw-Hill Book Company

Cluckie, I D, Smith, F J B (1980a) **Flood Forecasting Project for Wessex Water Authority (Avon and Dorset Division)** - Interim Report, Dept of Civil Engineering, University of Birmingham

Cluckie,I D, Smith, F J B(1980b) **Flood Forecasting Project for Wessex Water Authority (Avon and (Dorset Division)** - Final Report, Dept of Civil Engineering, University of Birmingham

Cluckie, I D, Owens, M D(1987) **Real-time Rainfall-Runoff Models and Use of Weather Radar Information.** Weather Radar and Flood Forecasting, John Wiley & Sons Ltd.

Cluckie, I D, Burne, S (1988) **Wessex Radar Information Project.** WRIP Report No.1

Cluckie, I D, Tilford, K A (1988) **An Evaluation of the Influence of Radar Rainfall Intensity Resolution for Real-Time Operational Flood Forecasting.** ARIP Report No2

Cluckie, I D, Han, D (1988) **Preminary Analysis of Upavon Radar Data.** WRIP Report No.3

Cluckie, I D, Han, D (1988) **Radar Data Quantisation, Sampling and Prelinminary Model Assessment using Upavon Data.** WRIP Report No.4

Cluckie, I D, Tilford, K (1989) **Transfer Function Models for Flood Forecasting in Anglian Water Authority.** Anglian Radar Information Project, Report No. 3

Cluckie, I D, Tilford, K and Shepherd, G (1989) **Radar Rainfall Quantisation and its Influence on Rainfall Runoff Models.** Proc. Int. Symp. on Hyd. App. of Weather Radar, University of Salford, U.K.

Cluckie, I D, Yu, P and Tilford, K (1989) **Real-Time Forecasting: Model Structure and Data Resolution.** Proc. Seminar on Weather Radar Networking, Brussels, Belgium

Cluckie, I D, Tilford, K and Han, D (1989) **The Influence of Signal Quantisation of Radar Precipitation Estimates on Real-Time Flood Forecasting.** Int. Workshop on Precipitation Measurement, St. Moritz, Switzerland

Coates, R F W (1982) **Modern Communication Systems.** University of Wales

Collier, C G, Larke P.R. & May B.R (1983) **A Weather Radar Correction Procedure for**

Real-time Estimation of Surface Rainfall, Quart. J.R. Met. Soc., Vol. 109, pp589 - 608

Collier, C G, Cluckie,I.D (1985) **A Hydrological Study of the Real-Time Calibration Radar Derived Rainfall Data',** Proc. Int. Symp. Advances in Water Engineering, University of Birminham, 15 - 19 July, Elsevier App. Sci. Pub

Collier, C G, Knowles J.M (1986) **Rainfall Estimates made by a Radar used in an Operational Rainfall and Flood Forecasting System, Part III: On the Sensitivity of River Catchment Flow Forecasts to Inaccuracies in Radar Estimates of Rainfall,** J. of Hydrology, Vol.83, pp237 - 249

Collier, C G (1986) **Accuracy of Real-time Radar Measurements.** Weather Radar and Flood Forecasting, pp71-95

Collier, C G (1989) **Applications of Weather Radar Systems - A Guide to Uses of Radar Data in Meteorology and Hydrology,** Ellis Horwood Limited

DeFatta, D, Lucas, J and Hodgkiss, W (1988) **Digital Signal Processing,** John Wiley & Sons

Dorf, R C (1986)**Modern Control Systems,** Addison-Wesley Publishing Company

English, E.J (1973) **A Objective Method of Calculating Areal Rainfall,** Meteorological Magazine, 102, pp292-298

Fishman,G S (1969) **Spectral Methods in Econometrics.** Harvard University Press

Gauss, K.F. (1809) **Theoria motus corporum celestium. English translation: Theory of the Motion of the Heavenly Bodies.** Dover, New York (1963)

Graham, S (1988) **Precipitation-Process and Analysis,** John Wiley & Sons

Grant, P M ets (1989) **Signal Processing and Coding.** Chartwell-Bratt Studentlitteratur

Gray, D (1970) **Handbook on the Principles of Hydrology.** Water Information Center, INC

Grimshaw, D and Wong, T (1980) **Radio Telemetry Flood Warning Scheme,** Document PD 048/01, Bristol Avon Division, Wessex Water Authority.

Hamming,R W (1980) **Coding and Information Theory.** Prentice-Hall, Inc.

Han, D (1988) **Brightband in U.K.** Internal Technical Report, University of Salford, U.K.

Han, D (1991) **Weather Radar Information Processor.** Software Profile, Technical Report, University of Salford, U.K.

Han, D (1991) **System To Obtain Radar rainfall Measurement (STORM).** Software Profile, Technical Report, University of Salford, U.K.

Han, D (1991) **Radar Communication Software (RADCOM).** Software Profile,Technical Report, University of Salford, U.K.

Harpin,R (1982) **Real Time Flood Routing with Particular Emphasis on Linear Methods and Estimation Techniques.** PhD Thesis, University of Birmingham

Harvey,A C (1981) **Time Series Models.** Philip Allan

Ingels,F M (1971) **Information and Coding Theory.** Intext Educational Publishers

Jenkins,M, Watts,D (1968) **Spectral Analysis.** Holden-Day

Jordan, E (1990) **Information System Design,** Prentice-Hall, Inc.

Jones, O (1988) **Introduction to the X Window System,** Prentice-Hall, Inc.

Kwmpthorne,O (1971)**Probability, Statistics, and Data Analysis.** The Iowa State University Folks, L Press, U.S.A

Ljung,L (1987) **System Identification.** Sweden, Prentice-Hall, Inc.

Martin, J (1991) **Signals & Processes, A Foundation Course.** Pitman Publishing

NERC (1975) **Flood Studies Report.** Natural Environment Research Council, London

O'Donovan,T M (1983) **Short Term Forecasting.** John Wiley & Sons

Owens,M D (1986) **Real-Time Flood Forecasting Using Weather Radar Data.** PhD Thesis, Dept of Civil Engineering, University of Salford

Powell, S M (1985) **River Basin Models for Operational Forecasting of Flow in Real-Time.** PhD Thesis, University of Birmingham

Proakis, J G (1989) **Digital Communications.** McGraw-Hill Book Company

Schwartz,M (1981) **Information Transmission, Modulation, and Noise.** McGRAW-HILL International Book Company

Shepherd,G W (1987) **On the Utilisation of Weather Radar in the Simulation of Urban Drainage Networks.** PhD. Thesis, University of Birmingham

Software Sciences (1987) **Flood Forecasting System User Guide.** Document WF/UG/01, Bristol Avon Division, Wessex Water Authority

Software Sciences (1987) **Flood Forecasting System VAX/VMS User Notes.** Document WF/UG/02, Bristol Avon Division, Wessex Water Authority

SOM Division (1973) **Somerset Local Land Drainage District - Land Drainage Survey Report, Water Act 1973 Section 24(5).** Somerset Division, Wessex Water Authority

Su,S G (1977) **Information Theory with Applications.** McGraw-Hill International Book Company

Sudman, S (1976) **Applied Sampling.** Academic Press

Tilford,K A (1987) **Real-Time Flood Forecasting using Low Intensity Resolution Radar Rainfall Data.** MSc Thesis, Dept of Civil Engineering, University of Birmingham

Tou, J T, Gonzalez, R C (1974) **Pattern Recognition Principles, Addison - Wesley** Publishing Company

Viner, D, Cluckie, I, Collier, C.G (1991) **A Preliminary Analysis of the Hydrological Utilisation of 'FRONTIERS' System,** COST-73 Seminar, Yugoslavia

Yu, P S (1987) **Real-Time Forecasting Using Radar Data.** PhD Qualifying Thesis, Dept. of Civil Engineering, University of Birmingham

APPENDIX

WRIP GUI (Graphical User Interface)

Some principal user interfaces are illustrated in the following pictures.

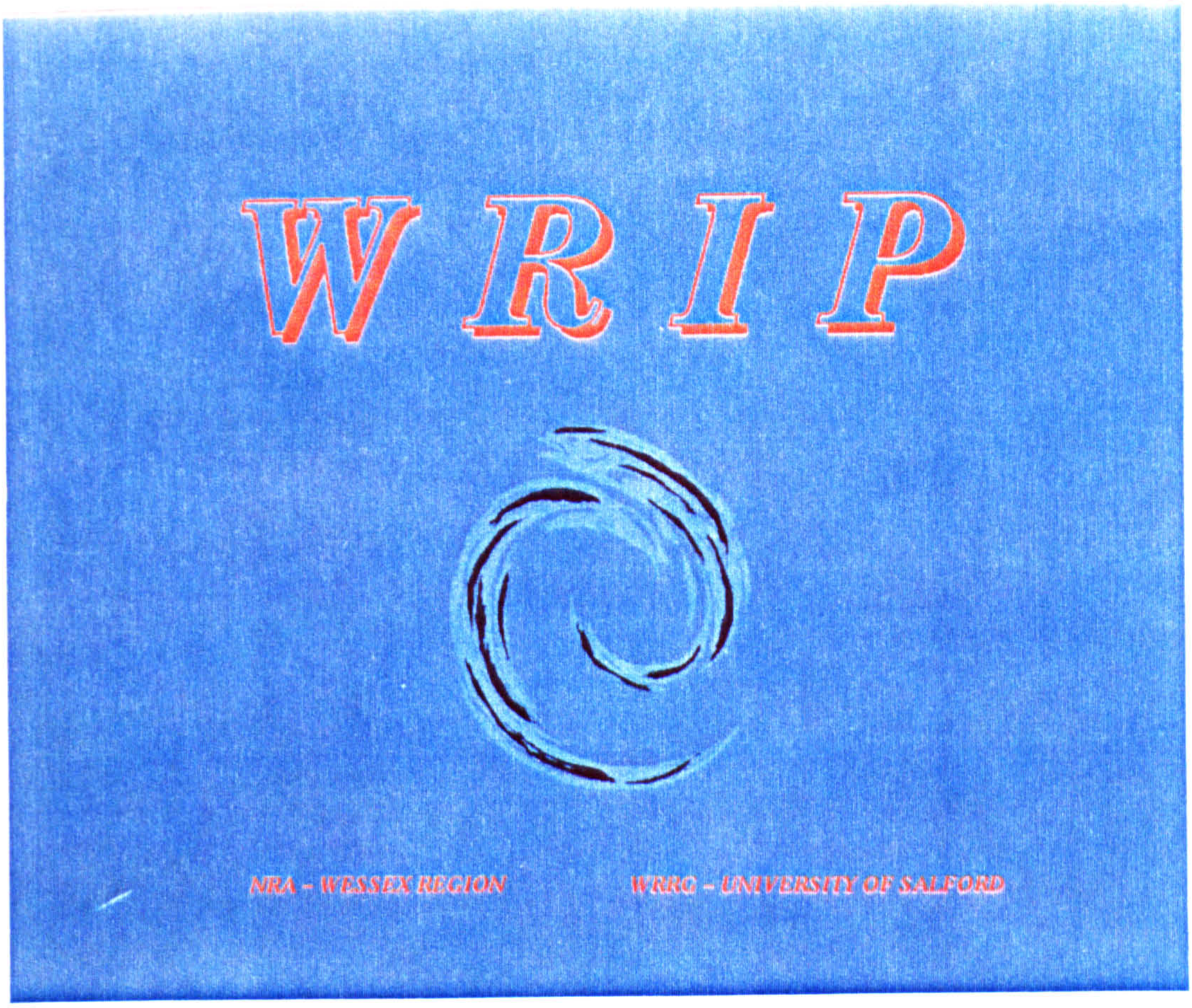

a) WRIP Start Screen

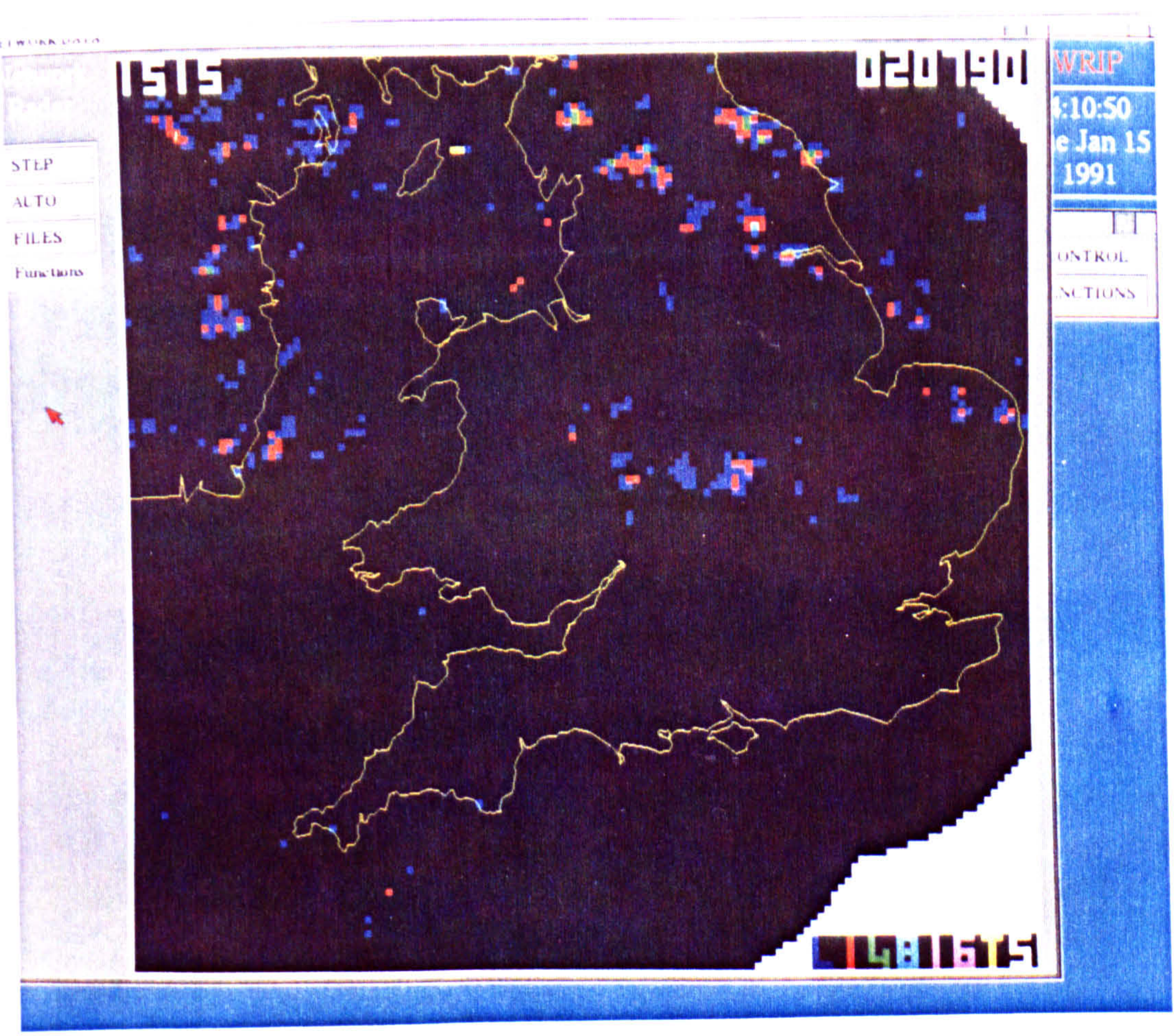

b) Network Radar Display Window

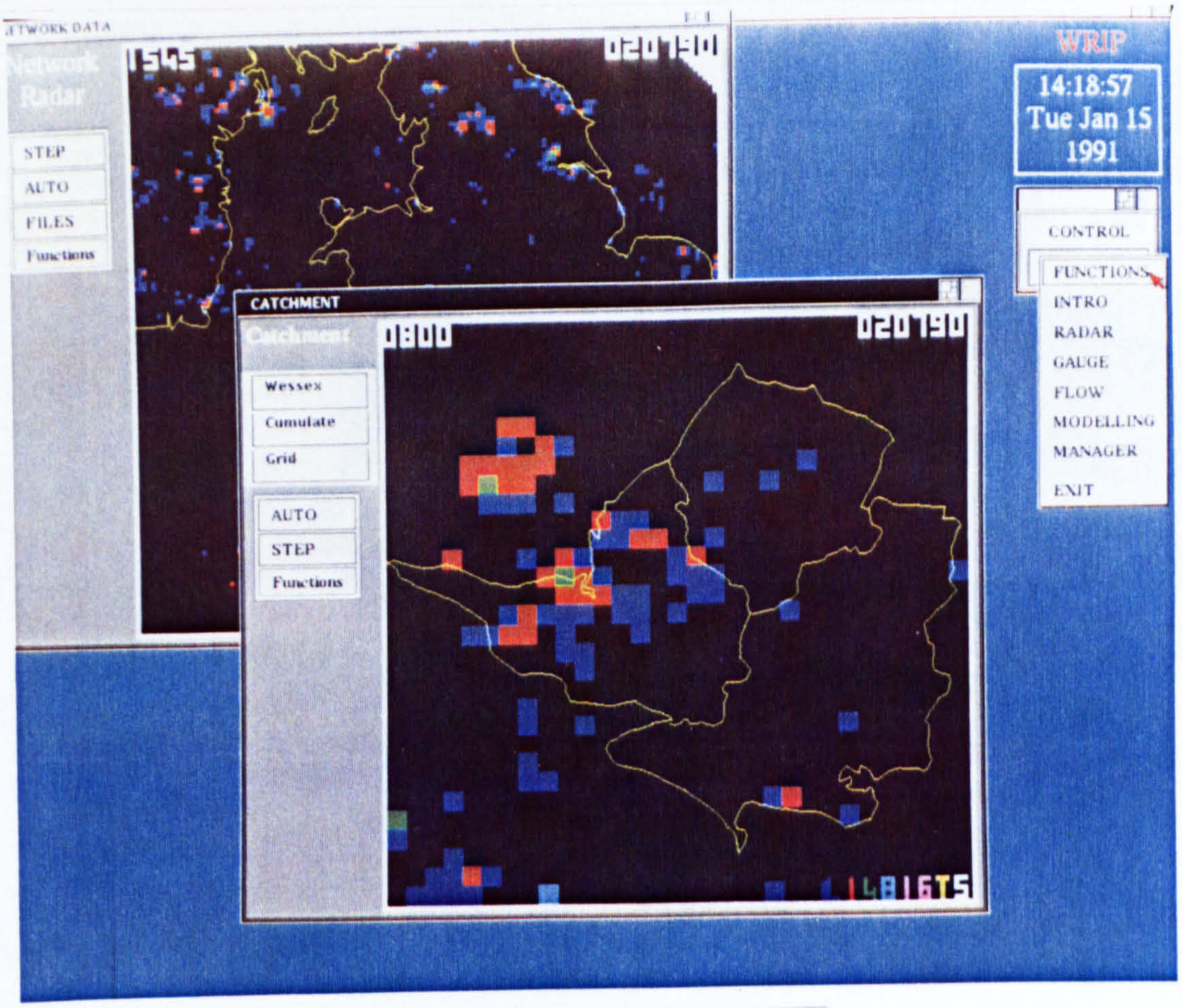

c) Catchment Zoom Window

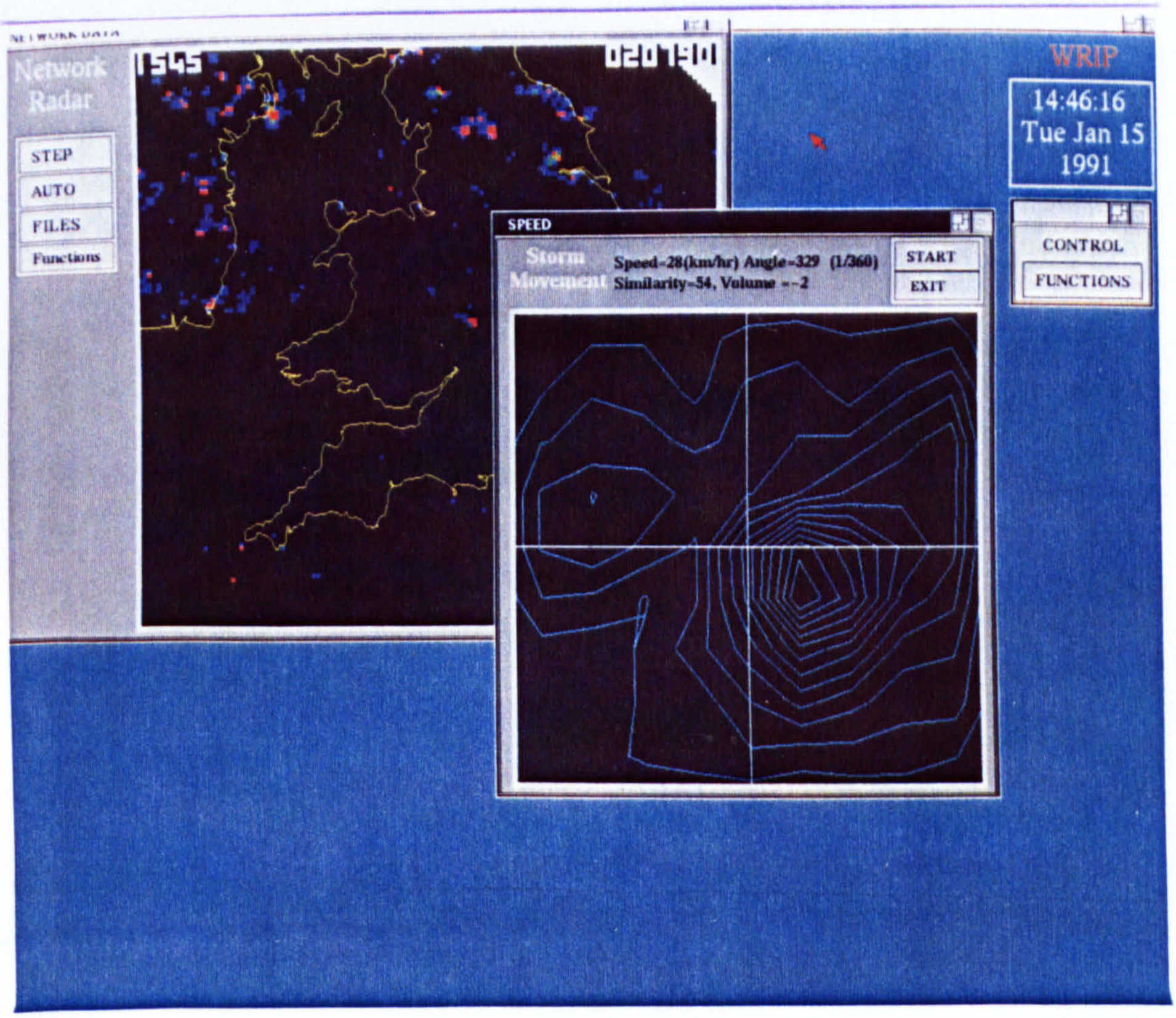

d) Storm Forecasting

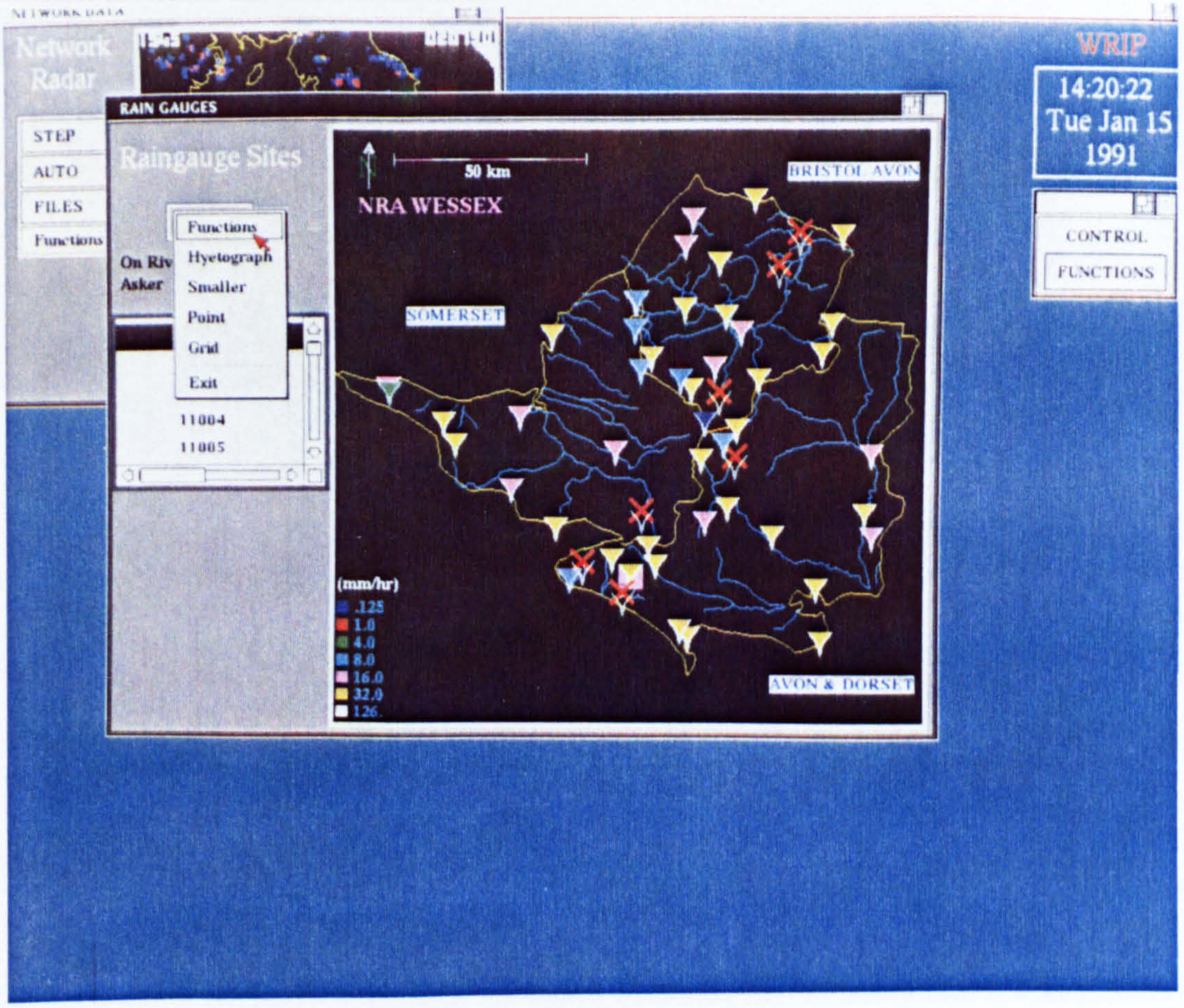

e) Raingauge Window

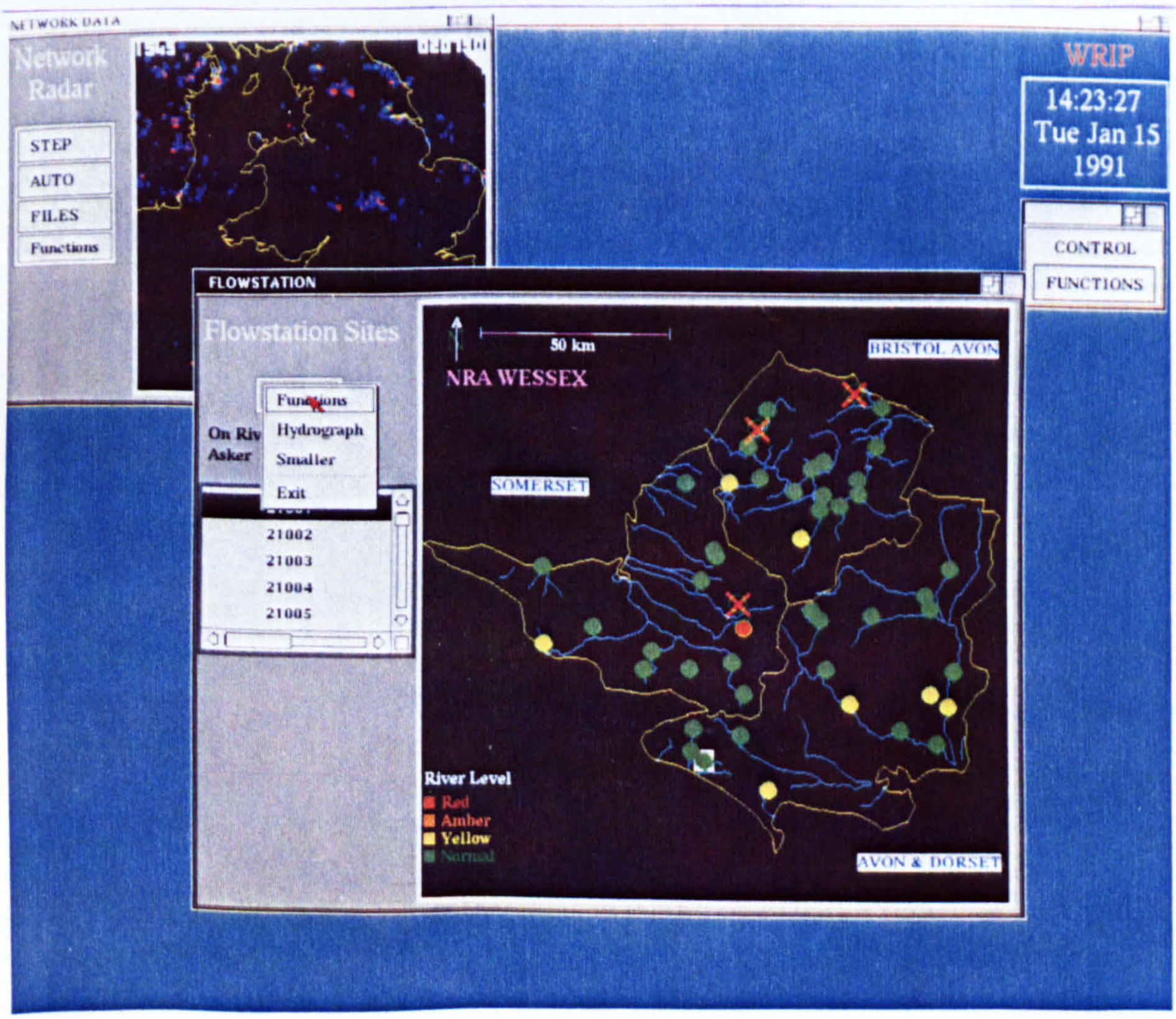

f) Flow Station Window

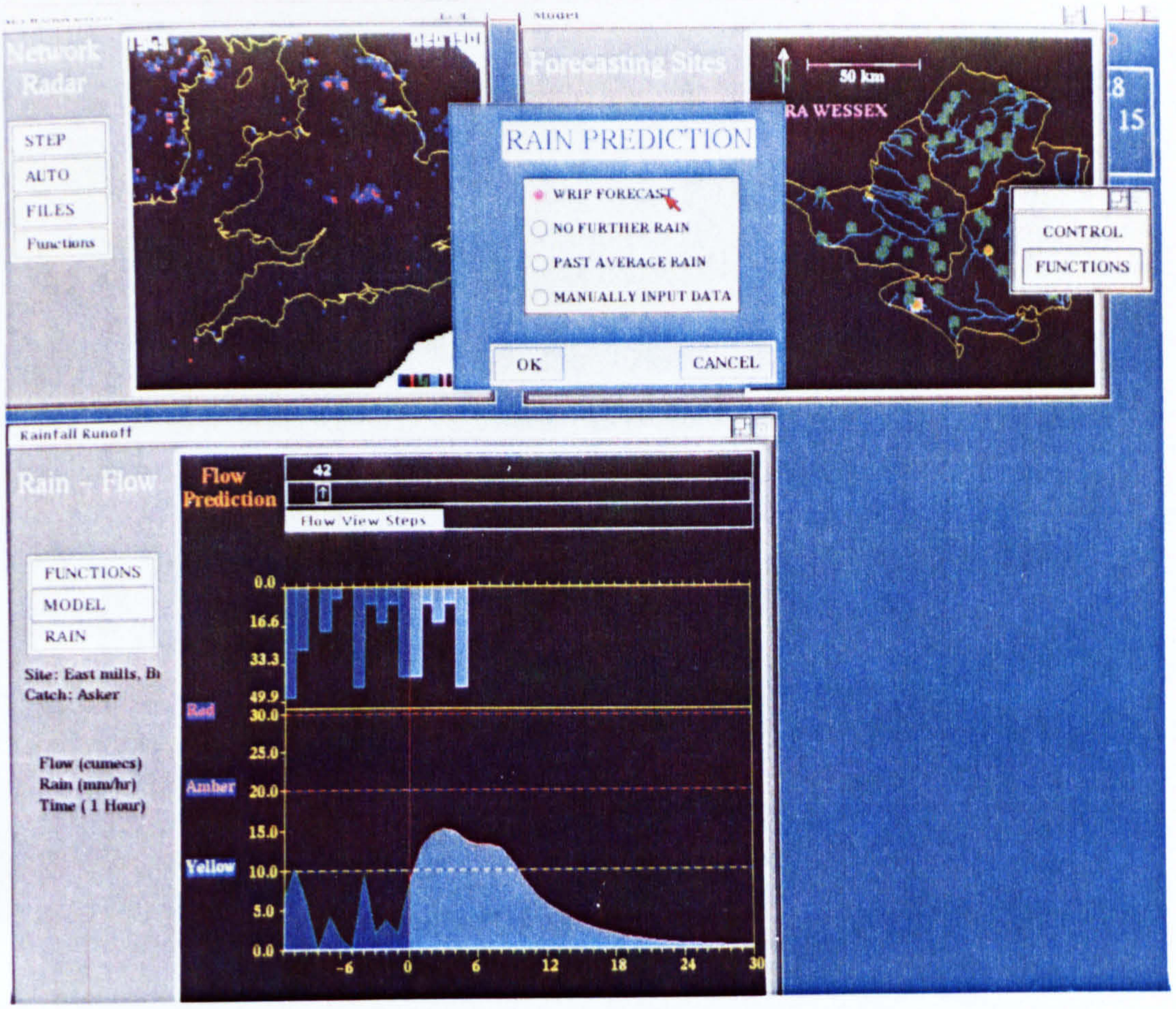

g) Flow Forecasting Window

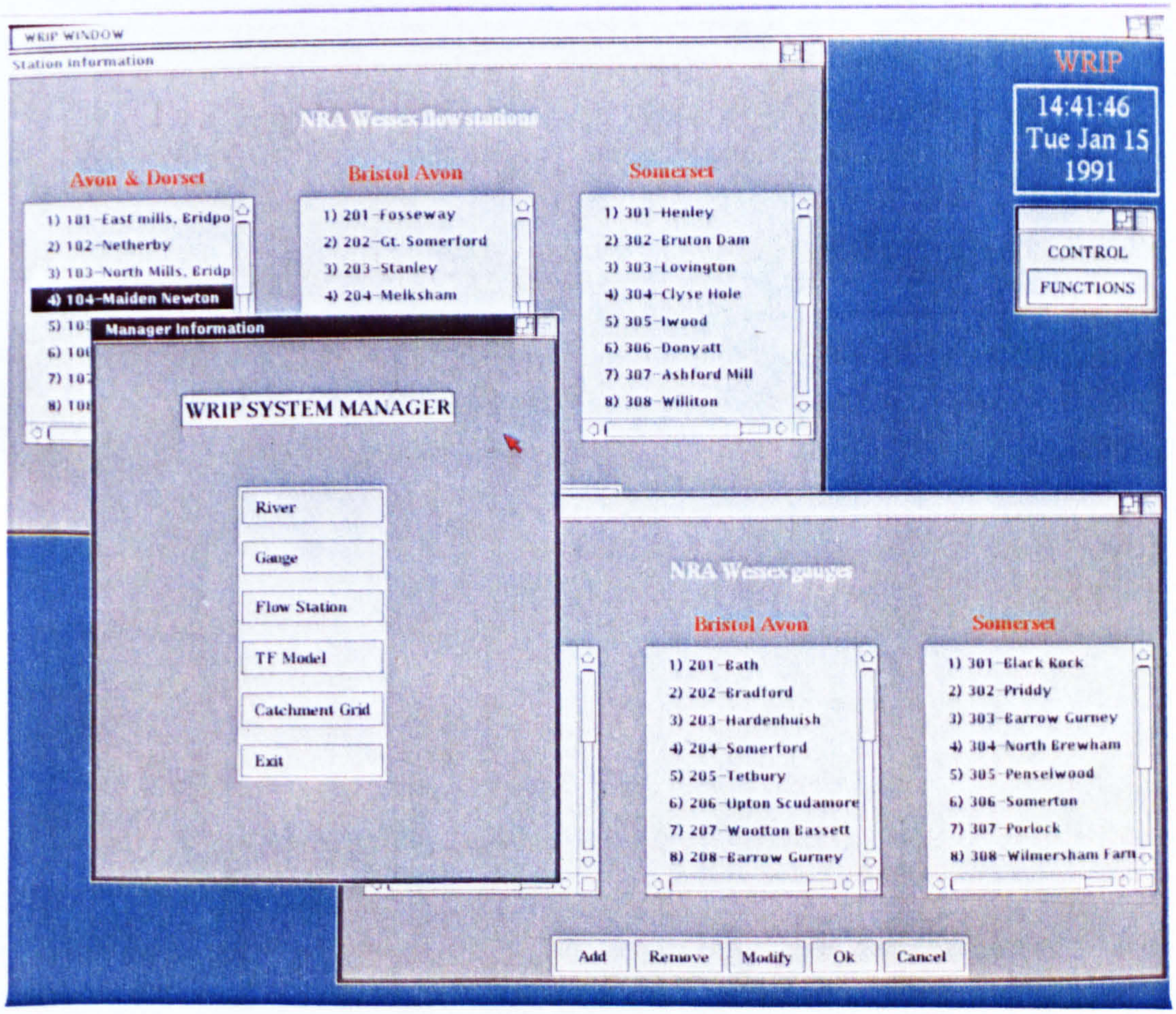

h) Database Management Window